WIND EFFECTS ON THE ROOF OF LOW-RISE STRUCTURES

A Thesis Submitted

in Partial Fulfilment of the Requirements for the

Degree of

DOCTOR OF PHILOSOPHY

in

CIVIL ENGINEERING

by

DEEPAK SHARMA

(Roll No.2K21/PHDCE/02)

Under the supervision of

PROF. SHILPA PAL & DR. RITU RAJ

Department of Civil Engineering

DELHI TECHNOLOGICAL UNIVERSITY

(Formerly Delhi College of Engineering)

Shahbad Daulatpur, Main Bawana Road, Delhi-110042, India

JUNE, 2025

ACKNOWLEDGEMENT

The work presented in this thesis would not have been possible without my close association with many people who were always there when I needed them the most. I take this opportunity to acknowledge them and extend my sincere gratitude for helping me make this thesis a possibility. At this moment of accomplishment, first of all, I would like to pay homage to the vice chancellor of Delhi Technological University, **Prof. Prateek Sharma**, who made this glorious temple to realize spiritual, technical and scientific knowledge about this vast existing universe.

I embrace the opportunity to express my deep sense of gratitude to my supervisors, **Prof. Shilpa Pal,** Department of Civil Engineering, Delhi Technological University, Delhi and **Dr. Ritu Raj**, Assistant Professor, Department of Civil Engineering, Delhi Technological University, Delhi, for their constant guidance, valuable suggestions and kind encouragement during my association with their research group. Their encouragement, constant support, intellectual stimulation, perceptive guidance, immensely valuable ideas, and suggestions from the initial to the final level enabled me to develop an understanding of the subject. Their scholarly suggestions, prudent admonitions, immense interest, constant help and affectionate behavior have been a source of inspiration for me. Their suggestions will remain with me as an inexhaustible source of scientific learning throughout my life.

I would like to express my sincere and wholehearted gratitude to the DRC members, **Prof. K.C. Tiwari**, Head of Department, Civil Engineering, Delhi Technological University, Delhi, **Prof. V.K. Minocha**, DRC Chairman, Department of Civil Engineering, Delhi Technological University, **Prof. M.S. Niranjan**, External Expert, Department of Mechanical Engineering, Delhi Technological University, **Prof. H.K. Sharma**, External University Expert, Department of Civil Engineering, NIT, Kurukshetra, **Prof. S.K. Verma**, External University Expert, Department of Civil Engineering, Punjab Engineering College, Chandigarh, for discussion during SRC and Pre-Ph.D. presentation and valuable suggestions given by them.

I would like to express my great appreciation and thanks to the staff of the Earthquake Engineering Laboratory and Computer-Aided Design Laboratory, Department of Civil Engineering Mr. Sanjay, Mr. Mahesh, Mr. Rakesh, Mr. Shashi Kant, Mr. Inder Singh, Mr. Vijay Sharma for their continuous assistance during the Ph.D. research work.

I am thankful to the unknown reviewers who have rejected my papers several times in some of the international conferences and journals. The comments that they provided helped to polish

our articles in better shape. But the bigger and nobler cause of thanking them is that the rejections have equipped me with a high level of patience and helped me a lot to exercise/implement my spiritual thoughts in practice.

My heartfelt thanks to my seniors **Dr. Rahul Kumar Meena, Dr. Nitin Lamba, Prateek Raushan, Dr. Vijay Kaushik, Kiran Cholak, Dharmendra Kumar** and fellow mates **Rishabh Tyagi, Shailesh Gupta, Shivangi Bharadwaj, Khyati Saggu, Payal Devi, Noopur Awasthi, Wesam Al-Agaha** for always being there and bearing with me the good and bad times during my wonderful days of my PhD. Also, I am thankful to **Amartya Sinha** (B.Tech Student) and **Nikhil Gaur** (M.Tech Student) for helping me in learning Ansys CFX, **Sudhanshu Pandey, Nitesh Thakur and Paras Nath** (B.Tech Students) for their kind support. I can see my thesis in good shape because of their help in formatting the entire thesis.

I will fail not only in my work rather in my life if I do not express my sincere thanks and gratitude to my parents, **Shri. R. S. Sharma** and **Smt. Lata Sharma** for their support, invaluable help and blessing to see this day. My special thanks to my sisters, **Jyoti Sharma, Arti Sharma** and **Pooja Sharma,** for always being with me in my good or bad times. I shall be grateful to my best friends, **Vibham Nayak** and **Venketshwar Rai,** for their efforts and support during this Ph.D. journey.

Last but not least, the bountiful blessings of the Omnipresent One are sought with reverence now and forever.

(DEEPAK SHARMA)

DELHI TECHNOLOGICAL UNIVERSITY
(Formerly Delhi College of Engineering)
Shahbad Daulatpur, Main Bawana Road, Delhi-42

CANDIDATE'S DECLARATION

I, **Deepak Sharma,** hereby certify that the work being presented in the thesis entitled **Wind Effects on the Roof of Low-Rise Structures** in partial fulfilment of the requirements for the award of the Degree of Doctor of Philosophy, submitted in the Department of **Civil Engineering**, Delhi Technological University is an authentic record of my own work carried out during the period from **02/08/2021** to **23/06/2025** under the supervision of **Prof. Shilpa Pal and Dr. Ritu Raj**.

The matter presented in the thesis has not been submitted by me for the award of any other degree of this or any other Institute.

Candidate's Signature

This is to certify that the student has incorporated all the corrections suggested by the examiners in the thesis and the statement made by the candidate is correct the best our knowledge.

Signature of Supervisor (s)   **Signature of External Examiner**

DELHI TECHNOLOGICAL UNIVERSITY
(Formerly Delhi College of Engineering)
Shahbad Daulatpur, Main Bawana Road, Delhi-42

CERTIFICATE BY THE SUPERVISOR(s)

Certified that **DEEPAK SHARMA** (2K21/PHDCE/02) has carried out their search work presented in this thesis entitled **"Wind Effects on the Roof of Low-Rise Structures"** for the award of **Doctor of Philosophy** from the Department of Civil Engineering, Delhi Technological University, Delhi, under my supervision. The thesis embodies results of original work, and studies are carried out by the student himself and the contents of the thesis do not form the basis for the award of any other degree to the candidate or to anybody else from this or any other University/Institution.

Signature   Signature

Prof. Shilpa Pal   **Dr. Ritu Raj**

(Professor, CED)   (Assistant Professor, CED)

Supervisor   Joint Supervisor

Date:

ABSTRACT

Severe windstorms, including tropical cyclones, cause significant damage globally, especially in coastal and inland regions of India. Roofs of low-rise buildings are particularly vulnerable, and wind loads on roofs have been a key area of research due to increasing public concern about windstorm damage. Roof geometry plays a critical role in wind pressure distribution but is often overlooked, resulting in conflicting and inadequate documentation in most Standards and Codes of Practice.

A review of existing literature highlights gaps in understanding wind pressures on roof projections, eaves, canopies, and open verandahs, emphasizing the need for detailed studies on diverse roof forms. Wind loading data is primarily derived from wind tunnel tests on scaled models, but recent comparisons with full-scale studies underline the importance of accurate flow simulation for better insights.

Additionally, wind standards of various nations have inadequate information to address the effects of nearby buildings on wind pressure patterns and magnitudes. Research in such interference scenarios is limited, with wind tunnel tests and CFD simulations being the main tools for analysis. This study aims to use CFD simulations to investigate wind effects on low-rise buildings with different roof designs, both in isolation and in the presence of neighbouring structures.

This study examines the wind flow patterns around low-rise buildings with various roof shapes through numerical simulations. Using Computational Fluid Dynamics (CFD), the research employs Reynolds-averaged Navier-Stokes simulations (RANS) and large eddy simulations (LES). The study uses scaled-down (1:50) models, and the results are compared with established codes to validate the simulations. With the rapid advancements in CFD, it has gained increasing acceptance in recent decades. The study also identifies critical flow regions around differently shaped buildings. These areas, which experience notably high positive and suction pressures, are more susceptible to partial structural failures compared to other sections, highlighting the need for careful consideration by wind engineers.

In the present study, low-rise buildings with four types of roof forms are considered namely dome roof, cylindrical roof, mono-slope roof and hip roof. A Dome roof building is considered to have a square plan. Buildings with other three roof forms are considered to have a rectangular plan. For interference conditions, there are three different configurations of interference considered i.e., rectangular pattern, T pattern and Z pattern in which the six isolated models of

low-rise buildings are arranged in the mentioned pattern with different spacing configurations i.e., 0, 0.5B, B, 1.5B and 2B where B is the width of building. The building models are considered to be situated in sub-urban terrain with well-scattered objects having heights between 1.5 m to 10 m, defined as terrain condition 2 in IS 875 (Part-3): 2015.

The wind pressure distribution and pressure coefficient (C_{pe}) on all the roofs are measured at different angles of wind incidences, namely 0° to 180° at 15° wind intervals. Depending upon the symmetry of the roof, the dome roof is only tested for 0°, and 45° wind angles, cylindrical and hip roofs are tested for 0° to 90°, and the mono-slope roof is tested for 0° to 180° wind incidence angles. Similarly, for interfering conditions, the buildings arranged in different patterns (rectangular, T and Z) with variable spacing configurations are subjected to various angles of wind incidences at an interval of 15°. The pressure contours, pressure coefficient (C_{pe}), interference factor (IF) and interference difference (ID) are evaluated and presented for different interfering conditions.

The results from the analysis showed that the overall effects of wind on the roof surface are suction in nature, which fluctuates due to the change in wind incidence angles. For cylindrical roofs, the small roof portion near the windward edge is subjected to the positive wind-induced pressure, and the rest of the roof portion is under suction, while the dome, mono-slope and hip roof are under only suction.

The effect of shielding plays a vital role in reducing the wind load on the interfering roof when the spacing between buildings and angles of wind incidence angles change. The reduction in suction for dome roof is 88.46%, 87.41% on cylindrical roof, 85.27% on mono-slope roof and 80.18% on hip roof. Also, it is observed from the CFD simulation that the rectangular pattern of arrangement with variable spacing is more beneficial and stable than that of T and Z patterns in reducing the wind-induced pressure on the different roofs of low-rise buildings.

The results presented in the thesis can be used in future for the revision of codal recommendations about wind loads on low-rise buildings with different roof forms. These can also be used by the designers while designing the roofs of similar low-rise buildings.

List of Publications

Journal

1. Sharma, D., Pal. S. and Raj, R. "Numerical Prediction of Proximity Effects on Wind Loads on Low-Rise Building with Cylindrical Roofs", Wind and Structure, An International Journal, 36 (4), April 2023, 277-292. https://doi.org/10.12989/was.2023.36.4.277. **(SCIE, IF-1.6)**

2. Sharma, D., Pal, S. and Raj, R. "Effect of spacing on wind-induced interference on the roof of low-rise buildings with cylindrical roof using CFD simulation," Sadhana - Acad. Proc. Eng. Sci., vol. 48, no. 4, 2023. https://doi.org/10.1007/s12046-023-02351-5. **(SCIE, IF-1.6)**

Conference Proceedings

1.	Sharma, D., Pal, S. and Raj, R. "CFD Simulation of Wind Effects on Cylindrical Roof of T-Plan Multi-Span Low-Rise Building" Advances in Construction Management, Proceedings of ICCRIP, 2023, Lecture Notes in Civil Engineering, Springer. **(Scopus)**

2.	Sharma, D., Raj, R. and Pal, S. "Effects of different types of roofs under wind loads for low-rise structures," AIP Conference Proceedings, 2024, vol. 030008. https://doi.org/10.1063/5.0192953. **(Scopus)**

3.	Sharma, D., Raj, R. and Pal, S. "Effects of Roof Shapes on Wind Pressure Distribution of Multi-Span Low-Rise Buildings," Proc. Int. Struct. Eng. Constr., vol. 10, no. 1, pp. 1–6, 2023, doi: 10.14455/10.14455/isec.2023.10(1).str-19. **(Scopus)**

Conference Participated

1. Sharma, D., Pal, S. and Raj, R. "Effects of Different Types of Roofs under Wind Loads for Low-Rise Structures". International Conference on Advances in Civil Engineering (ICACE 2022), 20-22 Dec. 2022. Organized by Technology Research and Innovation Centre, India and hosted by LSKBJ College of Engineering, Chandwad, Nashik, India.

2. Sharma, D., Pal, S. and Raj, R. "Effects of Roof Shapes on Wind Pressure Distribution of Multi-Span Low-Rise Buildings". The Twelfth International Structural Engineering and Construction Conference (ISEC-12), 14-18 Aug. 2023. Organized by the University of Illinois, Chicago.

3. Sharma, D., Pal, S and Raj, R. "CFD Simulation of Wind Effects on Cylindrical Roof of T-Plan Multi-Span Low-Rise Building". 7th International Conference on Construction, Real Estate, Infrastructure and Project Management (ICCRIP 2023), 11-12 Aug. 2023. NICMAR University, Pune. (Best Paper Award)

4. Sharma, D., Saggu, K., Raj. R. and Pal, S. "Optimizing Wind-Induced Interference on Mono-Slope Roofs: Insights from CFD Modeling and Machine Learning Validation" National Conference on Futuristic Structural Engineering (StructE NatCon 2024) organized by Indian Association of Structural Engineers, 8-10, November 2024, New Delhi, India.

5. Sharma, D., Raj, R. and Pal, S. "Wind Load Optimization on Multi-Span Mono-Slope Roofs of Low-Rise Buildings using CFD Simulation". Third International Conference on Construction Engineering, 23rd-24th February, 2025, Damascus University, Syria.

Journal Papers Communicated

1. Sharma, D., Pal, S. and Raj, R. "Boundary layer Aerodynamic Prediction over various Roof Shapes of Low-Rise Structures" **(Under Review)**

2. Sharma, D., Pal, S. and Raj, R. "Extrapolating Wind-Induced Interference on Mono-Slope Roof of Low-Rise Buildings: CFD Simulation Vs XG Boost Algorithm" **(Under Review)**

Table of Contents

List of Tables

List of Figures

List of Symbols

A	Effective Frontal Area of Building
B	Breadth of Building
H	Height of the Building
P_d	Design Wind Velocity Pressure
S	Spacing between Buildings
V	Mean Velocity of Wind at any Height
V_d	Design Wind Velocity
V_b	Base Wind Velocity
V_{ref}	Mean Wind Velocity measured at Boundary Layer Depth
α	Power Index
ρ	Density of Air
θ	Wind Direction
υ	Kinematic Viscosity of air
C_{pe}	External Wind Pressure Coefficient
C_p	Mean Wind Pressure Coefficient
FST	Free Stream Turbulence
k-ε	K-epsilon turbulence model
SST	Shear Stress Transport Turbulence Model
k-ω	K-omega Turbulence Model
DNS	Direct Numerical Simulation
BAF	Building Amplification Factor
LES	Large Eddy Simulation
FEM	Finite Element Method
TTU	Texas Tech University
GVE	Global Venturi Effect
LVE	Local Venturi Effect
CAARC	Commonwealth Advisory Aeronautical Council Building
RANS	Reynold Average Navier Stroke
PSD	Power Spectrum Density
CFD	Computational Fluid Dynamics

CHAPTER 1

INTRODUCTION

1.1 General

Wind serves a dual role, acting as both a valuable ally and a potential adversary. It proves beneficial when harnessed for energy production through wind turbines, where the wind's kinetic energy is converted into mechanical power to generate electricity. With a global installed power generation exceeding 440 GW in 2017 and expected to surpass 720 GW by 2020, wind energy continues to grow **(Blaabjerg and Ma, 2017)**. Additionally, wind plays a positive role in dispersing air pollutants from industrial chimneys, contributing to cleaner and healthier urban air. Throughout history, wind has aided sailors in navigating seas.

Conversely, the impact of wind flow on buildings can pose challenges, exerting loads on structures like roofs and walls, and causing discomfort for pedestrians at street level. In these scenarios, wind becomes adverse, necessitating careful consideration in the design of buildings and urban planning.

Since the 1960s, wind tunnel experiments on models of buildings in the atmospheric boundary layer have been the primary means of determining wind design loads. Due to the expense of conducting full-scale tests, engineers heavily rely on the ongoing advancements in wind tunnel testing for novel building shapes. This method remains crucial for establishing wind design codes that include wind pressure and force coefficients for various generic building shapes. Initial studies concentrated on structures with gable roofs by **Davenport et al., 1977** and mono-sloped roofs by **Stathopoulos and Mohammadian, 1991,** followed by investigations into the wind loads on hipped-roof buildings **(Meecham, 1992)**. These efforts were particularly significant for evaluating wind loads on low-rise structures. As architectural styles evolve, continuous wind tunnel studies are essential to update wind load regulations and validate existing provisions with the emergence of new information.

1.2 Types of Structures

Building design criteria vary based on height, distinguishing between low-rise and high-rise structures. Predicting wind load patterns and magnitudes proves more complex for low-rise buildings, situated in the lower part of the atmospheric boundary layer characterized by high wind velocity gradient, turbulence, and flow unsteadiness.

Buildings can be broadly categorized into low-rise and high-rise structures based on their height. Low-rise structures typically have a height of less than 20 m, while high-rise structures generally exceed 50 m above the average ground level within their boundaries. Mid-rise

buildings fall within the 20 m to 50 m height range. High-rise buildings may have further subcategories based on their height, such as sky-rise (150 m to 300 m), super-tall (300 m to 600 m), or mega-tall (above 600 m) structures.

The calculation of loads and design criteria for structures varies based on their height. Tall buildings, in particular, face elevated lateral wind loads on their vertical surfaces, especially at upper levels, resulting in substantial pressure and increased wind forces. Conversely, low-rise structures are situated within the atmospheric surface layer of the earth, where accurately assessing wind flow proves challenging.

1.3 Different Types of Roof Shapes for Low-Rise Structures

Low-rise buildings are equipped with a variety of roof designs, including flat roofs, canopy roofs, gable or pitched roofs, north light roofs, saw-tooth roofs, skylight roofs, hip roofs, domical roofs, cylindrical roofs, gambrel roofs, and more as shown in Fig. 1.1 to 1.13.

Fig. 1.1: Flat Roof (Los Angeles)
https://en.wikipedia.org/wiki/Flat_roof

Fig. 1.2: Canopy Roof
www.livingspaceltd.co.uk/commercial-canopies/curved-roof-canopies/

Fig. : Pitched Roof in Hugo
https://www.berkeleyheritage.com

Fig. 1.4: Multi-Span Gable Roof
https://www.geograph.org.uk

Fig. 1.5: Multi-Span North-Light Roof
https://www.geograph.org.uk

Fig. 1.6: Saw Tooth Roof of Museum
https://solaripedia.com

Fig. 1.7: Skylight Roof Lantern's
www.traditionalproductreports.com/doors-skylights

Fig. 1.8: Hip Roof House
htts://blog.davinciroofsapes.com/

Fig. 1.9: Single Dome Roof
https://hawkebackpacking.com/israel_jerusalem

Fig. 1.10: Multi Domes Roof
https://commons.wikimedia.org

Fig. 1.11: Cylindrical Roof
www.flickr.com/photos/trainplanepro

Fig. 1.12: Multi-Span Cylindrical Roofs
www.chinakingpeng.com

Fig. 1.13: MI Gambrel Roof
https://www.hansenpolebuildings.com/

1.4 Low-Rise Structures subjected to Extreme Wind Effects

In the past few years, there have been several instances of roof structure failures caused by powerful winds. For instance, in 2018, strong winds at Hobby Airport in Houston (Fig. 1.14) resulted in damage to the hangar roof, affecting parked airplanes. In India, the east coast and Gujarat region on the west coast frequently face cyclones, leading to substantial roof damages across various structures (Fig. 1.15). Additionally, in 2022, notable structures in London and Texas also suffered significant roof damage due to high-speed winds (Fig. 1.16 & Fig 1.17).

Moreover, a majority of structures worldwide are characterized as low-rise buildings, and the financial repercussions of wind-related damages to such structures are substantial. This underscores the crucial need to thoroughly examine wind loads on low-rise buildings to ensure the development of safe and cost-effective designs for these constructions. Fig. 1.18 illustrates roof damage on recently constructed low-rise buildings in Tasmania resulting from a windstorm in April 2017. Additionally, Fig. 1.19 depicts severe roof damage to a gabled roof building caused by strong winds in Chicago's Park in April 2016.

Fig. 1.14: Damaged Hangar, Hobby Airport
https://www.newindianexpress.com/world/201
8/apr/04/wind-gusts-cause
hangar-collapse-at-hobby-airport-in-houston-
1797010.html

Fig. 1.15: Damaged Petrol Pump, Gujrat
https://weather.com/news/news/2021-05-17-
india-cyclone-tauktae-preparing
landfall

Fig. 1.16: Damaged Roof, O2 Arena, London
https://www.timeout.com/london/news/storm-
eunice-london-the-roof-of-the
o2-has-literally-ripped-021822

Fig. 1.17: Arial View of Damaged Roofs, Texas
https://www.nytimes.com/2022/03/21/us/severe-
weather-forecast
tornadoes.html

Fig. 1.18: Roof Damage of new building due to wind storm in Tasmania, April 2017
http://www.abc.net.au/news/2017-04-27/the-roof-peeled-back-from-a-house-in-kingsmeadows/8475332

Fig. 1.19: Roof damage of gable roof building caused by heavy winds in Chicago, April 2016
http://www.skylinenewspaper.com/wind-storm-rips-roof-from-apartment-building/

1.5 Scope of the Study

Low-rise structures are commonly erected with a standard plan size, typically up to 60 m or 200 ft and height up to 20 m serving residential, industrial, and commercial needs. However, there is a subset of low-rise structures designed with expansive plan dimensions exceeding 60 m or 200 ft to fulfill specific functions that demand substantial space. These larger buildings often feature low-slope roofs (with a slope between 0° and 7°) or flat roofs. Examples of such structures include grain storage buildings, commercial poultry breeding facilities, and expansive shopping centers. In many cases, large low-rise buildings are characterized by the use of low-slope roofs.

To engineer low-rise buildings of this nature to withstand wind loads, structural designers must adhere to the guidelines and recommendations outlined in current codes and standards **(IS 875 (Part-3):2015, ASCE 7-16, MNBC:2020, NCH 432, GB 50,009:2001, NSCP:2015, EN 1991:1-4, ANZ 1170.0.2002).** Nevertheless, it's important to note that the wind provisions in these codes and standards were developed through extensive wind tunnel studies primarily focused on testing models of regularly sized low-rise buildings. Notably, very limited studies have specifically examined the wind effects on low-rise buildings with larger dimensions, multi-span roofs, variable spacing, and similar features.

Therefore, it becomes essential to investigate wind loads on buildings with expansive plan dimensions due to the fact that the wind provisions in the design code of India, and other nations, were formulated based on research focused on structures of standard size. A comprehensive wind tunnel study is necessary for large roof models to evaluate the

appropriateness of existing wind provisions in various design codes and standards concerning economic considerations and structural safety for large low-rise buildings.

1.6 Objectives

The primary focus of this current investigation is to assess the numerical results in relation to the codes and standards applicable to low-slope roofs in low-rise buildings with substantial configurations, as observed in various nations, including India. The specific objectives of this study are outlined in detail as follows:

1. To study the effects of different types of roofs under wind load for low-rise structures.
2. To study the wind effect on different configurations of the roof slope.
3. To study the effect of interference between clusters of buildings under variable spacing.
4. Identification of suitable roof types for low-rise structures under wind load.

1.7 Organization of the Thesis

Chapter 1 deals with the introduction of wind effects on structures in which the classification of structures based on height is discussed, and different types of roof shapes and their damages due to wind are illustrated. The chapter contains the scope and objectives of the study as well.

In Chapter 2, fundamental concepts in wind engineering are discussed, covering topics such as wind speed, atmospheric boundary layer, turbulence, wind spectrum, and the use of boundary layer wind tunnels and computational fluid dynamics. Additionally, the chapter explores the historical research contributions that have aided in understanding and identifying the impact of wind on buildings and structures.

Chapter 3 provides an in-depth exploration of computational fluid dynamics (CFD) simulations, delving into the details of the techniques for measuring wind speed and examining the characteristics of the wind speed profile. The chapter offers a comprehensive overview of the building models, outlining their specifications. Furthermore, it covers the pressure measurement system employed to capture wind pressures on the model roofs, and details the methodology utilized for analyzing the recorded wind pressures.

Chapter 4 presents the outcomes of the current investigation, showcasing contours of enveloped pressure, area-averaged pressure coefficients, interference factors, and interference differences for the dome roof. Additionally, the chapter includes comparisons with findings from earlier studies and data obtained from CFD simulations.

Chapter 5 presents the outcomes of the current investigation, showcasing contours of enveloped pressure, area-averaged pressure coefficients, interference factors, and interference differences for the cylindrical roof. Additionally, the chapter includes comparisons with findings from earlier studies and data obtained from CFD simulations.

Chapter 6 presents the outcomes of the current investigation, showcasing contours of enveloped pressure, area-averaged pressure coefficients, interference factors, and interference differences for the mono-slope roof. Additionally, the chapter includes comparisons with findings from earlier studies and data obtained from CFD simulations.

Chapter 7 presents the outcomes of the current investigation, showcasing contours of enveloped pressure, area-averaged pressure coefficients, interference factors, and interference differences for the hip roof. Additionally, the chapter includes comparisons with findings from earlier studies and data obtained from CFD simulations.

Chapter 8 includes the comparison of all four different roofs to find out the best suitable roof. Chapter 9 presents the conclusions drawn from the research and recommendations for further studies.

CHAPTER 2
LITERATURE REVIEW

2.1 General

This chapter provides a comprehensive review of the existing literature relevant to the wind effects on the roofs of low-rise structures, with the aim of situating the current study within the broader context. The literature review synthesizes key theories, concepts, and findings from previous research, highlighting both the progress made in the field and the gaps that remain. By critically analyzing wind standards of different nations and previous research, this chapter establishes the theoretical framework for the study and justifies the need for the current research, which seeks to contribute to the ongoing academic conversation.

2.2 Review of Wind Engineering

Wind engineering can be defined as the systematic consideration of the interplay between the atmospheric boundary layer's wind and human activities and structures situated on the Earth's surface **(Cermak, 1990).**

Wind engineering primarily focuses on assessing the pressures exerted by wind on structures. This involves the consideration of two key components: the wind itself, which is a gaseous fluid, and the structures. Consequently, a comprehensive understanding of fluid and structural mechanics is essential in wind engineering to grasp the interaction between wind flow and various civil engineering structures like buildings, chimneys, signboards, as well as mechanical engineering structures such as planes and cars.

Naturally, the airflow close to the Earth's surface is turbulent due to surface roughness. When the wind encounters obstacles like buildings or trees, the turbulence intensifies, leading to additional unpredictability in the wind flow pattern. This, in turn, results in heightened and fluctuating wind-induced pressures on structures. The complexity of the wind flow regime makes it challenging to quantify accurately. Consequently, relying on computer models, specifically computational fluid dynamics (CFD), for assessing wind-induced pressures on buildings is considered unreliable. The most trustworthy approach involves either conducting full-scale measurements of wind pressures or testing building models in wind tunnels that simulate the boundary layer. These techniques provide accurate reflections and simulations of the actual wind flow regime and its interaction with buildings.

The current national codes and standards incorporate wind provisions that were developed through comprehensive wind tunnel experiments conducted on a variety of structures.

2.3 Review of Boundary Layer Formation

In the scenario of an ideal fluid, the fluid particles can smoothly glide along the surfaces of immersed bodies without experiencing any loss in velocity from their original free stream velocity. However, in the context of real fluids, there is adhesion between the fluid particles and the surface, causing them to adhere and create a contact layer with zero relative velocity. Brownian Motion among fluid particles leads to a slowing down of momentum in the contact layer, affecting the immediate upper layer. This process continues until each layer reaches the free stream velocity. Consequently, the immersed body hinders the flow in its vicinity, resulting in what is known as viscous drag. The entire region of slowed flow is termed the boundary layer. When the momentum exchange between layers is solely due to Brownian motion, this boundary layer is referred to as a laminar boundary layer. This phenomenon is typically observed at low flow velocities and near the leading edges of immersed bodies. However, as the distance from leading edges increases and flow velocity rises, the boundary layer becomes unstable, giving rise to turbulent eddies. This turbulent boundary layer is thicker than the laminar counterpart and leads to increased viscous drag.

2.3.1 Flow Separation, Wake Formation and Vortex Shedding

Objects within a flow field are generally categorized into two types: streamlined bodies and bluff bodies. A bluff body causes separation of the flow over its surface, while a streamlined body prevents such separation. In air flow, most buildings act as bluff bodies. Achieving a perfectly streamlined body in wind flow is practically challenging, but structures resembling airfoils come close due to their streamlined surfaces with minimal boundary layer thickness. The disturbed flow region around a body is termed the wake region, which is narrower for streamlined bodies (see Fig. 2.1) due to the small boundary layer thickness, facilitating easier reattachment of flow. In contrast, for bluff bodies (see Fig. 2.1), reattachment is more challenging due to the development of a thin region with high shear and vorticity. The concentrated vortices formed by shear layers move along the surface of the bluff body and gradually lose energy, a phenomenon referred to as vortex shedding. The geometry of the bluff body influences the pattern and effectiveness of vortex shedding.

2.3.2 Atmospheric Boundary Layer

During the 1870s, British engineer William Froude conducted laboratory experiments involving the towing of a thin plate in calm water. His goal was to investigate the impact of the frictional resistance generated by the moving plate on the undisturbed water. Froude's research introduced the concept of the boundary layer to the scientific community.
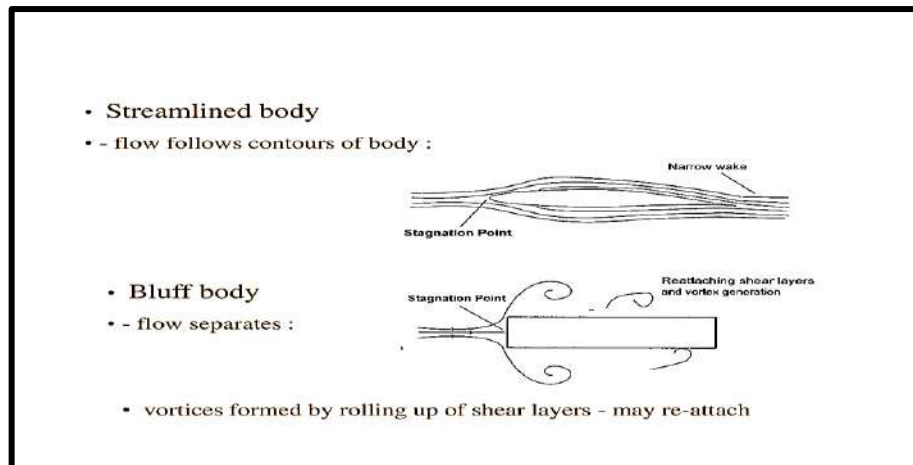
Fig. 2.1: Flow around Streamlined and Bluff body
https://slideplayer.com/13063812/79/images/slide_1.jpg

The term 'boundary layer' was first coined by the German scientist Ludwig Prandtl in 1905, following his thorough experimental investigations into the flow of low-viscosity fluids near a solid boundary. Defining the atmospheric boundary layer precisely has always posed a challenge. However, a practical working definition characterizes the boundary layer as the air layer immediately above the Earth's surface within a timescale of less than a day. This layer is marked by turbulent motion, and it plays a crucial role in carrying substantial fluxes of momentum, heat, or matter over distances approximately equal to or smaller than the depth of the boundary layer **(Garret, 1984).**

When analyzing a flow, it is typically separated into two interacting components. On one hand, there is the 'free fluid,' treated as if it were frictionless based on Helmholtz vortex theorems. On the other hand, there are the transition layers near solid walls. While these layers are influenced by the motion of the free fluid, they, in turn, contribute distinctive characteristics to the free motion through the emission of vortex sheets **(Prandtl, 1905).**

Put simply, the atmospheric boundary layer can be defined as the segment of air movement directly above the Earth's surface. This layer experiences the influence of ground roughness friction, resulting in the formation of a wind layer with variable speeds. Beginning with nearly zero wind speed in close proximity to the ground surface (at height = 0), the layer extends to a height where the wind speed matches that of the undisturbed wind flow, far from the Earth's surface.

The vertical profile of mean wind speed within the atmospheric boundary layer is illustrated in Fig. 2.2. The mean wind speed starts at zero at the Earth's surface and progressively increases with height (Z) in an exponential manner until it reaches a point where the air stream is no longer influenced by ground roughness as depicted. This specific height is referred to as the

gradient height (Z_G), and at this height, the mean wind velocity is termed gradient velocity ($\bar{V}_Z$). The gradient height serves as the boundary between the air flow affected by ground roughness and the free stream. Above the gradient height, it is assumed that the mean wind velocity remains constant and is equal to the gradient velocity.
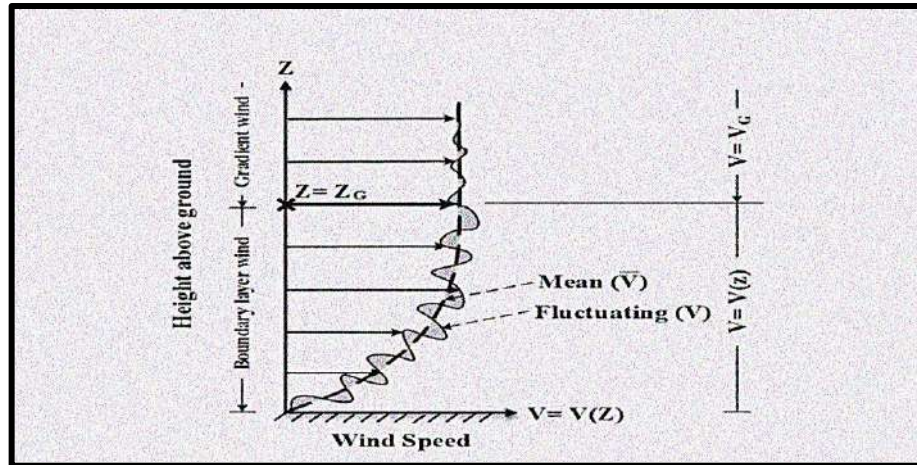
Fig. 2.2: Vertical Wind Velocity Profile in Atmospheric Boundary Layer
https://discover.hubpages.com/education/What-is-the-Atmospheric-Boundary-Layer

2.3.3 Turbulence

Irregular movement that typically occurs in gases or liquids when they move across solid surfaces, or when adjacent streams of the same fluid pass by or intersect with each other is called as turbulence **(Taylor, 1937).**

Mechanical turbulence arises in the atmospheric boundary layer due to the interaction between wind flow and the roughness of terrain, along with shear forces generated within the flow. While meteorological turbulence, resulting from convective air movements, plays a role in overall wind turbulence, its impact is relatively minor at high wind speeds in the atmospheric boundary layer.

The level of wind turbulence varies depending on the type of terrain it encounters. For example, wind passing over urban areas experiences higher turbulence compared to wind passing over open country. Additionally, as the height increases, turbulence decreases because the impact of ground roughness diminishes the further away from the surface of the earth.

2.3.4 Boundary Layer Wind Tunnel (BLWT)

In the initial stages, the assessment of wind impacts on structures and machinery relied on aeronautical wind tunnels, where the model being tested experienced consistent wind speeds across all its components. However, this methodology proved inadequate in predicting the genuine wind effects on structures as it failed to replicate the authentic wind flow above the Earth's surface. The necessity for a more precise simulation of natural wind within the

atmospheric boundary layer, asserting that the accurate model testing for wind phenomena must take place in a turbulent boundary layer, with the model-law specifying that this layer needs to be proportional in scale to the velocity profile **(Jensen, 1958).** This insight from Jensen highlighted the limitations of relying on uniform flow in aeronautical wind tunnels and underscored the importance of adopting a more realistic approach to capture the complexities of natural wind patterns.

Davenport and Isyumov, 1967 emphasized that the simulation of turbulence characteristics in the flow should encompass the intensities, probability distributions, and spectra encompassing both shape and scale of individual turbulence components and their higher order correlations, such as Reynolds stresses. It is evident that the simulation of a wind profile extends beyond merely replicating the similarity of vertical wind speed distribution between a wind tunnel and natural wind. Equally crucial is the need for the turbulence characteristics to closely align, ensuring a comprehensive representation of the complexities inherent in natural wind dynamics.

In both closed-circuit and open-circuit wind tunnels, there is a notable advantage in opting for longer tunnels; however, practical considerations such as cost and space availability often impose limitations on the dimensions. The effectiveness of a wind tunnel hinges on achieving a representative wind flow at the testing section, requiring an ample distance from the wind blower to the testing section. Furthermore, the cross-sectional dimensions of the wind tunnel must be carefully determined to minimize the impact of frictional forces between the wind flow and the tunnel's ceiling and sidewalls on the tested model's wind flow, ensuring accurate and reliable results.

The testing of buildings in wind tunnels necessitates the use of appropriately scaled building models, ensuring alignment with suitable length, time, and velocity scale factors. This ensures that the wind tunnel conditions meet the criteria for full-scale representation. Moreover, it is crucial to simulate the terrain exposure, a feat accomplished by incorporating suitable roughness elements on the wind tunnel floor. For instance, to replicate open country terrain exposure, the wind tunnel floor is adorned with a rough carpet, effectively emulating the impact of an unobstructed landscape on the building model under examination.

The primary purpose of boundary layer wind tunnels is to generate authentic insights into wind behavior and its effects on structures, encompassing factors such as wind pressure on buildings, wind speed variations, and wind patterns. The evolution of boundary layer wind tunnels has significantly advanced knowledge in the field of wind engineering, equipping structural engineers with indispensable information on wind loads. This wealth of data aids in the design

process, empowering engineers to create buildings that are both safe and economically efficient.

2.3.5 Computational Fluid Dynamics (CFD)

In the evolution of wind engineering, computational fluid dynamics (CFD) has emerged as a valuable adjunct to traditional methodologies, witnessing notable advancements and an increasing embrace by wind engineers over recent decades. CFD has demonstrated its efficacy, yielding satisfactory results in diverse realms such as the analysis of indoor and outdoor thermal environments **(Mochida and Lun, 2008; Moonen et al., 2012)**, assessment of pedestrian-level wind conditions **(Blocken et al., 2012; Blocken and Stathopoulos, 2013)**, and investigation into wind-driven rain phenomena **(Blocken and Carmeliet, 2004, 2010).** While CFD offers notable advantages, its simulation results' accuracy is heavily contingent on a myriad of simulation parameters determined by CFD users. Variations in parameters such as mesh resolutions, turbulence models, and boundary conditions can lead to significant discrepancies. Therefore, well-established guidelines play a crucial role in the effective application of CFD. In recent years, researchers have diligently compiled comprehensive best practice guidelines, elevating the precision of CFD applications to a higher standard **(Blocken et al., 2012) (Tamura, 2008; Blocken and Gualtieri, 2012; Blocken, 2014, 2015)**.

Researchers have significantly validated various simulation methods based on best practice guidelines. The focal point of the majority of these studies has been Reynolds-Averaged Navier-Stokes (RANS) simulation. This preference is incipiently imputed to the well-established guidelines cognate with RANS, its relatively lower computational cost, and its satisfactory performance in industrial applications. Richards and Norris **(Richards and Norris, 2011)** governed experiments to import various Reynolds-Averaged Navier-Stokes (RANS) turbulence models. They concretely maneuvered issues related to turbulence models referring to excessive turbulence generation near the ground and the over-prediction of stagnation pressure. In response, they suggested that establishing a consistent set of conditions involving the inlet, turbulence model, and boundary conditions at the ground and the top of the domain is crucial for mitigating these problems. **Akon and Kopp, 2016** conducted a study accentuating the significance of seeing the inlet condition in simulations. They found that the inlet flow intensity played a pivotal role in influencing both the size of flow separation and the separation length on the roof of low-rise buildings. Omitting any of these configurations was observed to lead to a reduction in the accuracy of simulation results. Additionally, certifying the clear-cut simulation of a horizontally homogeneous atmospheric boundary layer is decisive for achieving

accurate simulation results, particularly in studies musing on pollutant dispersion and deposition **(Ai and Mak, 2013)**.

Blocken et al., 2007 recommended several quick fixes to achieve horizontal homogeneity in atmospheric boundary conditions. When configured judiciously, Reynolds-Averaged Navier-Stokes (RANS) simulations steadily yield adequate performance, principally when focusing on time-averaged values **(Blocken et al., 2007; Kobayashi et al., 2010).** The virtue of diverse turbulence models varies substantially in reckoning different parameters when compared to results obtained from wind tunnel tests. **Tominaga et al., 2015** identified that the RNG k-ε model outperformed standard k-ε and k-ω SST models in reckoning turbulent kinetic energy. **Ozmen et al., 2016** observed that the realizable k-ε turbulence model endorsed good agreement with experimental data in predicting mean velocity and turbulence kinetic energy, while the standard k-ω model accurately predicted mean pressure coefficient. **Xing et al., 2018** validated the capability of the k-ω SST model in predicting mean pressure coefficient and recommended substantial overestimations of k-ε models in pressure coefficient around the stagnation point and flow separation region.

Nevertheless, the constraints of Reynolds-Averaged Navier-Stokes (RANS) become obvious when dealing with intricate flow problems, principally those involving high turbulence. **Tominaga et al., 2015** exposed a substantial deviation between simulation outcomes and actual measurements near buildings, attributing it to the large-scale transient fluctuations ascending from vortex shedding—a phenomenon beyond the capabilities of steady RANS. In instances where wind direction is oblique, **Montazeri and Blocken, 2013** observed significant disparities in wind pressure on leeward facades, prompting the necessity for large eddy simulation (LES). Given the computational constraints of Direct Numerical Simulation (DNS), LES and Detached Eddy Simulation (DES) emerge as pragmatic alternatives for handling complex flows. As in computing wind effects on a low-rise cube, LES accurately imitated transient lift and drag coefficients under varying downburst directions **(Haines and Taylor, 2018). Mo et al., 2013** achieved commendable congruity between axial velocity predictions from LES and experimental results behind a wind turbine. Large eddy simulation also authenticated its proficiency in evaluating wind loadings around buildings and structural responses, crucial for ensuring accurate and safe structural designs **(Janajreh and Simiu, 2012; Ricci, Patruno and de Miranda, 2017).** Notably, LES parameters—such as turbulence generation in the inlet flow and the selection of time step—were extensively deliberated to achieve precise simulation results at a more efficient computational cost **(Hu et al., 2015; Yan and Li, 2015; Zhiyin, 2015)**.
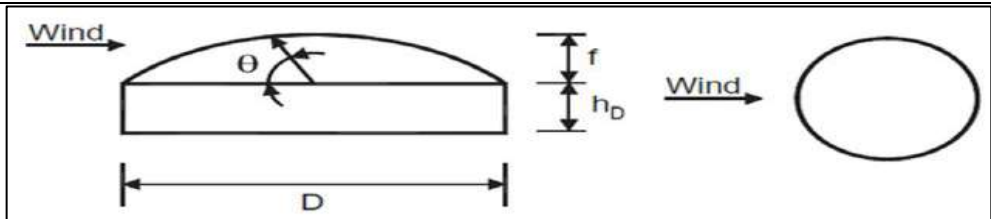
Numerous studies have marked the integration of various simulation methods to discourse the complexities of fluid dynamics. **Tamura et al., 1998** recommended an intensification of the $k-\varepsilon$ model as a simplified approach for intricate flows around low-rise structures, complemented by Large Eddy Simulation (LES) for handling unsteady scenarios. **Tominaga and Stathopoulos, 2010** undertook a provisional assessment of LES and Reynolds-Averaged Navier-Stokes (RANS) for dispersion issues around an isolated cubic building, concluding that LES consistently outperformed RANS in concentration distribution. **van Hooff et al., 2017** conducted a study to corroborate cross-ventilation flow within a generic enclosure using 5 distinct RANS turbulence models and LES. Meanwhile, **Liu and Niu, 2016** assessed the consummation of steady RANS, LES, and DES in simulating airflow in the vicinity of a building. Their findings identified that DES effectively seized wind flow features in the vicinity of the building and yielded results comparable to LES but with reduced mesh requirements and computational time. The comparative analysis of numerous simulation methods holds gravity in guiding the selection of the most opportune method for specific flow problems. Despite these valuable insights, there remains a scarcity of investigations in this domain. Therefore, additional studies in this area are deemed essential for a comprehensive understanding and application of simulation methods in diverse flow scenarios.

2.4 Review on codal provisions of various nations for different roofs

2.4.1 Buildings with Dome Roofs

The values of external pressure coefficients (C_{pe}) on a building with dome roof recommended by ASCE 7-16, IS 875 (Part-3):2015, MNBC:2020, NCh:432, GB 50,009:2001 and NSCP:2015 are shown below in Table 2.1.

Table 2.1. External Pressure Coefficient as per standards of different Nations

External Pressure Coefficients for Domes with Circular Base	
Standards of different Nations	**Pressure Coefficients (C_p)**
ASCE: 7-16	-0.9
IS 875 (Part-3):2015	-0.9
MNBC:2020	-0.9
NCh:432	-0.9
GB 50,009:2001	-0.8
NSCP:2015	-0.9

Where, h_D is the eave height, f is the apex height of the dome and D is the diameter of the dome, C_p is the pressure coefficient acting on the dome surface with positive and negative sign indicating that pressure is acting towards and away from the surface respectively.

2.4.2 Buildings with Cylindrical Roofs

As per the codal provisions given in AS/NZS 1170.2:2021, EN 1991-1-4:2005(E) and IS 875 (Part-3):2015, the cylindrical roof or arched roof is divided in three parts i.e., windward quarter, central half or apex and leeward quarter. The values of pressure coefficients are recommended for these three parts of the roof, shown in Table 2.2 and Fig 2.3.

For $0 \leq$ h/d <0.5, C_{pe} is Calculated by interpolation.

For $0.2 \leq$ f/d $\leq$0.3 and h/d$\geq$ 0.5, two values of C_{pe} are considered.

Reference Height = h+f
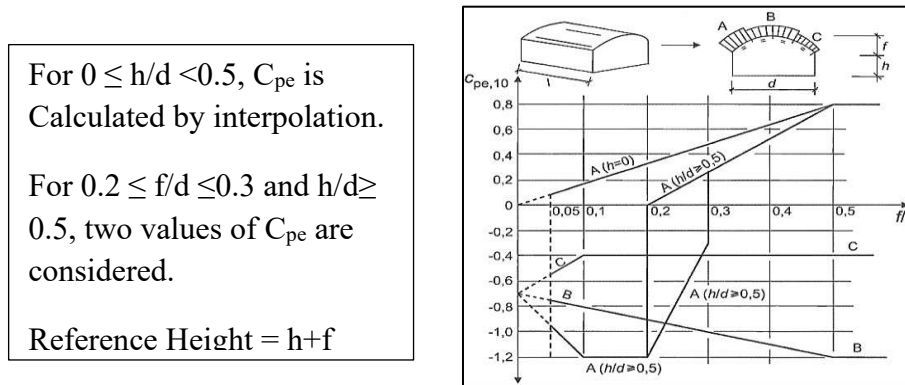
Fig. 2.3: Recommendations as per EN 1991-1-4:2005(E)

Table 2.2: Recommended values of AS/NZS 1170.2.2021 and IS 875(Part-3):2015

As per AS/NZS 1170.2.2021			As per IS 875(Part-3):2015	
Rise to Span Ratio (r/d or H/l)		Windward Quarter (U or C_2)	Central (T or C)	Leeward Quarter (D)
AS/NZS 1170.2.2021	0.18	(0.3-0.4 h/r) or 0	-(0.55+0.2 h/r)	-(0.25+0.2 h/r) or 0
	0.5	(0.5-0.4 h/r) or 0		-(0.1+0.2 h/r) or 0
IS 875(Part-3): 2015	0.1	-0.8	-0.8	-0.4
	0.2	-0.7	-0.9	-0.4
	0.3	-0.3	-1.0	-0.4
	0.4	+0.4	-1.1	-0.4
	0.5	+0.7	-1.2	-0.4

2.4.3 Buildings with Mono-Slope Roofs

The values of external pressure coefficients for the buildings with mono-slope roof are available in IS 875(Part-3):2015 shown in Table 2.3, ASCE 7-16 mentioned in Table 2.4 for square plan mono-slope roof and for rectangular plan mono-slope roof in which the roof is divided in three different zones i.e., zone 1 (central portion of the roof), zone 2 (near the windward, leeward, left and right edges of the roof and zone 3 (near the corners of leeward edges) respectively shown in Fig 2.4.

AS/NZS 1170.2.2021 provided the recommendations for multi-span mono-slope roof consisting of 5 spans as shown in Table 2.4, and the recommended values of pressure coefficient on mono-slope roof divided in different zones as per BS 6399-2:1997 and EN 1991-1-4:2005(E) are shown in Table 2.6. Where, a value is provided for interpolation purpose and b value is can be reduced linearly with area over which it is applicable. Also, for mono-slope roof, entire roof is surface is either windward or leeward depending upon the direction of wind.

Table 2.3: Pressure Coefficient of Mono-Slope Roof as per IS 875(Part-3):2015

Recommendations as per IS 875(Part-3):2015			
Roof Angle (°)	Solidity Ratio	Maximum (Largest +ve)	Minimum (Largest -ve)
0	ϕ=0	+0.2	-0.5
	ϕ=1	+0.2	-1.0
5	ϕ=0	+0.4	-0.7
	ϕ=1	+0.4	-1.1
10	ϕ=0	+0.5	-0.9
	ϕ=1	+0.5	-1.3
15	ϕ=0	+0.7	-1.1
	ϕ=1	+0.7	-1.4
20	ϕ=0	+0.8	-1.3
	ϕ=1	+0.8	-1.5
25	ϕ=0	+1.0	-1.6
	ϕ=1	+1.0	-1.7
30	ϕ=0	+1.2	-1.8
	ϕ=1	+1.2	-1.8

Table 2.4: Provisions for Mono-slope roof with square plan in ASCE 7-16
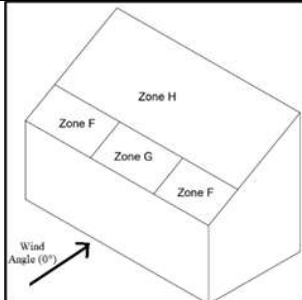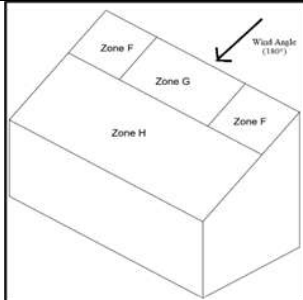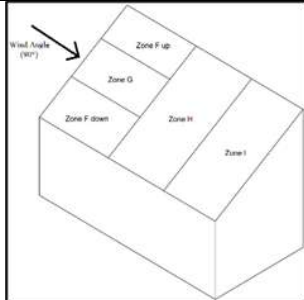
Wind Direction	h/L	Windward			Leeward	
		Roof Angle, θ(°)			Roof Angle, θ(°)	
		10	20	30	10	≥20
Normal to the ridge for θ≥10°	≤0.25	-0.7	-0.3	-0.2	-0.3	-0.6
		-0.18	0.2	0.3		
	0.5	-0.9	-0.4	-0.2	-0.5	-0.6
		-0.18	0.0ᵃ	0.2		
	≥1.0	-1.3ᵇ	-0.7	-0.3	-0.7	-0.6
		-0.18	-0.18	0.2		

Fig. 2.4: Provisions for rectangular plan Mono-Slope roof in ASCE 7-16

Table 2.5: Provisions for multi-span mono-slope roof in AS/NZS 1170.2.2021

Wind Angle (°)	Surface Reference for Pressure Coefficient								
	A	B	C	D	M	N	W	X	Y
0	0.7	-0.9	-0.9	-0.5,0.2	-0.5,0.5	-0.5,0.3	-0.3,0.5	-0.4	-0.2
180	-0.2	-0.2,0.2	-0.3	-0.2,0.2	-0.4	-0.4	-0.7	-0.3	0.7

Table 2.6: Provisions for mono-slope roof in BS 6399-2:1997 and EN1991-1-4-2005(E)

Wind Direction	Zone	BS 6399-2:1997	EN1991-1-4-2005(E)
0°	F	-0.5	-0.5
	G	-0.5	-0.5
	H	-0.2	-0.2
180°	F	-1.7	-1.7
	G	-1.0	-1.15
	H	-0.9	-0.8
90°	F_{up}	-1.7	-2.5
	F_{down}	-1.3	-1.65
	G	-1.2	-1.75
	H	-1.0	-1.15
	I	-0.8	-1.0

2.4.4 Buildings with Hip Roofs

The value of pressure coefficients for hip roof in isolated and closely spaced buildings are recommended in AS/NZS 1170.2.2021 on upwind, downwind and cross wind slopes are shown in Table 2.7 and 2.8. The key plan of hip roof divided in different zones as per BS 6399-2:1997 is shown in Fig 2.5 and recommended pressure coefficient values have been mentioned in Table 2.9. In the similar manner, the hip roof is divided in different zones in European code EN 1991-1-4:2005 (E) as shown in Fig 2.6 and Table 2.10 respectively.

Table 2.7: Upwind Pressure Coefficient on hip roof as per AS/NZS 1170.2.2021
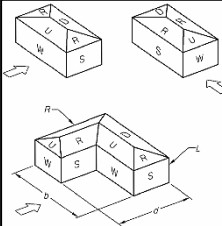
U- Upwind Slope
D- Downwind Slope
R- Crosswind Slope

Upwind Slope (U)	Ratio (h/d)	External Pressure Coefficient (C_{pe})		
		Roof Angle		
		10	20	30
α≥10°	≤0.25	-0.7,-0.3	-0.3,-0.2	-0.2,0.4
	0.5	-0.9,-0.4	-0.4,0.0	-0.2,0.3
	≥1.0	-1.3,-0.6	-0.7,-0.3	-0.3,0.2

Table 2.8: Crosswind & Downwind Pressure Coefficient on hip roof as per AS/NZS 1170.2.2021

Roof Type and Slope		Ratio h/d	External Pressure Coefficient		
Crosswind (R)	Downwind (D)		Roof Angle		
			10	20	≥25
α≥10°	α≥10°	≤0.25	-0.3	-0.6	For b/d <3; -0.6
		0.5	-0.5	-0.6	For 3< b/d <8; -0.06(7+b/d)
		≥1.0	-0.7	-0.6	For b/d>8; -0.9
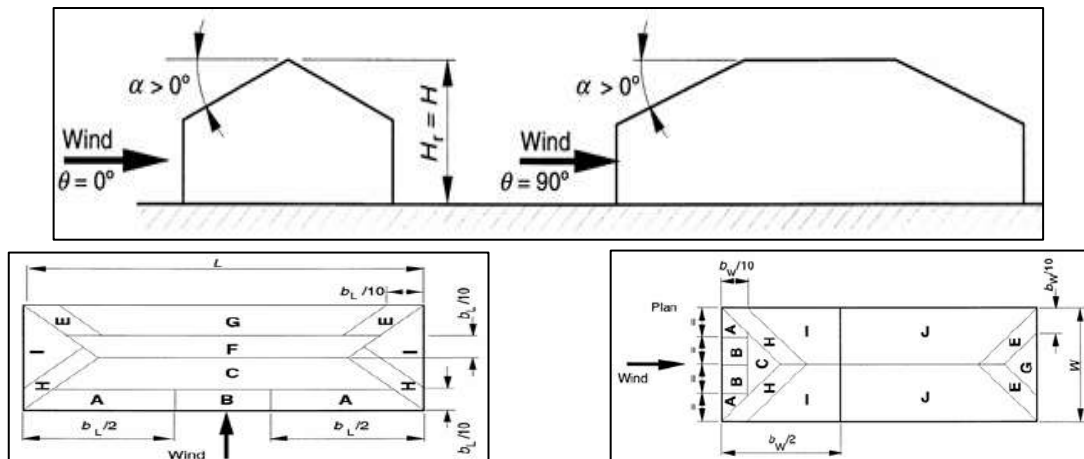
Fig. 2.5: Key plan of hip roof as per BS 6399-2:1997

Table 2.9: Pressure Coefficient of Hip Roof as per BS 6399-2:1997

Pitch angle α	Zone for θ = 0⁰ and θ = 90⁰								
	A	**B**	**C**	**E**	**F**	**G**	**H**	**I**	**J**
+5⁰	-1.8 +0.0	-1.2 +0.0	-0.6 +0.0	-0.8 -0.8	-0.6 -0.6	-0.6 -0.6	-1.1 +0.0	-0.6 +0.0	-0.6 +0.0
+15⁰	-1.3 +0.2	-0.8 +0.2	-0.5 +0.2	-1.4 -1.4	-1.3 -1.3	-0.6 -0.6	-0.9 +0.0	-0.6 +0.0	-0.4 +0.0
+30⁰	-0.5 +0.8	-0.5 +0.5	-0.2 +0.4	-1.3 -1.3	-0.8 -0.8	-0.6 -0.6	-1.0 +0.0	-0.6 +0.0	-0.5 +0.0
+45⁰	-0.0 +0.8	-0.0 +0.6	+0.0 +0.7	-0.7 -0.7	-0.4 -0.4	-0.4 -0.4	-1.1 +0.0	-1.15 +0.0	-0.4 +0.0
+60⁰	+0.8	+0.8	+0.8	-0.6	-0.3	-0.7	-1.2	-0.7	-0.6
+75⁰	+0.8	+0.8	+0.8	-0.6	-0.3	-1.2	-1.2	-0.5	-0.6
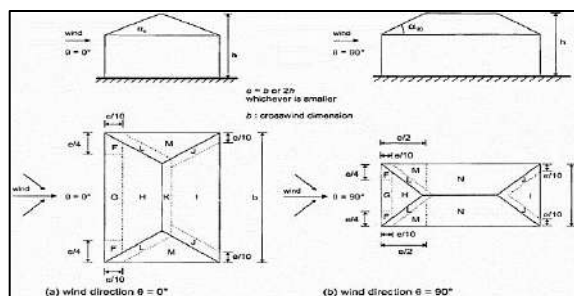
Fig. 2.6: Key plan of Hip Roof as per EN 1991-1-4:2005 (E)

Table 2.10: Pressure Coefficient of Hip Roof as per EN 1991-1-4:2005 (E)

Pitch angle α_0 for $\theta=0°$ α_{90} for $\theta=90°$	F $c_{pe,10}$	F $c_{pe,1}$	G $c_{pe,10}$	G $c_{pe,1}$	H $c_{pe,10}$	H $c_{pe,1}$	I $c_{pe,10}$	J $c_{pe,10}$	K $c_{pe,10}$	K $c_{pe,1}$	L $c_{pe,10}$	L $c_{pe,1}$	M $c_{pe,10}$	M $c_{pe,1}$	N $c_{pe,10}$
5°	-1,7 / +0,0	-2,5	-1,2 / +0,0	-2,0	-0,6 / +0,0	-1,2	-0,3	-0,6	-0,6		-1,2	-2,0	-0,6	-1,2	-0,4
15°	-0,9 / +0,2	-2,0	-0,8 / +0,2	-1,5	-0,3 / +0,2		-0,5	-1,0	-1,2	-2,0	-1,4	-2,0	-0,6	-1,2	-0,3
30°	-0,5 / +0,5	-1,5	-0,5 / +0,7	-1,5	-0,2 / +0,4		-0,4	-0,7	-0,5		-1,4	-2,0	-0,8	-1,2	-0,2
45°	-0,0 / +0,7		-0,0 / +0,7		-0,0 / +0,6		-0,3	-0,6	-0,3		-1,3	-2,0	-0,8	-1,2	-0,2
60°	+0,7		+0,7		+0,7		-0,3	-0,6	-0,3		-1,2	-2,0	-0,4		-0,2
75°	+0,8		+0,8		+0,8		-0,3	-0,6	-0,3		-1,2	-2,0	-0,4		-0,2

Note: For zone J, 15° has $c_{pe,1}$ = -1,5 and 30° has $c_{pe,1}$ = -1,2.

2.5 Review of previous research on wind effects on different types of roof forms

Stathopoulos, 1979 conducted a wind tunnel investigation to highlight the importance of height of the buildings in determining the roof pressure zones using pneumatic-average technique on 9 different models of low-rise buildings of different sizes and roof slopes considering two different terrain conditions. Before this research, the roof size was the only parameter considered in determining the roof pressure zones.

Stathopoulos and Surry, 1983 pointed out the effect of scaling while measuring the wind loads on low-rise buildings and concluded that the measured data got affected by 10% error just by changing the scale of the building model by factor of 2. After this study, there were several researchers like **Stathopoulos, 1984, Homes, 1983, Krishna, 1995, Kasperski, 1996** and **Uematsu and Isyumov, 1999** highlighted the state of the art and reviews on wind loads acting on low-rise buildings. **Stathopoulos, 1987** highlighted the other important parameters of buildings i.e., geometric scale, building height, terrain exposure etc., which affects the wind loads acting on the building.

Stathopoulos, 1987 pointed-out some discrepancies in the magnitude of pressure coefficients on edges and corners of the flat roof while comparing two researches i.e., **Kind and Wardlaw, 1979** with higher magnitude of pressure coefficient on edges and corners of flat roof and **Stathopoulos et al, 1981** with lower magnitude of pressure coefficients. These discrepancies were due to the different simulation conditions and different pressure tapping locations on the building roof.

Meecham et al, 1991 had done the experimental investigation to find out the magnitude and distribution of wind-induced pressures on hip and gable roof with the roof slope of 4:12, having aspect ratio of 2:1, scale of 1:100, model dimensions of 200mm X 100mm X 30mm and wind angle of 0° & 90° using wind tunnel simulation. It was stated that hip roof performed better than the gable roof during the cyclonic event since hip roof was having 50% less value of maximum negative pressure when compared with gable roof and there were 70% more chances of structural damage on gable roof compared to hip roof.

Kumar, 1991 aimed experimental research to investigate the impact of wind on convex cylindrical roofs. Models of considered buildings were fabricated at a scale of 1:240, corresponding to a plan of 120 m in length and 60 m in breadth. Three models were fabricated with rise-to-span ratios of 0, 0.06, and 0.12. The dimensions of each model were consistent, with lengths of 500mm, breadths of 250mm, and heights of 75mm. The findings suggest that the angle of wind incidence substantially influences the wind pressure coefficients across nearly all points of the building envelope.

Cochran and Cermak, 1992 conducted wind tunnel experiments on two models of the Texas Tech University (TTU) experimental building at Colorado State University, is a gabled roof low-rise structure with a roof slope of 1:60. Its dimensions are 9.8 m X13.7 m X 4 m. The geometric scales used for the models were 1:50 and 1:100. The collected data were compared with full-scale results of the TTU experimental building. The study pointed out that the mean pressure coefficients measured on both models aligned well with the full-scale data. However, discrepancies emerged when comparing peak suction values. Interestingly, Cochran and Cermak observed a reduction in peak suction pressures when considering the larger model (scaled at 1:50). This reduction was attributed to lower turbulence intensity at the eave height of the larger model.

Saathoff and Stathopouios, 1992 had done the investigation of wind pressure coefficients in the roof of saw-tooth roof buildings with single, double and four span having roof angle of 15° using wind tunnel simulation by considering the open country exposure condition with the scale of 1:400 subjecting the wind velocity of 13m/s with the model dimensions of 152mm X 48.5mm X 30mm and wind angle of 0° to 90° with the 15° interval. The spacing between the buildings were taken to be zero for the interference effect. They concluded that the maximum value of suction was found out to be in the higher corner of the roof. The maximum value of the negative pressure was found at the wind angle of 45° for single span and 30°-40° for multiple spans.

Stathopoulos and Yongsheng, 1993 computed the wind pressure on the surfaces of L-shaped buildings with plan view and cross-section view using wind tunnel simulation. The mean values of the pressure were computed by the numerical study using staggered grid system and having the scale of 1:400. They have shown the variation of Cp in the form of contours over the surfaces of the buildings. The pressure varies due to the step of the roof. The windward corners of the higher roof were subjected to the high positive pressure and the whole backwall was subjected to the negative pressure in case of cross-section plan view L-shape. The suction on the windward edges of sidewall and upwind backwall was found to be high.

Hoxeya et al., 1993 had done the investigation about the geometric parameters that affects wind load on low-rise building using full scale and CFD experiments. In this study the four parameters were considered for the investigation i.e., height, span length and roof pitch respectively. It was concluded that the average pressure was quite not affected by the height and span on the leeward roof slope. The windward side require more attention because the flow separation produces large negative pressure whose value is inversely proportional to the span. In case central part of long roof slopes, the pressure values were inversely proportional to the span. For ridge line region including 10% span to both sides of the ridge, there was drastic increase in suction with large span buildings or low eaves height buildings which is affected by height to span ratio.

Lin et al., 1995 performed wind tunnel experiments on five roof models to study wind loads. Three models had different heights (4, 8, 12 m) but identical plan dimensions (40 m x 40 m), and two were replicas of the TTU experimental building, with one having a flat roof and the other a 1:60 roof slope. All models were made at a 1:50 scale. The study found that the mean values of pressure coefficients from the experiments aligned well with full-scale data. However, discrepancies were noted in peak pressure coefficients. These differences were attributed to factors such as tap size, turbulence, scaling, and geometric details. Compared to **Cochran and Cermak, 1992**, **Lin et al, 1995** data showed better agreement with full-scale TTU building data. The critical wind direction was identified as 30° (± 5°), with symmetry at 60° (± 5°), relative to the wind perpendicular to the leading edge. No limits were set for wind load on flat roof corners, but the study observed very high suction pressures at the corners. It was also noted that the average suction pressure decreased with an increase in the considered tributary area.

Lin and Surry, 1998 analysed how wind load is distributed across the flat roofs of low-rise structures. They determined that the dimensions of the building's plan do not influence the size of the pressure zones on the roof. Instead, these zones' sizes are more accurately correlated

with the building's height, denoted as (H). Additionally, they found that the pressure coefficients in the corner zones are best described when the tributary area is standardized against (H^2). They also observed that the area-averaged pressure coefficients in the corner zones are reduced by half when the tributary area exceeds (0.1H X 0.1H).

Xu and Reardon, 1998 analysed the effect of roof pitch against wind loads on hip roof with three different roof pitches i.e., 15°, 20° and 30° additionally with geometrical scale of 1:50 and aspect ratio of 2:1. The obtained results were compared with the gable roof building with same plan as that of hip roof and concluded that 30° hip was subjected to some of the positive pressure on windward span of the roof and by increasing the roof pitch the overall suction on the roof got reduced.

Kumar and Stathopoulos, 2000 demonstrated the study for wind loads on low-rise building roof with flat, gable and mono-slope roof. The researchers had observed that most of the studies on low-rise buildings were concentrated on measurement of pressure i.e., mean, root mean square or peak values etc but not emphasised on the other variable component characteristics i.e., power spectrum, probability density function, crossing rates etc. In this study the flat roof, gable roof with 19° and 45° roof slope and mono-slope roof with 15° roof slope was used to carried out the research. It was concluded that pressure variations were there due to the dependence on tap location, wind direction, roof geometry and follows either the gaussian or non-gaussian distributions. The windward edges were more subjected to the non-gaussian wind pressure variations.

Ahmad and Kumar, 2001 examined the effect of interference on hip roof low-rise buildings by arranging similar type of buildings in 15 different interfering conditions. The roof surface was divided in 10 different zones win which zone zone 5 of the roof was under least shielding effect and zone 2 was having maxing shielding from the from the upstream interfering building and the enhancement in the value of pressure coefficient was observed by changing the interfering conditions.

Ginger and Holmes, 2003 carried out the wind tunnel investigation on low-rise building model with steep roof slope to find out the influence of building length in terms of different length to span ratios on the wind loads. It was found that by increasing the value of aspect ratio, the magnitude of suction on the leeward roof and walls also increased and the suction on the gable ends was maximum in magnitude.

Amreshwar, 2005 examined the wind effects on elevated structure having the curved roof in the form of semi-circle to find out the wind induced pressure distribution on the curved roof by reducing the height of building from 200 mm to 25 mm at the rate of 25 mm each. Different

rigid models were tested having various rise to height ratios subjected to different wind incidence angles at the rate of 15° interval. The model of building having 100 mm height and rise to height ratio of 1.2 was having maximum wind induced positive pressure coefficient and maximum wind induced negative pressure coefficient at 90° wind incidence.

Prasad et al., 2009 carried out the wind tunnel investigation to identify the wind effects on low-rise buildings with flat, gable and hip roof having the same eave height. The gable and hip roof were having different roof configurations in the form of slopes i.e., 15°, 20°, 30° and 45° respectively. The pressure coefficients on walls and roof were investigated and concluded that the suction on the roof got reduced as the slope of the roof increased. The performance of hip roof was found to be better than gable roof.

Faghih and Bahadori, 2010 investigated the wind flow pattern on dome roof to find out the wind pressure distribution using numerical simulations by applying k-ε turbulence model. There were 3 different opening conditions considered i.e., (a) the top of the dome was having a hole and windows were closed (b) the hole on top and windows both were opened and (c) the hole and windows were opened but the model was little shifted to 15° angle. It was concluded that the lowest portion of the dome was under maximum pressure and top-most portion of the dome was having minimum pressure.

Guha et al., 2012 compared the internal wind induced pressure in the low-rise buildings in which a single wall was having single and double closely spaced openings by carrying out the experimental and analytical investigation. The internal pressure got increased by increasing the opening ratios and reached to the most critical value of pressure i.e., almost equal in case of wall having single opening when the area of two openings became double the area of single critical opening.

Sun et al., 2013 conducted a wind tunnel experimental study that focused on the wind pressure spectra on spherical domes, crucial for designing dome cladding against wind loads on twelve dome models with varying geometric parameters. It was observed that despite differences in tap locations and dome shapes, the pressure spectra exhibited similar patterns and amplitudes. Three representative spectra were identified to illustrate the shift in spectral patterns from the windward to the leeward side of the domes. Based on these findings, a synthetic spectral model was developed to simulate local pressure fluctuations for the structural design of domes, aiding in both extreme weather and fatigue considerations.

Natalini et al., 2013 computed the mean wind loads on the vaulted canopy roof. In this study the measurement of coefficient of wind load had done on the roofs of vaulted canopy roof with the help of wind tunnel experiment. There were six models used for the study by varying the

length and eave height using the scale of 1:75. The angle of wind incidence were taken to be 60°, 75° and 90°. In case of 90° wind incidence angle, the maximum suction was found to be at the ridge line and also the flow separation takes place. In case of no blockage, the pressure on windward side span was positive but it converted in negative for the rest part of the roof. In case of full blockage, the pressure on upside span was to the enclosed duo-pitch buildings. During the full blockage arrangement, the pressure was changing from positive to negative on windward quarter span but remains unchanged on the rest of the part. It was found that the aspect ratio F/b does not have that much influence on the wind load as compared to the other aspect ratios.

Bitsuamlak et al., 2013 had done the aerodynamic mitigation of roof and wall corner suctions using simple architectural elements. In this study the aerodynamic modification devices were used to reduce the pressure acting on roof and wall corners of low-rise structure due to wind. The structural elements that were aerodynamically modified are trellises (pergolas), roof extensions of gable ends (gable end ribs), ridgeline extensions (ridge rib), sideways extensions of the walls (wall ribs) respectively. Residential house with gable roof and hip roof was tested in the wind tunnel. After modification it was found that 65% at gable end corners, 60% close to roof ridges, 45% at soffits, 35% at wall corners and 25% at eaves, the negative pressure was reduced.

Qiu et al., 2014 investigated the effects of Reynolds number ranging from 6.90 X 10^4 to 8.28 X 10^5 on cylindrical roof subjected to uniform wind flow having low turbulence while considering the different aspect ratios (rise to span) i.e., 1/2, 1/3 and 1/6 of the building with two different spans i.e., 0.2 m and 0.6m respectively and concluded that the adopted approach was found to be reliable for prediction of wind induced pressure distribution on curved roof i.e., cylindrical and dome roofs.

Irtaza et al., 2014 applied CFD technique to find out the wind effects on hip roof of low-rise buildings using two different models of turbulences i.e., (a) RNG k-ε turbulence (b) standard k-ε turbulence respectively and compared the data generated form CFD simulations with wind tunnel data. It was concluded that the CFD technique is the very good, reliable and alternative source in place of wind tunnel because it was less-time consuming, easy to handle and low-cost approach.

Tominaga et al., 2015 had done the wind tunnel study as well as CFD simulation to find out the wind effects of air flow around isolated gable-roof buildings with different roof pitches. The three different roof pitches of 3:10, 5:10 and 7.5:10 was considered in the study and the model dimension of 6.6m X 6.6m X 6m with the scale of 1:30 was used. For CFD simulations

they have used ANSYS FLUENT with steady RANS turbulence model. In conclusion it was stated that by increasing the roof pitch the negative Cp was changed into positive Cp for windward roof portion but the leeward roof was not that much affected by increasing the roof pitch. Also, by increasing the roof pitch the recirculation region became larger behind the building and it was found that the most critical roof angle was 18 because of the recirculation or reverse flow was occurring there.

Verma and Ahuja, 2015a had done the experimental research on the rectangular plan low-rise building with multiple domes to find out the wind pressure distribution. In the investigation they have considered three different models i.e., two, three and four dome models respectively with the dimension of 254mm X 508mm, 254mm X 762mm and 254mm X 1016mm having the eave height of 150mm and dome height of 84mm with the base of 254 mm. During the investigation the wind angle was considered as 0°. In conclusion it was stated that the positive pressure was found at windward edge of windward dome. Suction was decreased towards leeward edge. In case of multiple domes, it was concluded that the central dome was subjected to suction on the top and pressure on windward and leeward edges.

Verma and Ahuja, 2015b had computed the wind pressure distribution on domical roofs. In this research the rigid model of domical roof was subjected to open circuit boundary layer wind tunnel and pressure measurement was done over different pressure points on the roof. The model was consisting of two types i.e., one with single dome having square cross section and second with two domes having rectangular cross section. It was concluded that the wind pressure was suction in nature and maximum suction was found at the peak of the dome. The base of the dome was subjected to the positive pressure on windward side in case of single dome. The leeward portion of the windward dome was subjected to the small positive pressure in magnitude near the base. The suction near the base of leeward dome on leeward side is quite similar to that of the single dome building.

Verma and Ahuja, 2015c demonstrated the research study to find out the wind pressure distribution on low-rise buildings with cylindrical roof of single and multi-span. The information related to the wind pressure coefficients for cylindrical roof is limited to only single span. The information for multi-span is not in available in standards. Dimensions of the prototype rectangular plan low-rise building with circular cylindrical roof is assumed to have length of 20m, eave height of 7.5m and rise of 5m. The scale used in the study was 1:50 and the angle of wind incidence was taken from 0° to 90° with the interval of 15°. It was found that the very small portion of the single span near windward edge was subjected to the positive pressure otherwise entire roof surface was subjected to the suction. Maximum suction was

found at the apex on the windward side of the roof. In case of multiple spans, the pressure distribution on windward span is similar to that of the single span. There is an advantage of shielding by windward span on the wind pressure distribution on leeward span.

Alrawashdeh and Stathopoulos, 2015 marked the inaugural investigation into the wind loads impacting large-scale buildings. This study focused on how wind affects the edges and corners of flat roofs on low-rise buildings with substantial plan dimensions. At Concordia University's wind tunnel, nine models were tested, each crafted at a 1:400 scale with a square flat roof. These models represented full-scale buildings with dimensions of 60 m, 120 m, and 180 m. Three different building heights i.e., 5 m, 7.5 m, and 10 m were also examined. The study's findings were then evaluated against several standards, including the ASCE 7-10, NBCC 2010, EN 1994-1-4 (2005), and AS/NZS 1170.2 (2011). The research indicated that for substantial low-rise structures under 8 meters in height, the dimensions of the corner and edge zones should not adhere to the 4% rule based on the smallest horizontal plan dimension, as suggested by ASCE 7-10 and NBCC 2010. Instead, these zones should be confined to a maximum of 80% of the building's height. The study posited that adhering to the 4% rule could result in overly cautious and economically inefficient designs. Additionally, the study affirmed that the external pressure coefficients provided in ASCE 7-10 and NBCC 2010 are suitable for designing the large roofs of low-rise buildings.

Akon and Kopp, 2016 scrutinized the behavior of separated and reattaching flows around the leading edges of three-dimensional bluff bodies stationed within turbulent boundary layers. It was inspected how turbulence intensities and length scales within the incoming boundary layer influenced the mean length of the reattachment zone and surface mean pressure distributions for low-rise building roofs. It was observed that the mean pressure distribution relies on both the mean reattachment length and the turbulence intensity upstream. The authors also implied a technique for reckoning the mean reattachment length on low-rise building roofs using measured surface pressures and turbulence intensity at the roof height.

Zhang et al., 2016 pointed out the effects of shape modification on circular cylinder to investigate the flow pattern around the cylindrical. The modification of the cylinder was taking place in two different criteria (a) modification along the diameter and (b) modification along the length of the cylinder. The span wise modification was found to be more effective in reducing the aerodynamic forces.

Rani and Ahuja, 2017a computed the wind pressure distribution on circular canopy roof. In this investigation the wind pressure distribution was measured in the roof of single and multiple span circular canopy roof using boundary layer wind tunnel. The pressure measurement was

done on both upper and lower surfaces of the roof. The wind angle was taken to be 0° to 90° for isolated model and 0° to 180° for multiple span model with 15° and 30° interval respectively. The model dimension and scale were 300mm X 150mm X 150mm and 1:50 respectively. In conclusion it was stated that the ridge line was subjected to the maximum suction dur to maximum flow separation on upper roof surface. The suction value was higher for upper roof surface as compared with lower roof surface. In case of three span model the central roof was least subjected to the suction in contrast with windward and leeward span.

Rani and Ahuja, 2017b computed the effect of blockage of wind loads on mono-slope canopy roof. The author demonstrated the effect of various blocking conditions on the mono-slope canopy roof for wind pressure distribution. The open circuit wind tunnel, scale of 1:50 and wind incidence angle from 0° to 180° was used with the interval of 30° with 70 pressure points. In case of non-blocking condition, the interval of wind incidence was taken to be 15° while in blocking condition the wind incidence interval was 30°. Three blocking conditions were used i.e., 0B (0%), 0.5B (50%) and B (100%) blocking respectively. In conclusion it was stated that for 100% blocking of one panel, the high positive Cp was occurred. Also, in all the cases of blockage, the suction was higher over the upper roof surface when compared with lower roof surface and the roof was under suction at the corners as well.

Fouad et al., 2018 demonstrated the research study on the single span short gable structure with mono and double slopes, truss and domes to find out the wind loads using wind tunnel and CFD simulation for comparison. The gable roof with 3:10, 5:10 and 7.5:10 roof slope was investigated in the study. Six different models with varying height, diameter and height to diameter ratio was used for the study. The saw tooth roof with 15°, 30°, 45° and 60°, lattice structure with 3m X 3m X 6m dimensions and dome structures with varying height to diameter ratio i.e., 0.1, 0.2, 0.3, 0.4 and 0.5 were investigated. It was concluded that the most favourable gable roof was 30° roof slope. The value of Cp for mono-slope roof was over estimated in Eurocode but in ASCE code the Cp varies about 10% when compared with CFD. In case of domes the Cp values for windward and top zones were very much closed to Eurocode and for lattice structure the Cp was well matched with code values.

Kopp and Morrison, 2018 delved into the wind pressures on components and cladding of low-rise buildings with gently sloping roofs, concentrating on how wind pressures are distributed across roof surfaces and the intensity of the resulting pressure coefficients. The research included various building models with gabled roofs, all with slopes of 1:12 or less, tested in the University of Western Ontario's boundary layer wind tunnel II, simulating both open country and suburban terrains. Utilizing data from **Ho et al., 2005, Kopp and Morrison,**

2018 found that the external pressure coefficients for components and cladding as per ASCE 7-10 were lower than what their wind tunnel experiments suggested. It was proposed that pressure zone sizes should be based solely on building height, contrary to ASCE 7-10's method, which considers both height and the smallest plan dimension, advocated for an L-shaped corner zone rather than a square one and noted that despite slight variations due to turbulence and the unpredictable nature of peak pressures, the overall magnitude and spatial distribution of coefficients were consistent across different terrain exposures. ASCE 7 incorporated the findings of Kopp and Morrison (2018) by increasing the external pressure coefficients for components and cladding on low-rise buildings with low-slope roofs and by revising the size and shape of pressure zones in the ASCE 7-16 standards.

Xing et al., 2018 demonstrated the research study on isolated gable roof with variable roof pitches using BLWT and 3D steady RANS & LES simulation to find out the local wind pressure. Different roof pitches i.e., 1:5, 2:5 and 3:5 was investigated in BLWT and CFD analysis. Wind incidence angle, reduced scale, wind velocity and model dimensions were 0° to 90° with 15° interval, 1:20, 8.5m/s and 0.25m X 0.5m X 0.2m respectively. In conclusion it was stated that the critical roof slope was 2:5 at the wind incidence angle of 90° because the flow pattern changed mostly on this roof and RANS model gave more close values of pressure to BLWT results at the wind angle of 0° and 90°. The suction was reduced by increasing the roof slope from 1:5 to 3:5, therefore it can be concluded that flat roof is more prone to suction than the sloped roof.

Rani and Ahuja, 2018 computed the wind loads on the roof of multi-span mono-slope canopy roof. The angle of wind incidence was taken to be 0° to 180° with the interval of 30° and the angle of roof was considered as 30°. The model was tested for the wind velocity of 10m/s at 1m height from the wind tunnel floor level. The scale used in the study was 1:50 and there were 6 columns in the model from which 4 were attached to the corners and other 2 were attached at the centre of the eaves of the roof. The author concluded that there was similar suction acting on the all the span in case of 90° wind incidence angle. The suction on leeward edge was 3 times higher than the windward edge of the single span case at 0° wind angle. The suction was decreased form windward to leeward side for all cases on lower roof surface. Since the flow separation is more near the second span, therefore the second span was most affected span.

Shao et al., 2018 had done the wind tunnel study on the 4:12 sloped roof of rectangle, L and T shaped low-rise building to find out the wind pressure distribution on the roofs. The wind velocity, scale, roof slope and power law exponent were 11m/s, 1:200, 4:12 and 0.15 respectively. The wind incidence angle was taken as 0° to 180° with 5° interval and 0° to 360°

with 10° interval. It was found that the suction was reduced by almost 30% to 40% respectively along the leading edge and the maximum negative value of pressure was found near the roof eaves specially at 45° wind angle.

Singh and Roy, 2018 demonstrated the study to find out the wind pressure coefficients on pyramidal roof of square plan low-rise building of double storey with the help of CFD simulation. Different roof slopes were considered for the study i.e., 20°, 25°, 30°, 35° and 40° respectively and the angle of wind incidence was taken to be 0°. It was found that the maximum positive and maximum negative pressure coefficients were increased due to increase in the roof slope. The maximum positive pressure coefficient was found at windward side of the roof and maximum negative pressure coefficient was found at the peak point where wind upstream and downstream sides meets. At 20° roof slope, both maximum positive and maximum negative pressure were found.

Singh and Roy, 2019a demonstrated the research study to find out the pressure variations on the pyramidal roof of square plan low-rise building due to wind load having 15% wall opening with help of CFD simulation. There were 24 models of different roof slopes i.e., 0°, 10°, 20° and 30° at different wind incidence angle i.e., 0° to 75° with 15° interval were investigated. The Cp of building with opening were compared with Cp of building without opening and it was noted that the Cp of building without opening were twice or thrice the Cp of building with opening. It was concluded that there were better chances of survival of the building with 20° and 30° roof slope.

Singh and Roy, 2019b demonstrated the research study to find out the pressure distribution on the pyramidal roof with pentagonal and hexagonal plan low-rise single storey building with the help of CFD simulation. The roof slope was taken to be 20°, 25°, 30°, 35° and 40° respectively. The angle of wind incidence, power law coefficient, wind velocity and reduced scale were 0° to 45° with 15° interval, 0.14, 8m/s and 1:25 respectively. In conclusion it was stated that the pyramidal roofs were found to be better than other types in various disaster studies and can be considered as cyclonic shelter. It was found that the pyramidal roof with pentagonal plan having the roof slope of 40° to be most optimal from wind load point of view.

Zhou et al., 2018 had done the research study which entitled as "Study on wind load distribution on the surface of dome structure based on CFD Numerical simulation". It was based on Reynold's average navier-stokes equation. Researchers had considered 7 wind incidence angles i.e., 0° to 90° with 15° interval. The measurement of maximum negative pressure at the top of different winds was done and compared with wind tunnel data. It was

found that the wind force was very small when the wind was blowing at 90° to the building and north wind i.e., 0° was most unfavourable condition.

Chen et al., 2019 investigated the interference effects on wind loads of gable roof buildings with different roof slopes by varying the spacing between the buildings of low-rise gable roof using wind tunnel simulation. The roof slope of 10° & 35° was considered for the study and spacing (S/H) ratio was taken to be 0.25, 0.5, 1.0, 1.5, 2.0, 3.0, 4.0, 6.0 and 8.0 respectively. The wind attack angle was taken as 0° to 360° with 15° intervals. In conclusion, they stated that there were the similar effects of interference was observed on mean, standard deviation and peak Cp. There was shielding effects was acting on windward portion of central and downstream roof. By increasing the spacing between the buildings more than 3.0 spacing ratio, there was increase in negative Cp at leeward portion of upstream building and windward portion of central building.

Hoq and Judd, 2021 had done the comparative study between wind tunnel and wind force resisting system to find out the directional and envelope strategy which is based on the data provided by wind tunnel test for low-rise structure having gable shaped roof in open terrain (exposure C). the computed base shear was compared with the design base shear due to wind load in the direction of the horizontal component. The roof angle was taken to be 26.6° and wind angle was 0°, 40°, 45°, 50° and 90° respectively. The length and width of the model was 38.1m and 24.4m respectively. The two different eave heights were considered for the study i.e., 3.66m and 12.2m. In conclusion it was stated that the values of design base shear were found out to be larger in case of directional procedure when compared with envelop procedure. The reliability index β was larger in case of directional procedure and β provided by envelope procedure was not matched with the standard target β.

Sharma et al., 2023a investigated the proximity effects on wind induced pressure distribution on the roof of low-rise buildings with cylindrical roof arranged in rectangular pattern with variable spacing using CFD simulations and concluded that with increase in spacing between the buildings, the suction on the roof also increases. Additionally, some portion of the roof on the windward side was subjected to the positive wind induced pressure and left other portion was subjected to suction.

Sharma et al., 2023b conducted CFD investigation to find out the effect of interference on cylindrical roof to evaluate the interference factor (IF) and interference difference (ID) in which the shielding effect played a crucial role in reducing the negative wind induced pressure on the cylindrical roof under different interfering conditions and various angles of wind incidence.

Sharma et al., 2023c investigated the effects of roof shapes on wind load distribution on multi-span low-rise buildings in four different roof shapes were considered i.e., cylindrical roof, dome roof, hip roof and mono-slope roof. It was concluded that the middle roofs were under least suction as compared to windward roofs and leeward roofs. The streamline flow of the wind was observed on the multi-span cylindrical roof and dome roof. the flow separation was taking place on the sharp edges of the multi-span hip and mono-slope roof.

Sharma et al., 2024 pointed out the effects of wind loads on isolated low-rise buildings with different roof shapes and different roof angles and concluded that the 30° roof angle of hip and mono-slope roof was under least suction as compared to 10° and 20° roof angles. The overall effect of wind load is suction in nature on the roof and geometry of roof played a vital role in distribution of wind induced pressure on the roof.

2.6 Research Gaps

1. The information related to wind pressure coefficients for different roof is limited to only single span and it is not available for multi-span in Indian Standards.

2. Interference study has not got so much attention from researchers by arranging the low-rise buildings in different patterns with variable spacing between them.

3. The most of the wind pressure coefficients available in codes are given only for wind angle of 0° to 180° with the interval of 45° but not available for smaller wind angle interval.

4. Although it is well known fact that wind pressure distribution on both roof and wall surfaces get modified when more than one building are placed in close vicinity, information about wind pressure coefficients on closely spaced low-rise buildings with dome, mono-slope, cylindrical and hip roof is not available in standards on wind loads.

5. In few studies, code or standard, the values for pressure coefficients were found different from recent wind tunnel test results with a noticeable difference. Hence, codes, too, need a thorough rechecking of values and should be revised.

6. The flat and gable roofs have been investigated in more studies as compared to the other types of roofs. That may be because of their simple geometry, as studies shows that gable and flat roofs are found subjected to the higher uplift and suction forces.

7. Very few studies have been carried out on cylindrical roof, dome roof, saw-tooth roof, mono-slope roof and pyramidal roof buildings and they found highly capable of resisting extreme wind loads, that is why more studies have to be carried out on these roofs.

CHAPTER 3
METHODOLOGY

3.1 General

As described earlier, a CFD simulation is carried out in the proposed research work to evaluate the wind pressure coefficients on the roof of low-rise structures. This chapter deals with a detailed explanation of the methodology adopted for the present research. It includes the process of carrying out the numerical investigation using the Ansys CFX tool, i.e., geometry creation, selection of the suitable type of meshing, and applying boundary conditions.

3.2 CFD Technique

The branch of fluid mechanics that deals with the investigation of simulation of fluid flow characteristics is known as computational fluid dynamics (CFD) technique. In recent years, CFD is highly getting its acceptance by the researchers in the area of wind engineering. There are some advantages of CFD over several traditional methods e.g., on-site testing of full-scale building model, testing of reduced scale building model using wind tunnel. It is very difficult to control the boundary conditions in on-site model testing as well as the cost of wind tunnel testing is significantly higher. In contrast, the CFD technique is proved to be lower in cost as compared to on-site wind tunnel testing as well as there is great control over the boundary conditions in flow domain. The CFD technique is great alternative source in place of wind tunnel since it is more economical and time efficient than the wind tunnel, if the accuracy and reliability could be proved.

Although the prospect of CFD is up and coming, more research is still needed on this subject to make it more applicable. Since the results of CFD are susceptible to a wide range of parameters, users mainly define them. For example, the selections of computational size, computational grid, turbulence model, and boundary condition can all dramatically influence computational results. That is why the experimental results should constantly use to validate the simulation results. Therefore, well-developed guidelines are highly required for CFD to cope with different flow problems. Several guidelines had been proposed by **Blocken, 2015** to get the accurate and reliable results from RANS simulation method that had been achieved in last 15 years but needs to be achieved for LES simulations which is one of most crucial part of the applicability of LES simulations. There are several simulation methods available which proves to be very important part of investigation in the area of CFD e.g., DNS (Direct Numerical Simulation), RANS and LES from which the RANS and LES are more applicable as compared to DNS because of its non-suitability for industrial applications and low

processing speed. In case of transient fluid flow problems, the LES proves to be more accurate as compared to RANS simulation which leads to the higher simulation cost. Hence, for carrying out different fluid flow problems to obtain higher accuracy and lower computational cost, selecting the best suitable simulation is proved to be most critical in real industrial problems. The k-Ɛ turbulence model is used in the present research. This model has a well-documented capacity for prediction and has demonstrated stability and numerical dependability. With this approach, general-purpose simulations may be conducted with a precise balance of dependability. It is frequently used to imitate the properties of turbulent flow and is quite inexpensive.

3.2.1 Numerical Simulation

The numerical simulation involves the creation of a computational domain and grid sensitivity analysis to choose the meshing best suited for further simulation and apply boundary conditions and a detailed description of these parameters is given in this section.

3.2.1.1 Computational Domain

The computational domain is being created using Ansys CFX as per dimensions suggested in best practices guidelines by **Franke et al., 2007** and **Tominaga et al., 2015,** according to which the length of the upstream side of the domain should be 5H to 3H, the downstream side of the domain should be 15H and the sidewalls and top of the domain should be 5H, where is the total height of the building, as shown in Fig. 3.1. The domain is allowed to rotate at various angles to find out its effects on wind loads.
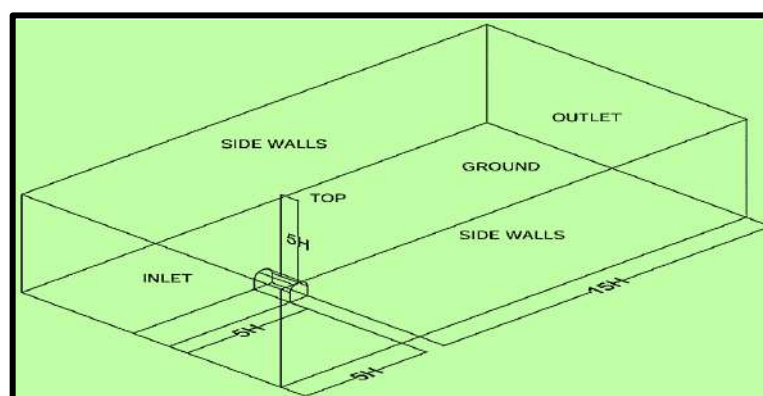
Fig. 3.1: Dimensions of the Computaional Domain
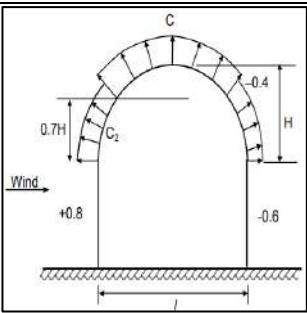
3.2.1.2 Meshing

Meshing plays a crucial role while performing any numeral simulation using various tools. Since the Ansys CFX is FEM based tool in which meshing is one of important factor to carry-out the research. In the meshing process, a complex geometric object is divided into several cells, each defined by a specific number of nodes. These cells have predictable shapes that

effectively represent the physical form of the object. CFD solvers can utilize structured, unstructured, or hybrid meshing techniques, creating 2D shapes (triangles, quadrilaterals) or 3D shapes (tetrahedrons, hexahedrons) with different densities during the meshing of a structure. The selection of meshing size depends upon the method called grid sensitivity in which the simulation is performed using different sizes ranging from coarse to fine size of the mesh.

3.2.1.3 Grid Sensitivity

Before performing a numerical investigation, it is necessary to conduct a grid sensitivity analysis, so that a suitable size of mesh can be decided to carry-out the further investigation. Four different types of meshes i.e., coarse (148790 elements), medium (687578 elements), fine (1146916 elements) and very fine (2023215 elements) mesh are used to conduct the grid independence test. The low-rise building model with cylindrical roof having H/l ratio of 0.5 is considered and the results of pressure coefficient on windward portion, leeward portion and top portion of the roof are examined and compared with IS 875(Part-3):2015 as shown in Table 3.2 and Fig. 3.2. From the results of grid independence test, the fine mesh is selected for the further investigation, since it is giving the closest value of pressure coefficient with respect to the IS 875 (Part-3):2015. Also, the values of the pressure coefficient start repeating by creating a finer mesh, which indicates that further reduction in mesh size will not influence the pressure coefficient. The size of fine mesh is taken as 0.0125 m on the faces of the buildings, 0.025 m size is used on the edges of the buildings, 0.05 m meshing is used on the ground surface after performing grid sensitivity as shown in Fig. 3.3.

Table 3.1: Pressure Coefficient for cylindrical roof in IS 875(Part-3):2015			
	H/l	C	C_2
	0.1	-0.8	-0.8
	0.2	-0.9	-0.7
	0.3	-1.0	-0.3
	0.4	-1.1	+0.4
	0.5	-1.2	+0.7
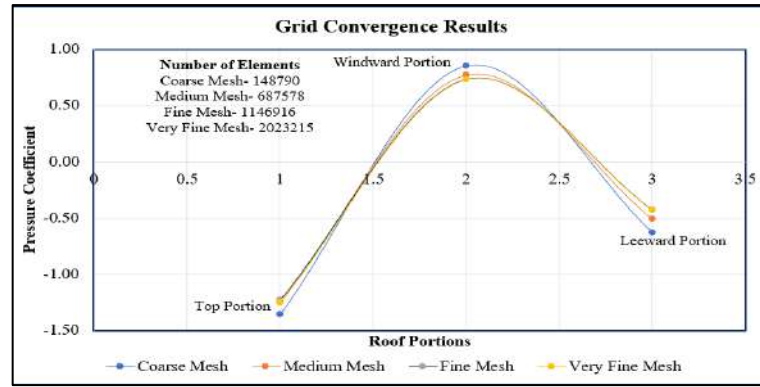
Fig. 3.2: Grid Sensitivity Analysis

Face Meshing

Edge Meshing

Ground Meshing

Inflation Layer
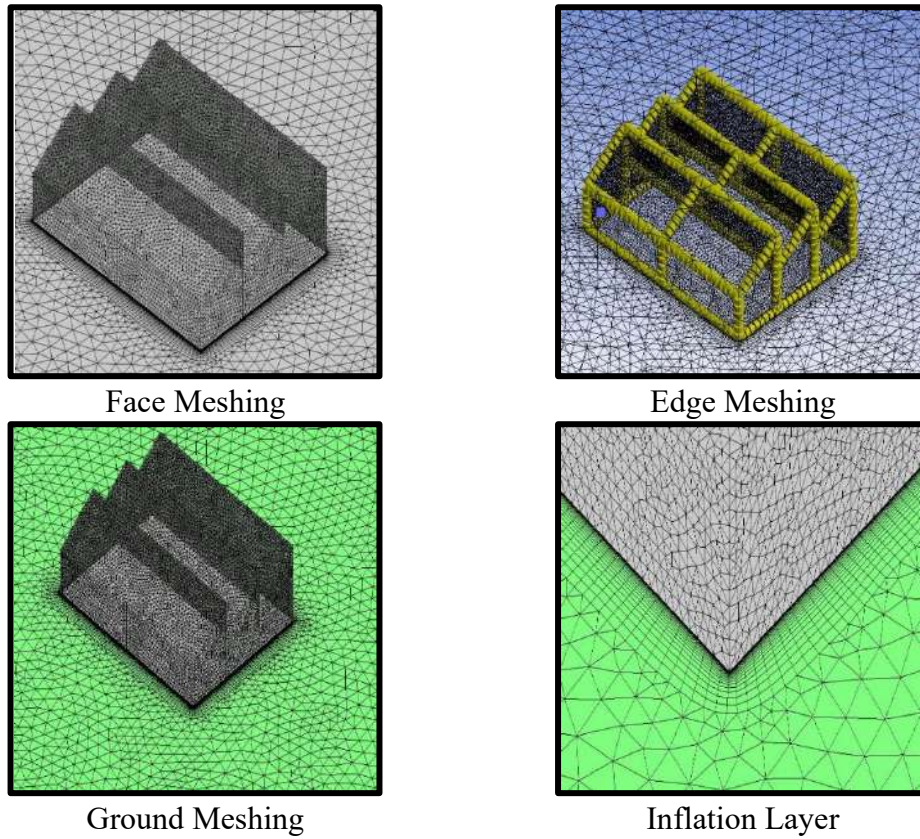
Fig. 3.3: Different Types of Meshing

3.2.1.4 Boundary Conditions

Since the low-rise building lies under the boundary layer in which the velocity fluctuations are very less as compared to the high rise building but the turbulence within the boundary layer is very much higher. To resemble the conditions of boundary layer in CFD with wind tunnel, the inlet velocity is provided with power-law which indicates that the velocity of air increases as the height of the building increases, as shown in equation 3.1, where V_{ref} is the reference velocity (10 m/s), Y_{ref} is the reference height (1 m) and α is the power-law coefficient (0.15) and V is the velocity at required height. The validation of velocity profile and turbulence intensity has been done by comparing the obtained wind profile and turbulence from Ansys

CFX by experimental wind profile and turbulence performed by **Verma et al., 2022** as shown in Fig. 3.4.

$$\frac{V}{V_{ref}} = \left(\left(\frac{Y}{Y_{ref}}\right)^{\alpha}\right) \dots\dots\dots\dots\dots\dots\dots\dots\dots\dots\dots\dots\dots\dots\dots\dots\dots\dots\dots\dots\dots\dots 3.1$$
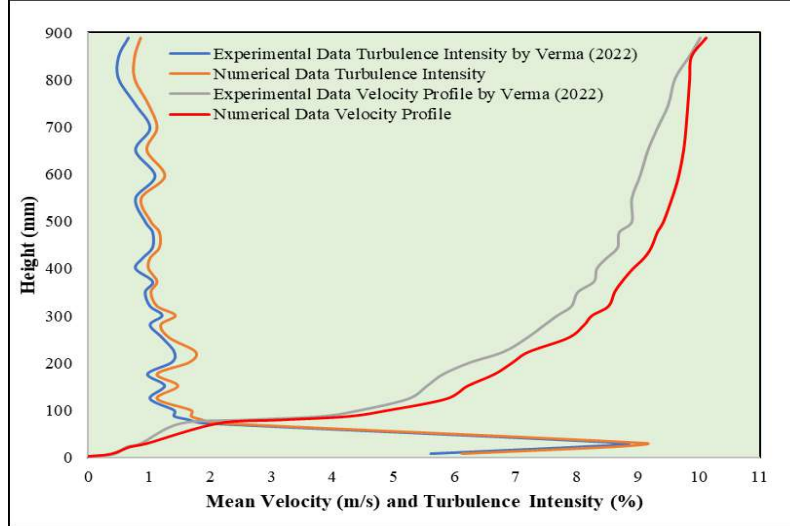
Fig. 3.4: Wind Profile and Turbulence Intensity: Ansys CFX Vs Experimental

The side and top walls of domain are assigned as free slip wall where the normal velocity and its gradient is zero and outlet of the domain is provided with zero static pressure. The faces of the building models are assigned as no-slip walls which indicates that the velocity of fluid flow is zero along the boundary wall. To solve the problems of complex fluid flow, the two-equation model is used, which is called the k-ε turbulence model that performs almost equally to the experimental problems and solves two different equations, i.e., (i) turbulent kinetic energy (k) and (ii) turbulent dissipation rate (ε) shown in equation 3.2 and 3.3 respectively.

$$k = \frac{3}{2}\left(U_{avg}I\right)^{2} \dots\dots\dots\dots\dots\dots\dots\dots\dots\dots\dots\dots\dots\dots\dots\dots\dots\dots\dots\dots\dots\dots\dots\dots 3.2$$

$$\varepsilon = \frac{C_{\mu}k^{2}}{v\left(\frac{\mu_{\tau}}{\mu}\right)} \dots\dots\dots\dots\dots\dots\dots\dots\dots\dots\dots\dots\dots\dots\dots\dots\dots\dots\dots\dots\dots\dots 3.3$$

Where, C_{μ} is a non-dimensional constant, k is the turbulent kinetic energy, μ_{τ}/μ is eddy viscosity ratio. There are certain equations which involves in the k-ε turbulence model i.e., continuity equation and momentum equation presented in equation 3.4 and 3.5 respectively.

$$\frac{\partial_{\rho}}{\partial_{t}} + \frac{\partial_{\rho_{i}}}{\partial_{x_{i}}} = 0 \dots\dots\dots\dots\dots\dots\dots\dots\dots\dots\dots\dots\dots\dots\dots\dots\dots\dots\dots\dots\dots 3.4$$

$$\frac{\partial(\rho u_{i})}{\partial t} = -\frac{\partial(\rho u_{i} u_{j})}{\partial x_{j}} - \frac{\partial P}{\partial x_{j}} + \frac{\partial}{\partial x_{j}}\left[\mu\left(\frac{\partial u_{i}}{\partial x_{j}} + \frac{\partial u_{j}}{\partial x_{i}}\right)\right] + F \dots\dots\dots\dots\dots\dots\dots\dots 3.5$$

In present investigation, the k-Ɛ turbulence model has been utilized which is based on two equations i.e., turbulence kinetic energy and turbulence dissipation rate, described as below:

(i) Equation for Turbulence Kinetic Energy:

$$\frac{\partial(\rho k)}{\partial t} + \frac{\partial}{\partial x_j}(\rho U_j k) = \frac{\partial}{\partial x_j}\left[\left(\mu + \frac{\mu_t}{\sigma_k}\right)\frac{\partial k}{\partial x_j}\right] + P_k - \rho\varepsilon + P_{kb} \ldots\ldots\ldots\ldots\ldots\ldots\ldots\ldots\ldots\ldots.3.6$$

(ii) Equation for Turbulence Dissipation Rate:

$$\frac{\partial(\rho\varepsilon)}{\partial t} + \frac{\partial}{\partial x_j}(\rho U_j\varepsilon) = \frac{\partial}{\partial x_j}\left[\left(\mu + \frac{\mu_t}{\sigma_k}\right)\frac{\partial\varepsilon}{\partial x_j}\right] + \frac{\varepsilon}{k}\left(C_{\varepsilon 1}P_k - C_{\varepsilon 2}\rho\varepsilon + C_{\varepsilon 1}P_{\varepsilon b}\right)\ldots\ldots\ldots\ldots\ldots.3.7$$

Where, $C_{\varepsilon 1} = 1.44$, $C_{\varepsilon 2} = 1.92$, $\sigma_k = 1.30$, $\sigma_\sigma = 1.00$ are constants **(Taha, 2005)**, the effects of buoyant forces are represented by P_{kb} and $P_{\varepsilon b}$ and viscous forces generating turbulence is denoted by P_k, the equation of which is given below:

$$P_k = \mu\left(\frac{\partial U_i}{\partial x_j} + \frac{\partial U_j}{\partial x_i}\right)\frac{\partial U_i}{\partial x_j} - \frac{2}{3}\frac{\partial U_k}{\partial x_k}\left(3\mu_t\frac{\partial U_k}{\partial x_k} + \rho k\right)\ldots\ldots\ldots\ldots\ldots\ldots\ldots\ldots\ldots\ldots\ldots.3.8$$

3.3. Methodology for Objective 1

"To study the effects of different types of roofs under wind load for low-rise structures"

From the literature survey, it is very clear that most of the wind investigation had been carried out on gable roof or on flat roof due to their geometrical simplicity. The information related to other types of roof forms is still scanty. Therefore, it is proposed to carry-out the research on wind flow characteristics of four more different types of roofs i.e., cylindrical roof, dome roof, hip roof and mono-slope roof as shown in Fig. 3.5.
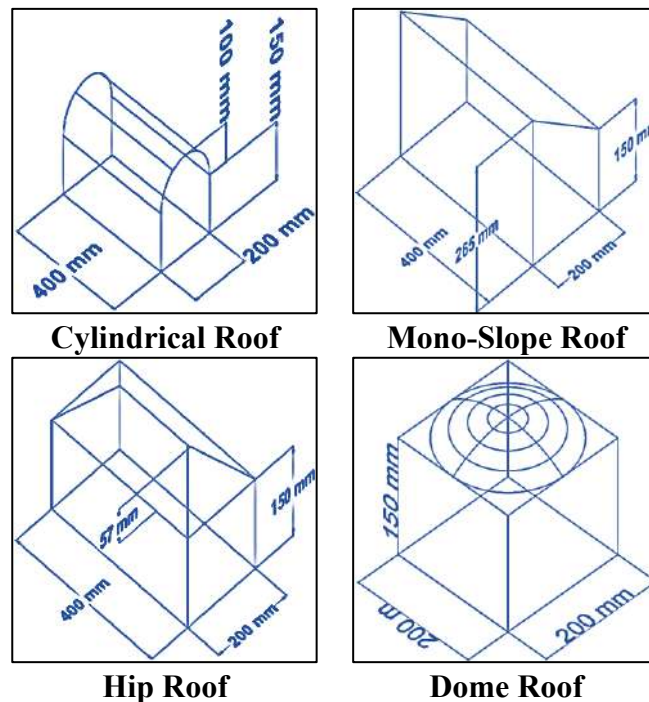

Fig. 3.5: Different Types of Roof Structures

All the considered roofs are subjected to different angles of wind attack depending upon the symmetry of the structures such as cylindrical roof and hip roof are subjected to 0° to 90° wind angles, mono-slope roof is subjected to 0° to 180° and dome roof is only subjected to 0° and 45° respectively, as shown in Fig. 3.6.
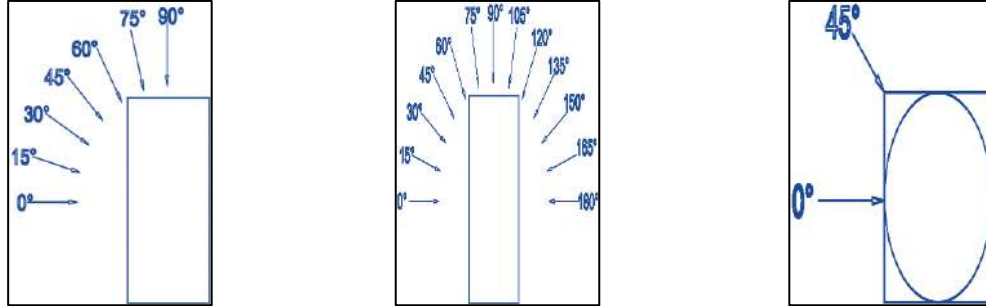
Fig. 3.6: Angle of Wind Attack for Different Roof Structures

3.4. Methodology for Objective 2

"To study the wind effect on different configurations of the roof slope."

The roof slope plays a vital role in changing the behaviour of wind on the roofs of low-rise structures. In some studies, it has been shown that increasing the roof slope reduces the wind-induced pressure coefficient. Therefore, the present research is proposed to investigate the effect of changing roof slopes on wind effects for low-rise structures. For this purpose, three different roofs are considered, i.e., 10°, 20° and 30° for hip roof and mono-slope roof subjected to different wind incidence angles i.e., 0° to 90° for hip roof and 0° to 180° for mono-slope roof, as shown in Fig. 3.7.

Fig. 3.7: Different Configurations of Roof Slopes

3.5. Methodology for Objective 3

"To study the effect of interference between clusters of buildings under variable spacing."

Wind loads measured on the isolated models of low-rise structures are not enough to obtain the expected results in actual practice. It is a well-known fact that wind pressure distribution on both roof and wall surfaces gets 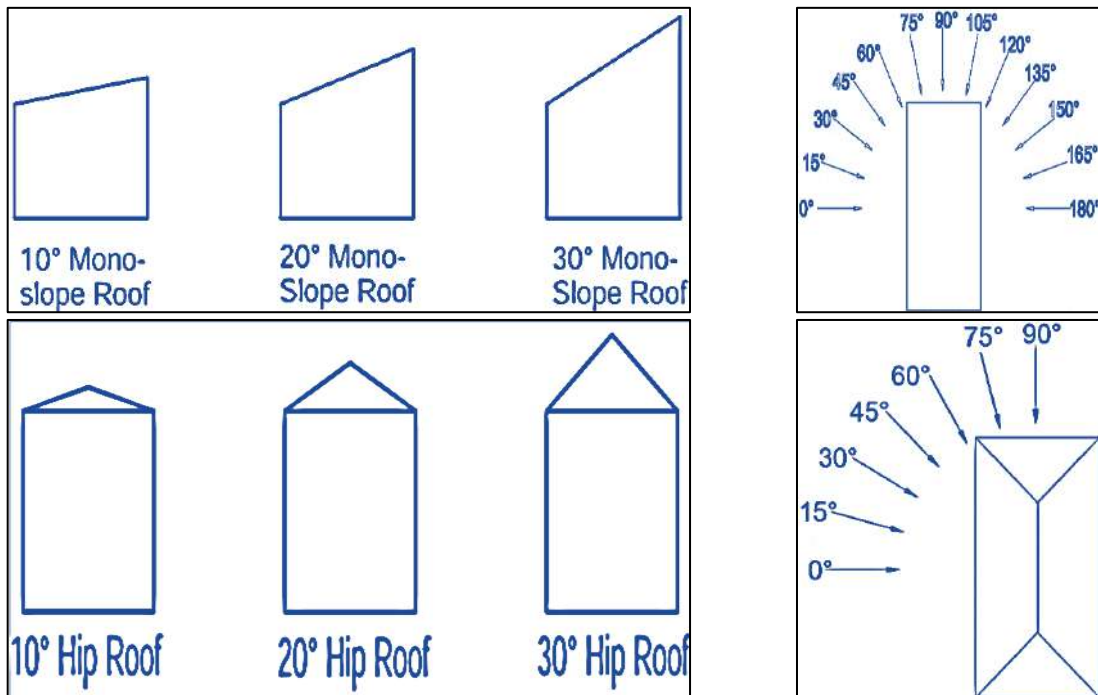modified when more than one building is placed in close vicinity, also known as the interference effect. Interference is a critical parameter that must be considered while designing a group of low-rise buildings. Information about wind-induced interference on closely spaced low-rise buildings with dome, mono-slope, cylindrical and hip roofs is not available in standards on wind loads. To investigate the effect of interference low-rise buildings with different roof forms, the low-rise building models are arranged in three different interfering conditions i.e., (i) rectangular pattern, (ii) T-pattern and (iii) Z-pattern. Additionally, the spacing between the buildings is varying with respect to the width of building i.e., 0, 0.5B, B, 1.5B and 2B (B is the width of building), as shown in Fig. 3.8 to Fig. 3.10.
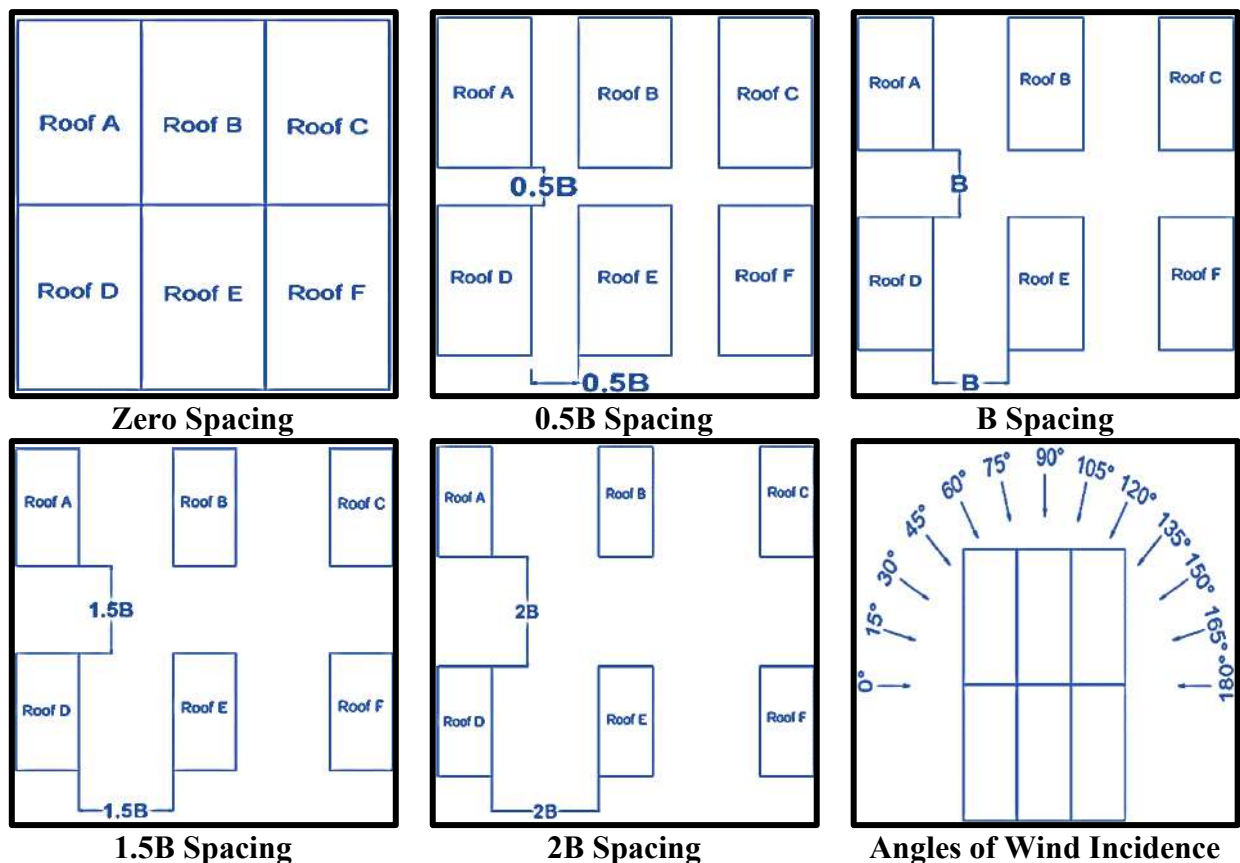
Fig. 3.8: Interference Conditions of Rectangular Pattern with Variable Spacing
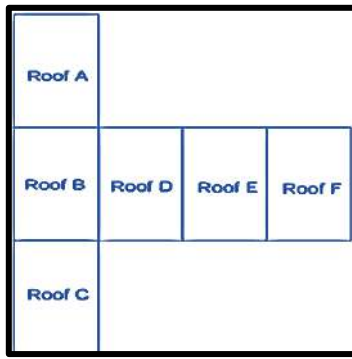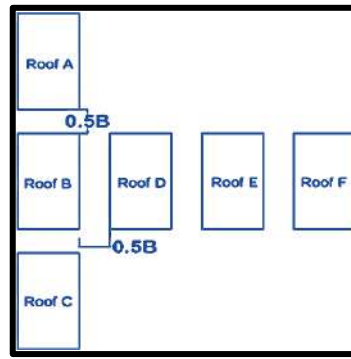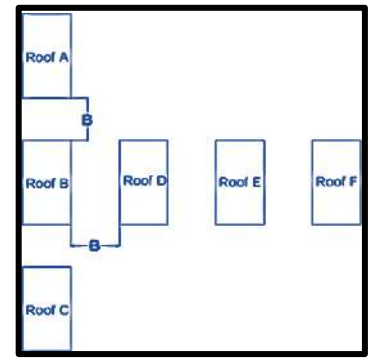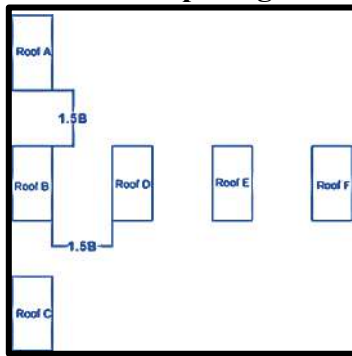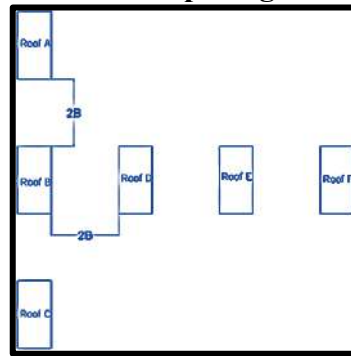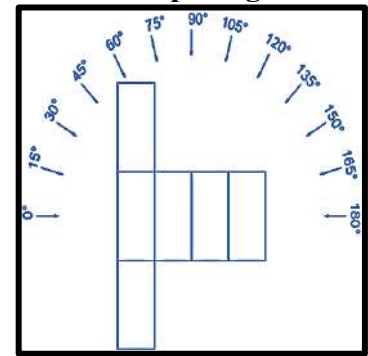
Fig. 3.9: Interference Conditions of T Pattern with Variable Spacing
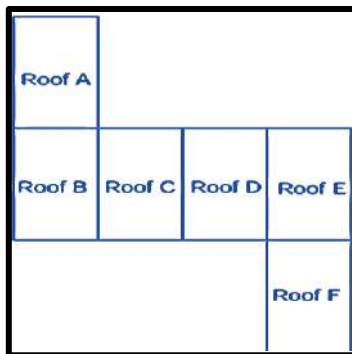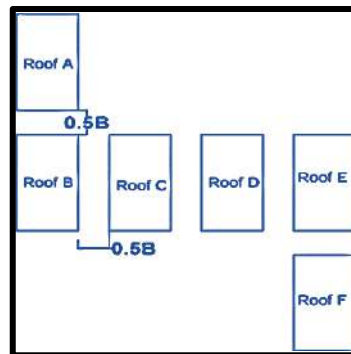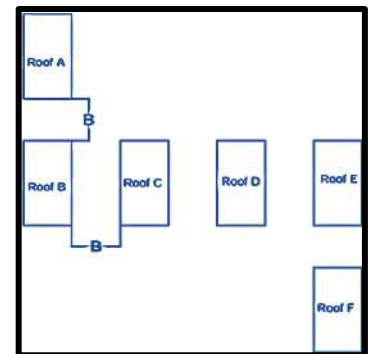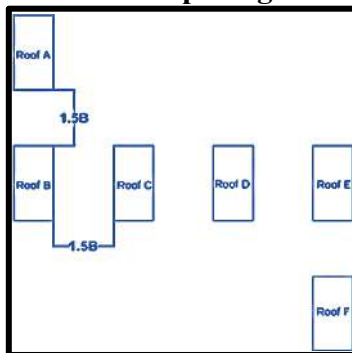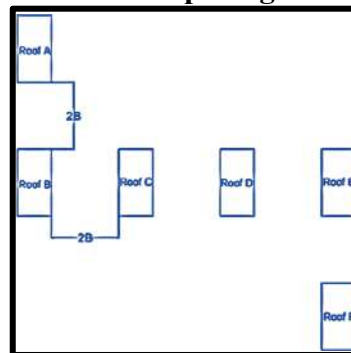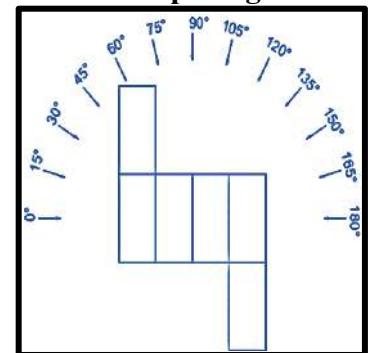
Fig. 3.10: Interference Conditions of Z Pattern with Variable Spacing

3.6. Methodology for Objective 4

"Identification of suitable roof types for low-rise structures under wind load."

The best-suited roof is decided based on objectives 1, 2 and 3 results by comparing the pressure coefficients (C_{pe}), drag and lift coefficient (C_d and C_l), as shown in fig. 3.11.

Comparison of the results obtained from Objective 1	→	Comparison of the results obtained from Objective 2	→	Comparison of the results obtained from Objective 3	→	Best suited roof will be decided based on results obtained from
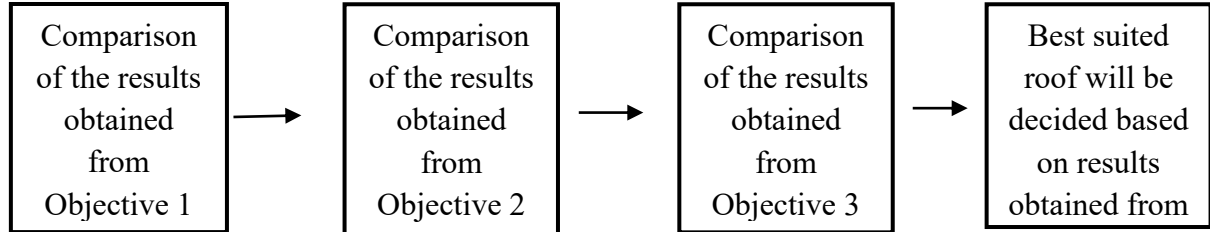
Fig. 3.11: Methodology for comparison of roofs

CHAPTER 4

RESULTS AND DISCUSSIONS FOR DOME ROOF

4.1 General

In this chapter, the results are typically organized around the key research questions or themes identified in the study, with clear presentation of data in the form of tables, figures, or descriptive summaries. This chapter not only reports the outcomes but also provides a detailed analysis of their significance, comparing them with existing literature, theories, and previous studies. A detailed discussion is being done about wind-induced pressure contours, pressure coefficient (C_{pe}), interference factor (*IF*) and interference difference (*ID*) over the dome roof in case of isolated and different interfering conditions. The variation of the mentioned coefficients concerning various angles of wind incidence is also discussed in this chapter.

4.2 Isolated Dome Roof

The low-rise building model with a dome roof with the plan dimensions of 200 mm X 200 mm, eave height of 150 mm and diameter of the dome roof of 200 mm is subjected to 0° and 45° wind incidence angles. The wind-induced pressure contours and variation of C_{pe} for isolated low-rise building with dome roof are discussed in section 4.2.1.

4.2.1 Pressure Contours

The wind induced pressure contours for isolated dome roof are shown in Fig. 4.1 in which it is very much clear that most part of the dome roof is under negative pressure and some portion is under positive pressure. During 0° wind angle in which the flow is perpendicular to the windward wall of the building, the bottom edge of the dome on the windward side is under maximum negative pressure and then due to the smooth wind flow, its magnitude reduces on the leeward potion. During 45° wind angle, the flow is diverted into two equal parts because of the sharp edge of the building in front of the flow which is responsible for the formation of two negative pressure zones on the both sides of the diagonal of roof. The dome roof is acting like streamline body which helps in reducing the pressure on the roof from higher negative magnitudes to lower negative magnitudes.

0° Pressure Contours   45° Pressure Contours
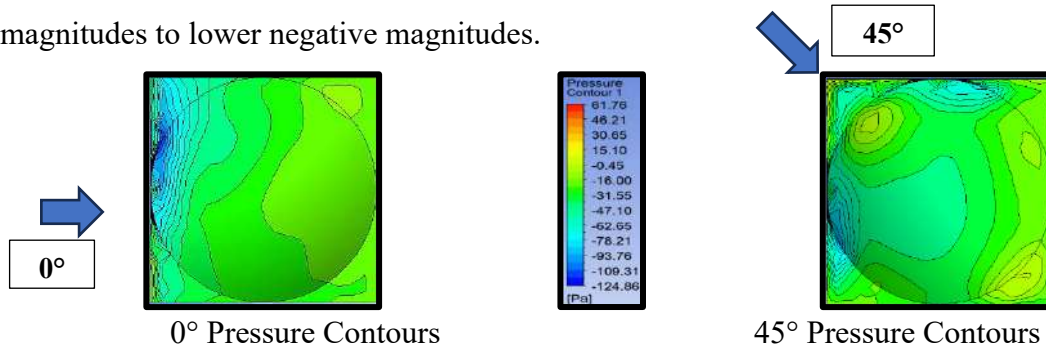
Fig. 4.1: Wind Induced Pressure Contours for Isolated Dome Roof

4.2.2 Pressure Coefficient

The external pressure coefficient on the dome roof is calculated using the equation 3.9 (**IS 875(Part-3):2015**).

$$C_{pe} = \frac{P - P_o}{\frac{1}{2}\rho U_H^2} \dots\dots\dots\dots\dots\dots\dots\dots\dots\dots\dots\dots\dots\dots\dots\dots\dots\dots\dots\dots\dots (3.9)$$

Where, P is the pressure derived from the simulation, P_o is the static pressure at reference height, ρ is the density of air i.e., 1.225 kg/m^3 and U_H is the reference velocity.

The validation of model is being done by comparing the value of C_{pe} at 0° wind incidence with code provisions of different nations (**ASCE 7-16, IS 875(Part-3):2015, MNBC:2020, NCH:432, GB50,009:2001 and NSCP:2015**) and the experimental studies which had been published earlier and shown below in Fig. 4.2. From Fig. 4.2, it can be seen that the C_{pe} values taken in the codal provisions are of higher magnitude 69.81% as compared to the values obtained experimental and CFD investigation which means that the codal value are overly estimated and less considerate for complex roof shapes e.g., dome roofs.

Since the model of low-rise building with dome roof is symmetrical about both axes i.e., x and y, therefore 0° and 45° angle of wind incidence are only considered as shown in Fig. 4.3. The overall impact of wind is negative which is creating suction on the roof and both the values of C_{pe} at 0° and 45° are coming out to be lesser than that of the codal provisions, hence the values are safer side. The values of maximum positive, negative and average C_{pe} are more or less equal at both the wind incidence angles 0° and 45° due to the symmetricity of the building about both axes.
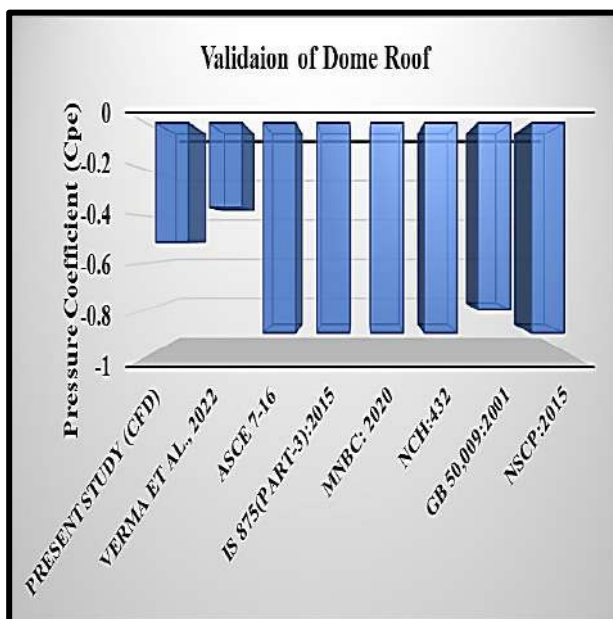
Fig. 4.2: Validation of the Dome roof model   **Fig. 4.3:** Pressure Coefficients for Dome Roof
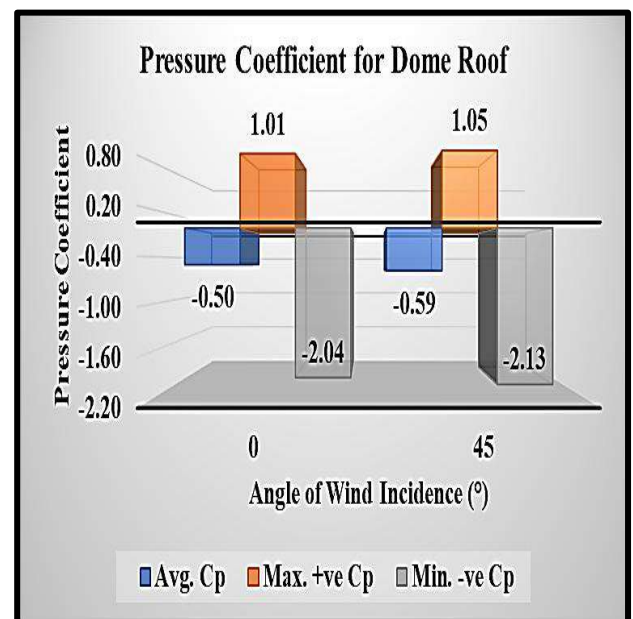
4.2.3 Wind Flow Pattern on Isolated Dome Roof

The wind flow pattern on isolated dome roof at 0° and 45° wind incidence angles is presented in Fig. 4.4. It is observed from the Fig. 4.4 that during 0° and 45° wind incidence angles, the wind flow is taking place very smoothly over the dome roof from the upstream side. The flow separation is taking is place at the apex of the dome and the started recirculating at the leeward portion of the dome and leeward wall of the building which is responsible for the higher suction at the leeward side of the building during 0° angle of wind incidence. The flow separation phenomenon is taking place near the leeward edge of the dome roof during 45° angle of wind incidence.

0°

45°
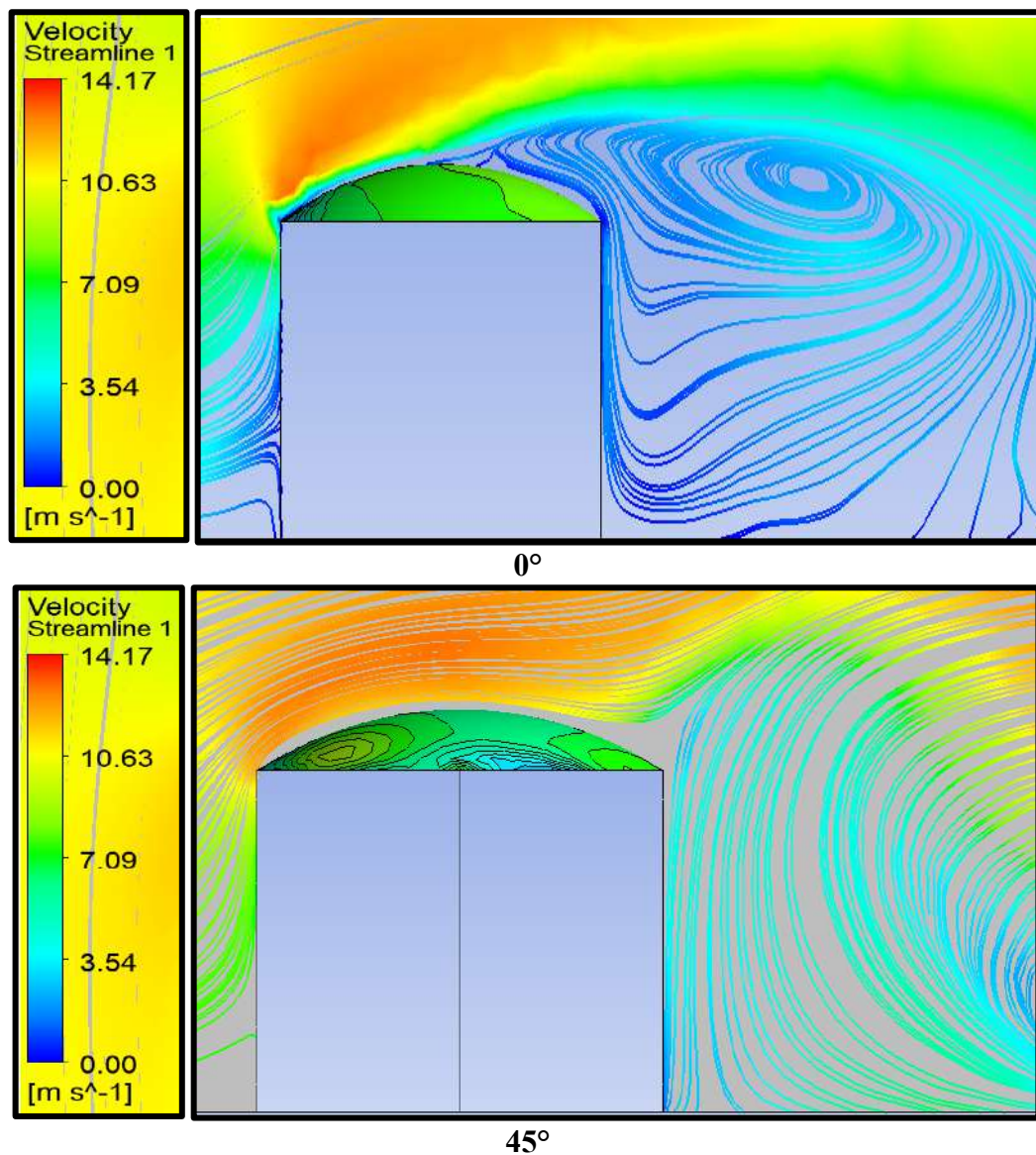
Fig. 4.4: Wind Flow Pattern over the Dome Roof

4.3 Interference

Due to the presence of nearby buildings in the close vicinity, the wind loads get modified on the roofs as well as on the wall of the low-rise buildings. In this section the effects of presence of nearby buildings are investigated in the form of interference factor (*IF*) and interference difference (*ID*) on the dome roof of low-rise structures arranged in rectangular pattern, T-pattern and Z- pattern with variable spacing i.e., 0, 0.5B, B, 1.5B and 2B where B is the width of the building.

4.3.1 Rectangular Pattern

To find out the effect of interference on dome roof, six low-rise building models with dome roof arranged in rectangular pattern placed nearby each other using different spacings. The wind generated pressure contours, IF and ID on all the six dome roofs due to interference have been studied.

4.3.1.1 Pressure Contours

The wind induced pressure contours for dome roof arranged in rectangular pattern with variable spacing are shown in Fig. 4.5 to 4.9. The pressure contours are shown for different wind incidence angles ranging from to 0° to 90° at 45° interval. All the six dome roofs have been given the different nomenclature as Roof A, Roof B, Roof C, Roof D, Roof E and Roof as already discussed and shown in shown in Fig. 3.8 of chapter 3. The Roofs A & D are acting as a windward roof, Roofs B & E are acting as a middle roofs and Roofs C & F are acting as a leeward roof.

In all cases of wind angles, the windward roofs are experiencing maximum wind induced pressure and middle and leeward roofs are least subjected to wind induced pressure due to shielding effects of the roofs. During 0° wind attack, the roofs which opposite to each other i.e., roof A & D, roof B & E and roof C & F are experiencing similar pressure distribution since the wind flow is equally divided into two halves. Similarly, in case of 90° wind attack, since the flow is dividing in to two equal halves, the roofs A, B and C are acting as a shield for roofs D, E and F.

Also, there is positive wind pressure distribution on the middle and leeward roofs which is possible due to the presence of windward roofs. Therefore, it can be said that interference plays vital role in reducing to the negative wind induced pressure to positive pressure.

The magnitude of wind-induced pressure is ranging between -56.24 to -3.38 Pa indicating the reduction in suction on roof as the spacing changes from 0 to 2B due to interference effect when the dome roofs are arranged in rectangular pattern.
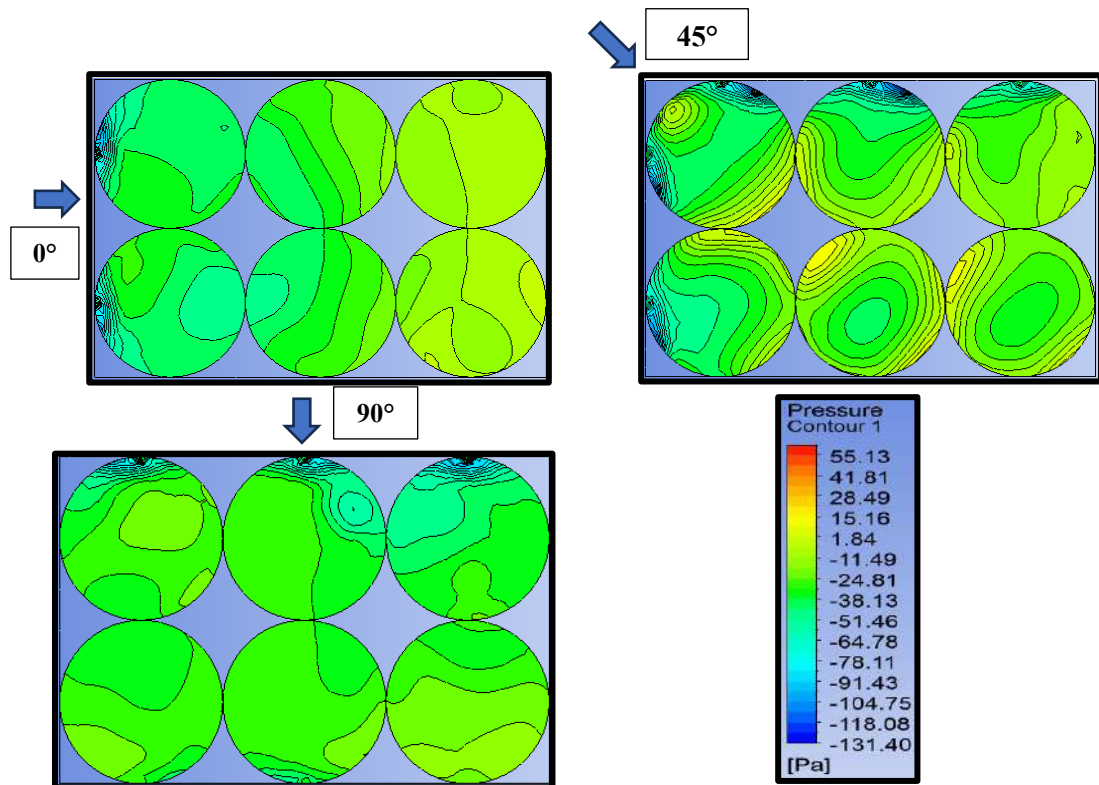
Fig. 4.5: Pressure contours of Rectangular Pattern with Zero Spacing
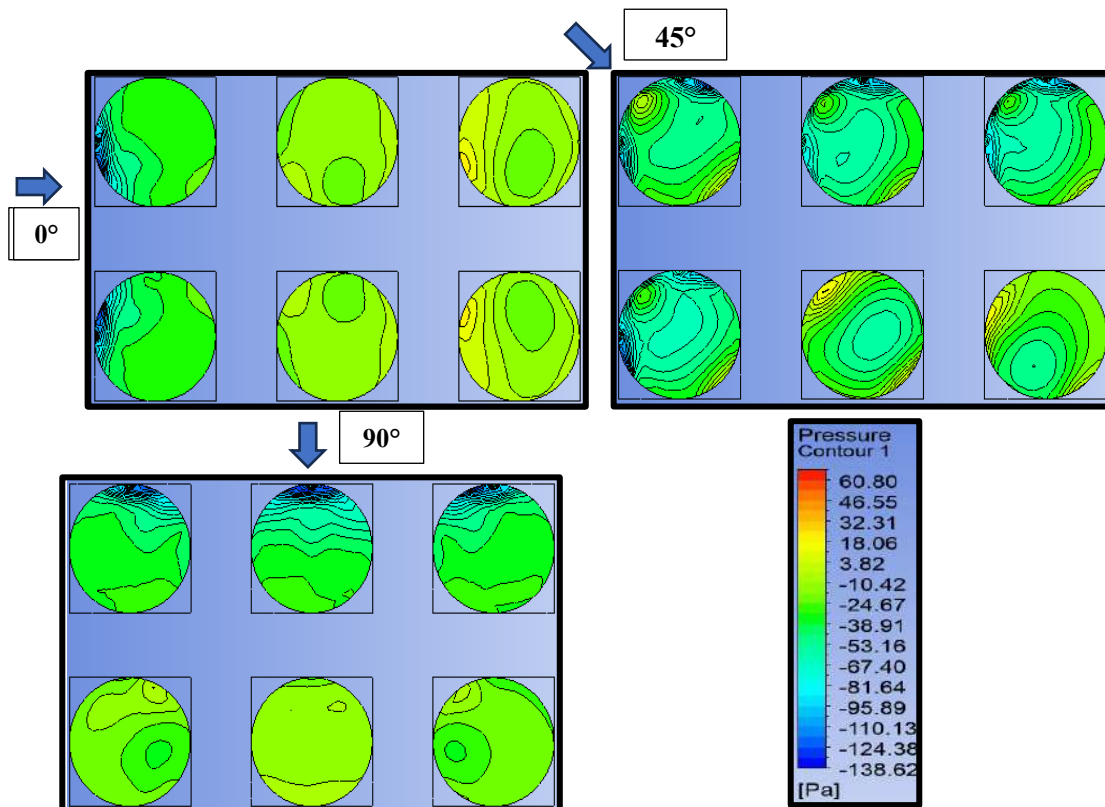
Fig. 4.6: Pressure contours of Rectangular Pattern with 0.5B Spacing
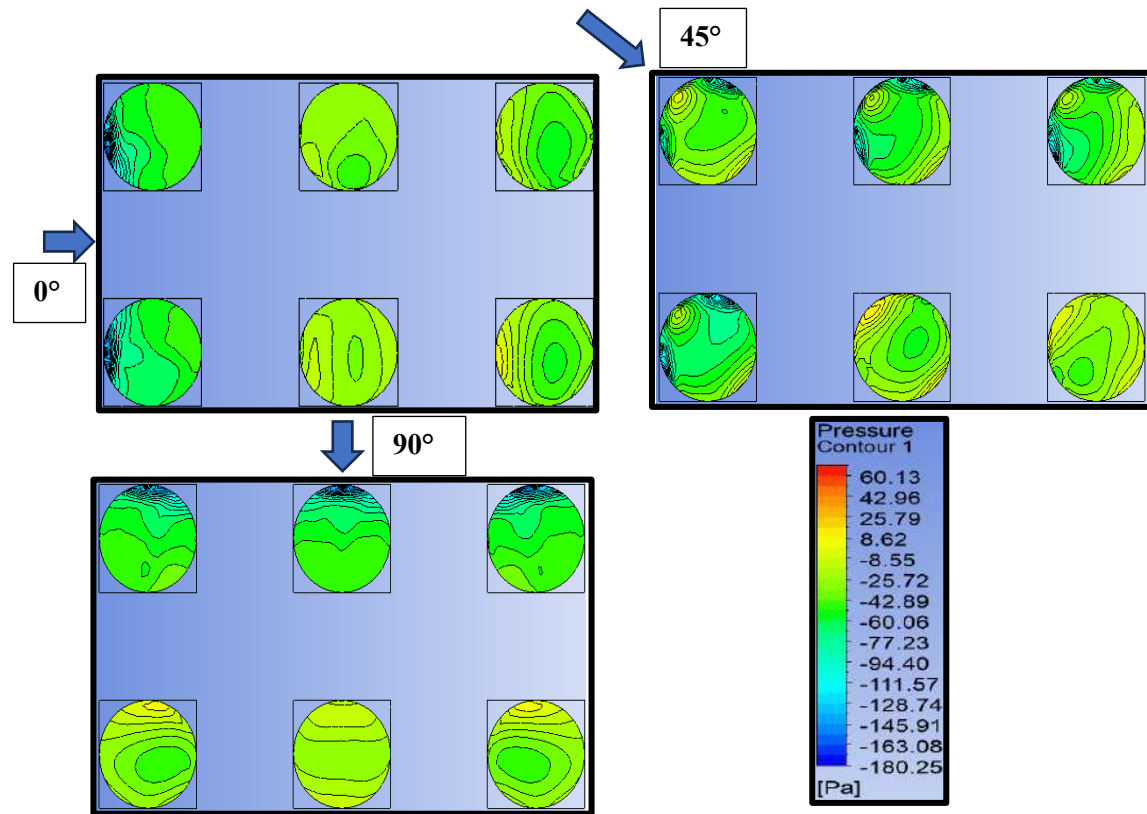
Fig. 4.7: Pressure Contours of Rectangular Pattern with B Spacing
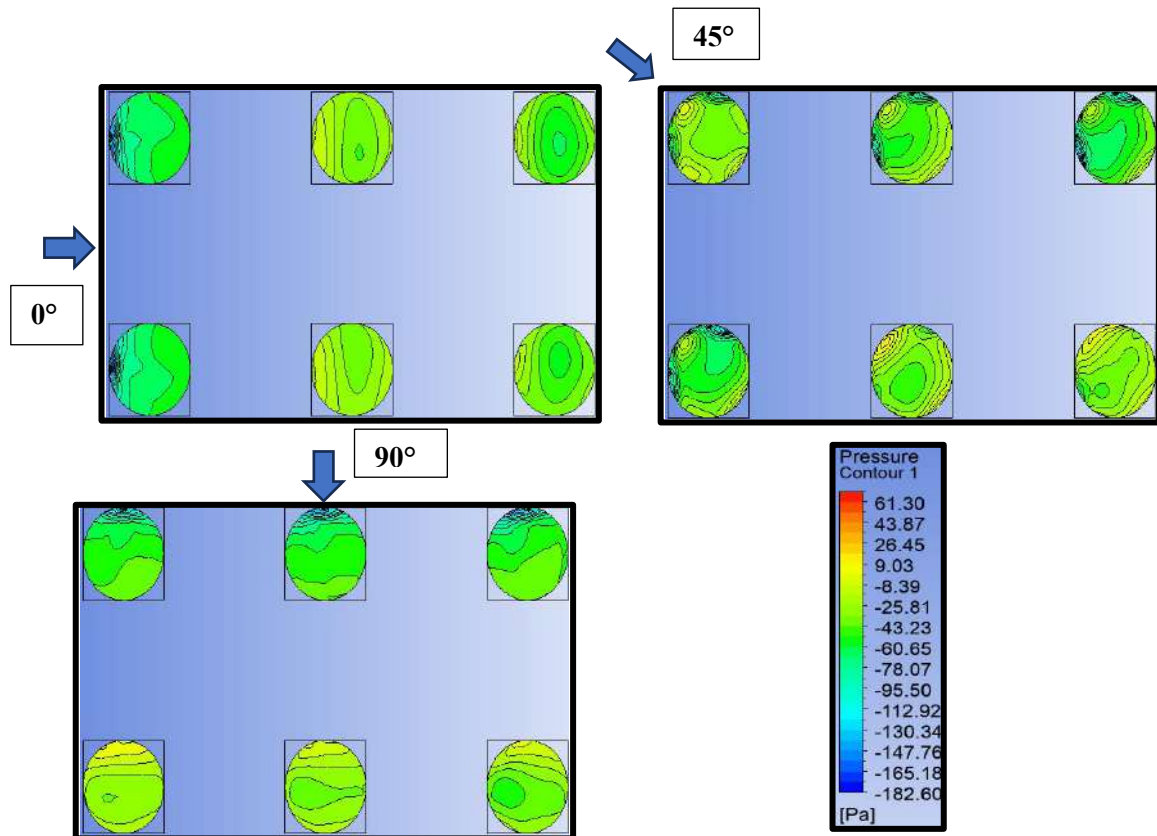
Fig. 4.8: Pressure Contours of rectangular pattern with 1.5B Spacing
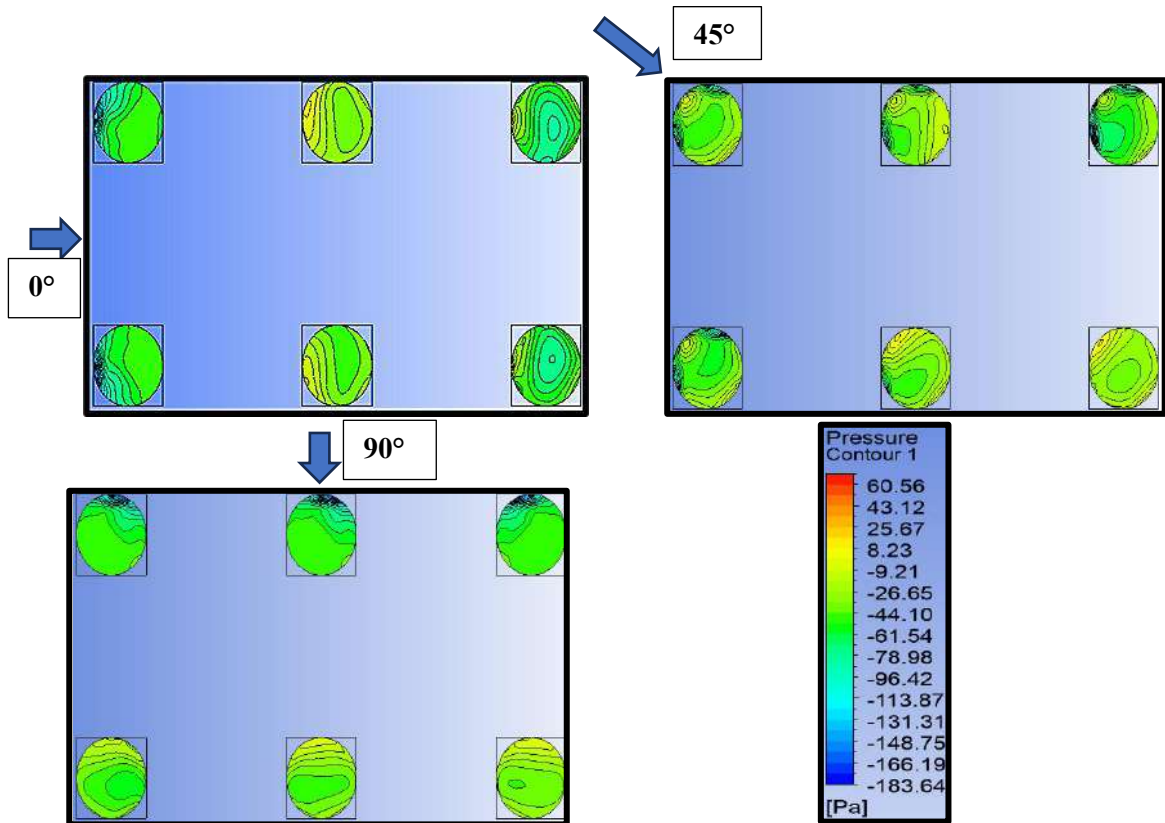
Fig. 4.9: Pressure Contours of Rectangular Pattern with 2B Spacing

4.3.1.2 Pressure Coefficient

The value of pressure coefficients for dome roof in case of rectangular interference conditions with variable spacing are shown in Fig. 4.10. The variation of C_{pe} for roof A & D follows the same trend during 0° wind incidence as it was reducing by increasing the spacing between the buildings which indicates that the suction on the windward roofs A & D (windward roofs) is reducing as the spacing increases. Similarly, the roofs B & E (middle roofs) and roofs C & F (leeward roofs) follows same pattern of variation of C_{pe} during 0° wind incidence.

Because of the shielding effect, the suction on the leeward roofs C and F is lesser than that of the middle roofs B & E and suction on the middle roofs B & E is lesser than the suction on the windward roofs A & D.

The maximum value of the suction is observed on roof A &D in case of interfering condition with zero spacing and minimum value of the suction is observed on roof B & E when the spacing is 2B between the buildings. During 90° wind angle, the behaviour of roofs A, B and C is similar to each other and acting as a shield for roofs D, E and F.

The magnitude of C_{pe} is ranging between -0.91 to -0.06 (75% increase when spacing is 0 and 88.46% reduce when spacing is 2B) indicating the reduction in suction on roof as the spacing changes from 0 to 2B when the dome roofs are arranged in rectangular pattern.
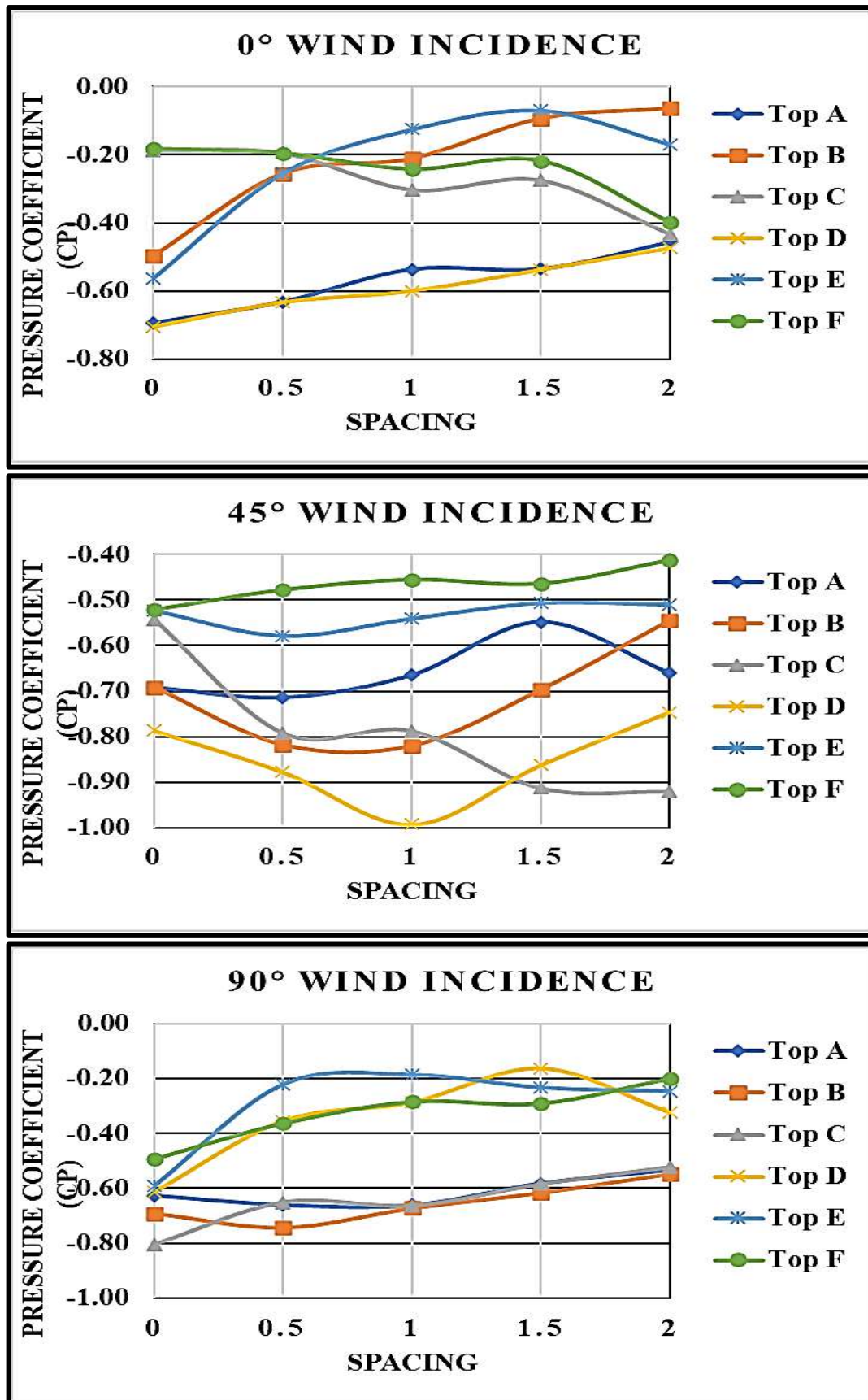
**Fig. 4.10:** Pressure Coefficient for Rectangular Pattern

4.3.1.3 Interference Factor (IF)

The ratio of C_{pe} obtained in interfering condition to the C_{pe} obtained in an isolated condition is known as Interference Factor (*IF*). It helps in clarifying the intricacies and to scrutinize the effect of interference on the roofs, which is given by equation 4.10. The cause of change in magnitude of *IF* means that either the wind induced positive or negative pressure is changed. And, when the symbol of *IF* is changed from either negative to positive or positive to negative, it implies that the nature of wind is changing on the roof. The range of *IF* varies between 1.7 to 0.12 when the spacing changing from 0 to 2B, in which the magnitude of *IF* $\geq$ 1 indicates the increased suction and *IF* $\leq$ indicates the reduced suction on the roof.

$$IF = \frac{C_{pe(interference)}}{C_{pe(isolated)}} \dots\dots\dots\dots\dots\dots\dots\dots\dots\dots\dots\dots\dots\dots\dots\dots\dots\dots\dots (4.10)$$
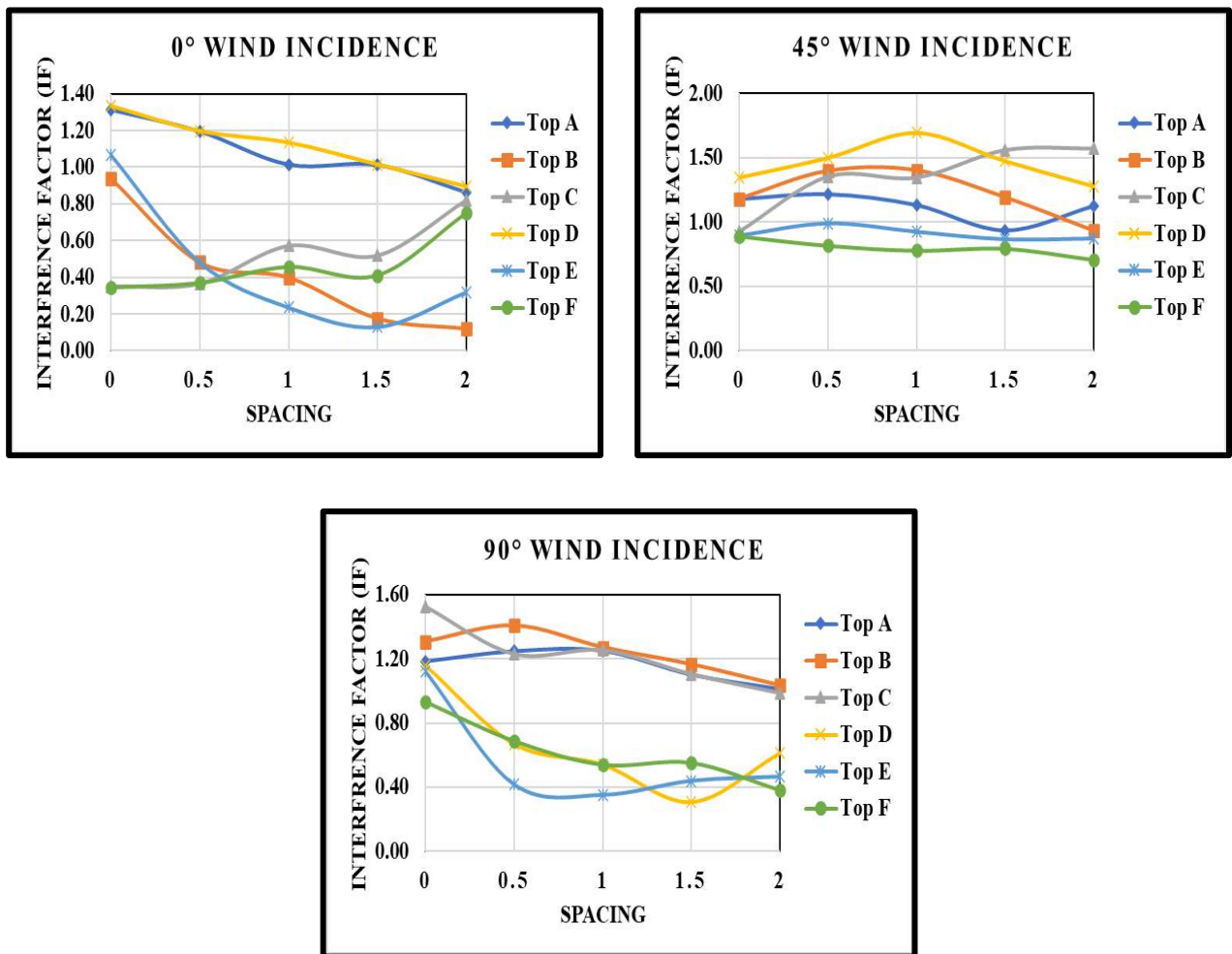
Fig. 4.11: Interference Factor for Rectangular Pattern

The variation of *IF* on dome roofs arranged in rectangular pattern with variable spacing is shown in Fig. 4.11. The magnitude of *IF* is reducing as the spacing between the buildings is increasing which indicates that either the suction or the positive pressure on the roof is

decreasing. This reduction in the magnitude of *IF* is due to the shielding effect which is occurring due to the presence of upstream buildings. Form the Fig. 4.11, it is clearly visible that middle roofs B & E and leeward roof C & F are highly protected due to interference effect of upstream buildings. During 0° and 90° wind incidence angles, the interference plays a critical role in reducing the wind induced positive or negative pressure on the roofs, while in case of 45°, there is no as such huge variation in *IF*.

4.3.1.4 Interference Difference (ID)

The influence of interference on the buildings can also be studied using another parameter also known as interference difference (*ID*) which is defined as the difference between the C_{pe} during interfering condition and C_{pe} during isolated condition, as it gives the exact idea of how much positive pressure or the suction on the roof is decreased or increased which proves out to be more precise than that the *IF*, shown in equation 4.11. The variation of *ID* for dome roof is shown in Fig. 4.12.

$$ID = C_{pe(interference)} - C_{pe(isolated)} \dots\dots\dots\dots\dots\dots\dots\dots\dots\dots\dots\dots\dots\dots\dots\dots\dots\dots\dots (4.11)$$
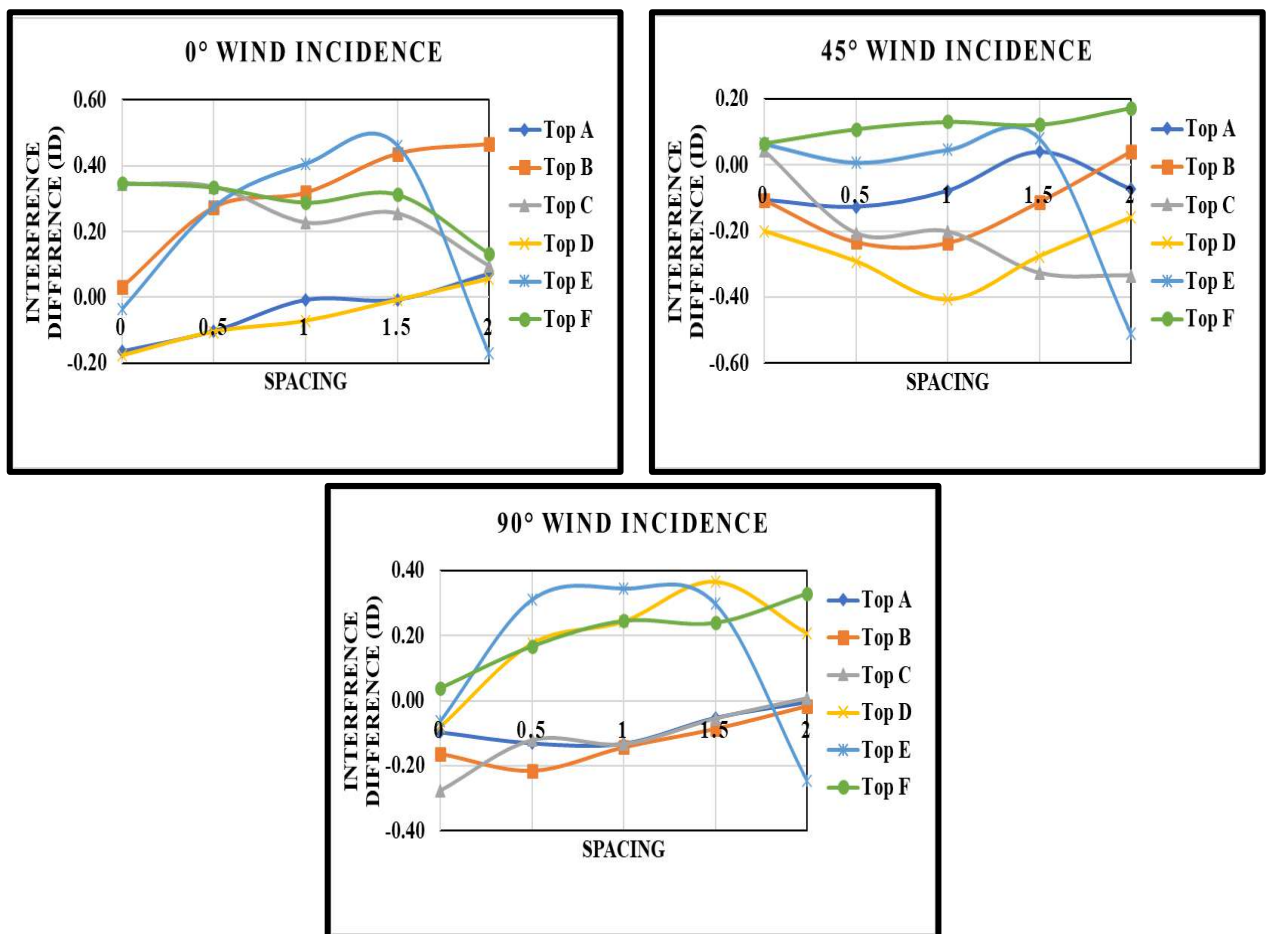
Fig. 4.12: Interference Difference for Rectangular Pattern

The range of *ID* is in between 0.47 to -0.51 which generates two different conditions of *ID* which helps in predicting the nature of wind on the roof, i.e., (a) when C_{pe} during isolated and interfering condition is less than 0 and *ID* is also less than 0, it implies that suction during interference condition is greater than the suction during isolated condition and (b) when C_{pe} is less than 0 but *ID* is greater than 0, therefore suction during interference condition is less than that of the suction during isolated condition. From Fig. 4.12, it is clearly predictable that the suction on the dome is reduced due to the interference of the upstream buildings. The value of *ID* is reducing with the increase in spacing between the buildings.

### 4.3.1.5 Wind Flow Streamlines

The wind flow streamlines for different interfering condition on dome roofs are shown in Fig. 4.13-4.16 for 0, 0.5B, B, 1.5B and 2B spacing respectively. In case of zero spacing between the buildings, the whole building model is acting as a multi-span isolated low rise building with dome roofs. The wind flow is not able to flow between the buildings and gets separated from the wall of the building, which is perpendicular to the wind flow in the upstream direction.

The maximum wind velocity of the flow is occurring near the upstream edges of the building which gets reduces on the leeward wall of the building during 0°, 45° and 90° wind incidence angles. The flow recirculation is taking place at the backside of the building in which the velocity of the is almost zero or negative which is responsible for the higher suction on the leeward side.

The streamlines for the interfering model with 0.5B spacing are shown in Fig. 4.14, in which it is clearly visible that the wind flow is trying to enter between the buildings but with a very low velocity due to less spacing between the buildings. A very small flow recirculation area is visible in between the windward roofs (A & D) and middle roofs (B & E).

As the spacing between the buildings is increasing, the wind flow which is separated due to the wall and edges of the windward buildings is trying to get converge in between the middle and leeward buildings. The velocity of wind flow is increasing from the upstream direction of the wind flow and get reduces towards to the downstream direction in between the building due to increase in the spacing.

Also, the vortex generation which is taking place behind the leeward walls of the building in case of zero spacing is now disappeared as the spacing is increased till 2B due to wind flow in between the buildings as shown in Fig. 4.13-4.17.
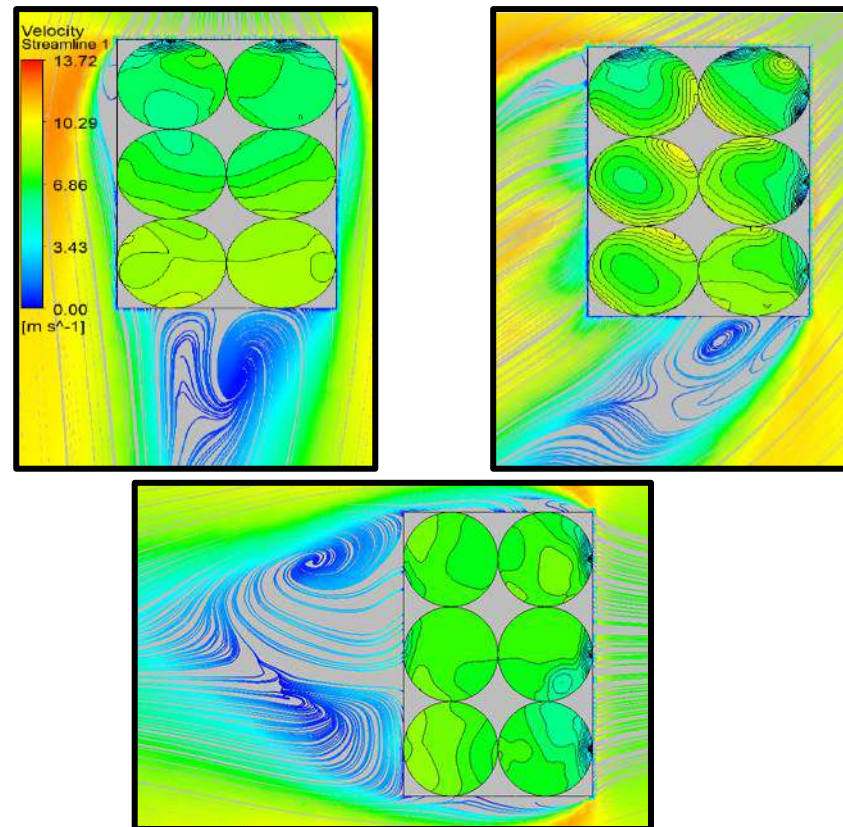
Fig. 4.13: Wind Flow Streamlines for Zero Spacing
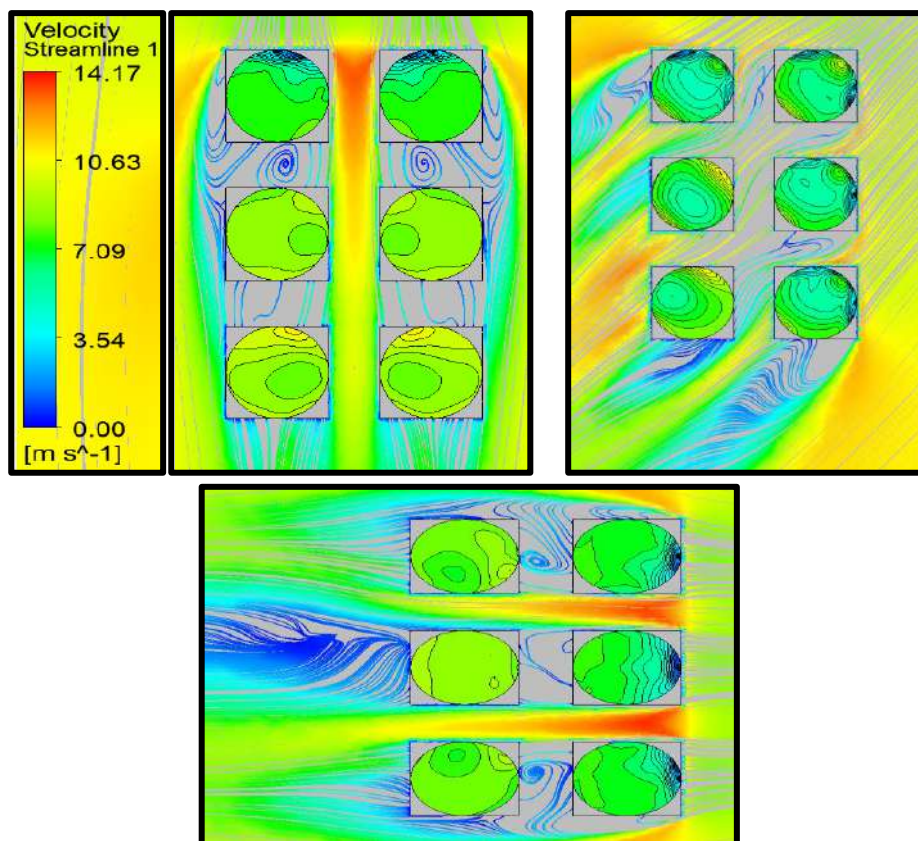

Fig. 4.14: Wind Flow Streamlines for 0.5B Spacing
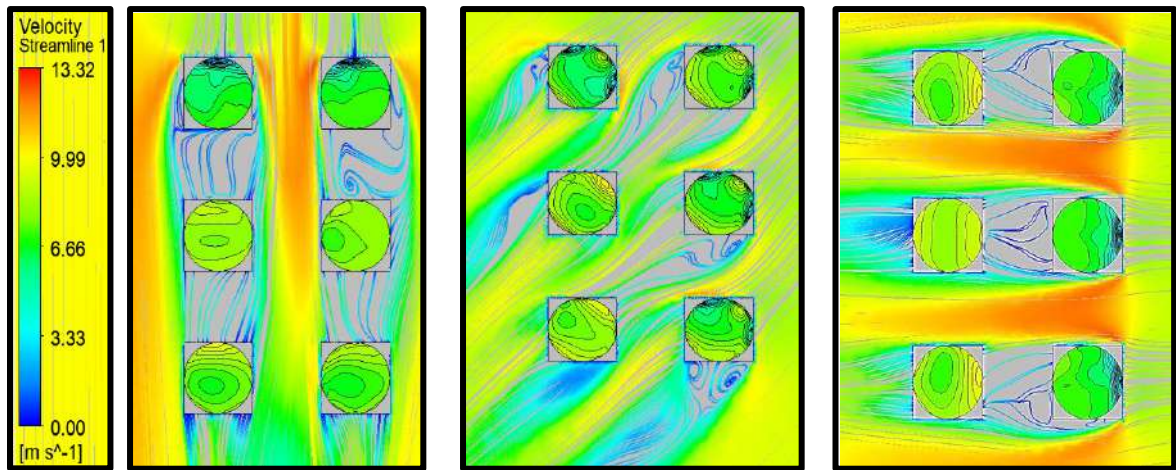
Fig. 4.15: Wind Flow Streamlines for B Spacing
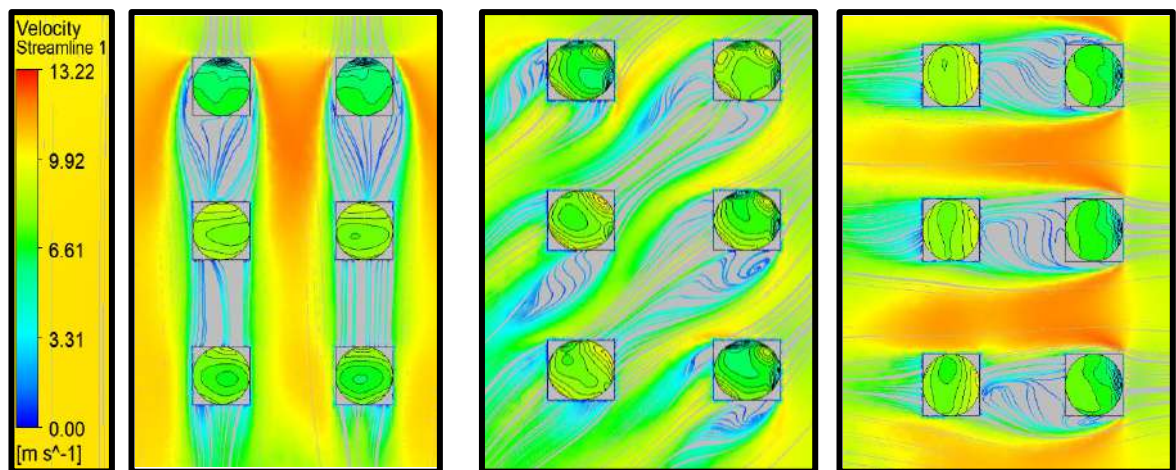
Fig. 4.16: Wind Flow Streamlines for 1.5B Spacing
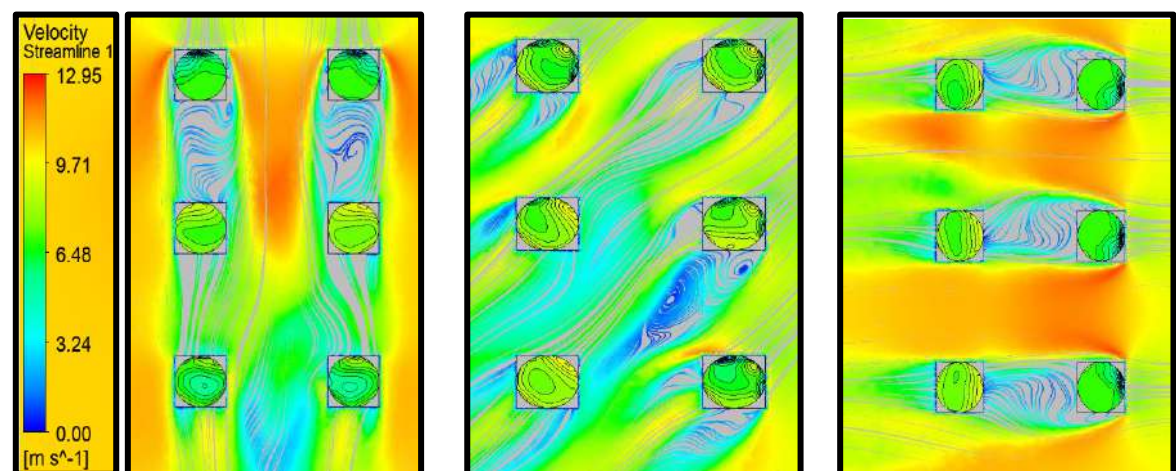
Fig. 4.17: Wind Flow Streamlines for 2B Spacing

4.3.2 Z Pattern

Similarly to the rectangular pattern, the dome roofs are now arranged in Z pattern of different interfering conditions with variable spacing of 0, 0.5B, B, 1.5B and 2B at different angles of wind attack to find out the wind effects on the dome roof, discussed below.

4.3.2.1 Pressure Contours

The pressure contours for dome roofs arranged in Z pattern at different angles of wind attack i.e., 0°, 45°, 90°, 135° and 180° are shown in Fig. 4.18-4.22. The wind induced pressure contours for 0° and 180° are similar to each other due to the symmetricity. It can be observed from Fig. 4.18-4.22 that the middle and leeward domes are under lesser suction as compared to the windward domes. The interfering model with 0 spacing is behaving like an isolated multi-span low-rise building having z shape and multiple domes.

During 45° and 135° wind attack, there are some portions on the dome roofs subjected to positive wind induced pressure. During 90° wind attack, the maximum suction is occurring at the upstream edge of the roof A, C, D and E just lying opposite to wind flow, shown in Fig. 4.18. When the spacing between the buildings is increased from 0 to 0.5B, the middle roof D is mostly under positive wind induced pressure during 0° wind attack. Also, the suction on all other roof is decreased on other dome roofs due to the distribution of the wind flow in between the buildings, shown in Fig. 4.18. The maximum reduction in negative wind pressure distribution on the dome roof is observed during 45° and 135° angles of wind attack shown in Fig. 4.18-4.22. The effect of interference is playing very crucial role in reducing the wind load on the dome roof in all the cases of Z pattern interference condition as compared to the isolated dome roof. The range of wind-induce pressure on dome roof when arranged in Z pattern with variable spacing is -51.8 Pa (0 spacing) to -23.1 Pa (2B spacing).
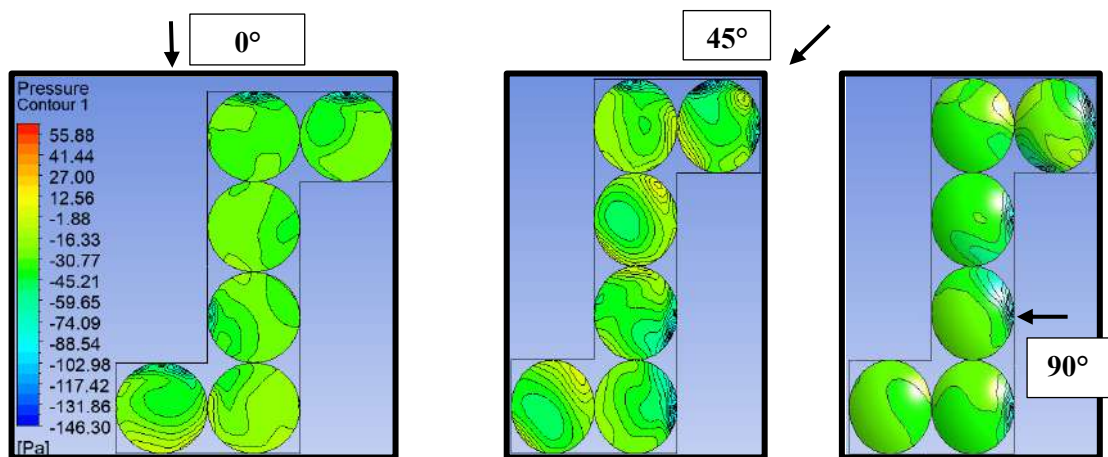
Fig. 4.18(a): Pressure contours of Z Pattern with Zero Spacing
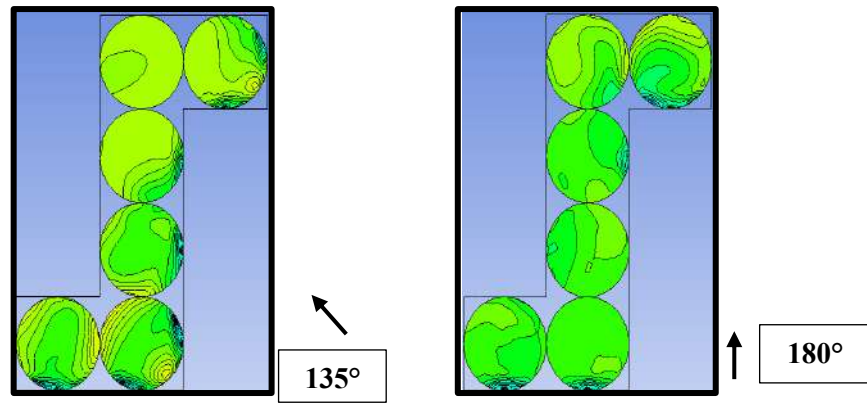
Fig. 4.18(b): Pressure contours of Z Pattern with Zero Spacing
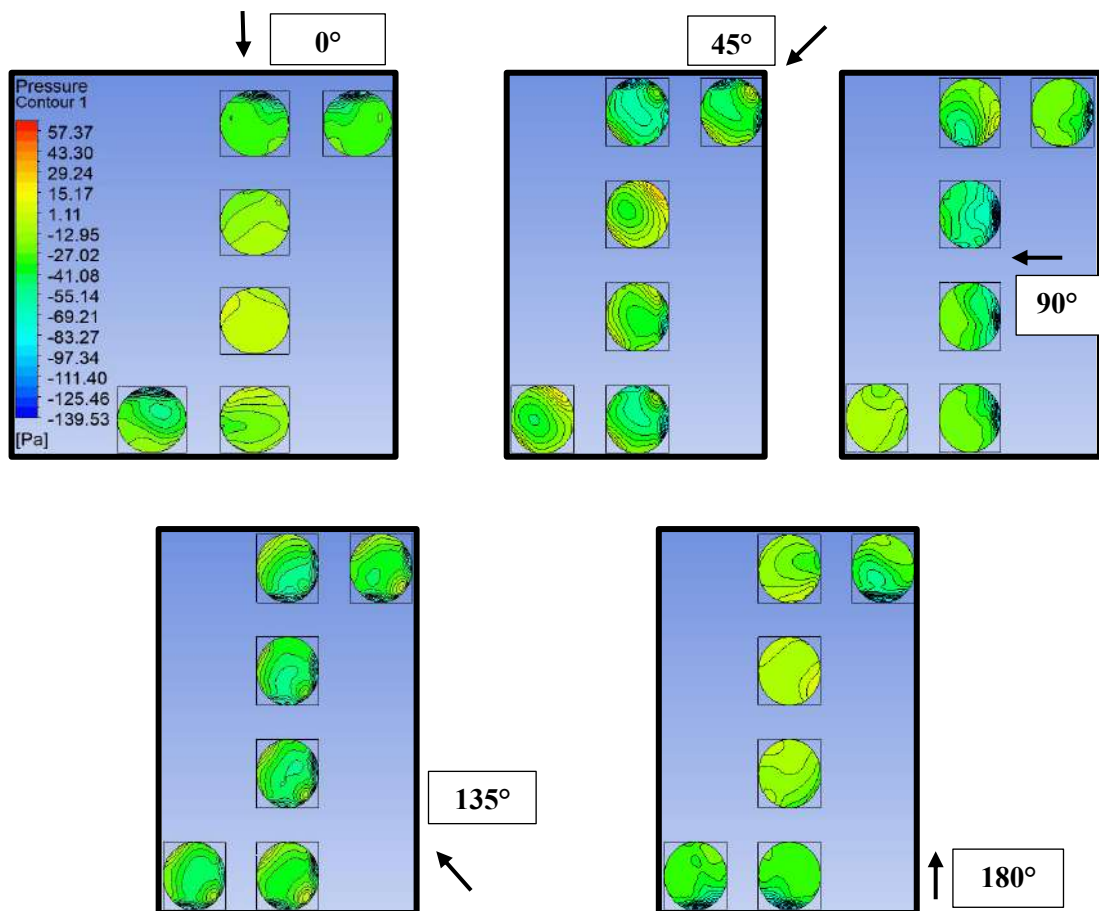
Fig. 4.19: Pressure contours of Z Pattern with 0.5B Spacing
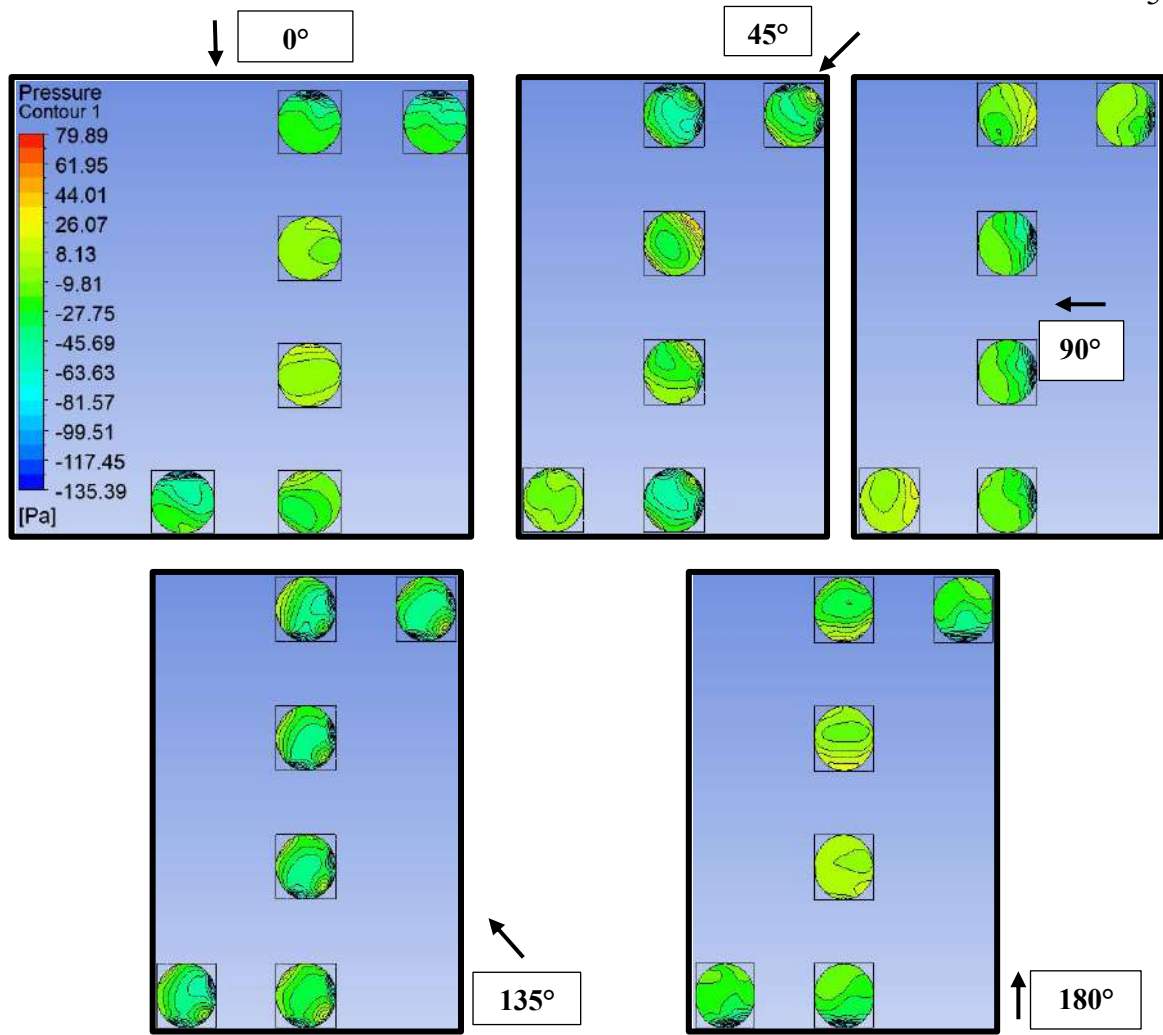
Fig. 4.20: Pressure contours of Z Pattern with B Spacing
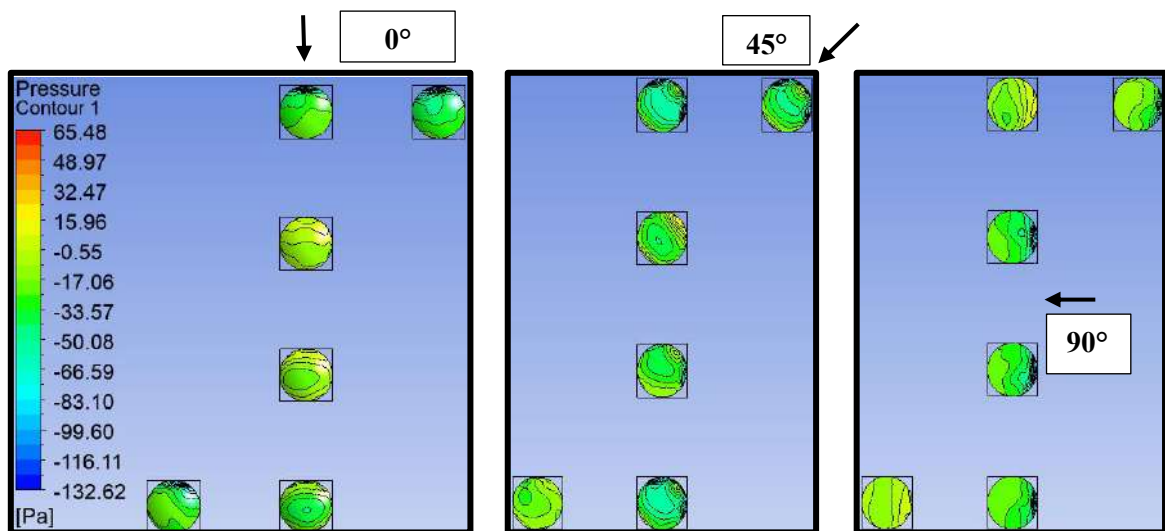
Fig. 4.21(a): Pressure contours of Z Pattern with 1.5B Spacing
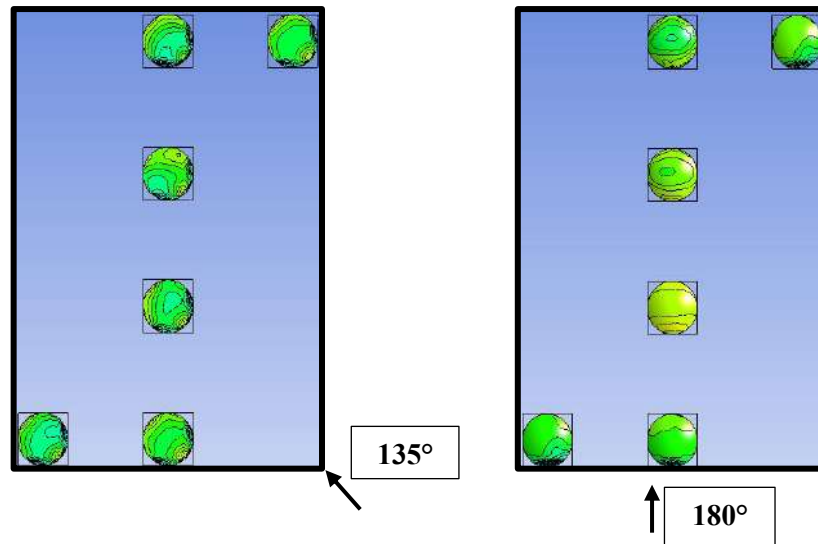
Fig. 4.21(b): Pressure contours of Z Pattern with 1.5B Spacing
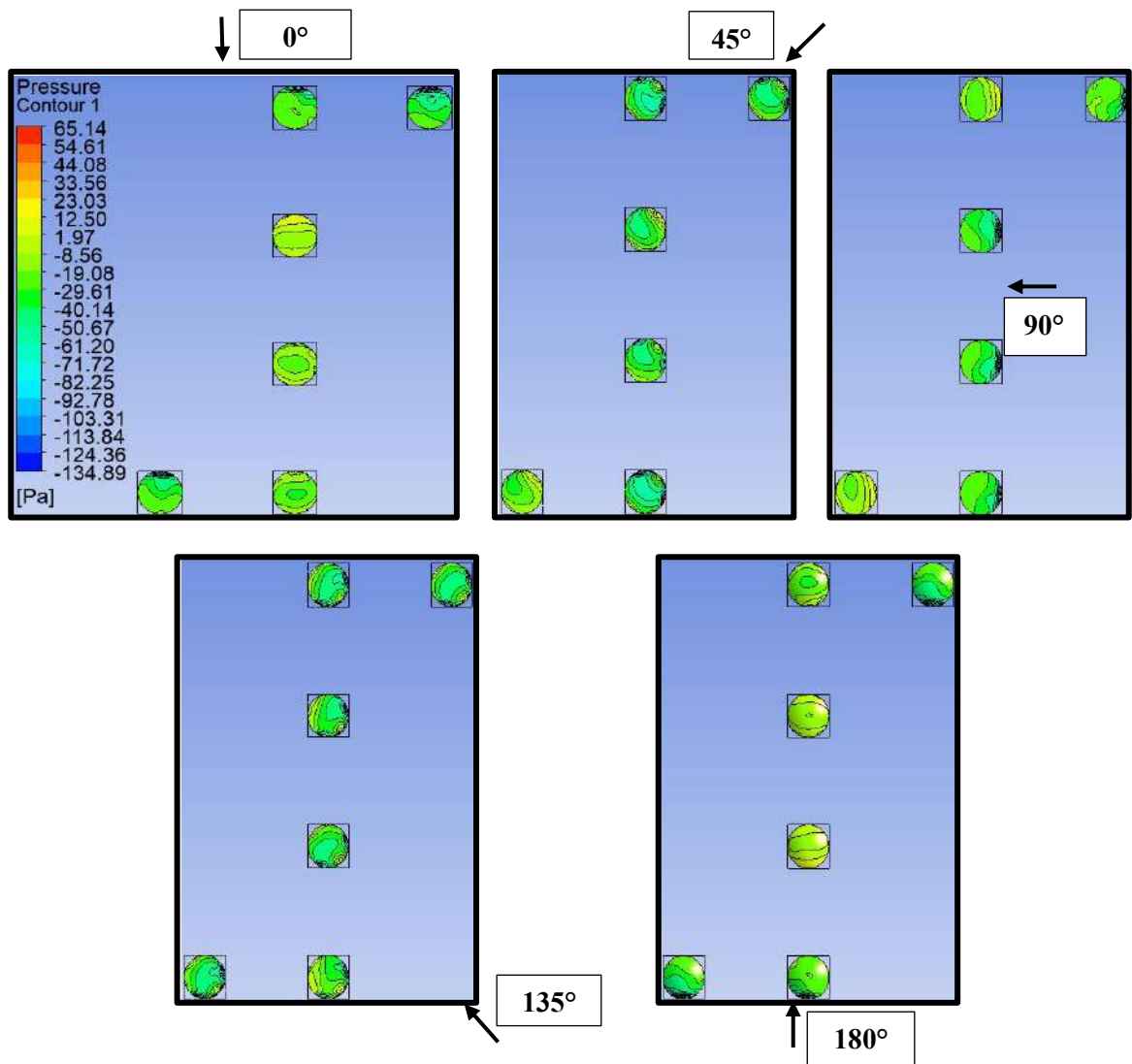
Fig. 4.22: Pressure contours of Z Pattern with 2B Spacing

4.3.2.2 Pressure Coefficient (C_{pe})

The variation of the pressure coefficient (C_{pe}) on dome roofs arranged in Z pattern are shown in Fig. 4.23 (a) and (b). Comparing to the rectangular pattern, it is observed that the value of C_{pe} is enhanced on the dome roof in case of z pattern which implies that the effect of interference is not that much effective. The effect of interference is generally visible only on the roofs B, C, D and E which are lying just behind each other in a single line of z pattern. The maximum increase in the value of C_{pe} is mostly occurring at 45°, 90° and 135° wind angles or it can be called most critical angles, on the dome roof shown in Fig. 4.23. During the wind incidence of 0° and 180°, the roofs C, D and E are getting shielding effect due to upstream roofs which is responsible for reduction in the value of C_{pe} on the dome roof similarly in case of 90°, the roofs B and F are getting shielded due to roof A and E respectively. The magnitude of pressure coefficient is ranging between -0.98 to -0.001 (88.46% increase when spacing is 0 and 98.9% reduce when spacing is 2B) indicating the reduction in suction on roof as the spacing changes from 0 to 2B when the dome roofs are arranged in Z pattern.
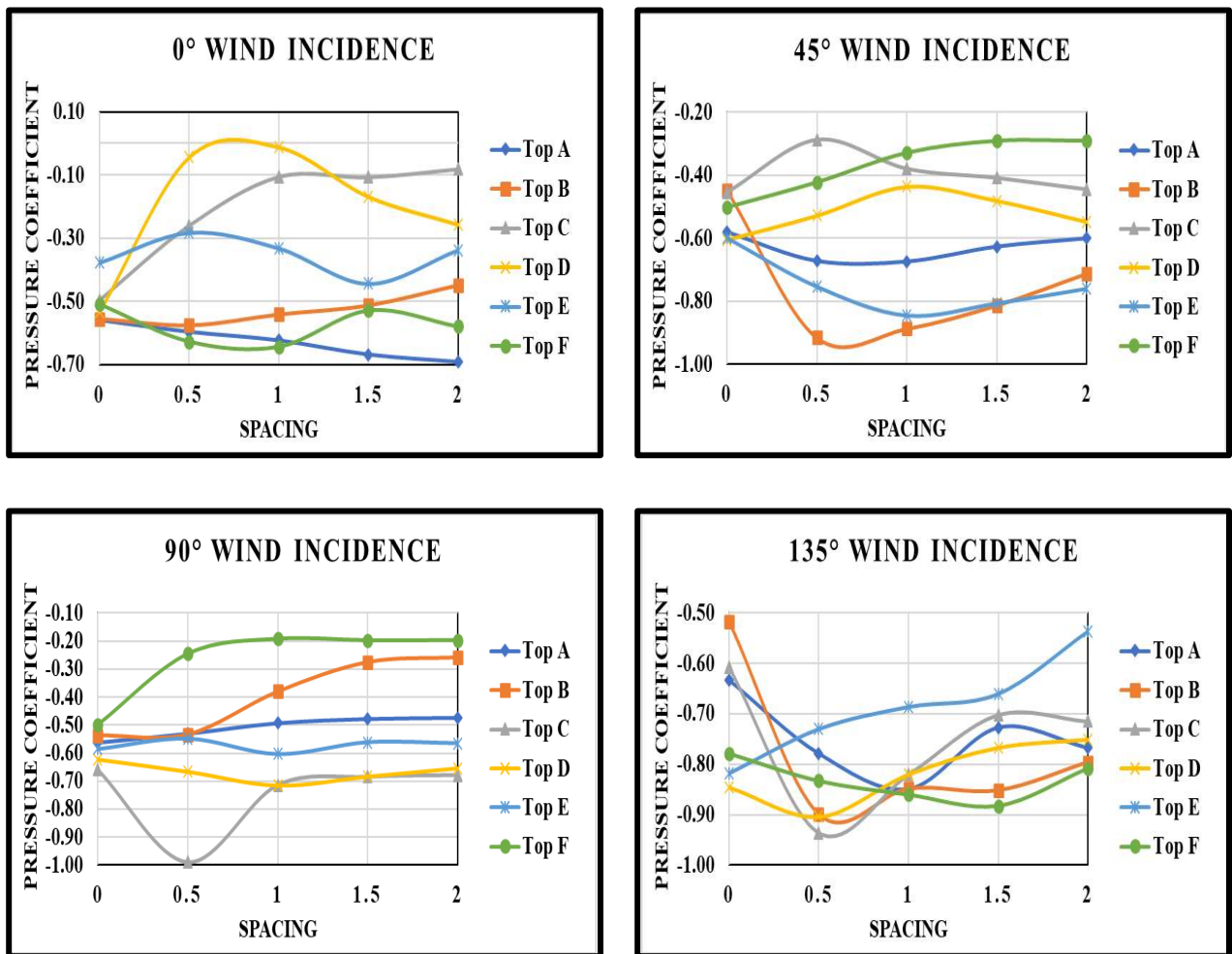
Fig. 4.23 (a): Pressure Coefficient for Z Pattern
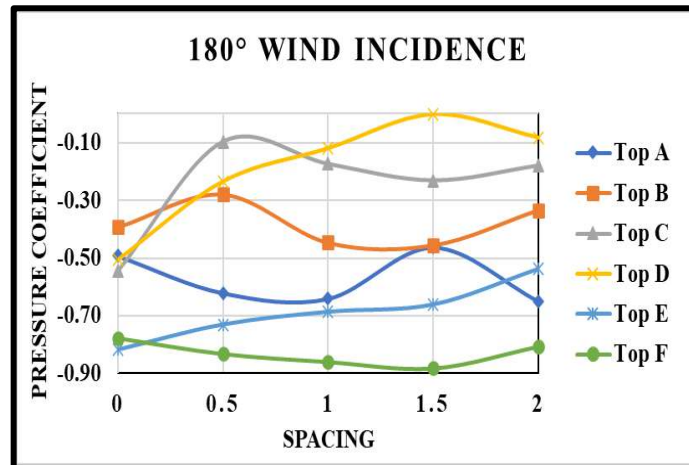
Fig. 4.23(b): Pressure Coefficient for Z Pattern

4.3.2.3 Interference Factor (IF)

By using equation 4.10, the *IF* is calculated for a dome roof arranged in a Z pattern with variable spacing at various angles of wind incidence discussed in this section and shown below in Fig. 4.24. The role of interference from the neighbouring buildings is quite reduced in the case of the Z pattern, such that the effect of interference is mostly noticeable only on roofs B, C, D and E during 0° and 180° angle of wind incidence and on roofs B and F during 90° angle of wind incidence. The value of *IF* is greater than 1 in magnitude, which indicates that the wind load on the roof is increased and the nature of the wind is still suction. During 0° wind incidence angle, the value of *IF* on roof A (windward roof) has increased by increasing the spacing form 0 to 2B, while in case of 45°, 90°, 135° and 180°, its value is increased when the spacing is increased from 0 to B and starts reducing until 2B spacing. The value of *IF* on top B (windward roof) is found to be less than 1 in most of the cases of wind angle and spacing variations implies that the wind load on roof B reduced due to interference effect of upstream roofs. The value of *IF* on roof C (middle roof) is greater than 1 only in case of 90° and 135° wind incidence angles while it is less than 1 in all other cases of wind incidence angles which is indicating that shielding effect is maximum on roof C. The roof D is experiencing the lesser suction as compared to the isolated condition with *IF* less than 1 in case of 0°, 45° and 180° wind incidence angles while its value is more than 1 in case of 90° and 135° wind angles. The range of *IF* varies between 1.87 to 0.01 when the spacing changing from 0 to 2B, in which the magnitude of *IF* ≥ 1 indicates the increased suction and *IF*≤ indicates the reduced suction on the roof.

The variation of *IF* with respect to the different spacing at various angles of wind incidence are shown in in Fig. 4.24.
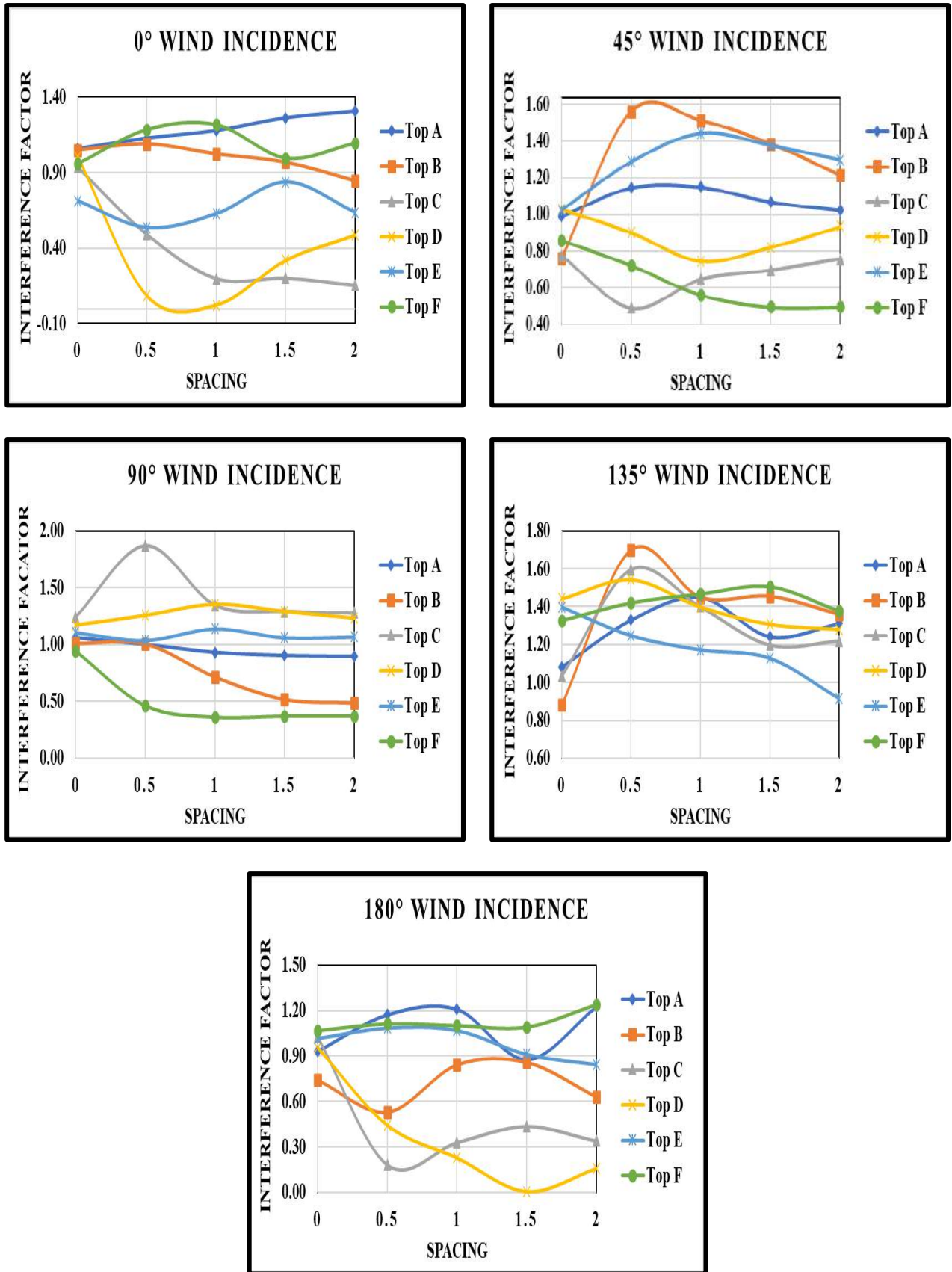
Fig. 4.24: Interference Factor for Z Pattern

4.3.2.4 Interference Difference (ID)

The variation of *ID* for dome roof in case of z pattern interference condition with variable spacing at different wind incidence angles is shown in Fig. 4.25 (a) and (b). From the Fig. 4.25, it is observed that the *ID* for roof A is positive in case of 90° wind incidence angles which implies that the suction on the dome roof A is reduced as compared to isolated dome roof, while on other angles such that 0°, 45°, 135° and 180°, the *ID* is less than 0 indicating that the suction is higher. The roof B is getting positive *ID* in case of 90° and 180° wind incidence angles. The roofs C and D have the positive value of *ID* during 0°, 45° and 180° wind incidence angles and roof F is subjected to positive *ID* during 45° and 90° incidence angles only. The range of *ID* is in between 0.53 to -0.46 in which the positive value of *ID* is indicating the reduction in the suction due to interference while negative value of *ID* is indicating that the suction on the roof is increased, shown in Fig. 4.25.
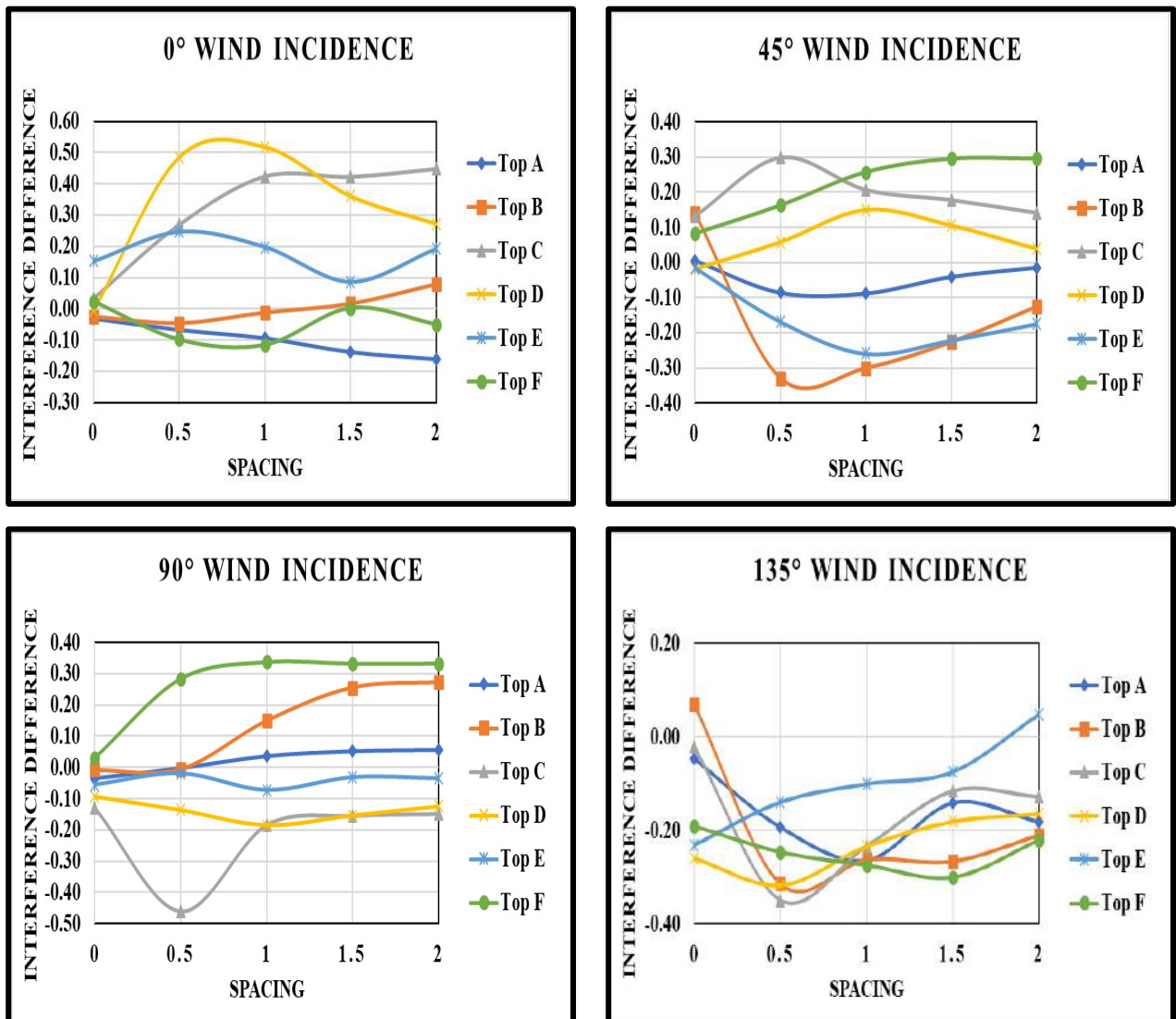
Fig. 4.25(a): Interference Difference for Z Pattern
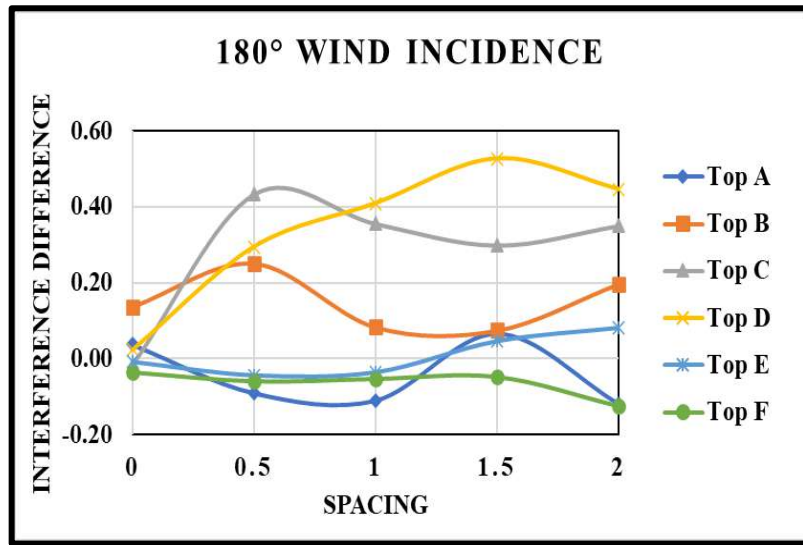
Fig. 4.25(b): Interference Difference for Z Pattern

4.3.2.5 Wind Flow Streamlines

The pattern of wind flow around and in between the buildings form dome roofs arranged in z pattern with variable spacing at various angles of wind incidence are shown in Fig. 4.26-4.30. The wind flow pattern for 0° and 180° wind incidence angles is exactly similar to each other. The only difference is that the behaviour of the roofs is interchanged such that the roof B initially acting as a windward roof during 0° wind incidence and started behaving as a leeward roof in case of 180° wind incidence angle.

The flow recirculation is taking place on both the sides of the middle vertical line of the roofs B, C, D and E. The flow recirculation is maximum in case of 90° wind angle taking place behind the building, shown in Fig. 4.26. The wake formation is reduced when the spacing between the buildings is increased from 0 to 2B.

The maximum wake region is formed in case of 90° wind incidence angle in the downstream direction of the wind flow on the roofs D, E and F only. As the spacing between the buildings is increasing, the wind flow gets separated from the leading edges and wall of the buildings and gets converge at the downstream location which is responsible for the flow recirculation and flow reattachment phenomenon as shown in Fig. 4.26-4.30.
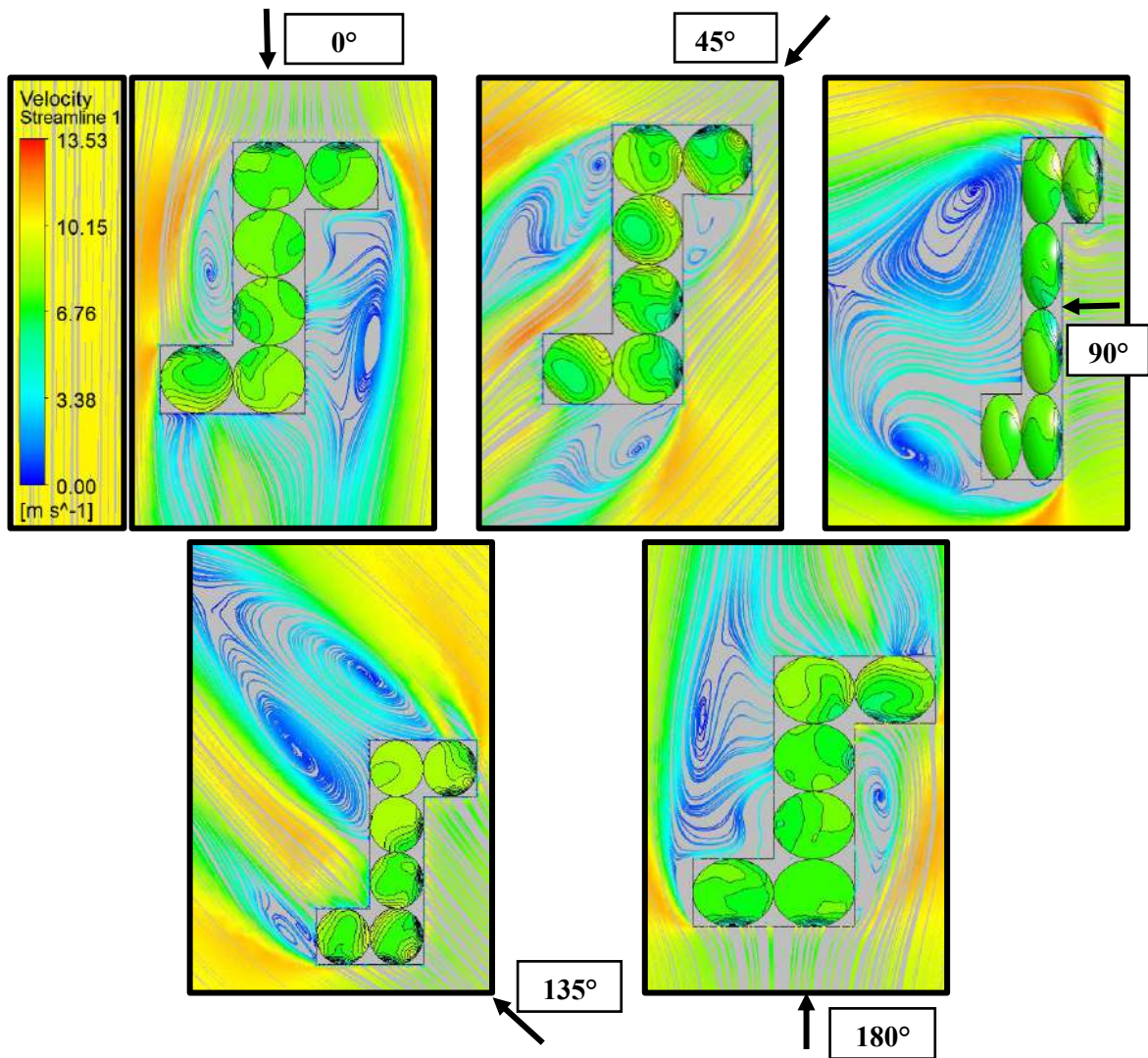
Fig. 4.26: Wind Flow Streamlines for Zero Spacing
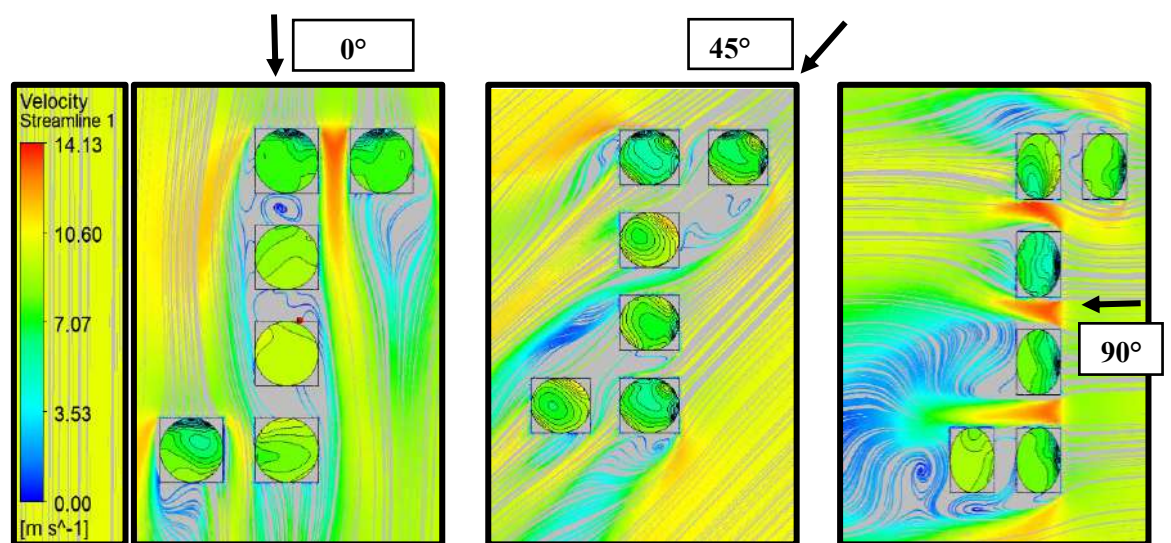
Fig. 4.27(a): Wind Flow Streamlines for 0.5B Spacing
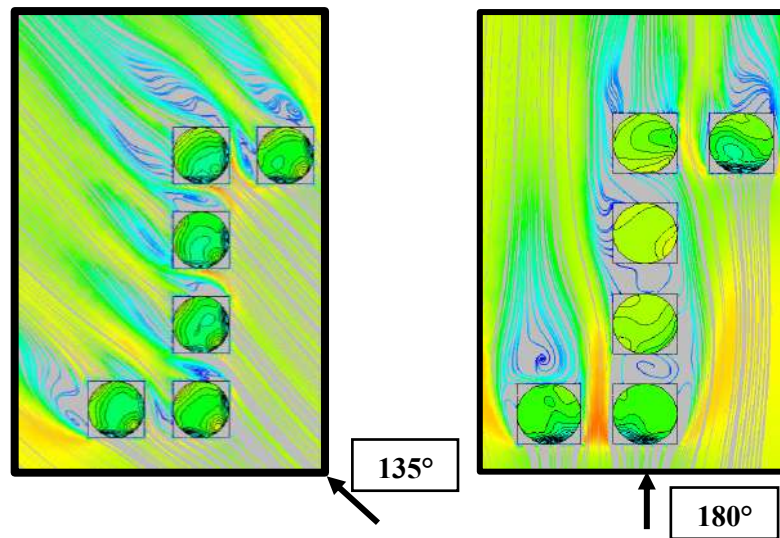
Fig. 4.27(b): Wind Flow Streamlines for 0.5B Spacing
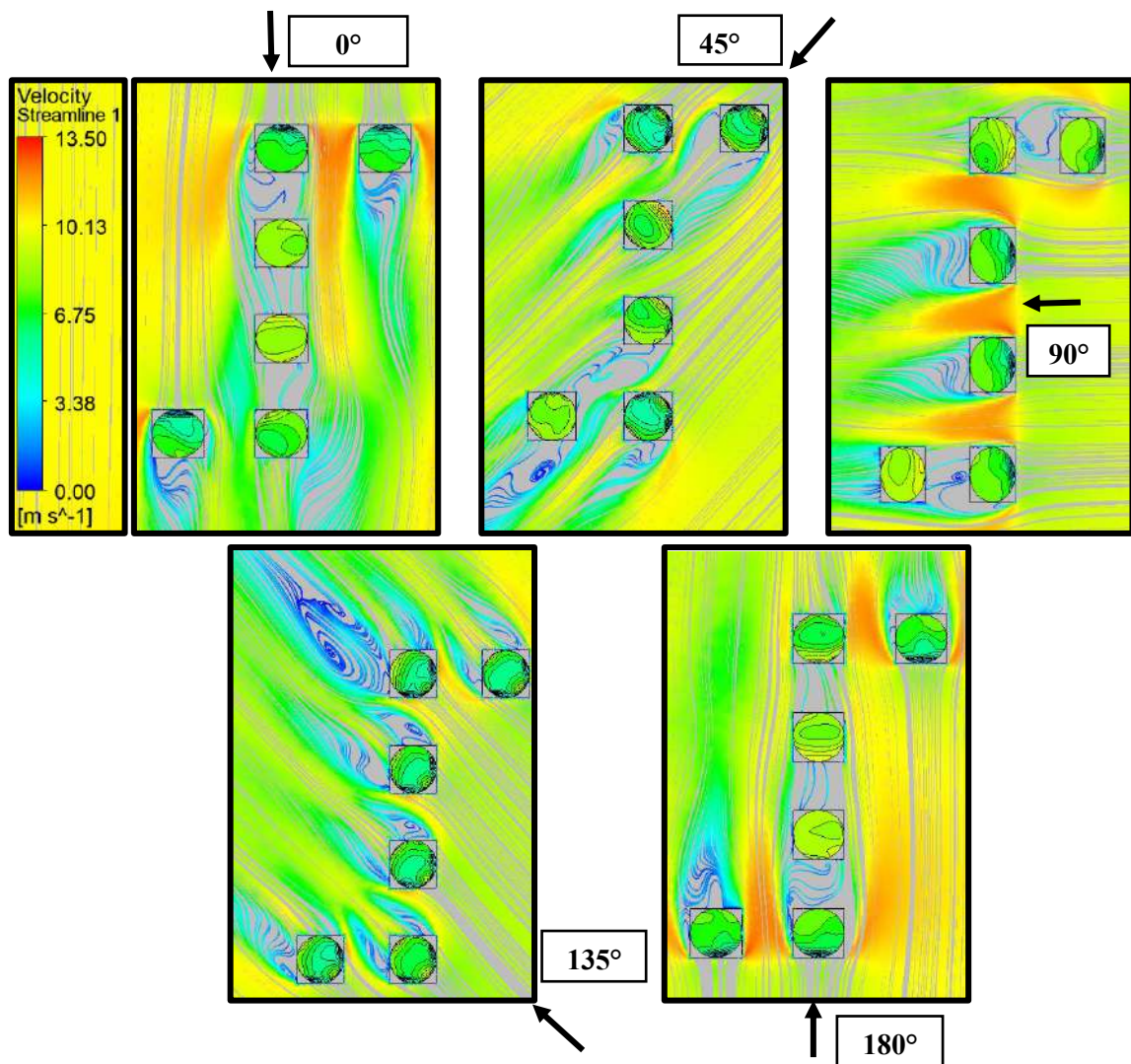
Fig. 4.28: Wind Flow Streamlines for B Spacing
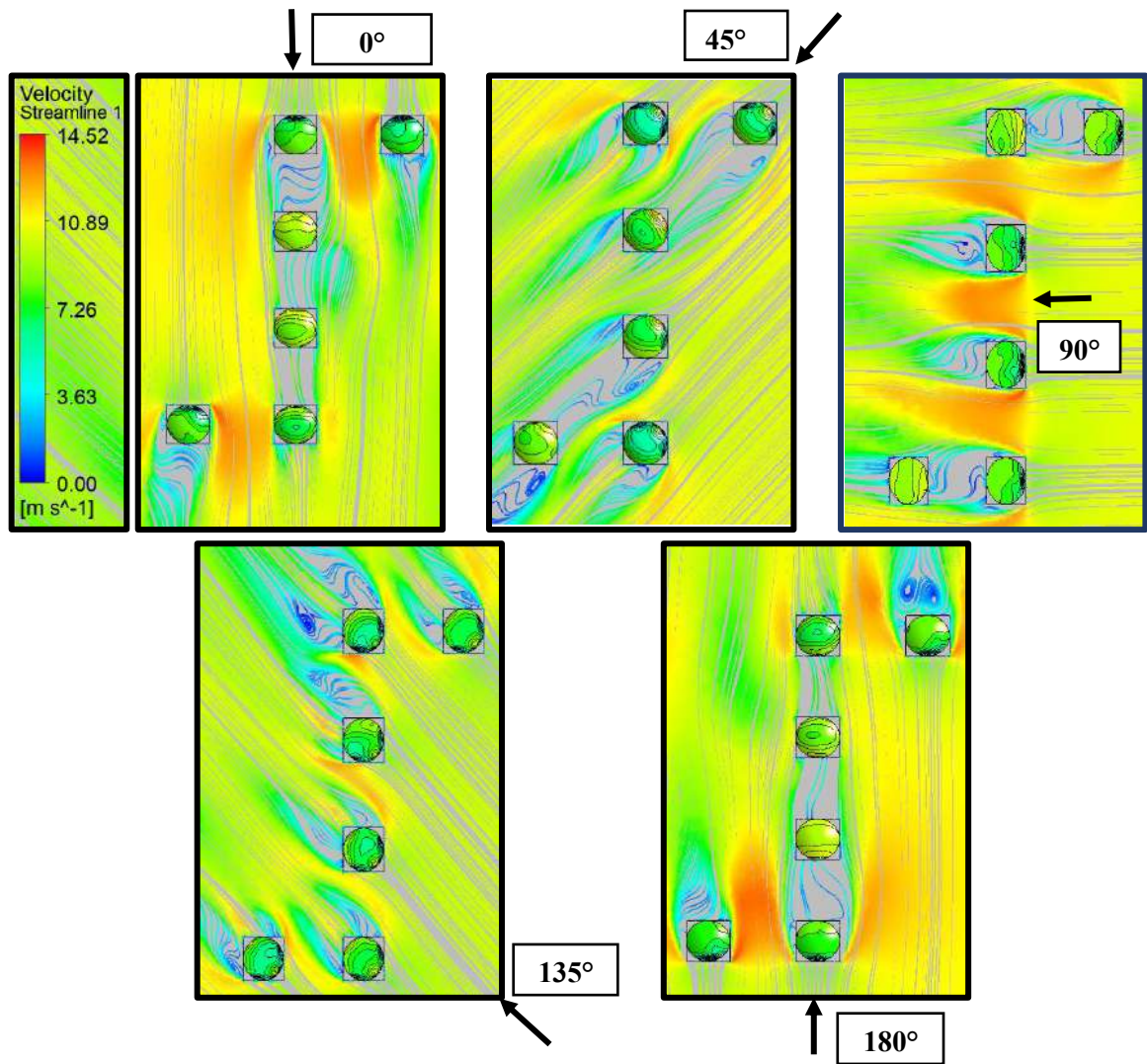
Fig. 4.29: Wind Flow Streamlines for 1.5B Spacing
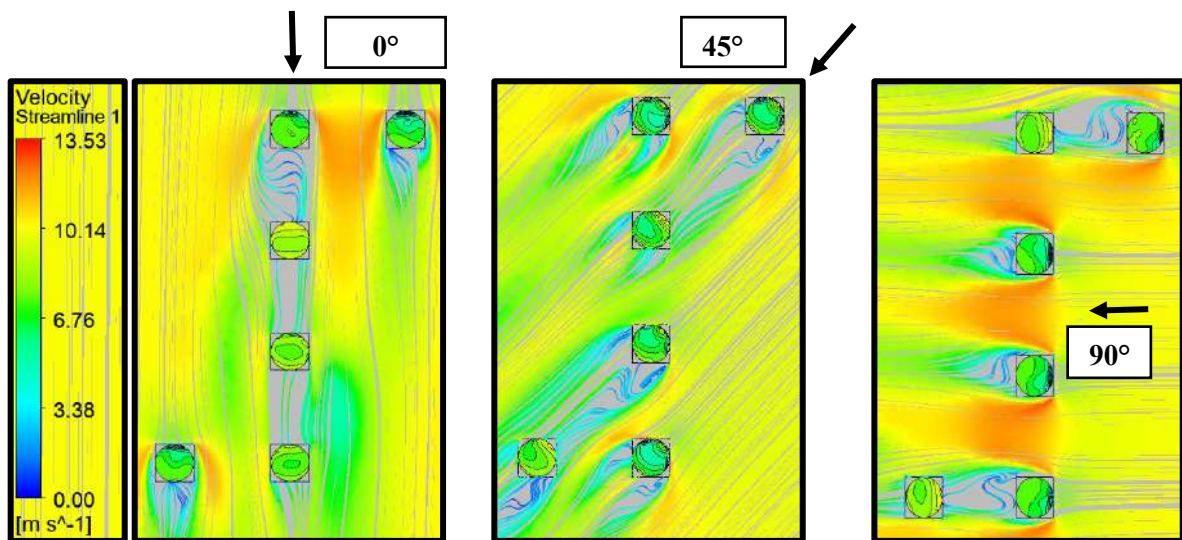
Fig. 4.30(a): Wind Flow Streamlines for 2B Spacing
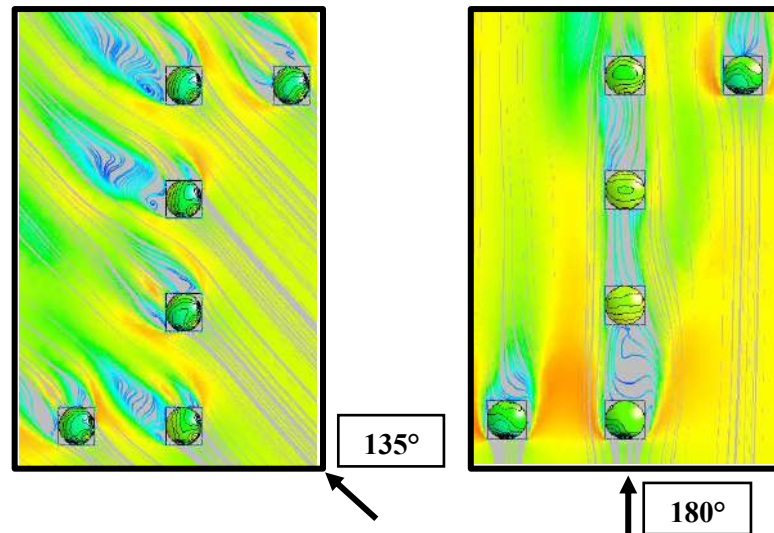
Fig. 4.30(b): Wind Flow Streamlines for 2B Spacing

4.3.3 T Pattern

This section contains a detailed description of the variation of pressure contours, pressure coefficients, *IF* and *ID* over the dome roofs arranged in a T pattern with variable spacing, i.e., 0, 0.5B, B, 1.5B and 2B at different angles of wind incidence such that 0°, 45°, 90°, 135° and 180° respectively.

4.3.3.1 Pressure Contours

The wind-induced pressure contours change with respect to wind incidence angle variable spacing, as shown in the Fig. 4.31-4.35. The dome roofs are arranged in a T pattern with the variable spacing of 0, 0.5B, B, 1.5B and 2B, where B is the width of the building (B = 200 mm) and subjected to different angles of wind incidences 0°,45°, 90°, 135° and 180°. In the case of 0° and 180° wind incidence angles, the distribution of wind-induced pressure is similar on roofs A and C. There is some portion on the roofs A, D and E, which is subjected to the positive wind pressure distribution during 45° wind incidence angle. The wind pressure distribution on dome roofs in a T pattern with zero spacing at various angles of wind incidences is shown in Fig. 4.31. In case of a T pattern with 0.5B spacing, the roofs E (middle) and F (leeward) are subjected to the lowest suction during 0° wind incidence angle, as shown in Fig. 4.32. The portion of roof D, lying just opposite to angle 45° is subjected to the positive wind pressure distribution since it gets a shielding effect from roof A (windward roof). During the 180° wind incidence angle, the nature of wind on roof D is completely positive, implying that the wind is dragging the downstream direction. The wind-induced pressure distribution on the dome roof in a T pattern with 0.5B spacing at various angles of wind incidence is shown in Fig. 4.32. the pressure is varying between -51.78 Pa (0 spacing) to 6.30 Pa (2B spacing), and it clearly visible

that the nature of wind has hanged from suction to pressure. The spacing between the building is playing very crucial role in changing the wind-induced pressure distribution on the dome roof of low-rise buildings as shown in Fig. 4.33-4.35.
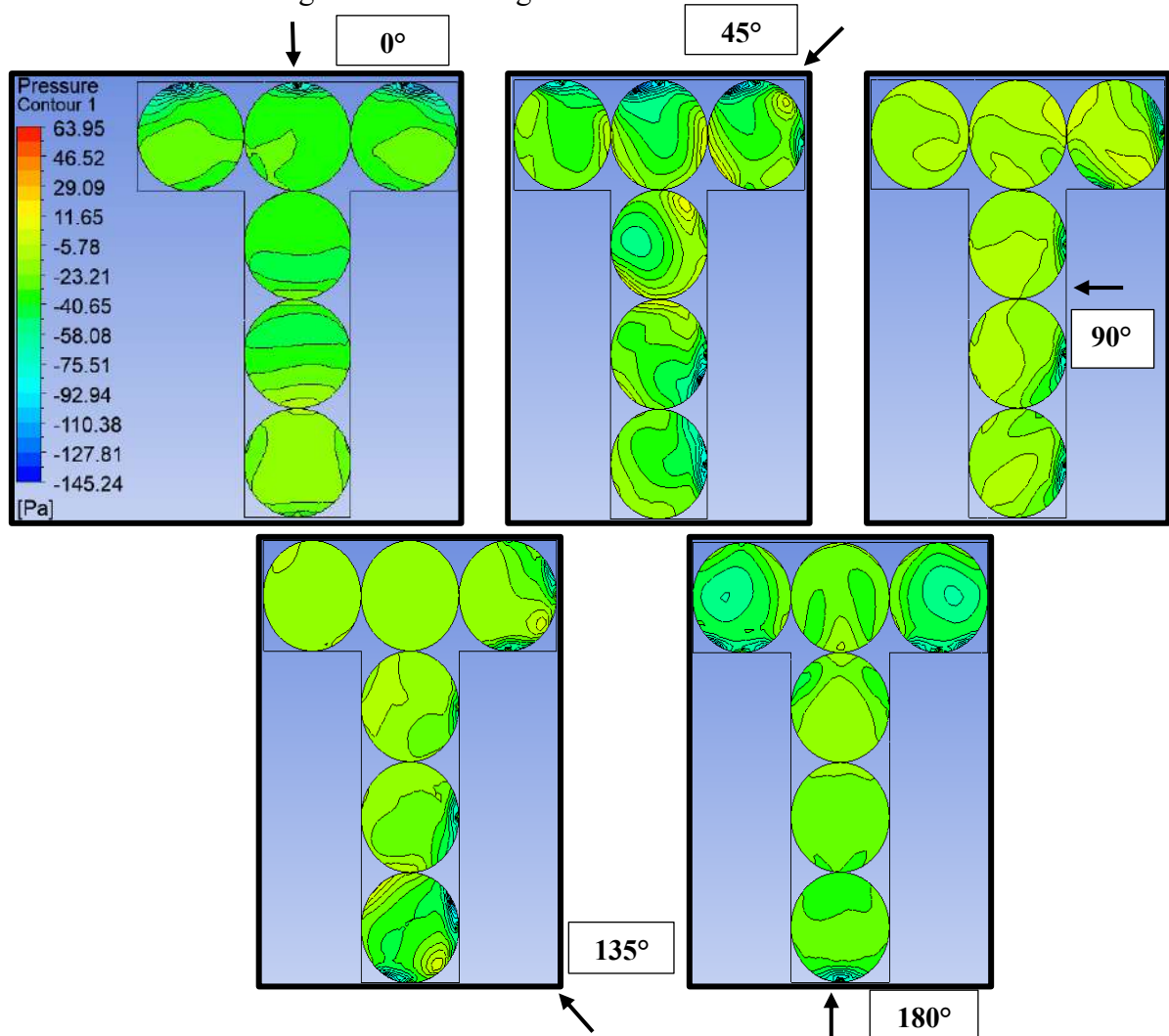
Fig. 4.31: Pressure contours of T Pattern with Zero Spacing
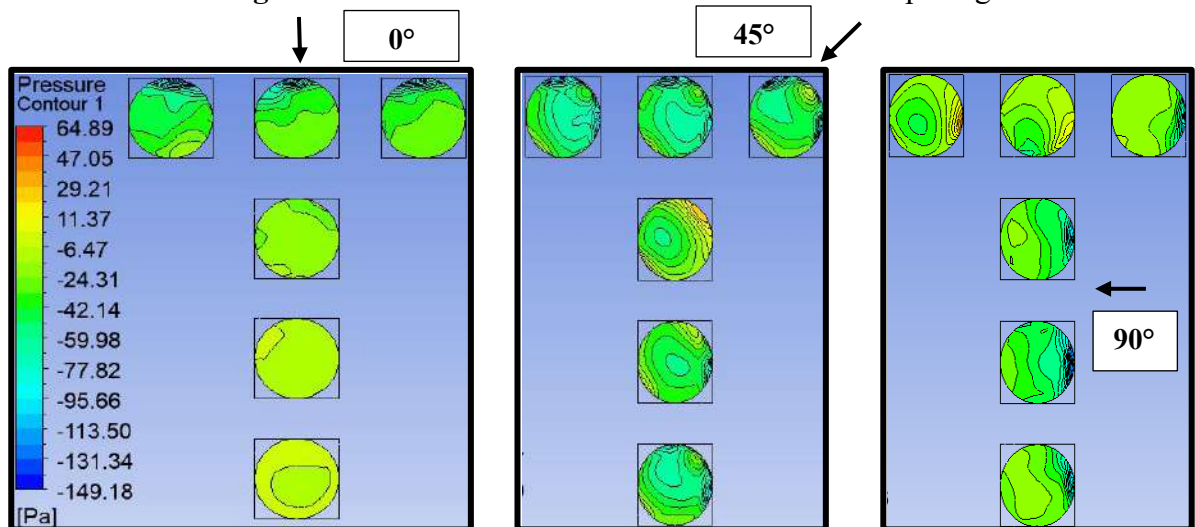
Fig. 4.32(a): Pressure contours of T Pattern with 0.5B Spacing
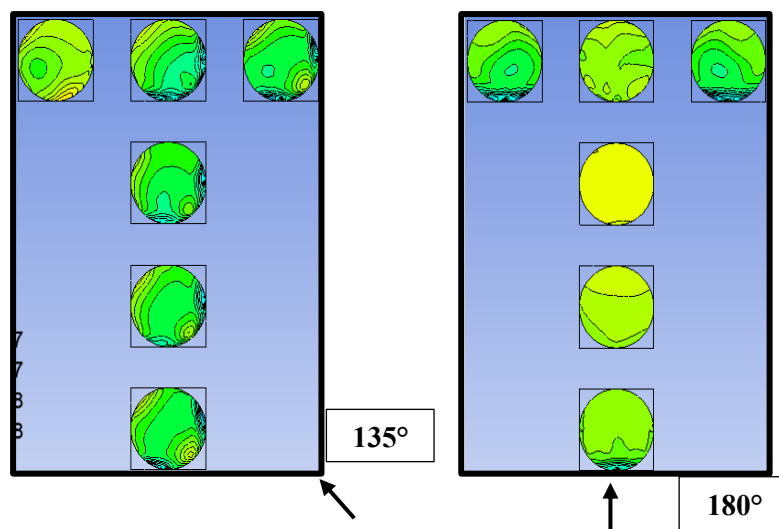
Fig. 4.32(b): Pressure contours of T Pattern with 0.5B Spacing
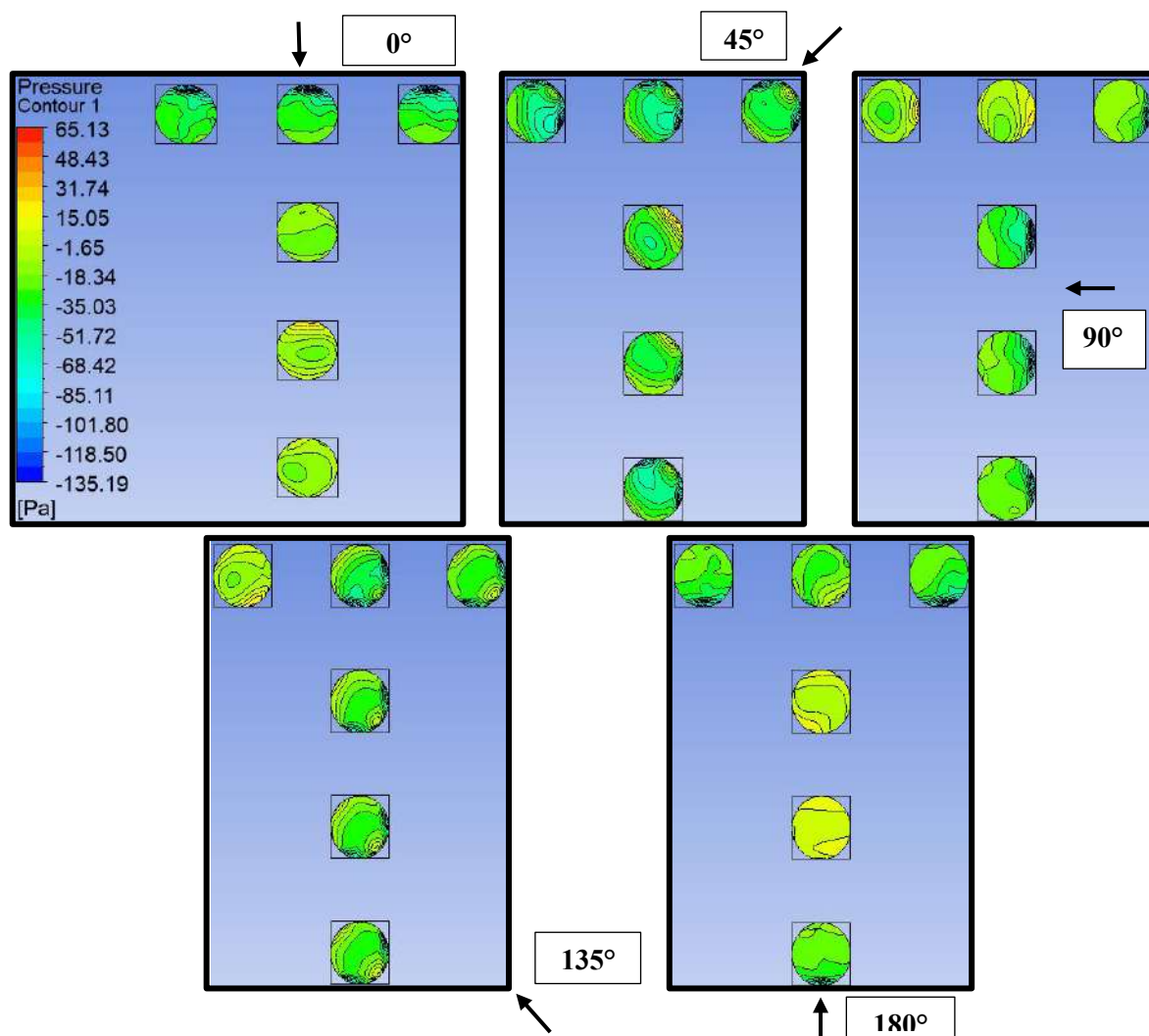
Fig. 4.33: Pressure contours of T Pattern with B Spacing
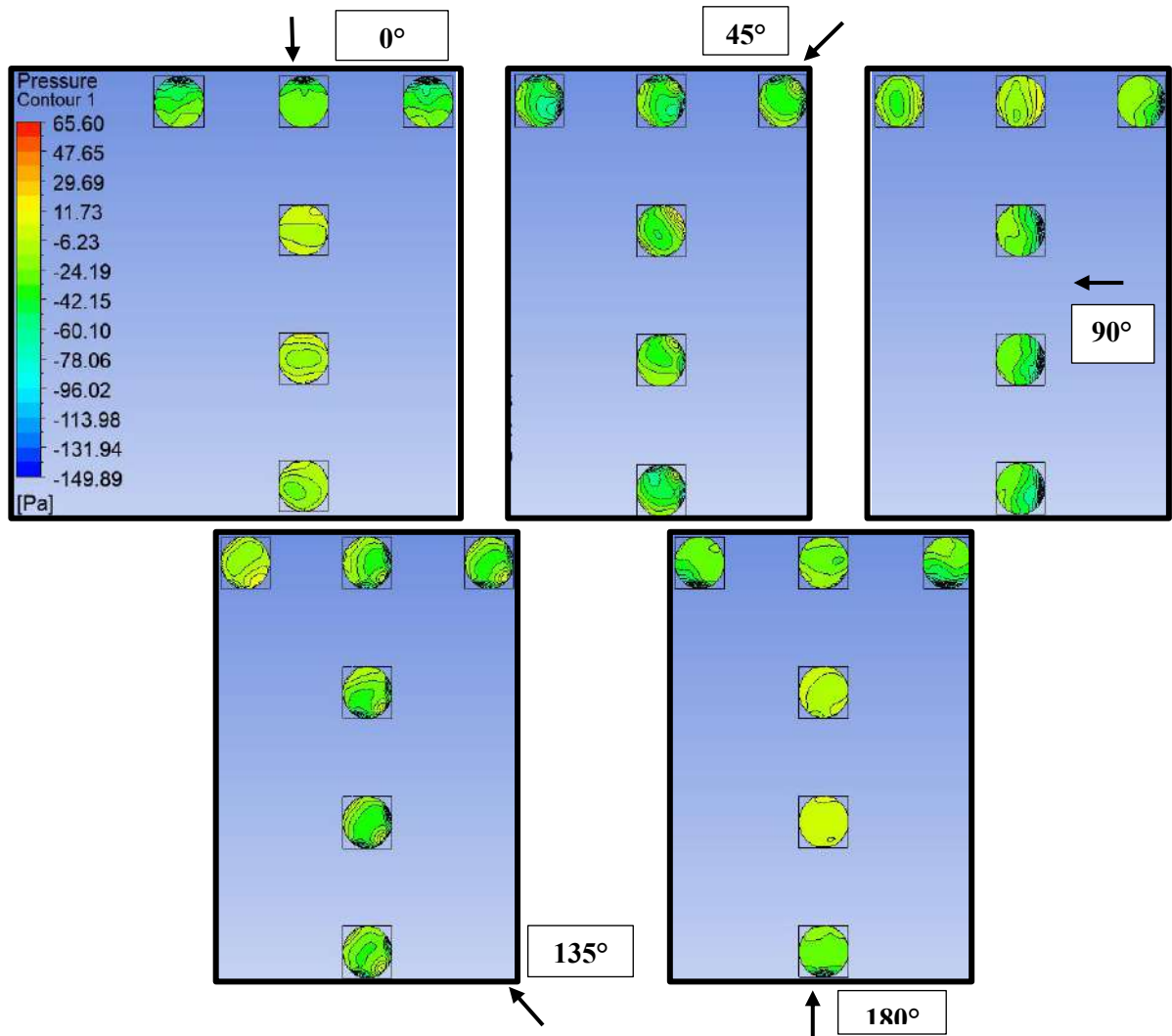
Fig. 4.34: Pressure contours of T Pattern with 1.5B Spacing
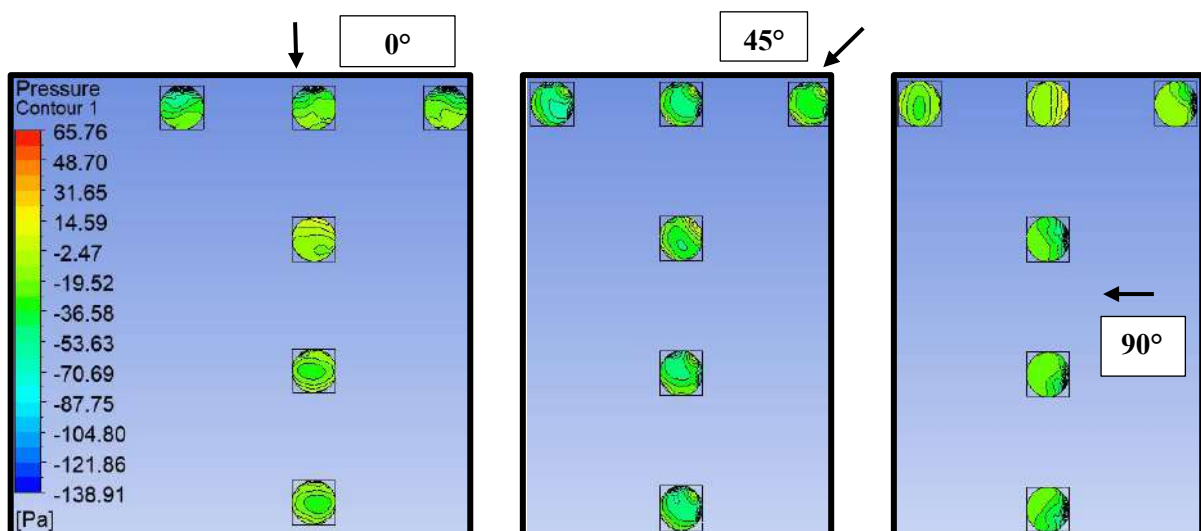
Fig. 4.35(a): Pressure contours of T Pattern with 2B Spacing
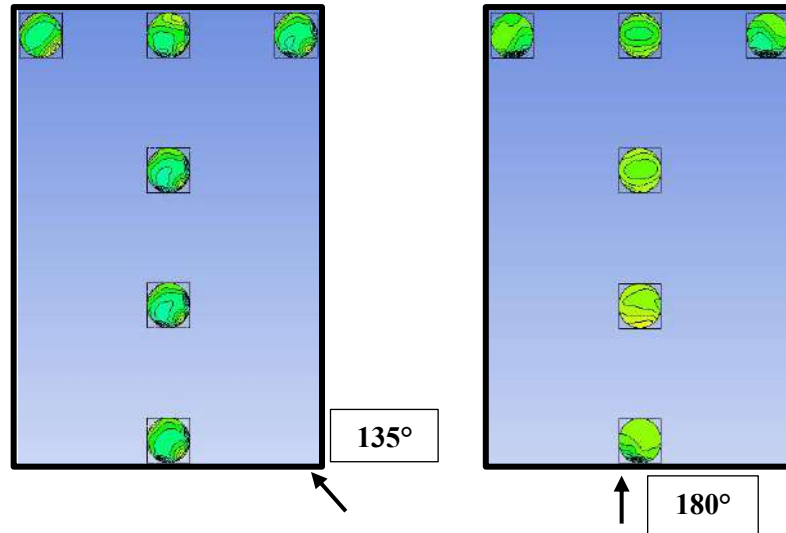
Fig. 4.35(b): Pressure contours of T Pattern with 2B Spacing

4.3.3.2 Pressure Coefficient (C_{pe})

The variation of C_{pe} over the dome roofs of low-rise structures arranged in a T pattern with variable spacing (0, 0.5B, B, 1.5B and 2B) between the buildings at different angles of wind incidence (0°, 45°, 90°, 135°, 180°) are shown in the Fig. 4.36.

The value of negative C_{pe} is increased on roofs A, B and C as compared to the isolated dome roof, while it is decreased on dome roofs D, E and F due to the shielding effect. During 0° and 180° wind incidence angles, roofs A and C experience the same magnitude of the negative C_{pe} due to the symmetry of a horizontal axis. In the case of a 90° wind incidence angle, the negative value of C_{pe} is reduced on roofs A, B and C, but it is increased on roofs D, E and F.

The minimum value of negative C_{pe} = -0.16 during spacing of 1.5B is observed on roof B since it is acting as a middle roof in case of a 90° wind incidence angle, and the maximum value of negative C_{pe}= -0.87 is observed on roof E during 0.5B spacing. In the case of the 135° angle of wind incidence, only roof C experiences the lowest value of negative C_{pe} compared to the other roofs.

The value of negative C_{pe} is greater on roofs A and C than on roofs B, D, E and F in the case of 180° wind incidence angle. There are some positive values of C_{pe} = 0.1 at 0.5B spacing and 0.5 at B and 1.5B spacing acting on roofs D and E respectively. The magnitude of pressure coefficient is ranging between -0.95 to 0.1 (82.69% increase when spacing is 0 and 100% reduce when spacing is 2B) indicating the reduction in suction on roof as the spacing changes from 0 to 2B when the dome roofs are arranged in T pattern.
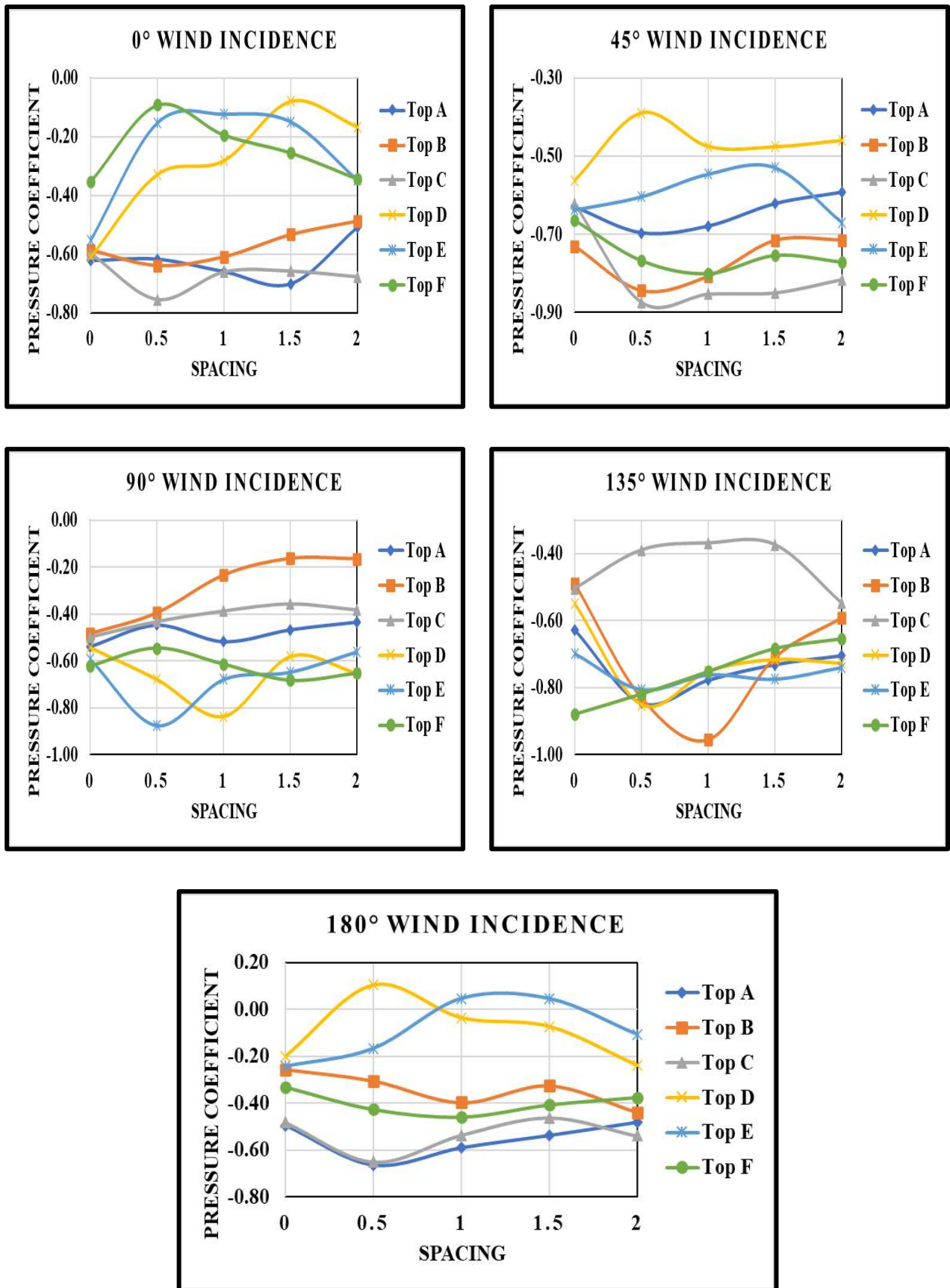
Fig. 4.36: Pressure Coefficient for T Pattern

4.3.3.3 Interference Factor (IF)

The variation of *IF* in the case of dome roofs arranged in a T pattern is shown in the Fig. 4.37(a) and (b). The role of interference from the neighbouring buildings is quite reduced in the case of the T pattern, such that the effect of interference is mostly noticeable only on roofs B, D, E and F during 0° and 180° angle of wind incidence and on roofs B and C during 90° angle of wind incidence. In most cases of wind incidence angles and variable spacing, the *IF* is observed to be greater than 1, which indicates that the nature of wind is still suction and the value of negative C_{pe} is increased on the dome roofs, although its value follows a decreasing trend indicating that the suction is getting reduced on roofs B, D, E and F during 0° wind incidence angle. The range of *IF* is varying between 1.65 to -0.19. The maximum value of *IF* = 1.65 is observed on roof E in case of 0.5B spacing and 90°angle of wind incidence, indicating that maximum suction is acting on E and minimum value of *IF* = -0.19 on roof D in case of 0.5B spacing and *IF* = -0.09 on roof E in case of B and 1.5B spacing at 180° angle of incidence implies that the nature of wind has changed from suction to positive pressure on these roofs.
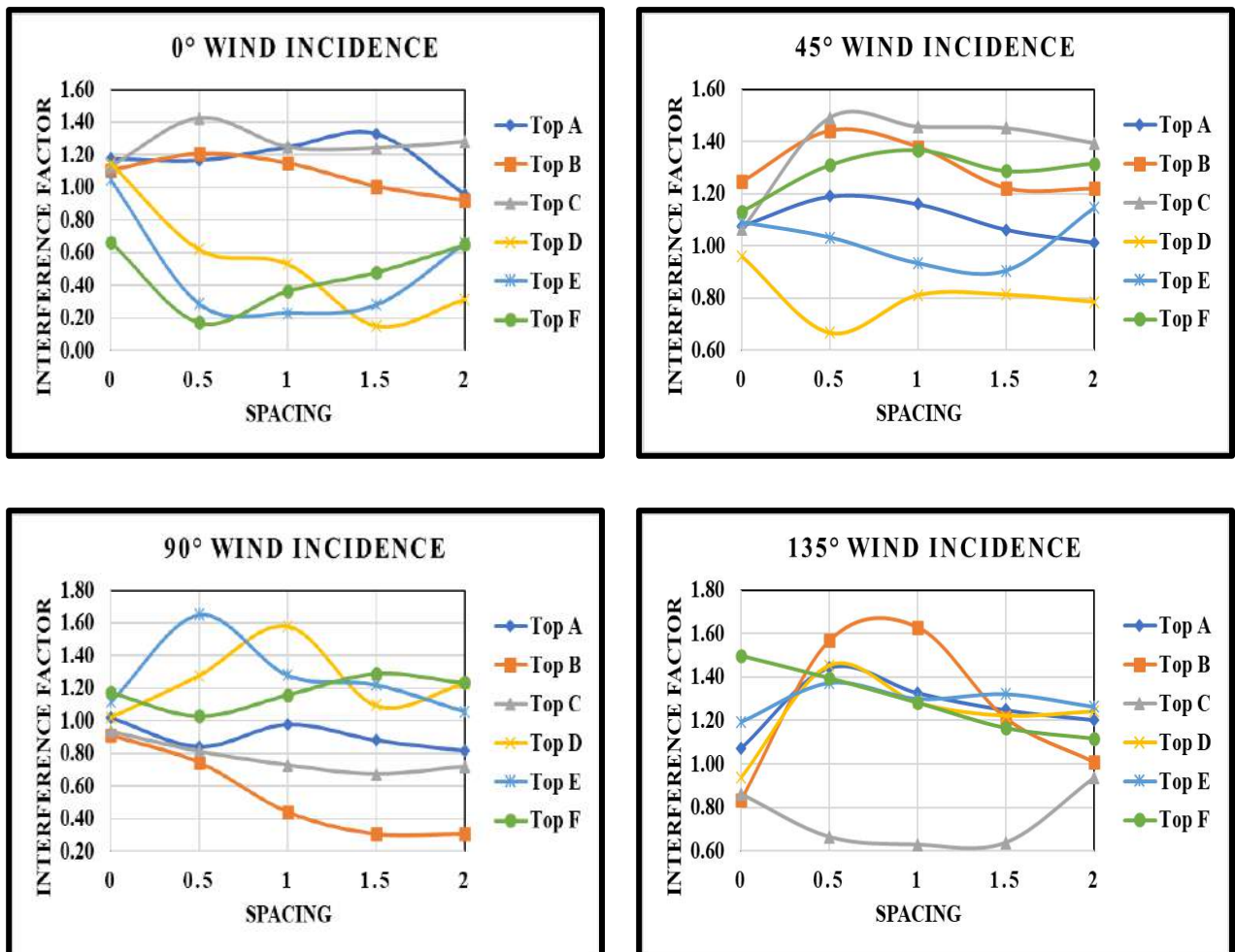
Fig. 4.37(a): Interference Factor for T Pattern
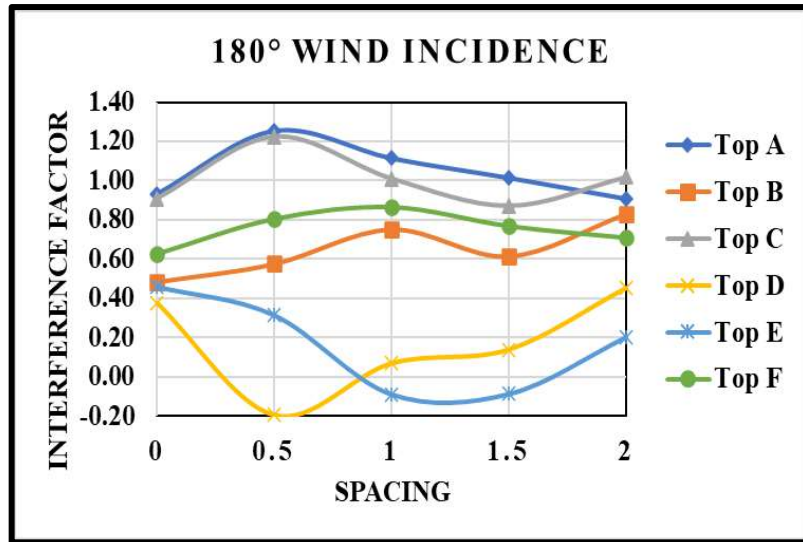
Fig. 4.37(b): Interference Factor for T Pattern

4.3.3.4 Interference Difference (ID)

The variation of *ID* with respect to variable spacing and angle of wind incidence when dome roofs are arranged in a T pattern is shown in Fig. 4.38. The idea of how much the wind-induced negative or positive pressure is increased or decreased on the dome roof due to interference can be taken from *ID*. The pattern of variation followed by *ID* is exactly similar to the pressure coefficient since it is directly proportional to C_{pe}.

As discussed in a variation of pressure coefficient, the value of negative C_{pe} has increased on roofs A, B and C, which is responsible for the higher *ID* during 0° wind incidence. The value of *ID* is ranging varying between -0.36 to 0.63. In the case of roofs D, E and F, the value of *ID* is positive which indicates that there is a drastic reduction in negative C_{pe} leads to the reduced suction on the roof due to the shielding effect of upstream roofs. The maximum negative *ID* = -0.17 is acting on roof A during 0° wind incidence angle at 1.5B spacing, and the maximum positive *ID* = 0.48 is acting on roof F at 0.5B spacing. It is clearly visible that the *ID* is influenced by to presence of neighbouring roofs, the value of *ID* coming out to be negative on all the dome roofs during 45° wind incidence with maximum negative *ID* = -0.29 on roof C at 0.5B spacing.

The effect of shielding is dominating during 0° and 180° angles of wind attack on roofs B, D, E and F in which roof F is behaving as a upstream roof and roof B is behaving as leeward roof and roofs D and E are behaving as middle roofs or vice versa as shown in Fig. 4.38.
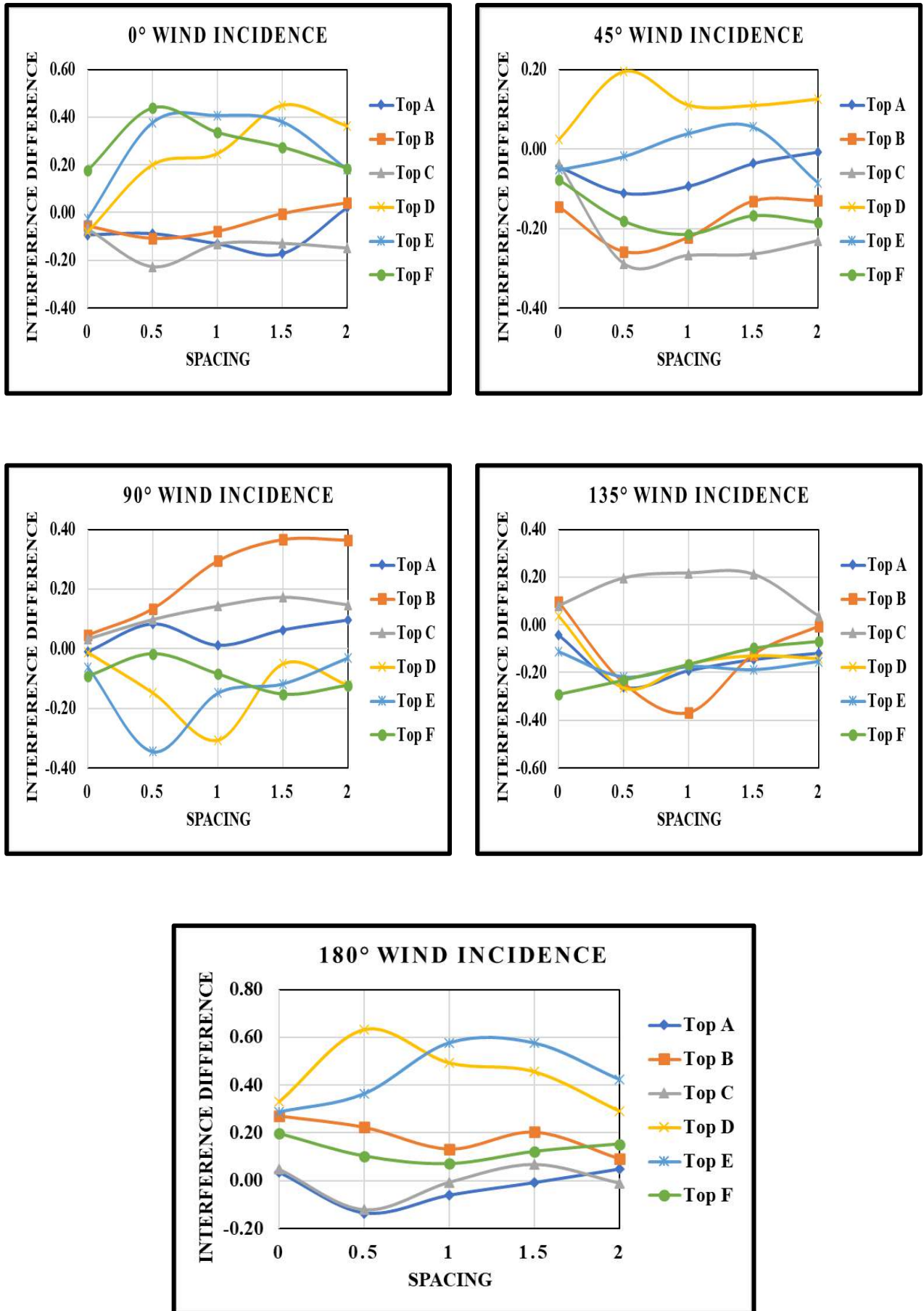
Fig. 4.38: Interference Difference for T Pattern

4.3.3.5 Wind Flow Streamlines

The wind flow recirculates on both sides of roofs D, E and F, which is initially separated from the windward sides of roofs A, B and C and gets reattached on both sides of roofs D, E and F during 0° wind incidence angle at zero spacing of the T pattern. In the case of a 90° angle of wind incidence, the flow recirculation and reattachment take place in the wake region, i.e., downstream sides of the wind flow behind the roofs D, E, and F. The wind flow streamlines for T pattern with zero spacing at various angles of wind incidence are shown in Fig. 4.39. The wind flow is distributed in between the buildings when the spacing is increased from zero to 2B, due to which the wake formation is reduced in the downstream direction as compared to the zero spacing model of the T pattern, as shown in Fig. 4.39 to 4.43, respectively. During 0° wind incidence angle, the wind flow with high velocity flows between roofs A, B and C, while in the case of 90° wind incidence, the maximum velocity flow is observed in between roofs D, E and F. The wind flow streamlines for B, 1.5B and 2B are shown in Fig. 4.41-4.43, in which it is clearly visible that the flow is taking place smoothly by increasing the spacing between the buildings, which is responsible for the increase or decrease in the pressure coefficient which in turn affect the ID and IF on the roofs.
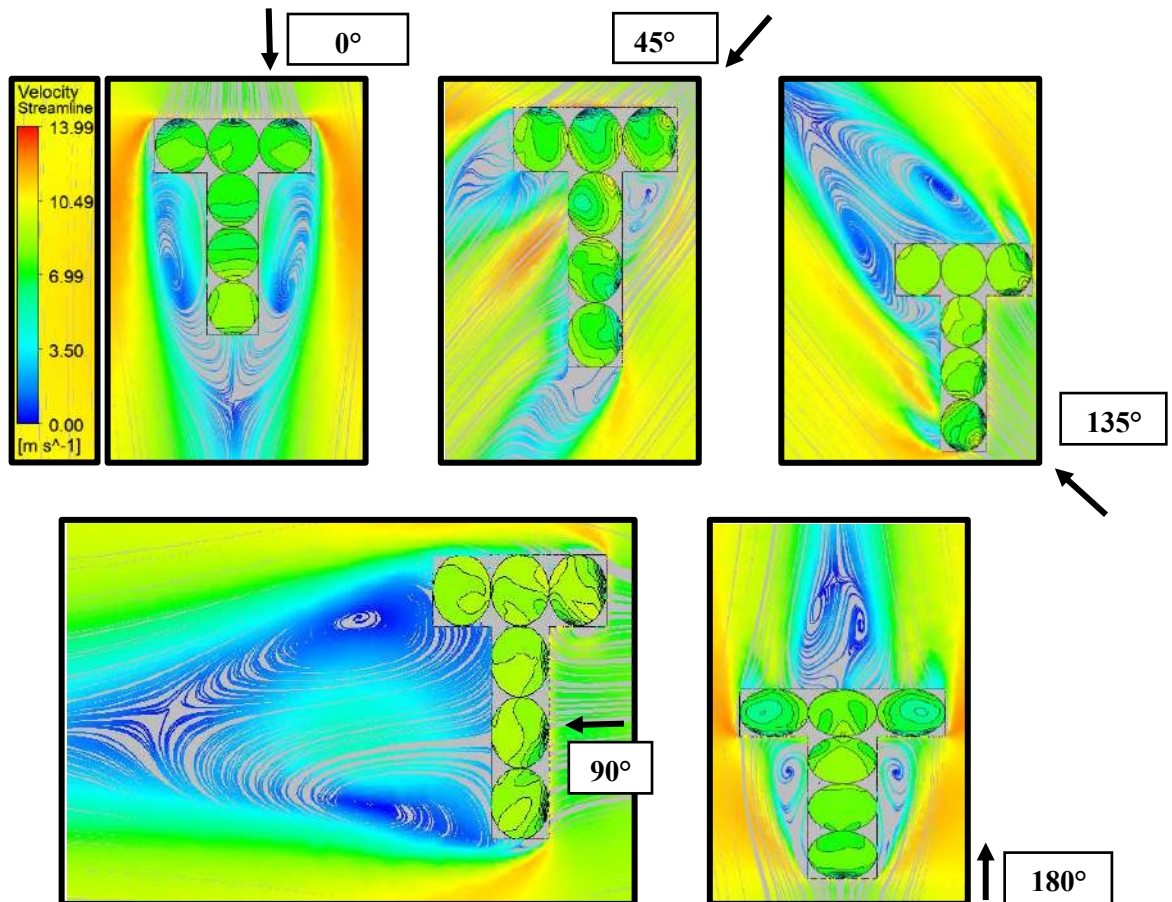
Fig. 4.39: Wind Flow Streamlines for Zero Spacing
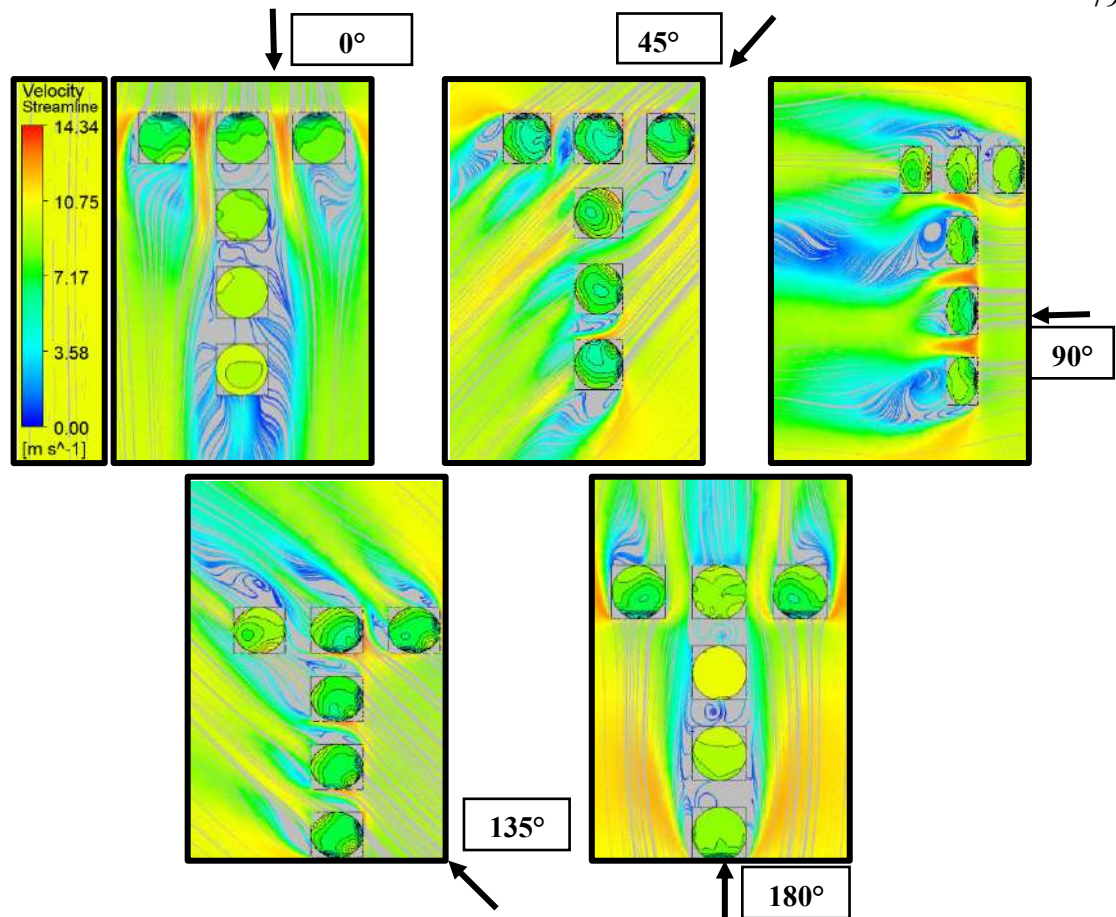
Fig. 4.40: Wind Flow Streamlines for 0.5B Spacing
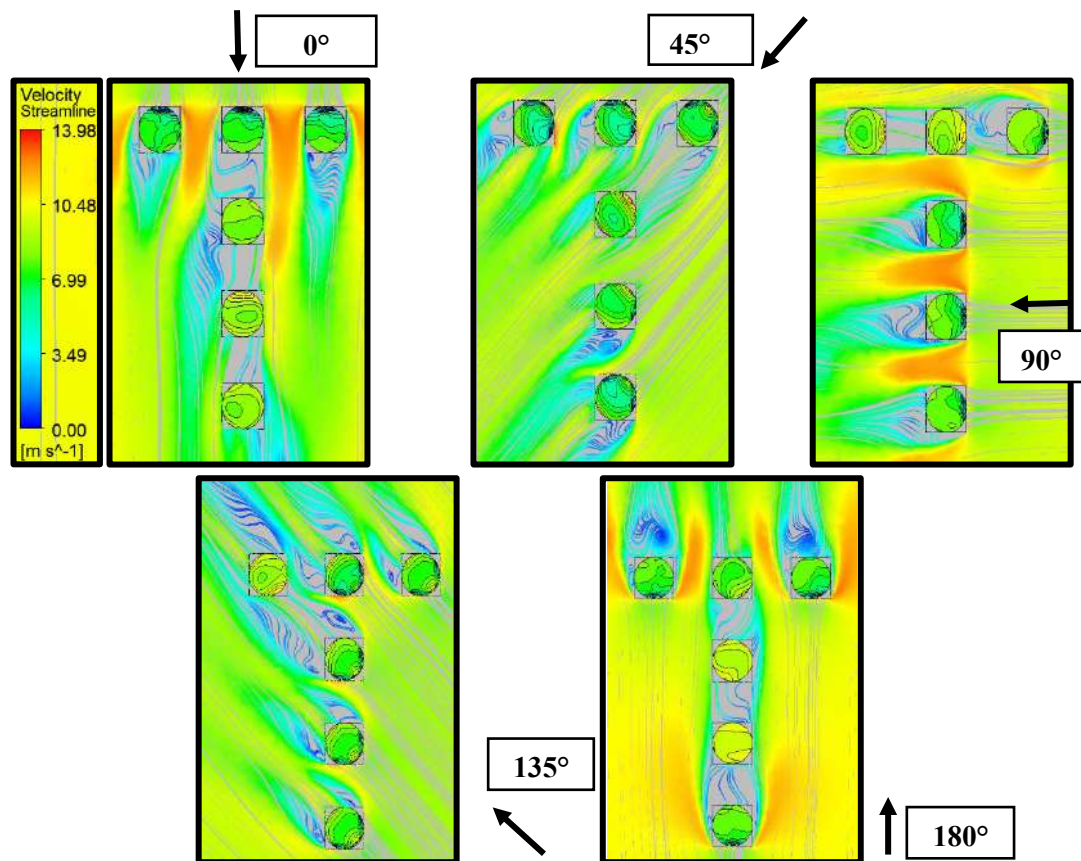
Fig. 4.41: Wind Flow Streamlines for B Spacing
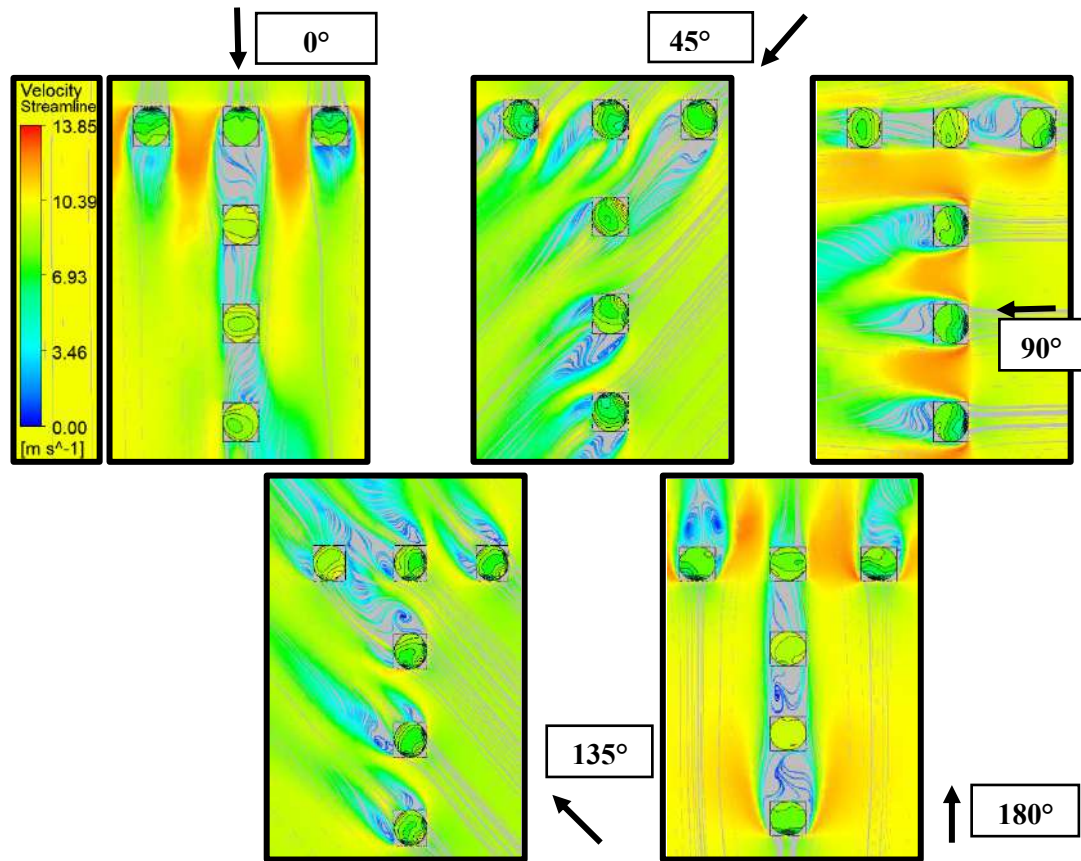
Fig. 4.42: Wind Flow Streamlines for 1.5B Spacing
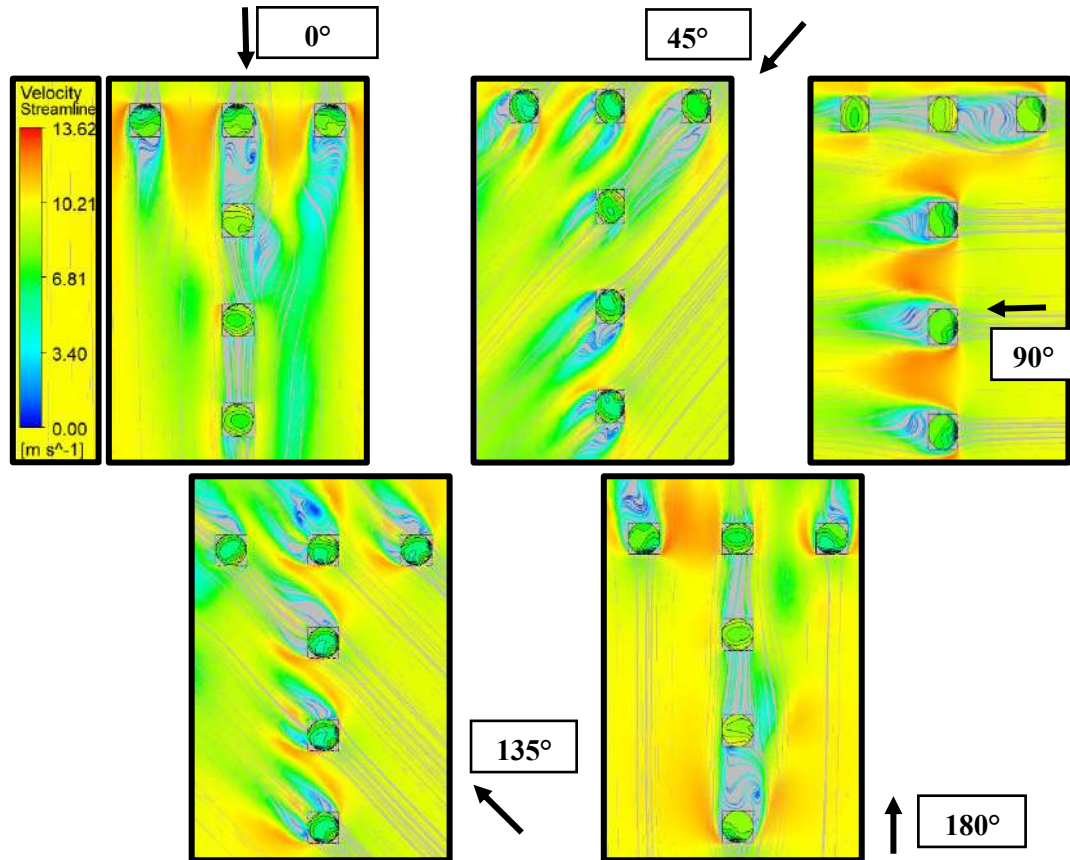
Fig. 4.43: Wind Flow Streamlines for 2B Spacing

4.4. Conclusions

In conclusion, the findings highlight the critical need for structural designers to address wind load effects comprehensively when designing low-rise domical roofs. Current wind load standards often fail to account for the complexities introduced by varying wind incidence angles and the influence of dome configurations, leading to potentially conservative and uneconomical designs. Key insights from the study include:

A. **Critical Wind Angle:** Designers must evaluate the worst-case wind scenarios to ensure structural integrity, as wind pressure coefficients (C_{pe}) are highly sensitive to wind incidence angles.

B. **Impact of Spacing and Arrangement:** Patterns such as rectangular, Z, and T arrangements exhibit varying pressure coefficient ranges (C_{pe}), interference factor (IF), and interference difference (ID). Increased spacing between buildings (0 to 2B) reduces these factors, highlighting the role of spacing in mitigating wind effects.

C. **Aerodynamic Benefits of Domes:** The streamlined nature of domical roofs reduces wind pressures, particularly on windward sides, but requires careful consideration of dome configuration to manage wind-induced forces effectively.

D. **Overestimation in Standards:** Codal provisions for C_{pe} values tend to overestimate pressures, sometimes up to 69.81%, making them less suited for complex roof geometries. Experimental and CFD investigations suggest the need for revised standards that better reflect real-world conditions.

E. **Interference Effects and Patterns:** Among tested configurations, the rectangular pattern demonstrates superior performance under interference, offering lower wind loads compared to T and Z patterns. Furthermore, by increasing the spacing between the roofs from zero to 2B, there was a reduction in suction on roofs, i.e., 88.46% in the rectangular pattern, 98.9% in the z pattern and 100% in the T pattern. Here, the 100% reduction indicates that the nature of wind is changed from suction to positive pressure.

F. **Positioning and Shielding Effects:** Domes directly exposed to wind experience lower pressures, while shielded domes (leeward) are subjected to higher forces, emphasizing the importance of dome positioning in multi-dome structures.

G. These findings underscore the need for a more nuanced approach to wind load analysis and design, encouraging designers to consider aerodynamic behavior, interference effects, and realistic wind pressure distributions to ensure the safety and efficiency of domical roof structures.

CHAPTER 5

RESULTS AND DISCUSSIONS FOR CYLINDRICAL ROOF

5.1 General

In this chapter, the results are typically organized around the key research questions or themes identified in the study, with clear presentation of data in the form of tables, figures, or descriptive summaries. This chapter not only reports the outcomes but also provides a detailed analysis of their significance, comparing them with existing literature, theories, and previous studies. A detailed discussion is being done about wind-induced pressure contours, pressure coefficient (C_{pe}), interference factor (*IF*) and interference difference (*ID*) over the cylindrical roof in case of isolated and different interfering conditions. The variation of the mentioned coefficients concerning various angles of wind incidence is also discussed in this chapter.

5.2 Isolated Cylindrical Roof

The low-rise building model with a cylindrical roof with the plan dimensions of 200 mm X 400 mm, eave height of 150 mm and diameter of the cylindrical roof of 200 mm is subjected to 0° to 90° angle of wind attack at an interval of 15°. The wind-induced pressure contours and variation of C_{pe} for isolated low-rise building with cylindrical roof are discussed in section 5.2.1.

5.2.1 Pressure Contours

The wind-induced pressure contours for the isolated cylindric roof are shown in Fig. 5.1(a) and (b) in which the roof is divided into three portions i.e., (a) windward portion (b) top or apex portion and (c) leeward portion. When the wind is flowing from 0°, 15° and 30°, a small portion on the windward side is subjected to the positive wind-induced pressure which converts into maximum negative pressure on the apex portion and then reduces on the leeward portion but still in negative nature. From the wind incidence angle of 45° to 90°, the cylindrical roof is fully under negative pressure with a lesser magnitude, as shown in Fig. 5.1.

| 0° | 15° | 30° |
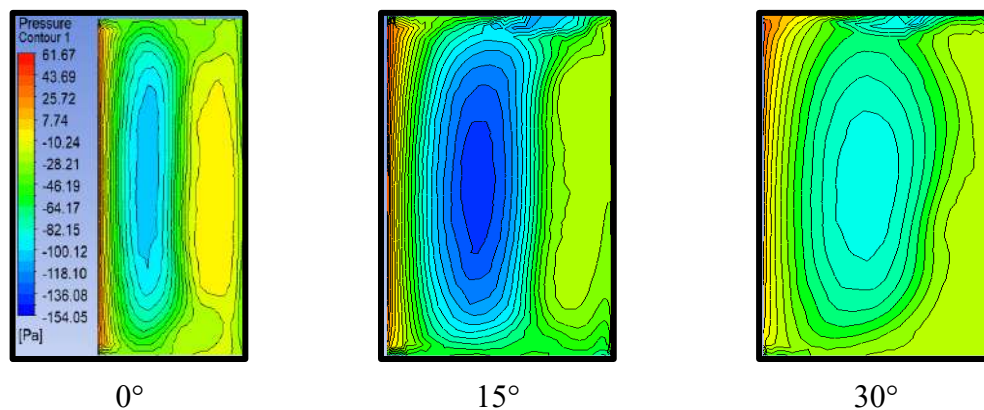
Fig. 5.1(a): Pressure Contours for Cylindrical Roof Low-Rise Building
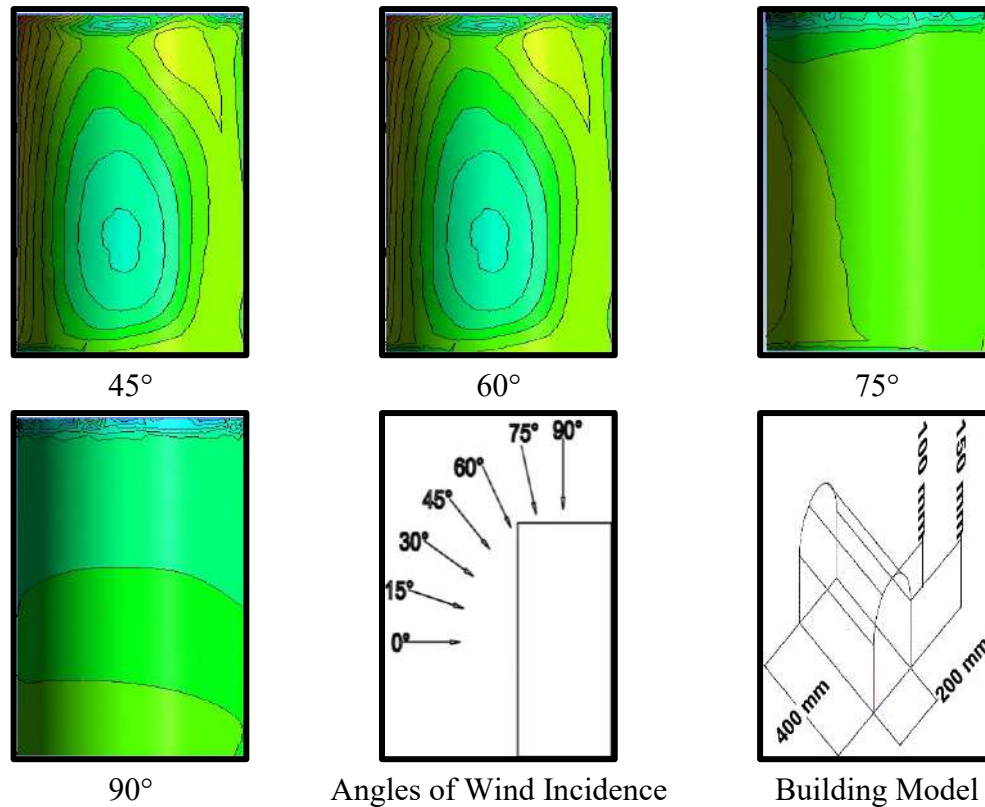
Fig. 5.1(b): Pressure Contours, Angle of Wind Incidence and Dimensions of Cylindrical Roof Low-Rise Building

5.2.2 Pressure Coefficient (C_{pe})

The C_{pe} for the cylindrical roof is calculated using CFD simulation by subjecting it to the different angles of wind incidence angles 0° to 90° at an interval of 15°. But before that, the model needs to be validated either with the wind standards of different nations or some previous research. In the present research, a low-rise building model with a cylindrical roof of an aspect ratio (rise to width) of 0.5 and a plan dimension of 200 mm X 400 mm is validated with some wind standards and previous experimental research as shown in Fig. 5.2. The Eurocode for wind actions in EN1991-1-4 further provides values of external pressure coefficients for curved roofs, for a range of rise height to span ratios from 0.05 to 0.5, for h/d = 0.0 and 0.5, for wind incidence on the eaves. The Australian and New Zealand code, on the other hand, in the span for external pressure coefficients for curved roofs, for rise height to span ratios r/d = 0.05, 0.2, 0.5, and for h/r = 0, when wind incidence is first on the eaves. For roofs with wind pressure incidence parallel to the ridge, the pitched data with is used completed considering the slope factor to reach the data for curved roofs. Regarding a single curved roof with a rise height to span ratio of 0.17 and a side wall height to span width ratio of 0.08, both the Canadian code and the US differ in that the former also contains data for wind onto eaves, while the second one contains data for parallel wind to eaves and parallel to ridge. The ASCE also contains data

for rise height to span ratios running from 0 to 0.6 for structures with and without side walls, but no data is provided in the last case concerning the influence on the side wall height. To estimate height to span ratios, Cook utilized data from Blessmann (1987a, b) in which categories were provided according to the specific data point, namely R/W of 0.1, 0.2, and 0.3 together with H/W of 0, 0.25, 0.5 among others. Additionally, there is some information for greenhouses both with and without side walls as indicated in EN13031. In case there are no side walls on the greenhouse then all h/s values are covered in only one dataset while in situations where side walls exist, h/r values range from 0.4 to less than 0.6. It is challenging to compare these data because they are presented in functions of different ridge height parameters, differences in average pressure coefficient areas and reference elevations. From the charts, the windward side of the roof has quite a wide range of C_{pe} values. The Fig. 5.2 show that there is a wide range of C_{pe} values, especially on the windward part of the roof. Typically, the difference between the smallest and largest values is at least two times or more while in certain cases the pressure coefficient sign differs from that of other data sets. These notable variations cannot only be ascribed to differences in area, reference height among others.
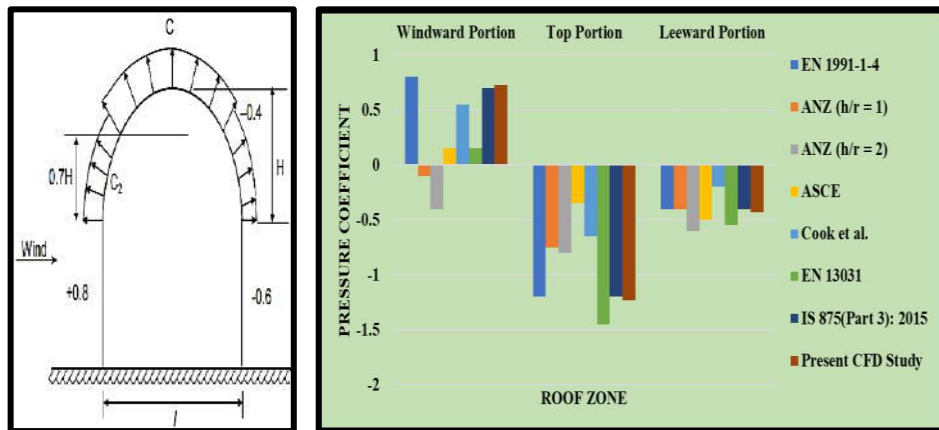
Fig. 5.2: Validation of Cylindrical Roof Model

After the validation of cylindrical roof model, the value of C_{pe} on the roof is measured at different angles of wind attack ranging from 0° to 90° at an interval of 15° each. The maximum value of -ve C_{pe} is obtained during 15° and 30° wind incidence angle i.e., -0.90 and -0.88 and the minimum value of -ve C_{pe} is -0.44 during 90° angle of wind incidence. The overall impact of wind on cylindrical roof is suction in nature but with some positive pressure on windward portion on the roof during 0°, 15° and 30° respectively. The variation of C_{pe} for cylindrical roof with respect to different angle of wind incidence is shown in Fig. 5.3.
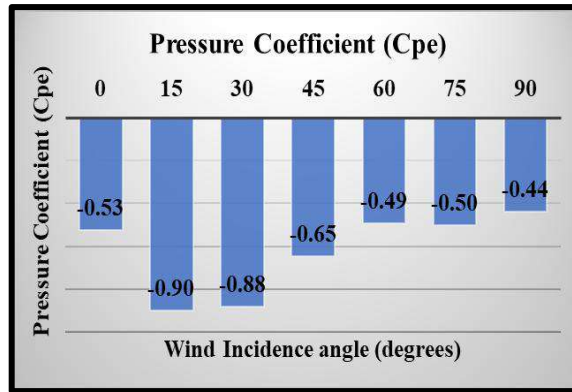
Fig. 5.3: C_{pe} variation w.r.t wind incidence angle for the cylindrical roof

5.2.3 Wind Flow Pattern on Isolated Cylindrical Roof

The wind flow pattern over an isolated cylindrical roof at various angles of wind incidence ranging between 0° to 90° at an interval of 15° each is shown in Fig. 5.4(a) and (b). The wind flow recirculation occurs at the cylindrical roof's leeward side during 0° to 45° wind incidence angle. The maximum wind flow velocity occurs at the roof's apex. The turbulence is maximum in case of 60°, 75° and 90° wind incidence angles because the flow directly hits the cross-wind roof edge, due to which the vortex shedding takes place. The flow reattachment is maximum in case of 0° angle of wind attack, as shown in Fig. 5.4.
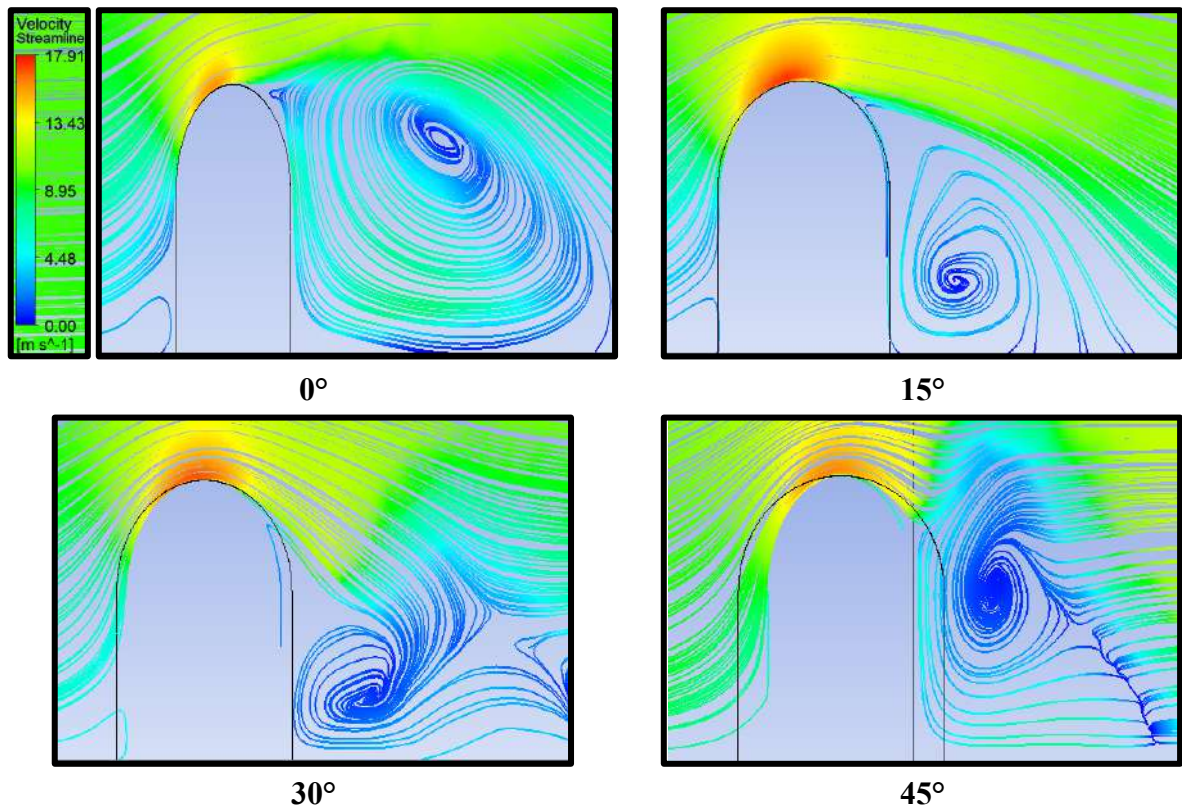
Fig. 5.4(a): Wind Flow Streamlines of Isolated Cylindrical Roof
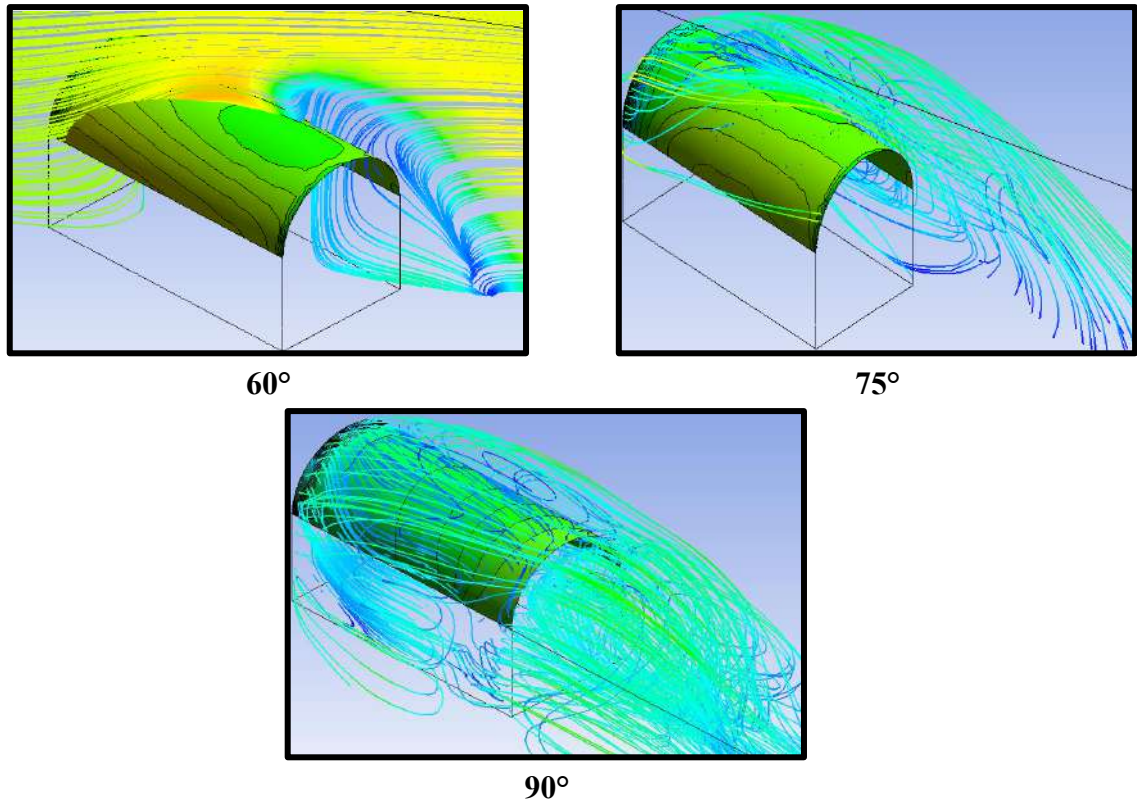
Fig. 5.4(b): Wind Flow Streamlines of Isolated Cylindrical Roof

5.3 Interference

In this section the effects of presence of nearby buildings are investigated in the form of interference factor (*IF*) and interference difference (*ID*) on the cylindrical roof of low-rise structures arranged in rectangular pattern, T-pattern and Z-pattern with variable spacing i.e., 0, 0.5B, B, 1.5B and 2B where B is the width of the building at various angles of wind incidence ranging between 0° to 90° at an interval of 15° each.

5.3.1 Rectangular Pattern

To find out the effect of interference on cylindrical roof, six low-rise building models with cylindrical roof arranged in rectangular pattern placed nearby each other using different spacings i.e., 0, 0.5B, B, 1.5B and 2B. The wind-generated pressure contours, *IF* and *ID* on all six cylindrical roofs due to interference are discussed below at different angles of wind incidence ranging between 0° to 90° at 15° intervals each.

5.3.1.1 Pressure Contours

The wind-induced pressure contours obtained for low-rise buildings with cylindrical roofs arranged in rectangular patterns with variable spacing and at different angles of wind incidence are shown in Figs. 5.5-5.9. The range of wind-induced pressure distribution on cylindrical roofs arranged in rectangular patterns with variable spacing is -62.55Pa to -13.92Pa. For the multi-span cylindrical roof model or zero spacing model, it was observed from Fig. 5.5 that in the

case of 0° wind angle, the suction on the leeward span is smaller than the suction on the upwind span, up to half the upwind span. The pressure distribution on windward span of multi-span roof was quite similar to that of the single span roof. The middle span was least subjected to suction when compared with windward and leeward span. In the wind pressure distribution of the leeward span, there is an advantage of the shield by the leeward span. During the 0° wind angle it was observed that the maximum negative pressure (suction) having approximately same magnitude was acting on the windward roofs A and D while other left roofs B, C, E and F were subjected to less negative pressure (suction) having the magnitude quite equal. The maximum negative pressure was recorded on the leeward roof C in case of 30° wind incidence angle. The pressure distribution on windward roofs A & D and middle roofs B & E was showing quite similar pattern with very less difference during wind incidence angle moving from 0° to 45° but it shows significant difference during the wind angle from 60° to 90°. But on the leeward roofs C & F it was observed that the pressure distribution was similar only for the wind angle of 0° and 60° otherwise it was having a noticeable difference for all other wind angles. The maximum negative pressure was observed on the leeward roof C during wind angle of 30°.

| 0° | 15° | 30° |

| 45° | 60° | 75° |

| 90° | Roof Nomenclature | Angle of Wind Incidence |
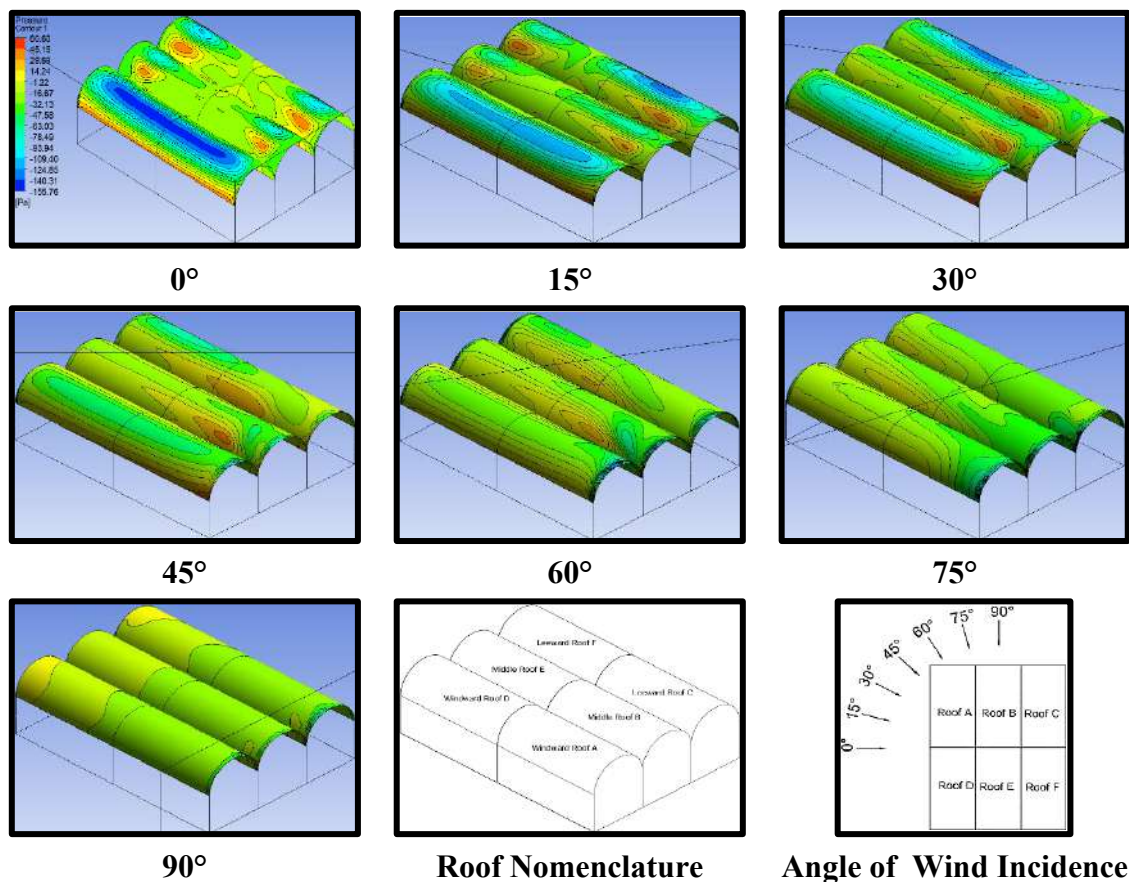
Fig. 5.5: Pressure Contours for Rectangular Patter with Zero Spacing

Fig. 5.6 depicts the contours created by pressure brought on by the disposition of wind loads on low-rise structures with cylinder roofs that are placed in a rectangular pattern with 0.5B spacing between them during the wind incidence angle of 0°. It was noticed that the maximum negative (suction) pressure was acting on the top of windward roofs A & D. The windward roofs A & D had similar kind of distribution of pressure. Furthermore, it was discovered that the negative pressure on windward roofs A & D of 0.5B spacing model was reduced when compared with zero spacing model. This implies that suction reduced on the windward roofs due to increase in the spacing between the buildings i.e., 0 to 0.5B. The middle roofs B & E were subjected to minimum negative pressure due to shielding effect. A very sliver portion of windward span of roof B & D was exposed to small magnitude of shielding effect. The negative pressure on leeward roofs C & F found greater than that of the middle roofs B & D. Although there is maximum shielding effect observed in the windward span of the roofs C & F. During 15° wind interval it was observed that the negative pressure on roofs A, B, E and F, reduced when compared with 0° incidence. On the other hand, the negative pressure on roofs C & D were increased when compared with 0° wind incidence. Shielding effect observed on windward span of middle and leeward roofs. It can be inferred that the wind shielding effect started getting reduced on the middle and leeward roofs. The negative pressure on roofs A, B, E and F were not affected that much when compared with 15° wind incidence. But on the roofs D & C, the pressure was highly suction in nature. The maximum changes in the pressure observed during the wind incidence angle of 0° to 30°, after that the suction on the roofs started getting reduced on all the roofs. In case of 90° angle of wind attack, the side faces of the roofs A, B and C were directed towards the wind direction due to which the roofs D, E and F were acting as leeward roofs. The pressure distribution on these leeward roofs found to be similar in nature and magnitude. Although the least suction noticed on these leeward roofs during 90° wind incidence angle when compared with all other wind incidence angles.

| 0° | 15° | 30° |

Fig. 5.6(a): Pressure Contours for Rectangular Patter with 0.5B Spacing

45°

60°

75°

90°

Fig. 5.6(b): Pressure Contours for Rectangular Patter with 0.5B Spacing

Fig. 5.7 shows the pressure contours for the models of B spacing. At an angle of 0° wind incidence, it was noticed that the maximum negative (suction) pressure was acting on the top of windward roofs A & D. The windward roofs A & D were having similar kind of disposition of pressure. Furthermore, it was discovered that the negative pressure on all the roofs A, B, C, D, E and F of B spacing model was reduced when compared with zero and 0.5B spacing model. This implies that suction was reduced on all the roofs due to increase in the spacing between the buildings i.e., 0 to B. When wind incidence angle is 15°, it was observed that the negative pressure on roofs A & F was reduced when compared with 0° wind incidence. On the other hand, the negative pressure on roofs B, C, D and E was increased when compared with 0° wind incidence. The effect of wind shielding was reduced on windward span of middle roofs (B & E) and leeward roofs (C & F). The pressure contours for 30° wind incidence angle shows that the suction dramatically increases from a wind incidence angle of 0° to 30°, it has been noticed that the windward roof D is most impacted by negative pressure. In other words, it can be said that the most critical wind incidence angle is 30°. The maximum changes in the pressure were observed during the wind incidence angle of 0° to 30°, after that the suction on the roofs started getting reduced on all the roofs. At an angle of 90° wind incidence, the side faces of the roofs A, B and C were directed towards the wind direction due to which the roofs D, E and F were acting as leeward roofs. The pressure distribution on these leeward roofs was to be similar in nature and magnitude. Also, the least suction was noticed on these leeward roofs during 90° wind incidence angle when compared with all other wind incidence angles.

Fig. 5.7: Pressure Contours for Rectangular Patter with B Spacing

Fig. 5.8 shows the pressure contours for the models of 1.5B spacing. During the wind incidence angle of 0°, it was noticed that the maximum negative (suction) pressure was acting on the top of windward roofs A & D. The windward roofs A & D were having similar kind of disposition of wind induced pressure. Furthermore, it was discovered that the negative pressure on all the roofs A, B, C, D, E and F of 1.5B spacing model was reduced when compared with zero, 0.5B and B spacing model. This implies that suction was reduced on all the roofs due to increase in the spacing between the buildings i.e., 0 to 1.5B. During 15° wind interval, there was drastic increase in the negative wind pressure on the windward roof D. It was observed that the negative pressure on roofs A & F was reduced when compared with 0° wind incidence. The leeward roof F was subjected to least negative pressure. On the other hand, the negative pressure on roofs B, C, D and E was increased when compared with 0° wind incidence. The effect of wind shielding was reduced on windward span of middle roofs (B & E) and leeward roofs (C & F). Since the suction dramatically increases from a wind incidence angle of 0° to 30°, it has been noticed that the windward roof D is most impacted by negative pressure. In other words, we can say that the most critical wind incidence angle is 30°. The maximum increase in the suction pressure is observed during wind incidence angle of 30° for all the roofs

except middle roof E. The maximum changes in the pressure were observed during the wind incidence angle of 0° to 30°, after that the suction on the roofs started getting reduced on all the roofs. Also, the least suction was noticed on these leeward roofs during 90° wind incidence angle when compared with all other wind incidence angles.
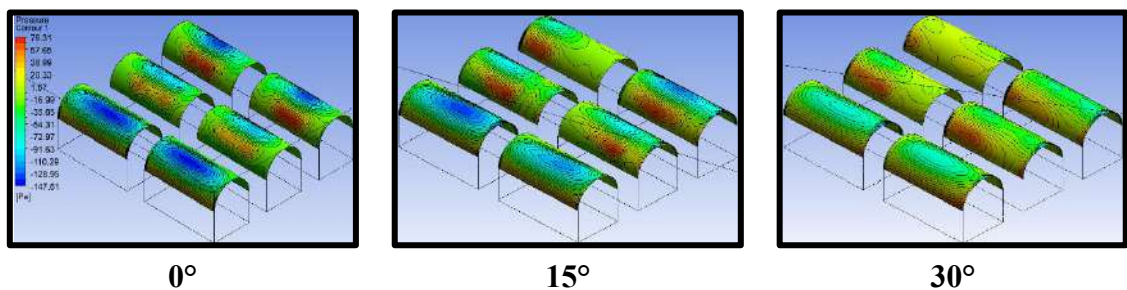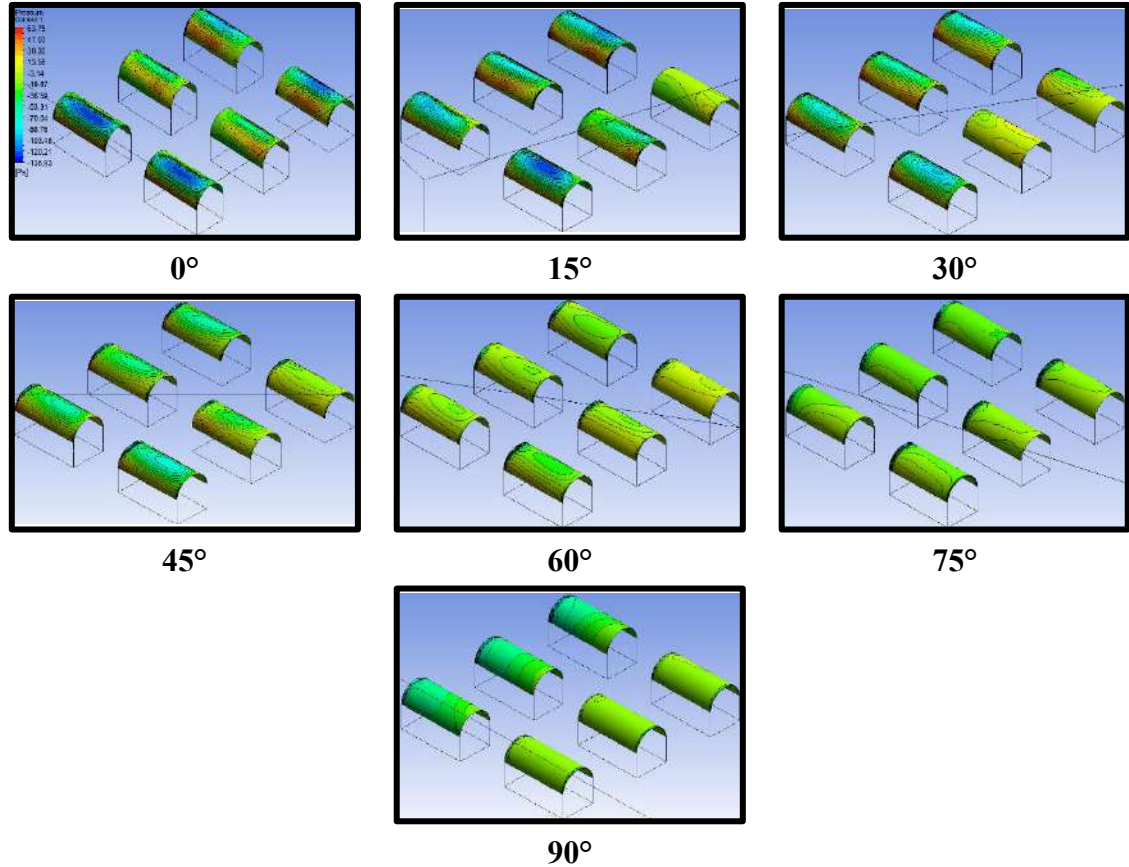

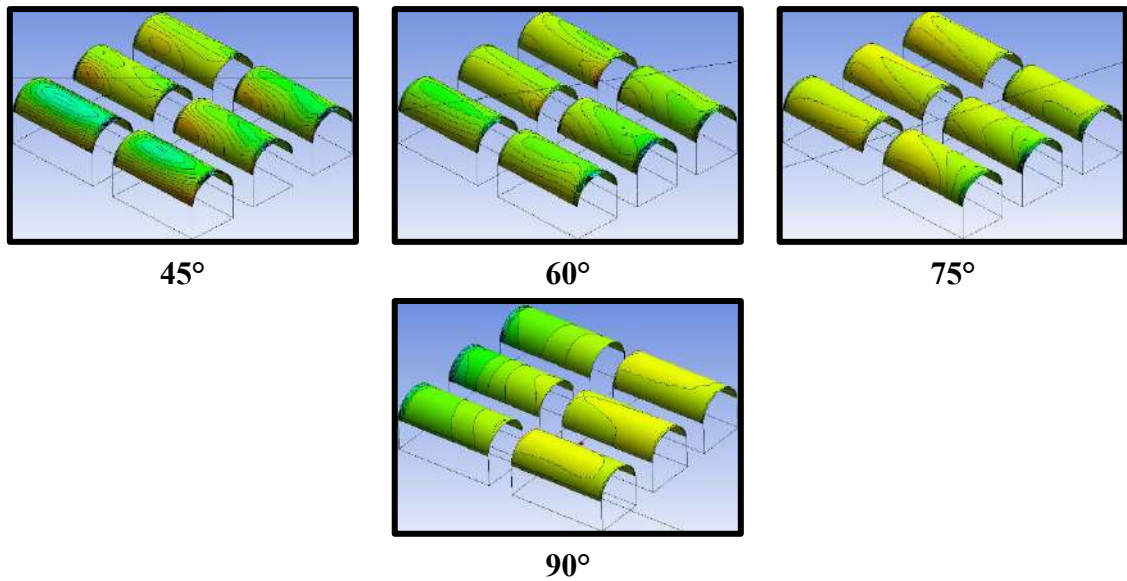**Fig. 5.8:** Pressure Contours for Rectangular Patter with 1.5B Spacing

Fig. 5.9 depicts the contours created by pressure brought on by the disposition of wind loads on low-rise structures with cylinder roofs that are placed in a rectangular pattern with 2B spacing between them during the wind incidence angle of 0° to 90° at 15° intervals. It was noticed during 0° wind incidence that the maximum negative (suction) pressure was acting on the top of windward roofs A & D. The windward roofs A & D were having similar kind of distribution of pressure. Furthermore, observed that the negative pressure on all the roofs A, B, C, D, E and F of 1.5B spacing model was reduced when compared with zero, 0.5B and B and 1.5B spacing model. This implies that suction was reduced on all the roofs due to increase in the spacing between the buildings i.e., 0 to 2B. During 15° wind interval, there was drastic increase in the negative wind pressure on the windward roof D. The windward roof D was subjected to maximum negative pressure as compared with other roofs. It was observed that the negative pressure on roofs A & F was reduced when compared with 0° wind incidence. The

leeward roof F was subjected to least negative pressure. On the other hand, the negative pressure on roofs B, C, D and E was increased when compared with 0° wind incidence. The effect of wind shielding was reduced on windward span of middle roofs (B & E) and leeward roofs (C & F). Since the suction dramatically increases from a wind incidence angle of 0° to 30°, it has been noticed that the windward roof D is most impacted by negative pressure. In other words, we can say that the most critical wind incidence angle is 30°. The maximum increase in the suction pressure is observed during wind incidence angle of 30° for all the roofs except middle roof E. The maximum changes in the pressure were observed during the wind incidence angle of 0° to 30°, after that the suction on the roofs started getting reduced on all the roofs. The pressure distribution on these leeward roofs was to be similar in nature and magnitude. Also, the least suction was noticed on these leeward roofs during 90° wind incidence angle when compared with all other wind incidence angles.
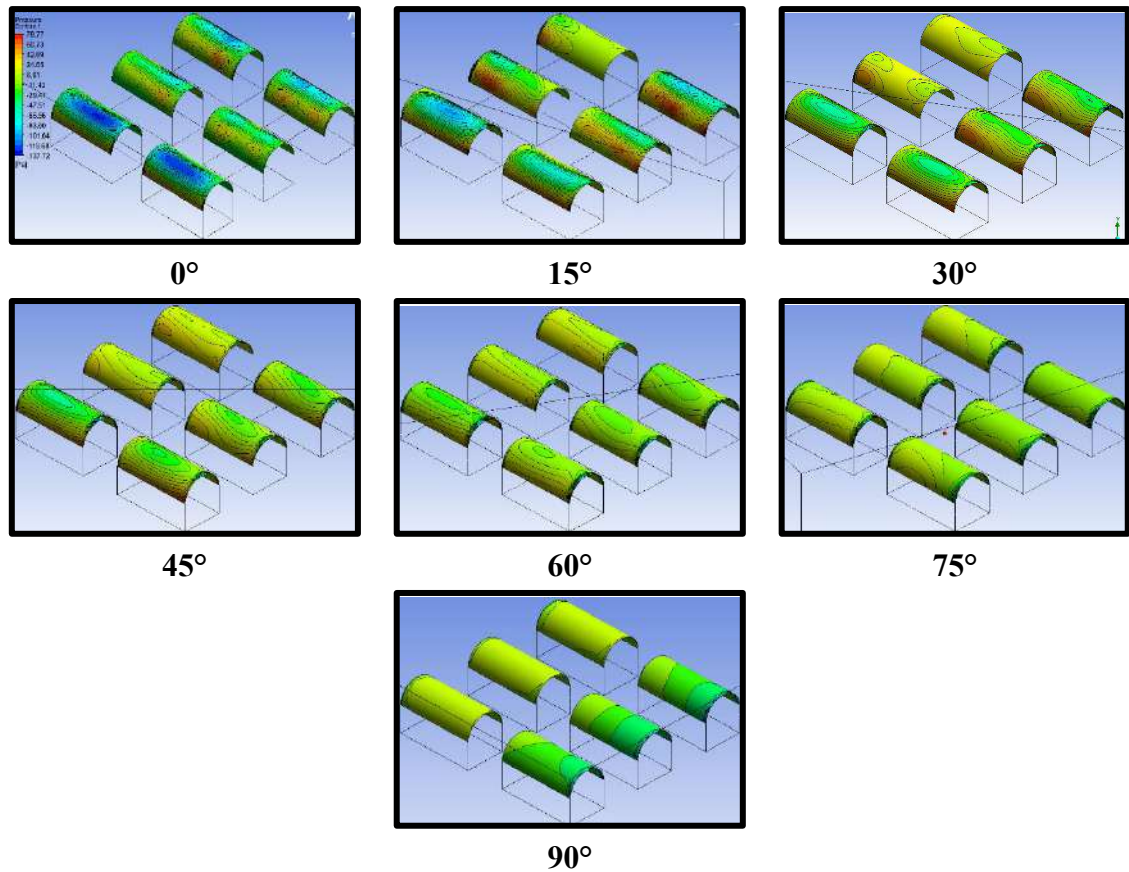

Fig. 5.9: Pressure Contours for Rectangular Patter with 2B Spacing

5.3.1.2 Pressure Coefficient

Fig. 5.10(a) and (b) depicts the variation of average C_{pe} of all the cylindrical roofs for different wind incidence angle i.e., 0° to 90° at 15° wind interval with variable spacing i.e., zero, 0.5B, B, 1.5B and 2B (where B=0.2m).

It is observed that the variation of C_{pe} for all the types of interfering model i.e., C_{pe} for roof A showed the similar trend of was gradually decreasing which indicates that the suction was reducing due to the interfering buildings. The maximum negative value of C_{pe} on roof A was noticed during zero spacing interfering model at 0° wind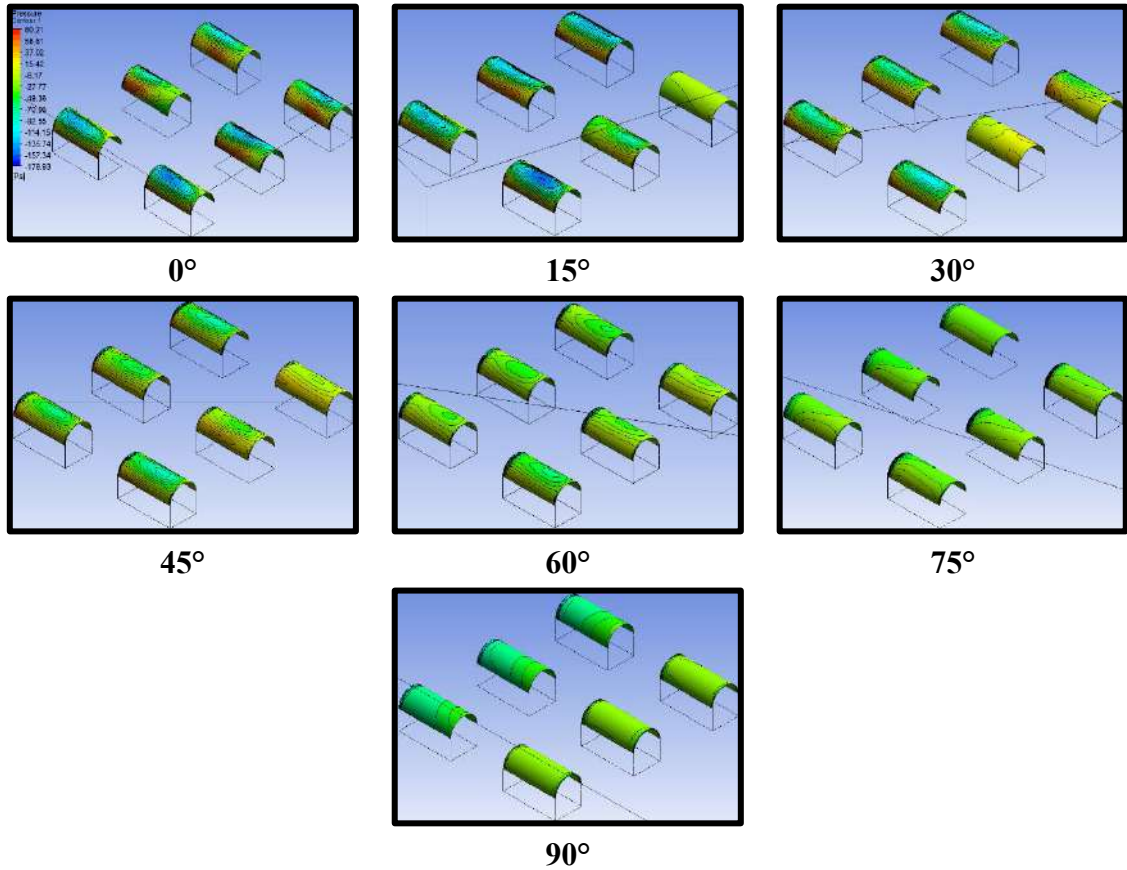 interval i.e., C_{pe} = -0.86 and minimum negative C_{pe} was observed for 2B interfering model at 90° wind incidence angle i.e., C_{pe} = -0.45.

The variation of C_{pe} for roof B is shown for different interfering model w.r.t to different wind incidence angle. The value of C_{pe} was increasing in magnitude towards negative value which indicates that the suction on roof B was increased for all the types of interfering model. The minimum suction i.e., C_{pe} = -0.23 was noticed on roof B during 0° wind incidence angle having 2B spacing while maximum suction with C_{pe} = -0.63 was found at 0°, 45°, and 75° wind interval for zero, 2B and 0.5B spacing interfering model.

The variation of C_{pe} for roof C was quite similar for 0.5B, B, 1.5B and 2B interfering model except for zero spacing model. For zero spacing model, it shows reduction in C_{pe} for 15° to 45° wind incidence angles after onwards, it started increasing till 90° whereas for other interfering models, the value of C_{pe} was gradually decreasing. The maximum negative value of C_{pe} was -0.91 during 30° wind incidence angle for 2B interfering model and minimum negative value of C_{pe} is -0.32 at 0° wind angle for zero spacing interfering model.

The value of C_{pe} on roof D kept on decreasing in magnitude for all types of interfering models when wind angle changes from 0° to 90° at 15° wind interval. The minimum negative value of C_{pe} = 0.09 was found on the roof D at 90° wind angle for 2B spacing model and maximum negative value of C_{pe} = -1.02 was found at 30° wind angle for 1.5B spacing model.

The maximum negative value of C_{pe} = -0.66 for 2B spacing model at 0° wind interval and minimum negative value of C_{pe} = -0.11 for 1.5B spacing model, were found respectively on roof E.

The maximum negative value of C_{pe} on roof F is -1.0 during 30° wind angle of incidence for zero spacing and minimum negative value of C_{pe} is -0.08 at 90° wind incidence angle for 2B interfering model, as shown in Fig. 5.10.

The pressure coefficient varies between -1.2 to -0.08, which shows the reduction in the magnitude of suction on cylindrical roofs up to 86.79% when the spacing is changed from zero to 2B.

94
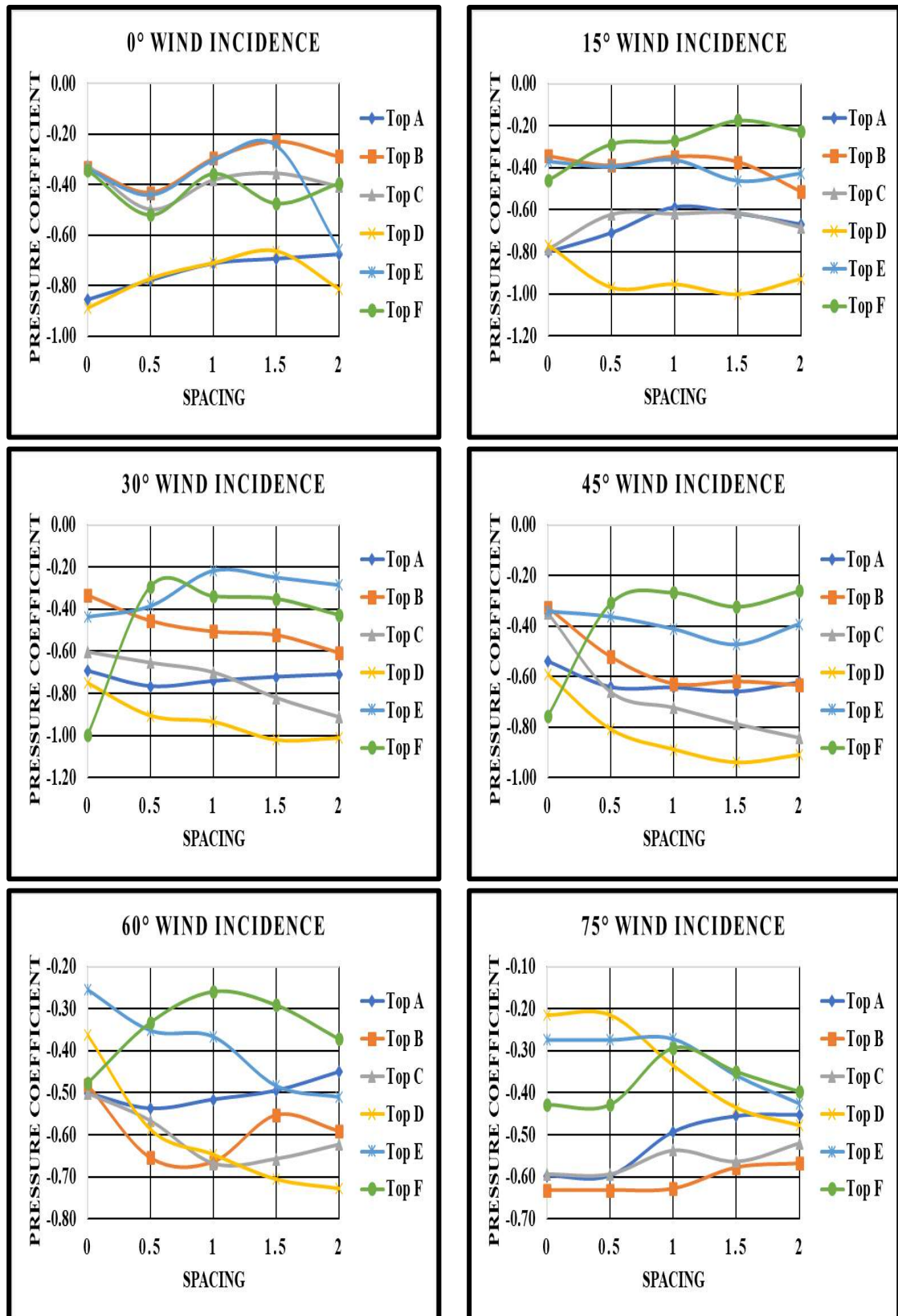
Fig. 5.10(a): Pressure Coefficient for Rectangular Patter of cylindrical roof
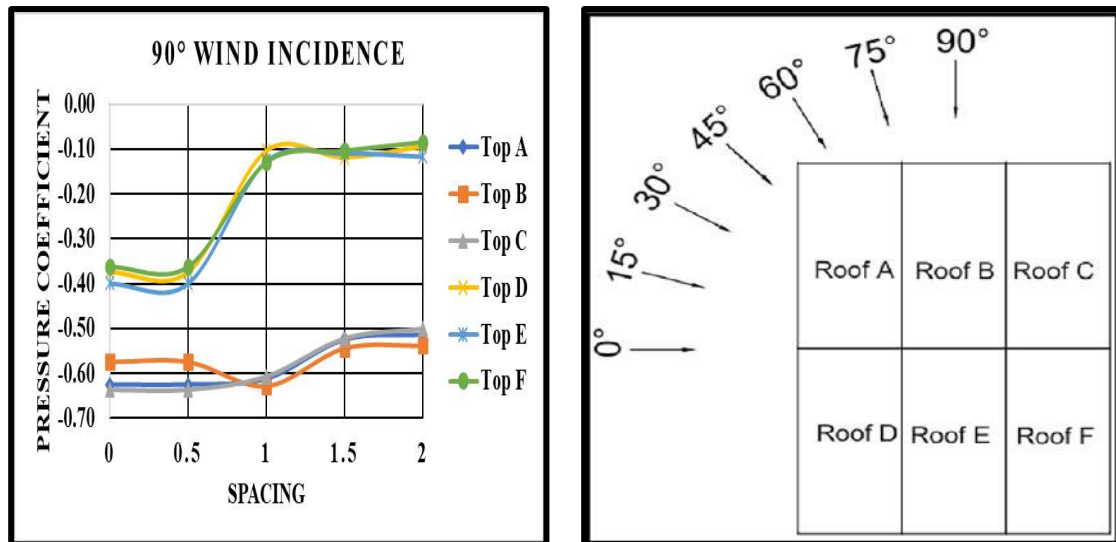
Fig. 5.10(b): Pressure Coefficient for Rectangular Patter of cylindrical roof

5.3.1.3 Interference Factor (IF)

For the numerical representation of the effects induced by the wind action due to interfering with the building under investigation, the *IF* can be utilized effectively. If the value of C_{pe} on the building under study is decreased due to interfering building which results in the reduction of *IF*, it indicates that the suction on the building is reduced due to the shielding effect of interfering building on the building under study, but the nature of wind action is same. The lower the value of *IF* lesser will the wind-induced action on the roof of the building under study. If there is a change in the sign of *IF* i.e., positive to negative then it implies that the wind action has changed its nature on the roof or the building under investigation. The *IF* on cylindrical roof is found to be varying between 1.63 to 0.19. The role of spacing and wind incidence angle plays a vital role in wind-induced action on all the roofs under investigation which results in variation of *IF* for all the roofs as shown in Fig. 5.11. For roofs A, B and C, there is a similar pattern has been observed in the variation of *IF*. The value of *IF* is decreased with respect to the spacing but keeps on gradually increasing with respect to the wind incidence angle. From 0° to 15° wind incidence angle, the magnitude of *IF* is decreased afterward it starts gradually increasing till 90°wind incidence. Since the value of *IF* is increasing with respect to wind incidence, it indicates that the major adverse effects of wind action are induced due to wind incidence angle on roofs A, B, and C respectively. The magnitude of *IF* is more than 1 on roofs A, B, and C indicating that these roofs are highly affected by wind loads. While in the case of Roofs D, E, and F, the *IF* is getting reduced with respect to spacing as well as wind incidence angle. The magnitude of *IF* in the case of roofs D, E and F are reduced to less than 1, indicating that these roofs are less affected by wind-induced actions.
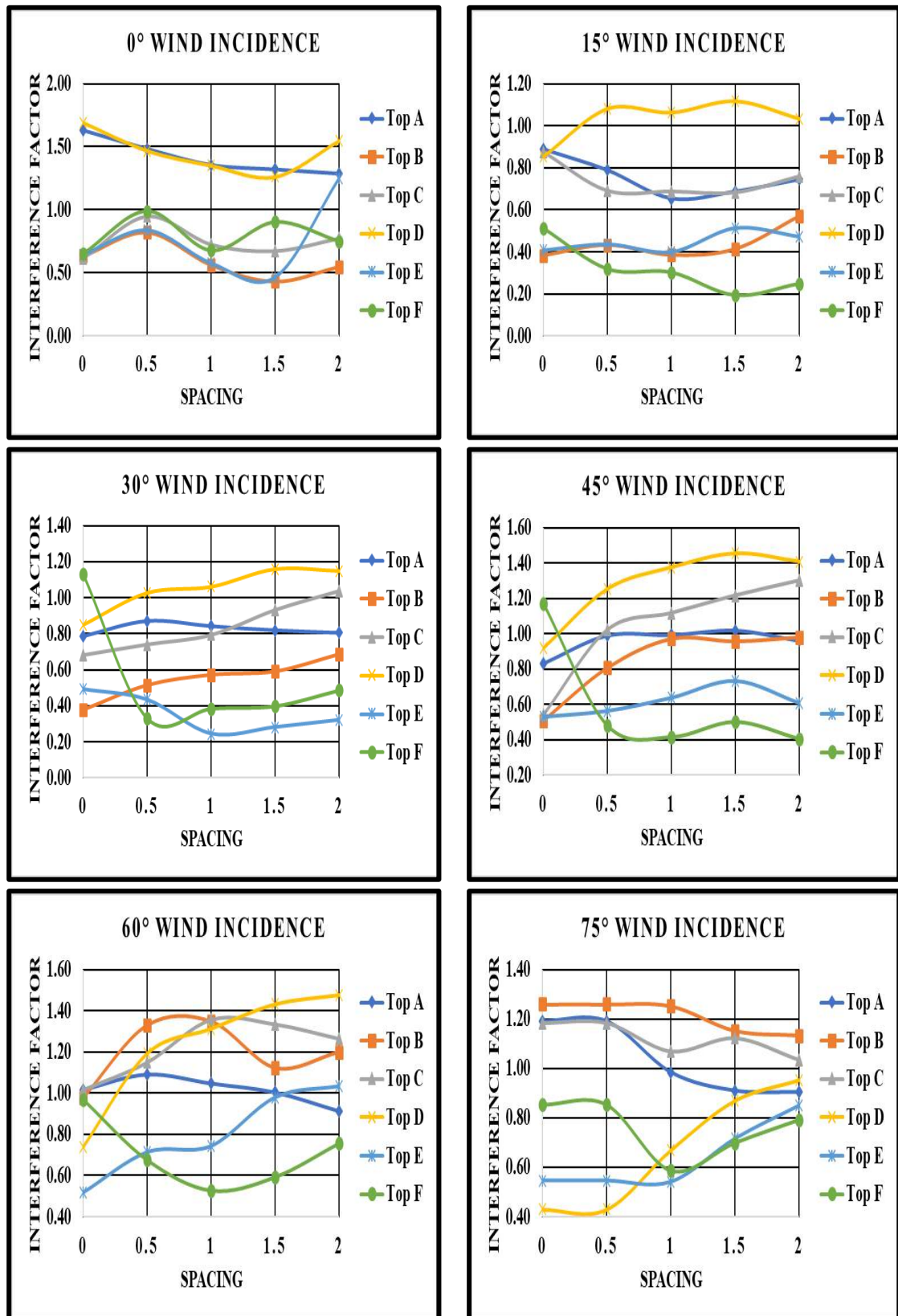
Fig. 5.11(a): Interference Factor for Rectangular Patter of cylindrical roof
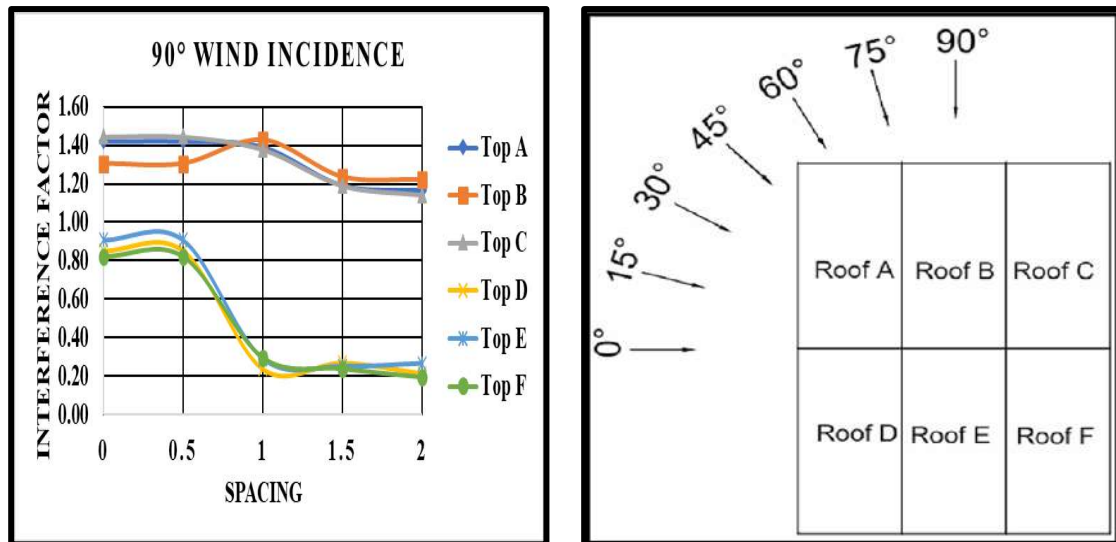
Fig. 5.11(b): Interference Factor for Rectangular Patter of cylindrical roof

5.3.1.4 Interference Difference (ID)

Sometimes it comes to knowledge that due to interference either pressure or suction on buildings gets reduced such as the action of shielding effect on the roof due to the presence of the interfering building in the upstream direction of the wind flow resulting in the reduction of the pressure or suction. The values of *ID* are calculated for all the cylindrical roofs under variable spacing and wind interval conditions presented in Fig. 5.12.

It was observed during the investigation of low-rise isolated building with cylindrical roof that the roof was under suction with respect to the wind incidence angles. Its value was kept on either increase or decrease under the wind load for various wind angles.

The range of variation of *ID* is found to be 0.73 to -0.36. So, there are two situations arises during the investigation of interference difference for cylindrical roofs. When C_{pe} during isolated and interference is less than 0 as well as *ID* is less than 0, we can infer that suction during interference is greater than that of the suction during isolated condition also there is change in wind induced action from acting as a positive pressure during isolated to the suction in interference condition.

Second condition says that C_{pe} is less than 0 but *ID* comes out to be greater than 0 indicating that suction on interfering building is less than the suction on isolated building or vice versa.

Therefore, from Fig. 5.12 it can be predicted for roofs A, B and C that the ID gradually increases and has the value more than 0˚ with respect to wind incidence angle till 45˚ which indicates that the suction was reducing gradually. After 45˚ wind incidence angle the positive *ID* changes into negative magnitude indicating that roofs are going under increased suction.

The variation of *ID* for roof D shows that during most of wind incidence angles the suction in interference was higher than the suction in an isolated condition. Only for wind incidence of 75˚ and 90˚ the *ID* changes from negative to positive indicates that suction is reduced on roof D during interference. Roofs E and F shows similar trend of variation in *ID*. The *ID* for both the roofs is more than 0 with respect to wind incidence angles.

It can be inferred that there is good amount of reduction in the suction due to interference. The maximum positive *ID* has been recorded on the roofs B, E and F during 15˚ and 30˚ wind incidence.
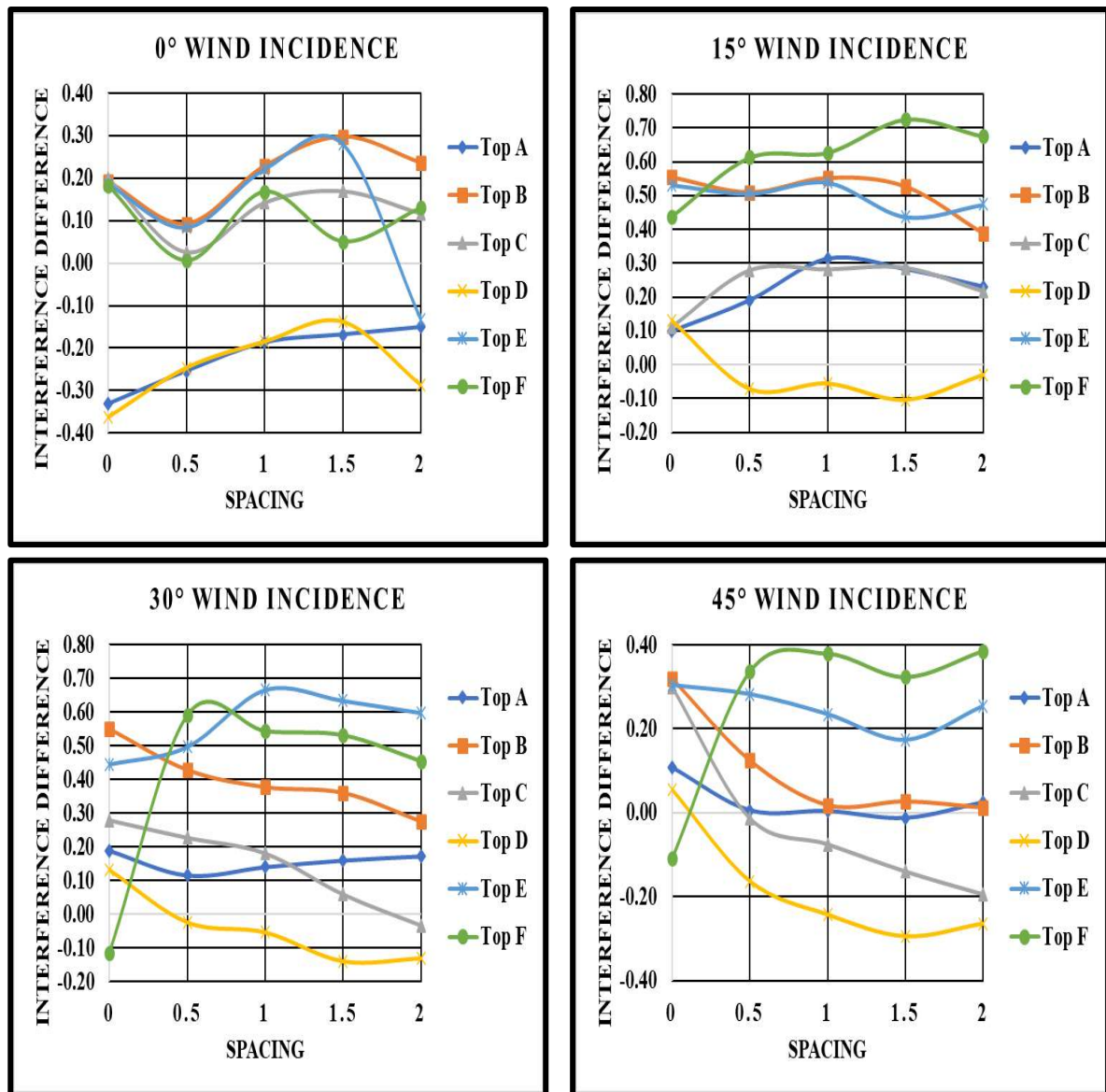
Fig. 5.12(a): Interference Difference for Rectangular Pattern of cylindrical roof
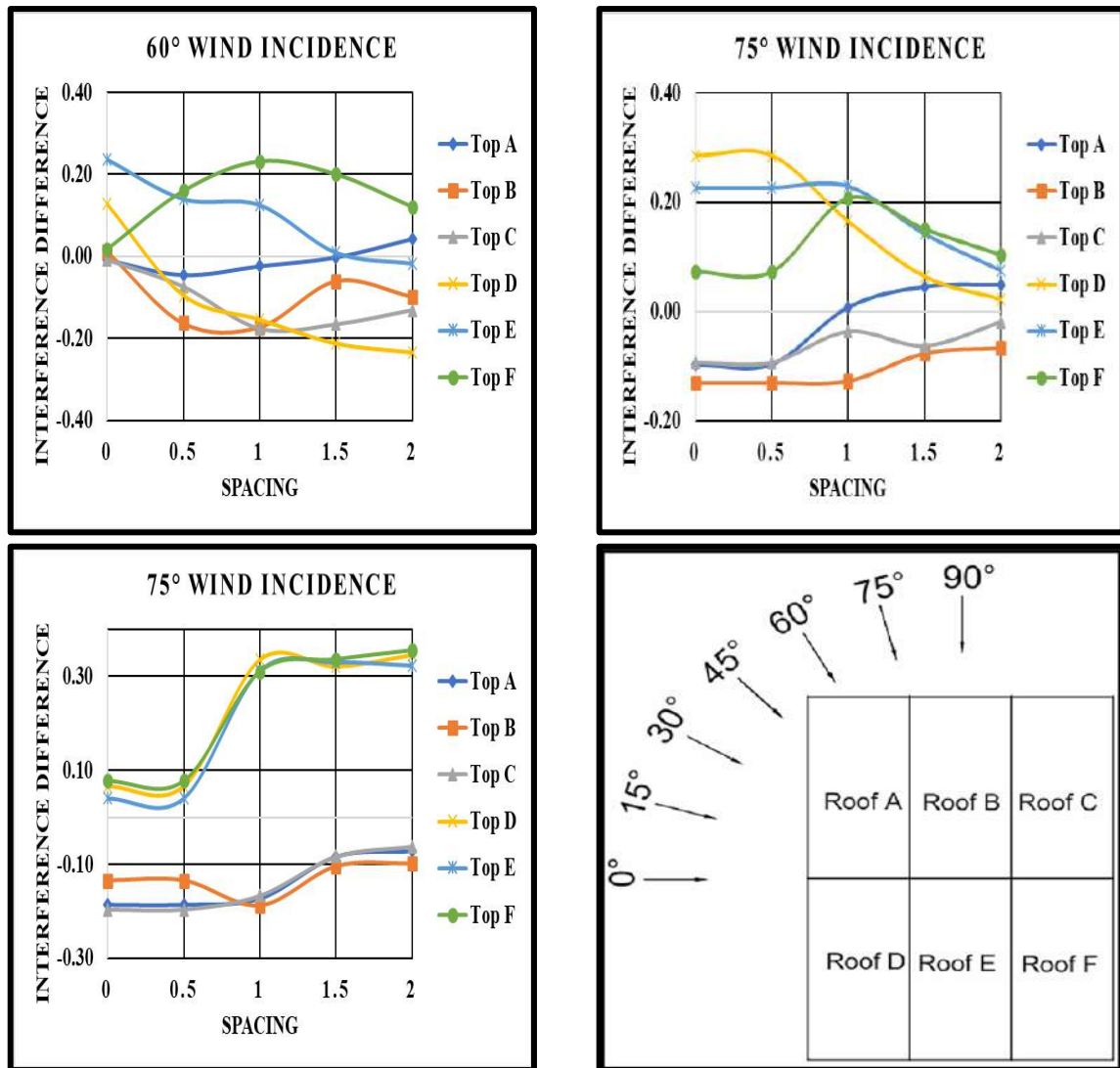
Fig. 5.12(b): Interference Difference for Rectangular Pattern of cylindrical roof

5.3.1.5 Wind Flow Streamlines

The wind flow streamlines for low-rise building with cylindrical roof arranged in rectangular pattern with variable spacing are shown in Fig. 5.13 at different angles of wind incidence ranging between 0° to 90° at an interval of 15°. The streamlines are generated for different wind induced interference conditions by creating a plane at an eave height of the building i.e., 150 mm. It is clearly seen from Fig. 5.13 that in the case of 0° wind incidence the three (left, right and leeward) sides of 0 spacing model is subjected to the suction while only area which is directly opposite to the wind flow was under positive pressure and same is the case of 90° wind incidence but the front, left and right are under negative wind induced pressure and leeward portion under positive pressure. Also, the flow separation zone maximum in area in case of 0° wind incidence angle as compared to 45° and 90° shown in Fig. 5.12. The spacing between the buildings has been increased to 0.5B for which the streamlines are shown in Fig.

5.14. During 0° wind incidence the flow separation zone has been increased in case of 0.5B spacing when compared with 0 spacing model which indicates that the wind flow is getting space to flow in between the buildings creating enhanced pressure between them. Also, all six buildings were under negative pressure from all the side but during 90° wind incidence angle the only front three buildings were under negative pressure from surroundings. The effect of Shielding is getting reduced when the spacing between the buildings is increased. It is seen from the Fig. 5.15, 5.16 and 5.17 that the effect of interference is getting influenced by the spacing as well as the angle of wind incidence. In terms of average wind-induced pressure, the roofs of all the six buildings under investigation are found to be under negative pressure but some of the windward portions of the all the roofs are getting exposed to positive pressure during 0° and 45° wind incidence angles due to interference.

Fig. 5.13(a): Wind Flow Streamlines for Rectangular Pattern with zero Spacing
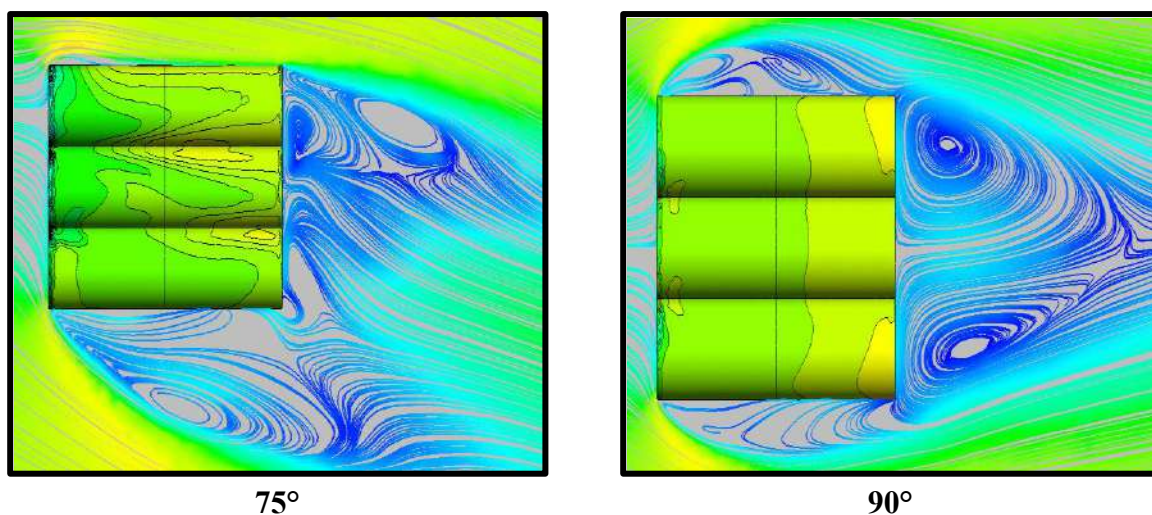
Fig. 5.13(b): Wind Flow Streamlines for Rectangular Pattern with zero Spacing

Fig. 5.14(a): Wind Flow Streamlines for Rectangular Pattern with 0.5B Spacing

90°

Fig. 5.14(b): Wind Flow Streamlines for Rectangular Pattern with 0.5B Spacing

0°   **15°**   **30°**

45°   **60°**   **75°**

Fig. 5.15(a): Wind Flow Streamlines for Rectangular Pattern with B Spacing

90°

Fig. 5.15(b): Wind Flow Streamlines for Rectangular Pattern with B Spacing

0°   **15°**   **30°**
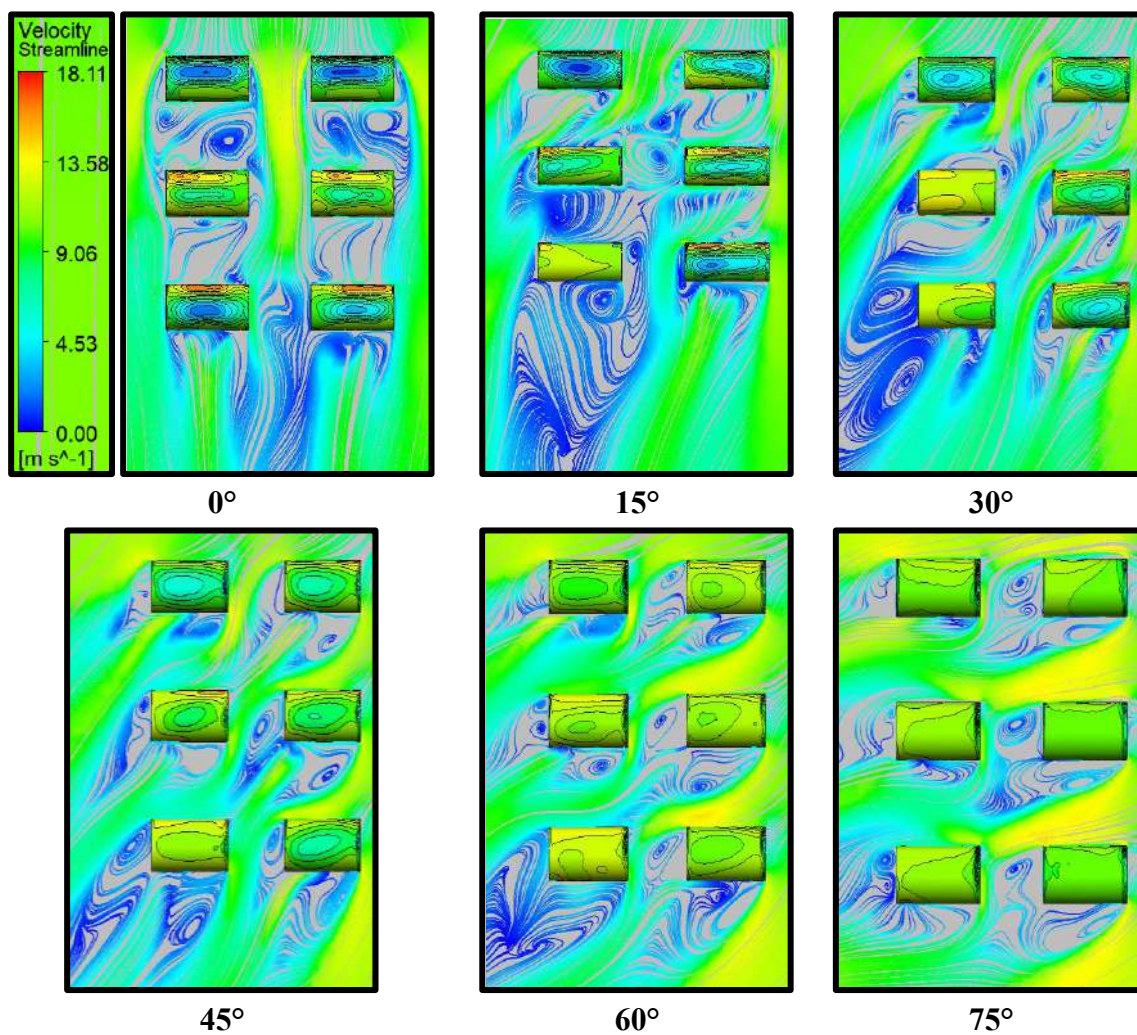
45°   **60°**   **75°**

Fig. 5.16(a): Wind Flow Streamlines for Rectangular Pattern with 1.5B Spacing
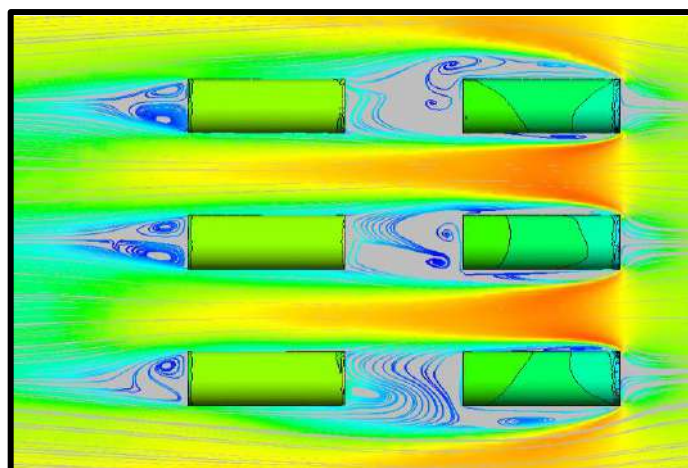
90°

Fig. 5.16(b): Wind Flow Streamlines for Rectangular Pattern with 1.5B Spacing

0°   **15°**   **30°**
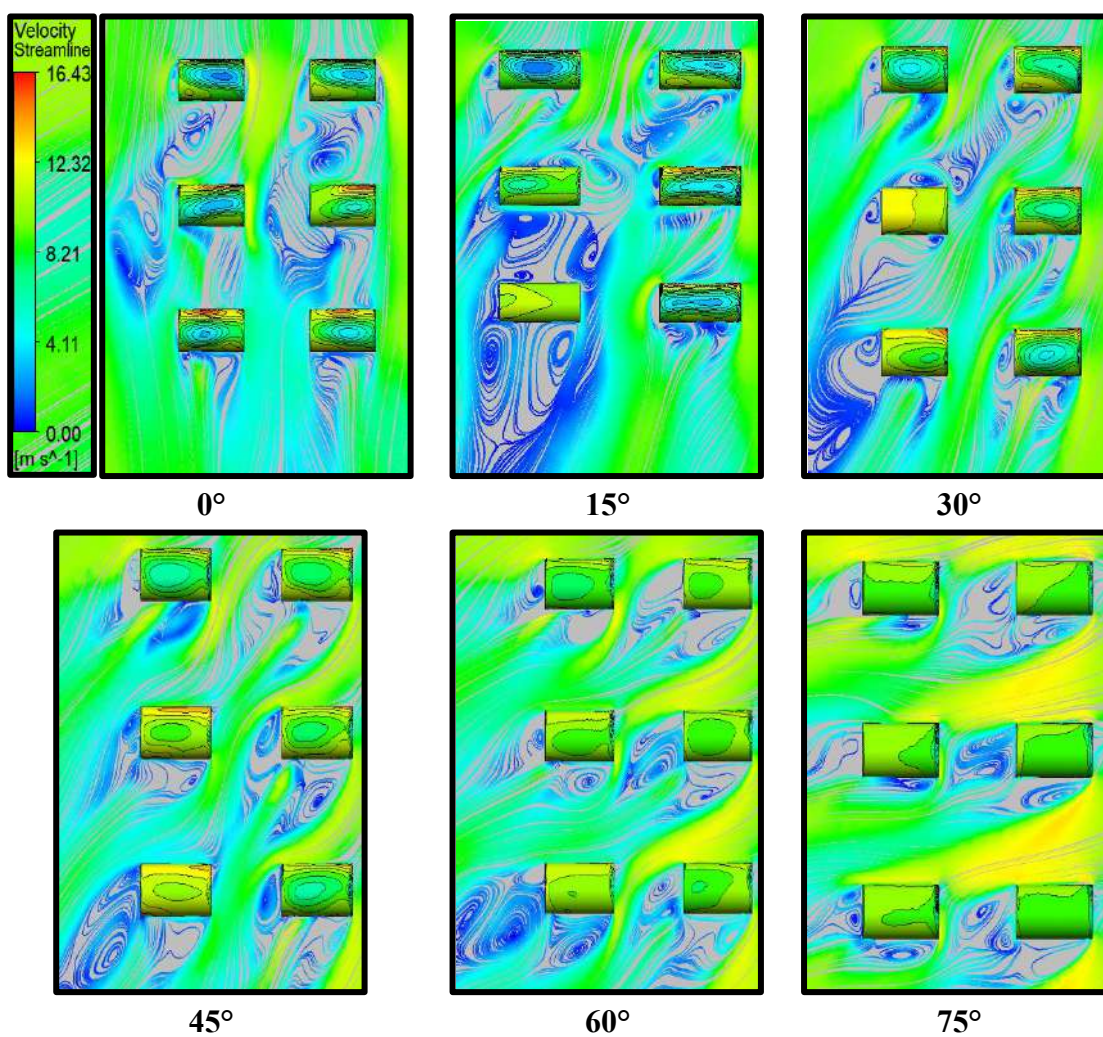
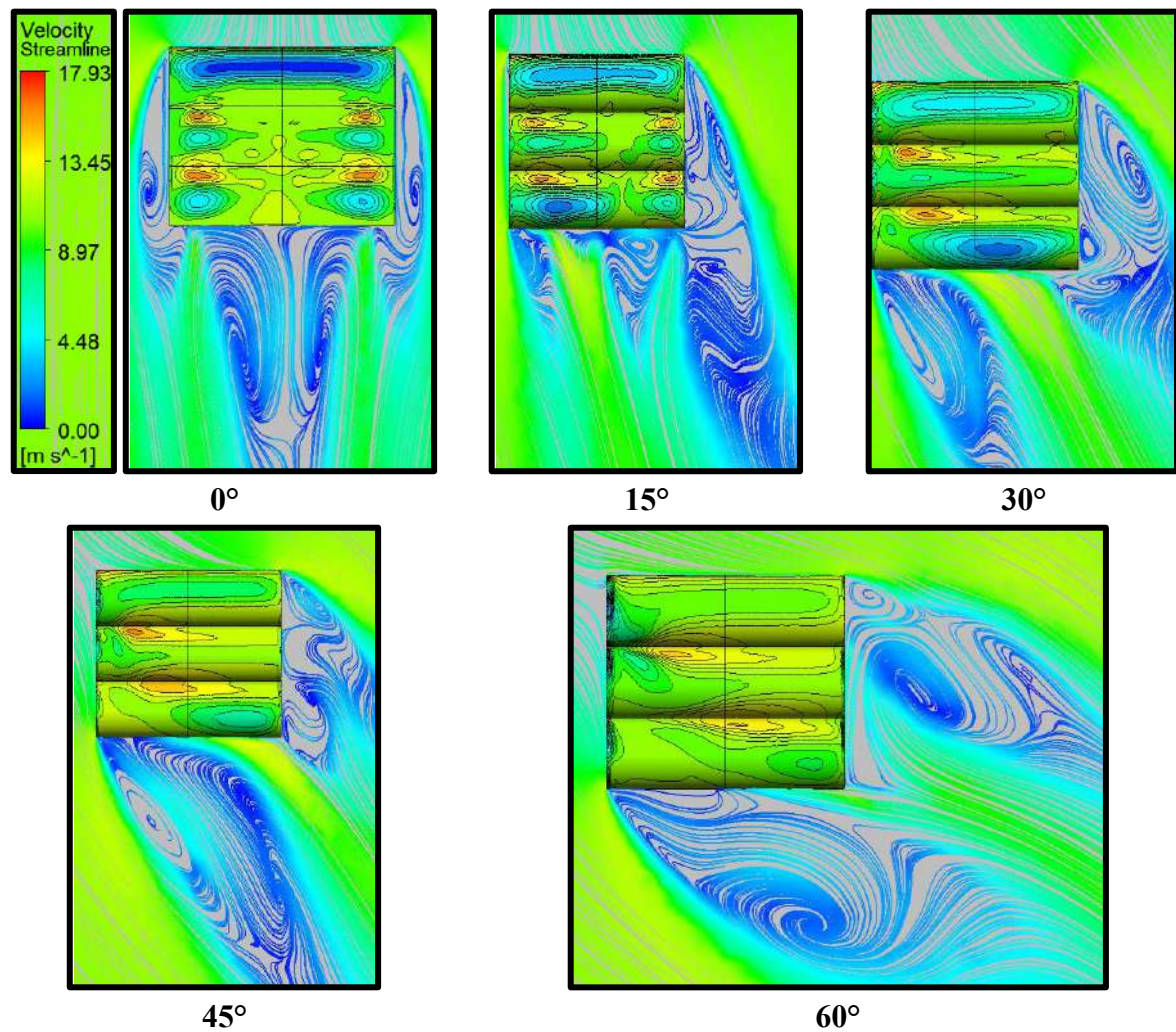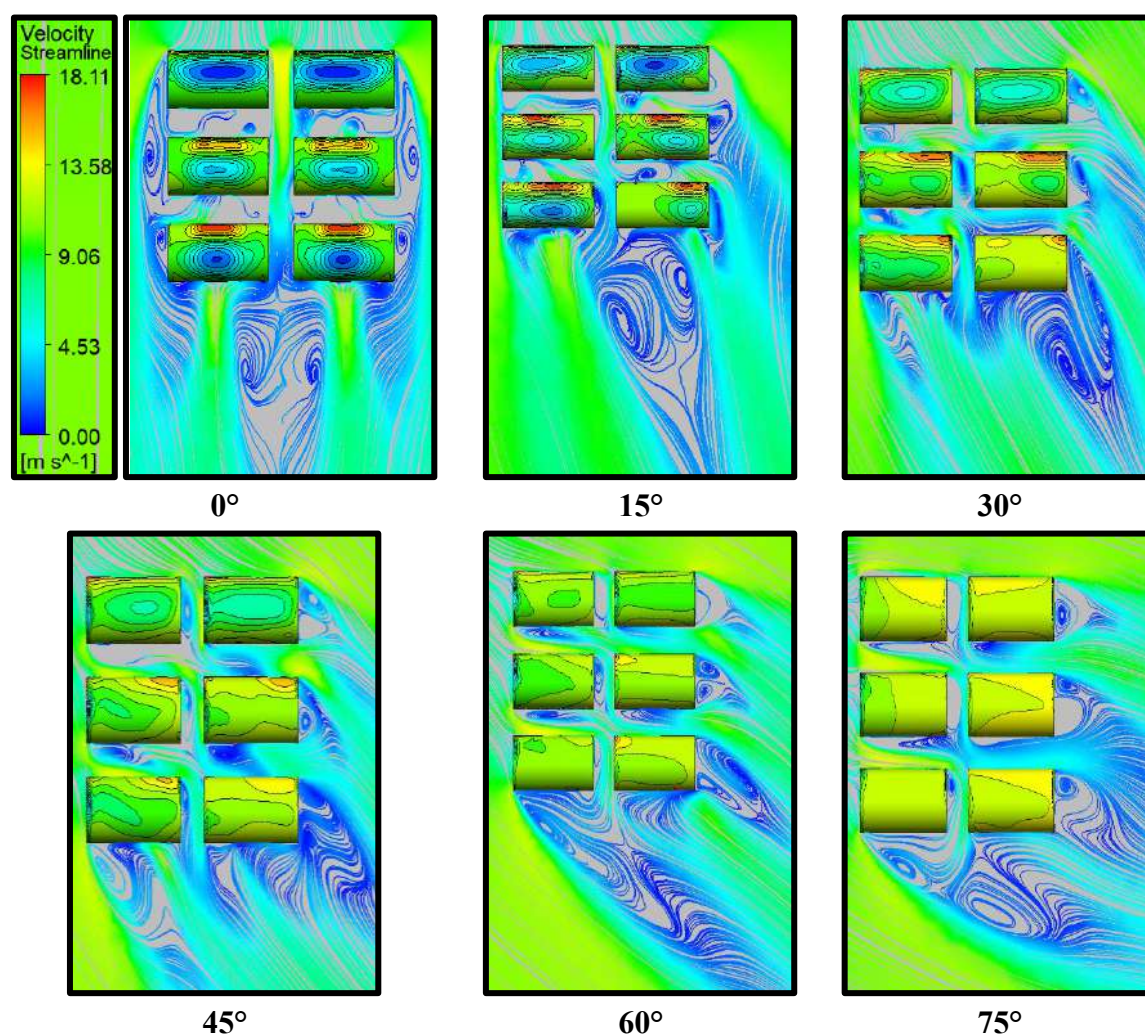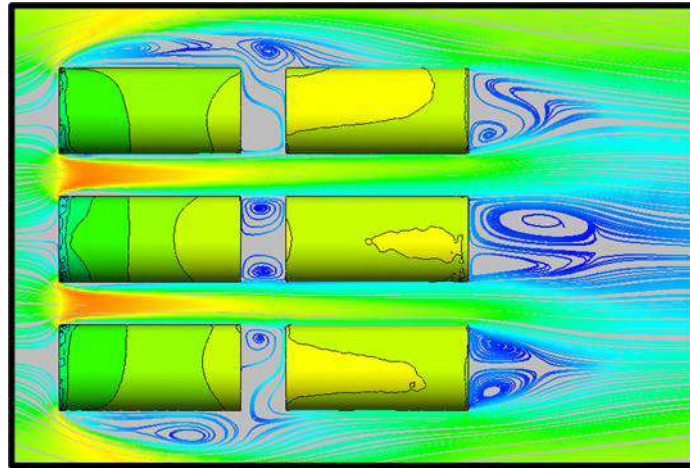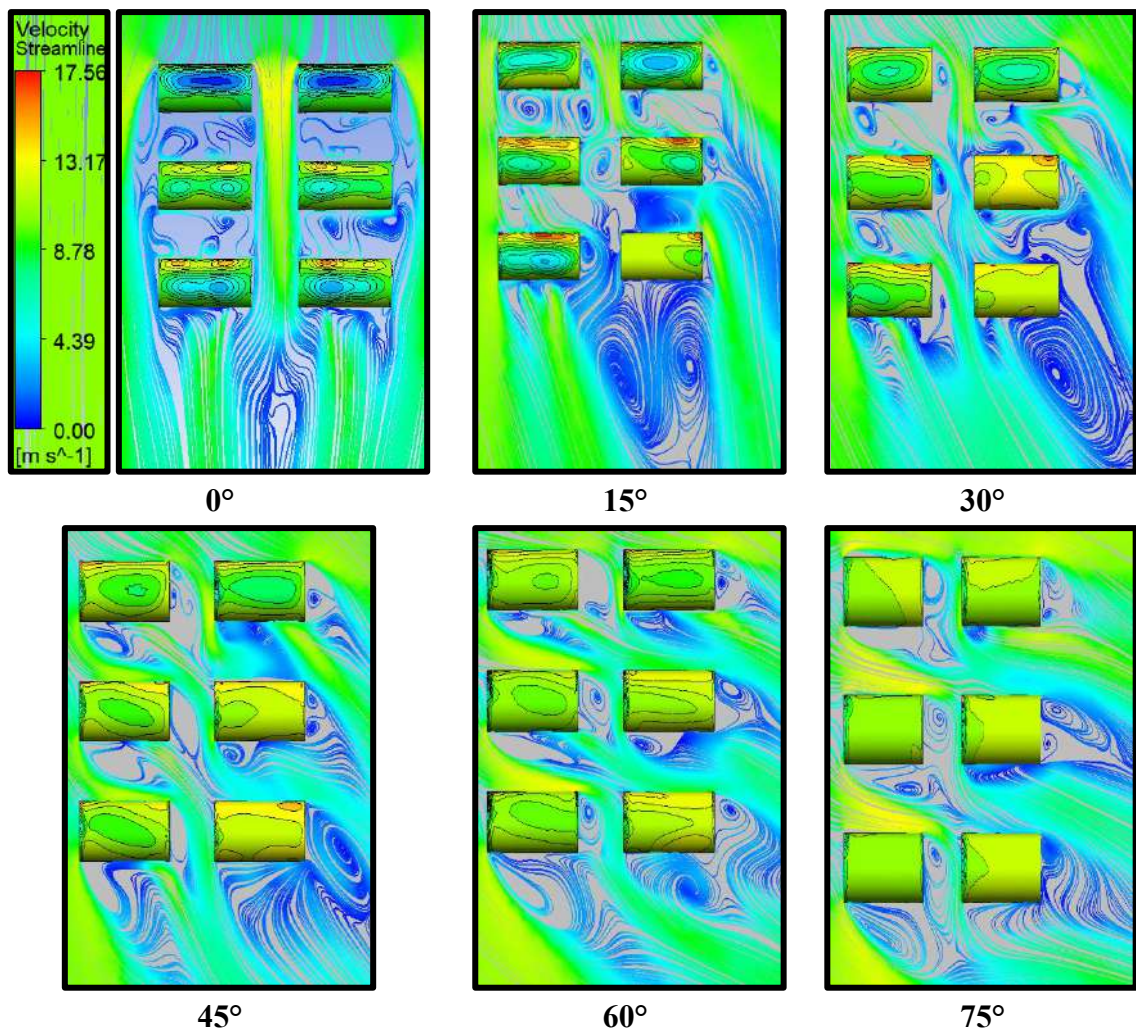**45°**   **60°**   **75°**

Fig. 5.17(a): Wind Flow Streamlines for Rectangular Pattern with 2B Spacing

90°
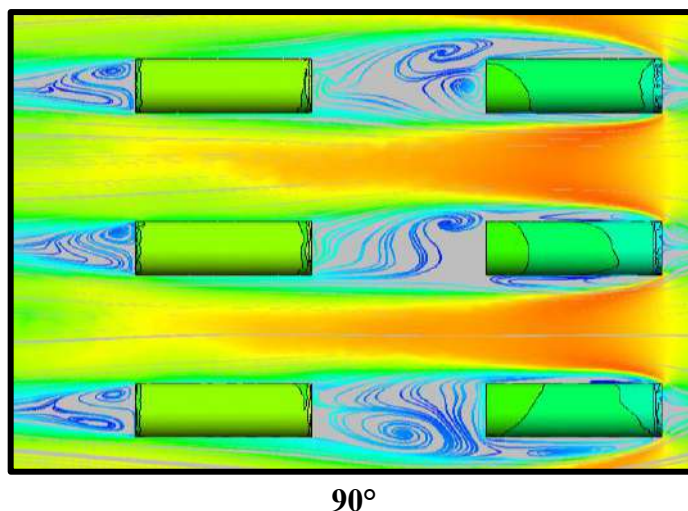
Fig. 5.17(b): Wind Flow Streamlines for Rectangular Pattern with 2B Spacing
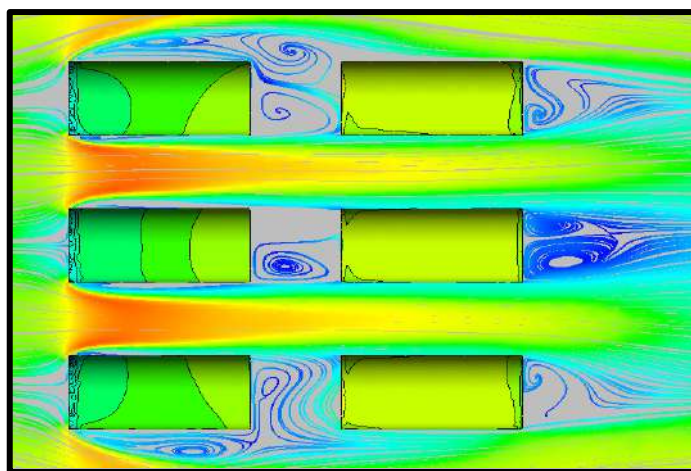
5.3.2 Z Pattern

Similarly to the rectangular pattern, the dome roofs are now arranged in Z pattern of different interfering conditions with variable spacing of 0, 0.5B, B, 1.5B and 2B at different angles of wind attack i.e., 0° to 180° at 15° each interval to find out the wind effects on the cylindrical roof, discussed below.

5.3.2.1 Pressure Contours

The wind-induced pressure contours on the cylindrical roof of low-rise structures are investigated by arranging the low-rise building models in a Z pattern with variable spacing (0, 0.5B, B, 1.5B and 2B) using CFD simulation are discussed here in this section. The pressure contours, roof nomenclature and angles of wind incidences for the zero spacing model are shown in Fig. 5.18 in which it is observed that during 0° to 45° wind incidence, a very small windward portion of all the roofs is subjected to positive wind-induced pressure while other is subjected to negative pressure due to which the overall impact of the wind on the cylindrical roof is negative. Due to the shielding effect, roofs C, D and E experience less pressure than roofs A, B, and F. There is almost a uniform negative pressure distribution on roofs C, D, and E during 90° wind incidence. The pressure contours obtained for 0° and 180° wind angles are exactly similar to each other, with the only difference being that the behaviour is changed from windward to leeward or vice versa, such that roofs A and B are behaving as leeward roofs in case of 180° wind angle, and roofs E and F are behaving as leeward roofs in case of 0° wind angles. By increasing the spacing between the buildings, the area of positive pressure on the windward side of the roofs is also increased at 0°, 15° and 30° angles of wind attack. During 90° wind attack, the wind pressure distribution on roofs C, D and E is almost divided into three portions i.e., the windward edges are under higher suction, middle portion is subjected to less

suction than the windward edge and leeward edge is under least suction when the spacing is increased from 0.5B to 2B respectively as shown in Figs. 5.19-5.22 respectively. The variation in magnitude of wind-induced pressure is in the range of -60.68Pa to -3.06Pa when the spacing is changed from zero to 2B.

| 0° | 15° | 30° |

| 45° | 60° | 75° |

| 90° | 105° | 120° |

| 135° | 150° | 165° |

| 180° | | **Roof Nomenclature and Wind Angles** |

Fig. 5.18: Pressure Contours for Z pattern with Zero Spacing

0°

15°

30°

45°

60°

75°

90°

105°

120°

135°

150°

165°

180°

Roof Nomenclature and Wind Angles
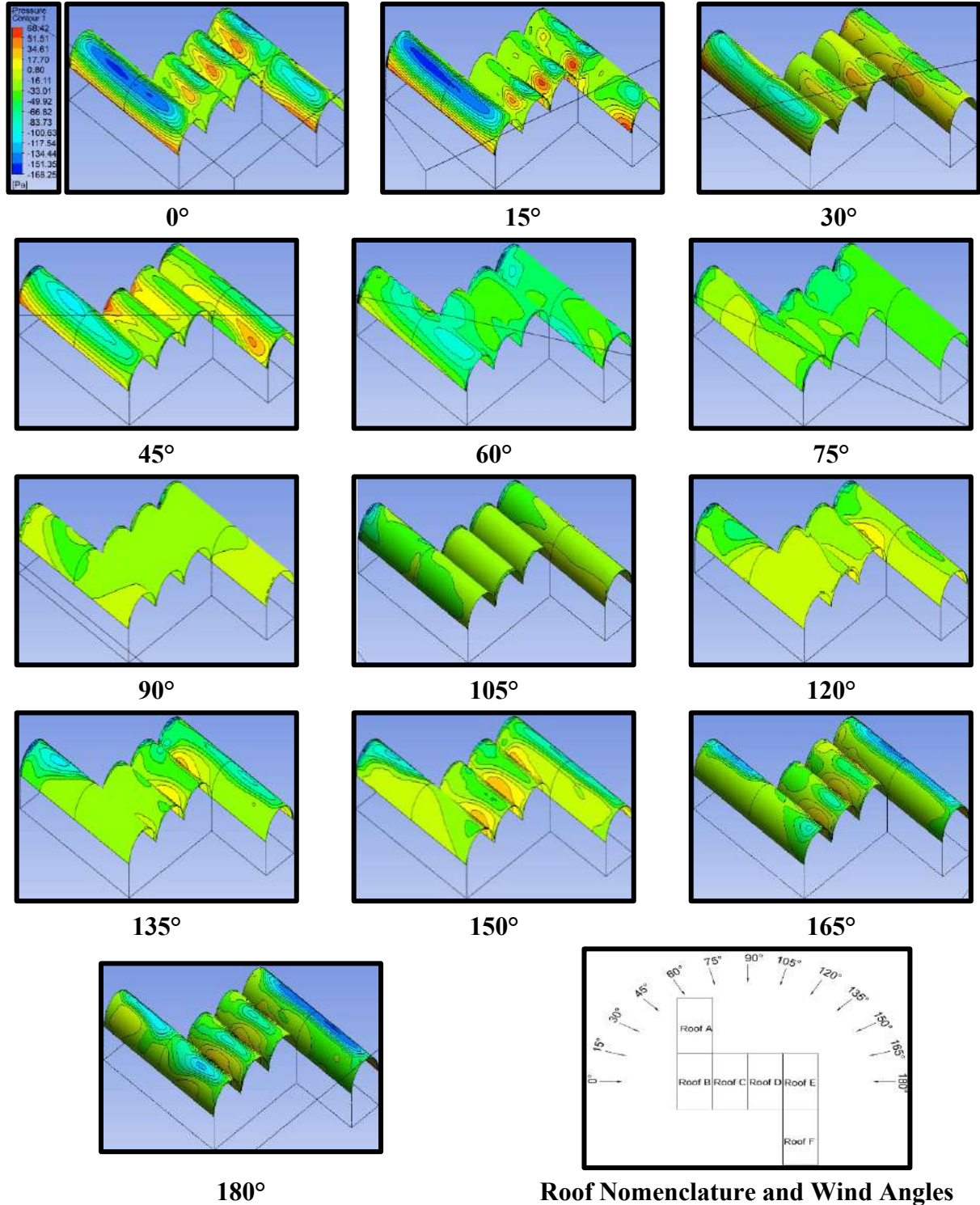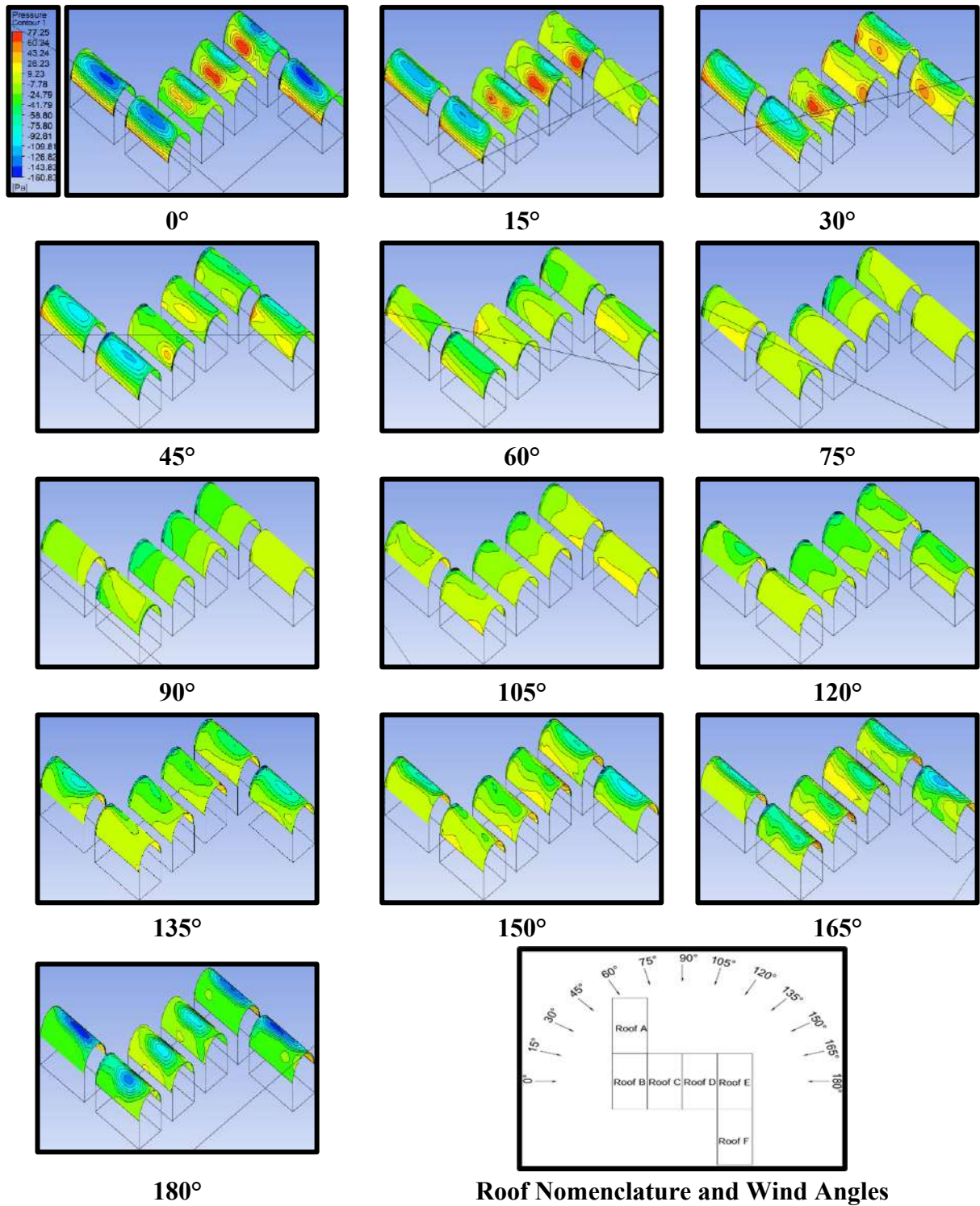
Fig. 5.19: Pressure Contours for Z pattern with 0.5B Spacing

0°

15°

30°
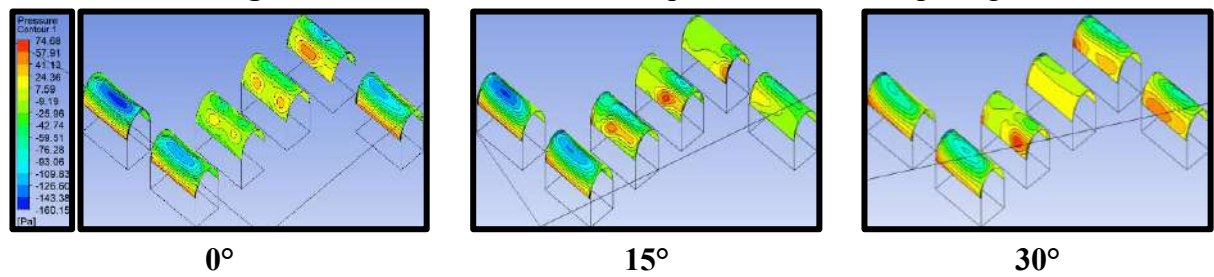
Fig. 5.20(a): Pressure Contours for Z pattern with B Spacing
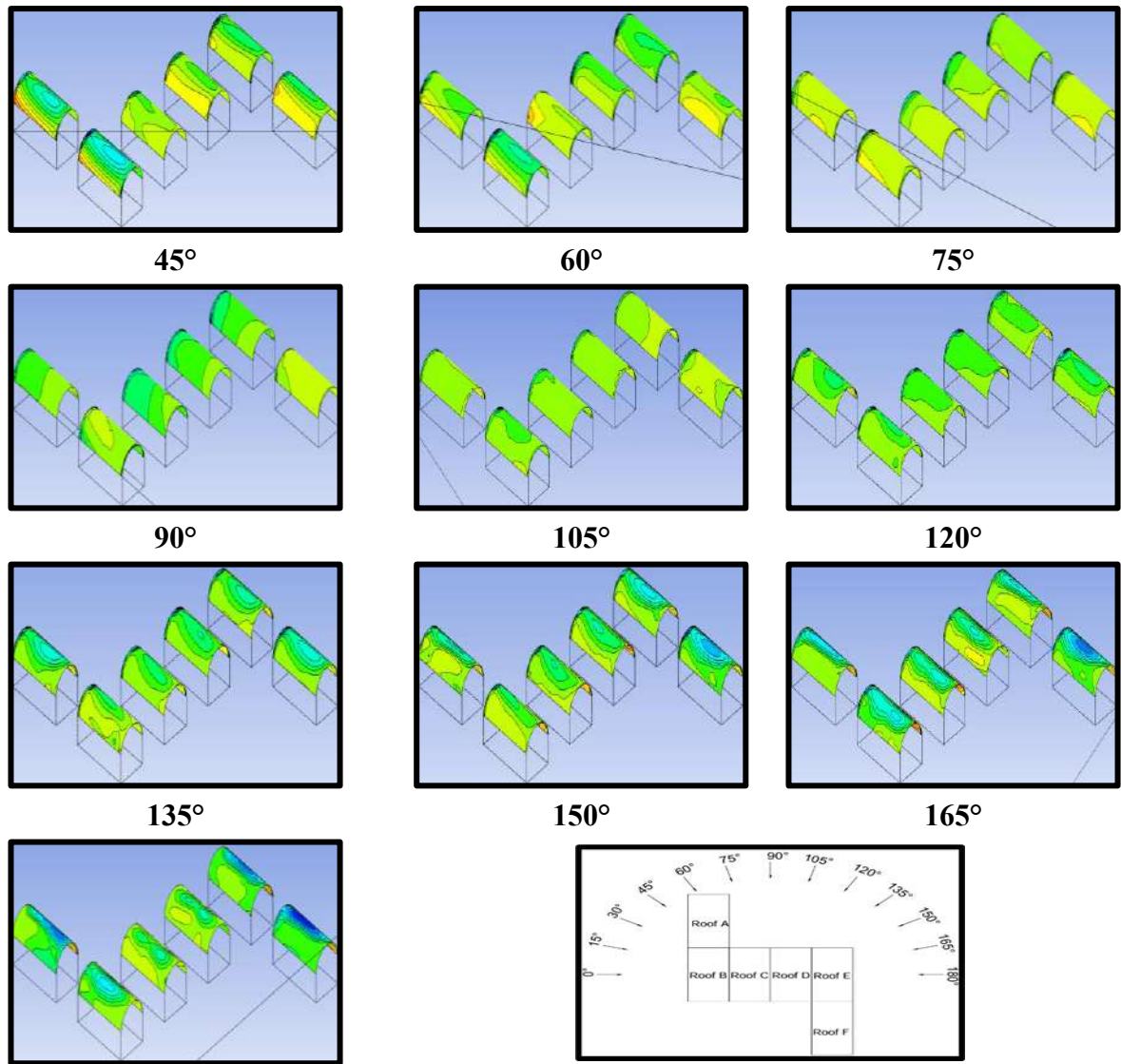
Fig. 5.20(b): Pressure Contours for Z pattern with B Spacing

Fig. 5.21(a): Pressure Contours for Z pattern with 1.5B Spacing

90°   **105°**   **120°**

135°   **150°**   **165°**

180°   **Roof Nomenclature and Wind Angles**

Fig. 5.21(b): Pressure Contours for Z pattern with 1.5B Spacing

0°   **15°**   **30°**

45°   **60°**   **75°**

90°   **105°**   **120°**

Fig. 5.22(a): Pressure Contours for Z pattern with 2B Spacing

| 135° | 150° | 165° |

180°   **Roof Nomenclature and Wind Angles**
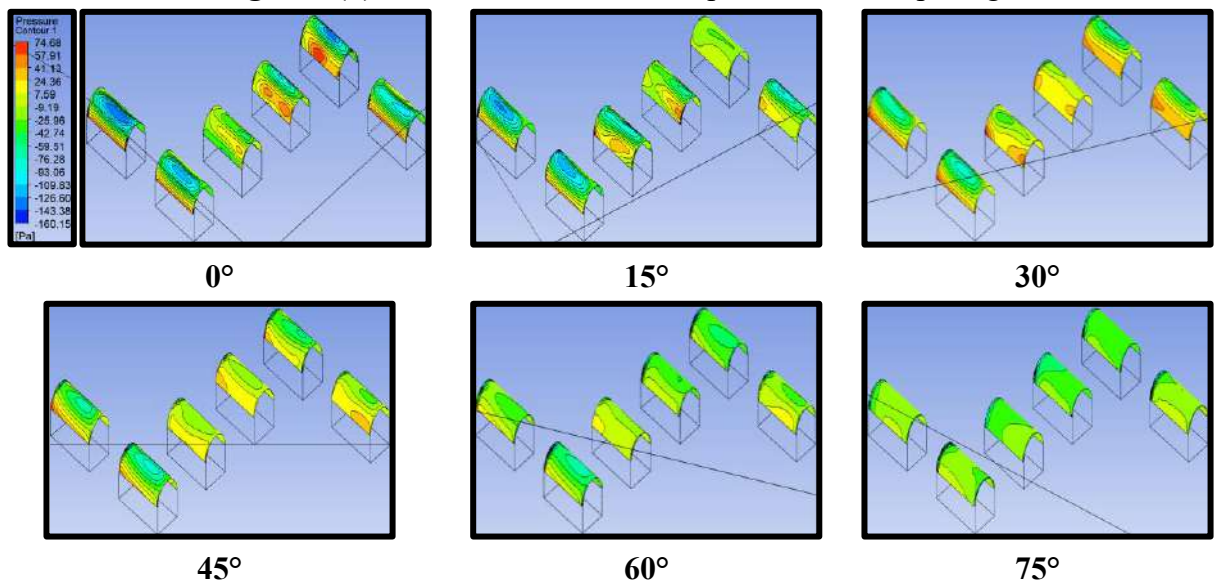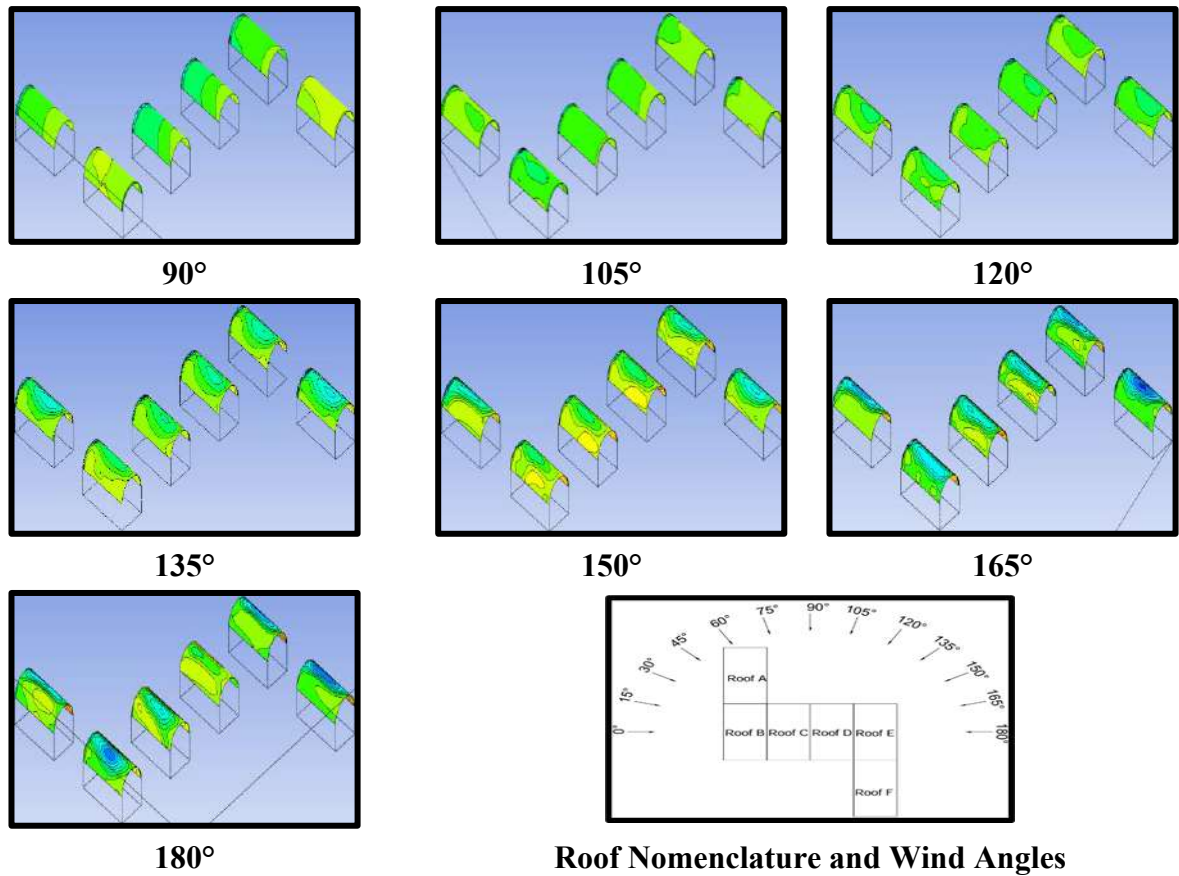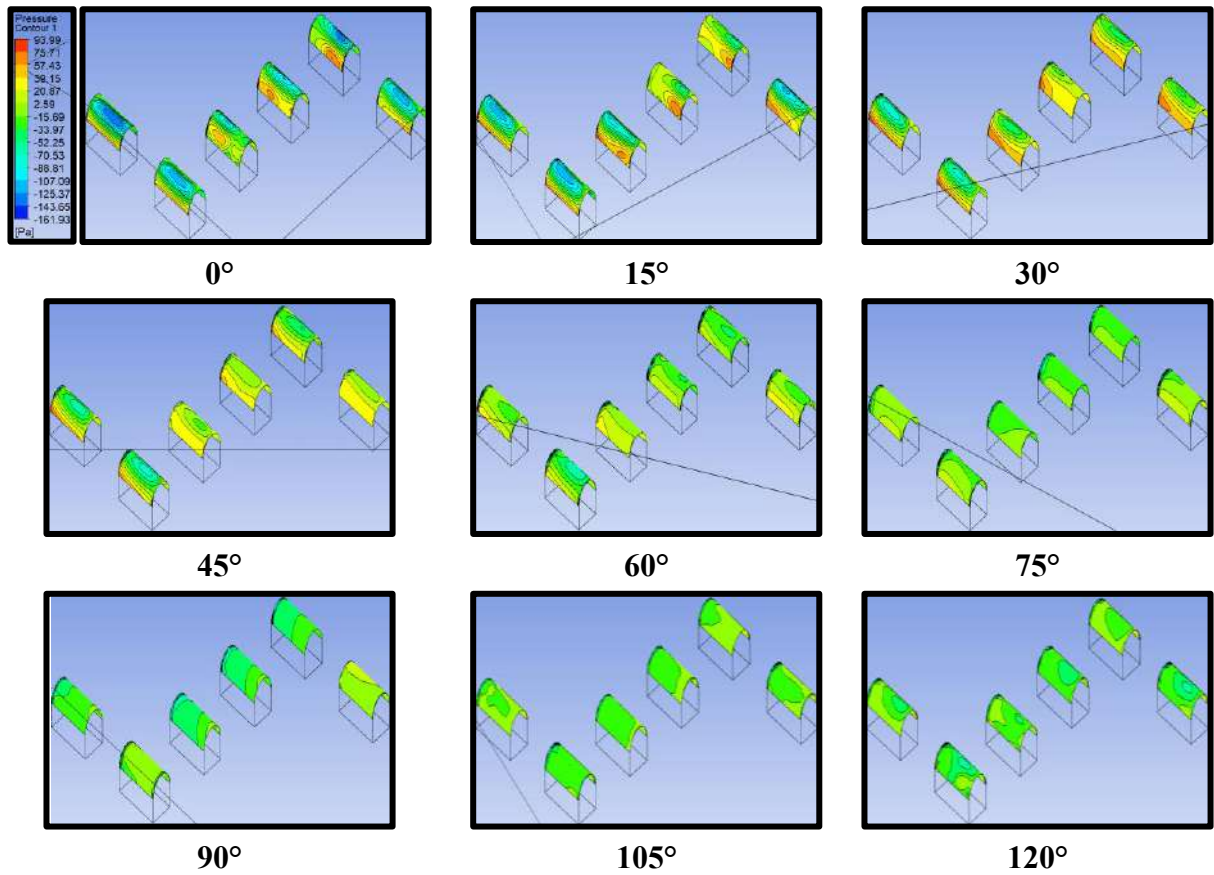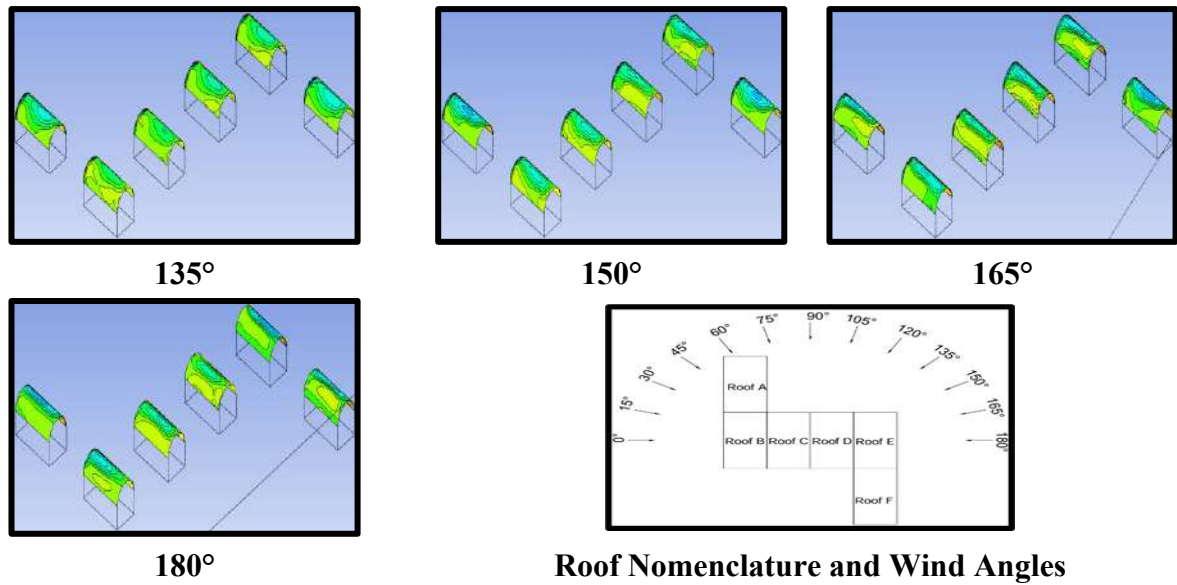
Fig. 5.22(b): Pressure Contours for Z pattern with 2B Spacing

5.3.2.2 Pressure Coefficient (C_pe)

The variation of C_{pe} on the cylindrical roof of six low-rise buildings arranged in z pattern with variable spacing of zero, 0.5B, B, 1.5B and 2B at different angles of wind interval ranging between 0° to 180° having an interval of 15° each, is shown in Fig. 5.23. The overall variation of C_{pe} on cylindrical roofs arranged in z pattern with different spacing is -1.29 to -0.05 which shows the reduction in magnitude of suction by 90.56% when there is increase in spacing.

The variation of C_{pe} on roof A is lying between -0.28 to -0.96 in which the maximum negative C_{pe} is -0.96 and it gets reduces to -0.75 when the spacing is increased from 0 to 2B at 0° wind angle. The minimum value of negative C_{pe} is observed during 60° and 75° angles of wind attack i.e., -0.28 at 60° and -0.32 at 75°. On comparing the roofs A, B, C, D, E and F, the minimum negative C_{pe} is obderved on roofs C and D during 0° wind angle ranging btetween -0.22 to -0.44. In case of 15° angle of wind attack, the value of C_{pe}= -0.17 which is the least value among all the roofs acting at roof D during 2B spacing. There is a drastic reduction in value of negative C_{pe} on roofs B and F during 90° wind incidence angle i.e. ranging between -0.59 to -0.17 (roof B) and -0.46 to -0.05 (roof F) as shown in Fig. 5.23.

As compared to the rectangular pattern of cylindrical roof, the value of negative C_{pe} is observd to higher in case of z pattern with variable spacing. The overall variation of C_{pe} with respect to wind angle and variable spacing over the cylindrical roof arranged in z pattern us shown below in Fig. 5.23.
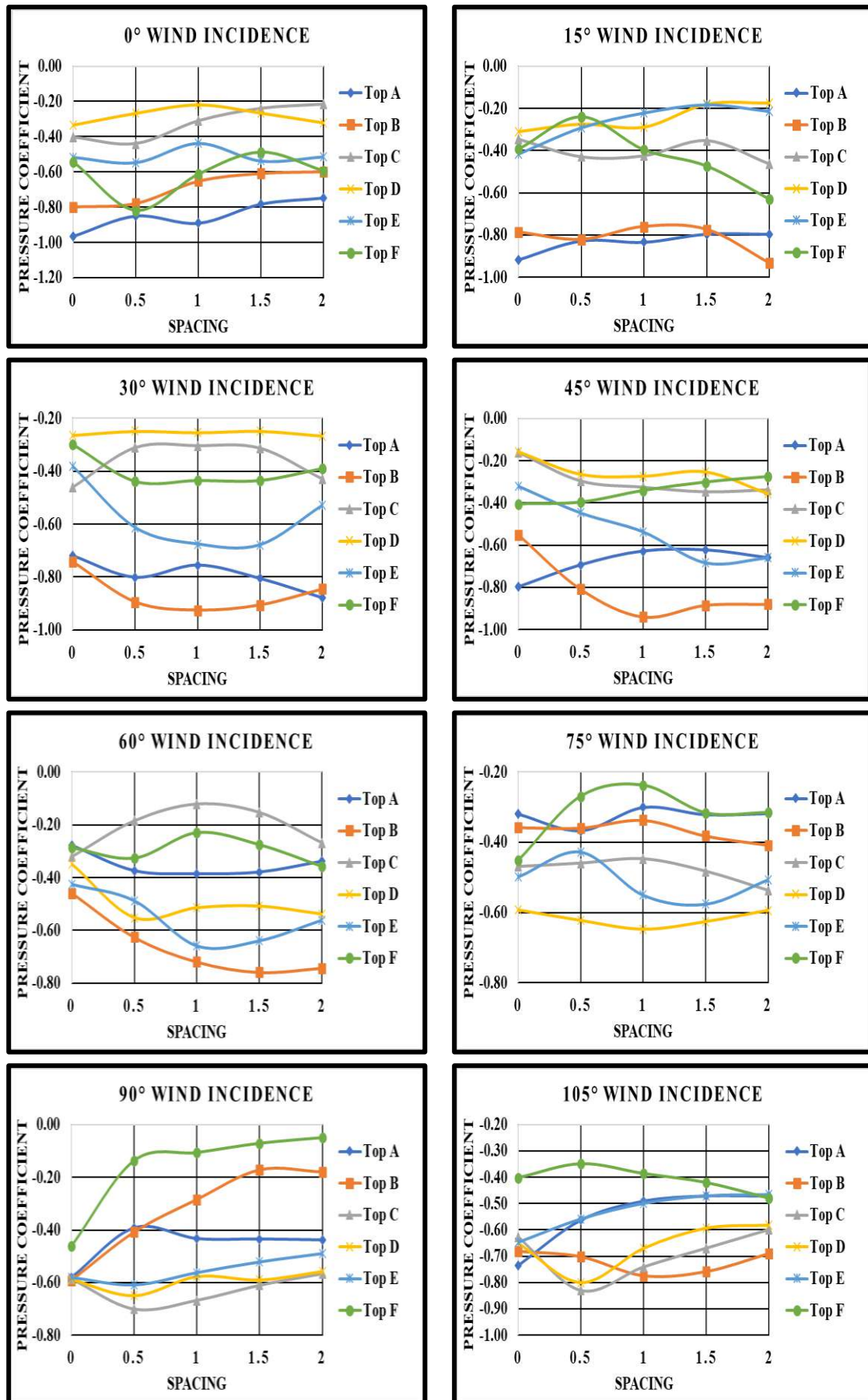
Fig. 5.23(a): Pressure Coefficient for Z pattern of Cylindrical Roof
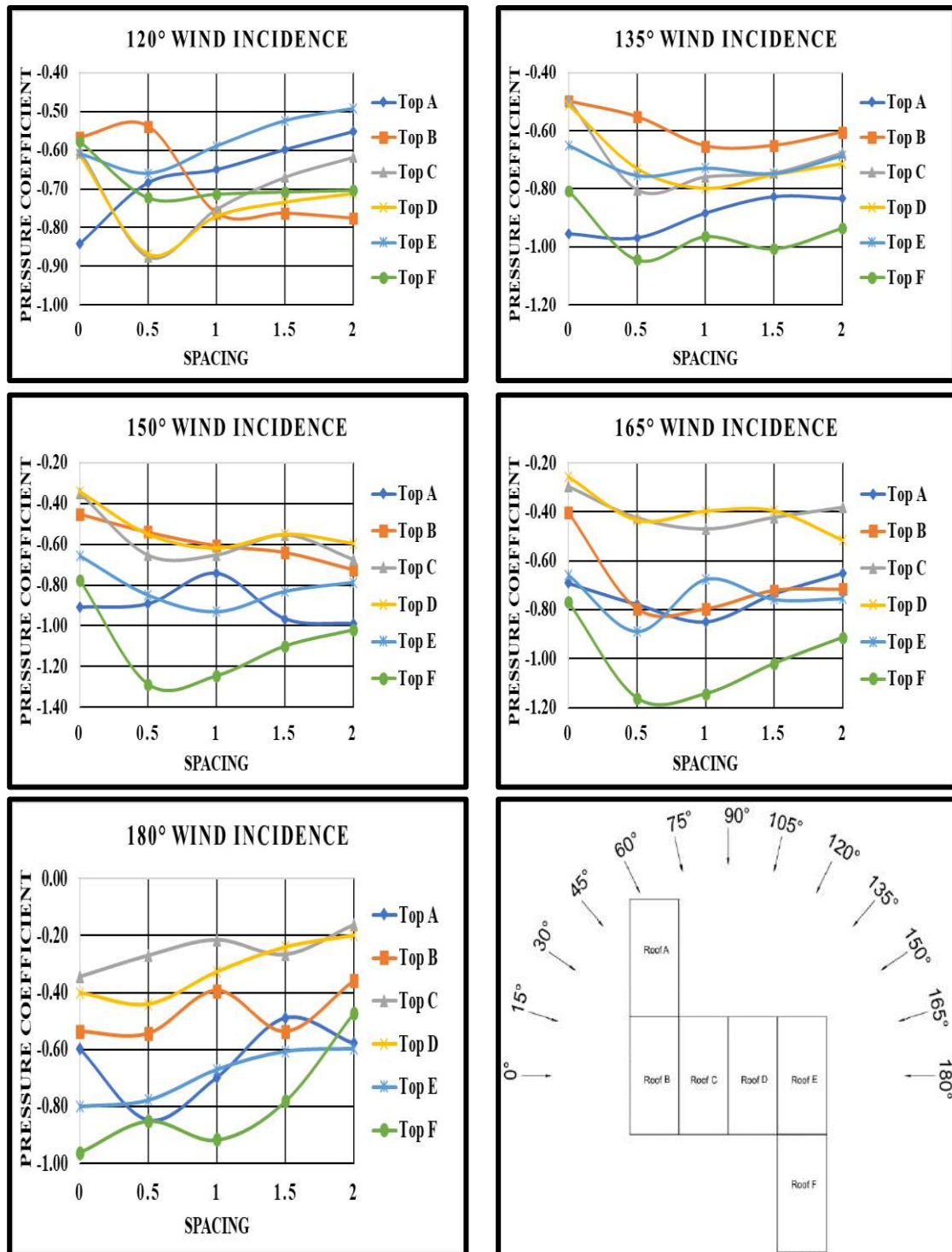
Fig. 5.23(b): Pressure Coefficient for Z pattern of Cylindrical Roof

5.3.2.3 Interference Factor (IF)

The idea of enhancement or reduction of suction or pressure on the roof is given by interference factor (*IF*) due to the presence of low-rise structure in the vicinity. The value of *IF* gets modified with respect to the spacing between the buildings and angles of wind attack. The varying magnitude of IF on cylindrical roof arranged in z pattern with variable spacing (0,0.5B,

B, 1.5B and 2B) at various angles of wind attacks i.e., 0° to 180° at 15° interval is shown in Fig. 5.24. The magnitude of *IF* is varying between the range of 1.84 to 0.11 which keeps that shows the reduction in suction on cylindrical roof by introducing the spacing between the roofs arranged in z pattern. During 0° wind angle, the value of *IF* on roof A, B and F is coming out to be more than 1 indicating that the suction on the roof is increased and on roofs C, D and E, the value if *IF* is less than 1 indicating the reduced suction on roofs during interference as compared to the isolated condition. During 15° wind angle, all the cylindrical roofs i.e., A, B, C, D, E and F are experiencing reduced suction as compared to isolated cylindrical roof. During 30° and 45° wind incidence, the only roof B is under enhanced suction (*IF* ≥1) while other roofs are under reduced suction (*IF*≤1). Till 105° angle of wind incidence, mostly the value if *IF* is less than 1 on cylindrical roofs arranged in z pattern with variable spacing. The pattern of variation of *IF* for 0° and 180° wind angles is similar to each other with only changed in behaviour of roofs i.e., the roofs which are acting as windward roofs during 0° angle of wind attack now started behaving as leeward roofs in case of 180° wind incidence angle as shown in Fig. 5.24.
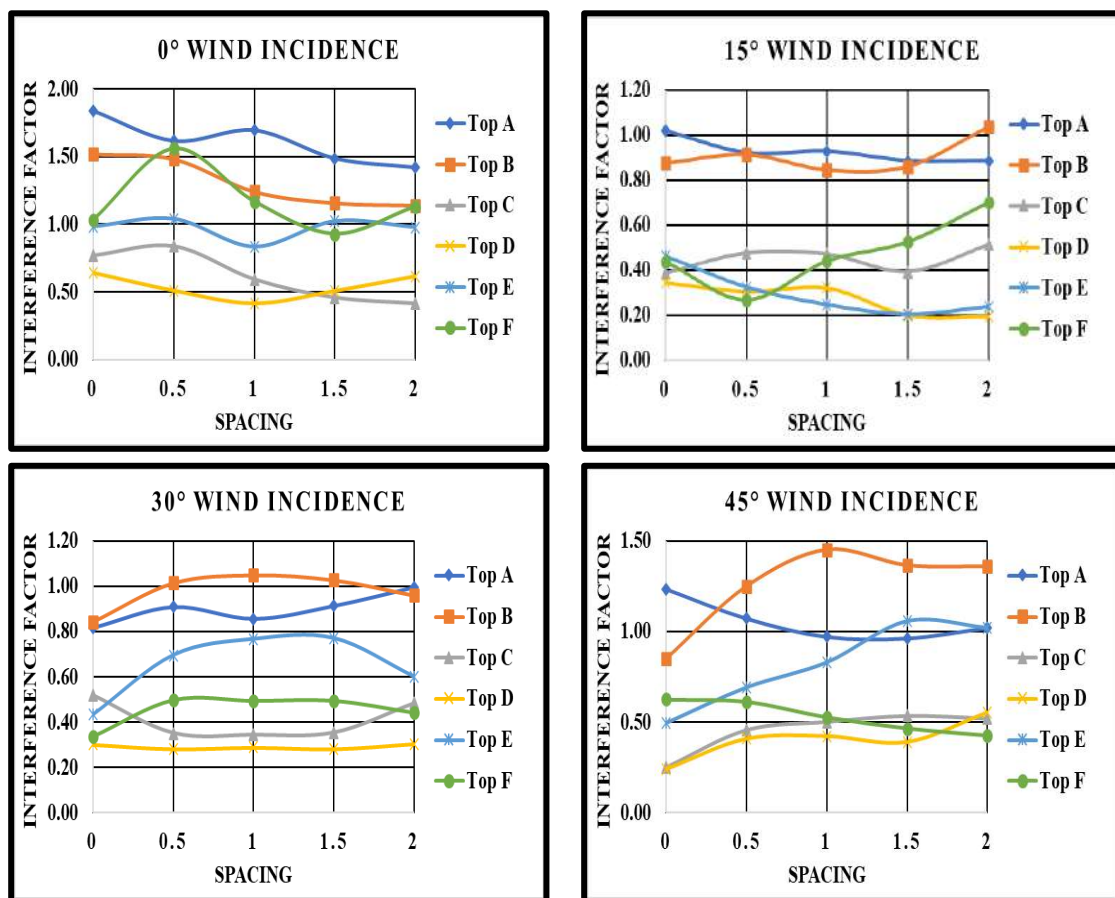
Fig. 5.24(a): Interference Factor for Z Pattern of Cylindrical Roof
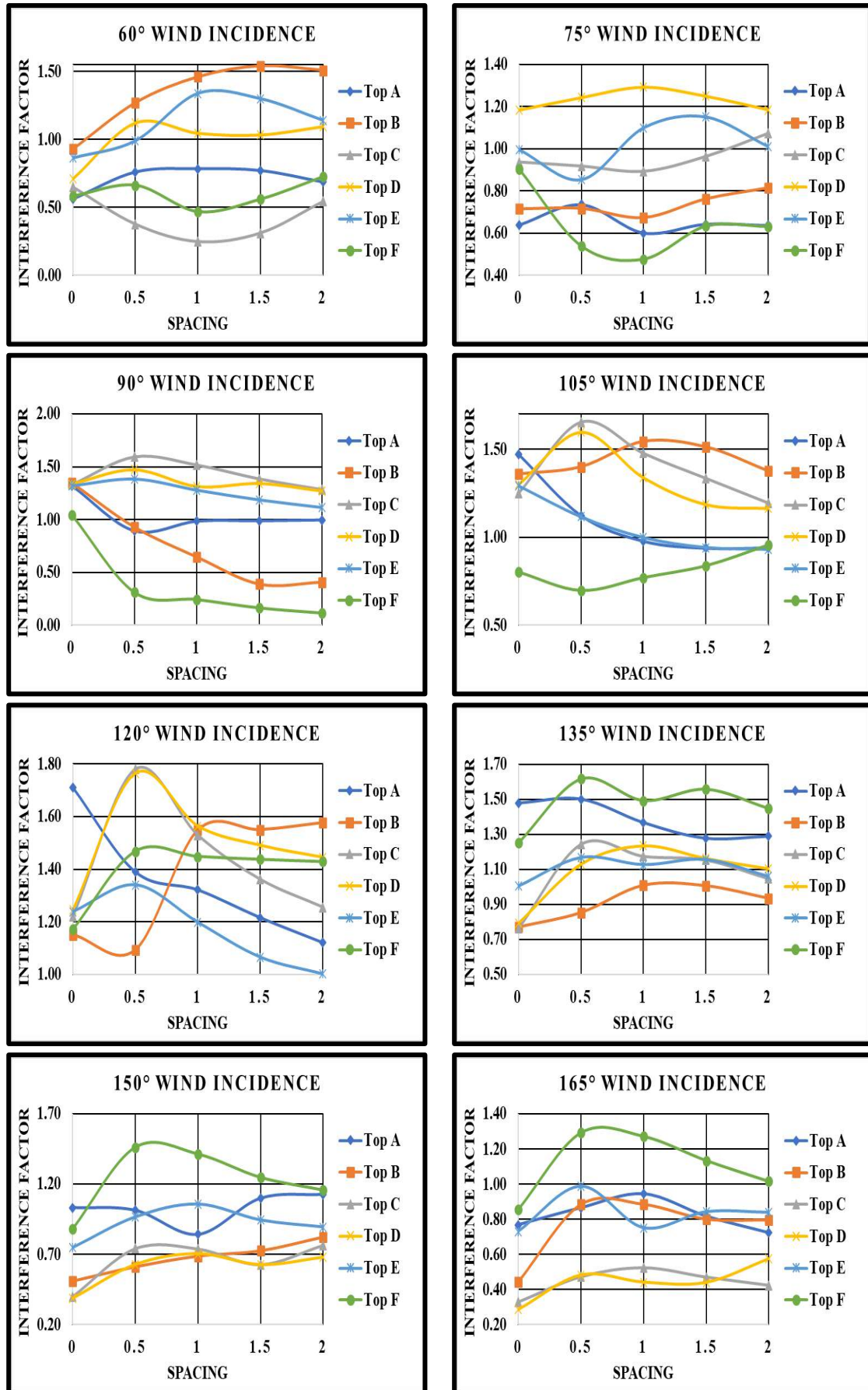
Fig. 5.24(b): Interference Factor for Z Pattern of Cylindrical Roof
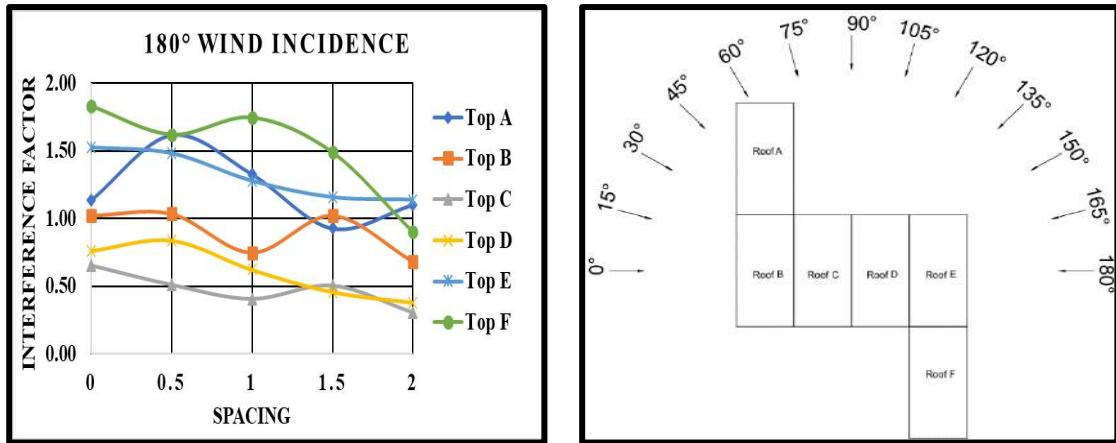
Fig. 5.24(c): Interference Factor for Z Pattern of Cylindrical Roof

5.3.2.4 Interference Difference (ID)

The difference between C_{pe} obtained during an interfering condition and C_{pe} obtained during an isolated condition is called as interference difference (*ID*), which gives an exact idea of enhancement or reduction in the wind-induced positive or negative pressure coefficient on the roofs. The variation of *ID* on cylindrical roofs arranged in a z pattern with different spacing ranging between 0 to 2B (where B is the width of a low-rise building) and at various angles of wind incidences ranging between 0° to 180° at 15° intervals is shown in Fig. 5.25. When the magnitude of negative C_{pe} on the roof is increased during interfering conditions, then the value of *ID* comes out to be negative, indicating the increased suction on the roof during interfering conditions, while the value of *ID* is positive, but the magnitude of C_{pe} is still negative on the roofs indicates that the suction on the roof is reduced due to interference of vicinity buildings. The variation of *ID* with respect to variable spacing is in the range of -0.44 to 0.76. During 0° wind angle, the value of *ID* is positive on roofs C, D and E, indicating the reduced suction on the roof due to the shielding effects of upstream buildings for all the cases of spacing i.e., 0 to 2B respectively. In case of 15° wind angle, the value of *ID* is positive on all the roofs due to the interference of nearby low-rise buildings. The only roof B is experiencing the negative *ID* at 0.5B, B and 1.5B spacing during 30° angle of wind incidence while there is positive *ID* on all other roofs. The maximum negative value of *ID* is -0.44 on roof A during 0° wind incidence at 0 spacing and on roof F during 180° wind incidence at 0 spacing respectively. Also, the maximum positive value of *ID* is 0.73 is observed on roof D during 15° wind incidence at 2B spacing. The variation of *ID* and C_{pe} of the cylindrical roof in z pattern with variable spacing and at various angles of wind incidences is similar to each other as shown in Fig. 5.25.
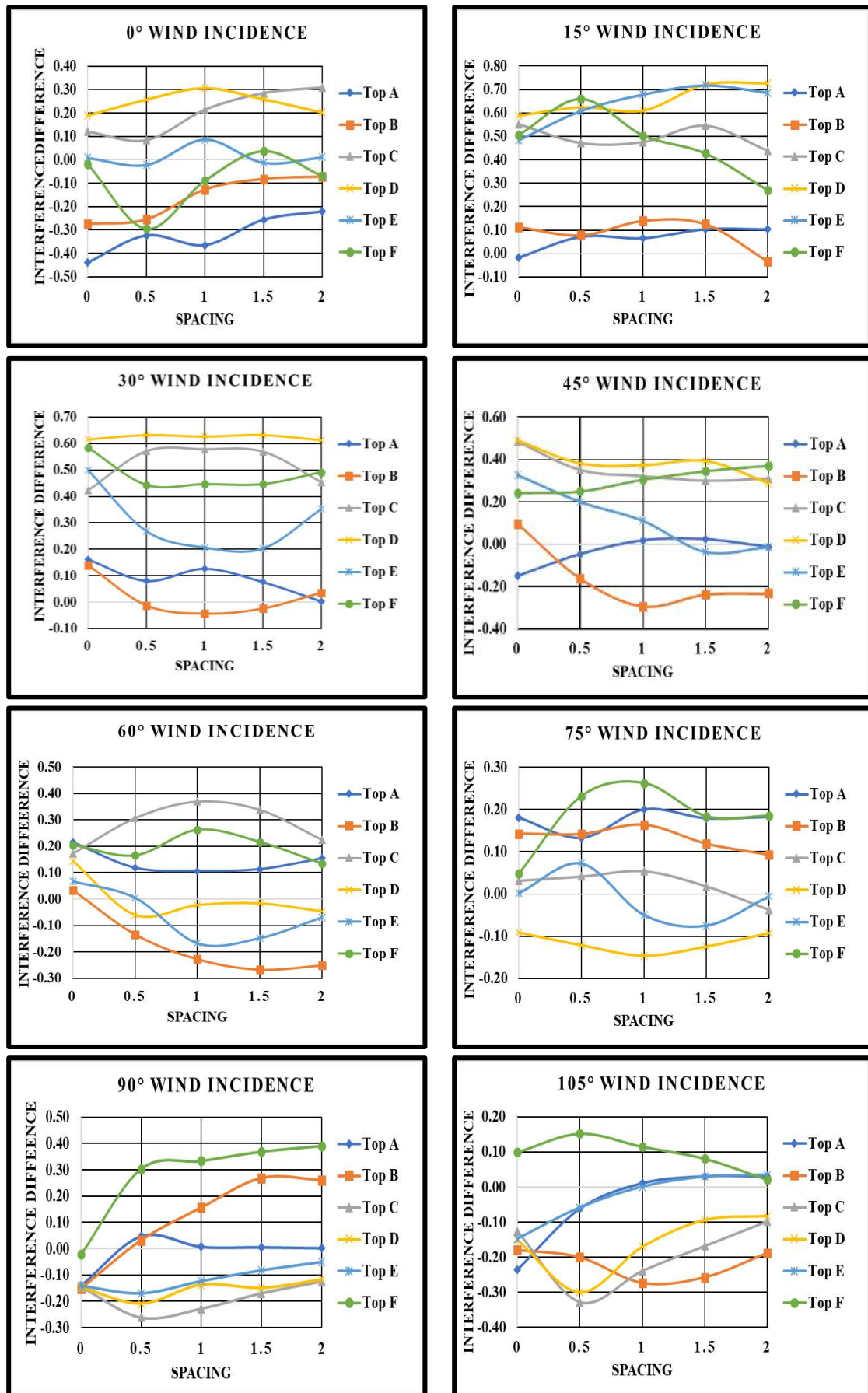
Fig. 5.25(a): Interference Difference for Z Pattern of Cylindrical Roof
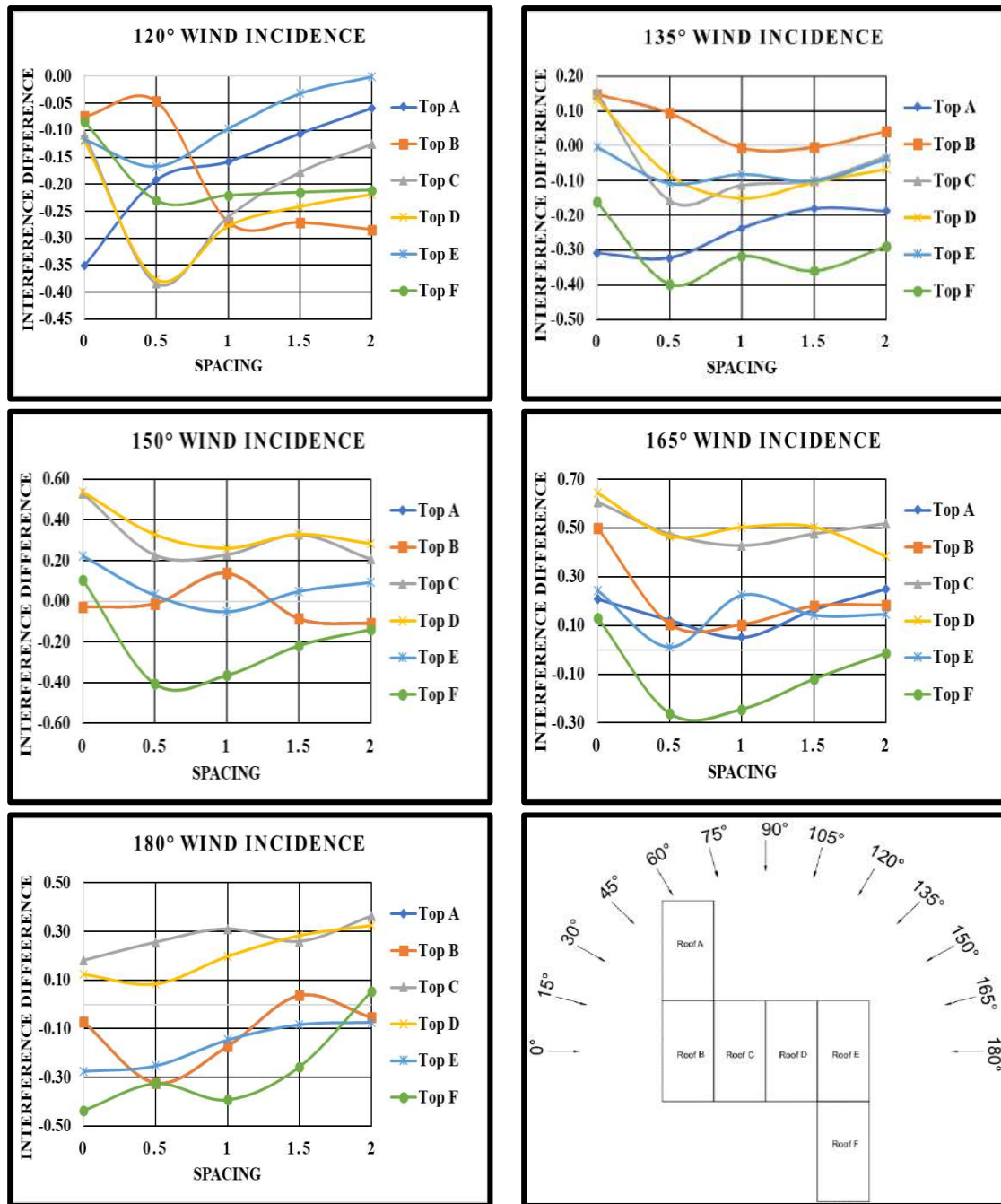
Fig. 5.25(b): Interference Difference for Z Pattern of Cylindrical Roof

5.3.2.5 Wind Flow Streamlines

The wind flow streamlines show how the wind flows around the buildings and is responsible for wind actions on the building walls and roofs. The streamlines for a z-pattern of low-rise buildings with cylindrical roofs at 15° wind intervals are shown in Figs. 5.26 – 5.30. The streamlines for cylindrical roofs are obtained at the eave height (150 mm) of the low-rise structures to analyse the wind effects on the roofs. When the wind strikes the wall and roof surface of the structures, it gets separated from the windward or upstream side, which is responsible for the generation of eddies around the building, after which the flow recirculation

and reattachment take place in the wake region of the building or downstream side. In the case of zero spacing, the eddies formation occurs on all sides of the building model other than the windward side. The building model with zero spacing behaves like a single building with multi-spans of cylindrical roofs. The length of the wake region in the downstream direction depends upon the angle of the wind attack and the pattern of the arrangement of the building, in which it is clearly predictable that the length of the wake region is lesser in the case of a rectangular pattern as compared to z pattern. The turbulence in the wind flow pattern is induced in between the buildings when spacing is increased from 0 to 2B, due to which the length of the wake region is reduced as shown in Figs. 5.26-5.30 respectively.
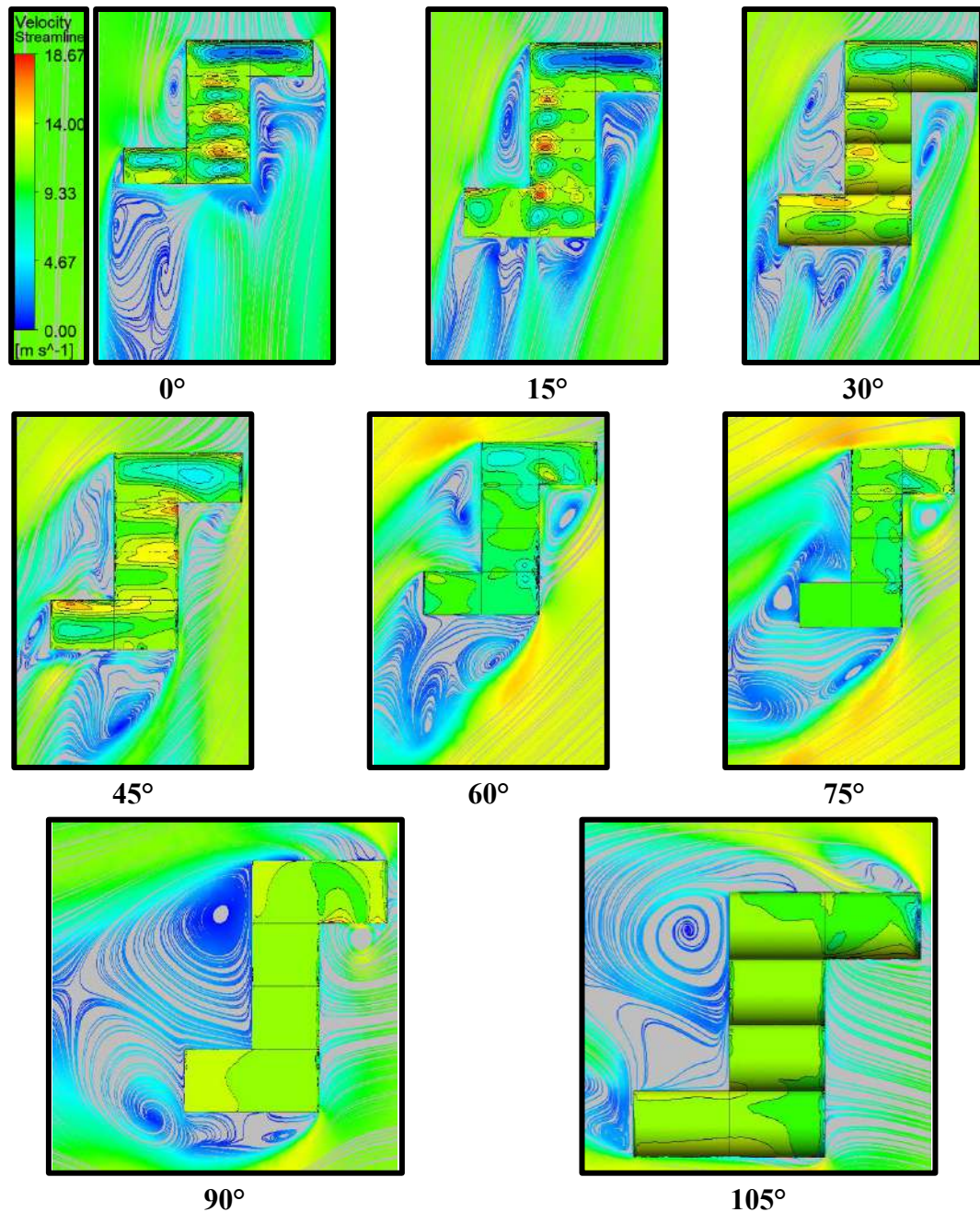
Fig. 5.26(a): Wind Flow Streamlines for Z pattern with Zero Spacing
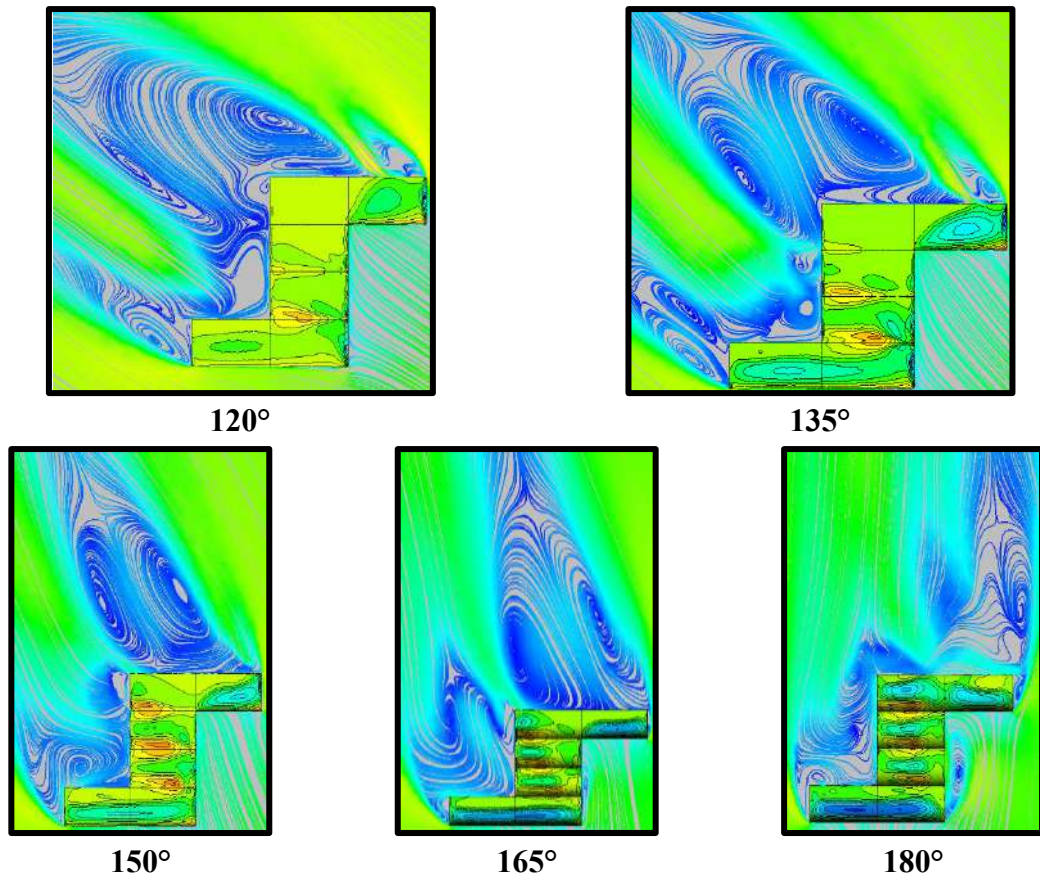
Fig. 5.26(b): Wind Flow Streamlines for Z pattern with Zero Spacing
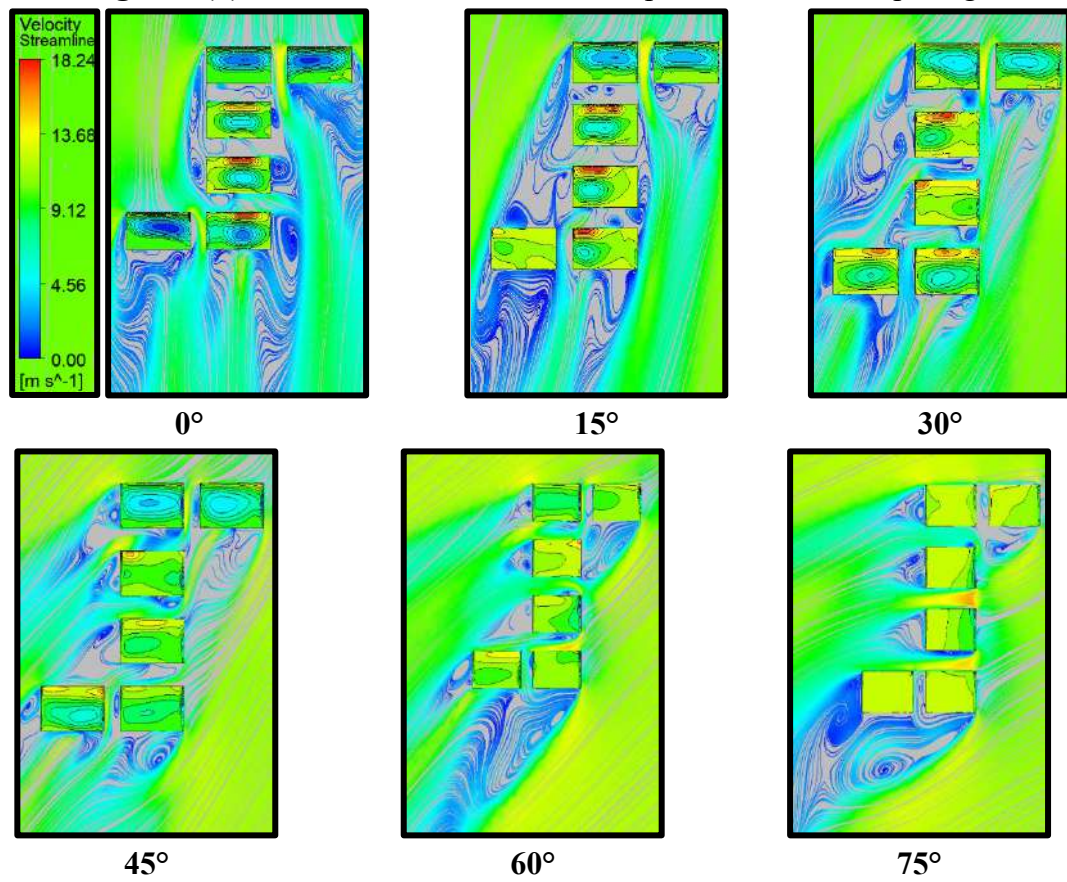
Fig. 5.27(a): Wind Flow Streamlines for Z pattern with 0.5B Spacing

90°

105°

120°

135°

150°

165°

180°
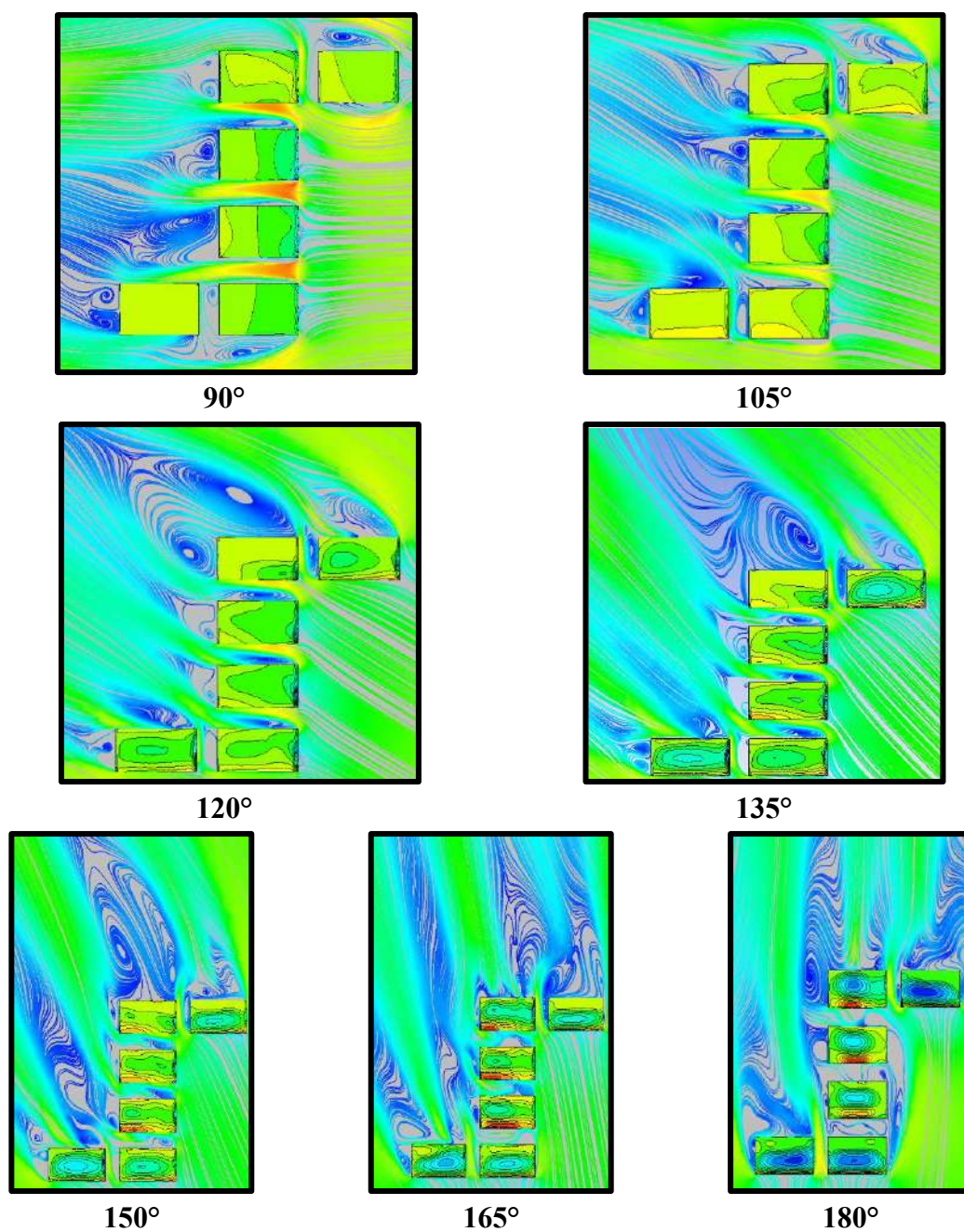
Fig. 5.27(b): Wind Flow Streamlines for Z pattern with 0.5B Spacing

0°

15°

30°

Fig. 5.28(a): Wind Flow Streamlines for Z pattern with B Spacing

45°

60°

75°

90°

105°

120°

135°

150°

165°

180°
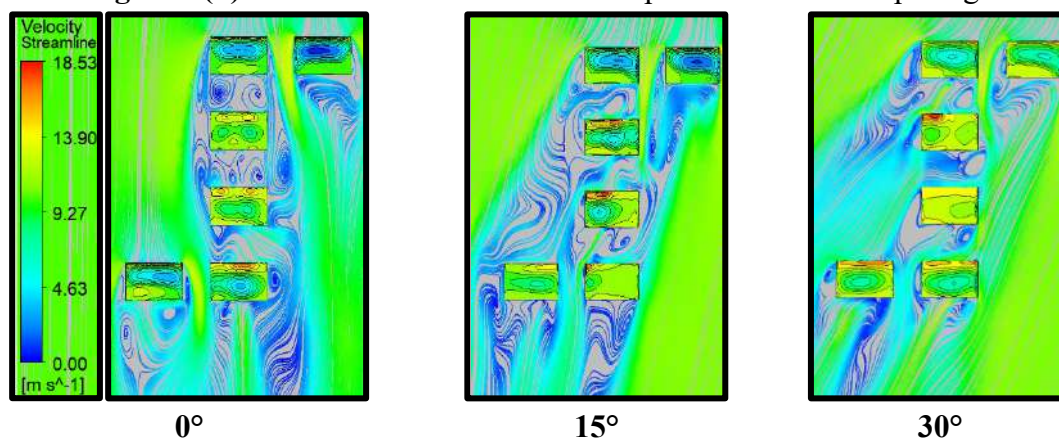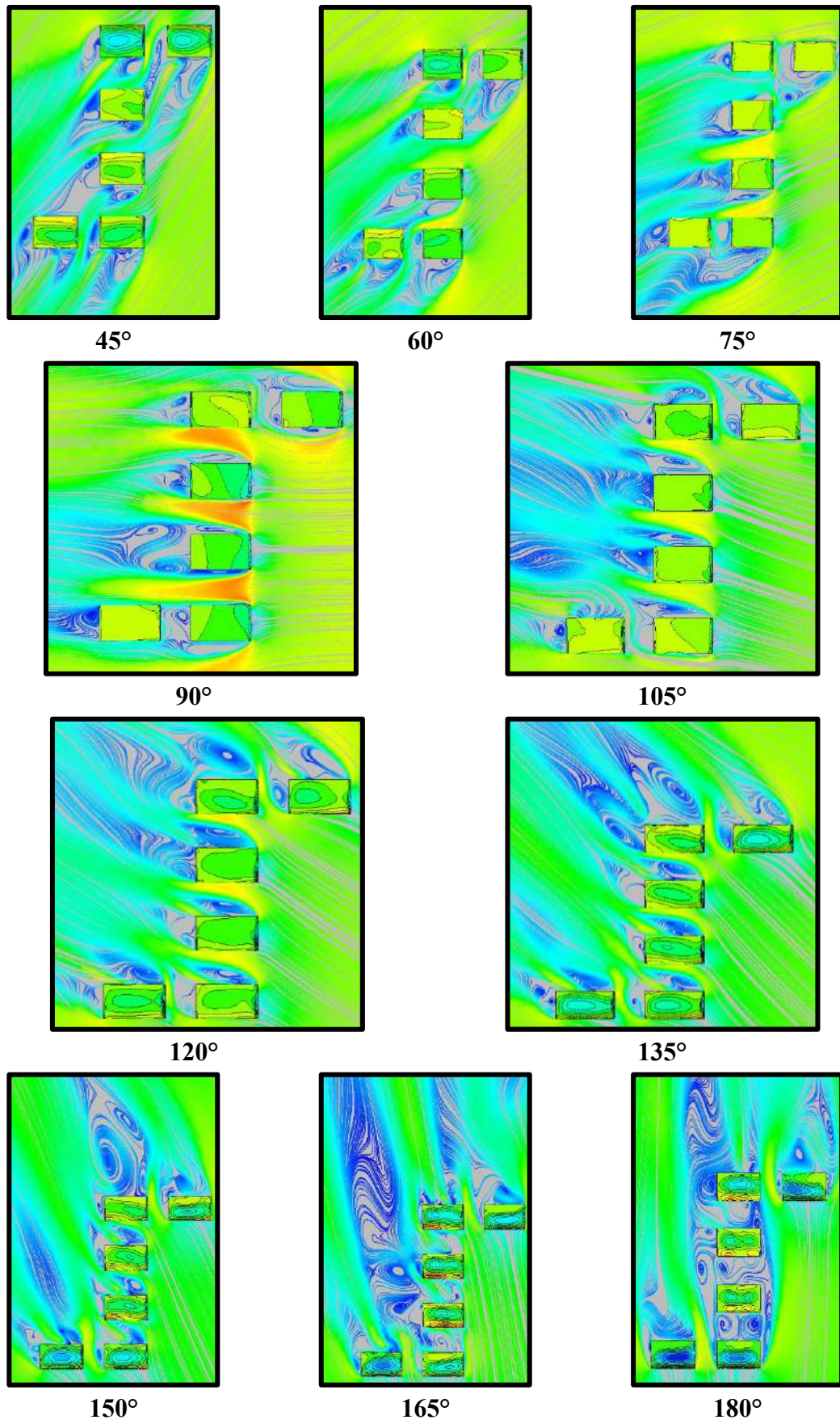
Fig. 5.28(b): Wind Flow Streamlines for Z pattern with B Spacing
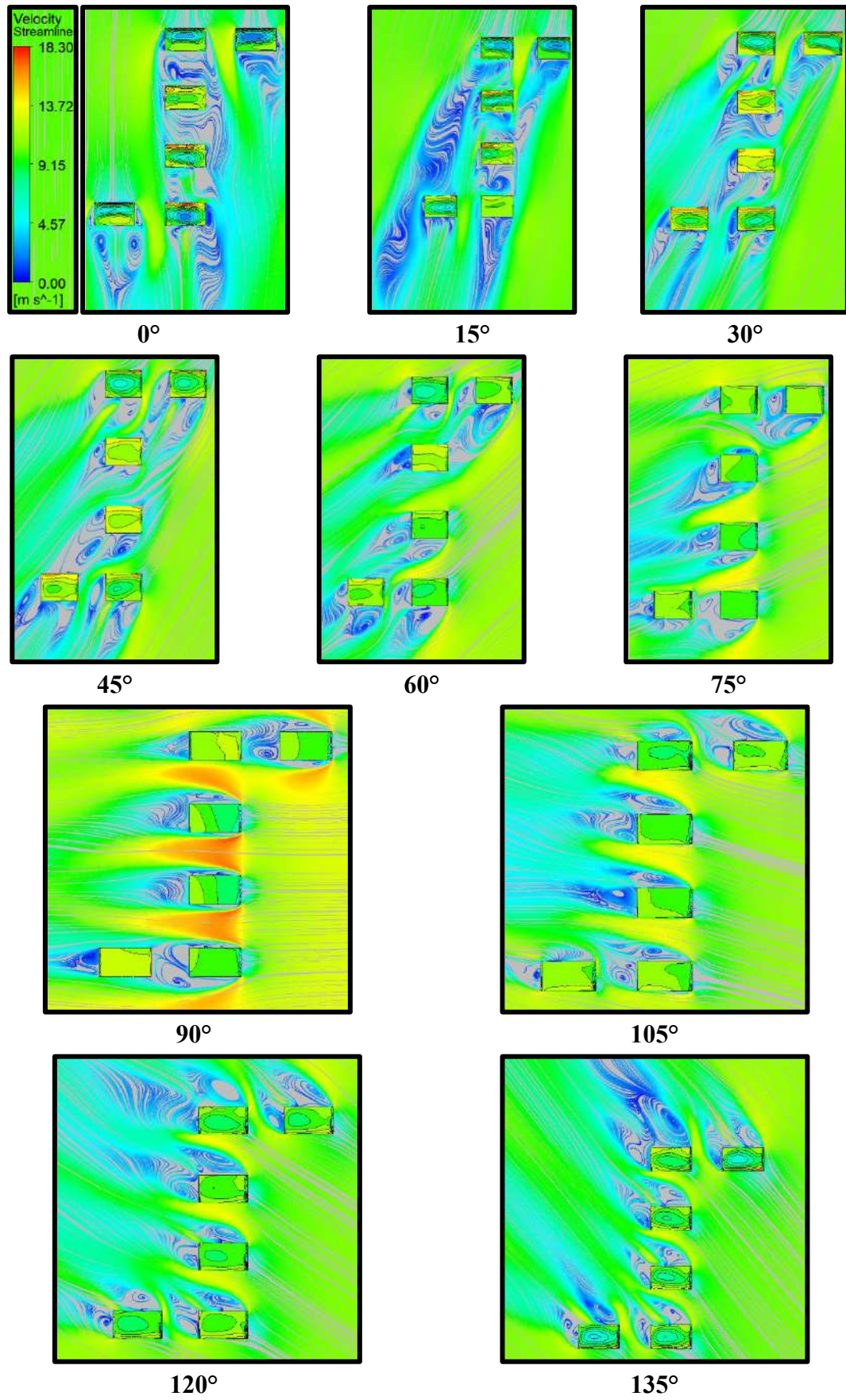
Fig. 5.29(a): Wind Flow Streamlines for Z pattern with 1.5B Spacing

Fig. 5.29(b): Wind Flow Streamlines for Z pattern with 1.5B Spacing

150°   165°   180°

0°   15°   30°

45°   60°   75°

90°   105°
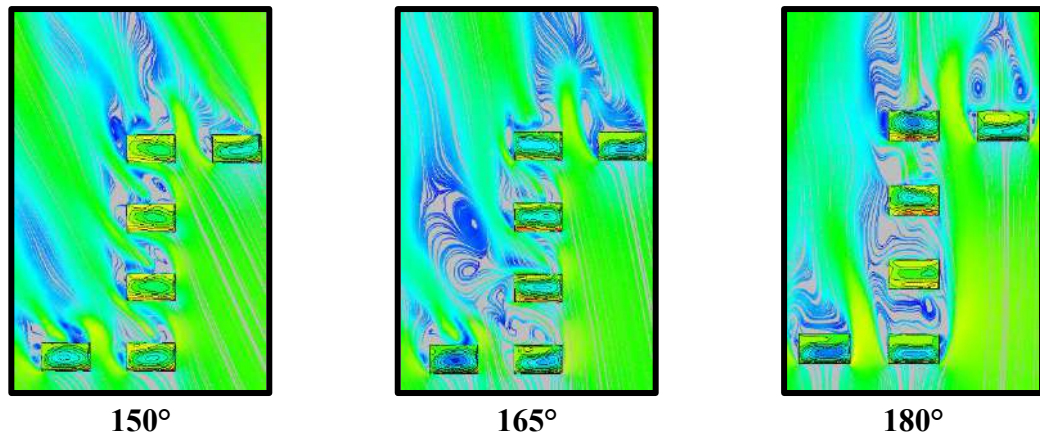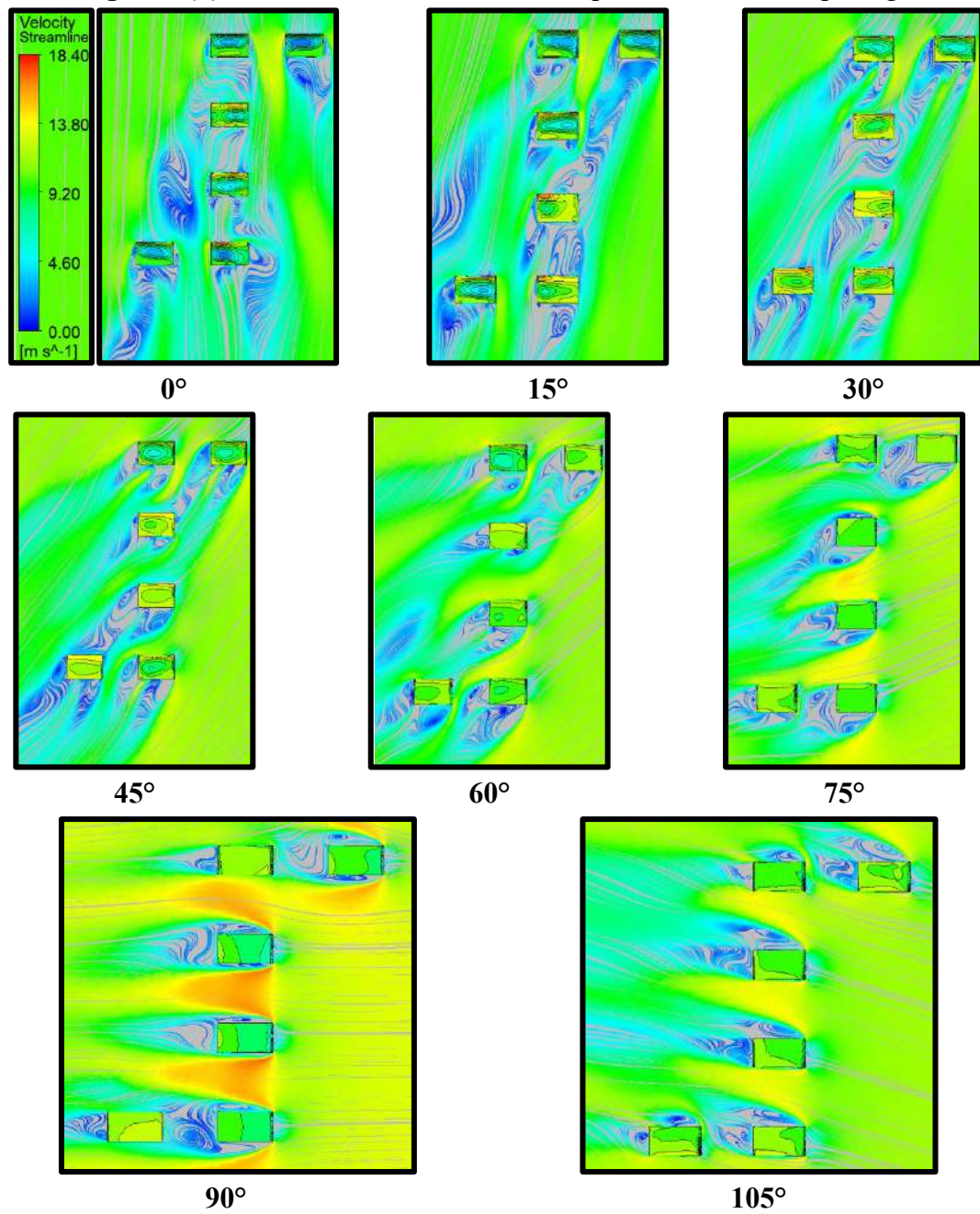
Fig. 5.30(a): Wind Flow Streamlines for Z pattern with 2B Spacing
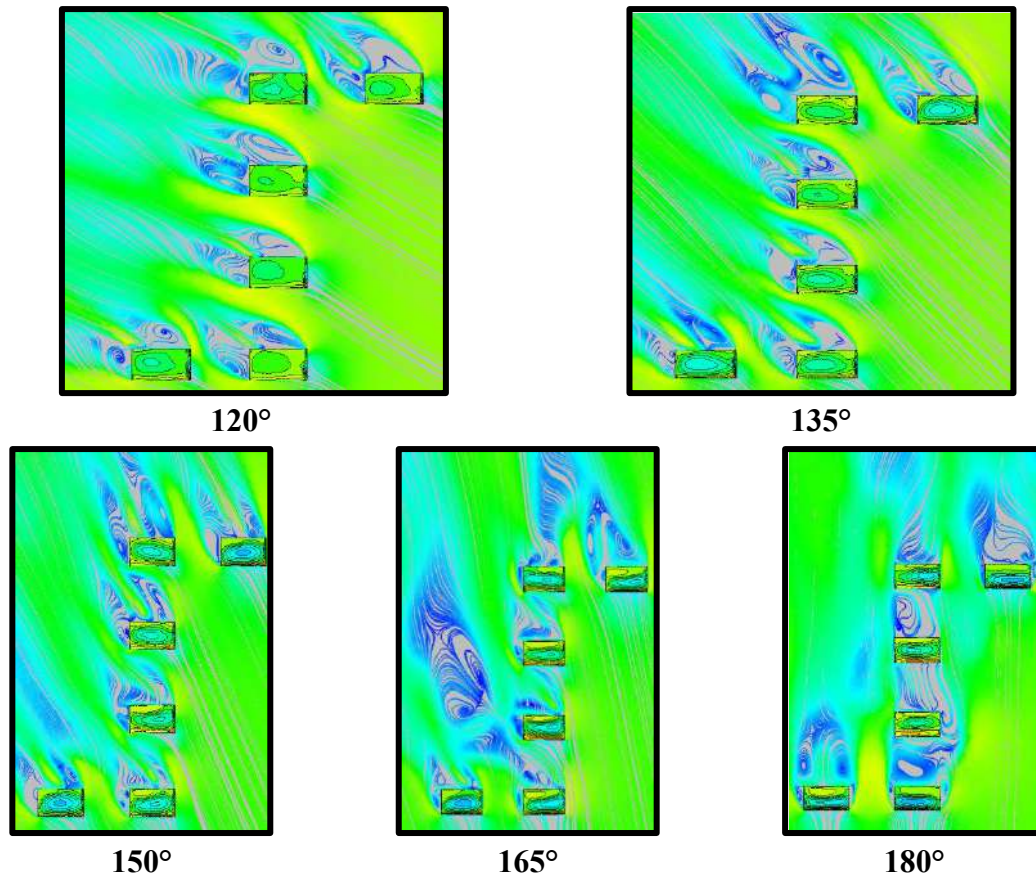
Fig. 5.30(b): Wind Flow Streamlines for Z pattern with 2B Spacing

5.3.3 T Pattern

This section contains a detailed description of the variation of pressure contours, pressure coefficients, IF and ID over the cylindrical roofs arranged in a T pattern with variable spacing, i.e., 0, 0.5B, B, 1.5B and 2B at different angles of wind incidence such that 0° to 180° at 15° wind interval.

5.3.3.1 Pressure Contours

The pressure distribution on cylindrical roofs arranged in a T pattern with zero spacing is shown in Fig. 5.31, in which the maximum suction is acting on the apex portion of roofs A, B and C during 0° and 15° wind intervals. The wind-induced pressure on the cylindrical roof arranged in a T pattern varies between the range of -71.50Pa to -3.16Pa. After comparing the pressure on cylindrical between isolated and interfering conditions, it is found that the negative pressure got reduced by 86.53% when the spacing is 2B. There are small portions on the roofs subjected to the positive wind pressure distribution from the upstream side, and this pressure completely vanishes when the wind angle changes from 60° to 105° indicating that the whole roof is only experiencing the negative pressure. During a 90° angle of wind attack, there is uniform pressure distribution on roofs D, E and F. When the wind angle changes from 135° to 180°, the leeward

portion of roof F, the small area on the junction of roofs F and E, E and D, D and B, leeward portion of roofs A and C. The pressure distribution is similar of roofs A and C during 180° angle of wind attack due to symmetrical wind flow on both sides of roofs D, E and F. The role of interference is mainly attributed to the roof B, D, E and F, since these roofs are under a single line placed back-to-back each other that is why when the spacing is varying, the pressure contours also change on these roofs. When the spacing is increased to B, the magnitude of positive pressure distribution which is acting on windward portions of all the roofs is increased as compared to zero spacing model of T pattern. During 75° wind angle of 0.5B spacing model, the overall impact of wind pressure is positive on all the cylindrical roofs and this positive impact is converted into negative pressure distribution when spacing is B and 1.5B respectively at 75° angle of wind attack. The wind pressure distribution on cylindrical roofs arranged in T pattern with variable spacing (0, 0.5B, B, 1.5B, 2B) at different angles (0° to 180°) of wind incidence at 15° interval is shown in Figs. 5.31-5.35.
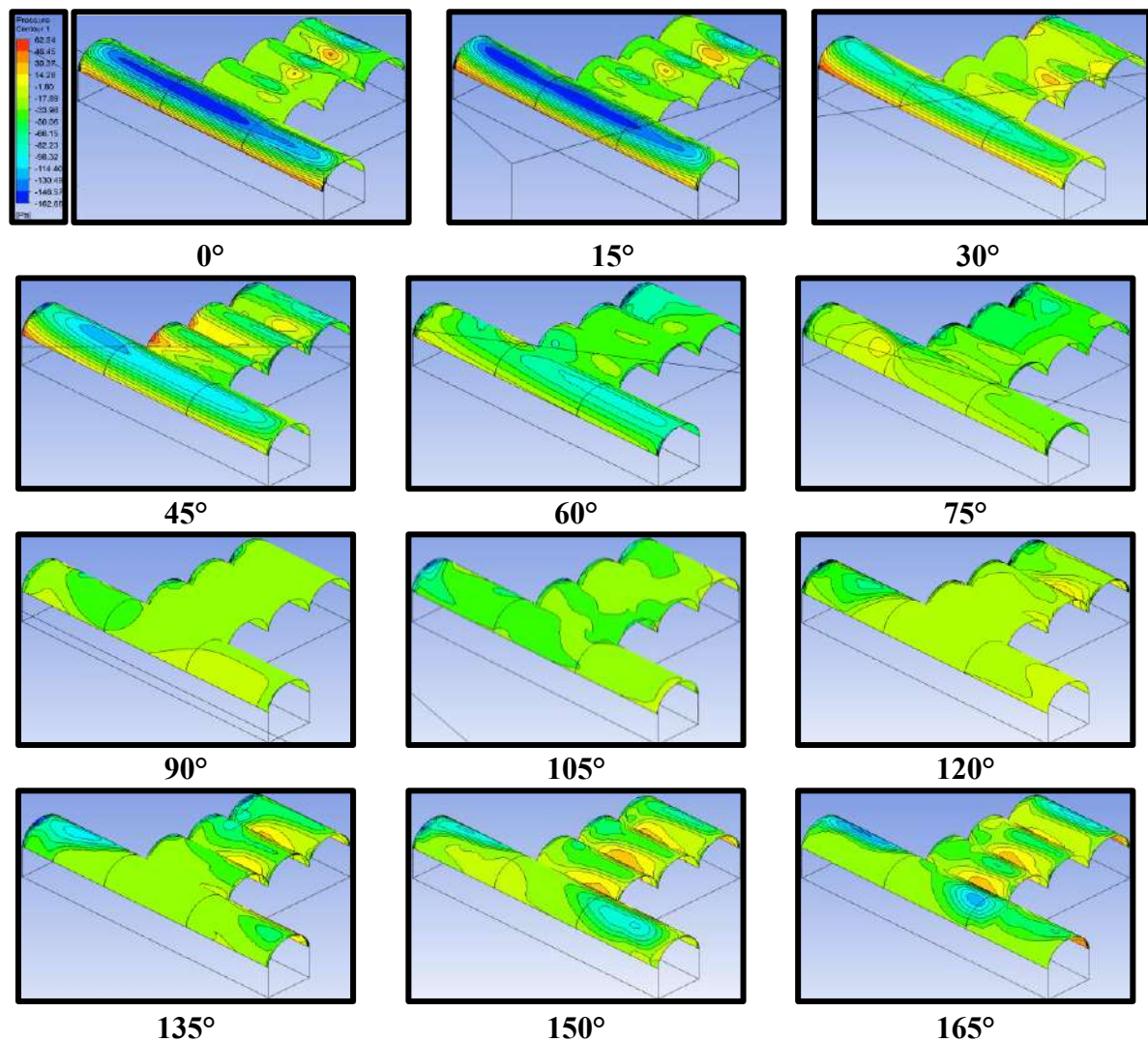
Fig. 5.31(a): Pressure Contours for T pattern with Zero Spacing
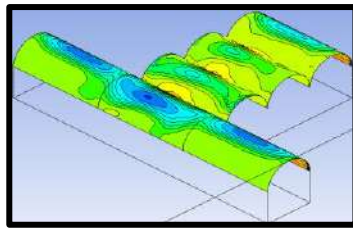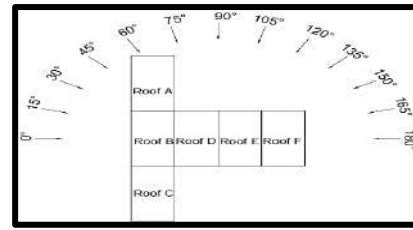
180° **Roof Nomenclature and Wind Angles**

Fig. 5.31(b): Pressure Contours for T pattern with Zero Spacing

0° **15°** **30°**

45° **60°** **75°**

90° **105°** **120°**

135° **150°** **165°**

180° **Roof Nomenclature and Wind Angles**
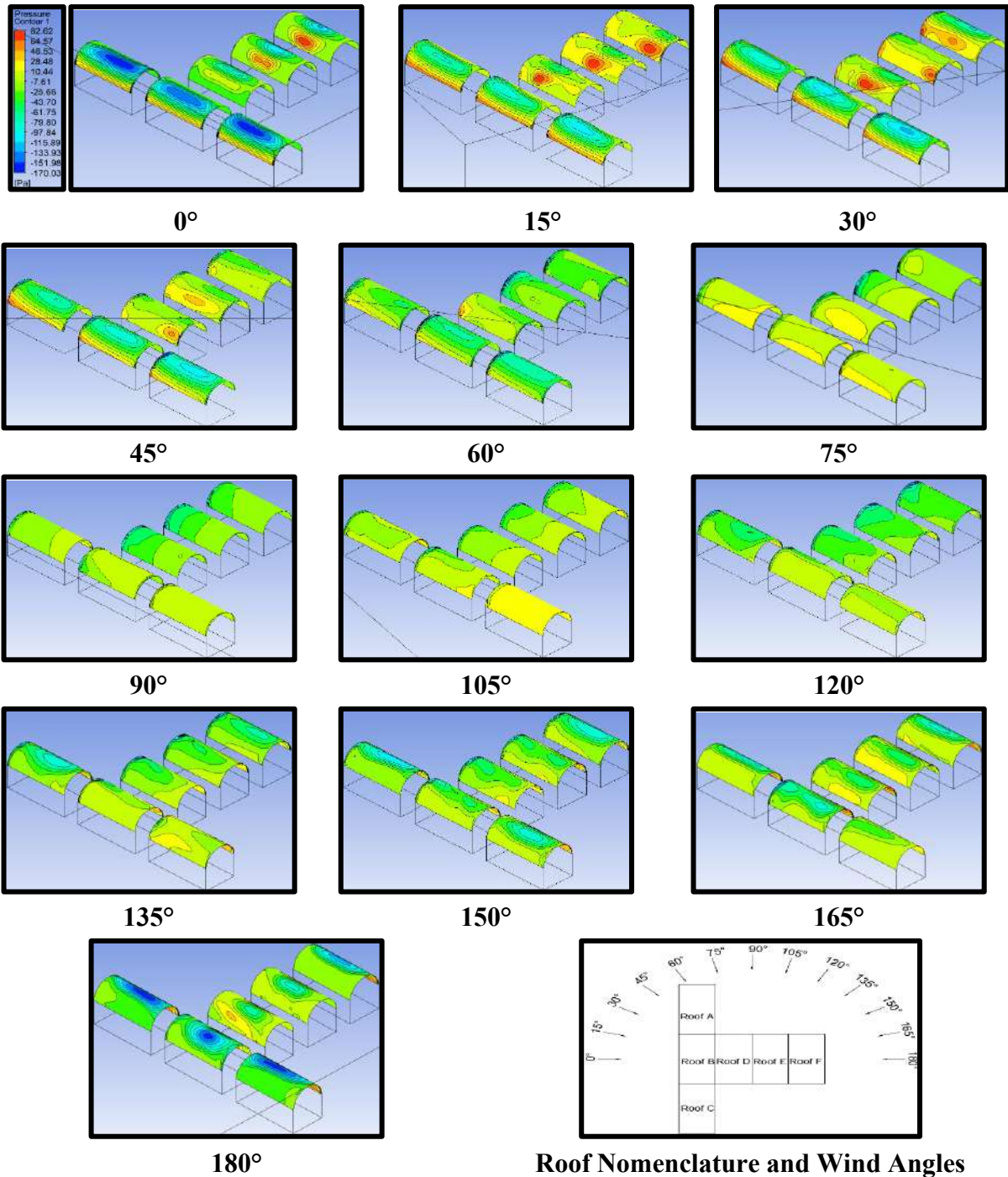
Fig. 5.32: Pressure Contours for T pattern with 0.5B Spacing
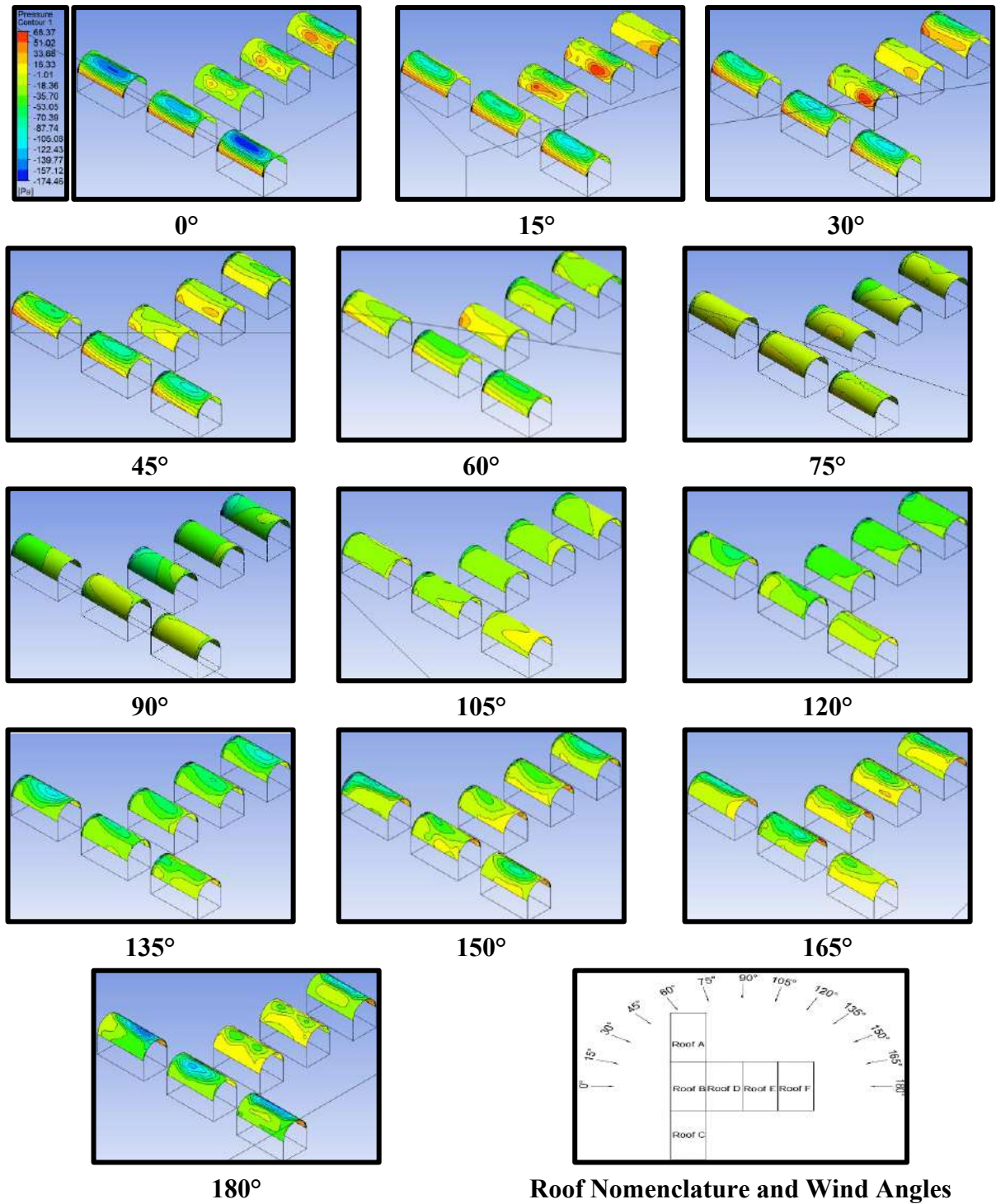
Fig. 5.33: Pressure Contours for T pattern with B Spacing

Fig. 5.34(a): Pressure Contours for T pattern with 1.5B Spacing

45°

60°

75°

90°

105°

120°

135°

150°

165°

180°

Roof Nomenclature and Wind Angles
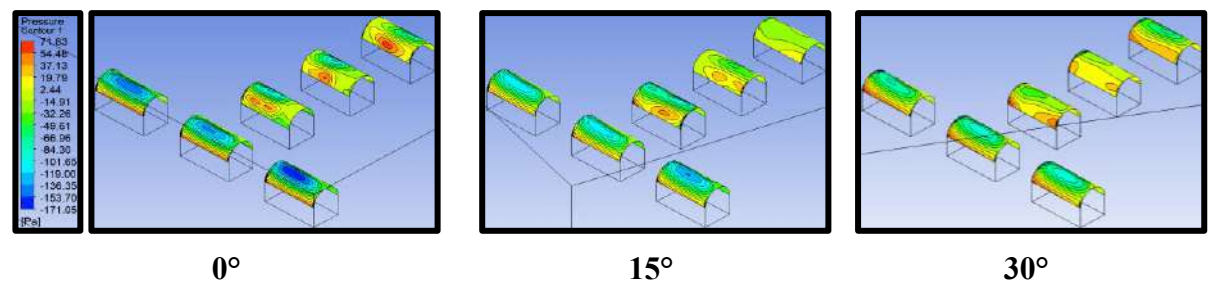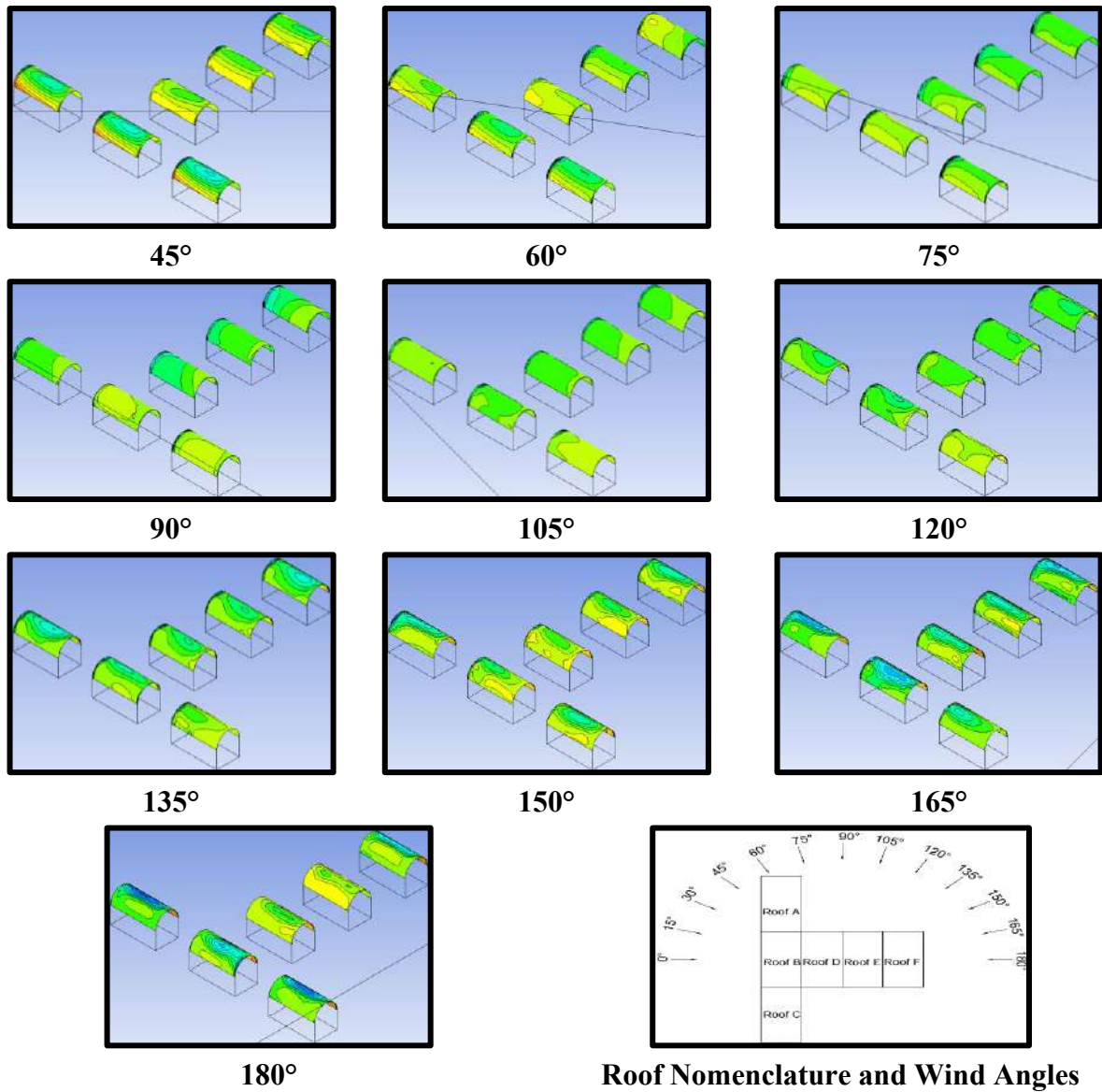
Fig. 5.34(b): Pressure Contours for T pattern with 1.5B Spacing

0°

15°

30°

45°

60°

75°

Fig. 5.35(a): Pressure Contours for T pattern with 2B Spacing

90° **105°** **120°**

135° **150°** **165°**

180° **Roof Nomenclature and Wind Angles**
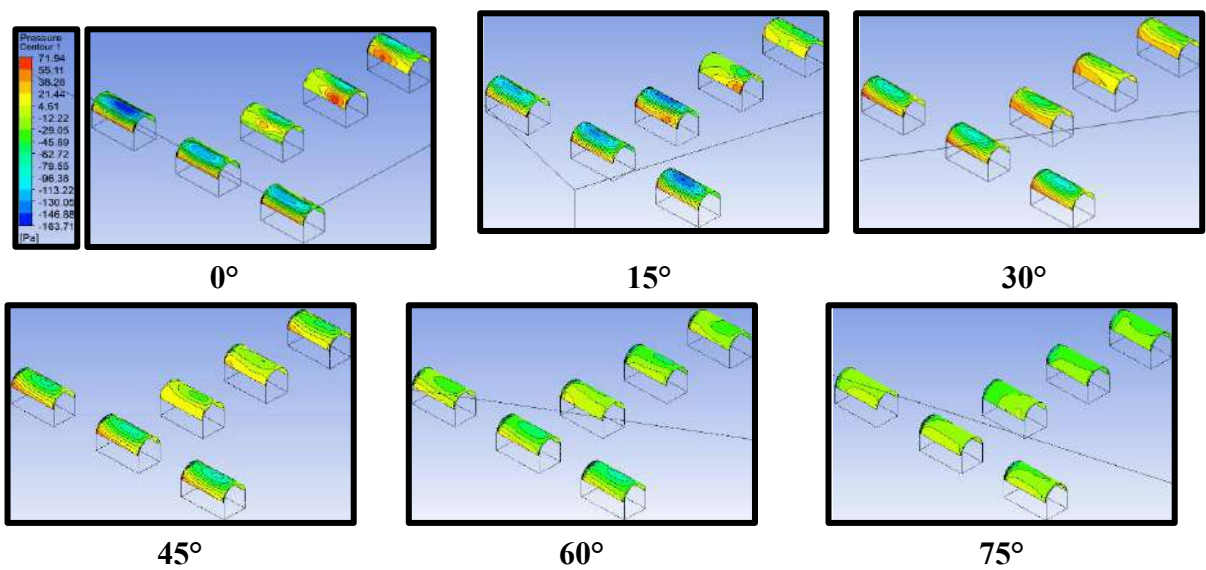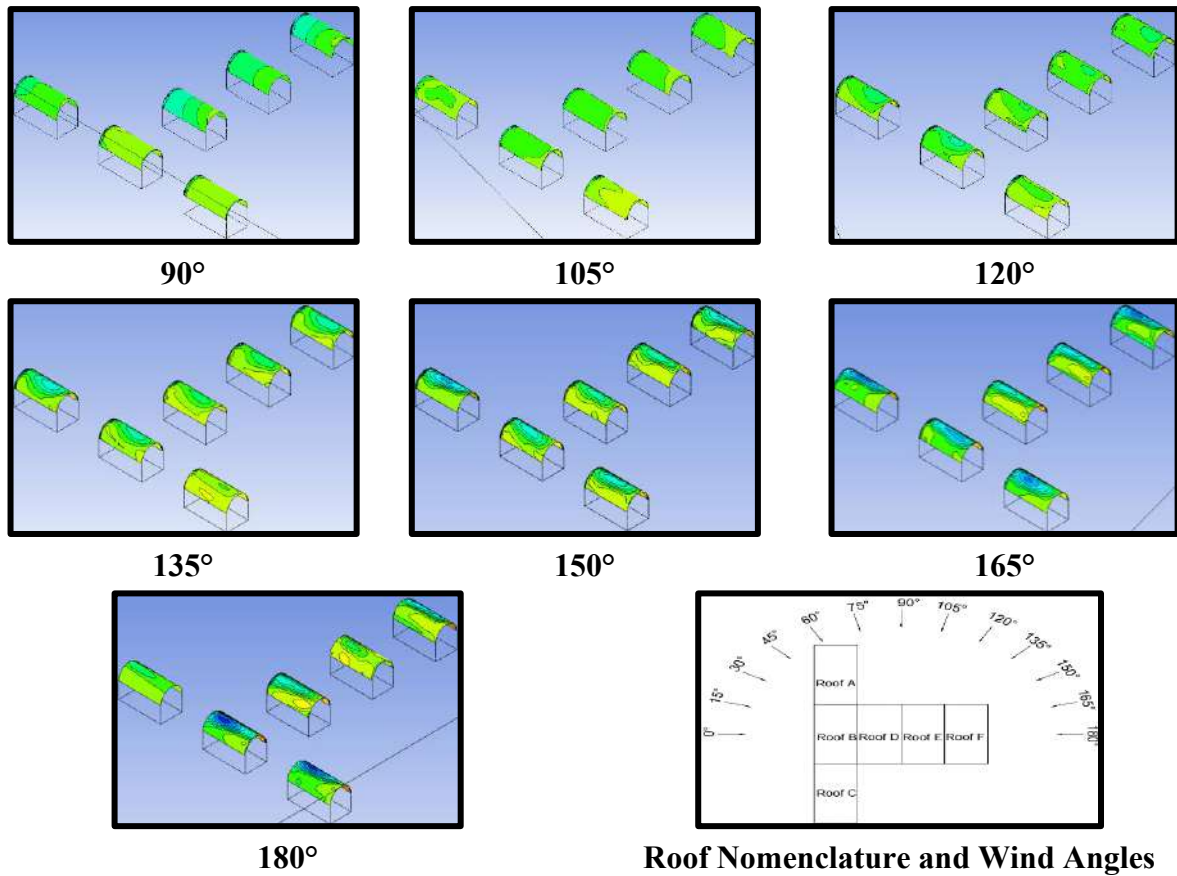
Fig. 5.35(b): Pressure Contours for T pattern with 2B Spacing

5.3.3.2 Pressure Coefficient (C_{pe})

While comparing the C_{pe} of interfering cylindrical roofs with an isolated cylindrical roof, the C_{pe} on roofs A, B, and C is increased in the T pattern of the zero spacing model since these roofs are windward and are under direct wind attack. The reduction in C_{pe} is observed on cylindrical roofs arranged in T pattern i.e., -1.17 to -0.07 (86.79% reduction), when the spacing is increased from zero to 2B. However, the C_{pe} on roofs D, E, and F is reduced due to interference from roofs A, B, and C. The increased value of C_{pe} on roofs A and B started decreasing when the wind angles changed from 45° to 105°. The maximum suction on roof A with C_{pe}= -1.01 is noted at 15° wind attack in the zero spacing model, and the minimum suction is when C_{pe}= -0.29 during 75° wind angle in the B spacing model. When the wind incidence angle is in between 90° to 135°, the suction on roofs D and E is increased as compared to isolated cylindrical roof. the maximum negative C_{pe}= -0.81 on roofs D and -0.84 on roof E during 120° angle of wind attack. The overall variation of C_{pe} with respect to wind incidence angles and variable spacing is shown in Fig. 5.36. The role of interference is mainly attributed to the roof B, D, E and F, since these roofs are under a single line placed back-to-back each

other that is why when the spacing is varying, the pressure coefficient also changes on these roofs.
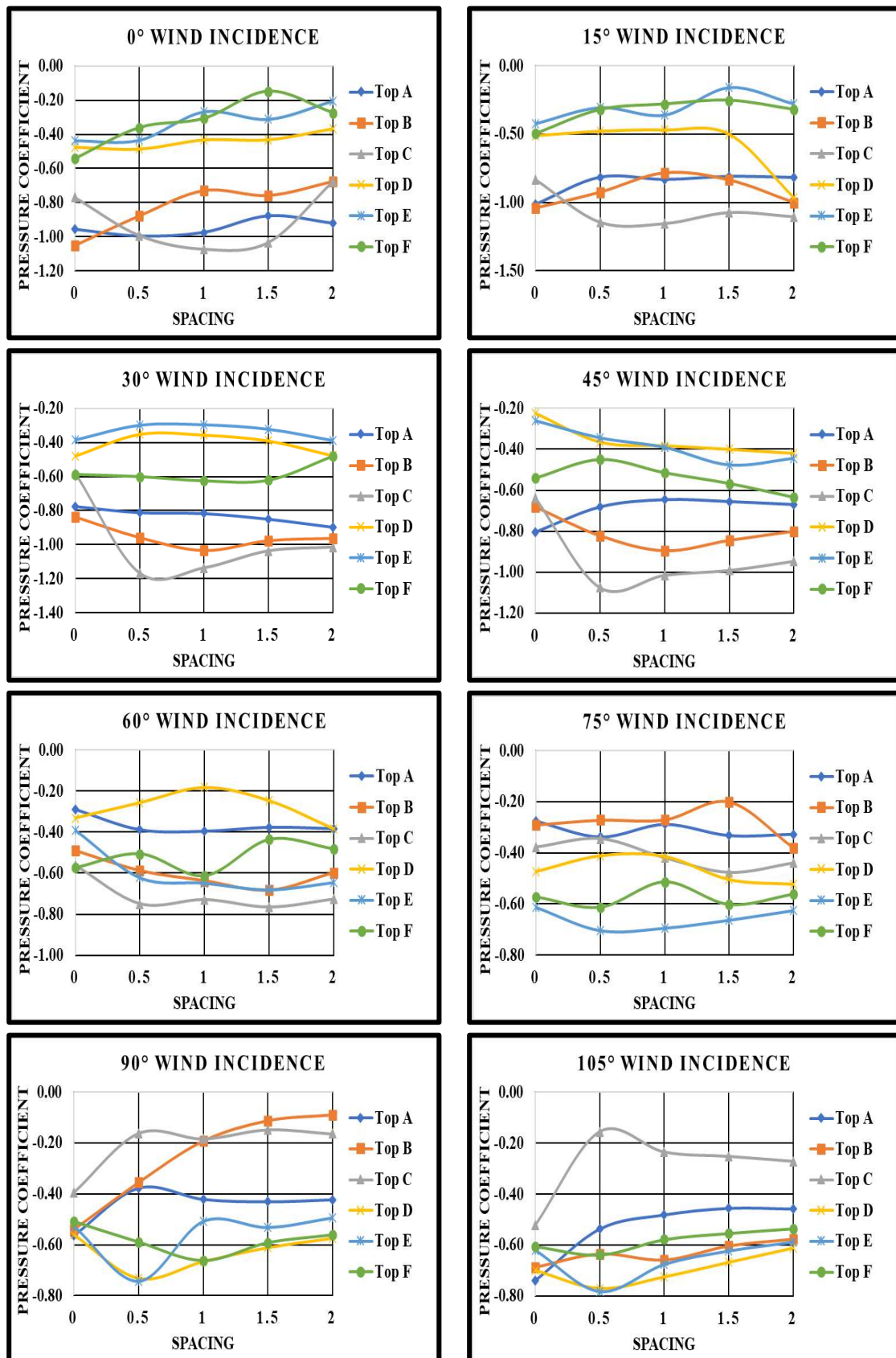
Fig. 5.36(a): Pressure Coefficient for T pattern with variable Spacing
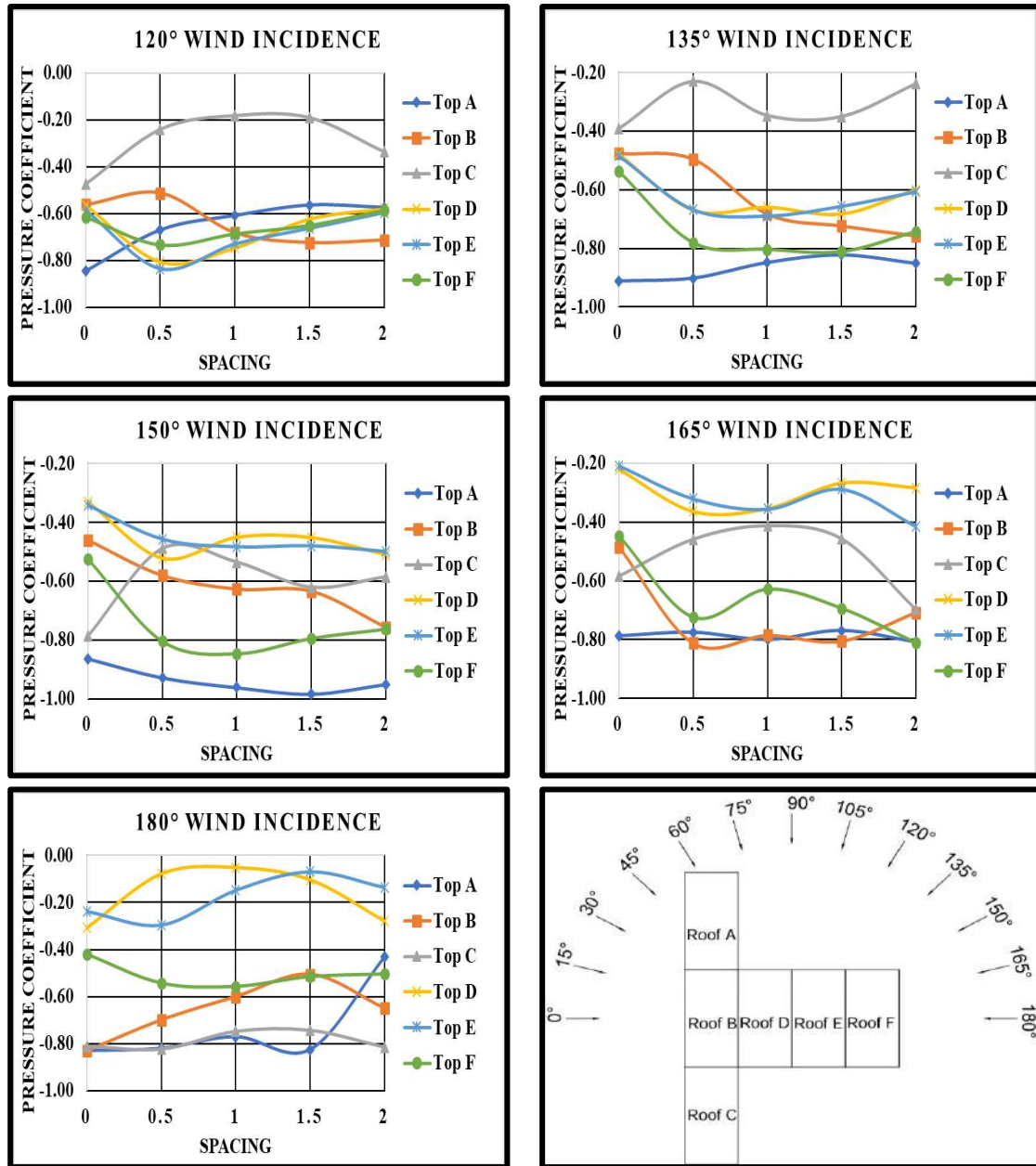
Fig. 5.36(b): Pressure Coefficient for T pattern with variable Spacing

5.3.3.3 Interference Factor (IF)

The ratio of $C_{pe(interfering)}$ to $C_{pe(isolated)}$, i.e., *IF*, varies with respect to variable spacing and angle of wind incidence when low-rise structure with cylindrical roofs is arranged in a T pattern as shown in Fig. 5.37. The range of variation of *IF* lies between 2.05 and 0.1, which keeps on reducing by changing the spacing between cylindrical roofs from zero to 2B. As already mentioned, the suction on roofs A, B and C is increased as compared to an isolated cylindrical roof, due to which the value of *IF* is coming to be more than 1, denoting the increased suction on roofs. The maximum value of *IF* is 1.90 on roof A in case of 0.5B spacing at 0° wind incidence, and the minimum value of *IF* is 0.55 when the spacing is zero at 75° wind incidence.

The roofs D, E and F are under less suction than the isolated cylindrical roof, which, in turn, is responsible for *IF* less than 1. The value of *IF* on roof D is more than 1 only in the case of 90°, 105° and 120° wind angles, while on other angles, the *IF* is less than 1. The roofs E and F experiences the *IF* less than 1 when the wind angle ranges between 0° to 45° and 150° to 180° respectively.
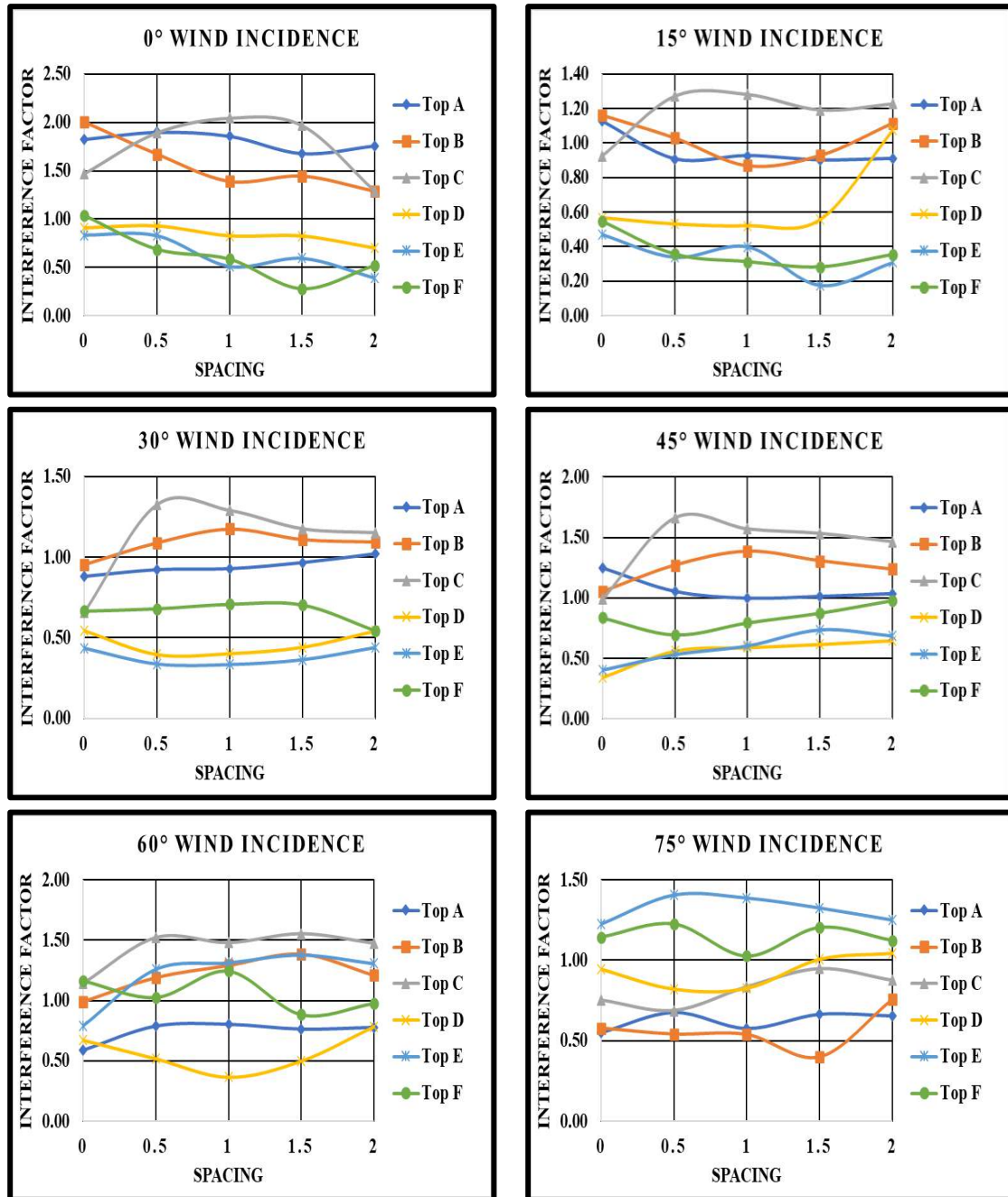
Fig. 5.37(a): Interference Factor for T pattern with variable Spacing
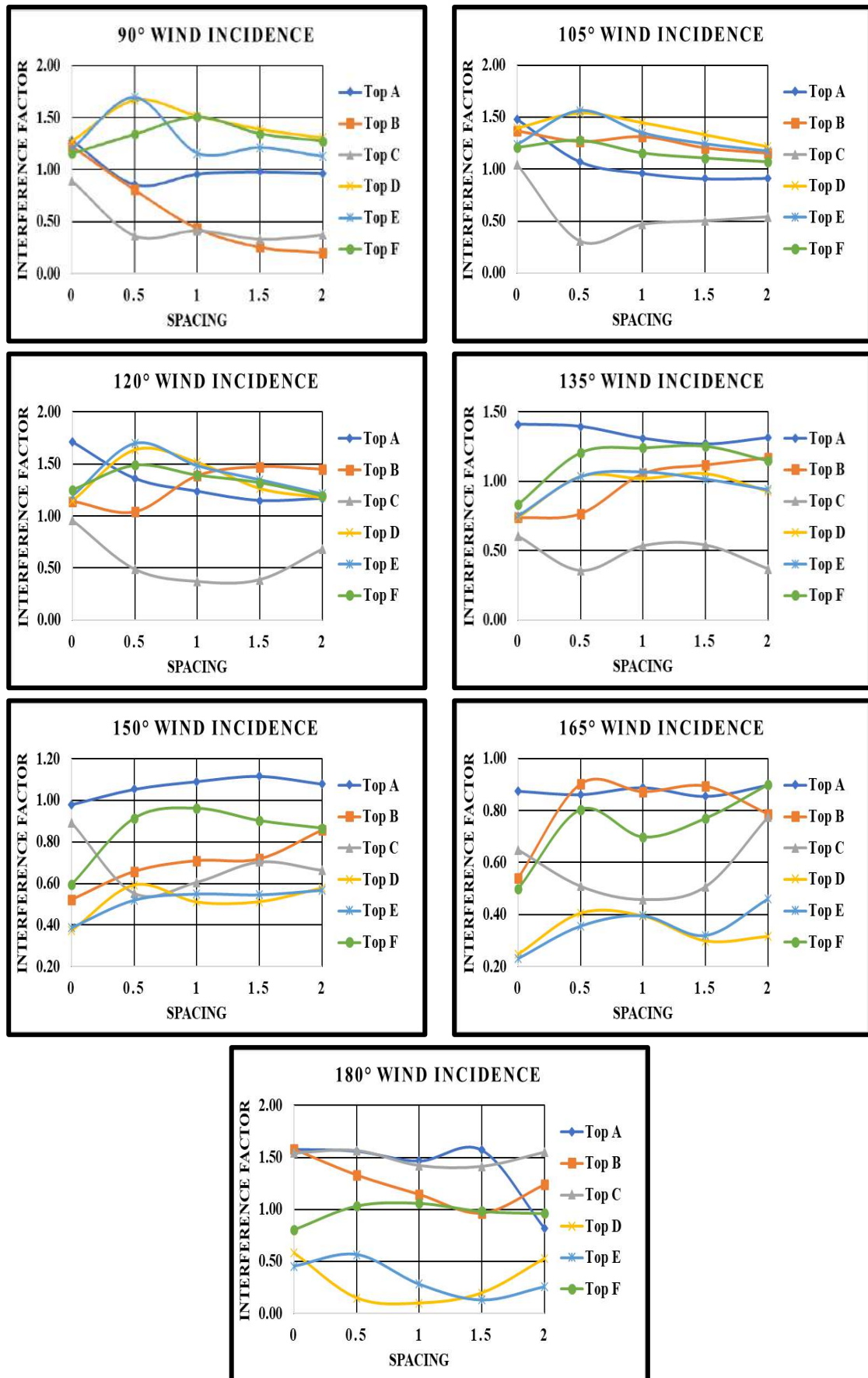
Fig. 5.37(b): Interference Factor for T pattern with variable Spacing

5.3.3.4 Interference Difference (ID)

ID gives the idea of the magnitude of wind-induced suction or positive pressure and how much it increases or decreases during interference conditions. The value of *ID* varies between -0.36 and 0.73. When C_{pe} in an isolated and interference condition is less than 0, and *ID* is less than 0, then there will be an increase in suction on the roof during interference. On the other hand, if C_{pe} is in an isolated and interference condition and *ID* is less than 0, it means that the suction on the roof is reduced during the interference condition. The nature of wind on roofs A, B and C is observed as suction, and the value of *ID* is less than 0, denoting that during interference conditions, the suction is increased on roofs A, B and C while the suction on roofs D, E and F is reduced due to interference with the value of *ID* less than 0. At 15°, 30°, 60°, 75°, 90° and 165° wind intervals, the value of *ID* is greater than 0 on roof A for all the spacing variations, 75°, 90°, 135° 150° and 165° for roof B and 75° to 165° for roof C respectively. The roofs D, E, and F experience ID greater than 0 during most of the angles of wind attack as the wind effect is reduced due to the shielding phenomenon. The variation of ID on cylindrical roofs arranged in a T pattern with variable spacing at different angles of wind incidences is shown in Fig. 5.38. The maximum negative value of *ID* is noted for roof C, i.e., -0.55 at 0° wind angle at B spacing, and the maximum positive value of *ID* is 0.69 on roof E during 165° wind angle in case of zero spacing.
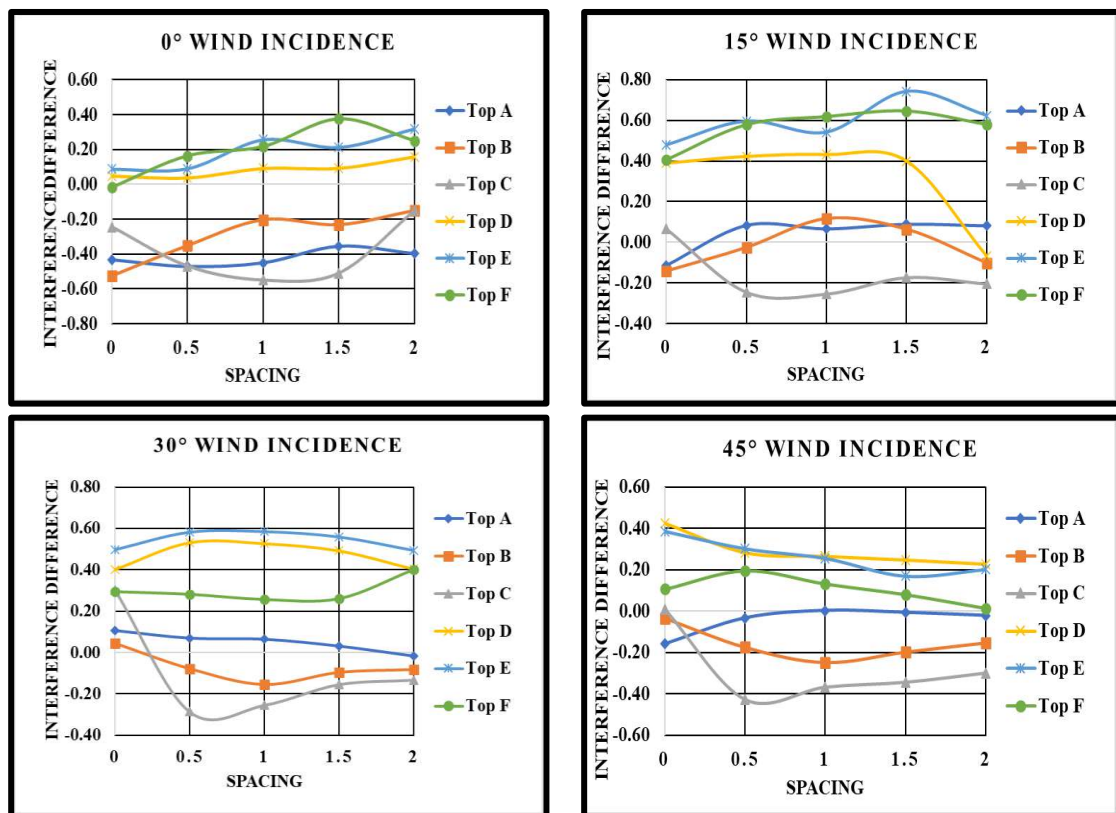
Fig. 5.38(a): Interference Difference for T pattern with variable Spacing
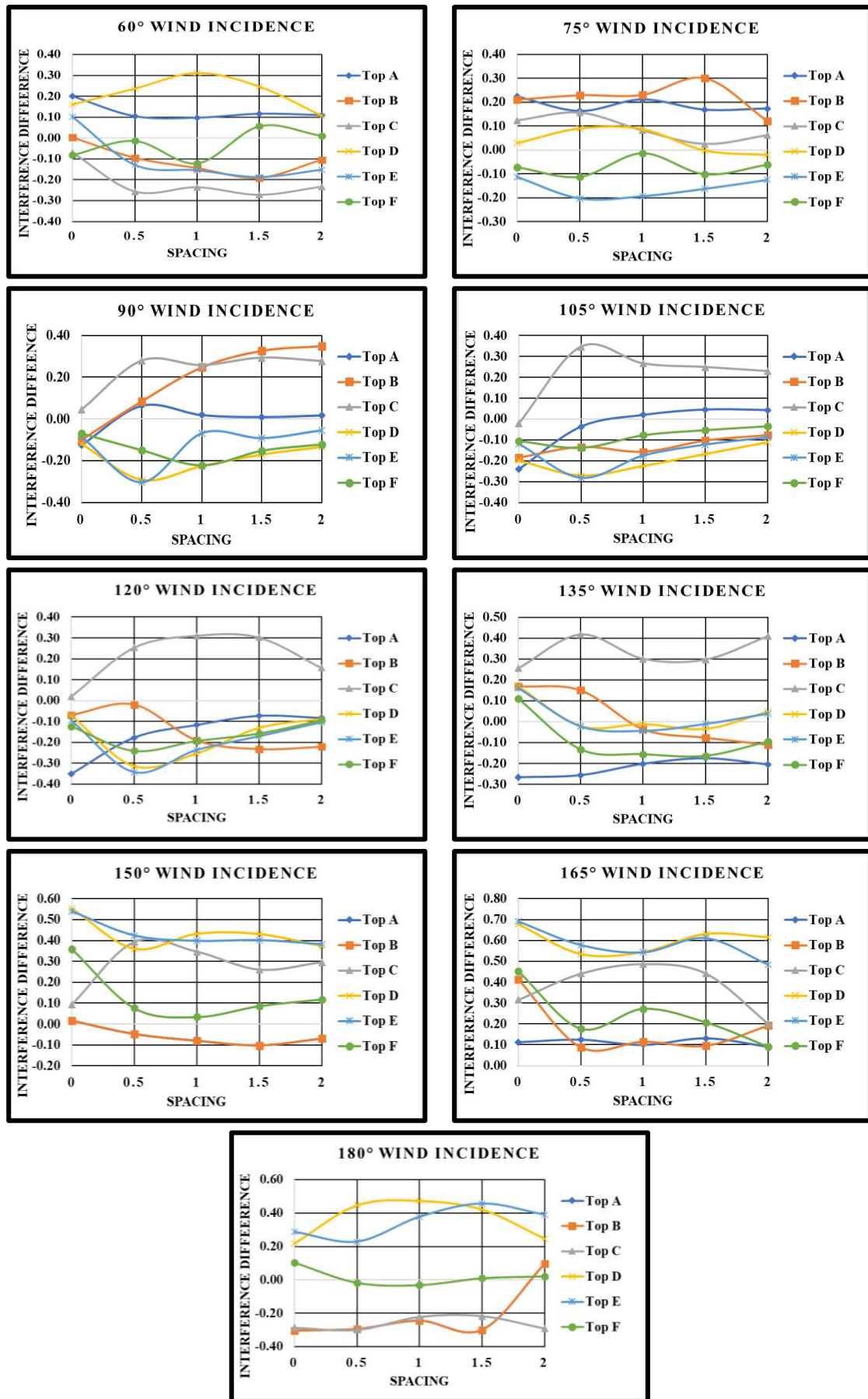
Fig. 5.38(b): Interference Difference for T pattern with variable Spacing

5.3.3.5 Wind Flow Streamlines

The pattern of wind flow around the low-rise structure with cylindrical roofs arranged in a T pattern with variable spacing (0, 0.5B, B, 1.5B and 2B) and at different angles of wind attack (0° to 180° at 15° interval) is shown in Fig. 5.39-5.43. As the wind is flowing around the building, there is a formation of vortex generation in the wake region after striking and separating from the upstream direction at the stagnation point. The formation of wake region is depending upon the angle of wind attack and spacing between the structures. The wake formation is reduced when the spacing between the buildings is increased from 0 to 2B as the wind flow is getting inserted in between the buildings. When there is zero spacing between the buildings, the vortex generation takes place only in the surrounding of the buildings in the downstream direction, but when the spacing is increased from zero to 2B, the flow is inserted between the buildings, resulting in reduced eddies formation and vortex generation in the wake region.

Fig. 5.39(a): Wind Flow Streamlines for T pattern with Zero Spacing
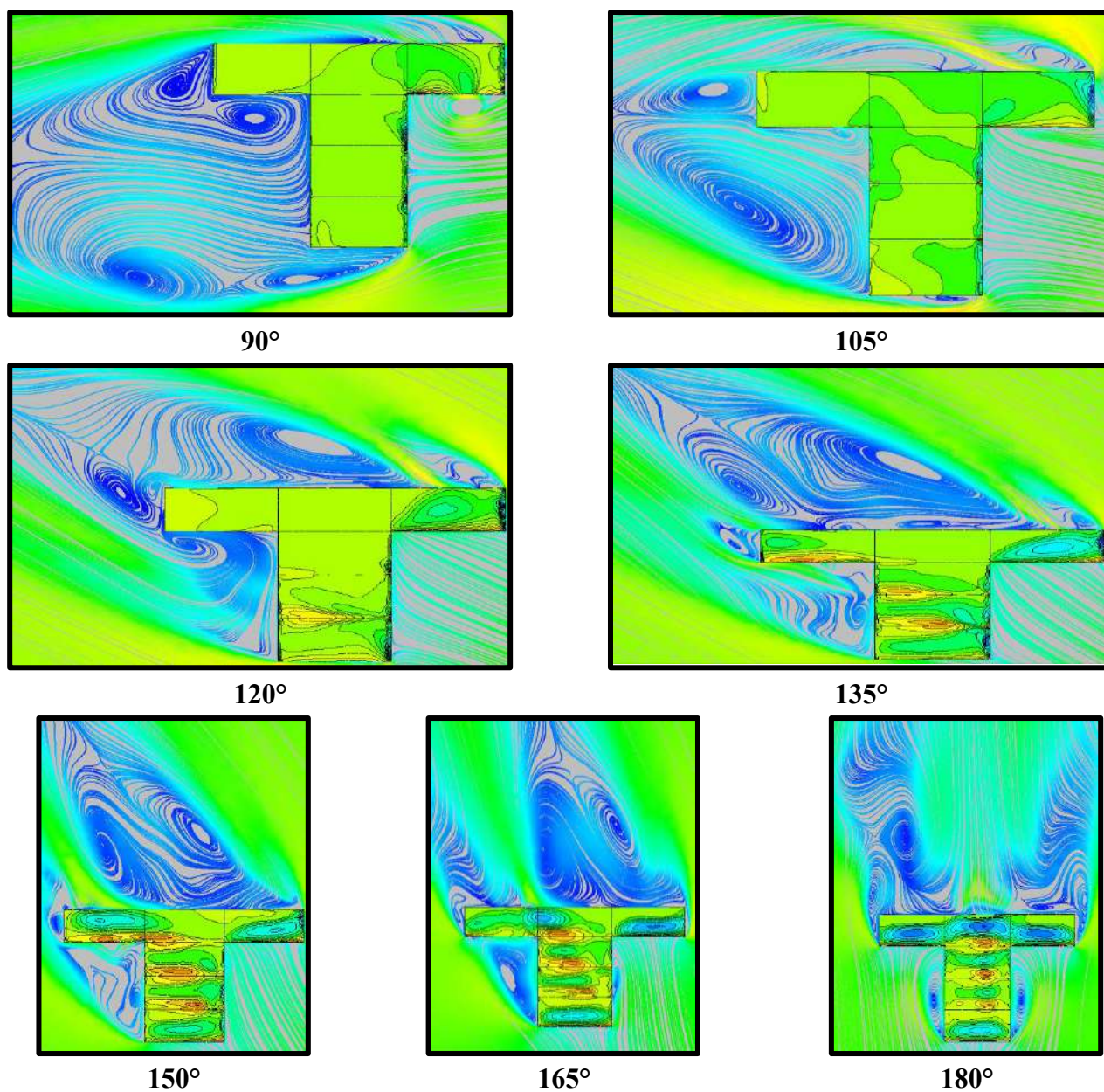
Fig. 5.39(b): Wind Flow Streamlines for T pattern with Zero Spacing

Fig. 5.40(a): Wind Flow Streamlines for T pattern with 0.5B Spacing

45°

60°

75°

90°

105°

120°

135°

150°

165°

180°
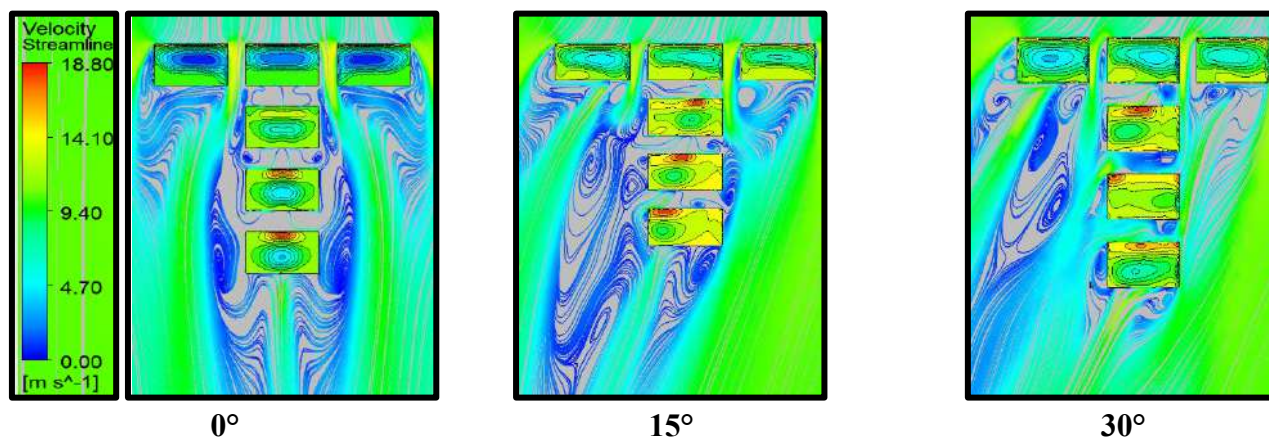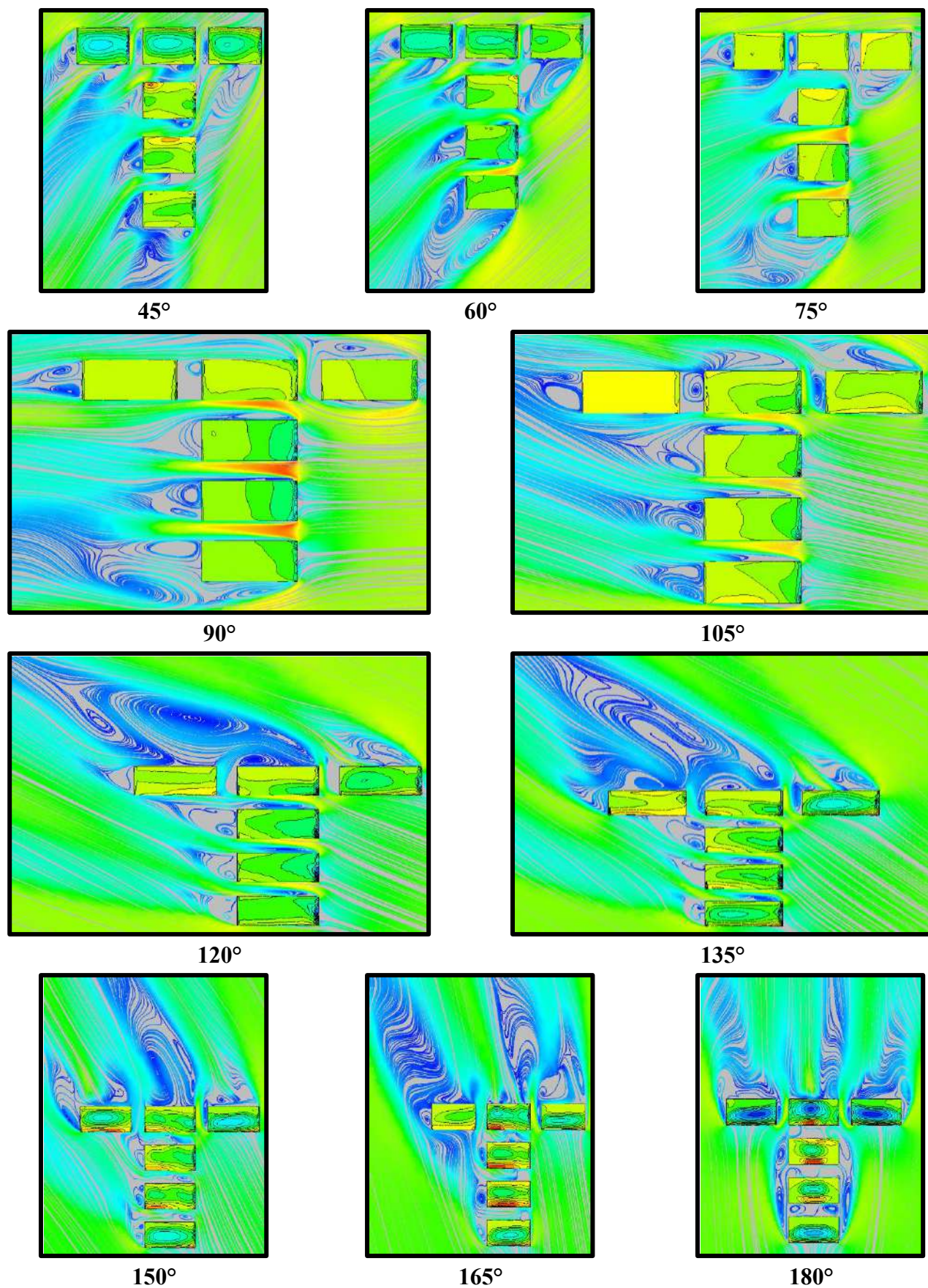
Fig. 5.40(b): Wind Flow Streamlines for T pattern with 0.5B Spacing
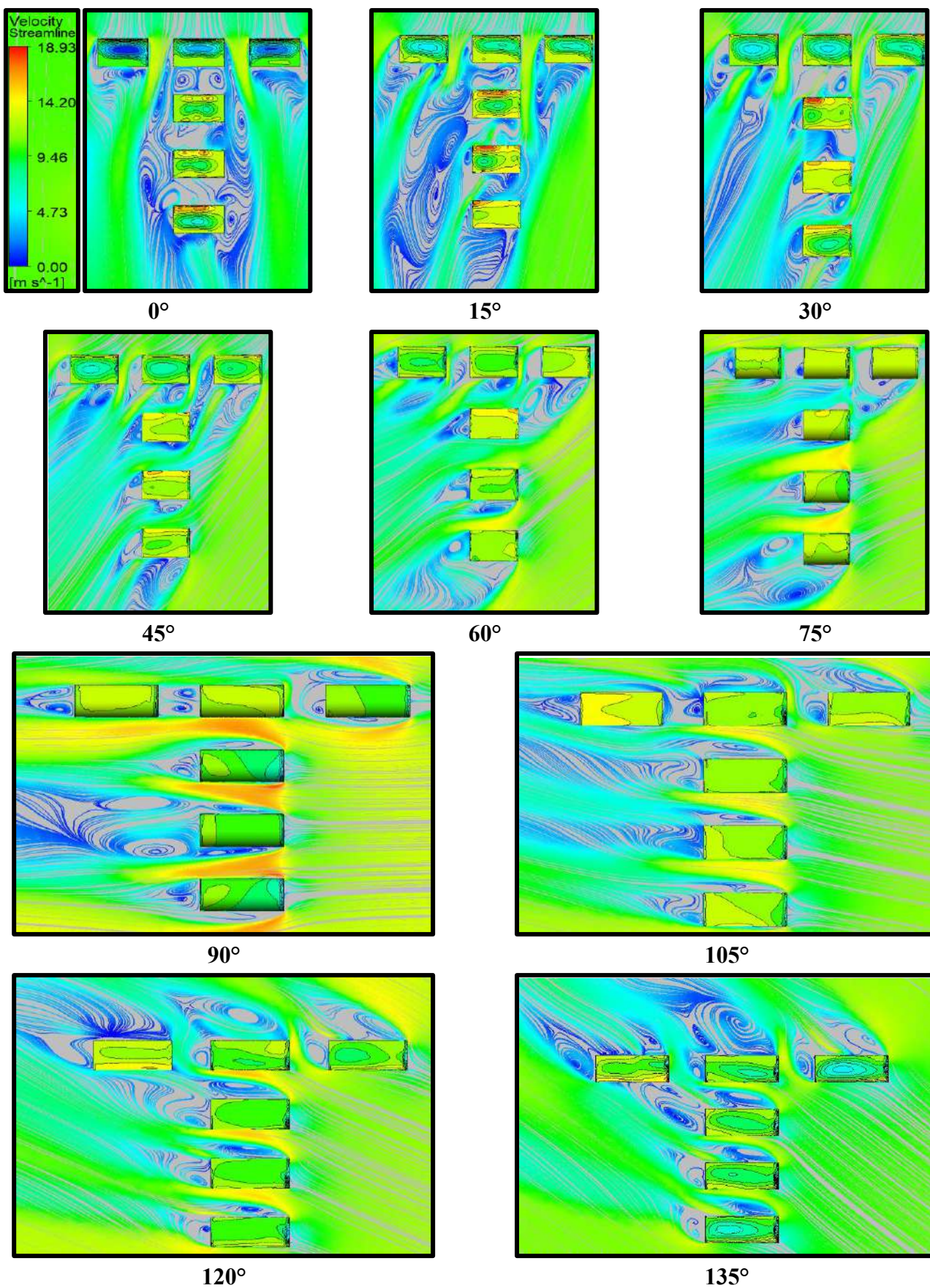
Fig. 5.41(a): Wind Flow Streamlines for T pattern with B Spacing
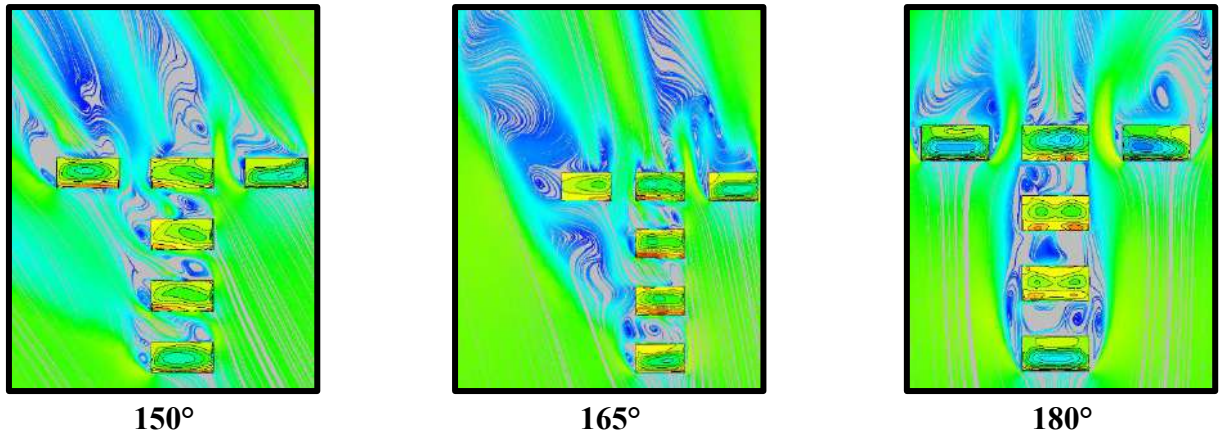
Fig. 5.41(b): Wind Flow Streamlines for T pattern with B Spacing
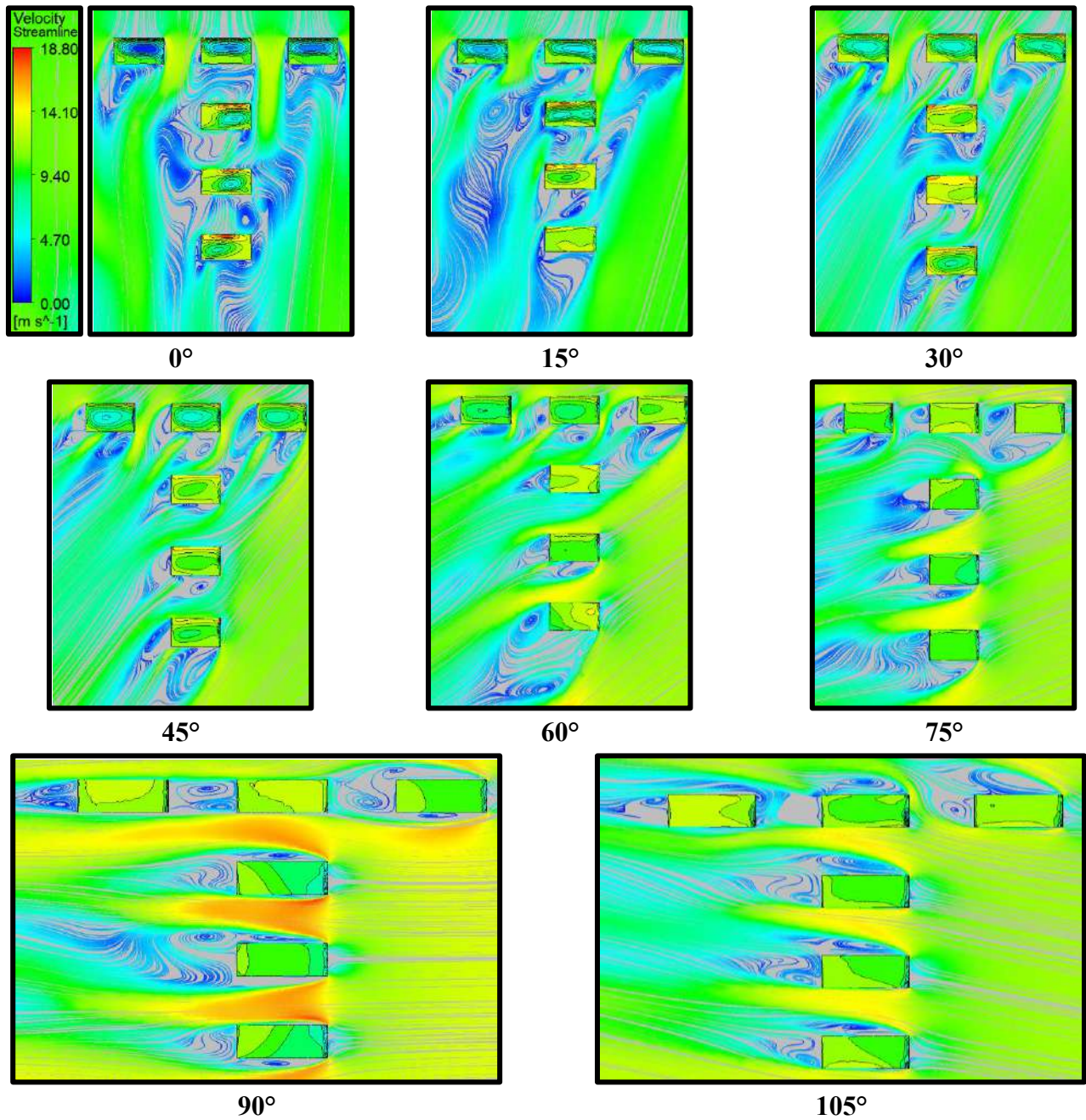
Fig. 5.42(a): Wind Flow Streamlines for T pattern with 1.5B Spacing

120°

135°

150°

165°

180°
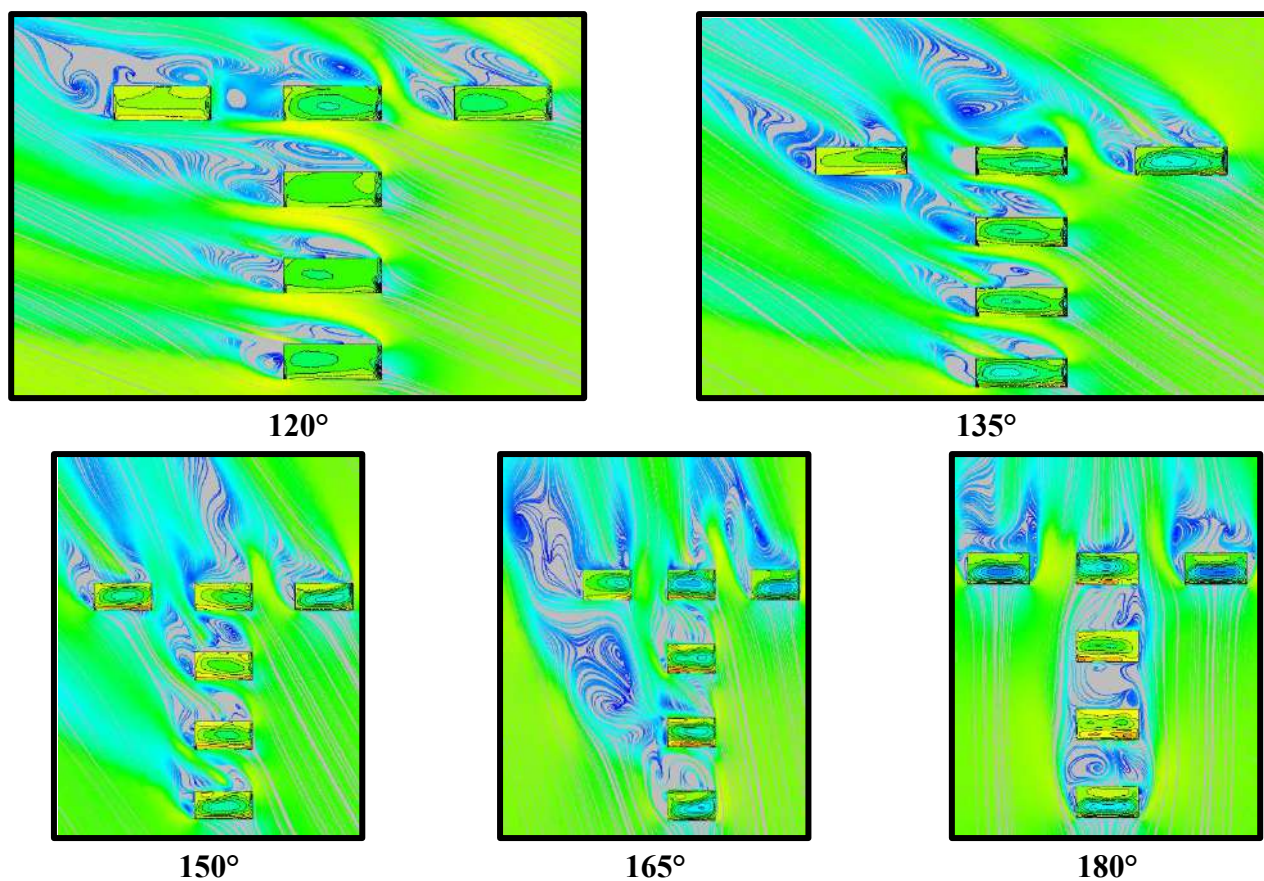
Fig. 5.42(b): Wind Flow Streamlines for T pattern with 1.5B Spacing

0°

15°

30°

45°

60°

75°
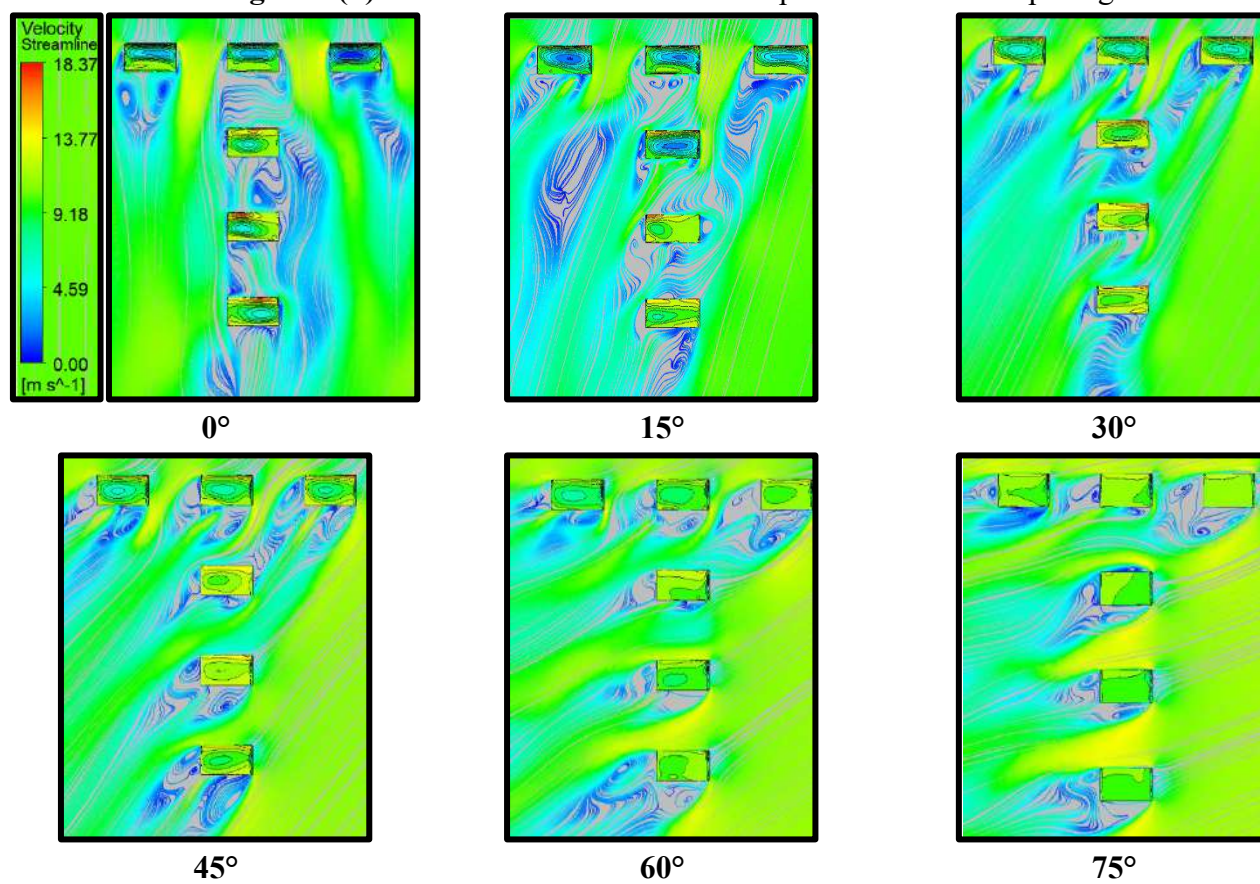
Fig. 5.43(a): Wind Flow Streamlines for T pattern with 2B Spacing
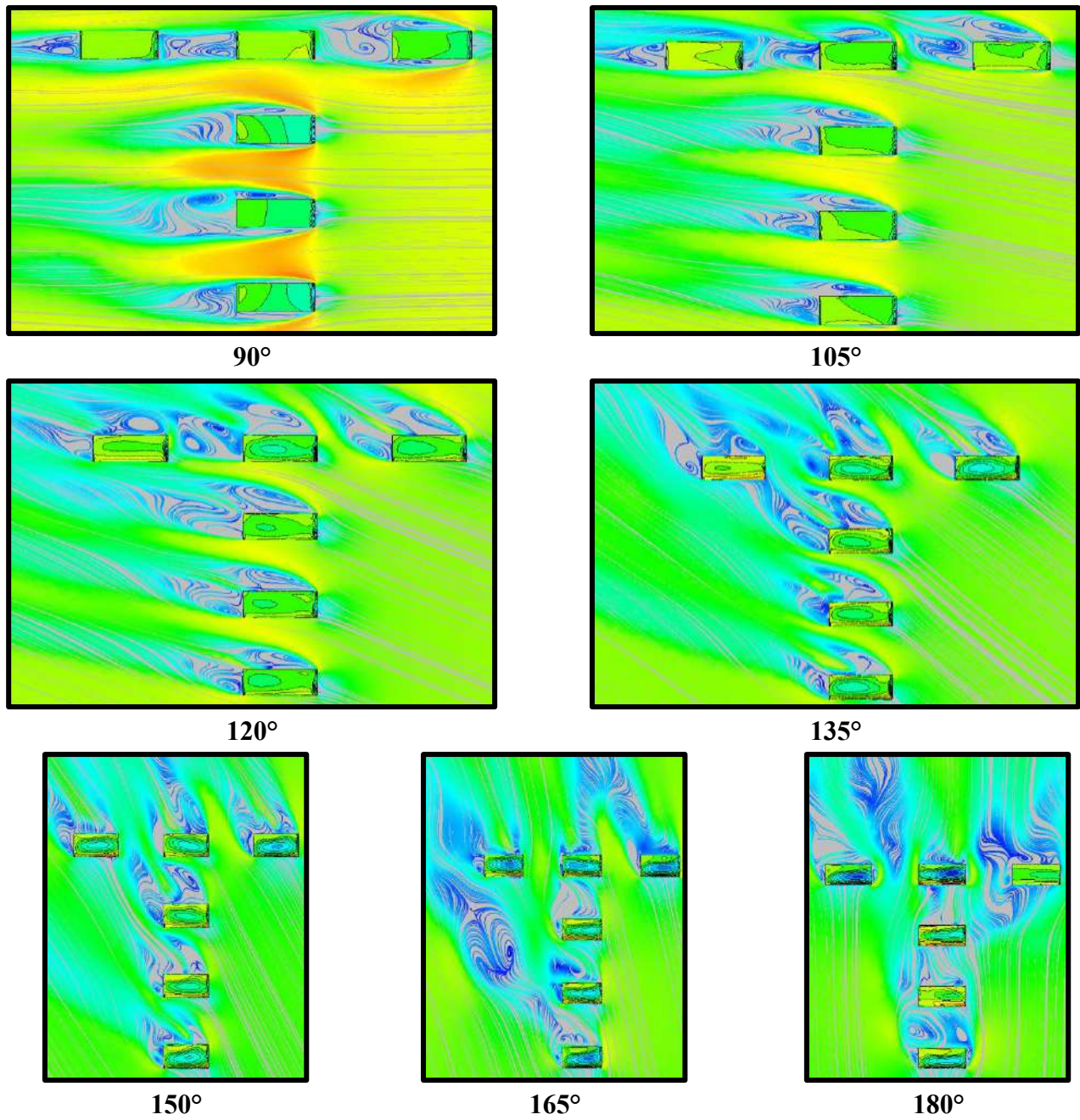
Fig. 5.43(b): Wind Flow Streamlines for T pattern with 2B Spacing

5.4. Conclusions

In conclusion, the aerodynamic behavior of cylindrical roofs under wind forces is influenced by several factors, including roof geometry, wind direction, building arrangement, and spacing. Key findings are as follows:

A. **Suction Forces on Cylindrical Roofs:** Cylindrical roofs predominantly experience suction forces, particularly at the roof's top near the windward edge. These forces are critical to consider in design for structural stability and safety.

B. **Building Patterns and Spacing Effects:** The interference from adjacent buildings reduces the suction forces on the cylindrical roof, as evidenced by changes in the pressure coefficient (C_{pe}), interference factor (*IF*), and interference drag (*ID*) across rectangular, T, and Z patterns. Increased spacing between buildings further diminishes the suction impact, i.e., 84.90% (in the rectangular pattern), 86.79% (in T pattern) and 90.56% (in Z pattern) reduction when the spacing is 2B.

C. **Variation of parameters:** C_{pe} varies between -1.02 to -0.08 for the rectangular pattern, -1.17 to -0.07 for the T pattern and -1.29 to -0.05 for the Z pattern. Based on C_{pe}, the value of *IF* varies between 1.63 to 0.17 for the rectangular pattern, 2.05 to 0.1 for the T pattern and 1.84 to 0.11 for Z pattern.

D. **Wind Pressure Distribution:** While the windward side experiences high wind pressure, the leeward side shows a relatively uniform suction, with the windward side providing a shielding effect.

E. **Critical Wind Angles:** The wind incidence angle significantly affects the pressure distribution. The most critical wind angles for isolated cylindrical roofs are 15° and 30°, where maximum suction occurs. Angles of 0°, 90°, and 180° result in a dominant shielding effect on the windward span.

F. **Design Implications:** The variability in wind pressure coefficients highlights the importance of evaluating critical wind directions for structural design. Designers must ensure that the structural system accounts for the most severe wind-induced forces, particularly on curved surfaces like cylindrical roofs, to ensure long-term stability and safety.

G. These insights emphasize the need for meticulous wind load analysis and interference consideration in the design and construction of cylindrical roofs and nearby structures.

CHAPTER 6

RESULTS AND DISCUSSIONS ON MONO-SLOPE ROOF

6.1 General

There are several types of roof forms provided for low-rise structures, and one of them is the mono-slope roof. The mono-slope roof is provided with a slope on one side of the roof due to which the windward and leeward edges are not at the same height. This chapter deals with the detailed discussion of wind-induced pressure contours, pressure coefficient (C_{pe}), interference factor (*IF*), and interference difference (*ID*) over the mono-slope roof in isolated and different interfering conditions. It also discusses the variation of the mentioned coefficients concerning various angles of wind incidence.

6.2 Isolated Mono-Slope Roof

The low-rise building model shown in Fig. 6.1, with a mono-slope roof, plan dimensions 200 mm X 400 mm, eave height 150 mm, and different roof slopes 10°, 20°, and 30°, is subjected to a 0° to 180° angle of wind attack at an interval of 15°. The wind-induced pressure contours and variation of C_{pe} for isolated low-rise buildings with mono-slope roofs of different roof slopes i.e., 10°, 20° and 30° are discussed here below in this section.
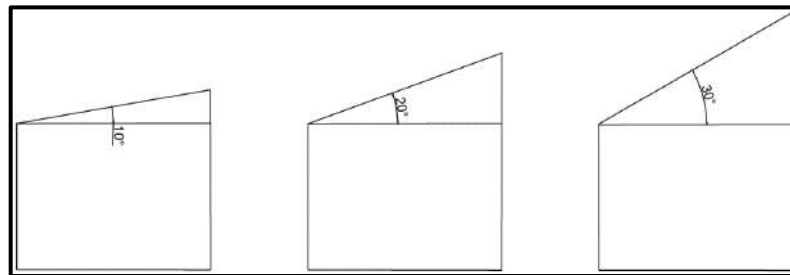
Fig. 6.1: Isolated Mono-Slope Roof with 10°, 20° and 30° Roof Slope

6.2.1 Pressure Contours

The wind-induced pressure contours for the isolated mono-slope roof 10°, 20° and 30° roof slope are shown in Fig. 6.2, 6.3 and 6.4, respectively. The deviation of wind-induced pressure on mono-slope roof with 10° roof pitch when subjected to angle of wind attack from 0° to 180° at 15° interval is shown in Fig. 6.2. When the angle of wind attack changes from 0° to 90°, the average pressure on the roof is changing higher to lower negative pressure afterwards it starts increasing till 180° angle of wind attack. As compared to 10° dome roof, the 10° mono-slope roof pitch is exposed to less negative pressure in magnitude. A small vicinity near windward edge is subjected under negative pressure during the wind incidence angle of 0° to 30°. The minimum pressure that is negative in nature is acting on the roof during 90° incidence angle as shown in Fig. 6.2. Fig. 6.3 shows the contours of pressure induced due to wind on the mono-

slope roof of 20° roof pitch. The magnitude of the pressure is getting reduced on the mono-slope roof with 20° roof pitch in comparison to the 10° mono-slope roof. The pressure is getting reduced as the angle of wind incidence is increasing from 0° to 90° also less than that of the 10° mono-slope roof. The pressure started increasing afterwards from 90° wind incidence angle also less than the 10° mono-slope roof. From the Fig. 6.3, it can be observed that the negative pressure is highly reduced as the roof pitch is increase from 10° to 30°. The negative pressure on the mono-slope roof of 30° roof pitch is the least among 10° and 20° roof pitch of mono-slope roof. The pressure on the mono-slope roof is inversely proportional to the roof pitch of mono-slope roof. The pressure contours obtained from 30° mono-slope roof while subjecting to 0° to 180° angle of attack with 15° interval shown in Fig. 6.3.
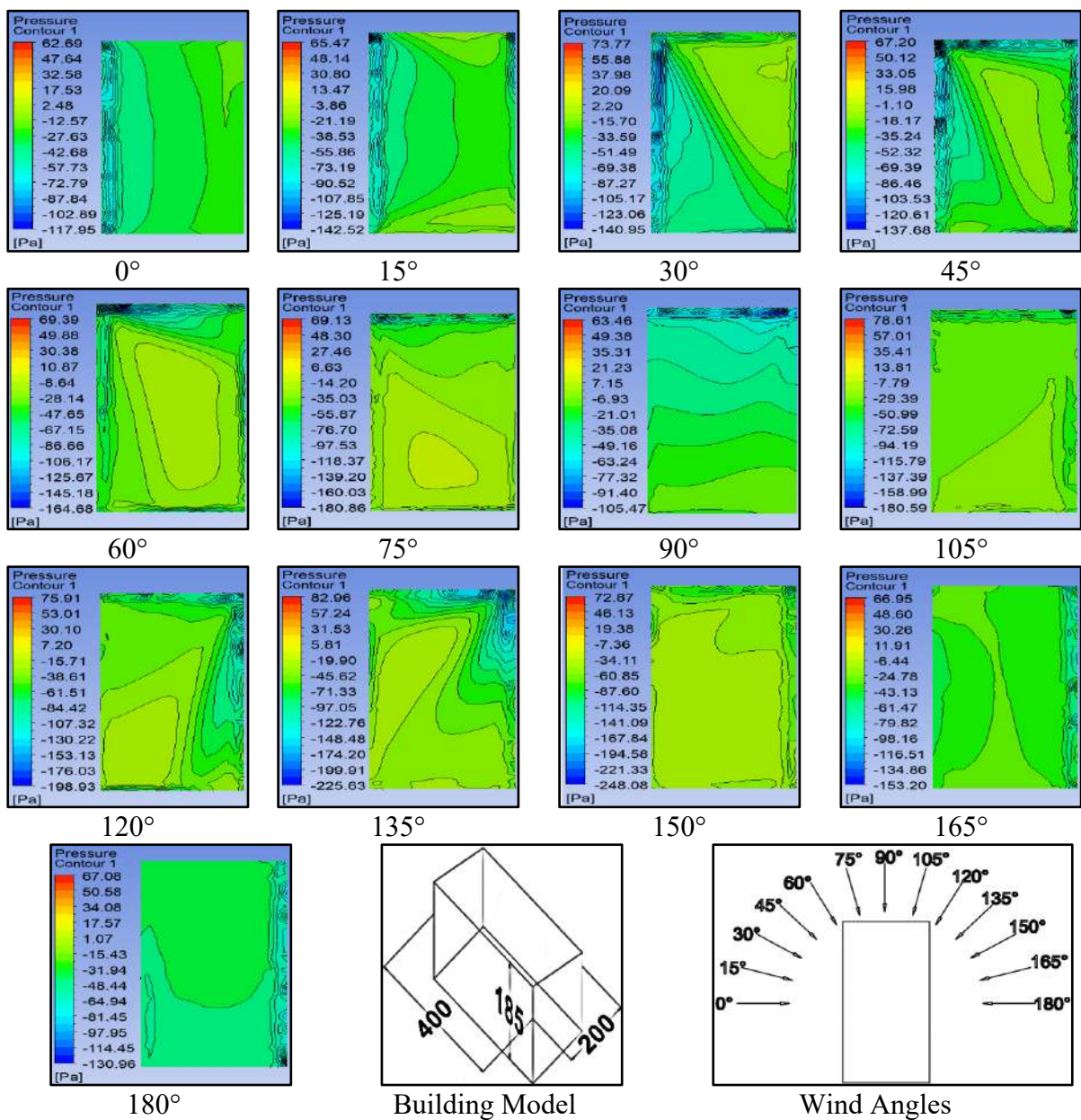
Fig. 6.2: Pressure Contours for 10° Mono-Slope Roof
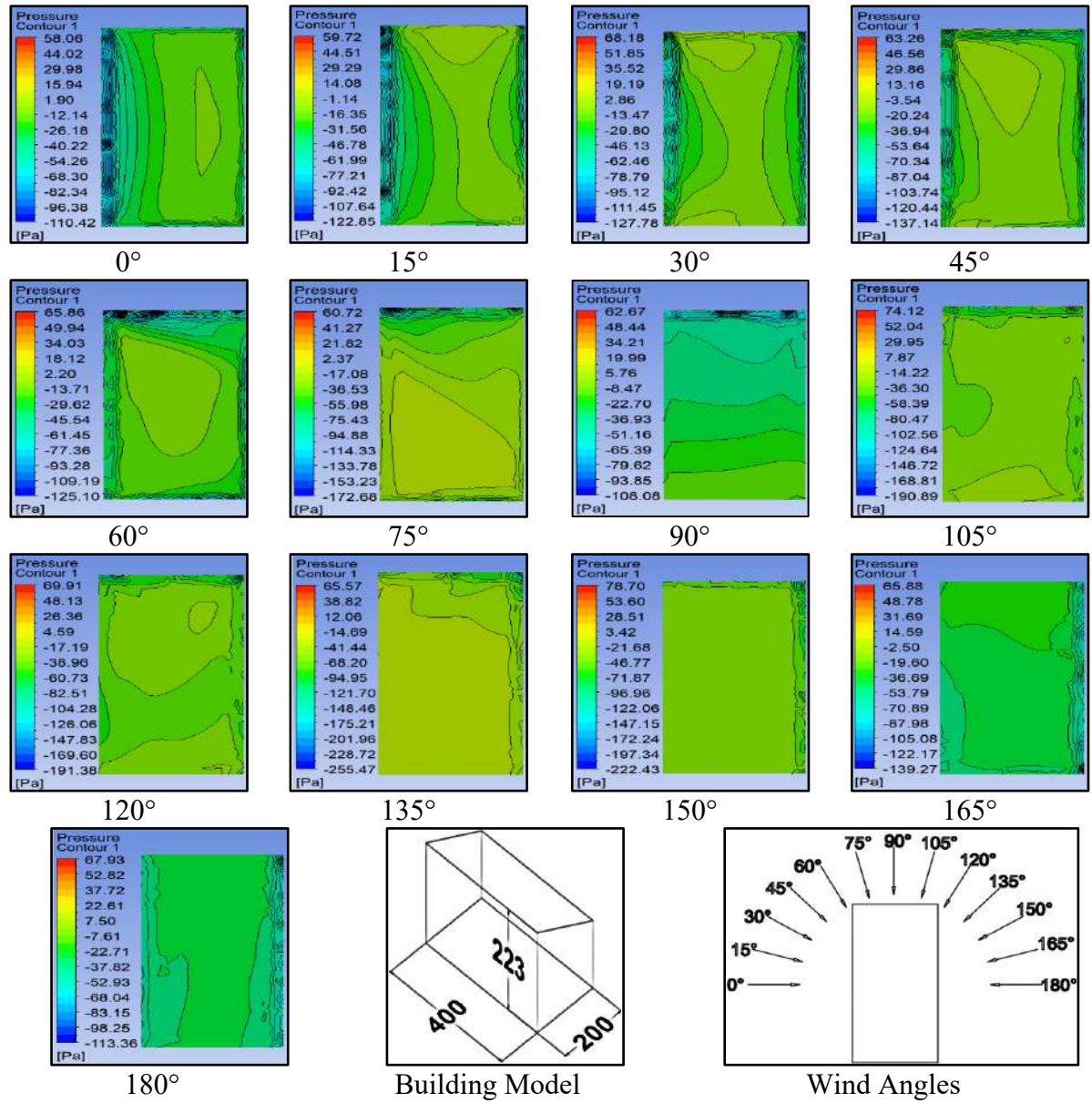
Fig. 6.3: Pressure Contours for 20° Mono-Slope Roof
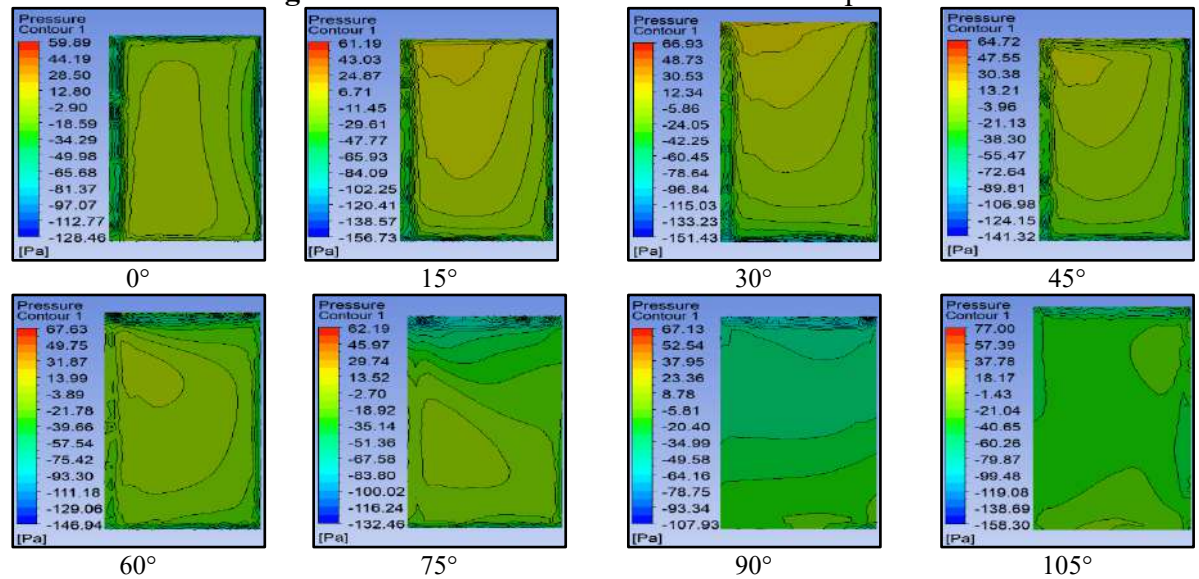
Fig. 6.4(a): Pressure Contours for 30° Mono-Slope Roof
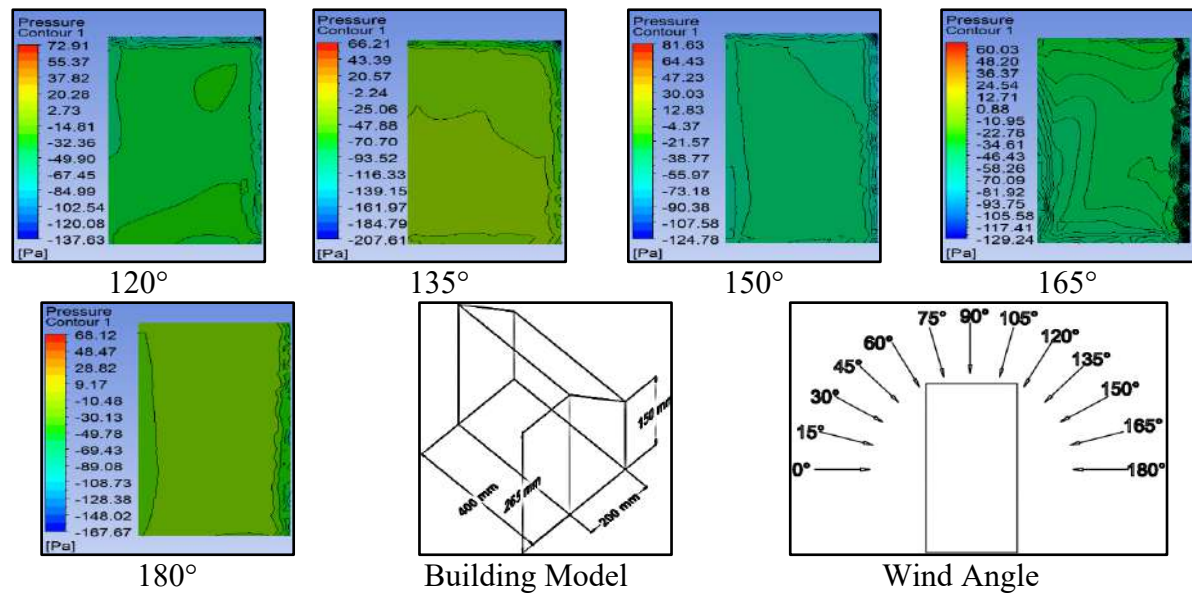
Fig. 6.4(b): Pressure Contours for 30° Mono-Slope Roof

6.2.2 Pressure Coefficient (C$_{pe}$)

The C_{pe} for the mono-slope roof with 10°, 20° and 30° roof slope is calculated using CFD simulation by subjecting it to the different angles of wind incidence angles 0° to 180° at an interval of 15°. But before that, the model needs to be validated either with the wind standards of different nations or some previous research.

In the present research, a low-rise building model with a mono-slope roof of 30° roof slope and a plan dimension of 200 mm X 400 mm is validated with some wind standards and previous experimental research as shown in table 6.1. Stathopoulos & Mohammadian conducted a wind study on mono-slope roof to find out the local and area average wind pressure acting on the roof of low-rise building with mono-slope shape using BLWT having the roof slope of 1:12 using 1:200 model scale. The values of area average C$_{pe}$ obtained for different wind incidence angles i.e., 0°, 30°, 45°, 60°, 90°, 120°, 150° and 180° respectively, were compared with present study.

Kumar & Stathopoulos have conducted an experimental study on mono-slope roof to find out the wind effects using stochastic perspective. The building models were subjected to 0° and 45° wind incidence angles and exposed to an open and sub-urban terrain condition.

The compared values of area average C_{pe} from the study conducted by Stathopoulos & Mohammadian, 1991 and Kumar & Statholpoulos, 2000 are mentioned below in table 6.1.
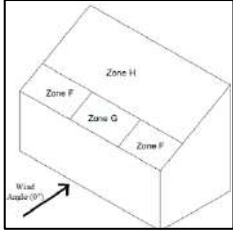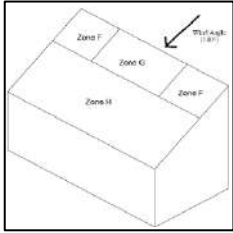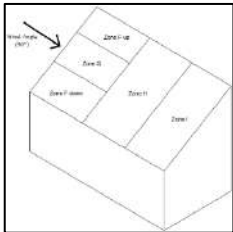
Table 6.1: Comparison of C_{pe} values with experimental studies

Wind Incidence Angles	0°	30°	45°	60°	90°	120°	150°	180°
C$_{pe}$ by Stathopoulus Mohammadian Study	-0.39	-0.59	-0.89	-0.87	-1.07	-2.37	-4.03	-1.06
C$_{pe}$ by Kumar and Statholpoulos Study	-1.11	-	-5.31	-	-	-	-	-
C$_{pe}$ by Present CFD Study	-0.19	-0.17	-0.22	-0.28	-0.46	-0.56	-0.66	-0.47

Fouad et al., performed CFD investigation on different roof roofs to predict the wind effects. The different types of roof forms considered for the investigation are gable, mono-slope, silo, dome and lattice structure. Particularly, for mono-slope roof, the roof was divided into different zones shown in Table 3, and the values of C_{pe} obtained at 0°, 90° and 180° wind incidences for different zones of the roof were compared with the Eurocode. The values of C_{pe} obtained from the present CFD investigation are compared with study performed by Fouad et al., and Eurocode are shown below in table 6.2. After comparing the values of C_{pe} obtained from present CFD investigation for mono-slope roof with Stathopoulos & Mohammadian, Kumar & Stathopoulos, Fouad et al and Eurocode, it was observed that the obtained values were smaller than that of the experimental studies and Eurocode, thus are on safer side.

The variation of C_{pe} with respect to various wind incidence angles for mono-slope roof with different roof pitches i.e., 10°, 20° and 30° respectively is shown in Fig. 6.5. In all the cases of mono-slope roof, the most vulnerable roof pitch is 10° because it is under suction with large magnitude as compared to other roof pitches of mono-slope roof. By increasing the roof pitch of mono-slope roof from 10° to 20° and 30° results in decrease the value of suction on the roof. The 30° mono-slope roof is the safest roof in all the cases considered for mono-slope roof.

Table 6.2: Comparison of C_{pe} with CFD Study and Eurocode

Wind Incidence Angle	Zone	Fouad et al., 2018	Eurocode	Present Study	Roof Zone
0°	F	-0.85	-0.50	-0.55	
	G	-0.85	-0.50	-0.55	
	H	-0.12	-0.20	-0.12	
180°	F	-0.61	-1.70	-0.67	
	G	-0.65	-1.15	-0.53	
	H	-0.83	-0.80	-0.67	
90°	F_{up}	-1.58	-2.50	-0.94	
	F_{down}	-0.85	-1.65	-0.73	
	G	-1.40	-1.75	-0.73	
	H	-1.37	-1.15	-0.53	
	I	-0.99	-1.00	-0.73	
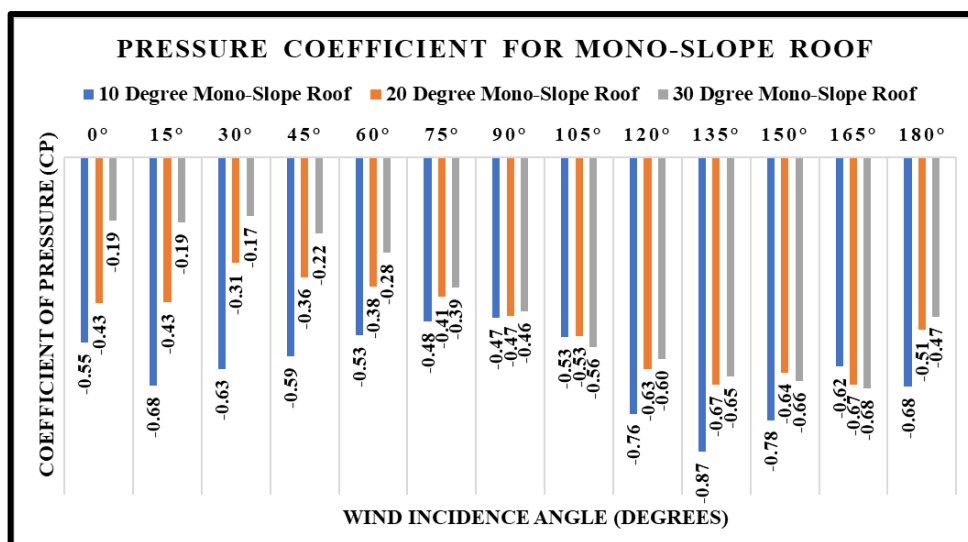
Fig. 6.5: C_{pe} variation w.r.t wind incidence angle for the Mono-slope roof

6.2.3 Wind Flow Pattern on Mono-Slope Roof

The wind flow pattern over an isolated mono-slope roof with 10°, 20° and 30° roof slope at various angles of wind incidence ranging between 0° to 180° at an interval of 15° each is shown in Figs. 6.6, 6.7 and 6.8 respectively.

The wind flow pattern over the 10° mono-slope roof at various angles of wind attack is shown in Fig. 6.6. During a 0° wind attack, the flow is separated from the windward edge of the roof and then recirculates exactly over the roof as well as on the leeward side of the building.

The flow is also getting separated from the corner existing at the junction of the windward edge and side edge of the building during a 45° wind attack, while in case of 135° wind angle, the flow is separated from the corners existing at the junction of leeward edge and the side edge. During a 90° wind angle, the wind flow completely engulfs the building, resulting in maximum flow turbulence all around the building. During a 180° wind attack, the flow is reattached to the surface lying in the downstream direction. By increasing slope of the roof from 10° to 20° and 30°, the flow separation phenomenon is reduced on the roof during 45° and 135° angles of wind incidence as shown in Figs. 6.7 and 6.8 respectively.

In case of mono-slope roof with 30° roof slope, the wind flow is completely attached to the roof surface while it gets detached or recirculate over the mono-slope of 10° and 20° roof slope. The mono-slope roof with 10° roof slope is more acting like a flat roof as compared to the 20° and 30° mono-slope roof.

0°

45°

90°

135°

180°
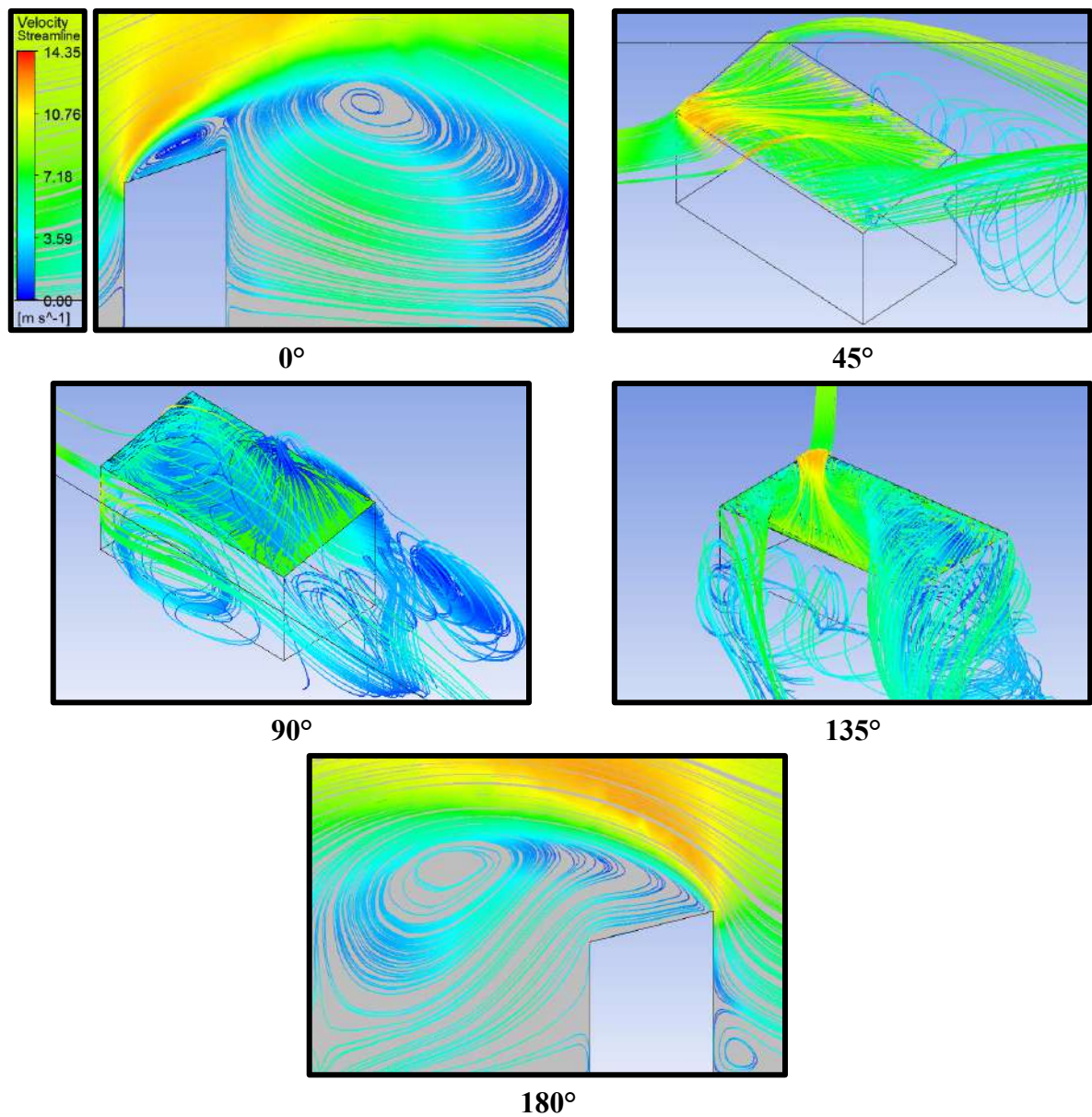
Fig. 6.6: Wind Flow Streamlines of 10° Mono-Slope Roof

0°

45°
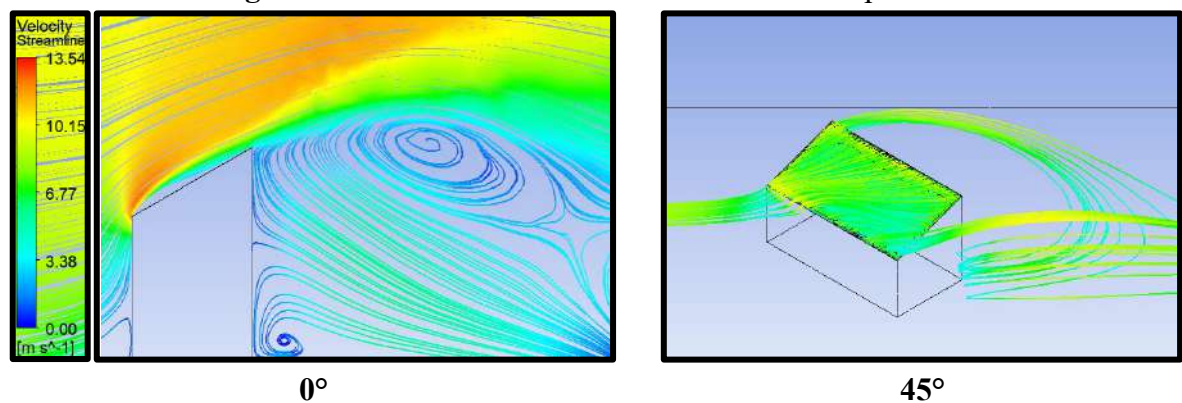
Fig. 6.7(a): Wind Flow Streamlines of 20° Mono-Slope Roof

90°

135°

180°
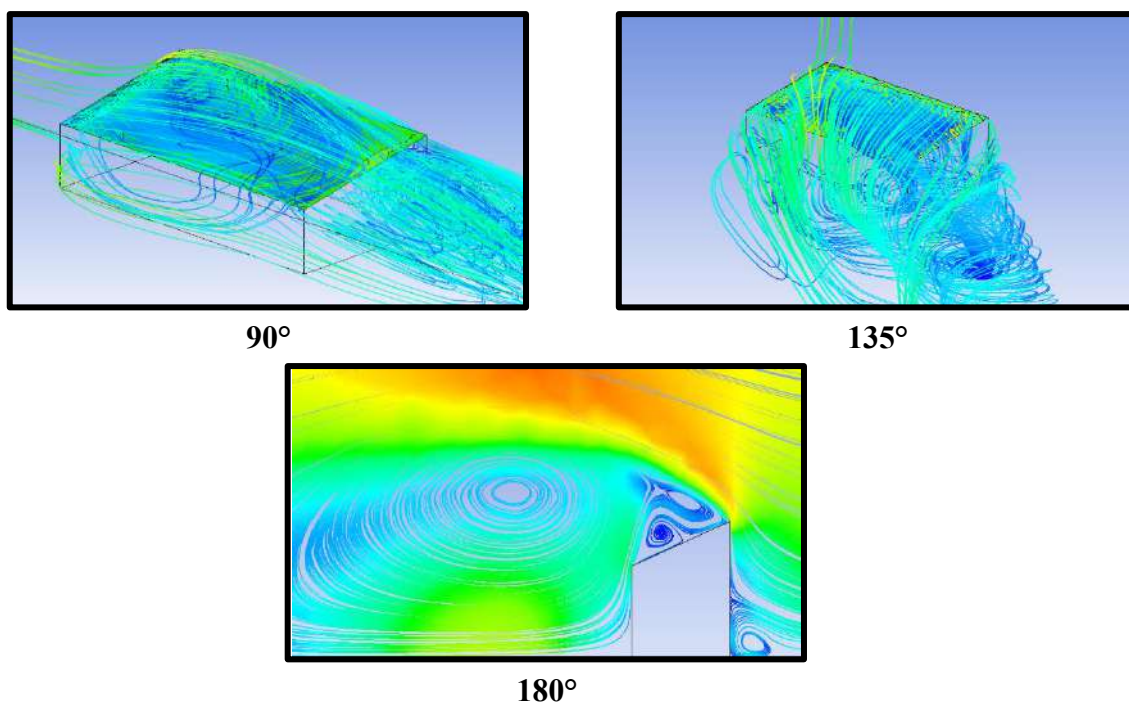
Fig. 6.7(b): Wind Flow Streamlines of 20° Mono-Slope Roof

0°

45°

90°

135°

180°
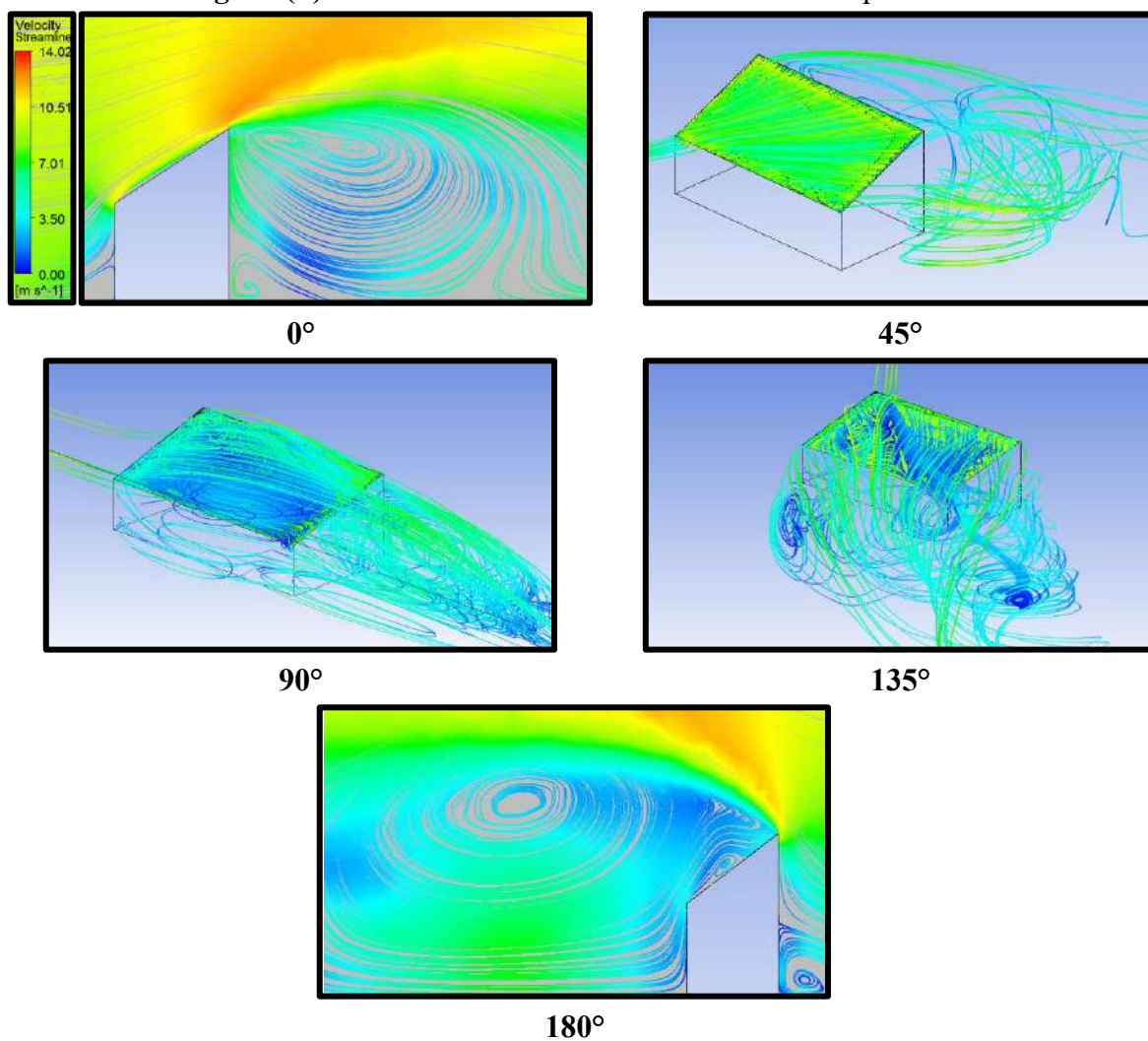
Fig. 6.8: Wind Flow Streamlines of 30° Mono-Slope Roof

6.3 Interference

In this section the effects of presence of nearby buildings are investigated in the form of interference factor (*IF*) and interference difference (*ID*) on the mono-slope roof with 30° roof slope of low-rise structures arranged in rectangular pattern, T-pattern and Z-pattern with variable spacing i.e., 0, 0.5B, B, 1.5B and 2B where B is the width of the building at various angles of wind incidence ranging between 0° to 180° at an interval of 15° each.

6.3.1 Rectangular Pattern

To find out the effect of interference on 30° mono-slope roof, six low-rise building models with mono-slope roof arranged in rectangular pattern placed nearby each other using different spacings i.e., 0, 0.5B, B, 1.5B and 2B. The wind-generated pressure contours, *IF* and *ID* on all six 30° mono-slope roofs due to interference are discussed below at different angles of wind incidence ranging between 0° to 180° at 15° intervals each. The rectangular pattern with 30° mono-slope roof and wind angles are shown in Fig. 6.9.

| Zero Spacing | 0.5B Spacing | B Spacing |

| 1.5B Spacing | 2B Spacing | Wind Angles |
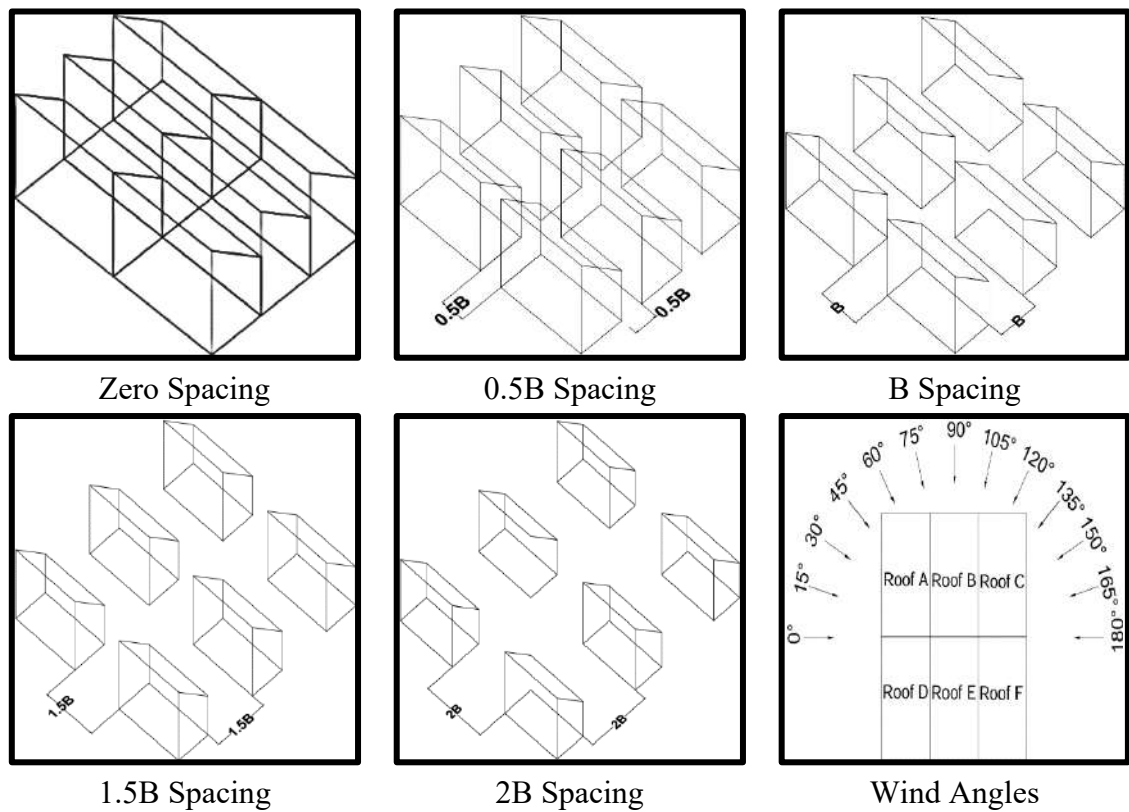
Fig. 6.9: Rectangular Pattern and Wind Angles of 30° Mono-Slope Roof

6.3.1.1 Pressure Contours

The wind-induced pressure contours obtained for low-rise buildings with 30° mono-slope roofs arranged in rectangular patterns with variable spacing and at different angles of wind incidence are shown in Figs. 6.10-6.14. During a 0° wind attack, there is a uniform wind pressure distribution over the central portion of roofs A & D, B & E and C & F, respectively. The impact

of wind pressure during 15°, 30° and 45° wind angle is mostly positive in nature on all the roofs. This positive wind-induced pressure started converting into negative when the angle of wind incidence changed from 60° to 180°, as shown in Fig. 6.10. When the spacing between the buildings is zero, the whole structure acts as a single or isolated building with a multi-span 30° mono-slope roof.

Fig. 6.11 depicts the contours created by pressure brought on by the disposition of wind loads on low-rise structures with 30° mono-slope roofs that are placed in a rectangular pattern with 0.5B spacing between them. By increasing the spacing between the buildings from 0 to 0.5, it is observed that the central portion of the roofs A & D is subjected to the positive wind induced pressure during 0° wind attack. From 0° to 180° there are several portions on the roofs subjected to the positive wind induced pressure due to the dominance of shieling effect as shown in Fig. 6.11. During 90° wind attack, the pressure is distributed on roofs A, B and C in similar pattern as well as on the roofs D, E and F.

In Fig. 6.12, the positive wind-induced pressure distribution occurs only at 15°, 30°, and 45° angles of wind incidence in the case of B spacing between the buildings, while at other angles, there is a negative wind-induced pressure distribution on all the roofs. The pressure distribution on the roof is symmetrical when the wind incidence angles are 0° and 180°, respectively. The pressure distribution on the roof keeps changing with respect to the angle of wind incidence, ranging between 0° to 180° at 15° intervals. The wind-induced negative pressure is maximum near the edges of the mono-slope roof as compared to the other portion of the roofs as shown in Fig. 6.10-6.14.

Fig. 6.10(a): Pressure Contours for Rectangular Pattern with 0 Spacing

90°   105°   120°

135°   150°   165°

180°   Wind Angles
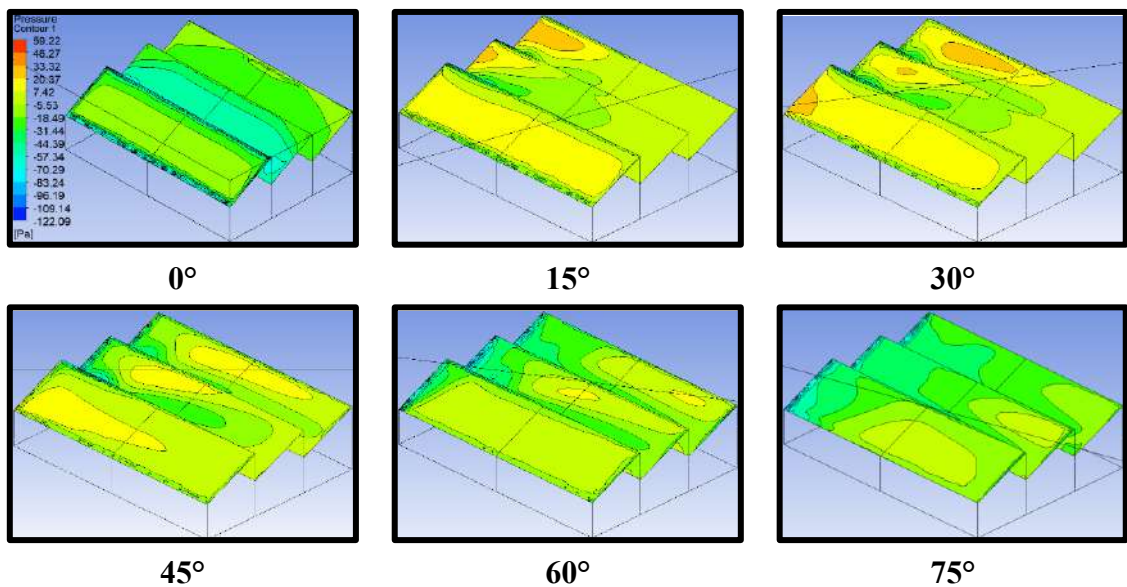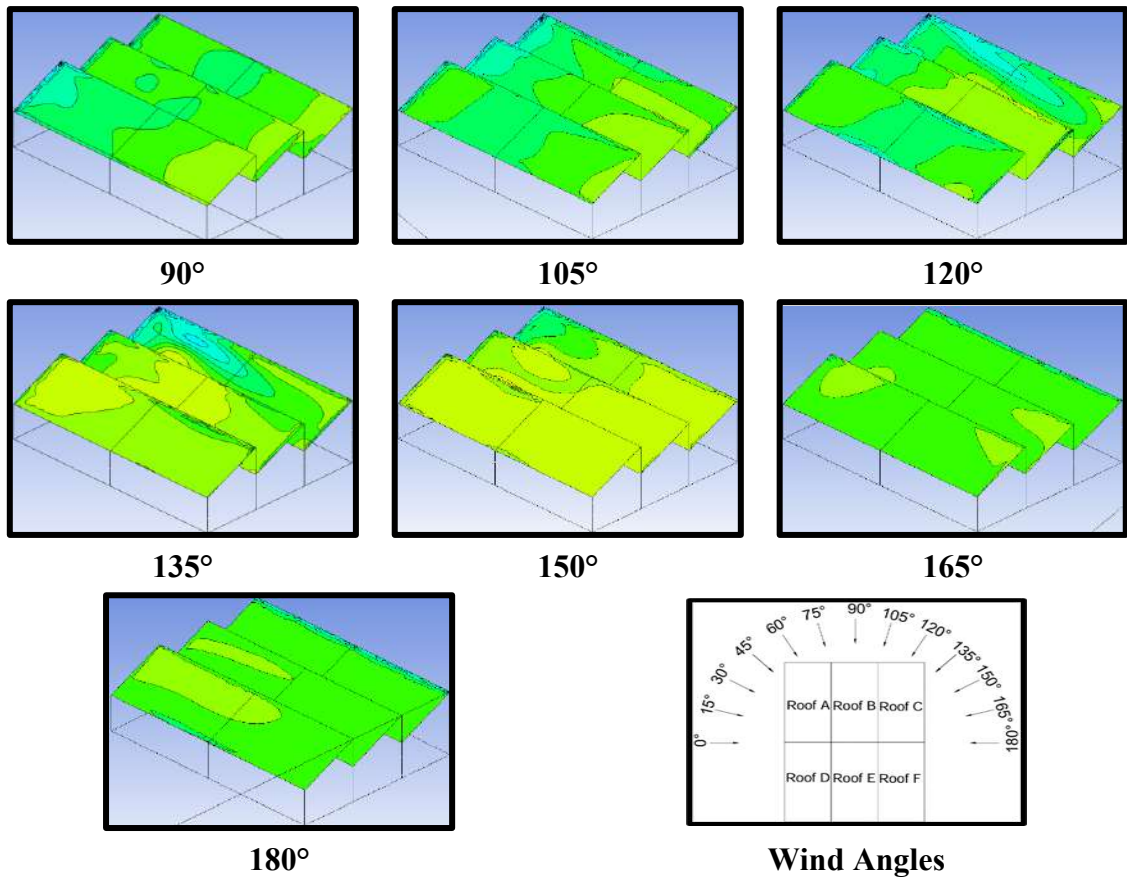
Fig. 6.10(b): Pressure Contours for Rectangular Pattern with 0 Spacing

0°   15°   30°

45°   60°   75°

90°   105°   120°

Fig. 6.11(a): Pressure Contours for Rectangular Pattern with 0.5B Spacing

135° **150°** **165°**

180° **Wind Angles**

Fig. 6.11(b): Pressure Contours for Rectangular Pattern with 0.5B Spacing

0° **15°** **30°**

45° **60°** **75°**

90° **105°** **120°**

135° **150°** **165°**
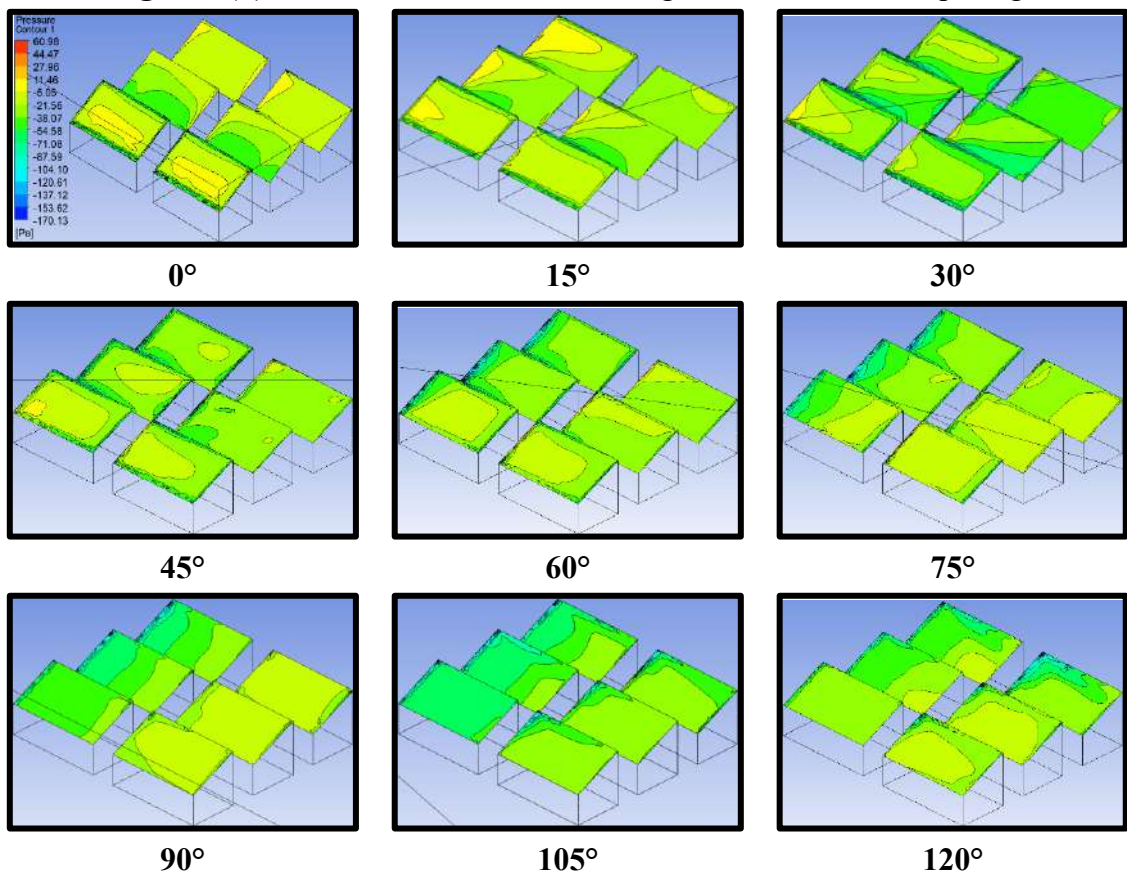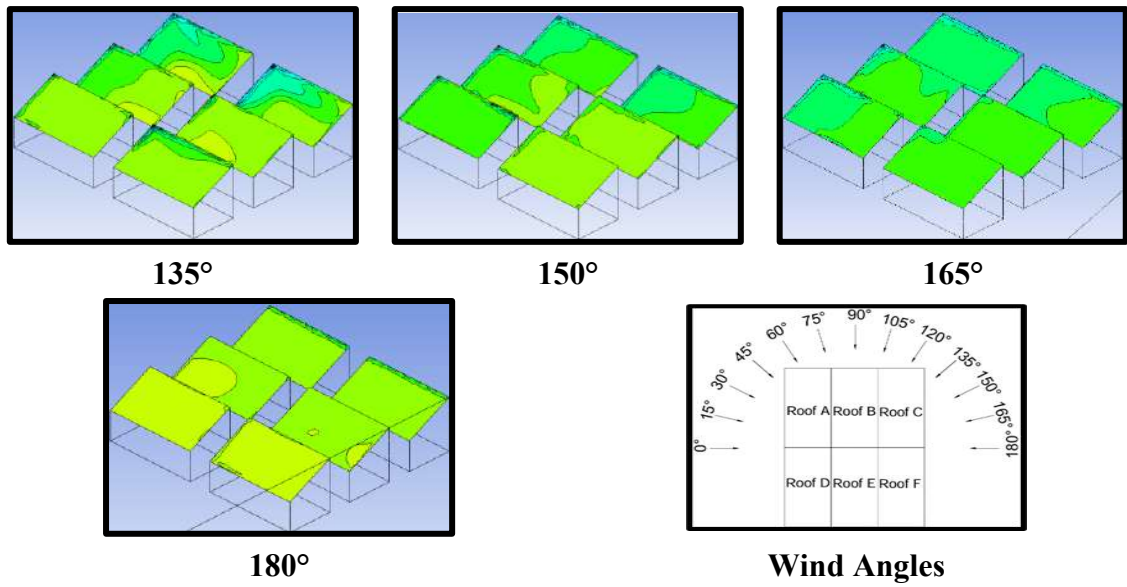
Fig. 6.12(a): Pressure Contours for Rectangular Pattern with B Spacing

180°
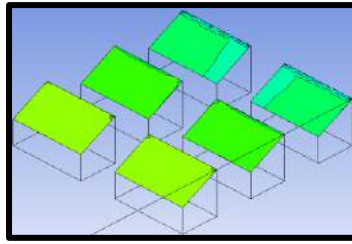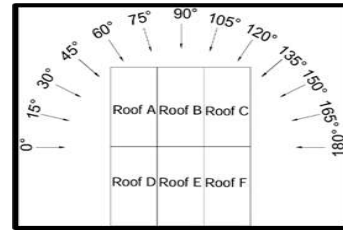
Wind Angles

Fig. 6.12(b): Pressure Contours for Rectangular Pattern with B Spacing

0°

15°

30°

45°

60°

75°

90°

105°

120°

135°

150°

165°

180°
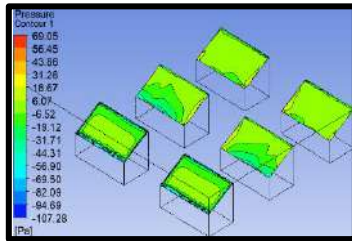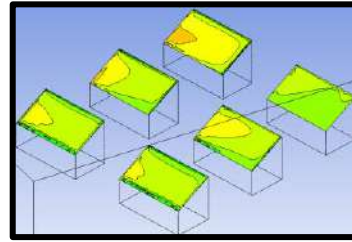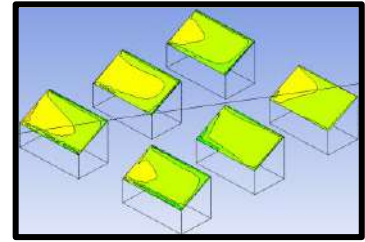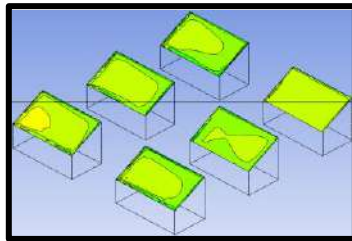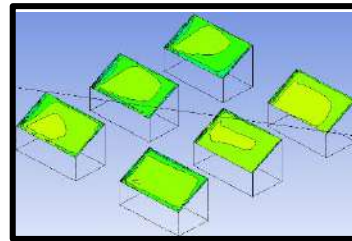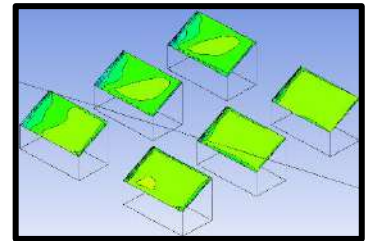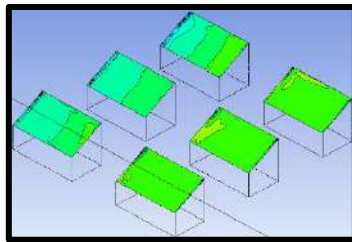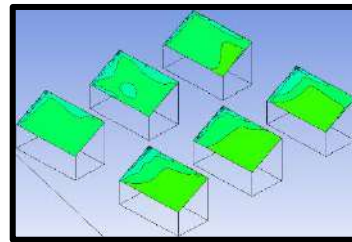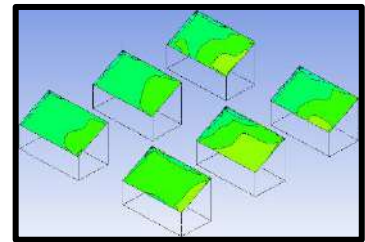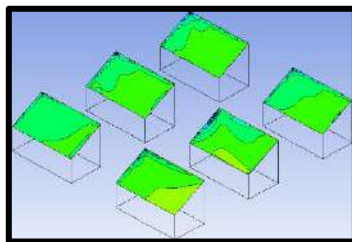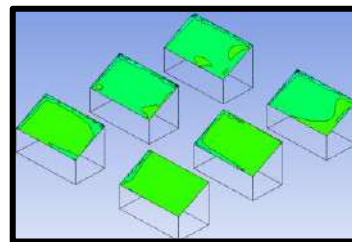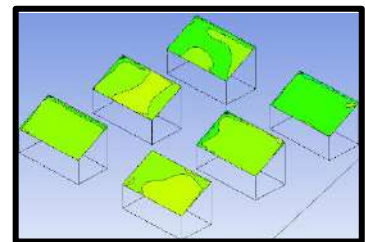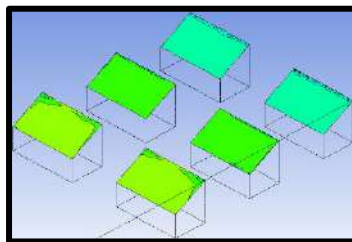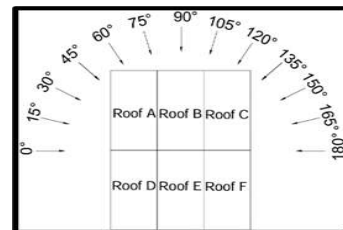
Wind Angles

Fig. 6.13: Pressure Contours for Rectangular Pattern with 1.5B Spacing
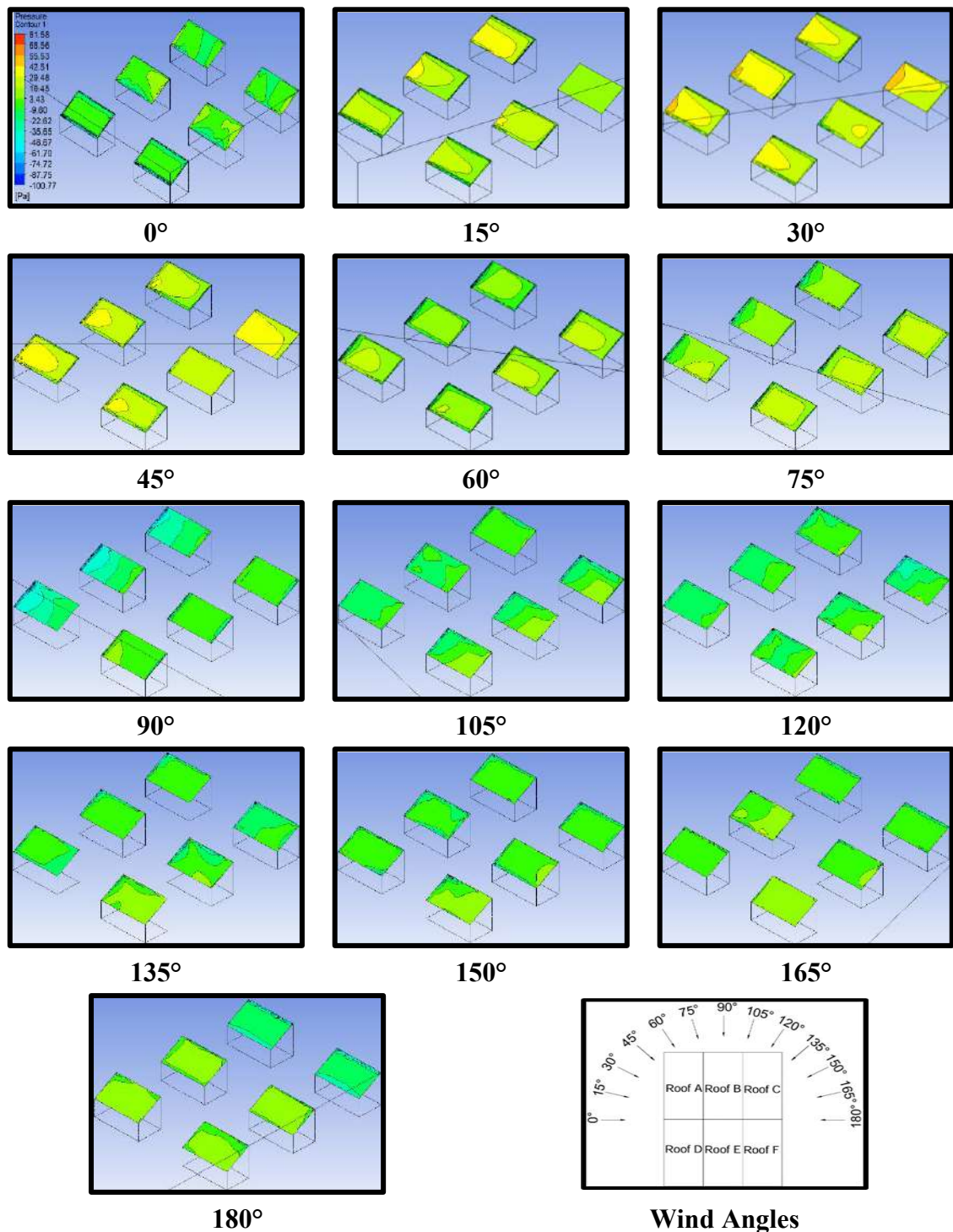
Fig. 6.14: Pressure Contours for Rectangular Pattern with 2B Spacing

6.3.1.2 Pressure Coefficient

Fig. 6.15 depicts the variation of average C_{pe} of all the mono-slope roofs for different wind incidence angles i.e., 0° to 180° at 15° wind intervals with variable spacing i.e., zero, 0.5B, B, 1.5B and 2B (where B=0.2m). Pressure on the mono-slope roof with a 30° roof slope is reduced with respect to the spacing and angle of wind incidence in rectangular patterns when compared

with cylindrical and dome roofs. The value of C_{pe} on all the roofs A, B, C, D, E and F is reduced, indicating the reduced suction on the roof by increasing the spacing between the buildings when the angle of wind attack ranges between 0° to 90° respectively, as shown in Fig. 6.15. The pattern of C_{pe} variation followed by roofs A, B, and C is similar to each other, as well as roofs D, E and F show a similar pattern of variation of C_{pe}. The value of C_{pe} is more or less same for roofs A&D, B&E and C&F at 180° angle of wind attack during variable spacing. The maximum negative value of C_{pe} is observed as -0.74, -0.62, -0.59, -0.57, -0.64, -0.67 on roof B during 0°, 15°, 30°, 45°, 60°, 75° wind attack, -0.73 on roof A dung 90° wind attack, -0.72 on roof B during 105° wind attack, -0.87, -1.14, -1.07, -0.82 on roof C during 120°, 135°, 150°, 165° wind attack, -0.81 on roofs C and F during 180° angle of wind attack.
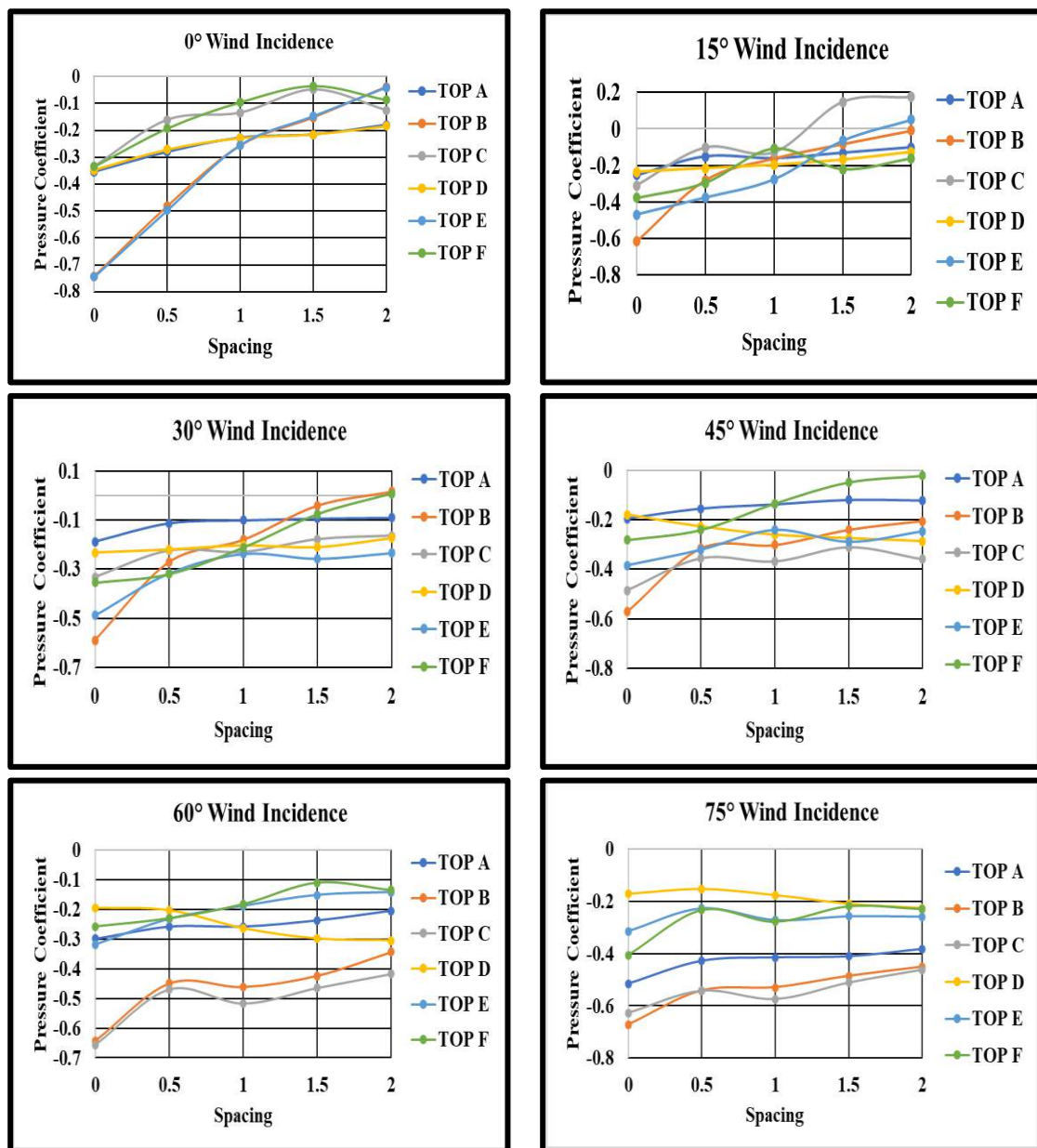
Fig. 6.15(a): Pressure Coefficient for Rectangular Pattern of mono-slope roof

159
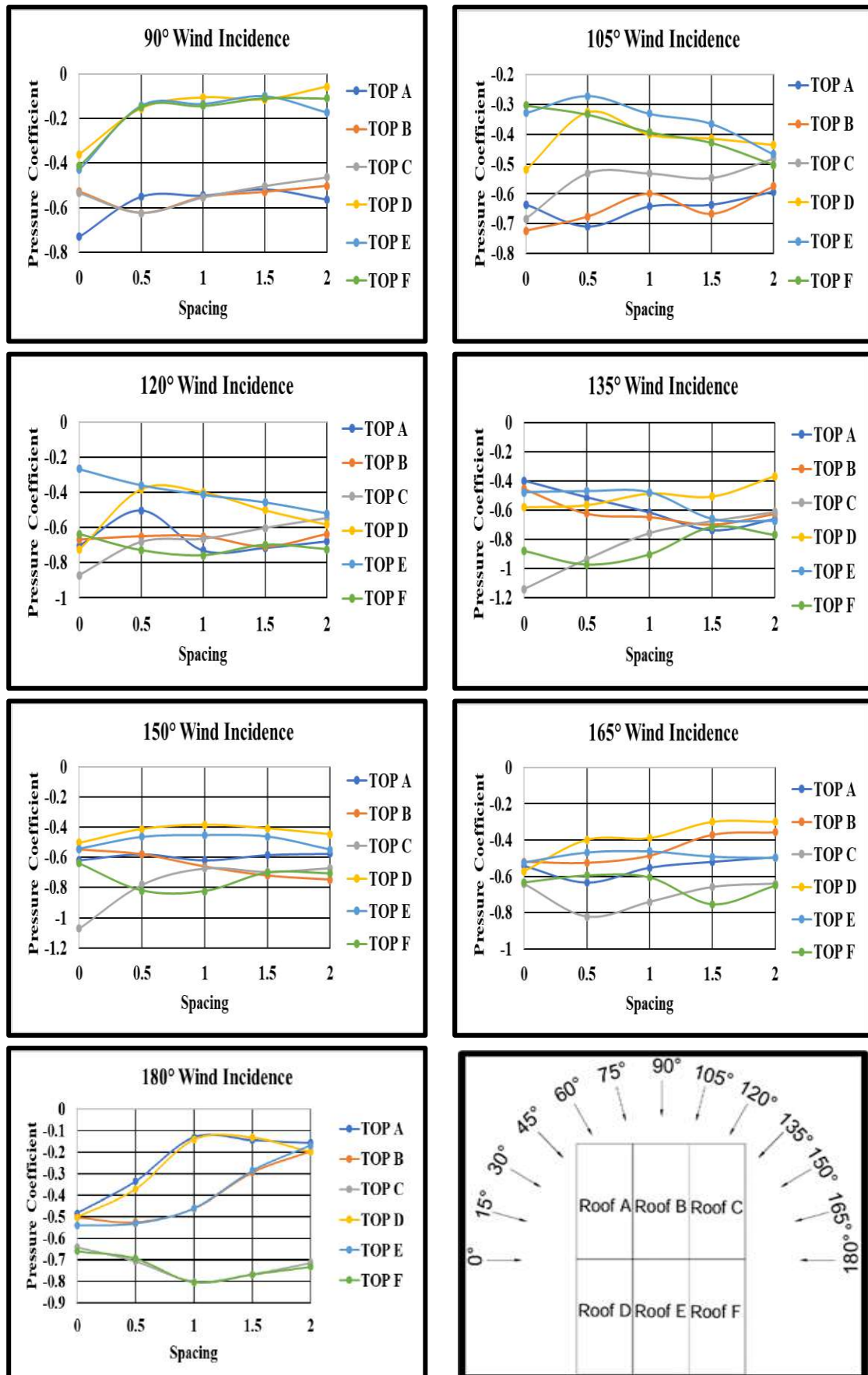
Fig. 6.15(b): Pressure Coefficient for Rectangular Pattern of mono-slope roof

6.3.1.3 Interference Factor (IF)

For the numerical representation of the effects induced by the wind action due to interfering with the building under investigation, the *IF* can be utilized effectively. If the value of C_{pe} on the building under study is decreased due to interfering building which results in the reduction of *IF*, it indicates that the suction on the building is reduced due to the shielding effect of interfering building on the building under study, but the nature of wind action is same.

The lower the value of *IF* lesser will the wind-induced action on the roof of the building under study. If there is a change in the sign of *IF* i.e., positive to negative then it implies that the wind action has changed its nature on the roof or the building under investigation. The role of spacing and wind incidence angle plays a vital role in wind-induced action on all the roofs under investigation which results in variation of *IF* for all the roofs as shown in Fig. 6.16.

In all the conditions of spacing between buildings, the *IF* is moving towards reduced value i.e., from a value of greater than 1 to less than 1, which is proved to be beneficial due to interference. During 0° wind incidence angle, roofs C and F are undergoing maximum reduced suction (*IF* less than 1) due to interference as compared to the other roofs. The value of *IF* on roof A is greater than 1 at 75°, 90°, 105° and 120° angles of wind attack, while *IF* is less than 1 at other angles i.e., 0° to 60° and 135° to 180° indicated the reduced suction on roof due to interference. The range of *IF* for roof B is between 3.97 (maximum suction) to -0.66 (least suction), in which the *IF* is less than 1 only at 135°, 150° and 165° angle of wind attack. The maximum increase in suction on roof C during interference is at 60° angle of wind attack with 0 spacing, during which the value of *IF* is 2.33, while the maximum reduction in suction on roof C takes place when *IF* is -0.91 at 15° wind angle with 2B spacing during which the nature of wind is changed from suction to positive pressure.

The maximum value of *IF* is 1.86 at 0° wind angle with 0 spacing interference and minimum value of *IF* is -0.68 at 165° angle of wind attack with 1.5B spacing. Just like roof B, the value of *IF* is 3.98 on roof E at 0° angle of wind attack with 0 spacing, indicates the maximum increase in suction the roof and *IF* is -0.26 when the spacing is 2B and angle of wind attack is 15° resulting in change of nature of wind on roof E from negative to positive.

The variation of *IF* for rectangular pattern arrangement of 30° mono-slope roofs with different spacing and at different angles of wind attack is shown in Fig. 6.16. The overall range of variation of *IF* is lying in between 3.97 to -0.90, in which the magnitude of *IF*≥1 indicates the suction on roof and *IF*≤1 indicates the changed nature of wind from suction to positive pressure.
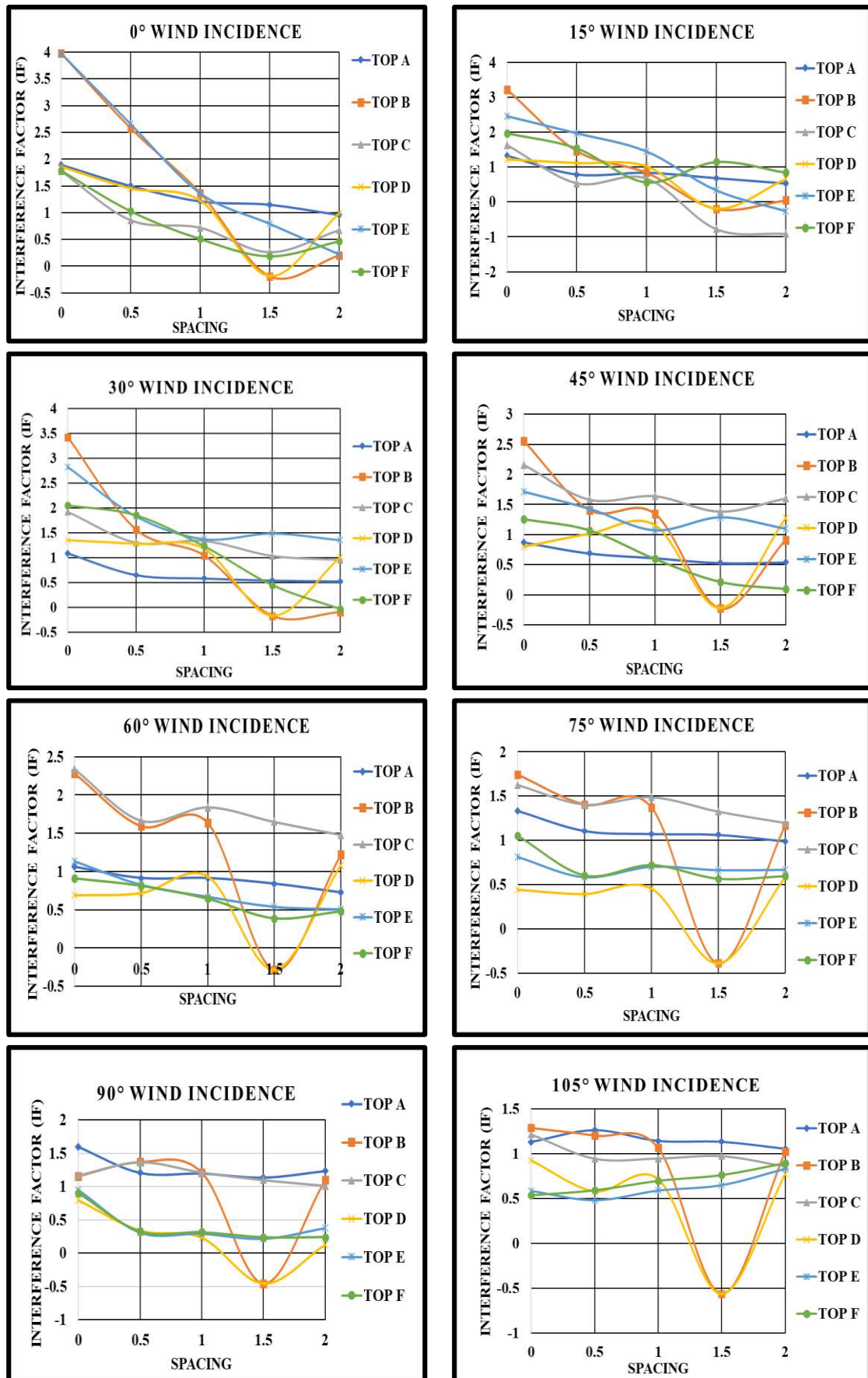
Fig. 6.16(a): Interference Factor for Rectangular Pattern of 30° Mono-slope roof
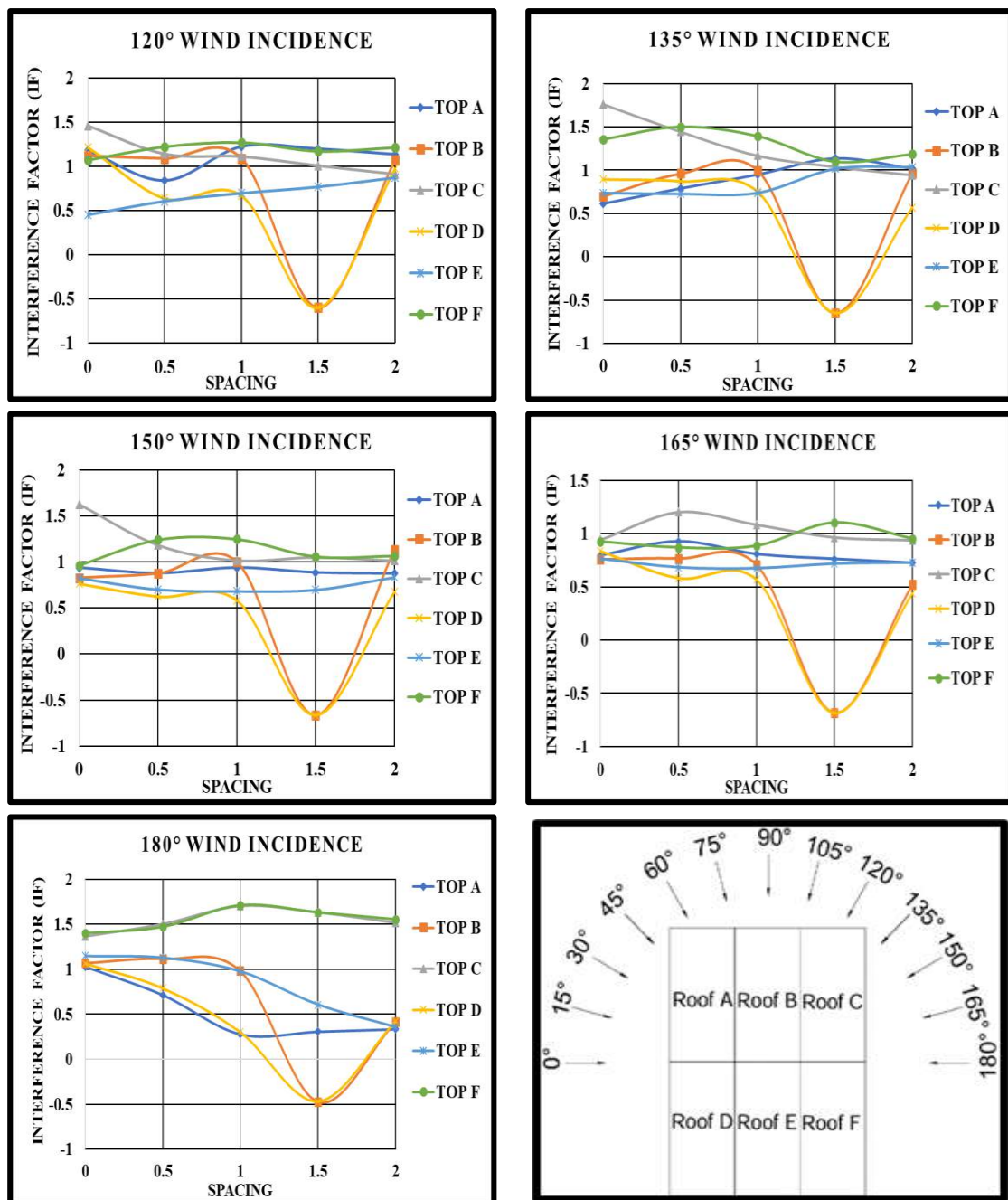
Fig. 6.16(b): Interference Factor for Rectangular Pattern of 30° Mono-slope roof

6.3.1.4 Interference Difference (ID)

Sometimes it comes to knowledge that due to interference either pressure or suction on buildings gets reduced such as the action of shielding effect on the roof due to the presence of the interfering building in the upstream direction of the wind flow resulting in the reduction of the pressure or suction. The values of *ID* are calculated for all the 30° mono-slope roofs under variable spacing and wind interval conditions presented in Fig. 6.17. The pattern of variation of *ID* for a 30° mono-slope roof is exactly similar to the variation of pressure coefficient with respect to the variable spacing and different angles of wind attack because *ID* denotes the

difference between the pressure coefficient during interfering conditions and isolated conditions. The negative sign of *ID* indicates the increased suction on the roofs due to interference of the upstream or side buildings, and the positive sign of *ID* denotes the reduced suction on the roof. Since it is clearly visible from Fig. 6.17, that initially at 0 spacing, the value of *ID* is less than 1 for all the roofs at all the angles of wind incidences, but it starts moving towards the reduced value i.e., *ID* becomes greater than or equal to 0 resulting in the reduced suction on the roof when spacing is increased from 0 to 0.5B, B, 1.5B and 2B at all the wind incidence angles. The overall range of variation of *ID* is lying between -0.55 to 0.40 indication the nature of wind changed from suction to positive pressure when the spacing is varying between zero to 2B.
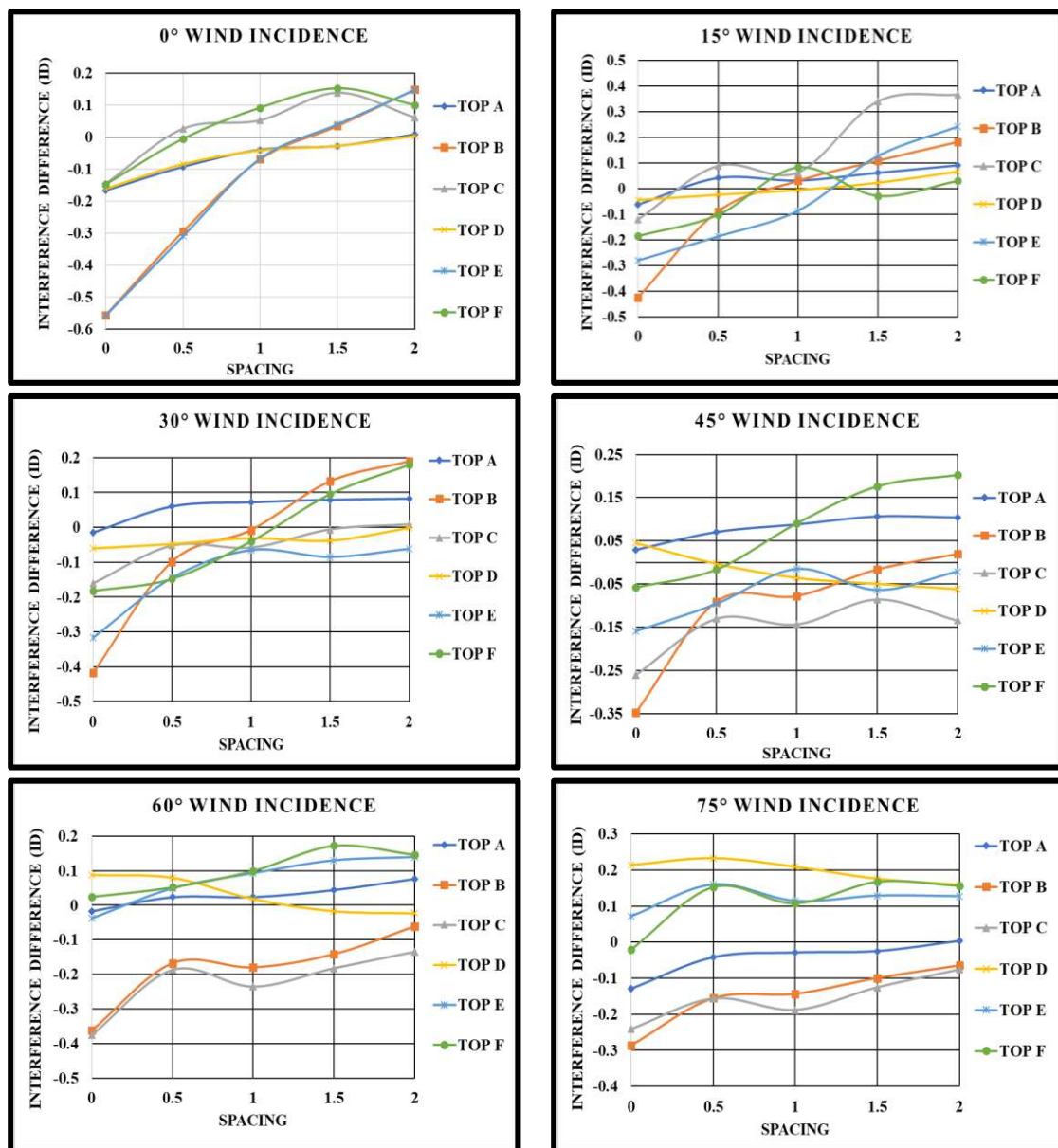
Fig. 6.17(a): Interference Difference for Rectangular Pattern of cylindrical roof
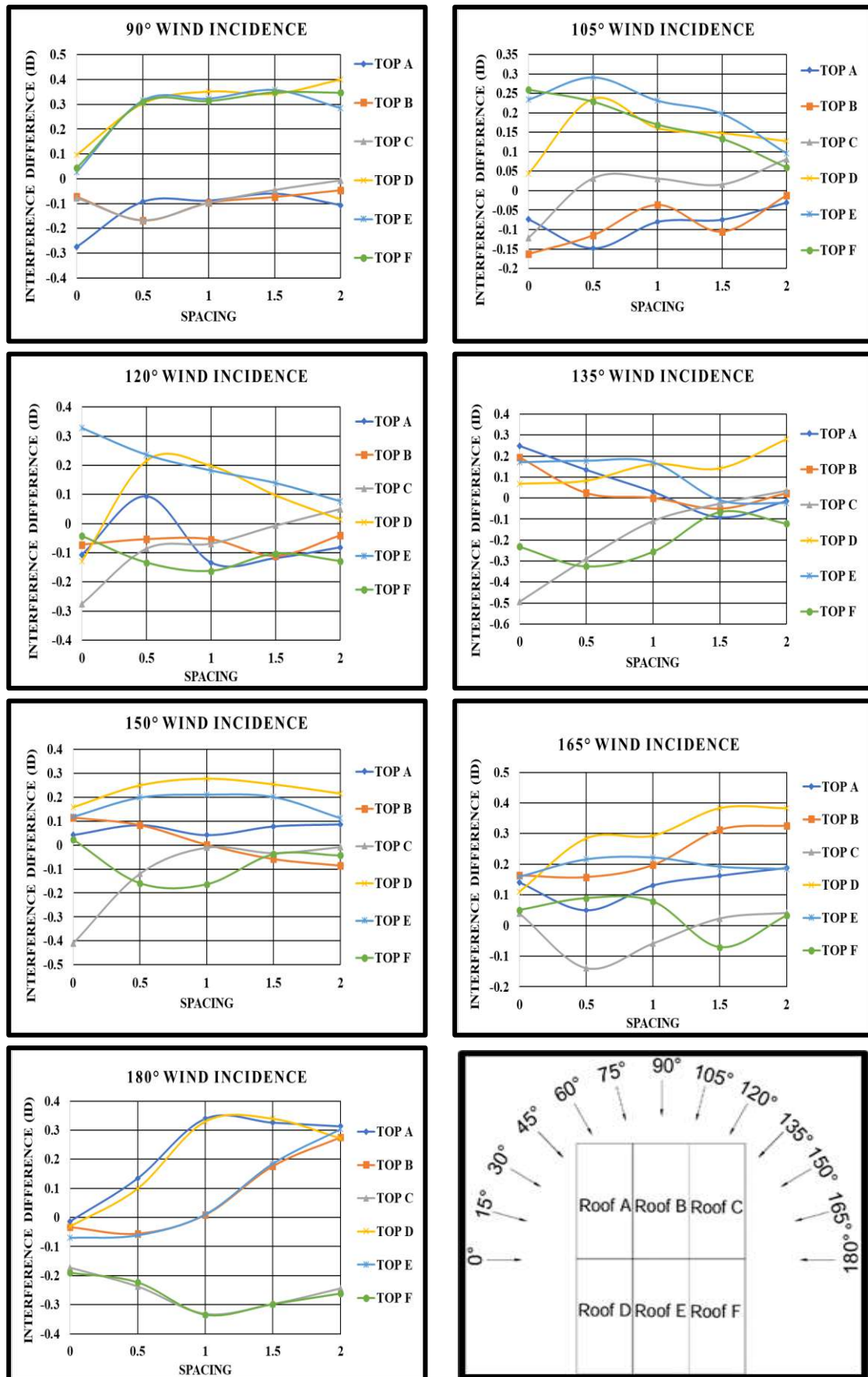
Fig. 6.17(b): Interference Difference for Rectangular Pattern of cylindrical roof

6.1.3.5 Wind Flow Streamlines

The wind flow streamlines for low-rise building with 30° mono-slope roof arranged in rectangular pattern with variable spacing are shown in Fig. 6.18 to 6.22 at different angles of wind incidence ranging between 0° to 180° at an interval of 45°. The streamlines are generated for different wind induced interference conditions by creating a plane at an eave height of the building i.e., 150 mm. It is clearly seen from Fig. 6.18 that in the case of zero spacing between the buildings, the wind flow is separated from the upstream wall in a uniform pattern and gets recirculated and the merged in downstream direction or in wake region. By increasing the spacing in between the buildings from zero to 0.5B, B, 1.5B and 2B, the wind starts flowing in between the buildings resulting in reduction of flow circulation in wake region. When the spacing is B, 1.5B and 2B, it is observed that the flow is recirculating in between the buildings during 0°, 45° and 180° angles of wind incidence. The spacing between buildings i.e., 0, 0.5B, B, 1.5B and 2B is proved to beneficial in reducing the vortices due to wind flow pattern.

Fig. 6.18(a): Wind Flow Streamlines for Rectangular Pattern with zero Spacing

180°
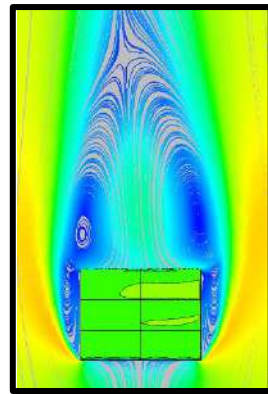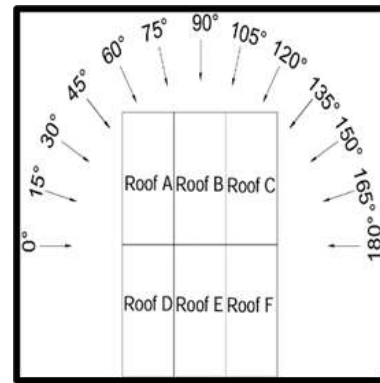
Wind Angles

Fig. 6.18(b): Wind Flow Streamlines for Rectangular Pattern with zero Spacing

0°

45°

90°

135°

180°
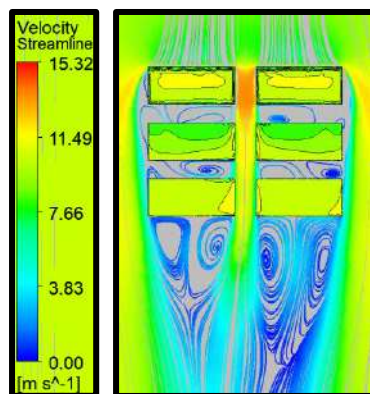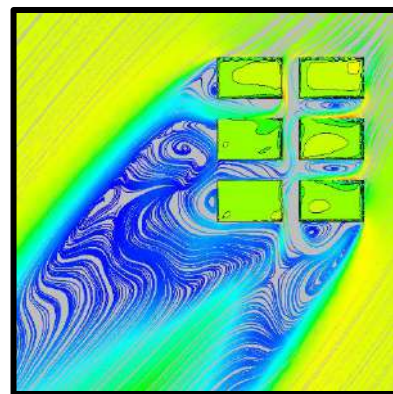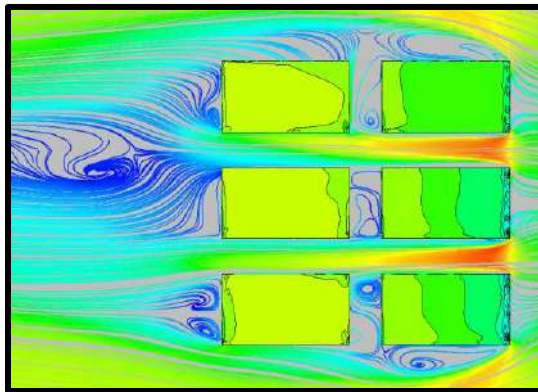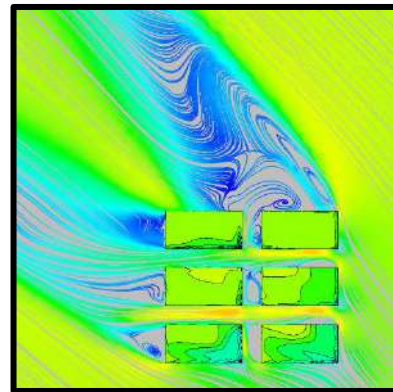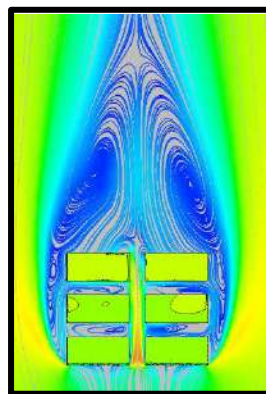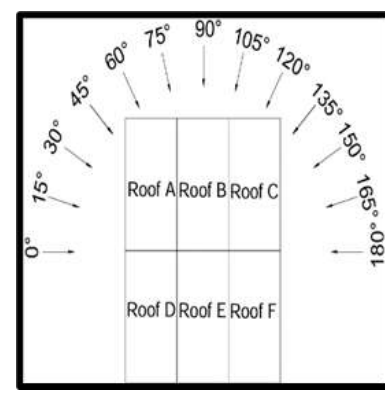
Wind Angles

Fig. 6.19: Wind Flow Streamlines for Rectangular Pattern with 0.5B Spacing

0°

45°

90°

135°

180°

Wind Angles
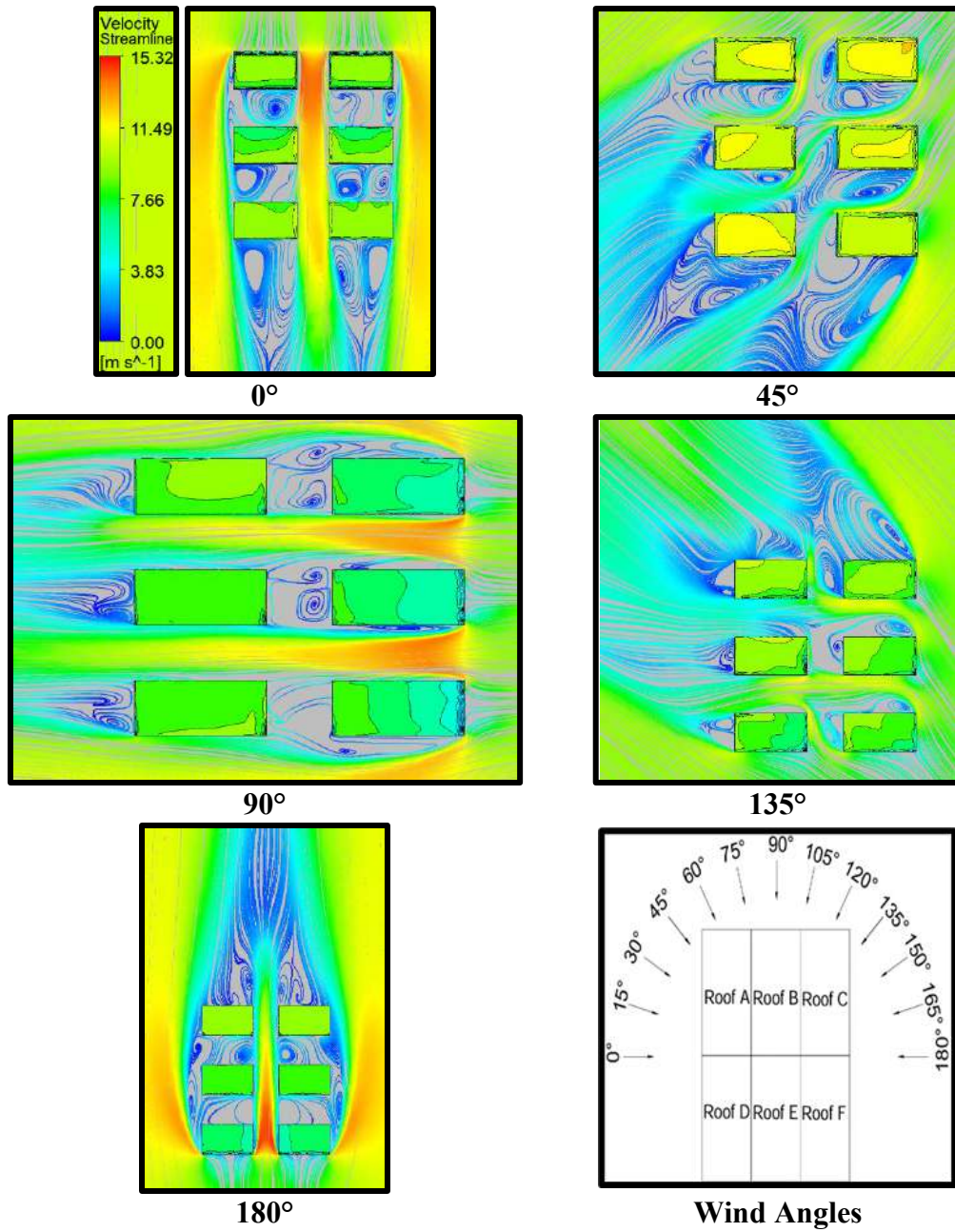
Fig. 6.20: Wind Flow Streamlines for Rectangular Pattern with B Spacing

0°

45°
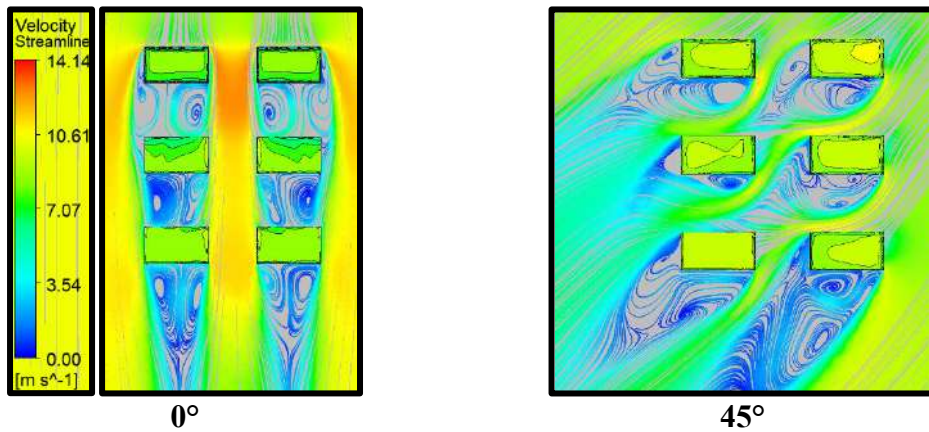
Fig. 6.21(a): Wind Flow Streamlines for Rectangular Pattern with 1.5B Spacing

90°

135°

180°

Wind Angles
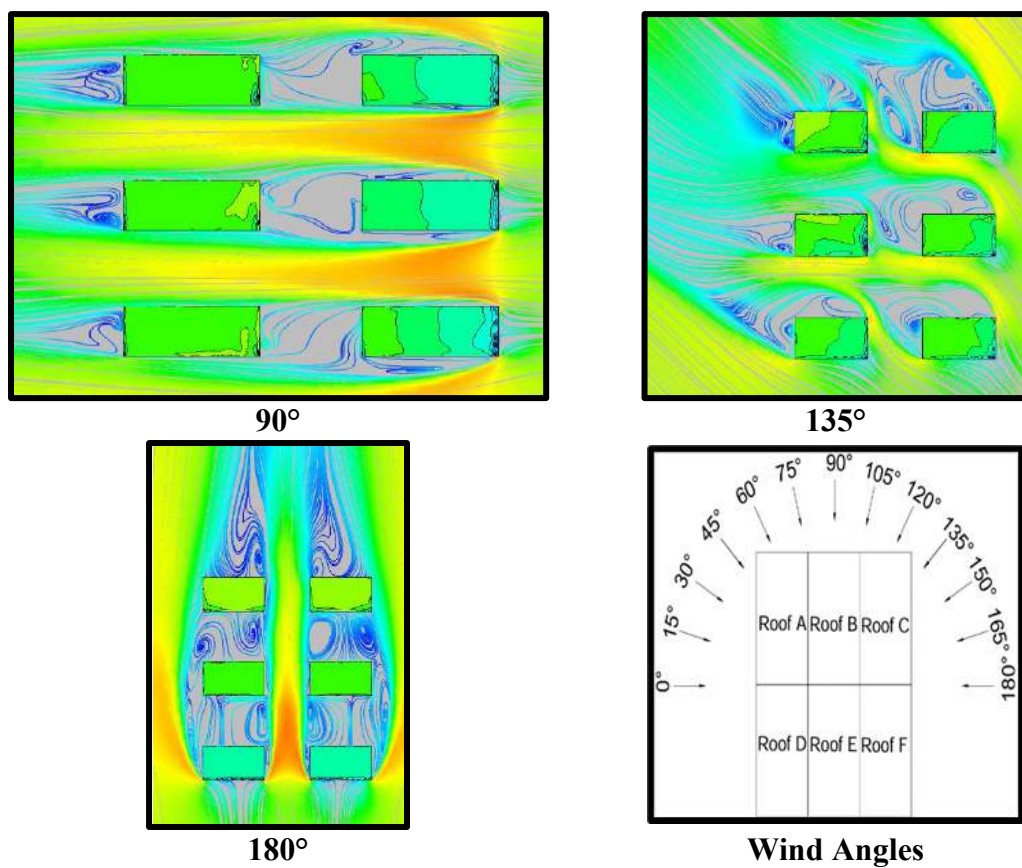
Fig. 6.21(b): Wind Flow Streamlines for Rectangular Pattern with 1.5B Spacing

0°

45°

90°

135°
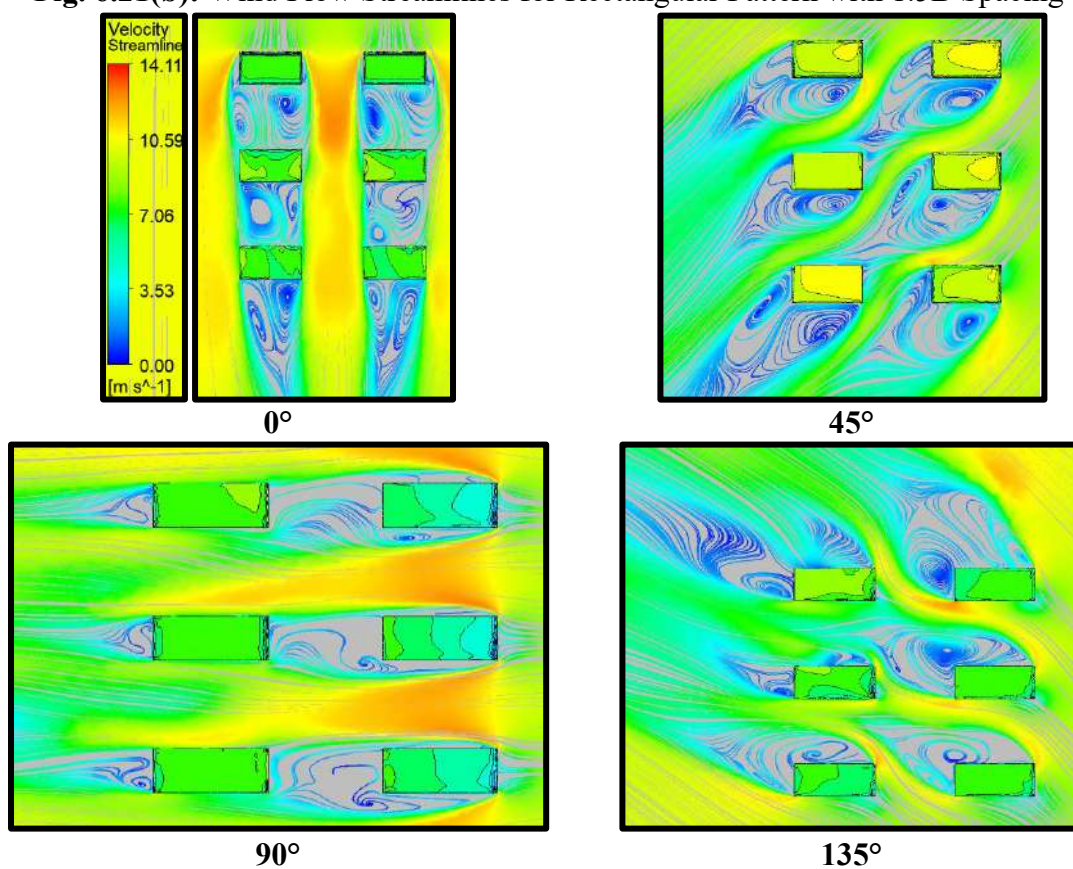
Fig. 6.22(a): Wind Flow Streamlines for Rectangular Pattern with 2B Spacing

| 180° | Wind Angles |
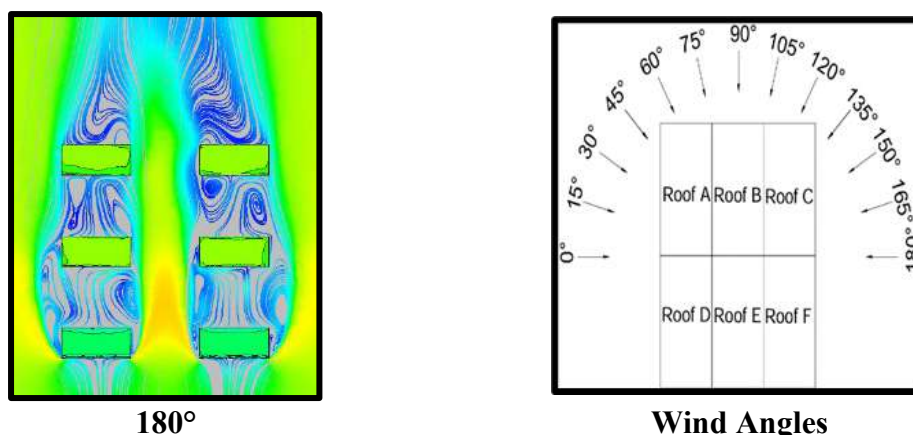
Fig. 6.22(b): Wind Flow Streamlines for Rectangular Pattern with 2B Spacing

6.3.2 Z Pattern

Similarly to the rectangular pattern, the 30° mono-slope roofs are now arranged in Z pattern of different interfering conditions with variable spacing of 0, 0.5B, B, 1.5B and 2B at different angles of wind attack i.e., 0° to 180° at 15° each interval to find out the wind effects on the roof, discussed below.

6.3.2.1 Pressure Contours

The wind-induced pressure contours on the 30° mono-slope roof of low-rise structures are investigated by arranging the low-rise building models in a Z pattern with variable spacing (0, 0.5B, B, 1.5B and 2B) using CFD simulation are discussed here in this section. The pressure contours, roof nomenclature and angles of wind incidences for all the spacing configurations are shown in Figs. 6.23-6.27.

It is clearly predictable from Figs. 6.23-6.27, that the 30° mono-slope roof is under negative wind induced pressure distribution during all the wind attacks i.e., ranging between 0° to 180° at 15° intervals. Spacing between the mono-slope roof from i.e., 0, 0.5B, B, 1.5B and 2B is beneficial in reducing the pressure distribution on the roofs as shown in Figs. 6.23-6.27 respectively.

It is also noticed that the edges (windward, leeward and side edges) of the 30° mono-slope roofs are under higher negative pressure as compared to the central portion of the roofs. The effects of interference are mostly visible from the roofs which are lying in the single central line of the z-pattern also when the angle of wind attack is 0°, 90° and 180° respectively.

The maximum change in wind pressure distribution i.e., conversion of negative pressure into positive pressure on the roof is noticed during 0.5B and B spacing between the buildings as shown in Figs. 6.24 & 6.25 respectively. The overall pressure variation when mono-slope roof is arranged in Z pattern is -76.29Pa to 13.70Pa.

0°   15°   30°

45°   60°   75°

90°   105°   120°

135°   150°   165°

180°   Roof Nomenclature and Wind Angles
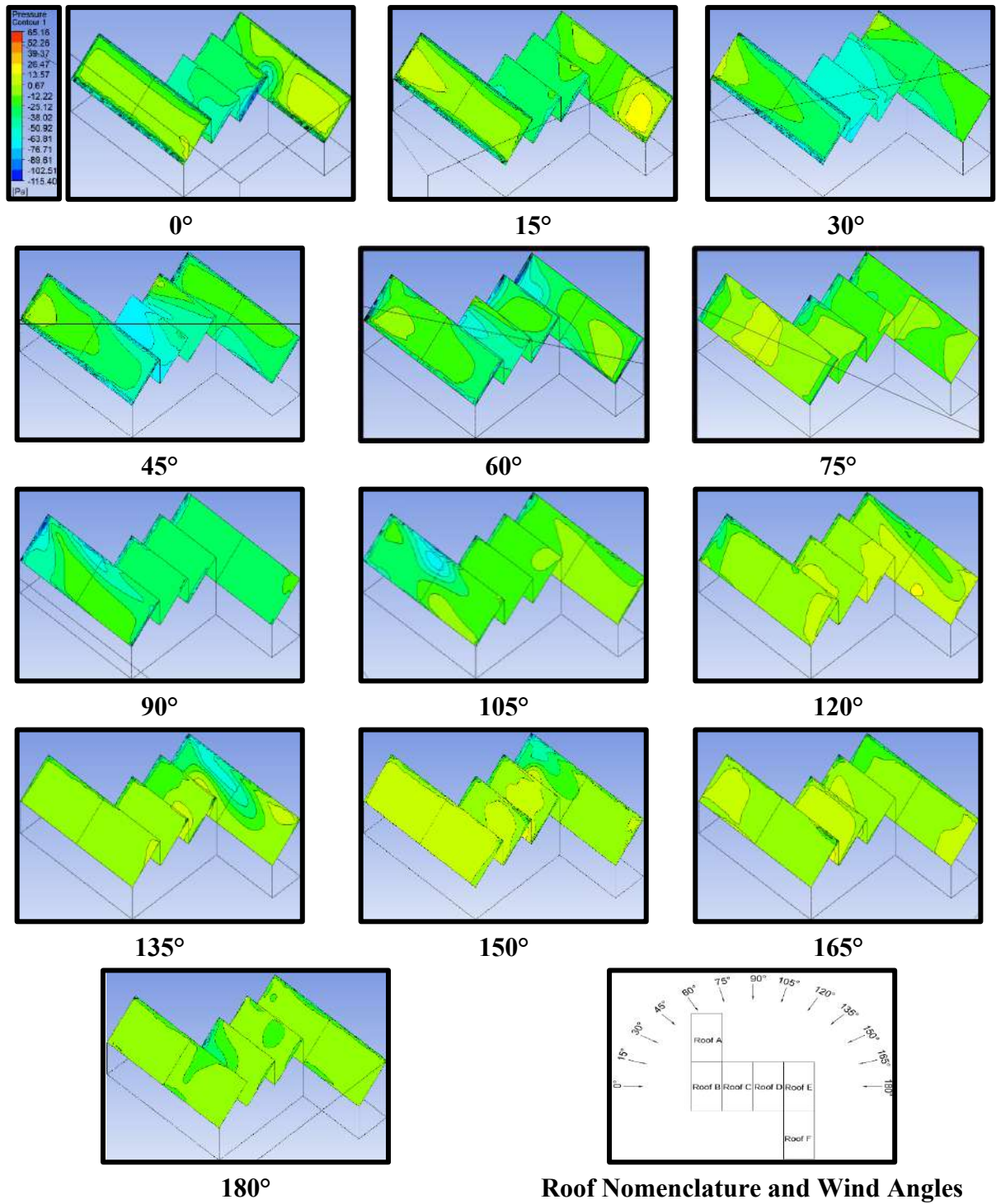
Fig. 6.23: Pressure Contours for Z pattern with Zero Spacing

0°   15°   30°

Fig. 6.24(a): Pressure Contours for Z pattern with 0.5B Spacing

45°

60°

75°

90°

105°

120°

135°

150°

165°

180°

Roof Nomenclature and Wind Angles
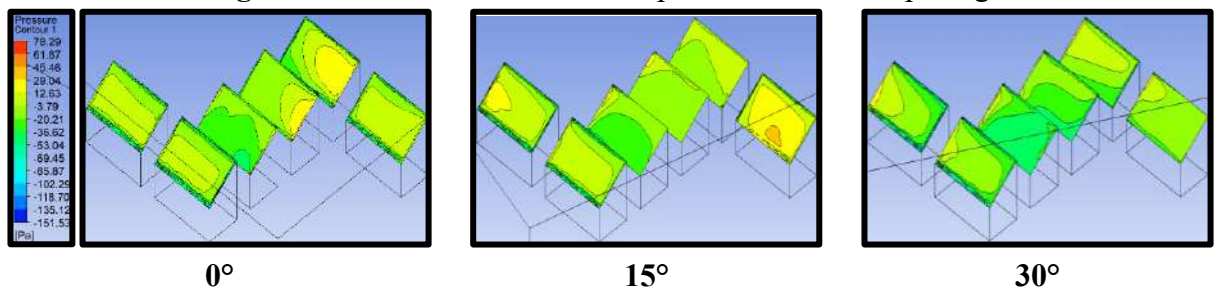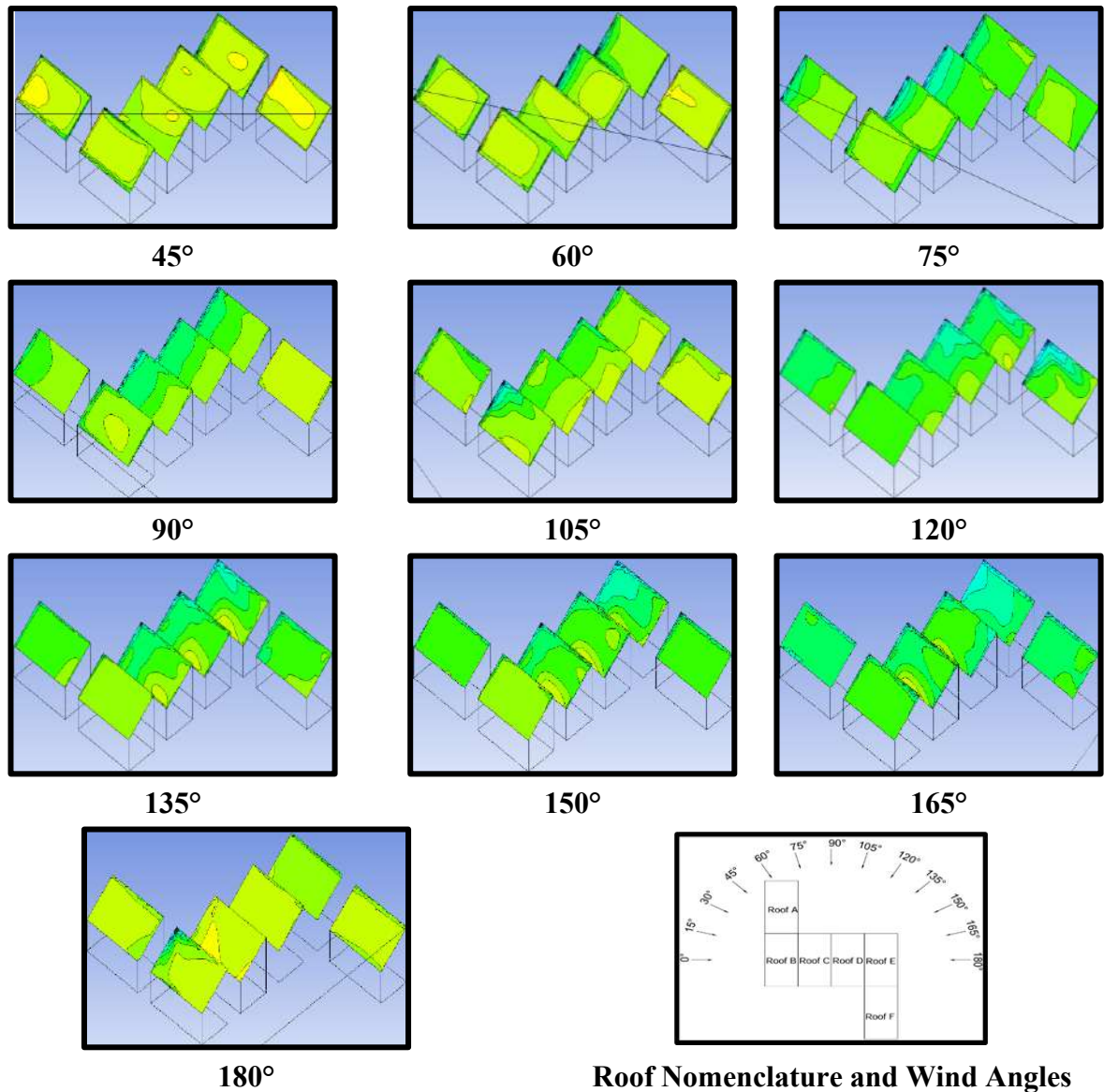
Fig. 6.24(b): Pressure Contours for Z pattern with 0.5B Spacing

0°

15°

30°

45°

60°

75°

Fig. 6.25(a): Pressure Contours for Z pattern with B Spacing
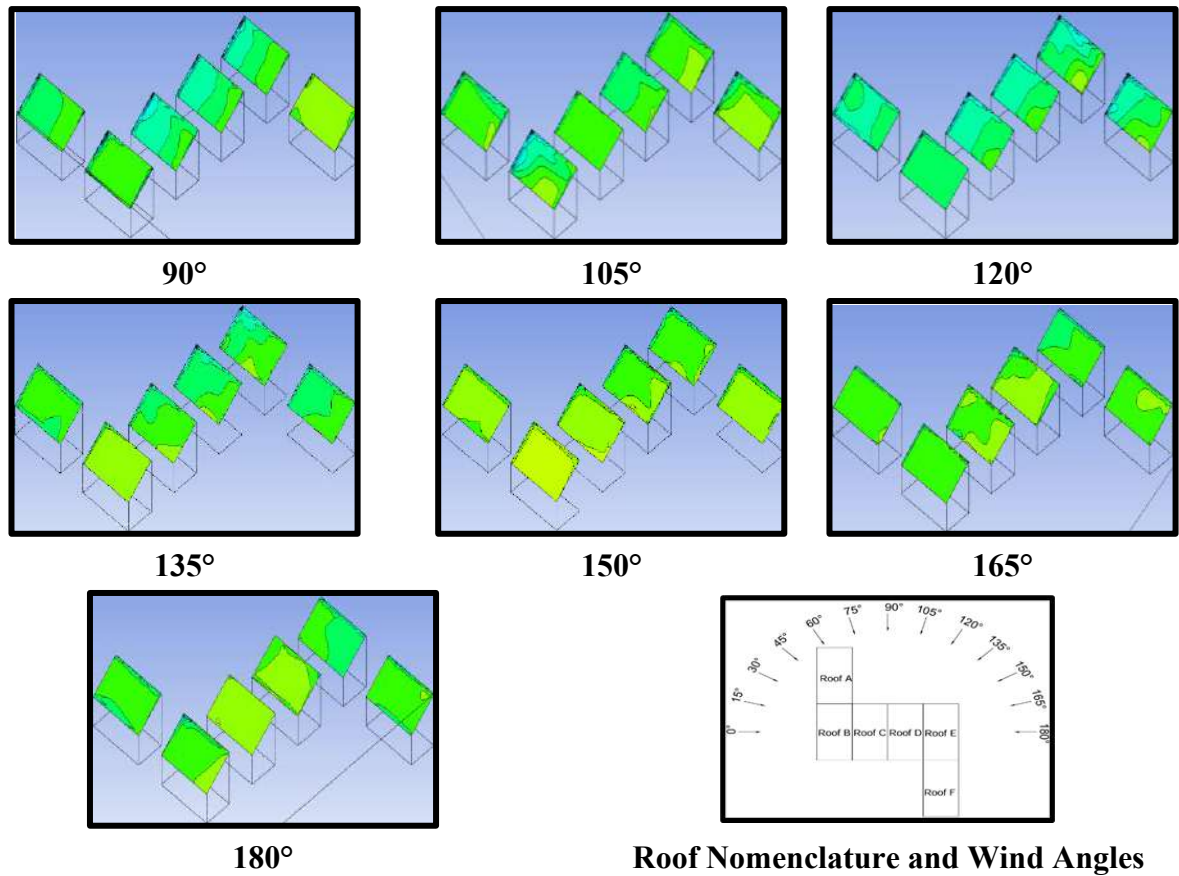
90°

105°

120°

135°

150°

165°

180°

Roof Nomenclature and Wind Angles

Fig. 6.25(b): Pressure Contours for Z pattern with B Spacing

0°

15°

30°

45°

60°

75°

90°

105°

120°

Fig. 6.26(a): Pressure Contours for Z pattern with 1.5B Spacing

135° **150°** **165°**

180° **Roof Nomenclature and Wind Angles**

Fig. 6.26(b): Pressure Contours for Z pattern with 1.5B Spacing

0° **15°** **30°**

45° **60°** **75°**

90° **105°** **120°**

135° **150°** **165°**
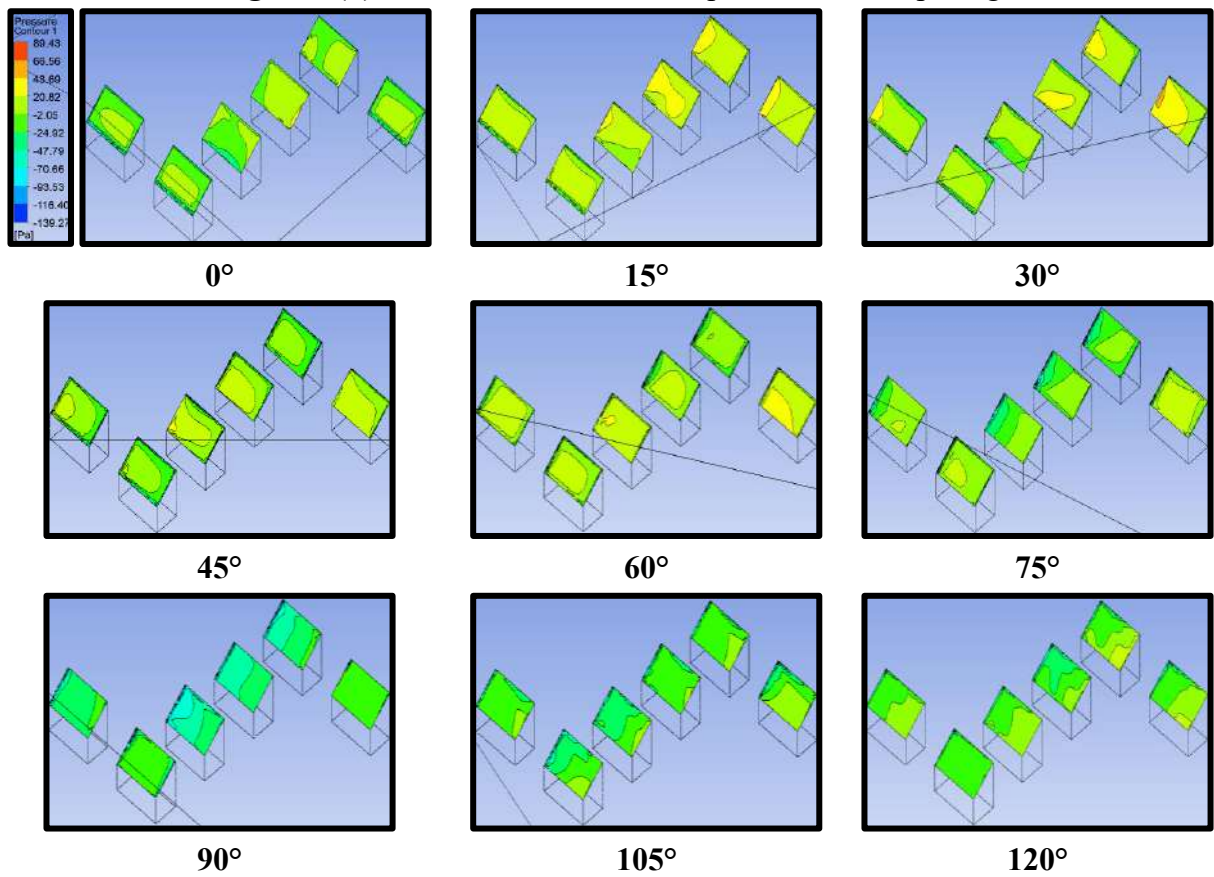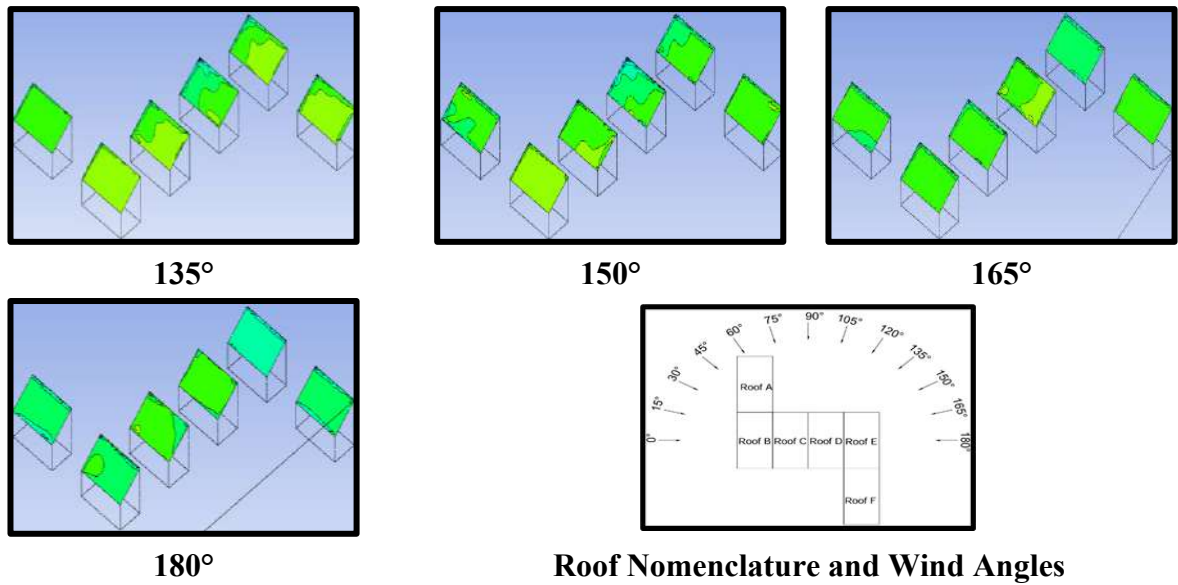
Fig. 6.27(a): Pressure Contours for Z pattern with 2B Spacing
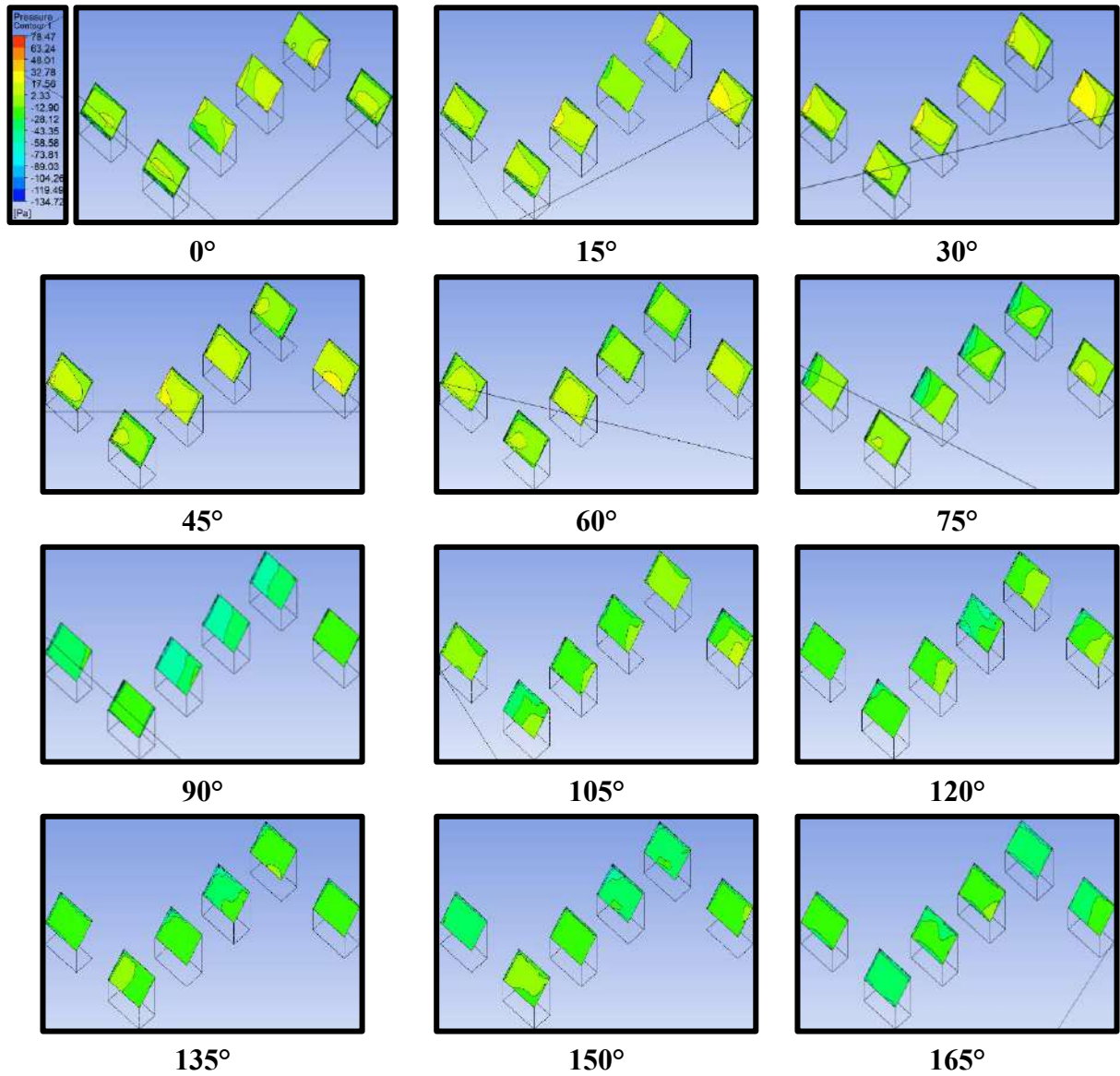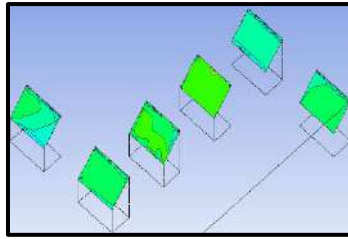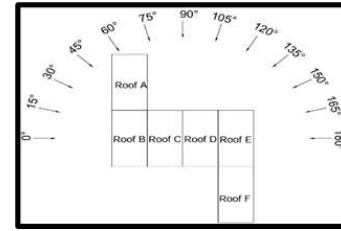
| 180° | Roof Nomenclature and Wind Angles |

Fig. 6.27(b): Pressure Contours for Z pattern with 2B Spacing

6.3.2.2 Pressure Coefficient (C_{pe})

The variation of C_{pe} on the 30° mono-slope roof of six low-rise buildings arranged in z pattern with variable spacing of zero, 0.5B, B, 1.5B and 2B at different angles of wind interval ranging between 0° to 180° having an interval of 15° each, is shown in Fig. 6.28. At each interval of wind incidence, it is observed that the value of C_{pe} is negative in magnitude on all the 30° mono-slope roofs in the case of different spacings between the buildings. The range of C_{pe} on roof A is -0.94 to -0.07 indicating that there is only suction on the roof in which the maximum suction is occurring during 120° angle of wind incidence with zero spacing between the buildings, while the minimum suction on roof A is observed during 30° wind incidence with 2B spacing between the buildings. The maximum and minimum suction on roof B is observed when the value of C_{pe} is -0.84 at 105° wind angle with B spacing and -0.13 at 15° wind angle with 2B spacing. The maximum value of negative C_{pe} on roofs C, D, E and F is occurring during 135° angle of wind incidence i.e., -0.82 with 0.5B spacing on roof C, -0.99 with 1.5B spacing on roof D, -1.25 with zero spacing on roof E and -0.86 with 0.5B & B spacing on roof F respectively. The value of C_{pe} is noticed as positive in magnitude which indicates that the negative pressure changed into positive pressure due to interference on roof C i.e., +0.05 at 45° wind angle with 2B spacing, +0.10 at 15° wind interval with 1.5B spacing on roof D, +0.04 at 30° wind interval with B & 1.5B spacing on roof E and +0.22 at 30° wind incidence with 1.5B spacing on roof F.
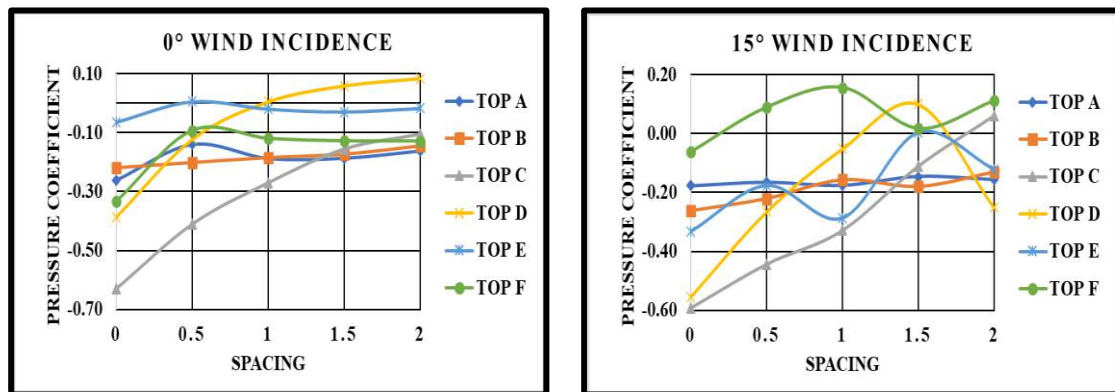
Fig. 6.28(a): Pressure Coefficient for Z pattern of 30° mono-slope Roof
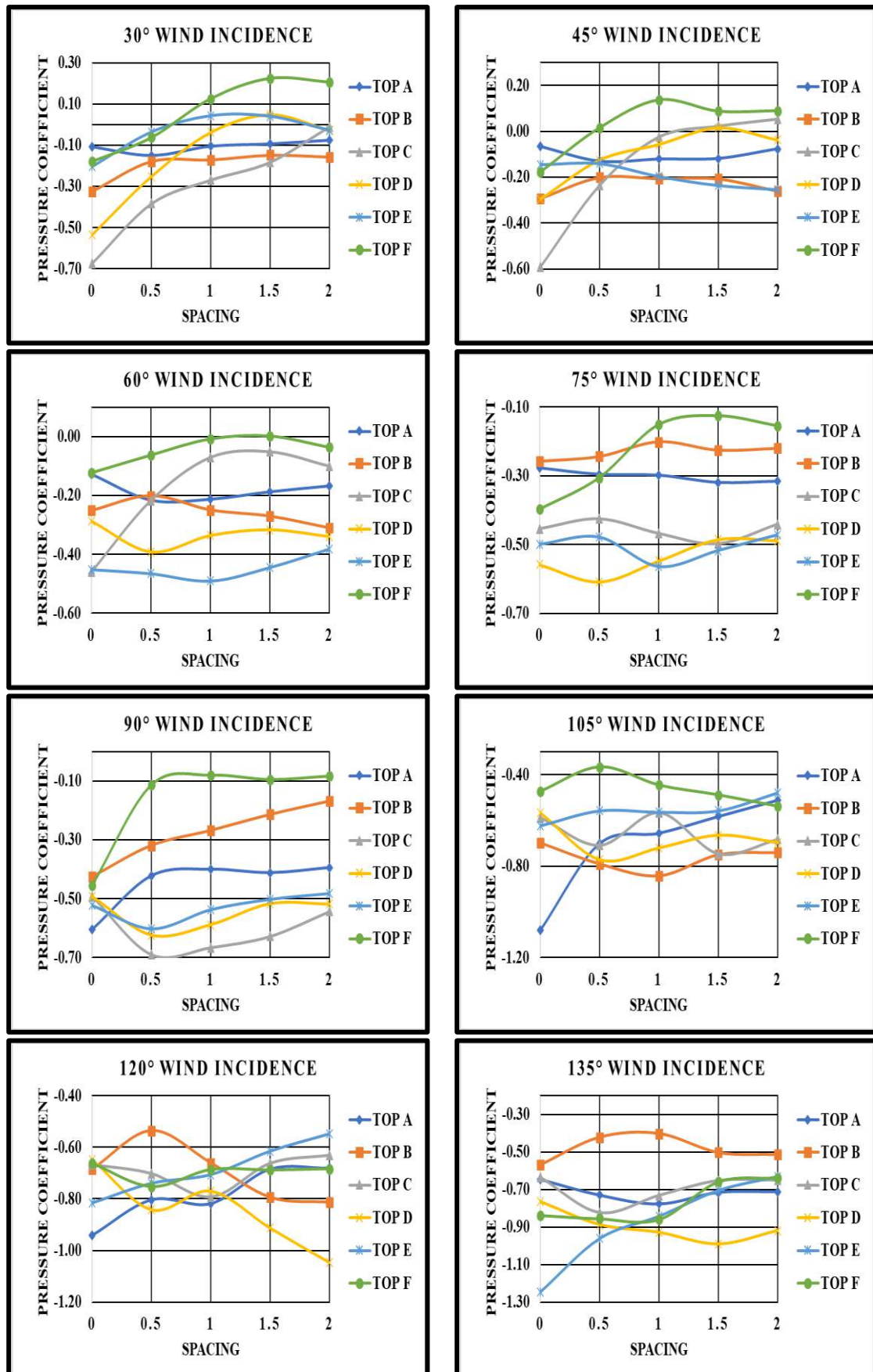
Fig. 6.28(b): Pressure Coefficient for Z pattern of 30° mono-slope Roof
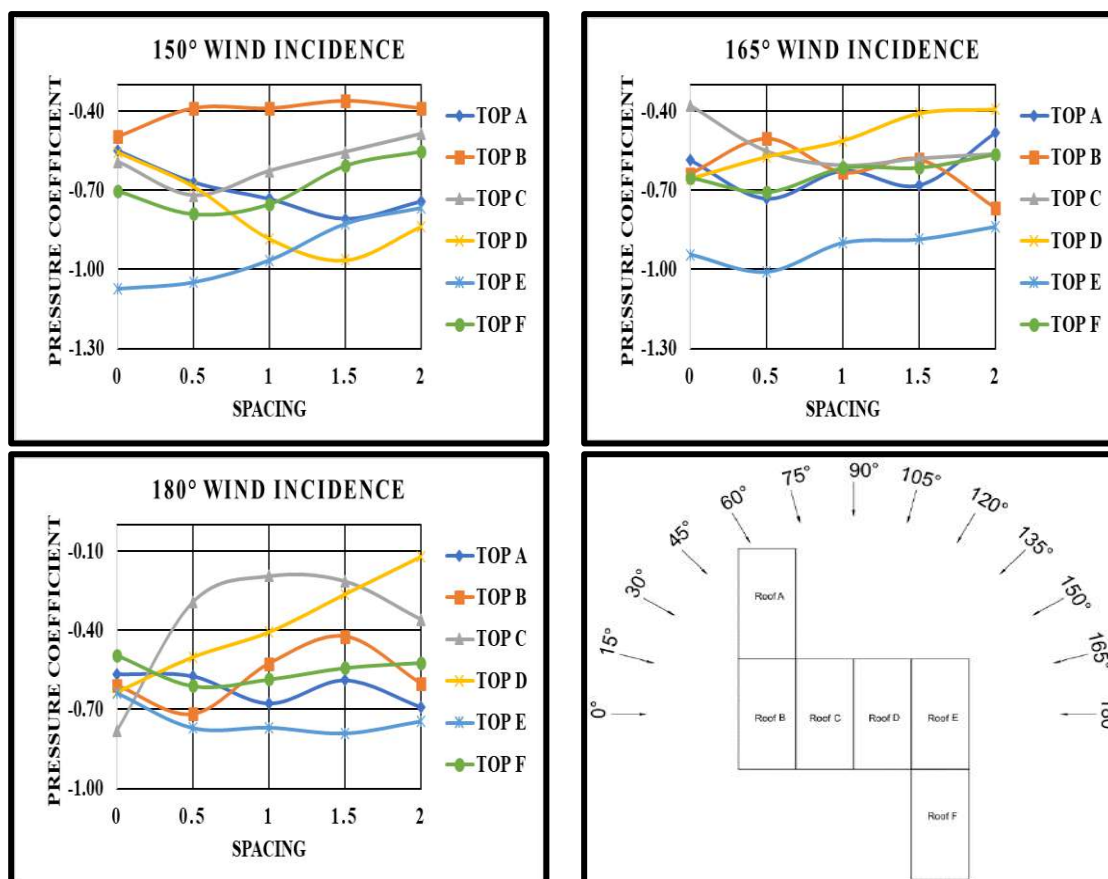
Fig. 6.28(c): Pressure Coefficient for Z pattern of 30° mono-slope Roof

6.3.2.3 Interference Factor (IF)

The idea of enhancement or reduction of suction or pressure on the roof is given by interference factor (*IF*) due to the presence of low-rise structure in the vicinity. The value of If gets modified with respect to the spacing between the buildings and angles of wind attack. The varying magnitude of *IF* on a 30° mono-slope roof arranged in a z pattern with variable spacing (0,0.5B, B, 1.5B and 2B) at various angles of wind attacks, i.e., 0° to 180° at 15° intervals is shown in Fig. 6.29. The value of *IF* on the roof A keeps on reducing with an increase in spacing from 0 to 2B. Initially, the value of *IF* comes out to be more than 1, indicating the increased suction on roof A at 0°, 60°, 90°, 105°, 120° and 135° angles of wind incidence with zero spacing, but it gets reduced while increasing the spacing till 2B at which *IF* becomes less than 1 indicating the reduced suction on roof A. On the rest of the wind incidence angles i.e., 15°, 30°, 45°, 75°, 150°, 165° and 180°, the value of *IF* is already less than 1 for roof A. Similarly to the IF of roof A, the value of *IF* for roof B follows the same trend in which its value comes out to be more than 1 when the angles of wind attack are 0°, 15°, 30°, 45°, 60°, 105° and 165° respectively and starts reducing when spacing between the building in increased from 0 to 2B. Also, the maximum reduction in *IF*, i.e., reduced suction on roof B, is observed at 1.5B spacing

at all the wind incidence angles, i.e., 0° to 180° at 15° intervals, as shown in Fig. 6.29. A drastic reduction in the value of *IF* for roof C is observed at 0°, 15°, 30°, 45°, 60° and 180° angles of wind incidence when the spacing is changed from 0 to 2B, during which *IF* changed from more than 1 to less than 1, indicating the reduced suction on roof C. But, on the rest of the wind incidence angles, the value of *IF* already comes out to be less than 1 and not much changed with respect to the spacing. The variation of *IF* on roof D follows the same pattern as that of roof B when wind incidence angles are 75°, 90°, 105°, 135°, 150° and 165°, at which the maximum reduction of *IF* takes place when the spacing is 1.5B between the buildings. The value of *IF* for roof E is less than 1 only in cases when the angle of wind incidence is 0°, 30° and 45°, indicating the reduced suction on roof E due to interference. The reduction in value of *IF* for roof F with respect to the spacing is observed when the angle of wind incidence is ranging between 0° to 105° and 165° respectively as shown in Fig. 6.29. The variation of spacing between the buildings is proved to be beneficial which helps in reducing the suction on the roof and greatly influences the nature of wind on roofs. The angle of wind incidence also plays a vital role in changing the magnitude of *IF* on the roof or low-rise structure with mono-slope roof.

Fig. 6.29(a): Interference Factor for Z Pattern of 30° mono-slope Roof
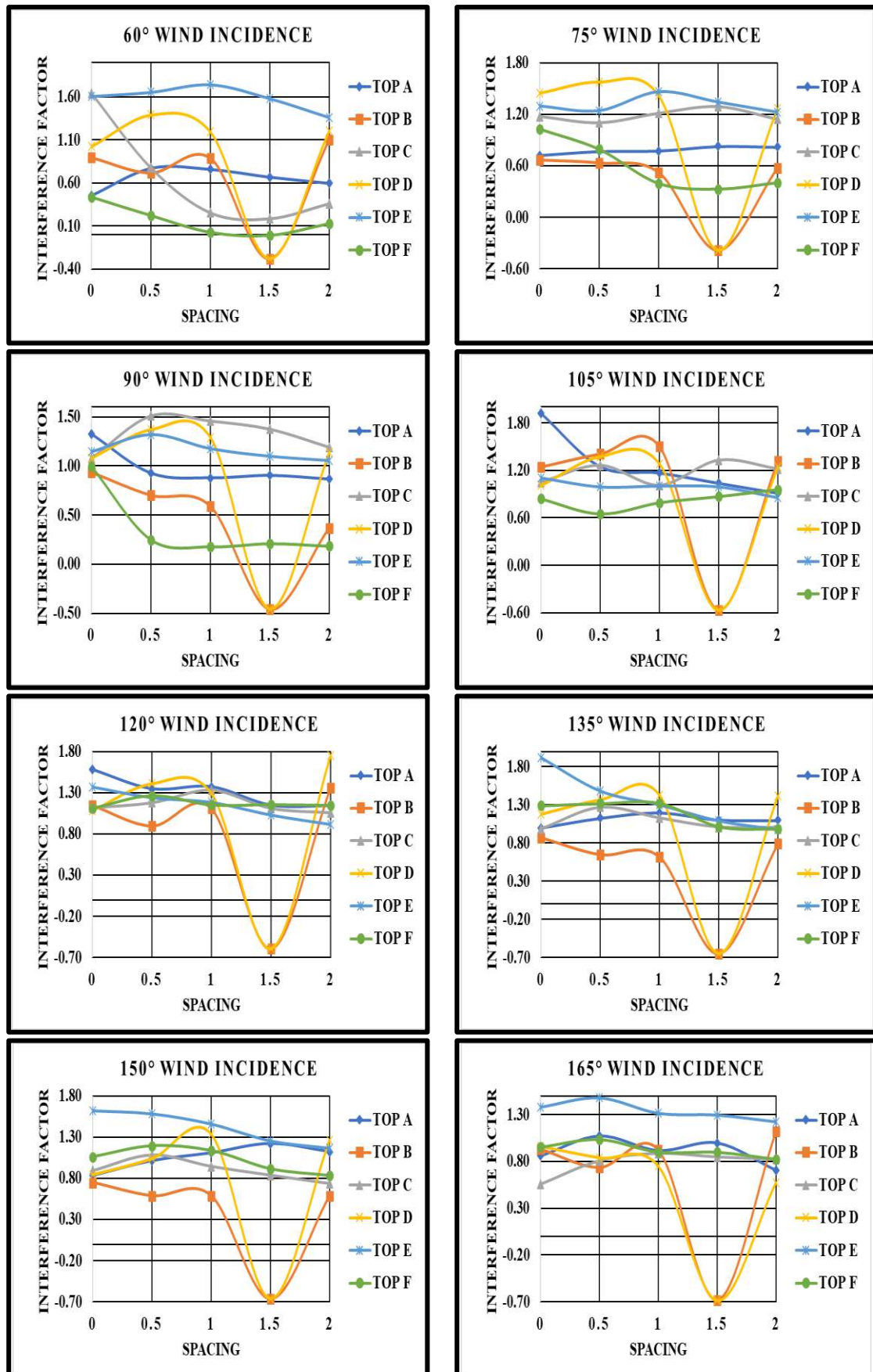
Fig. 6.29(b): Interference Factor for Z Pattern of 30° mono-slope Roof
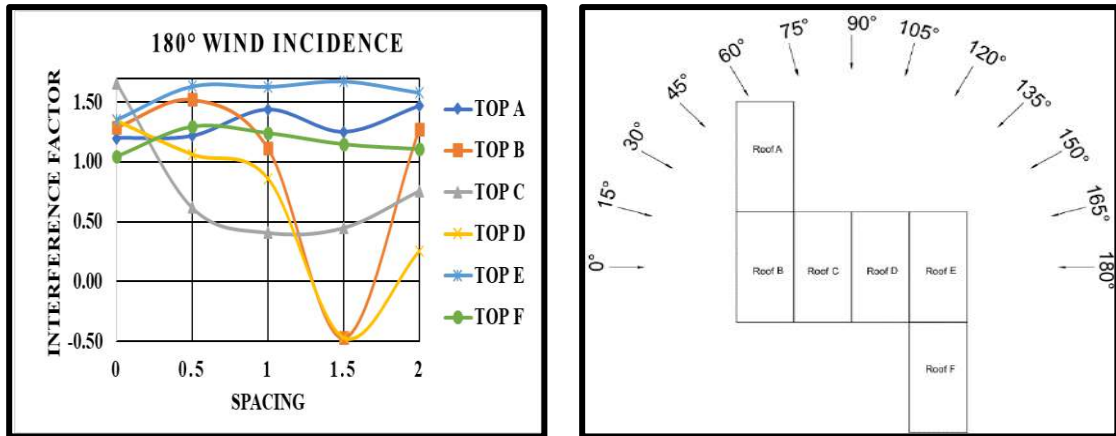
Fig. 6.29(c): Interference Factor for Z Pattern of 30° mono-slope Roof

6.3.2.4 Interference Difference (ID)

The difference between C_{pe} obtained during an interfering condition and C_{pe} obtained during an isolated condition is called as interference difference (*ID*), which gives an exact idea of enhancement or reduction in the wind-induced positive or negative pressure coefficient on the roofs. The variation of *ID* on 30° mono-slope roofs arranged in a z pattern with different spacing ranging between 0 to 2B (where B is the width of a low-rise building) and at various angles of wind incidences ranging between 0° to 180° at 15° intervals is shown in Fig. 6.30. When the magnitude of negative C_{pe} on the roof is increased during interfering conditions, then the value of *ID* comes out to be negative, indicating the increased suction on the roof during interfering conditions, while the value of *ID* is positive, but the magnitude of C_{pe} is still negative on the roofs indicates that the suction on the roof is reduced due to interference of vicinity buildings. This variation of *ID* on 30° mono-slope roof arranged in z pattern with variable spacing with respect to different angles of wind incidences is shown in Fig. 6.29 below. The overall variation of *ID* when mono-slope roofs are arranged in Z pattern is 1.23 to -0.44 in which the positive sign indicates the wind nature as suction on roof and negative sign indicates the changed nature of wind from suction to positive pressure.
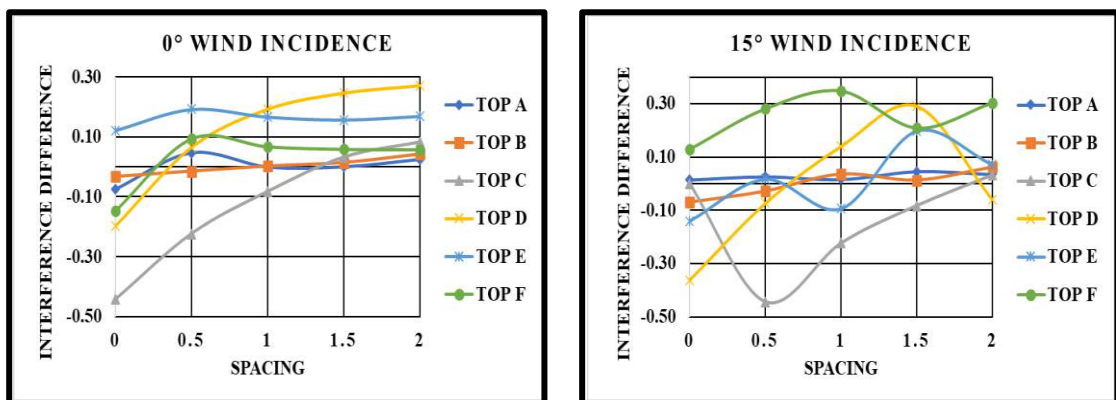
Fig. 6.30(a): Interference Difference for Z Pattern of 30° mono-slope Roof
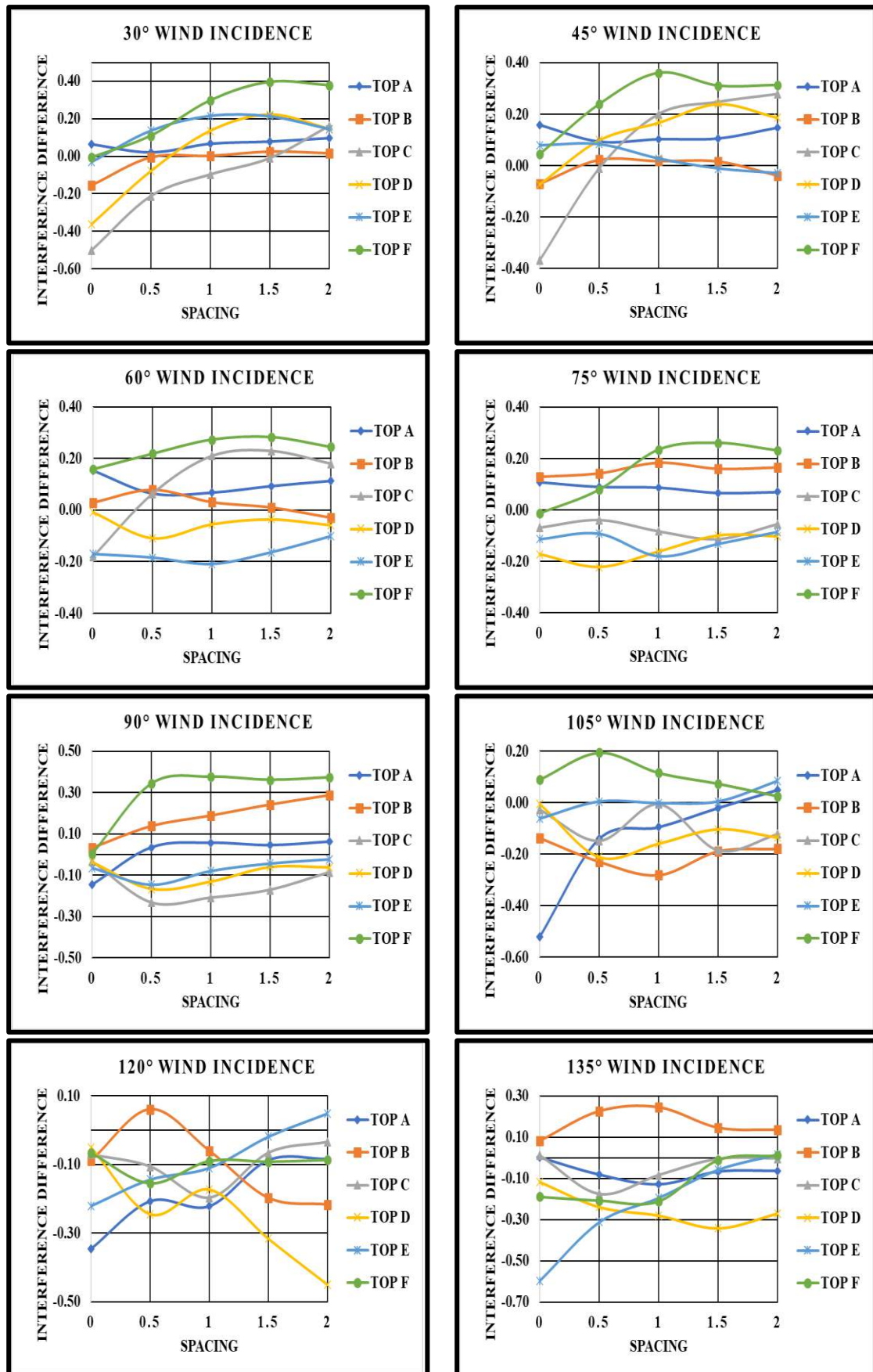
Fig. 6.30(b): Interference Difference for Z Pattern of 30° mono-slope Roof
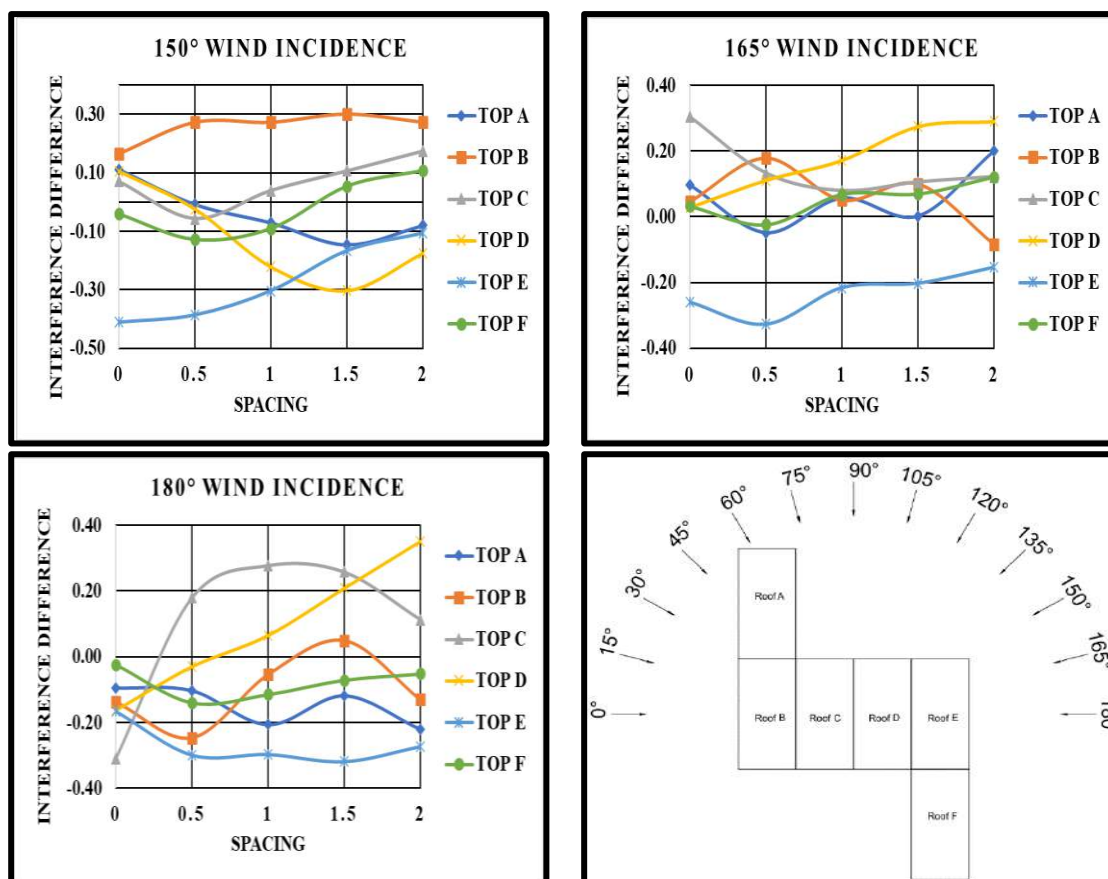
Fig. 6.30(c): Interference Difference for Z Pattern of 30° mono-slope Roof

6.3.2.5 Wind Flow Streamlines

The wind flow streamlines show how the wind flows around the buildings and is responsible for wind actions on the building walls and roofs. The streamlines for a z-pattern of low-rise buildings with 30° mono-slope roofs at 15° wind intervals are shown in Fig. 6.31 – 6.35. The streamlines for 30° mono-slope roofs are obtained at the eave height (150 mm) of the low-rise structures to analyse the wind effects on the roofs. When the wind strikes the wall and roof surface of the structures, it gets separated from the windward or upstream side, which is responsible for the generation of eddies around the building, after which the flow recirculation and reattachment take place in the wake region of the building or downstream side. In the case of zero spacing, the eddies formation occurs on all sides of the building model other than the windward side. The building model with zero spacing behaves like a single building with multi-spans of 30° mono-slope roofs. The length of the wake region in the downstream direction depends upon the angle of the wind attack and the pattern of the arrangement of the building, in which it is clearly predictable that the length of the wake region is lesser in the case of a rectangular pattern as compared to z pattern. The turbulence in the wind flow pattern is induced

in between the buildings when spacing is increased from 0 to 2B, due to which the length of the wake region is reduced as shown in Fig. 6.31-6.35 respectively.

0°

45°

90°

135°

180°

Angles of Wind Incidence

Fig. 6.31: Wind Flow Streamlines for Z pattern with Zero Spacing

0°

45°

90°

135°

180°

Angles of Wind Incidence
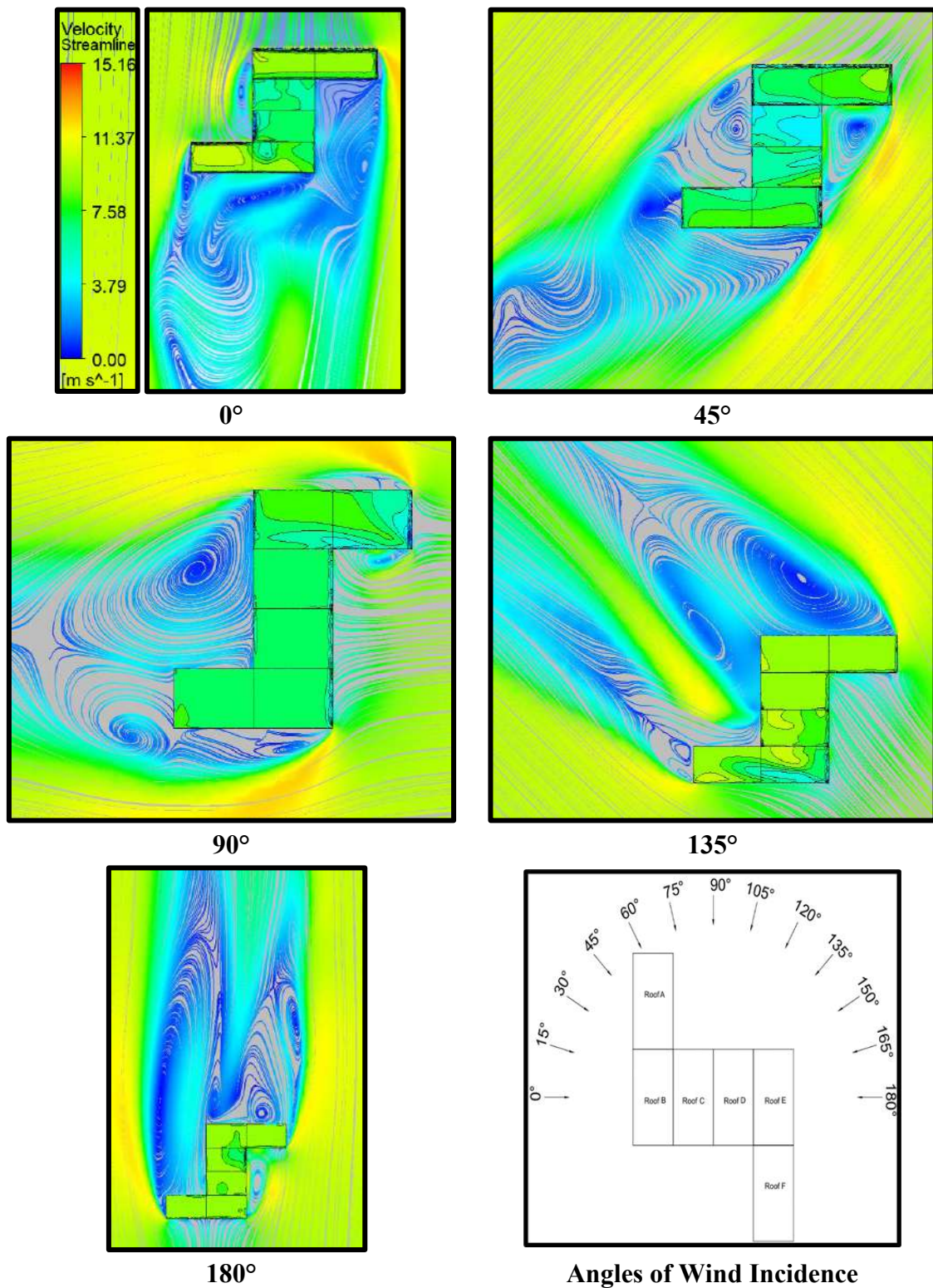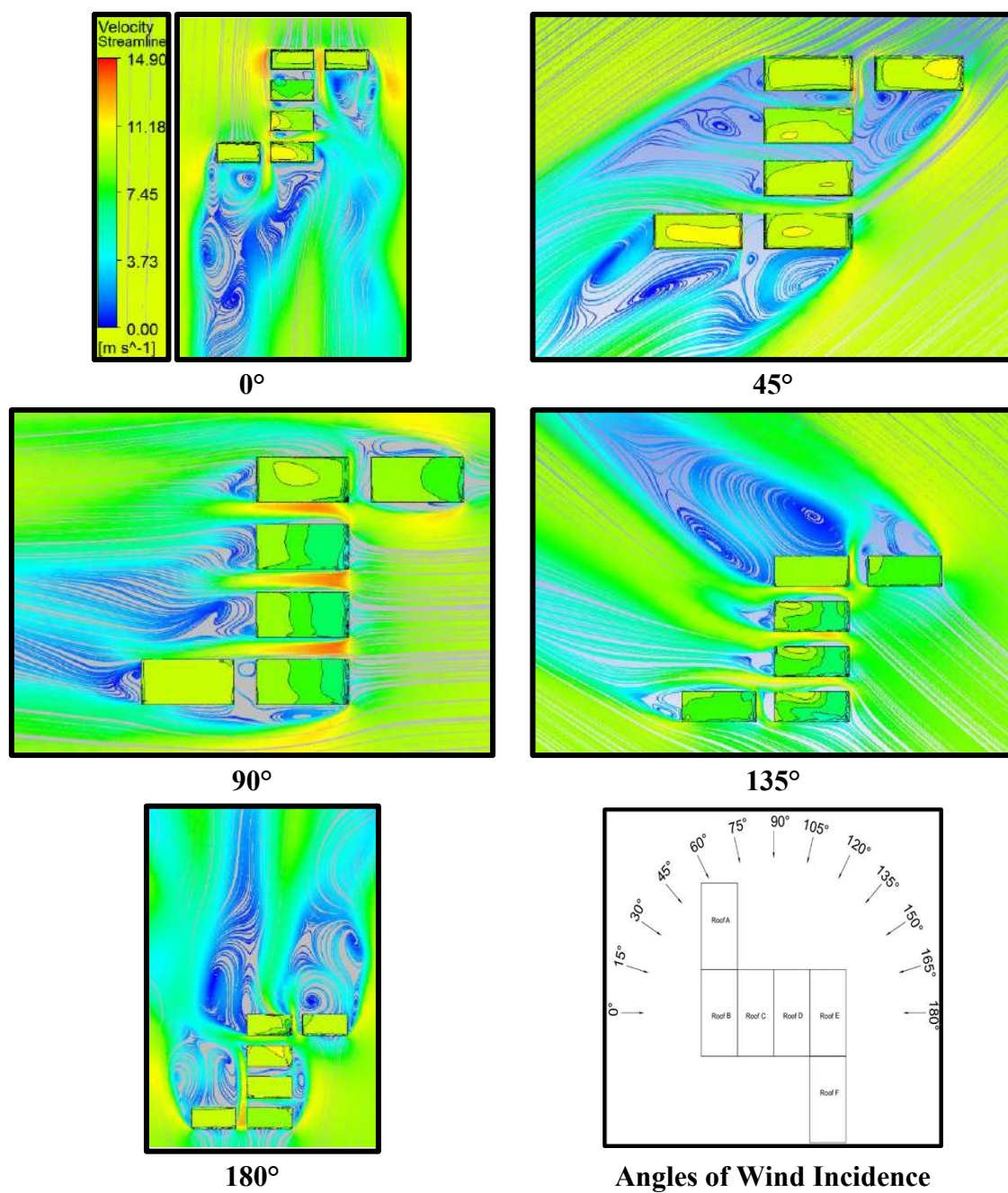
Fig. 6.32: Wind Flow Streamlines for Z pattern with 0.5B Spacing

0°

45°

Fig. 6.33(a): Wind Flow Streamlines for Z pattern with B Spacing

90°

135°

180°
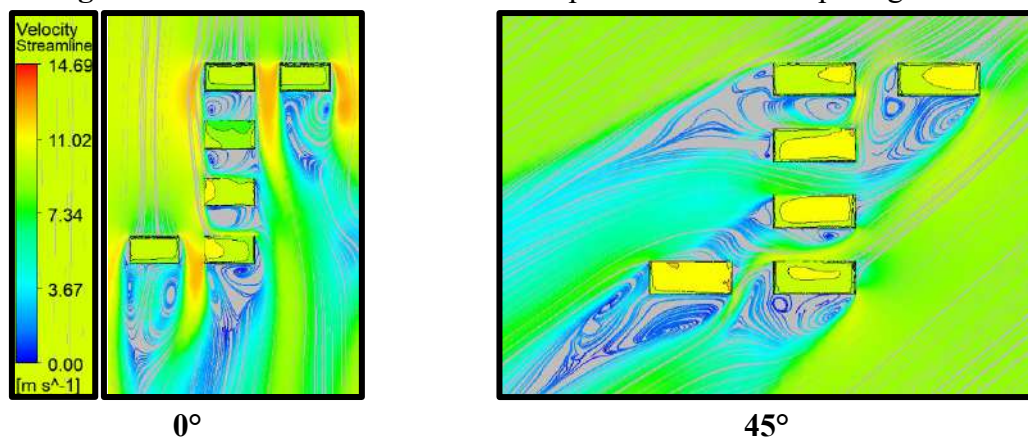
Angles of Wind Incidence
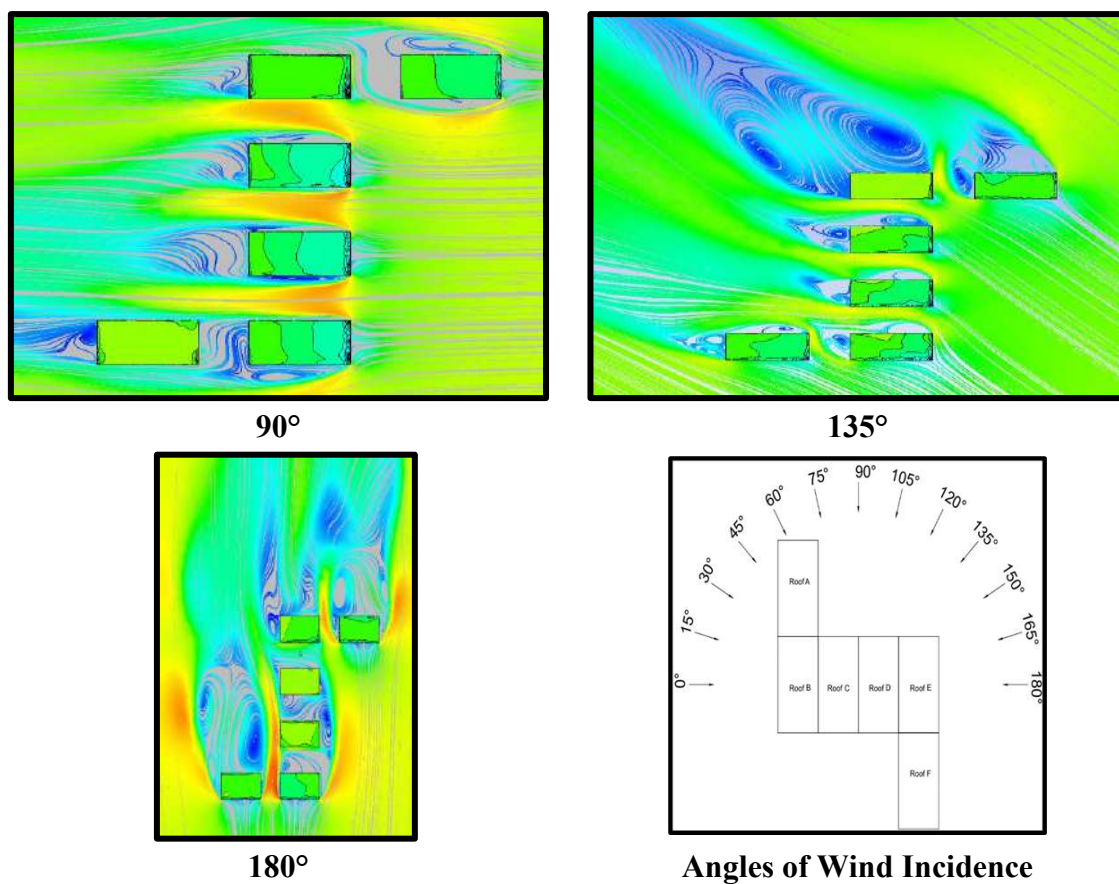
Fig. 6.33(b): Wind Flow Streamlines for Z pattern with B Spacing

0°

45°

90°

135°
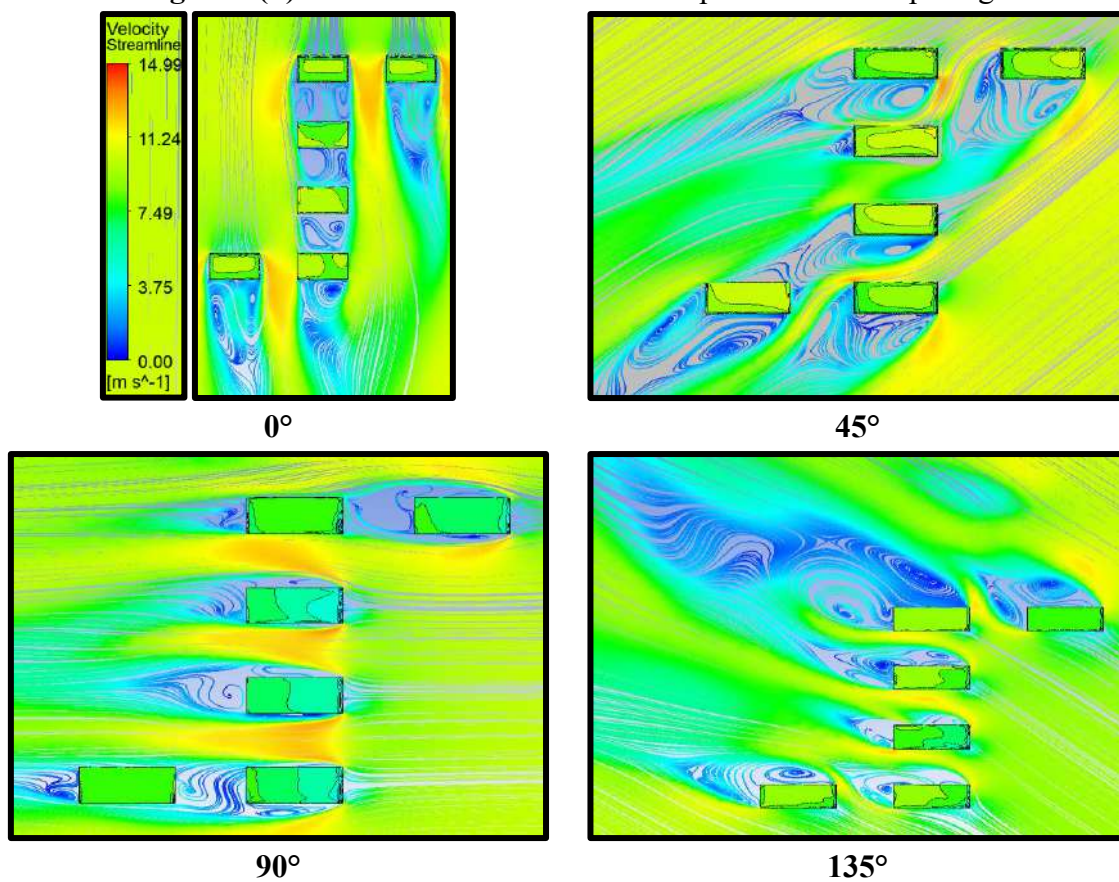
Fig. 6.34(a): Wind Flow Streamlines for Z pattern with 1.5B Spacing

180°
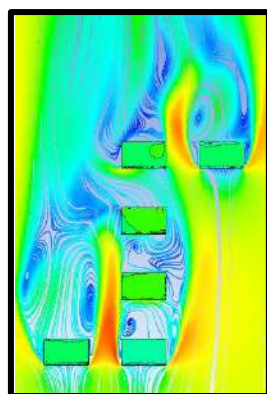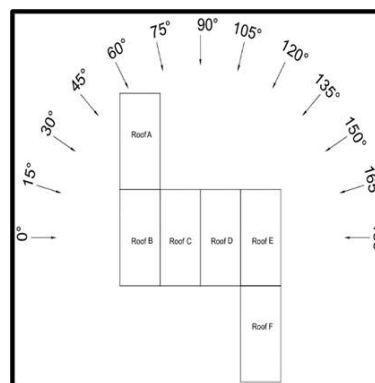
Angles of Wind Incidence

Fig. 6.34(b): Wind Flow Streamlines for Z pattern with 1.5B Spacing

0°

45°

90°

135°

180°
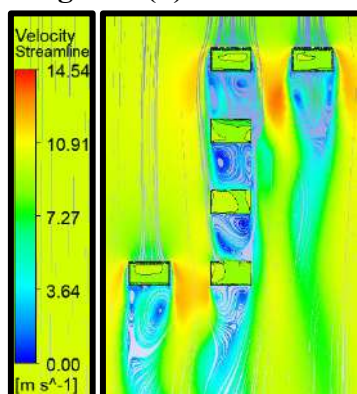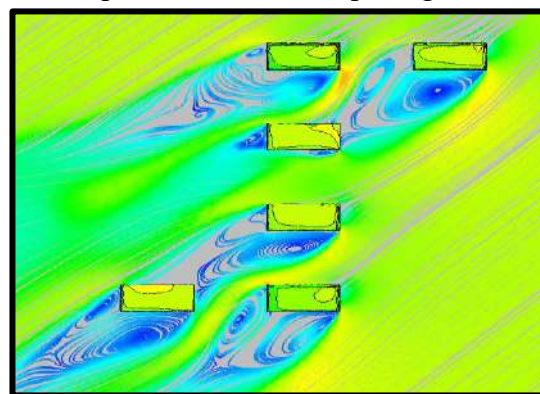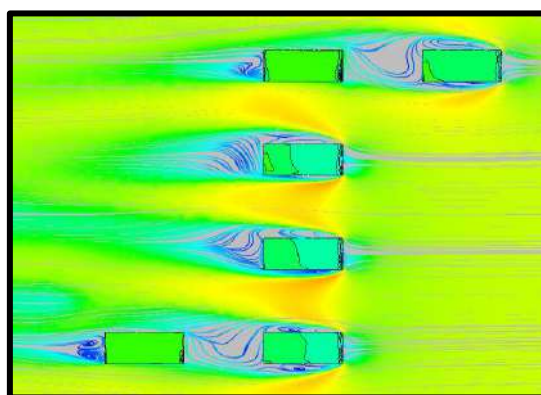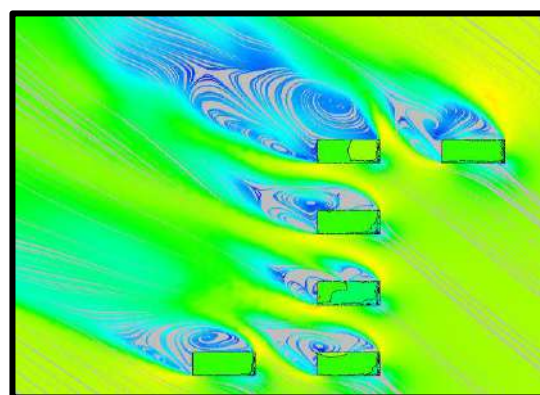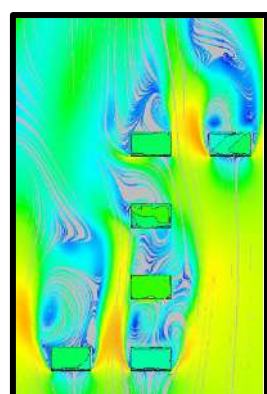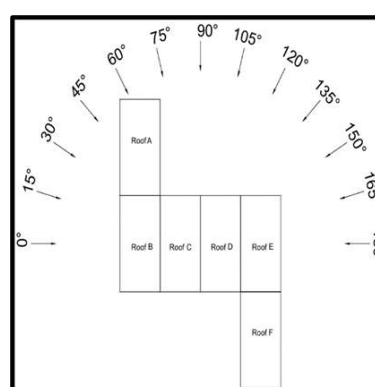
Angles of Wind Incidence

Fig. 6.35: Wind Flow Streamlines for Z pattern with 2B Spacing

6.3.3 T Pattern

This section contains a detailed description of the variation of pressure contours, pressure coefficients, IF and ID over the 30° mono-slope roofs arranged in a T pattern with variable spacing, i.e., 0, 0.5B, B, 1.5B and 2B at different angles of wind incidence such that 0° to 180° at 15° wind interval.

6.3.3.1 Pressure Contours

The wind-induced pressure contours on the 30° mono-slope roof of low-rise structures are investigated by arranging the low-rise building models in a T pattern with variable spacing (0, 0.5B, B, 1.5B and 2B) using CFD simulation are discussed here in this section. The pressure contours, roof nomenclature and angles of wind incidences for all the spacing configurations are shown in Figs. 6.36-6.40. It is clearly visible from Figs. 6.36-6.40, that the 30° mono-slope roof is under negative wind induced pressure distribution during all the wind attacks i.e., ranging between 0° to 180° at 15° intervals. Spacing between the mono-slope roof from i.e., 0, 0.5B, B, 1.5B and 2B is beneficial in reducing the pressure distribution on the roofs as shown in Figs. 6.36-6.40 respectively. It is also noticed that the edges (windward, leeward and side edges) of the 30° mono-slope roofs are under higher negative pressure as compared to the central portion of the roofs. The effects of interference are mostly visible from the roofs which are lying in the single central line of the T-pattern also when the angle of wind attack is 0°, 90° and 180° respectively. The maximum change in wind pressure distribution i.e., conversion of negative pressure into positive pressure on the roof is noticed during 0.5B and B spacing between the buildings as shown in Fig. 6.37 & 6.38 respectively. The overall variation of wind pressure on mono-slope roofs arranged in T pattern is lying between -61.43Pa to 6.68Pa.

Fig. 6.36(a): Pressure Contours for T pattern with Zero Spacing

90° **105°** **120°**

135° **150°** **165°**

180° **Roof Nomenclature and Wind Angles**
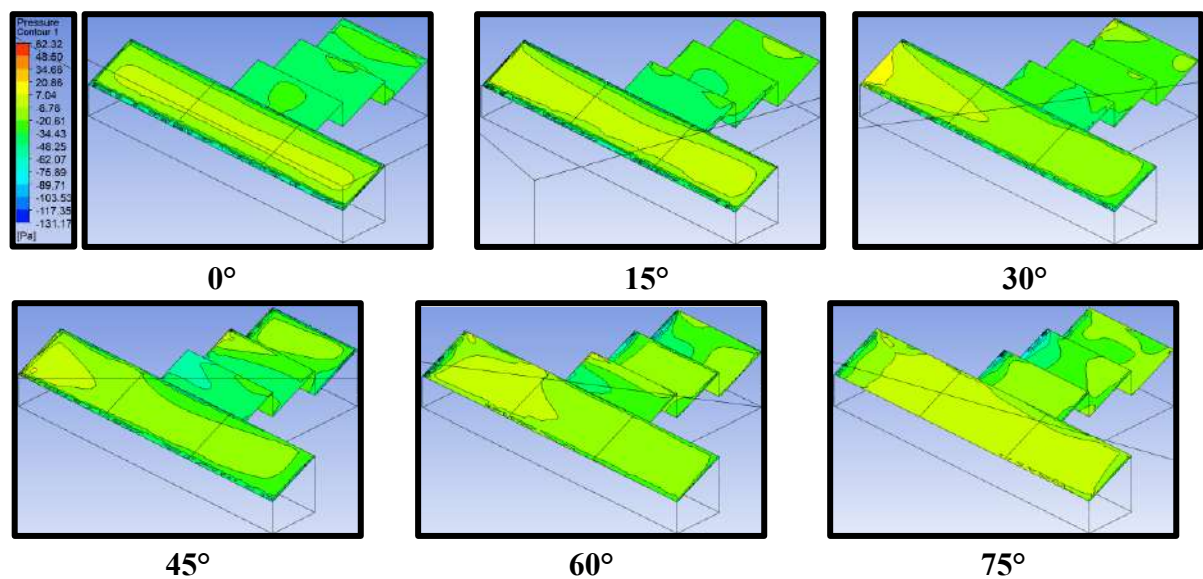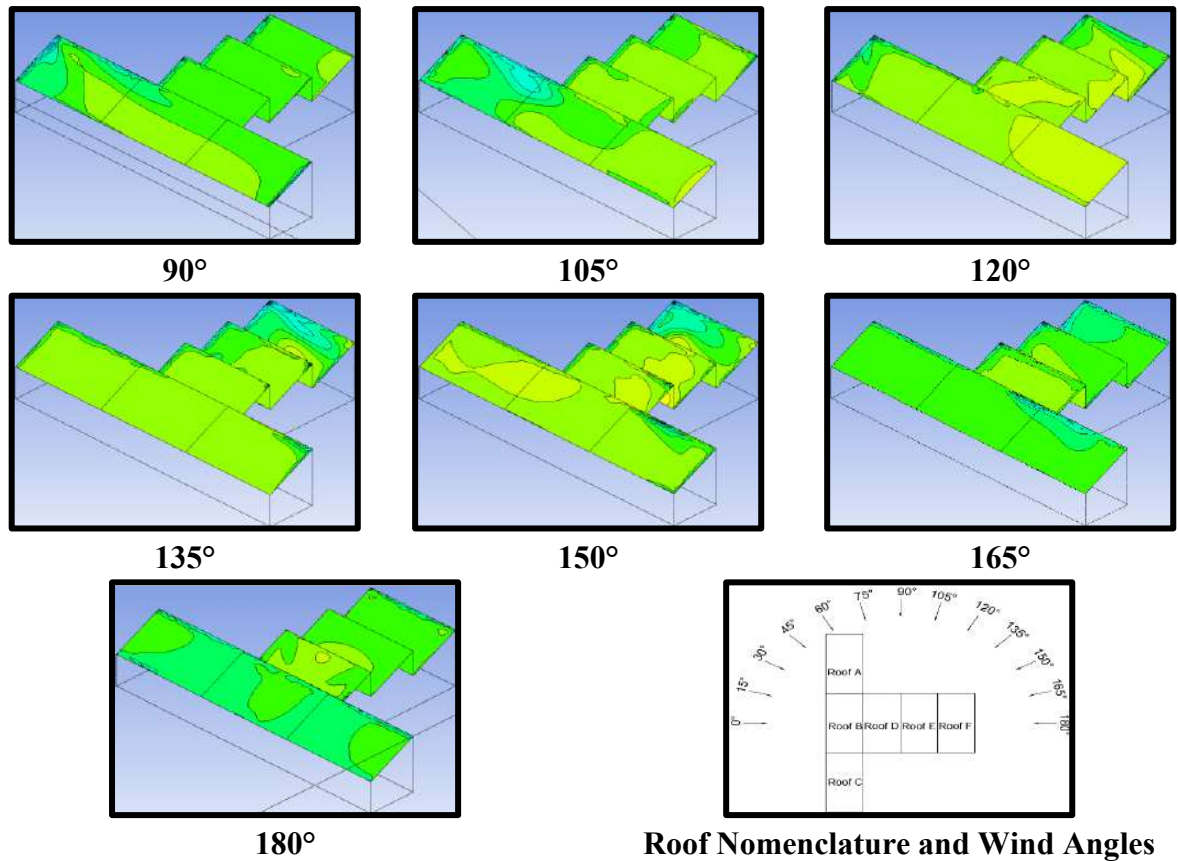
Fig. 6.36(b): Pressure Contours for T pattern with Zero Spacing

0° **15°** **30°**

45° **60°** **75°**

90° **105°** **120°**

Fig. 6.37(a): Pressure Contours for T pattern with 0.5B Spacing
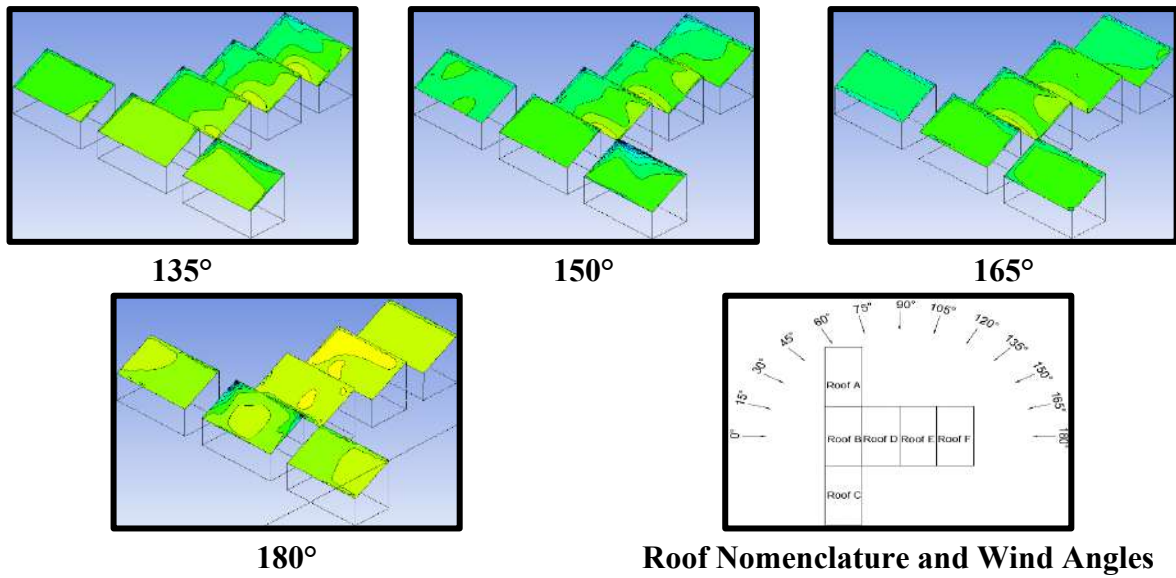
135°

150°

165°

180°

Roof Nomenclature and Wind Angles

Fig. 6.37(b): Pressure Contours for T pattern with 0.5B Spacing

0°

15°

30°

45°

60°

75°

90°

105°

120°

135°

150°

165°

Fig. 6.38(a): Pressure Contours for T pattern with B Spacing
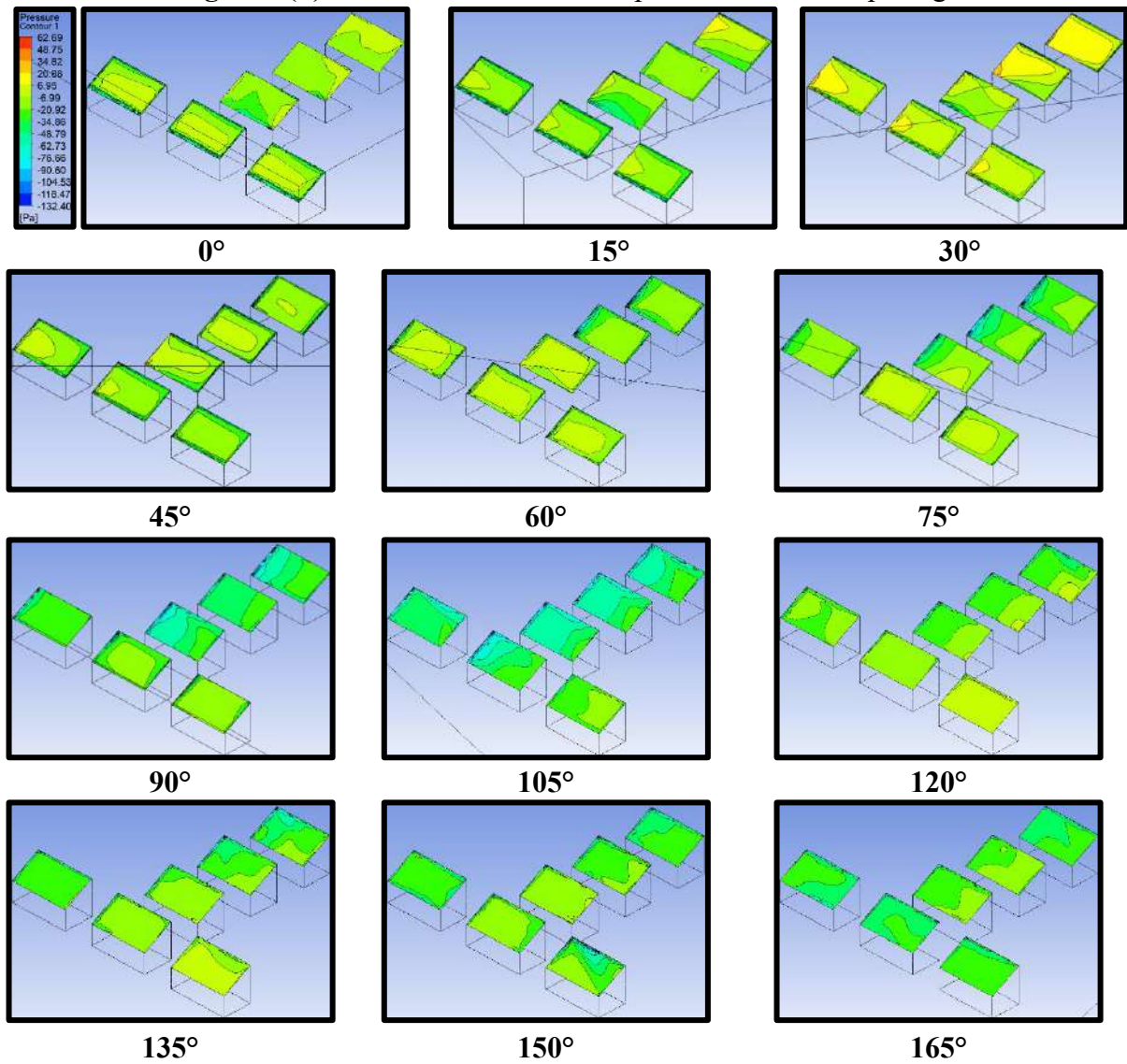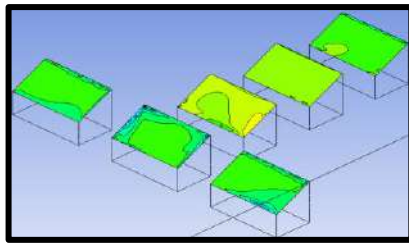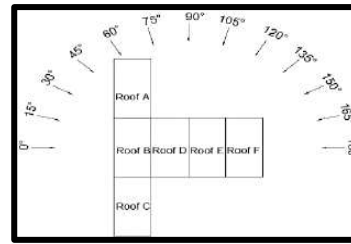
180° | **Roof Nomenclature and Wind Angles**

Fig. 6.38(b): Pressure Contours for T pattern with B Spacing
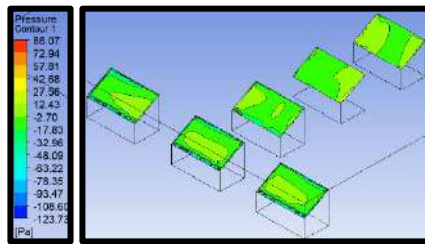
0° | **15°** | **30°**
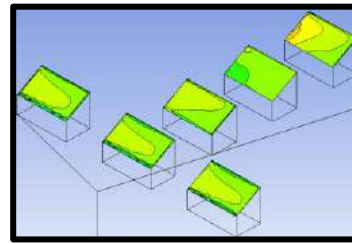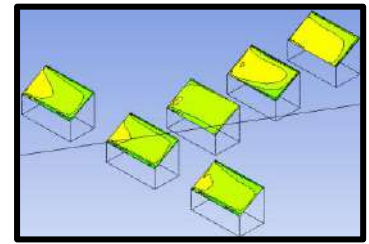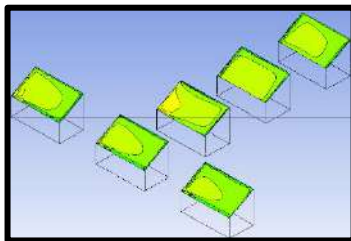
45° | **60°** | **75°**
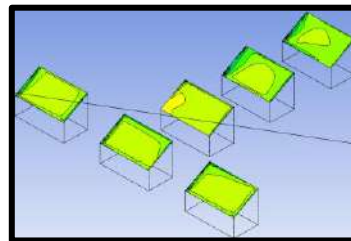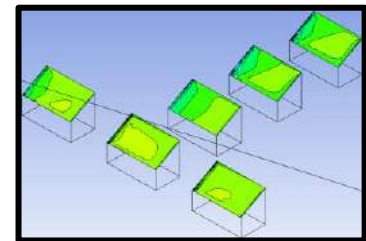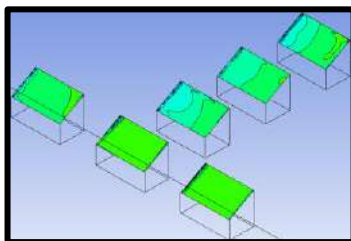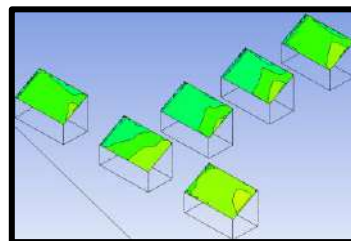
90° | **105°** | **120°**
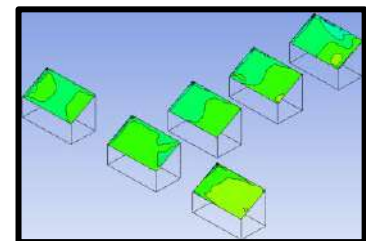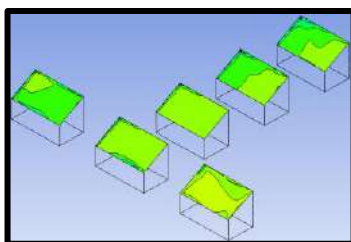
135° | **150°** | **165°**
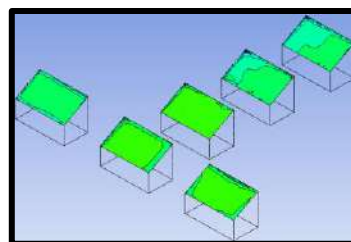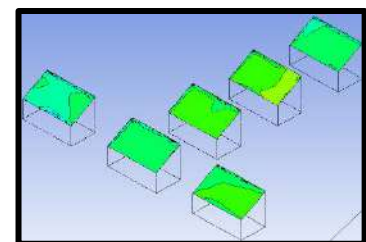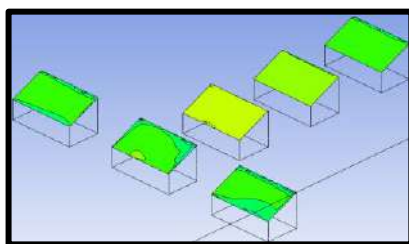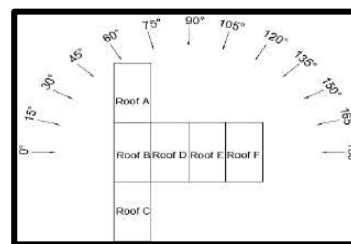
180° | **Roof Nomenclature and Wind Angles**

Fig. 6.39: Pressure Contours for T pattern with 1.5B Spacing

0°

15°

30°

45°

60°

75°

90°

105°

120°

135°

150°

165°

180°

Roof Nomenclature and Wind Angles
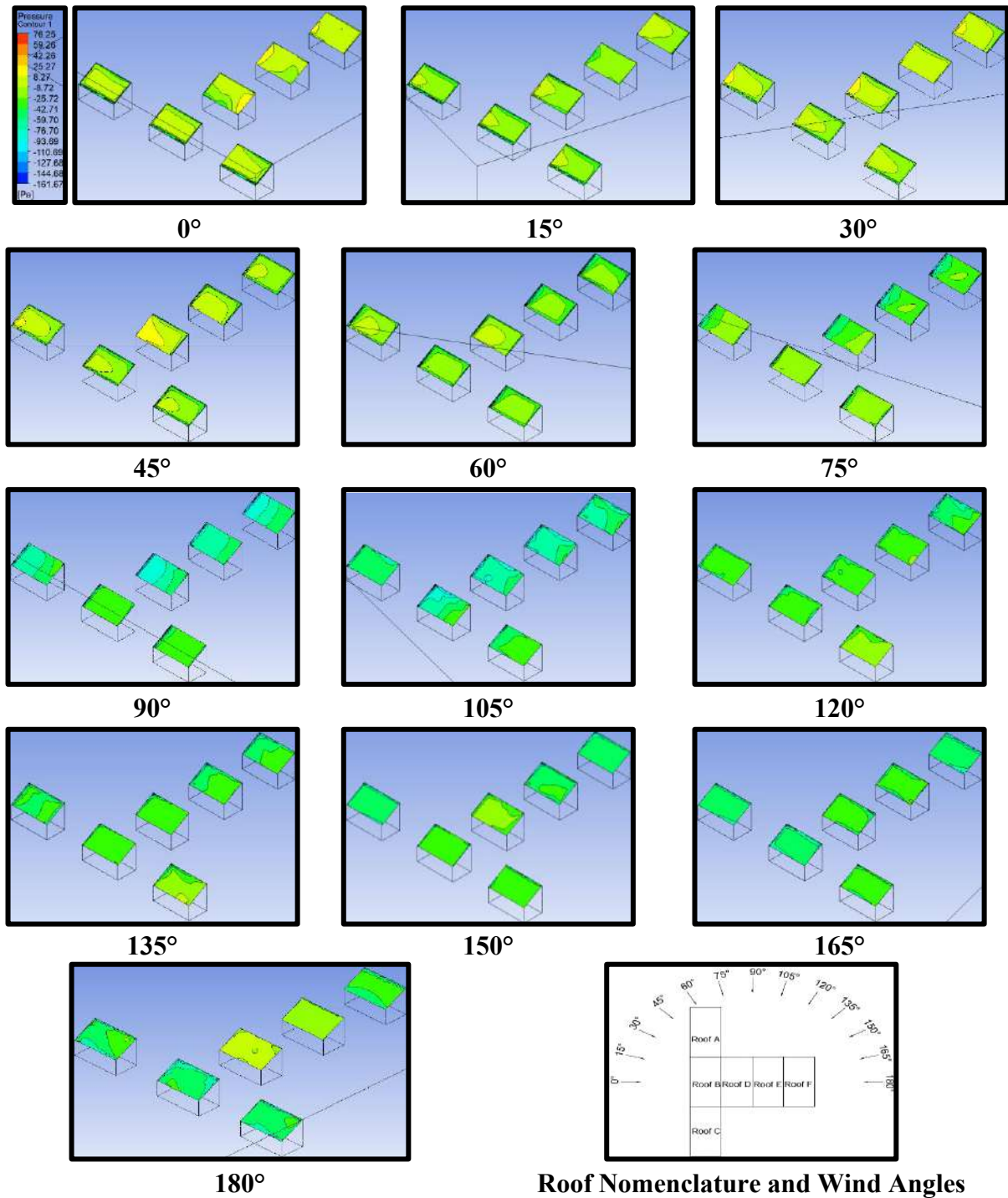
Fig. 6.40: Pressure Contours for T pattern with 2B Spacing

6.3.3.2 Pressure Coefficient (C$_{pe}$)

The variation of C_{pe} on the 30° mono-slope roof of six low-rise buildings arranged in T pattern with variable spacing of zero, 0.5B, B, 1.5B and 2B at different angles of wind interval ranging between 0° to 180° having an interval of 15° each, is shown in Fig. 6.41. At each interval of wind incidence, it is observed that the value of C_{pe} is negative in magnitude on all the 30° mono-slope roofs in the case of different spacings between the buildings. The range of C_{pe} on

roof A is -1.0 to -0.06 indicating that there is only suction on the roof in which the maximum suction occurs during 105° angle of wind incidence with zero spacing between the buildings, while the minimum suction on roof A is observed during 30° wind incidence with 2B spacing between the buildings. The maximum and minimum suction on roof B is observed when the value of C_{pe} is -0.85 at 180° wind angle with 0.5B spacing and -0.12 at 90° wind angle with 2B spacing. The maximum value of negative C_{pe} on roofs C, D, E and F is occurring during 150°, 105°, 120°, 30°, 135° angle of wind incidence i.e., -0.71 with B spacing on roof C, -0.77 with 0.5B spacing on roof D, -0.78 with 0.5B spacing on roof E and -0.94 with zero spacing on roof F respectively. The value of C_{pe} is noticed as positive in magnitude which indicates that the negative pressure changed into positive pressure due to interference on roof D i.e., +0.09 at 45° wind angle with 2B spacing, +0.03 at 30° wind interval with 1.5B & 2B spacing on roof E, +0.11 at 30° wind interval with 1.5B spacing on roof F.
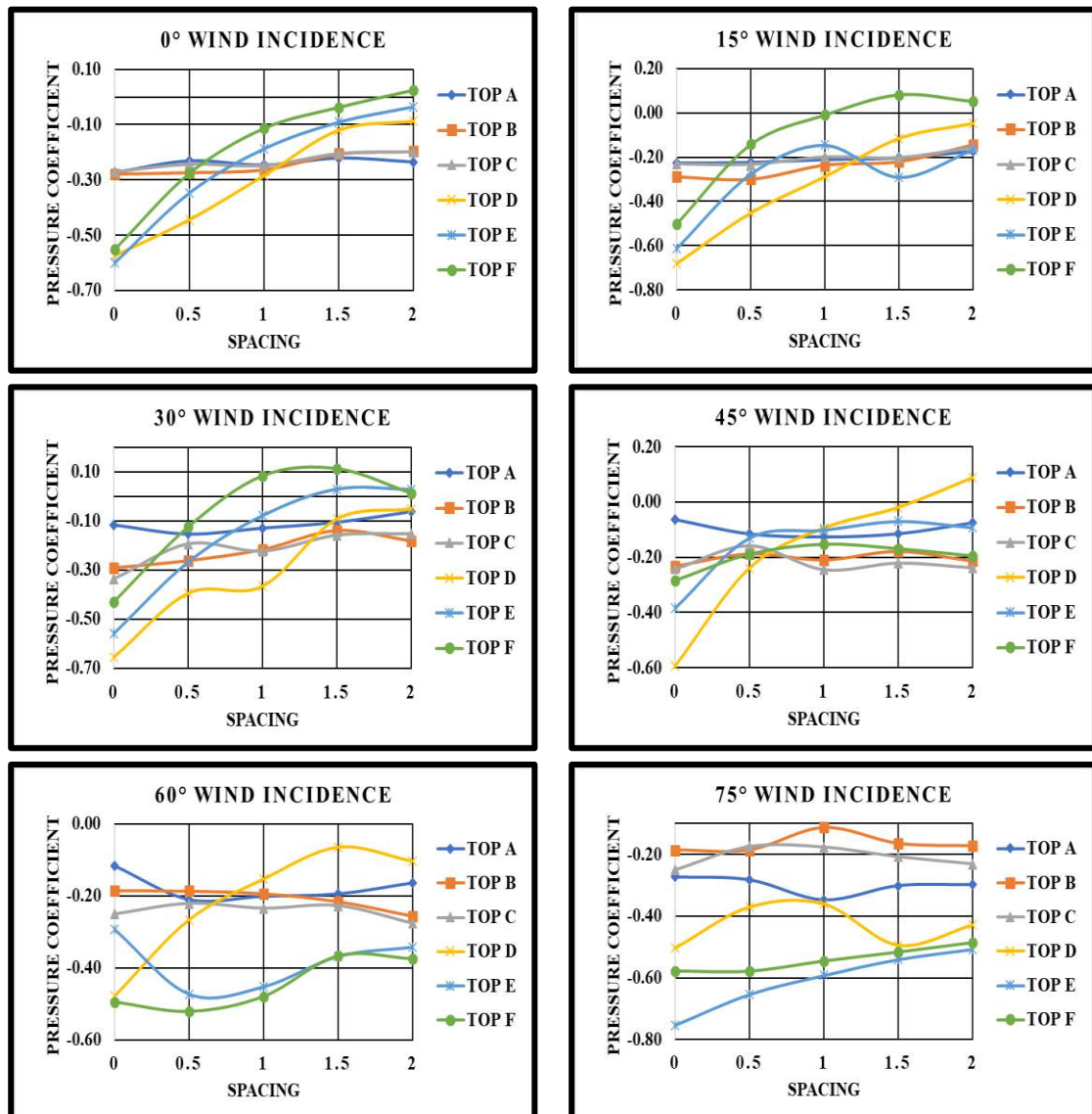
Fig. 6.41(a): Pressure Coefficient for T pattern with variable Spacing
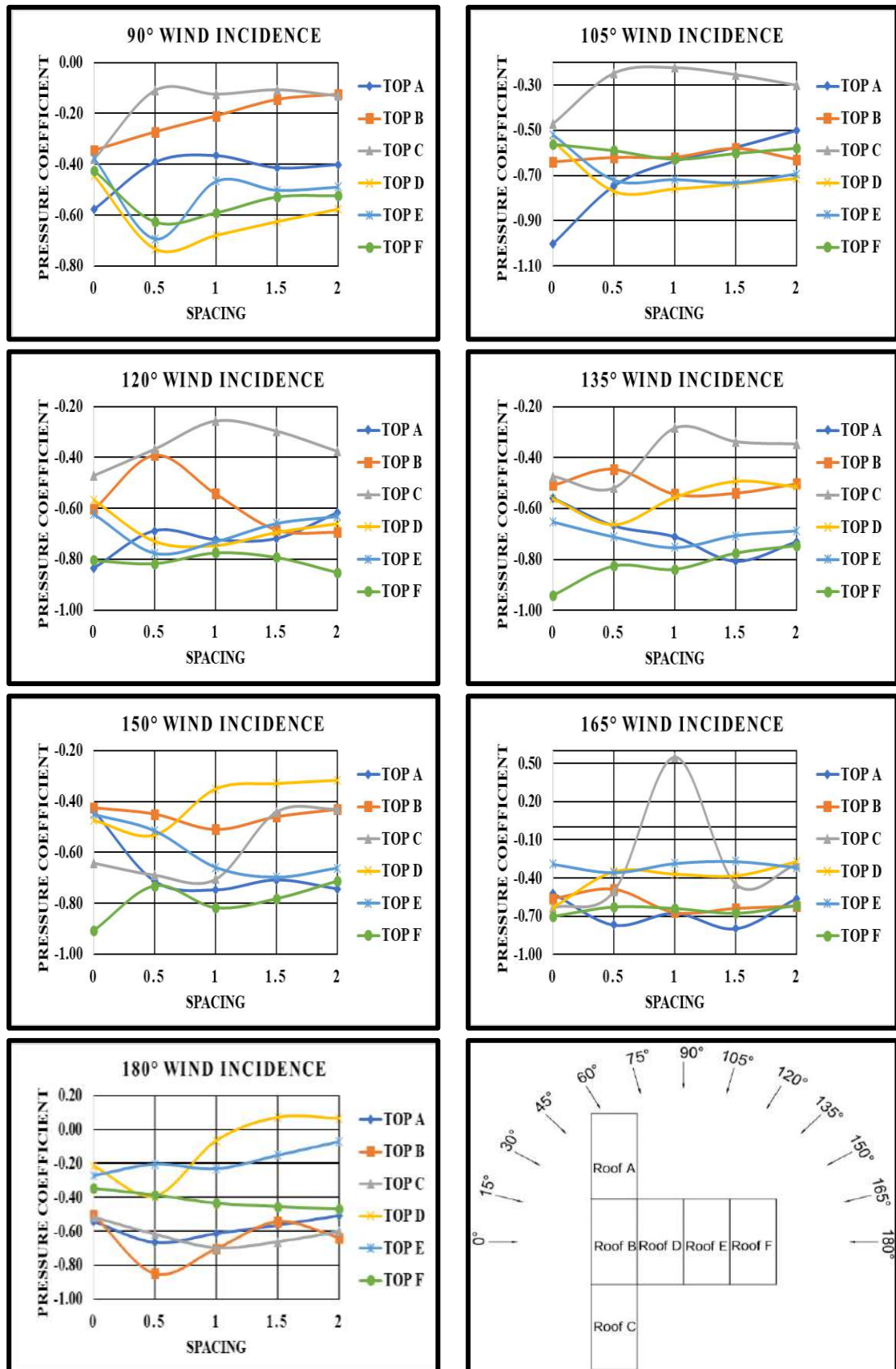
Fig. 6.41(b): Pressure Coefficient for T pattern with variable Spacing

6.3.3.3 Interference Factor (IF)

The idea of enhancement or reduction of suction or pressure on the roof is given by interference factor (*IF*) due to the presence of low-rise structure in the vicinity. The value of *IF* gets modified with respect to the spacing between the buildings and angles of wind attack. The varying magnitude of *IF* on a 30° mono-slope roof arranged in a T pattern with variable spacing (0,0.5B, B, 1.5B and 2B) at various angles of wind attacks, i.e., 0° to 180° at 15° intervals is shown in Fig. 6.42. The value of *IF* on the roof A keeps on reducing with an increase in spacing from 0 to 2B. Initially, the value of *IF* comes out to be more than 1, indicating the increased suction on roof A at 0°, 60°, 90°, 105°, 120° and 135° angles of wind incidence with zero spacing, but it gets reduced while increasing the spacing till 2B at which *IF* becomes less than 1 indicating the reduced suction on roof A. On the rest of the wind incidence angles i.e., 15°, 30°, 45°, 75°, 150°, 165° and 180°, the value of *IF* is already less than 1 for roof A. Similarly to the *IF* of roof A, the value of *IF* for roof B follows the same trend in which its value comes out to be more than 1 when the angles of wind attack are 0°, 15°, 30°, 45°, 60°, 105° and 165° respectively and starts reducing when spacing between the building in increased from 0 to 2B. Also, the maximum reduction in *IF*, i.e., reduced suction on roof B, is observed at 1.5B spacing at all the wind incidence angles, i.e., 0° to 180° at 15° intervals, as shown in Fig. 6.29. A drastic reduction in the value of *IF* for roof C is observed at 0°, 15°, 30°, 45°, 60° and 180° angles of wind incidence when the spacing is changed from 0 to 2B, during which *IF* changed from more than 1 to less than 1, indicating the reduced suction on roof C. But, on the rest of the wind incidence angles, the value of *IF* already comes out to be less than 1 and not much changed with respect to the spacing. The variation of *IF* on roof D follows the same pattern as that of roof B when wind incidence angles are 75°, 90°, 105°, 135°, 150° and 165°, at which the maximum reduction of *IF* takes place when the spacing is 1.5B between the buildings. The value of *IF* for roof E is less than 1 only in cases when the angle of wind incidence is 0°, 30° and 45°, indicating the reduced suction on roof E due to interference. The reduction in value of *IF* for roof F with respect to the spacing is observed when the angle of wind incidence is ranging between 0° to 105° and 165° respectively as shown in Fig. 6.29. The variation of spacing between the buildings is proved to be beneficial which helps in reducing the suction on the roof and greatly influences the nature of wind on roofs. The angle of wind incidence also plays a vital role in changing the magnitude of *IF* on the roof or low-rise structure with mono-slope roof. The overall variation of *IF* is ranging between 1.78 to -0.44 with respect to different spacing when mono-slope roofs are arranged in T pattern.
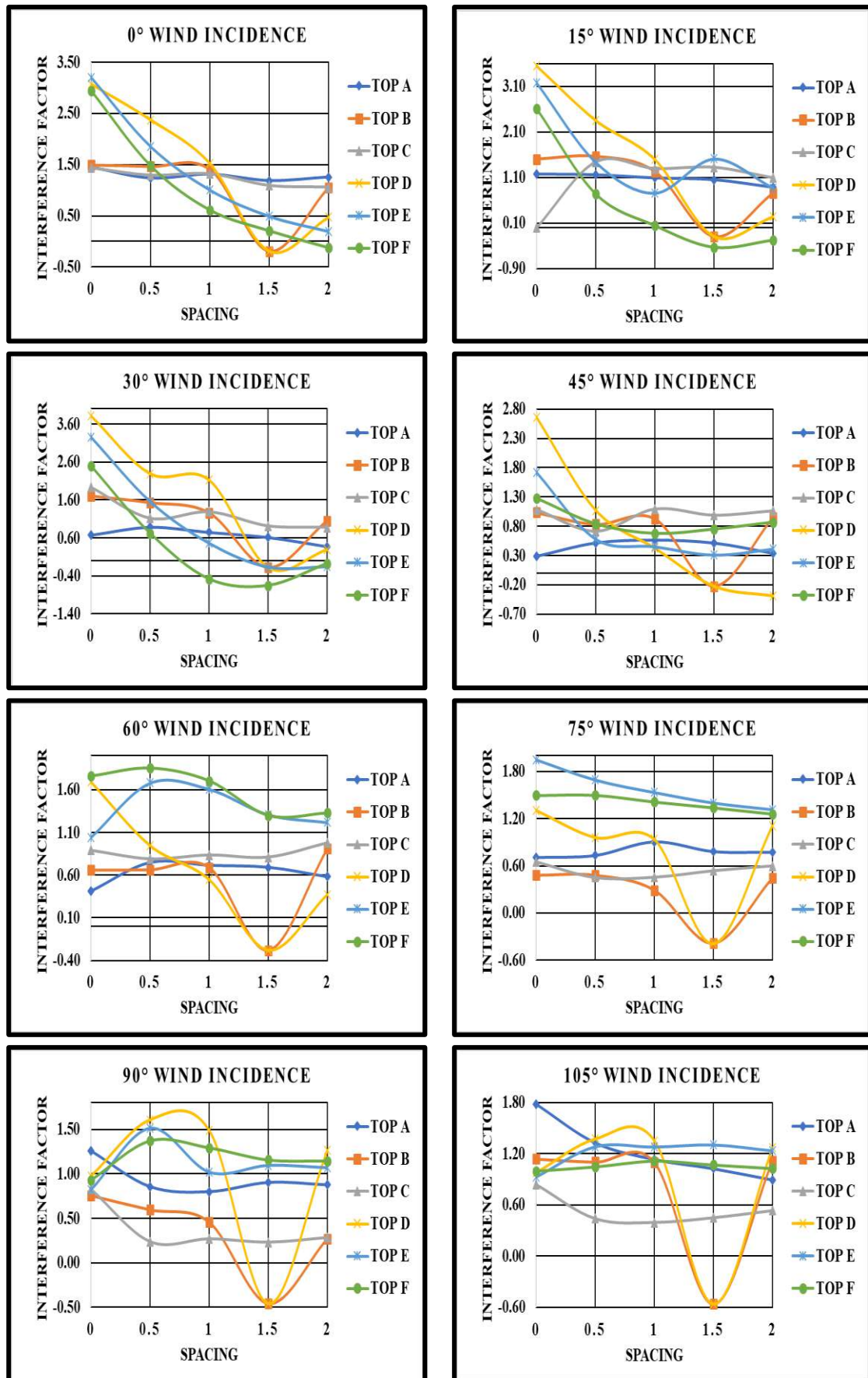
Fig. 6.42(a): Interference Factor for T pattern with variable Spacing
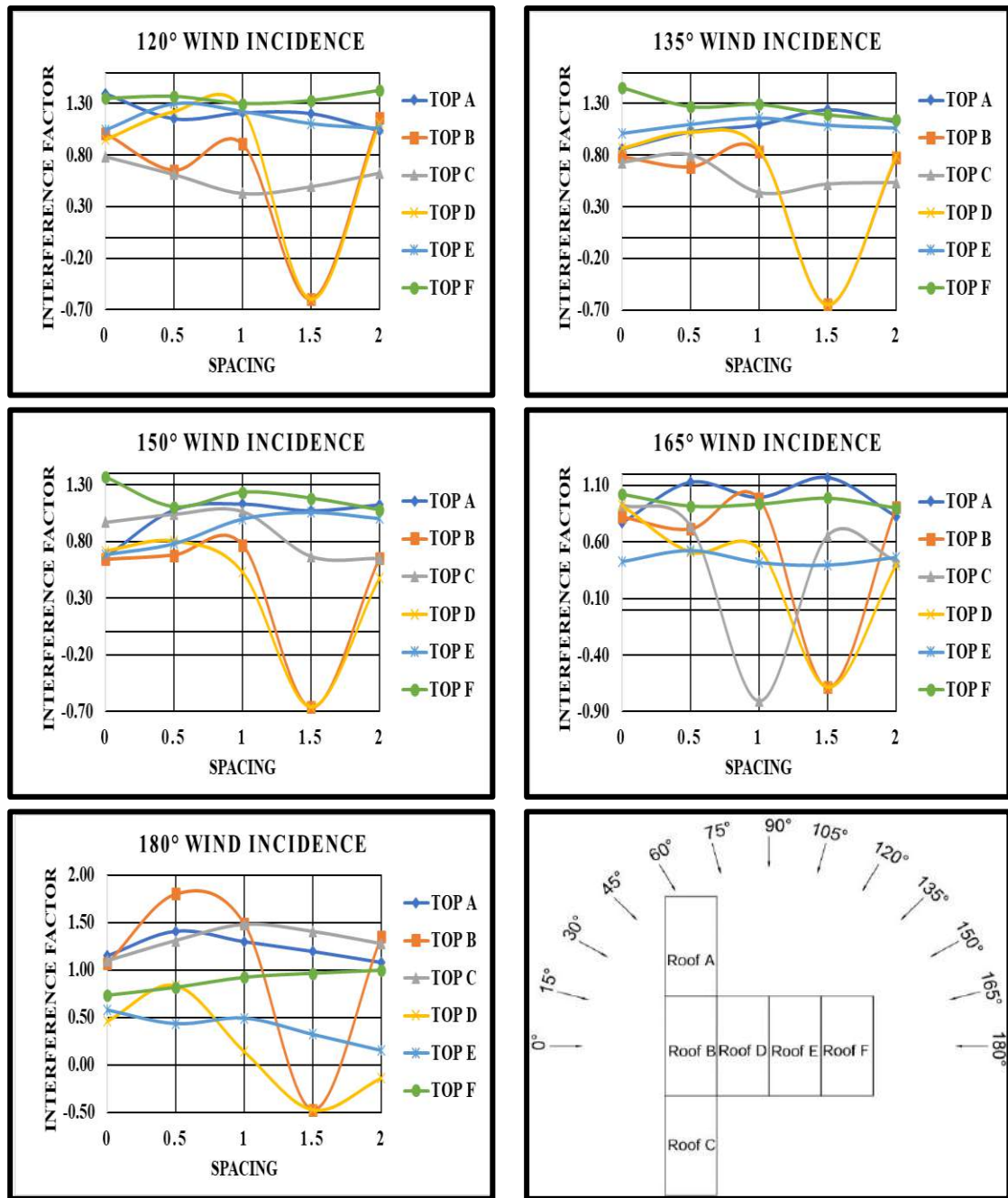
Fig. 6.42(b): Interference Factor for T pattern with variable Spacing

6.3.3.4 Interference Difference (ID)

The difference between C_{pe} obtained during an interfering condition and C_{pe} obtained during an isolated condition is called as interference difference (*ID*), which gives an exact idea of enhancement or reduction in the wind-induced positive or negative pressure coefficient on the roofs. The variation of *ID* on 30° mono-slope roofs arranged in a T pattern with different spacing ranging between 0 to 2B (where B is the width of a low-rise building) and at various angles of wind incidences ranging between 0° to 180° at 15° intervals is shown in Fig. 6.43. When the magnitude of negative C_{pe} on the roof is increased during interfering conditions, then

the value of *ID* comes out to be negative, indicating the increased suction on the roof during interfering conditions, while the value of *ID* is positive, but the magnitude of C_{pe} is still negative on the roofs indicates that the suction on the roof is reduced due to interference of vicinity buildings. This variation of *ID* on 30° mono-slope roof arranged in T pattern with variable spacing with respect to different angles of wind incidences is ranging between 0.11 to -0.1002 in which positive sigh in indicating the suction on roof and negative sign is indicating the changed nature of wind from suction to pressure as shown in Fig. 6.43 below.
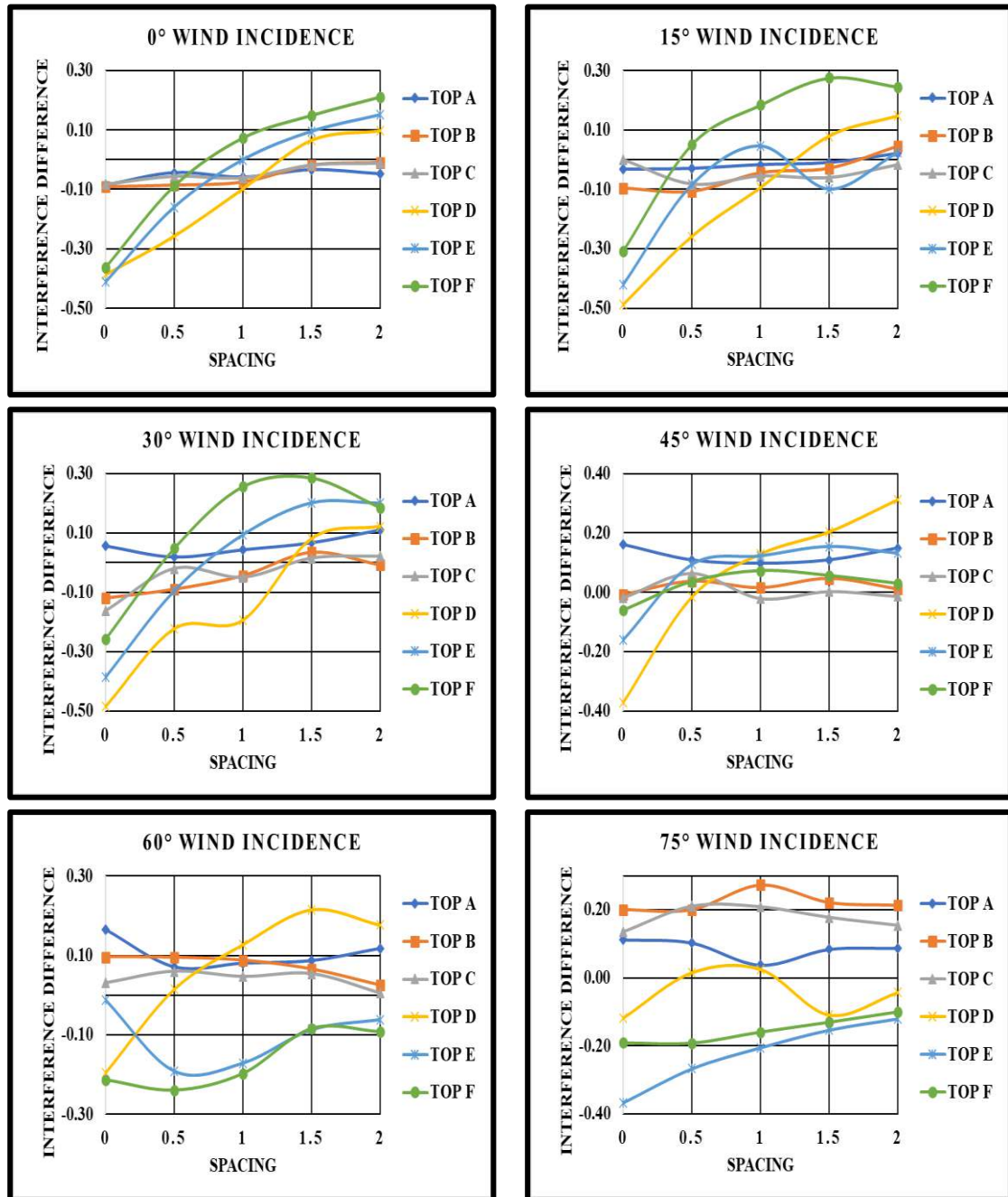
Fig. 6.43(a): Interference Difference for T pattern with variable Spacing
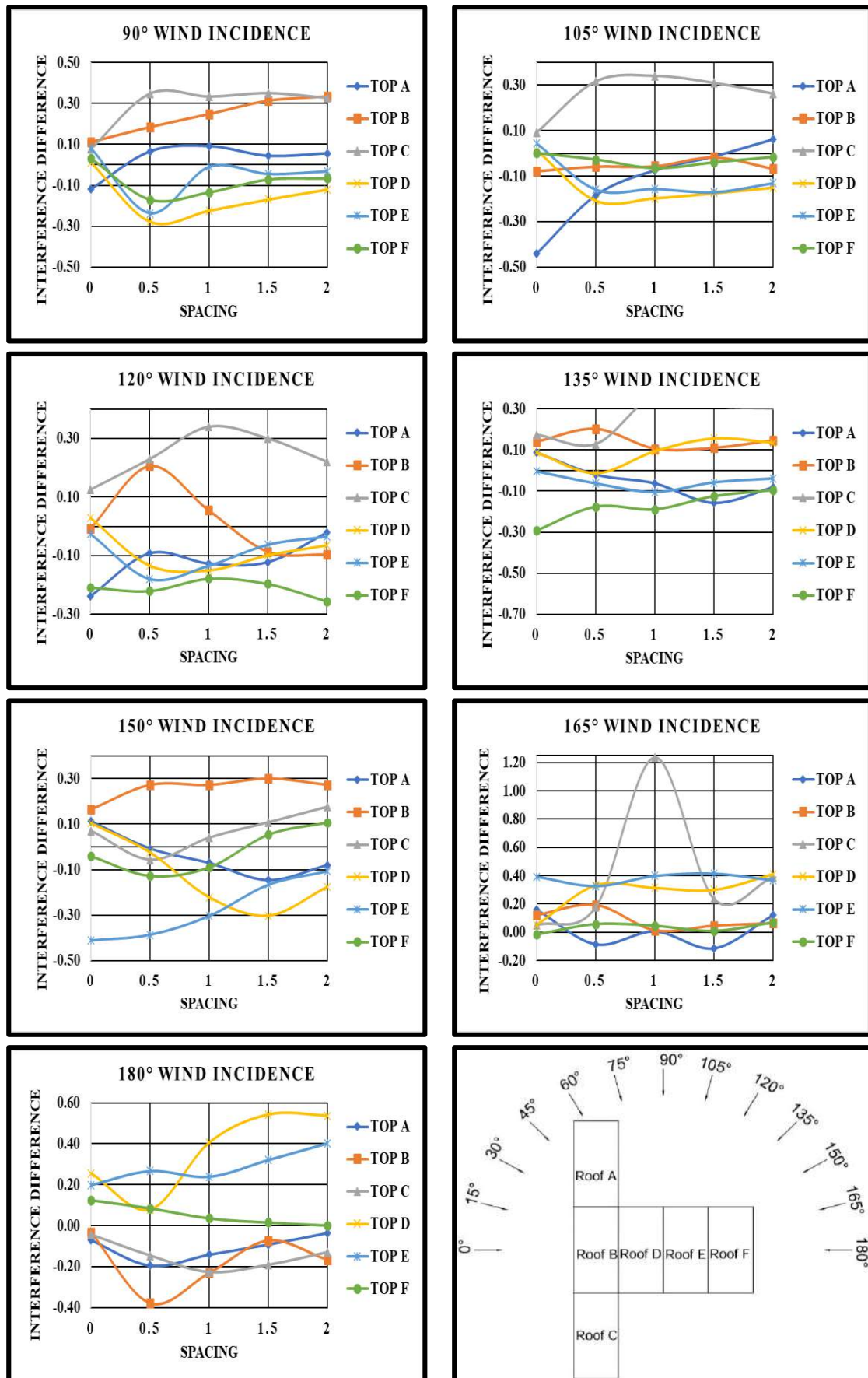
Fig. 6.43(b): Interference Difference for T pattern with variable Spacing

6.3.3.5 Wind Flow Streamlines

The pattern of wind flow around the low-rise structure with cylindrical roofs arranged in a T pattern with variable spacing (0, 0.5B, B, 1.5B and 2B) and at different angles of wind attack (0° to 180° at 15° interval) is shown in Fig. 6.44-6.48. As the wind is flowing around the building, there is a formation of vortex generation in the wake region after striking and separating from the upstream direction at the stagnation point. The formation of wake region is depending upon the angle of wind attack and spacing between the structures. The wake formation is reduced when the spacing between the buildings is increased from 0 to 2B as the wind flow is getting inserted in between the buildings. When there is zero spacing between the buildings, the vortex generation takes place only in the surrounding of the buildings in the downstream direction, but when the spacing is increased from zero to 2B, the flow is inserted between the buildings, resulting in reduced eddies formation and vortex generation in the wake region.

0°

45°

90°

135°

Fig. 6.44(a): Wind Flow Streamlines for T pattern with Zero Spacing

180°   **Angles of Wind Incidence**

Fig. 6.44(b): Wind Flow Streamlines for T pattern with Zero Spacing

0°   **45°**
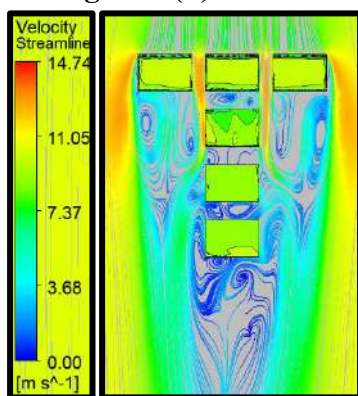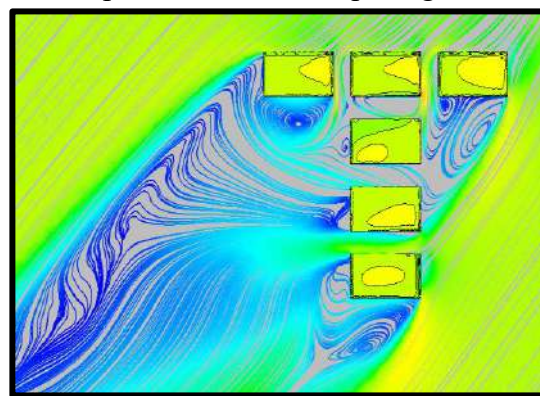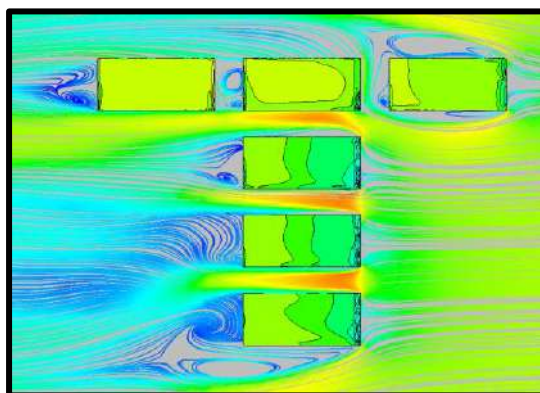
90°   **135°**
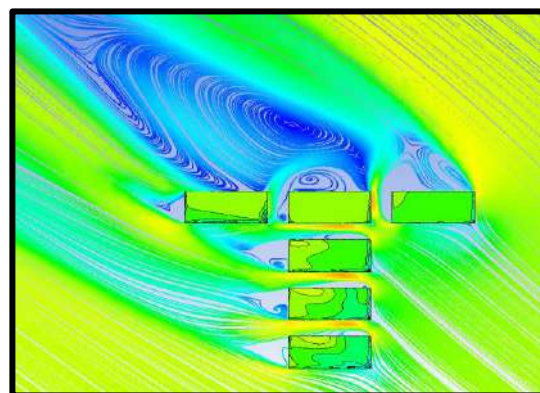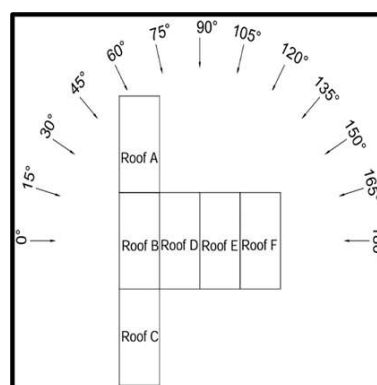
180°   **Angles of Wind Incidence**

Fig. 6.45: Wind Flow Streamlines for T pattern with 0.5B Spacing

0°

45°

90°

135°

180°

Angles of Wind Incidence
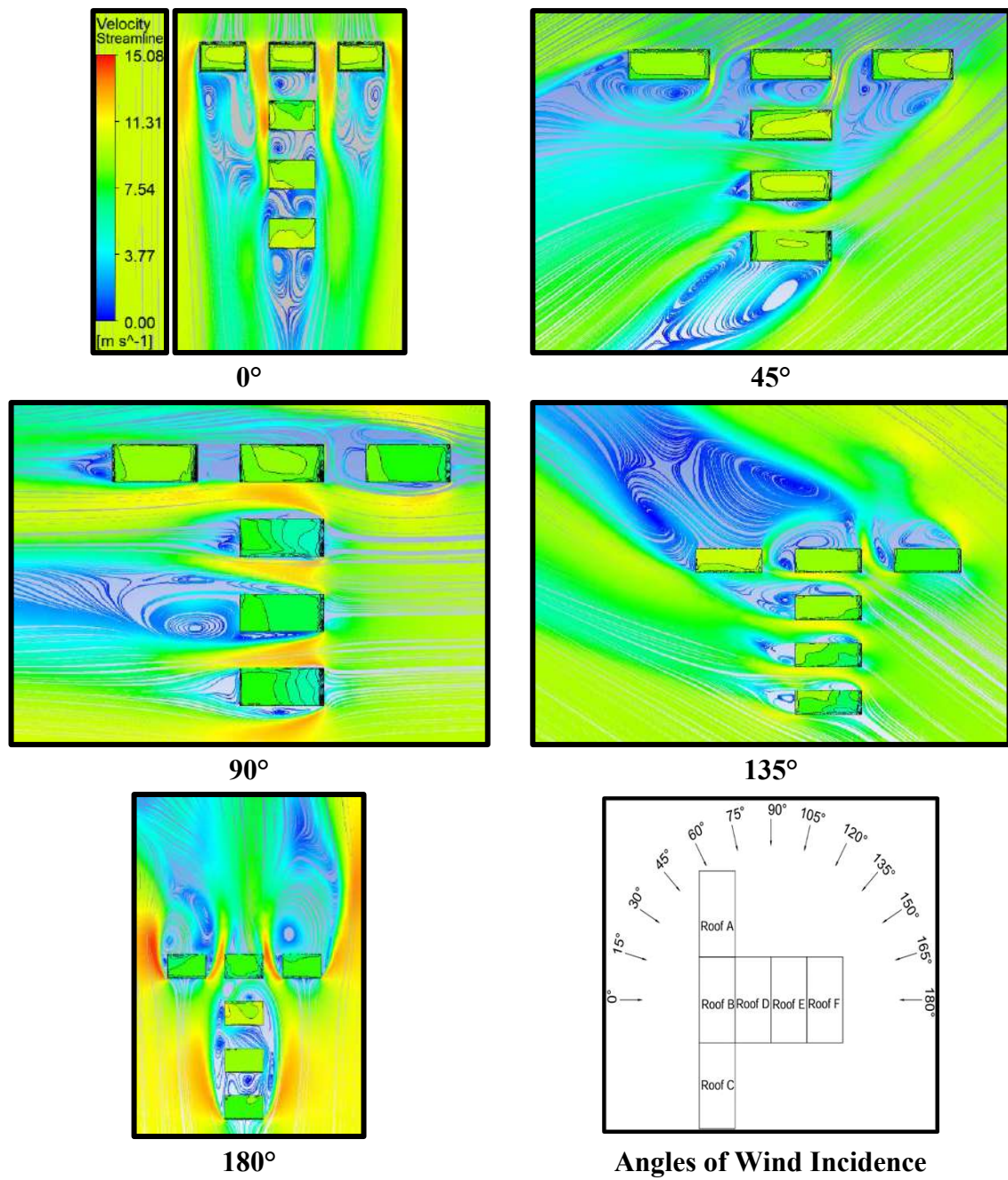
Fig. 6.46: Wind Flow Streamlines for T pattern with B Spacing

0°

45°

Fig. 6.47(a): Wind Flow Streamlines for T pattern with 1.5B Spacing

90°

135°

180°

Angles of Wind Incidence
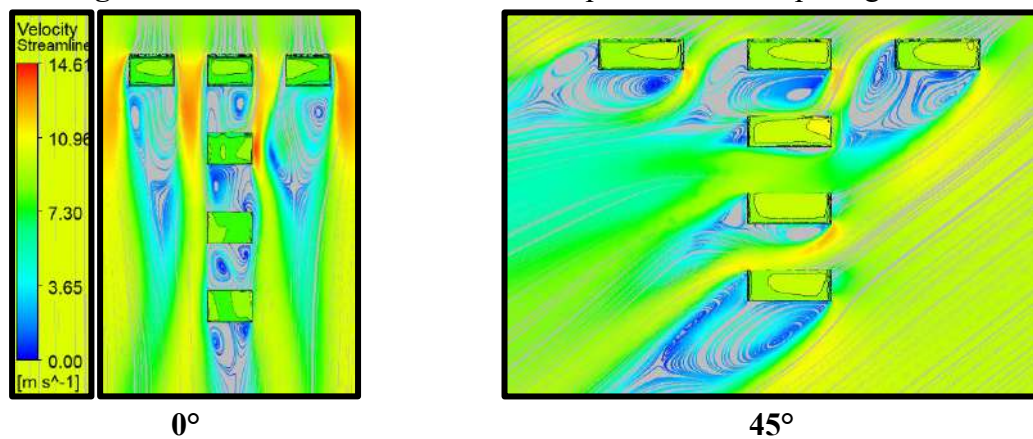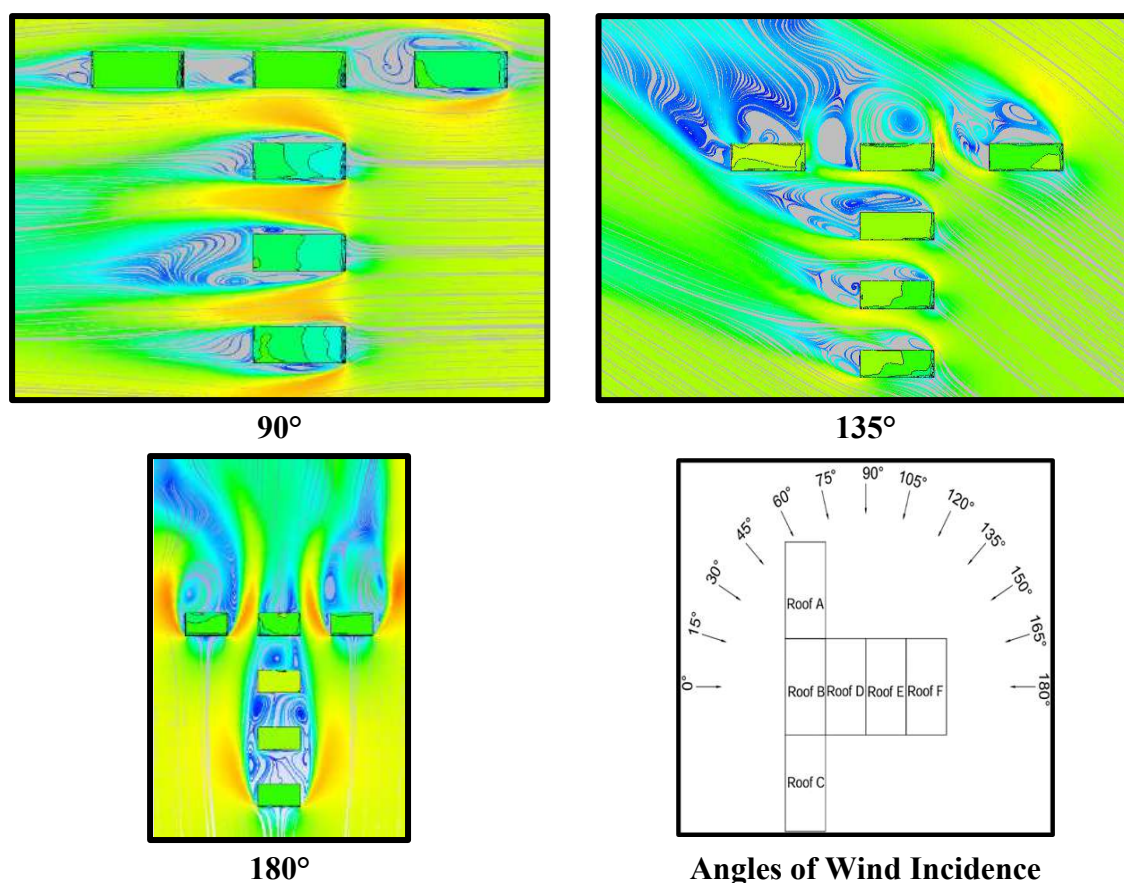
Fig. 6.47(b): Wind Flow Streamlines for T pattern with 1.5B Spacing

0°

45°

90°

135°

Fig. 6.48(a): Wind Flow Streamlines for T pattern with 2B Spacing

| **180°** | **Angles of Wind Incidence** |
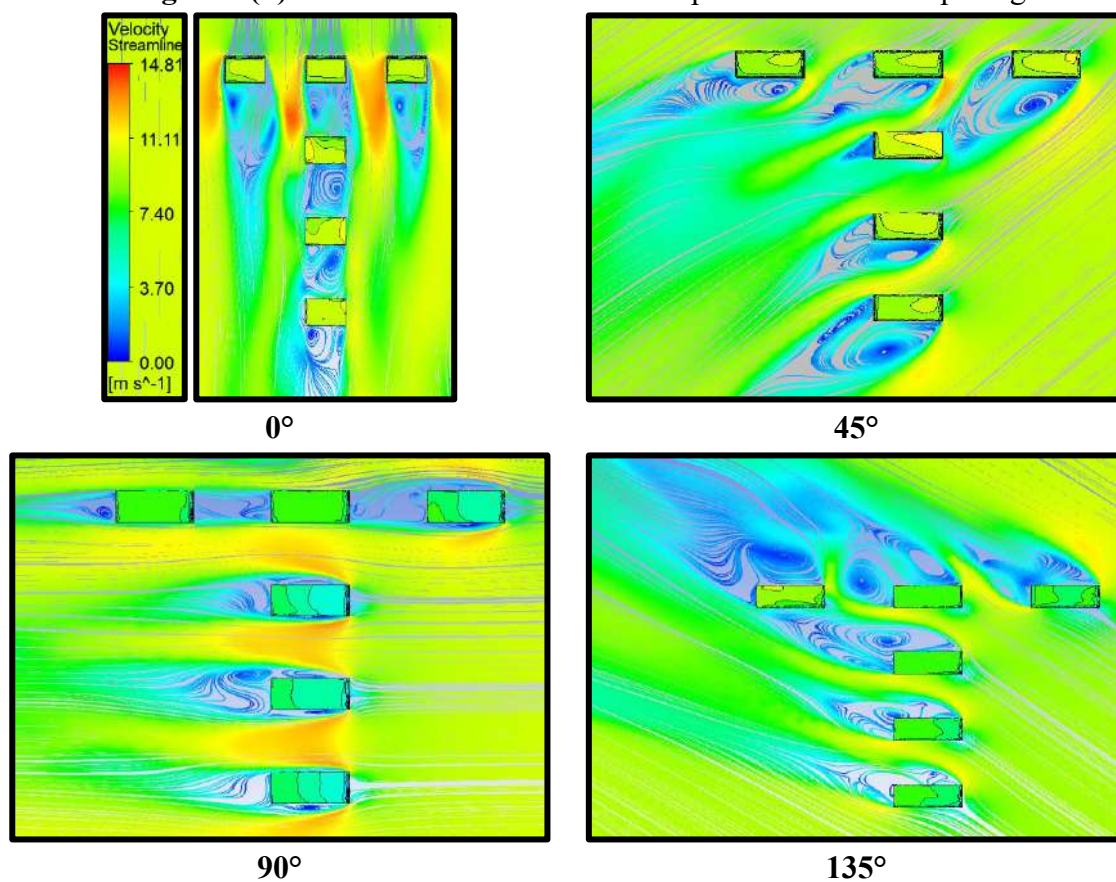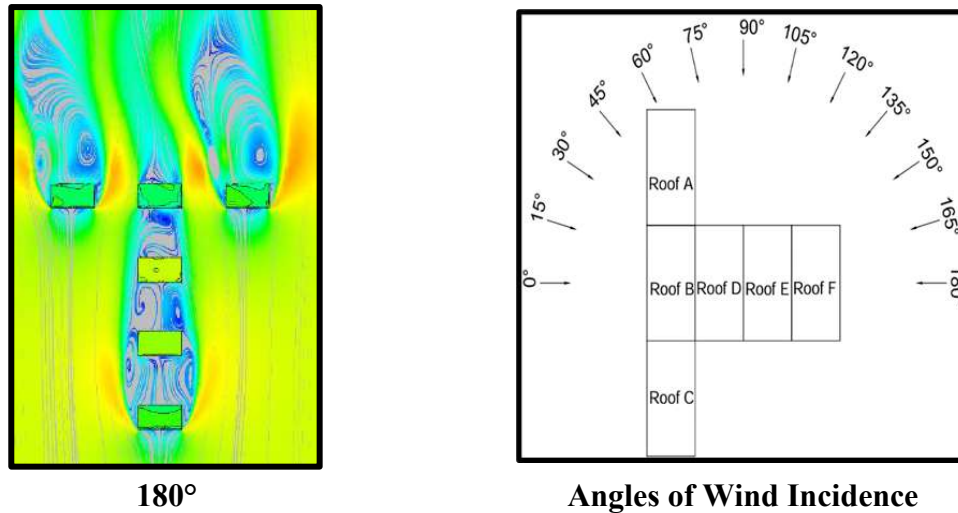
Fig. 6.48(b): Wind Flow Streamlines for T pattern with 2B Spacing

6.4. Conclusions

In conclusion, the study of pressure distribution and aerodynamic performance of mono-slope roofs under varying conditions has yielded several critical insights:

A. **Pressure Distribution and Roof Slope Impact**: Mono-slope roofs predominantly experience suction pressure.

B. Increasing the roof slope (from 10° to 30°) reduces the pressure coefficient (C_{pe}), with the minimum C_{pe} observed at a 30° slope, making it the safest configuration. The 10° roof slope is the most vulnerable, experiencing the largest suction magnitude.

C. **Building Interference Effects:** When buildings are closely spaced (zero spacing), the structure behaves like a single unit, and interference effects are minimized.

D. Increased spacing between buildings (from 0 to 2B) reduces suction due to interference, as reflected in changes to C_{pe}, Interference Factor (IF), and Interference Difference (ID) values. The reduction in pressure coefficient (C_{pe}) is observed to be 84.69% in rectangular pattern, 82.03% in Z pattern and 89.11% in T pattern.

E. **Pattern Suitability:** Among the three arrangements (rectangular, Z, and T patterns), the rectangular pattern offers the most aerodynamic benefit, with lower suction and better performance overall.

F. **Key Observations:** $IF > 1$ and positive ID indicate increased suction, while reduced suction corresponds to $IF < 1$ and negative ID values.

G. The variation of C_{pe}, IF, and ID with wind angles and spacing highlights the dynamic influence of interference on roof performance.

H. Recommendation: For optimal aerodynamic performance and reduced suction, a 30° mono-slope roof in a rectangular building pattern with increased spacing is the most effective configuration.

CHAPTER 7

RESULTS AND DISCUSSIONS FOR HIP ROOF

7.1 General

There are several types of roof forms provided for low-rise structures, and one of them is the hip roof. The hip roof is divided into 4 different portions, i.e., windward and leeward, both in the form of a trapezoidal section and 2 side slopes in the form of a triangular section. The same slope of the roof is provided from all four sides which makes it symmetrical about both the centrelines. This chapter deals with a detailed discussion of wind-induced pressure contours, pressure coefficient (C_{pe}), interference factor (*IF*), and interference difference (*ID*) over the hip roof in isolated and different interfering conditions. It also discusses the variation of the mentioned coefficients concerning various angles of wind incidence.

7.2 Isolated Hip Roof

The low-rise building model shown in Fig. 7.1, with a hip roof, plan dimensions 200 mm X 400 mm, eave height 150 mm, and different roof slopes 10°, 20°, and 30°, is subjected to a 0° to 90° angle of wind attack at an interval of 15°. The wind-induced pressure contours and variation of C_{pe} for isolated low-rise buildings with hip roofs of different roof slopes i.e., 10°, 20° and 30° are discussed here below in this section.
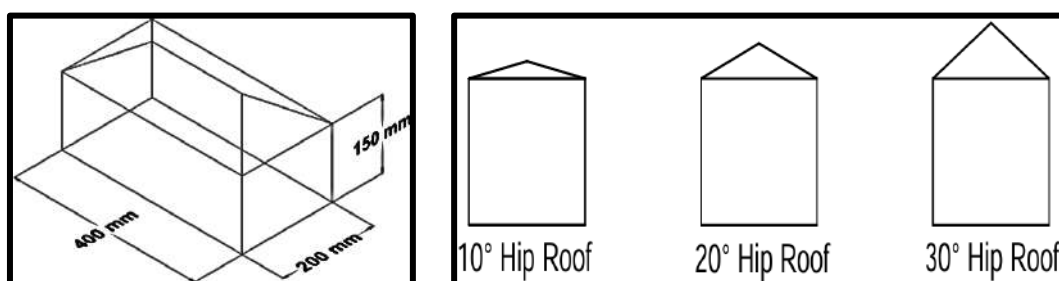
Fig. 7.1: Isolated Hip Roof with 10°, 20° and 30° Roof Slope

7.2.1 Pressure Contours

The wind-induced pressure contours for the isolated hip roof 10°, 20° and 30° roof slope are shown in Figs. 7.2, 7.3 and 7.4, respectively. The deviation of wind-induced pressure on hip roof with 10° roof pitch when subjected to angle of wind attack from 0° to 90° at 15° interval is shown in Fig. 7.2. It can be deduced from Fig. 7.2 that, as compared to other portions of the roof, the maximum negative pressure occurs at the windward edge. During the 30° angle of wind attack, the corner edge point where the windward and top right portion meet is under maximum suction, as shown in Fig. 7.2. Due to the wind flow separation at the junction of the windward and the top-right portion of the roof, the maximum negative wind-induced pressure

is generated. The almost full edge of the top right portion and half edge of the windward roof portion are subjected to higher negative wind-induced pressure. The edge of the top right portion, which is in the upstream direction of wind flow, is suffering the higher negative pressure in contrast with another portion of the roof. Also, the negative pressure that was acting on the windward edge of the windward roof portion during wind incidence angle ranging from 0° to 45° is now converted into nearly half of the magnitude in case of a 60° wind incidence angle. It can also be predicted that the amplitude of wind-induced suction is diminishing substantially. In the case of a 90° angle of wind attack, when the wind is blustering at 90° to the top right portion of the roof, the higher negative pressure is generated on the edge, which is in the upstream direction of wind flow. Major portion of the top left roof is subjected to the positive pressure during 90° wind incidence.

Fig. 7.3. shows the contours of wind-induced pressure on 20° hip roof. It is observed during the 0° wind incidence angle that the negative pressure on the edge of windward roof portion increased due to increase in roof pitch which results in the formation of sharp edge as compared to 10° roof pitch. Also, the pressure on top left & right and leeward potion reduced due to increase in roof pitch from 10° to 20°. When the wind is blowing at 15°, 30°, 45° and 60° respectively, the top edge of the hip roof of 20° roof pitch undergoes higher negative pressure due to an increase in the sharpness of the roof at the edges when compared with hip roof with 10° roof pitch. But for the other portions of the roof, it can also be said that the negative pressure is getting reduced due to increase in roof pitch. In case of 90° wind incidence angle, almost whole roof is subjected to reduced negative pressure as compared to 10° roof pitch.

Fig. 7.4. shows the contours of wind-induced pressure for the hip roof of 30° roof pitch with respect to various angles of wind incidence. It can be inferred that value of negative pressure on the roof get drastically reduced due to increase in roof slope. It is found that different portions of the 30° hip roof that were subjected to negative pressure in case of 10° and 30° roof are now subjected to positive pressure which enables that the 30° hip roof is quite safe as compared to 10° and 20° hip roofs. The pressure contours for 30° hip-roof subjected to different angles of wind attack i.e., 0° to 90° are shown below in Fig. 7.4. During 0° wind attack, the windward top portion of hip roof has shown some positive wind induced pressure while there is only suction acting on leeward top portion of the hip roof. There is maximum value of negative pressure is observed on the area just behind the ridge line of the roof. The pressure distribution during 45° wind attack is on hip roof is completely differs from 0° wind attack angle. Due to high turbulence and vorticity, the development of thin shear layer is taking place on the ridge line which is parallel to wind direction. The whole hip roof appears like it is divided

in two halves i.e., windward and leeward slopes respectively. The distribution of pressure contours on either windward or leeward portion is in continuous form. The area behind two hip ridges which are at the right angle to the wind flow and the roof ridge was under maximum average suction during 45° wind attack. During the wind attack at an angle of 45°, because of the development of separation bubbles of large size due to high roof slope, the area of roof which is lying behind the two hip ridges normal to wind direction is experiencing small wind induced mean suction. In case of 90° angle of wind attack, the leading eave edge experiences wind induced positive mean pressure. Also, there is a uniform distribution of wind induced pressure along the long edge over most of two side slopes. There is highest mean suction appears on the area which is closed to roof corners of behind windward hip ridge.
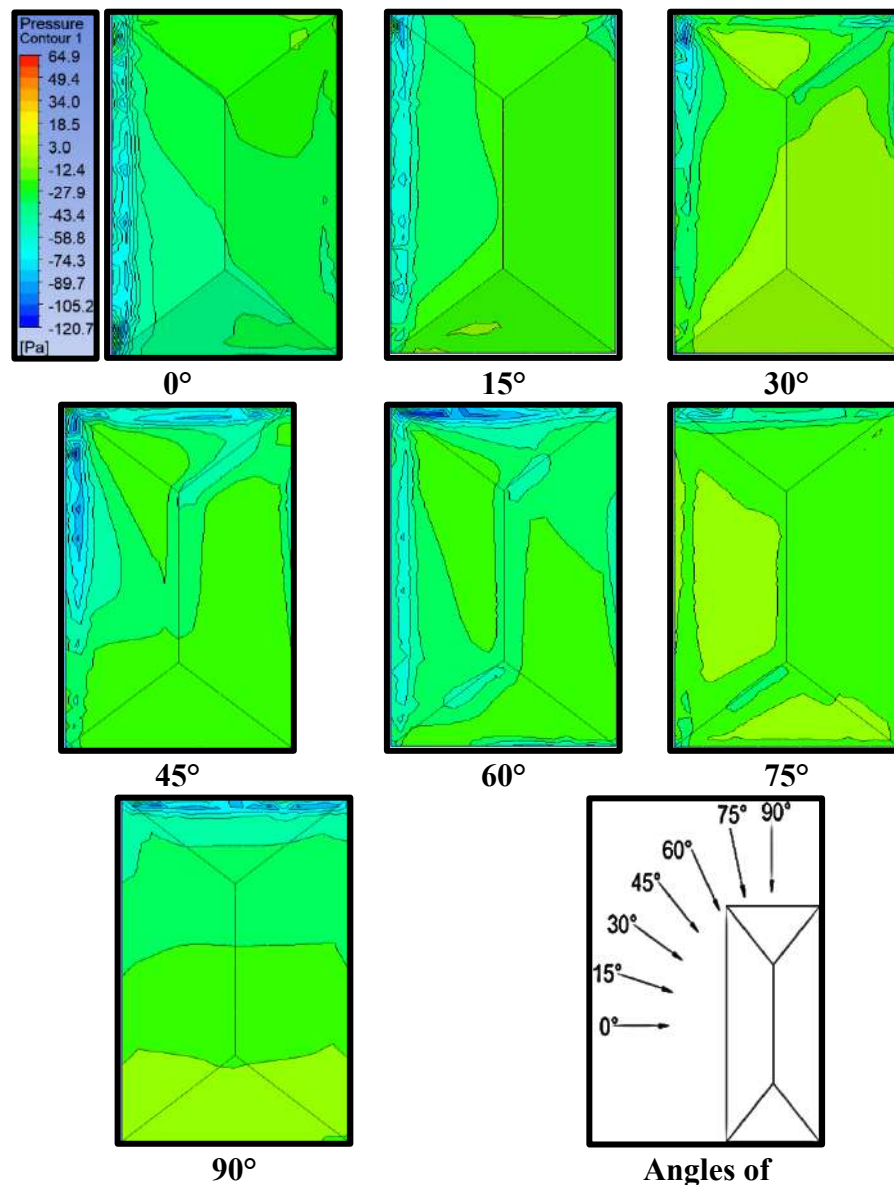
Fig. 7.2: Pressure Contours for 10° Hip Roof
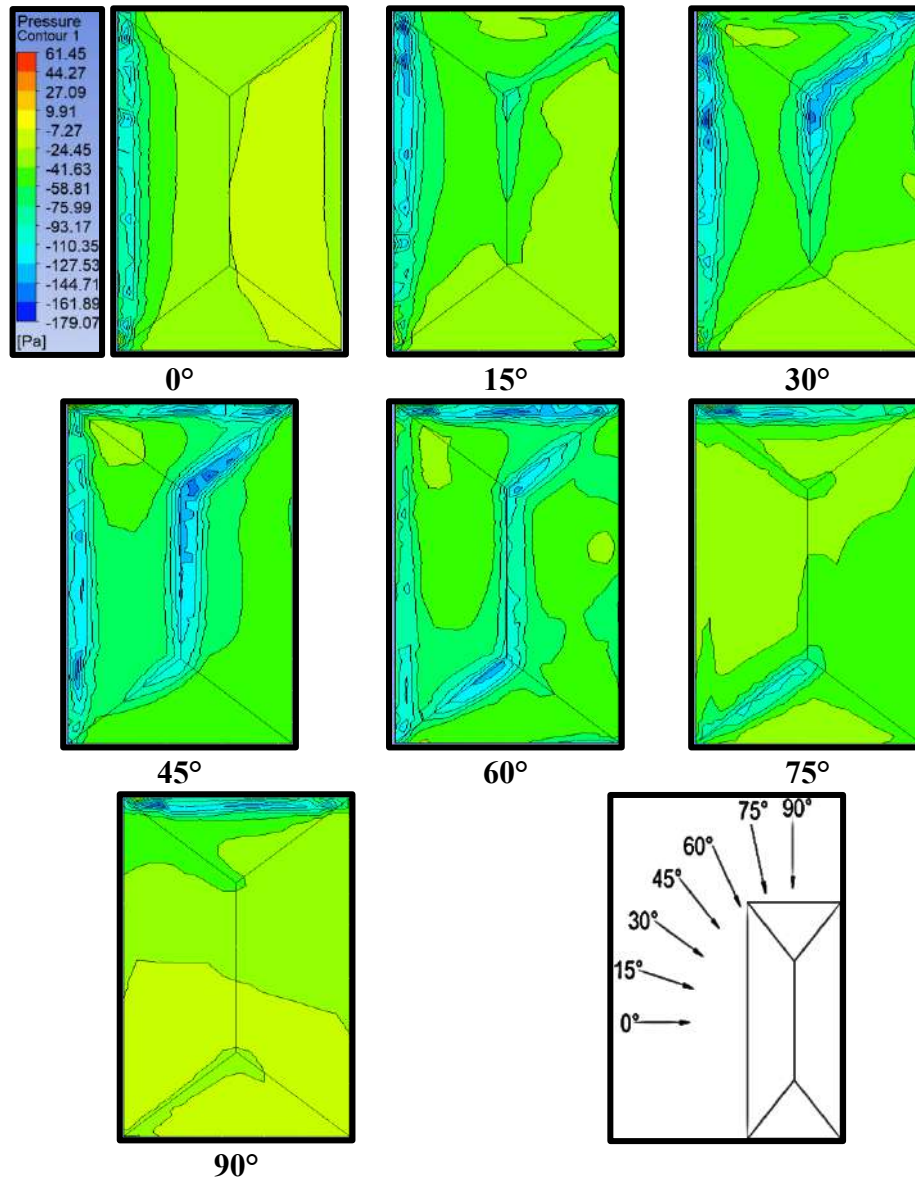
Fig. 7.3: Pressure Contours for 20° Hip Roof
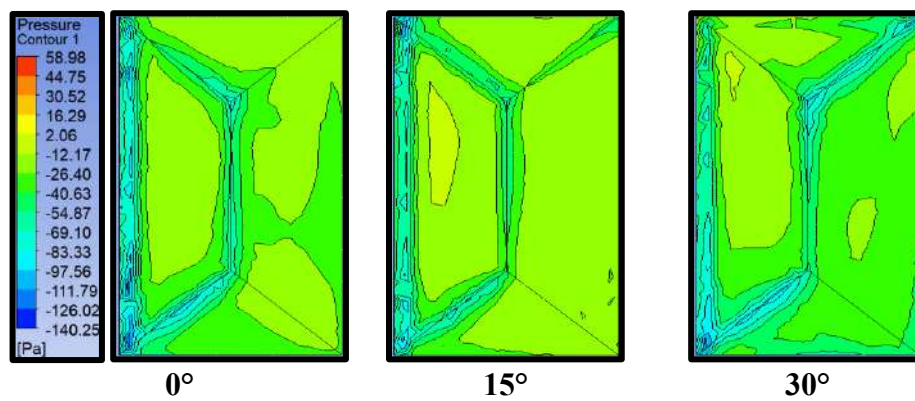
Fig. 7.4(a): Pressure Contours for 30° Hip Roof
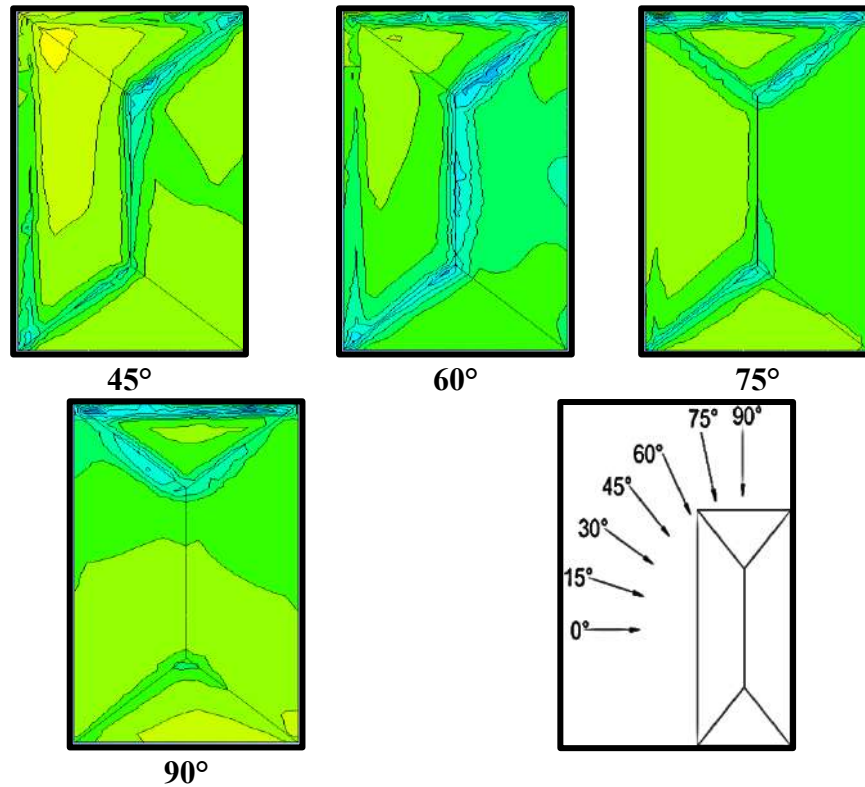
Fig. 7.4(b): Pressure Contours for 30° Hip Roof

7.2.2 Pressure Coefficient (C_{pe})

The C_{pe} for the hip roof with 10°, 20° and 30° roof slope is calculated using CFD simulation by subjecting it to the different angles of wind incidence angles 0° to 90° at an interval of 15°. But before that, the model needs to be validated either with the wind standards of different nations or some previous research.

In the present research, a low-rise building model with a hip roof of 30° roof slope and a plan dimension of 200 mm X 400 mm is validated with some wind standards and previous experimental research.

Fig. 7.5 shows the C_{pe} variation for hip roof of different roof pitches (10°, 20° and 30°) at different angles of wind attack (0° to 90° at 15° interval). The maximum suction is observed for hip roof of 20° roof pitch as compared to 10° and 30° hip roof.

It indicates that the most critical angle of the roof in case of hip roof is 20° from all the three cases of roof considered for the study. Now the minimum suction is observed in case of hip roof with 30° roof pitch in between 10° and 30° hip roof. The safest roof pitch is 30° for hip roof in all the three cases.
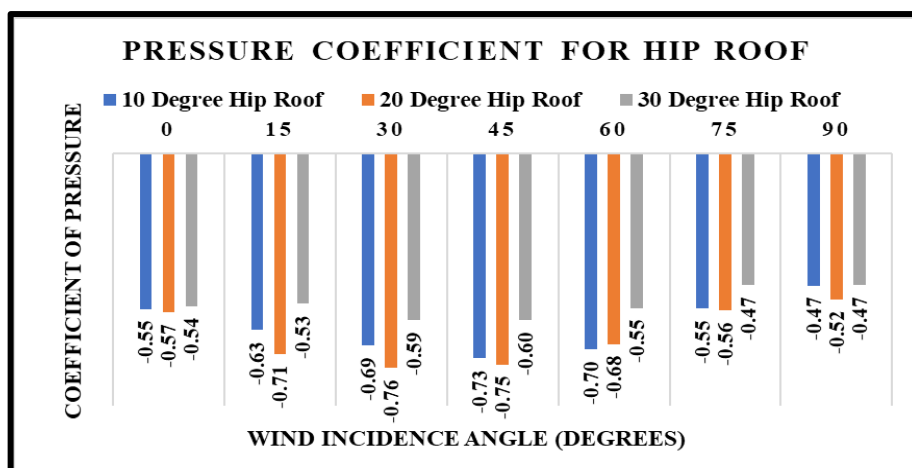
Fig. 7.5: C_{pe} variation w.r.t wind incidence angle for the Hip roof

7.2.2.1. Comparison with Holmes, 1981 and Xu & Reardon, 1998 work

Holmes, 1981 conducted an experimental wind investigation over the gable roof with three different roof pitches i.e., 15°, 20° and 30° respectively (Homes, 1983, 1983) and the only data provided in report was roof pressure. Xu & Reardon, 1998 also conducted the wind tunnel investigation on hip roof with 15°, 20° and 30° roof pitch having the model dimensions same as that of Holmes work. Holmes provided the results only for wind incidence angle of 0° and 90° whereas Xu & Reardon, 1998 provided the results for 0°, 45° and 90° respectively.

In present study, the CFD investigation has been conducted on 30° hip roof for different angles of wind incidences at an interval of 15° i.e., 0° to 90° and the wind induced pressure contours are provided for all the angles. It has been found out in Holmes, Xu and present investigation that is the pressure distribution on gable and hip roof is completely different from each other except for 0° wind attack. It was mentioned in Homes work that gable roof with 15° roof pitch was experiencing the maximum mean suction and that to over the roof area which is lying just behind the ridge nearer to gable end. The maximum value of wind induced pressure coefficient was -1.0 (Holmes, 1981). Holmes found that during 45° wind incidence, the maximum value of mean suction was C_{pe}=-2.73 acting on small area closer to gable end or roof ridge. The leading eaves of the roof were subjected to maximum suction of C_{pe} =-1.33 during 90° wind incidence.

Xu concluded that the 30° hip roof was experiencing the highest mean suction with C_{pe} = -1.0 over the roof area which is just behind windward hip ridge during 0° wind incidence. The mean suction got reduced over 30° hip roof during 45° wind incidence because of the generation of flow separation bubble of large size and also the half of windward slope was experiencing the positive pressure. The maximum value of mean suction was recorded as C_{pe} = -1.0 at the downward corners of the roof of front hip ridge (Xu & Reardon, 1998).

In present study it is found that the mean suction of C_{pe} = -0.54, maximum positive C_{pe} = 0.96 and maximum negative C_{pe} = -2.29 during 0° wind attack. In case of 45° wind attack the maximum positive, maximum negative and average C_{pe} are 1.03, -2.87 and -0.60 respectively. During 90° wind attack it was observed that maximum positive, maximum negative and mean C_{pe} are 0.96, -2.19 and -0.47 respectively.

7.2.3 Wind Flow Pattern on Hip Roof

The wind flow pattern over an isolated hip roof with 10°, 20° and 30° roof slope at various angles of wind incidence ranging between 0° to 90° at an interval of 45° each is shown in Figs. 7.6, 7.7 and 7.8 respectively.

During 0° wind incidence, the wind flow is responsible for negative wind-induced mean pressure on all 10°, 20° and 30° hip roofs, but there is some portion on the windward slope of the 30° hip roof which is under positive pressure.

By increasing the roof pitch from 20° to 30°, the region of positive wind-induced pressure also increases. The wind flow pattern in the wake region is changing as the direction of the wind changes.

During 45° angle of wind incidence, the wind flow is separated from the windward slope till the leeward slope of the 10° hip roof and then recirculated in the wake region, creating a very high suction region in the leeward direction but the wind flow is separated from the windward slope of the 20° hip roof which gets reattached to the leeward slope and then recirculating in the wake region while the wind flows on 30° hip roof is still attached to the windward slope of the roof and gets separated at the ridge of the roof creating a zone of low velocity while circulating in the wake region.

The low-velocity zone is forming on the sideways of the building as compared to the roof, due to which the suction on the roof is lesser than that of the side roof edges.

0°
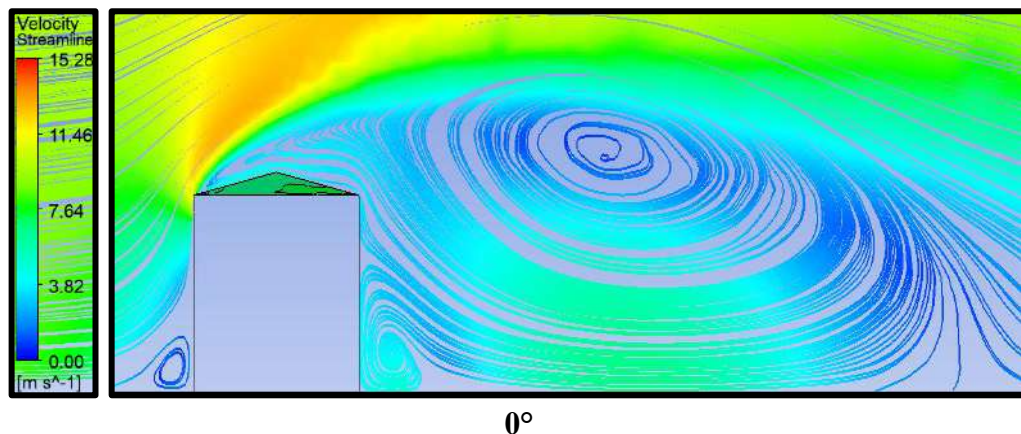
Fig. 7.6(a): Wind Flow Streamlines of 10° Hip Roof

30°   **90°**
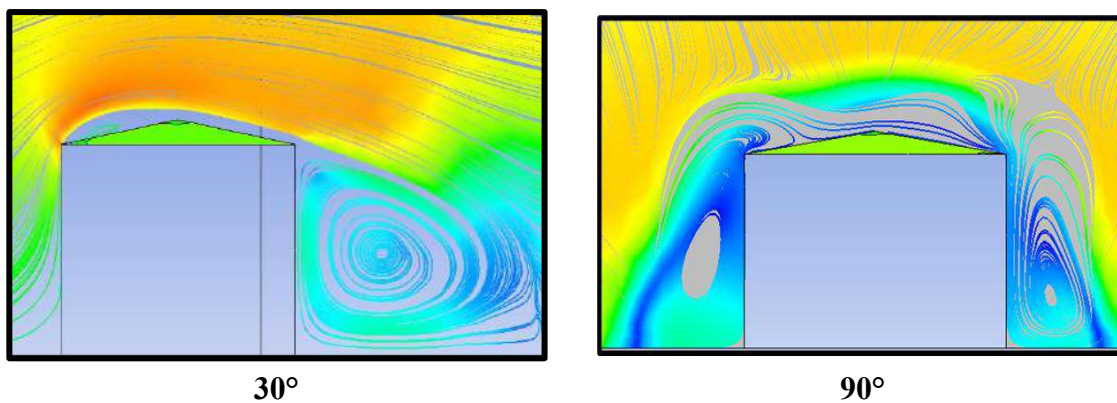
Fig. 7.6(b): Wind Flow Streamlines of 10° Hip Roof

0°

45°   **90°**
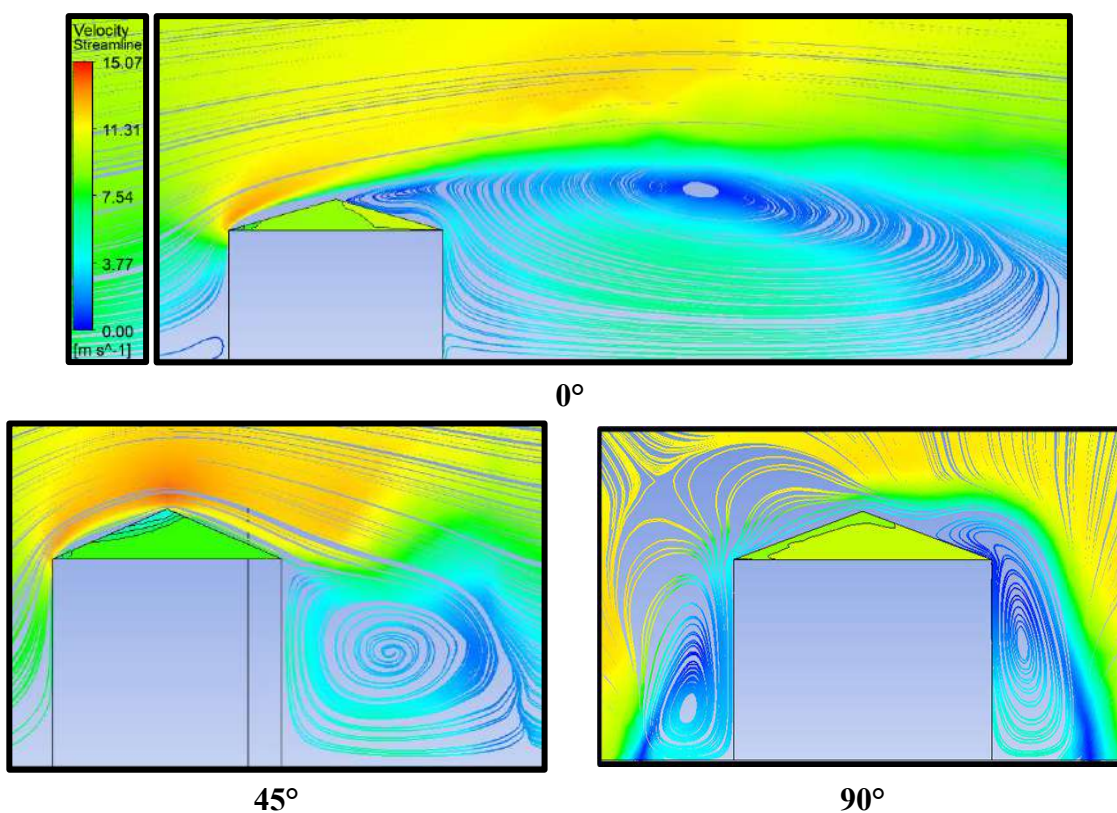
Fig. 7.7: Wind Flow Streamlines of 20° Hip Roof

0°
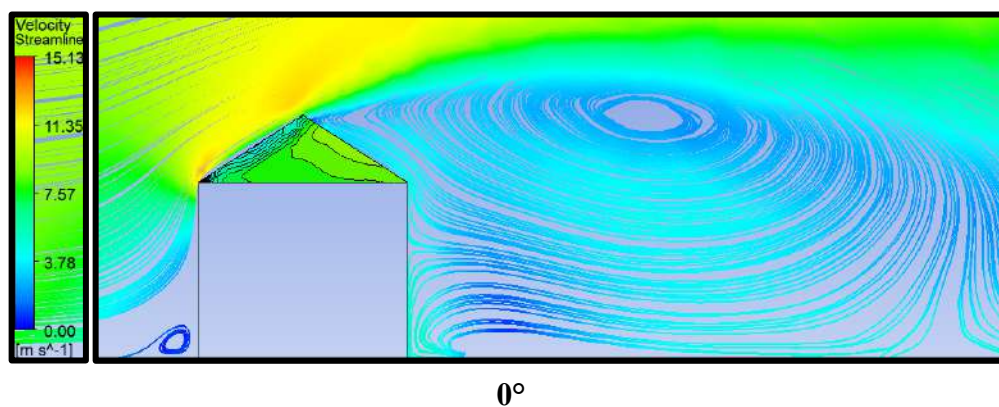
Fig. 7.8(a): Wind Flow Streamlines of 30° Hip Roof

| 45° | 90° |
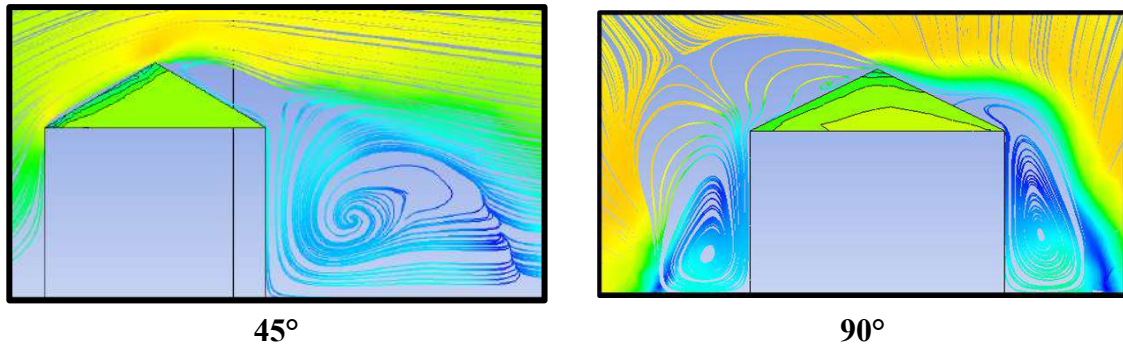
Fig. 7.8(b): Wind Flow Streamlines of 30° Hip Roof

7.3 Interference

In this section the effects of presence of nearby buildings are investigated in the form of interference factor (*IF*) and interference difference (*ID*) on the hip roof with 30° roof slope of low-rise structures arranged in rectangular pattern, T-pattern and Z-pattern with variable spacing i.e., 0, 0.5B, B, 1.5B and 2B where B is the width of the building at various angles of wind incidence ranging between 0° to 180° at an interval of 15° each.

7.3.1 Rectangular Pattern

To find out the effect of interference on 30° hip roof, six low-rise building models with hip roof arranged in rectangular pattern placed nearby each other using different spacings i.e., 0, 0.5B, B, 1.5B and 2B. The wind-generated pressure contours, IF and ID on all six 30° hip roofs due to interference are discussed below at different angles of wind incidence ranging between 0° to 90° at 15° intervals each. The rectangular pattern with 30° hip roof and wind angles are shown in Fig. 7.9.

| Zero Spacing | 0.5B Spacing | B Spacing |

| 1.5B Spacing | 2B Spacing | Wind Angles |

Fig. 7.9: Rectangular Pattern and Wind Angles of 30° Mono-Slope Roof

7.3.1.1 Pressure Contours

The wind-induced pressure contours obtained for low-rise buildings with 30° hip roofs arranged in rectangular patterns with variable spacing and at different angles of wind incidence are shown in Figs. 7.10-7.14. When the spacing between buildings is zero, the structure acts as a single building with multi-span hip roofs, which is responsible for making the structure more stable as compared to the single span isolated hip roof loo-rise structure. When the angle of wind incidence ranges between 0° to 30°, the windward edge of hip roofs A and D is subjected to the maximum wind-induced negative pressure as compared to the other parts of the roof. The leeward slope of roofs C and F is under least negative pressure during 0° wind incidence angle. The windward slope of roofs B and C is subjected to the positive wind pressure distribution during 15° and 30° wind angles. The ridge of hip roofs is undergoing negative wind pressure when the wind angle changes from 30° to 60°. In case of 75° and 90° wind angles, the edges of side slope of roofs A, B and C are under higher negative pressure and roofs D, E and F are under less negative pressure. The spacing between buildings up to 2B proves to be beneficial, due to which the pressure distribution tends to be in a balanced manner on the hip roof due to the interference. It is observed that there is both positive and negative wind-induced pressure distribution on the hip roof when arranged in a rectangular pattern with variable spacing, which makes the roof more stable and responsible for the reduction in mean wind pressure on the roof. The wind-induced pressure distribution on hip roofs arranged in rectangular patterns with variable spacing, i.e., 0, 0.5B, B, 1.5B and 2B with respect to different wind angles ranging between 0° to 90° having an interval of 15°, is shown in Fig. 7.10 to 7.14, respectively.
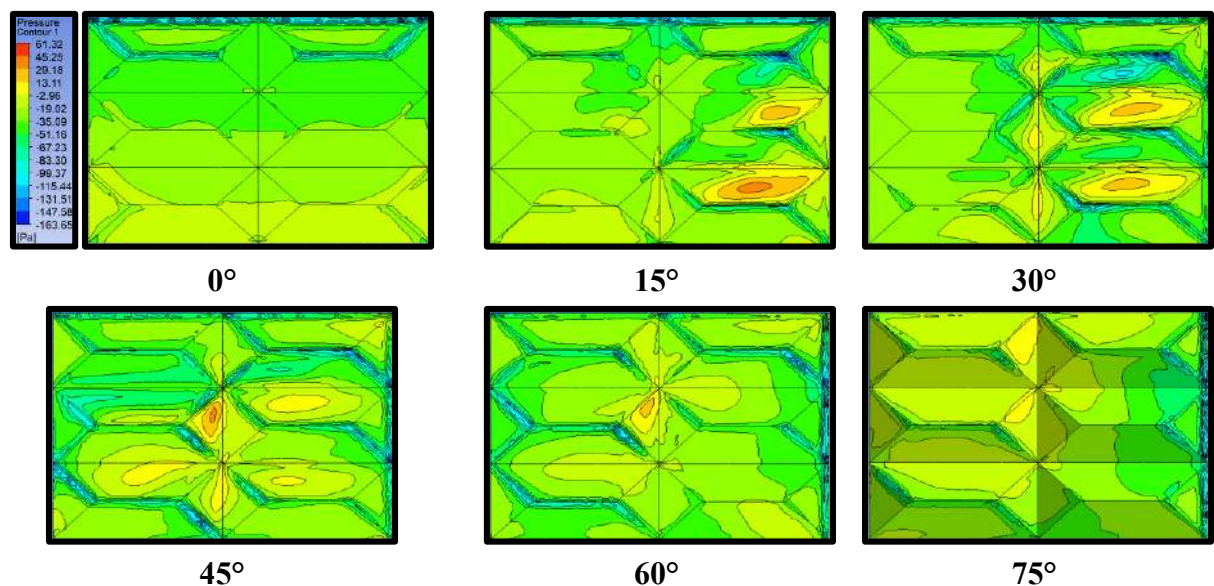
Fig. 7.10(a): Pressure Contours for Rectangular Patter with zero Spacing

90°
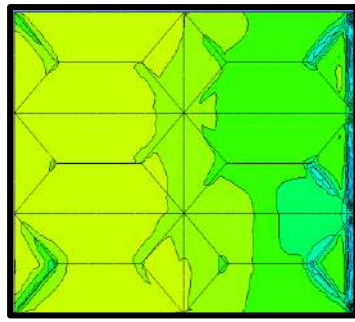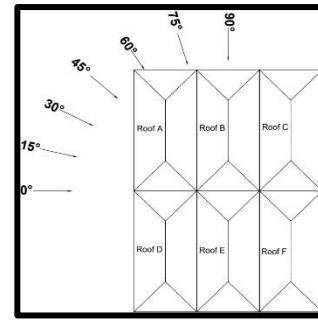
Wind Angles

Fig. 7.10(b): Pressure Contours for Rectangular Patter with zero Spacing

0°

15°

30°

45°

60°

75°

90°
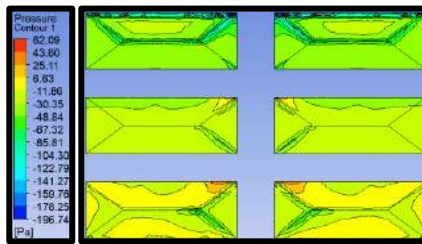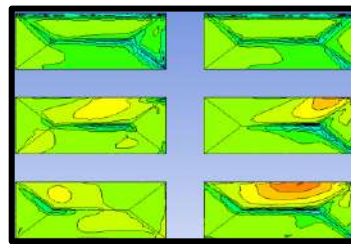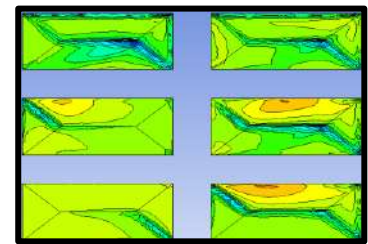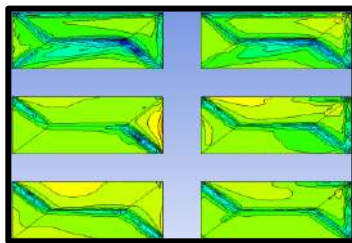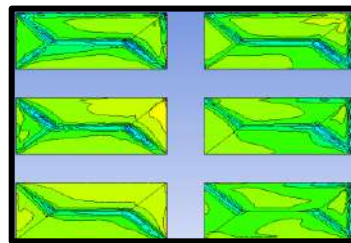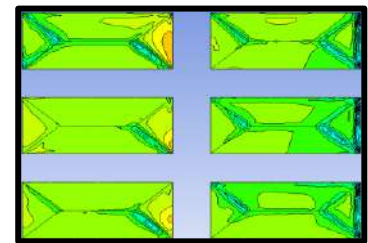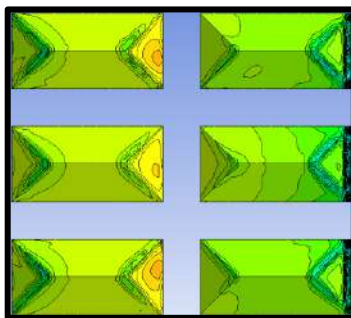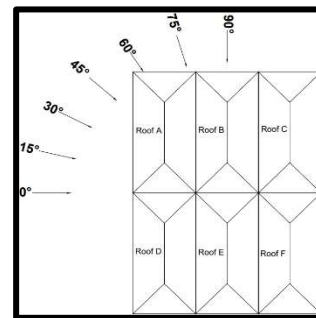
Wind Angles

Fig. 7.11: Pressure Contours for Rectangular Patter with 0.5B Spacing
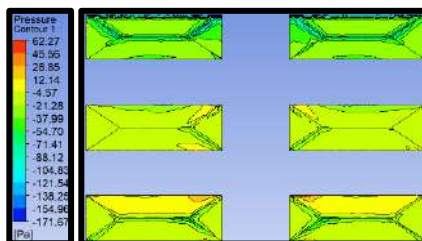
0°
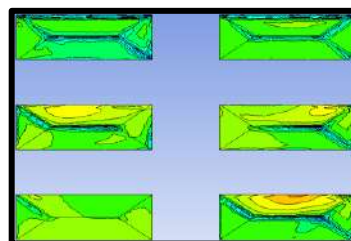
15°
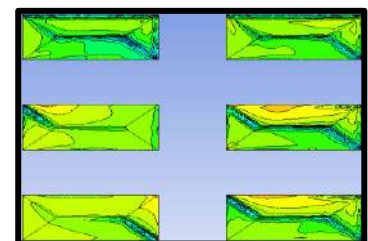
30°

Fig. 7.12(a): Pressure Contours for Rectangular Patter with B Spacing

45° **60°** **75°**

90° **Wind Angles**

Fig. 7.12(b): Pressure Contours for Rectangular Patter with B Spacing

0° **15°** **30°**

45° **60°** **75°**

90° **Wind Angles**
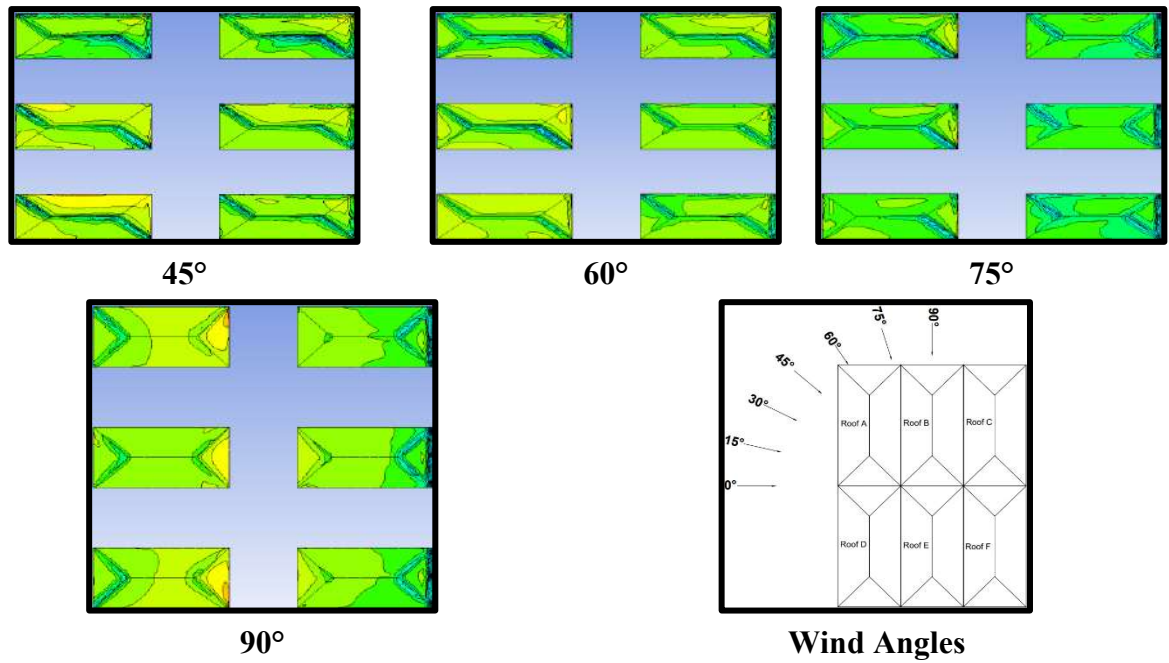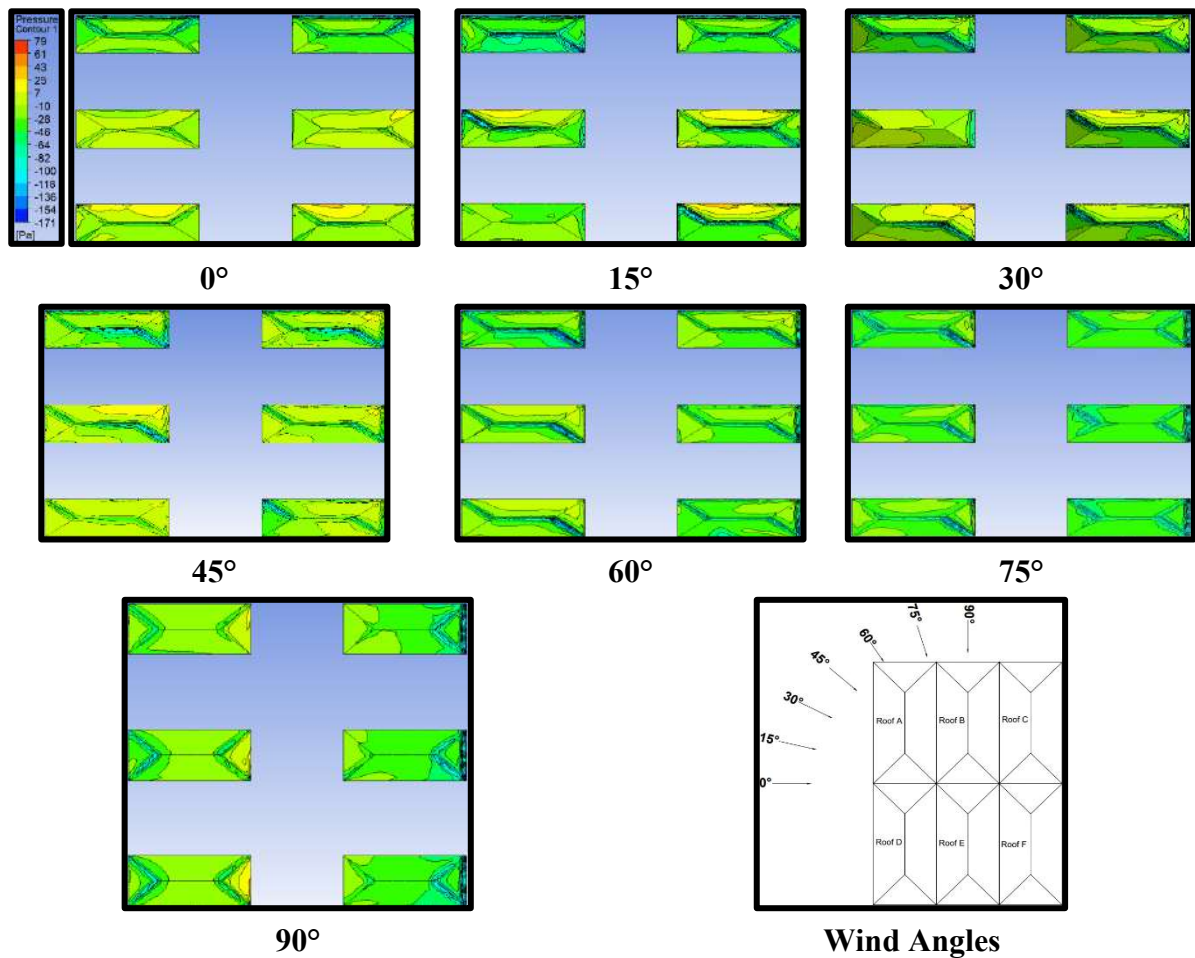
Fig. 7.13: Pressure Contours for Rectangular Patter with 1.5B Spacing
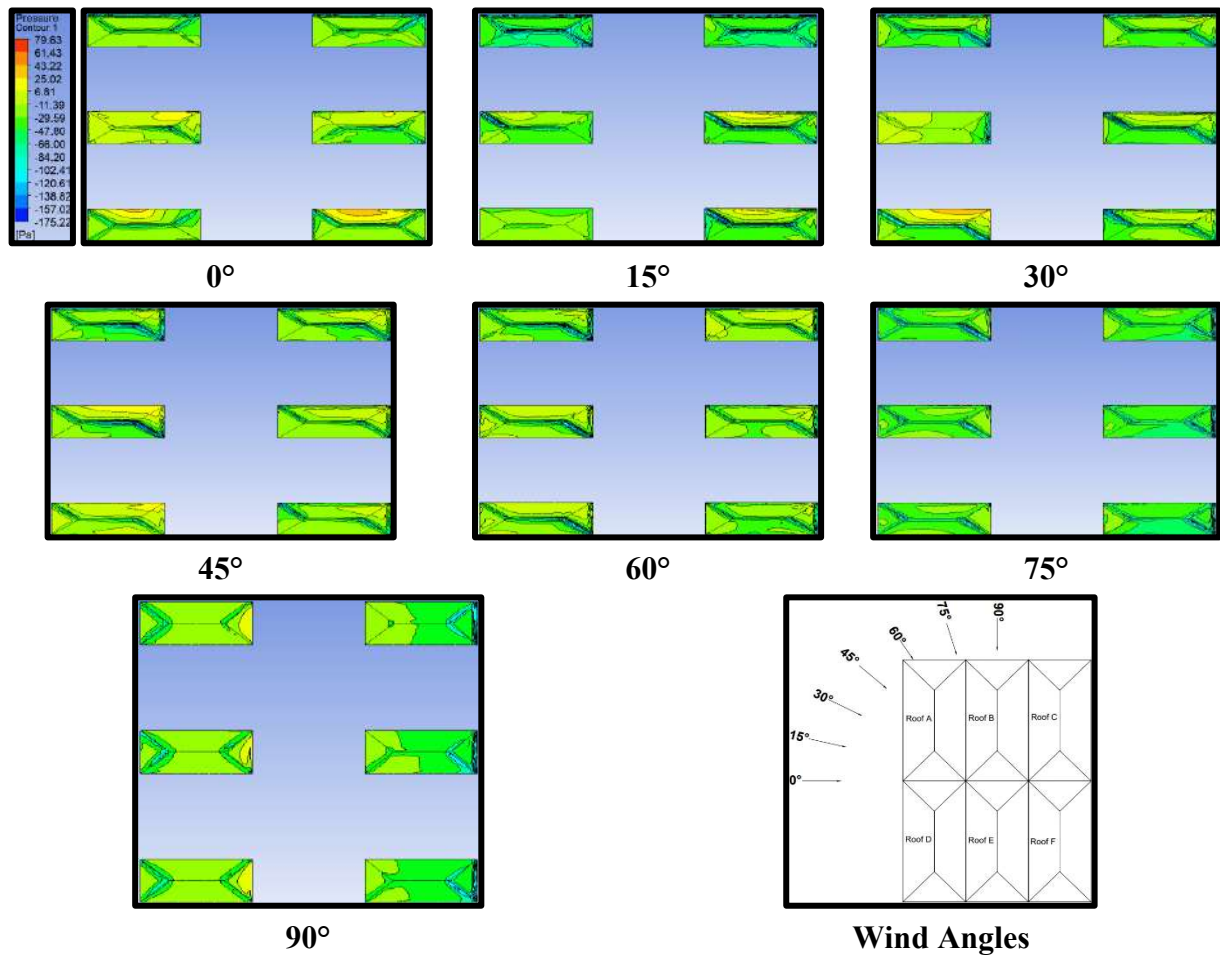
Fig. 7.14: Pressure Contours for Rectangular Patter with 2B Spacing

7.3.1.2 Pressure Coefficient

Fig. 7.15 depicts the variation of average C_{pe} of all the hip roofs for different wind incidence angles i.e., 0° to 90° at 15° wind intervals with variable spacing i.e., zero, 0.5B, B, 1.5B and 2B (where B=0.2m). Pressure on the hip roof with a 30° roof slope is reduced with respect to the spacing and angle of wind incidence in rectangular patterns when compared with cylindrical, dome and mono-slope roofs. The value of C_{pe} on all the roofs A, B, C, D, E and F is reduced, indicating the reduced suction on the roof by increasing the spacing between the buildings when the angle of wind attack ranges between 0° to 90° respectively, as shown in Fig. 7.15. The pattern of C_{pe} variation followed by roofs A, B, and C is similar to each other, as well as roofs D, E and F show a similar pattern of variation of C_{pe}. The maximum negative value of C_{pe} is observed as -0.81 on roofs A and D during 0° angle of wind incidence at zero spacing due to the symmetrical pressure distribution, while the minimum value of negative C_{pe} is observed on roof F i.e., -0.11 during 15° angle of wind attack and 2B spacing. The value of C_{pe} on roofs B, C, E and F comes out to be smaller than that of the isolated hip roof due to the effect of shielding during interference. Since the overall impact of wind on the hip roof is

suction in nature, also because of the slope provided from all four sides, the hip roof is more stable or safe as compared to the other roof forms.
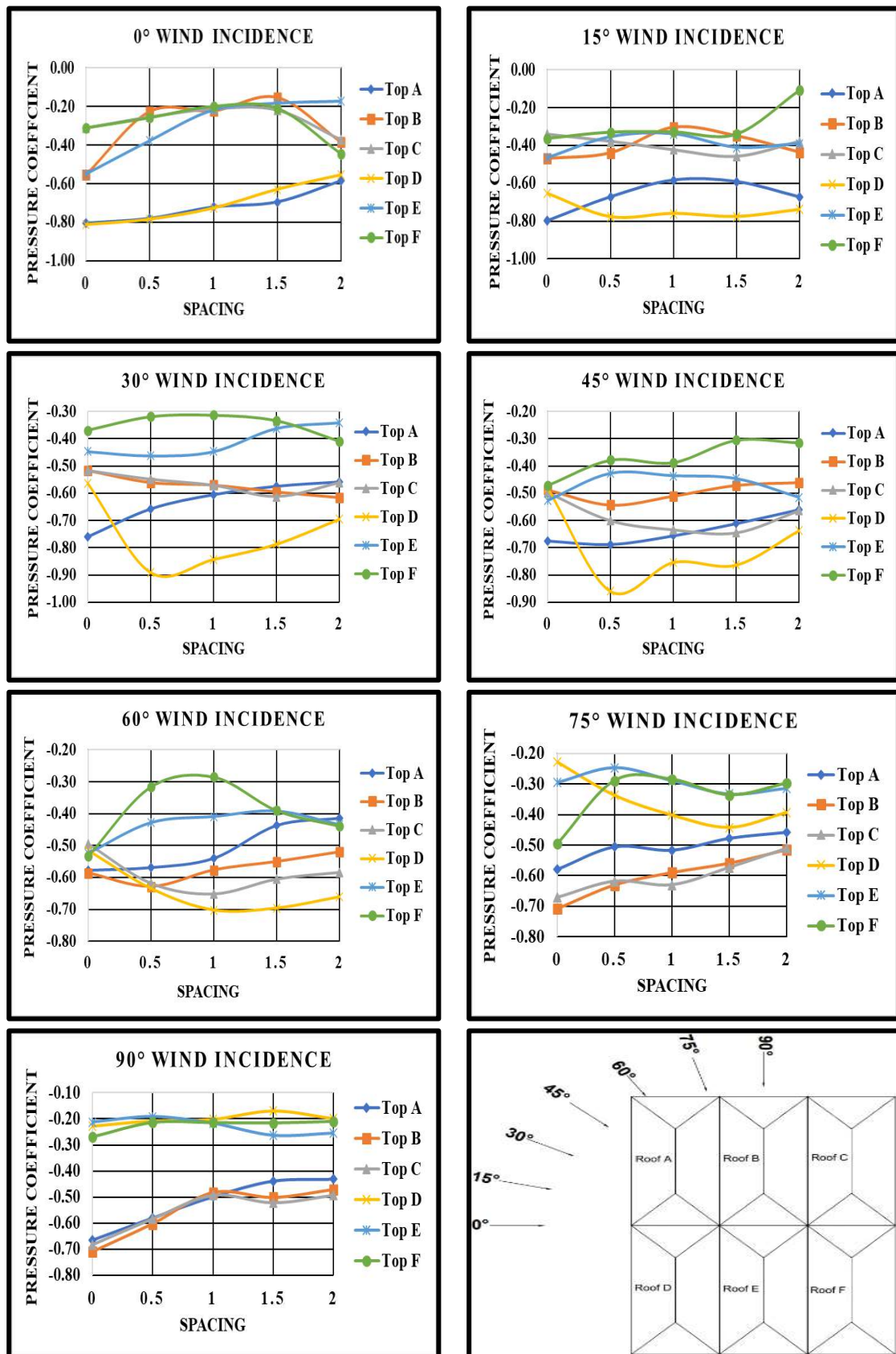
Fig. 7.15: Pressure Coefficient for Rectangular Patter of Hip roof

6.3.1.3 Interference Factor (IF)

For the numerical representation of the effects induced by the wind action due to interfering with the building under investigation, the *IF* can be utilized effectively. If the value of C_{pe} on the building under study is decreased due to interfering building which results in the reduction of *IF*, it indicates that the suction on the building is reduced due to the shielding effect of interfering building on the building under study, but the nature of wind action is same. The lower the value of *IF* lesser will the wind-induced action on the roof of the building under study. If there is a change in the sign of *IF* i.e., positive to negative then it implies that the wind action has changed its nature on the roof or the building under investigation. The role of spacing and wind incidence angle plays a vital role in wind-induced action on all the roofs under investigation which results in variation of *IF* for all the roofs as shown in Fig. 7.16. In all the conditions of Spacing between buildings, the IF is moving towards reduced value i.e., from a value of greater than 1 to less than 1, which is proved to be beneficial due to interference. During 0° wind incidence angle, roofs C and F are undergoing maximum reduced suction (*IF* less than 1) due to interference as compared to the other roofs. Also, the value of *IF* is less than 1, indicating the reduced suction on roofs B, C, E and F due to the shielding effects when the angle of wind attack ranges between 0° to 75°, as shown in Fig. 7.16. The value of *IF* on the roof A is greater than 1 at almost all the wind angles i.e., 0° to 90° but it keeps on reducing indicating the reduced suction on the roof when the spacing between the buildings is increased from 0 to 2B, while *IF* on roof D is greater than 1 and reduced by the increase in spacing when the angle of wind incidence is changed from 0° to 60°. The value of IF on roofs B, C, E and F is observed to be less than 1 denoting the reduced suction on the mentioned roofs due to interference of the surrounding buildings.
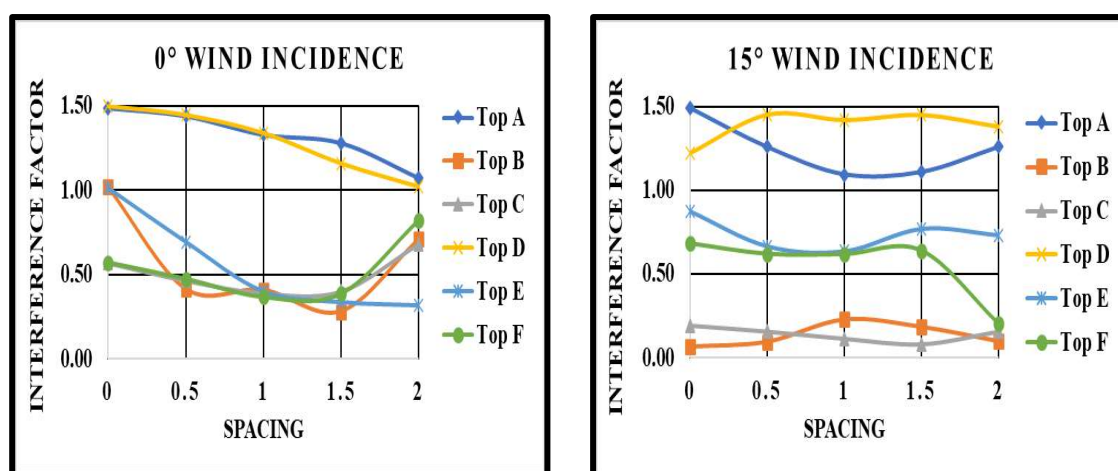
Fig. 7.16(a): Interference Factor for Rectangular Patter of 30° Hip roof
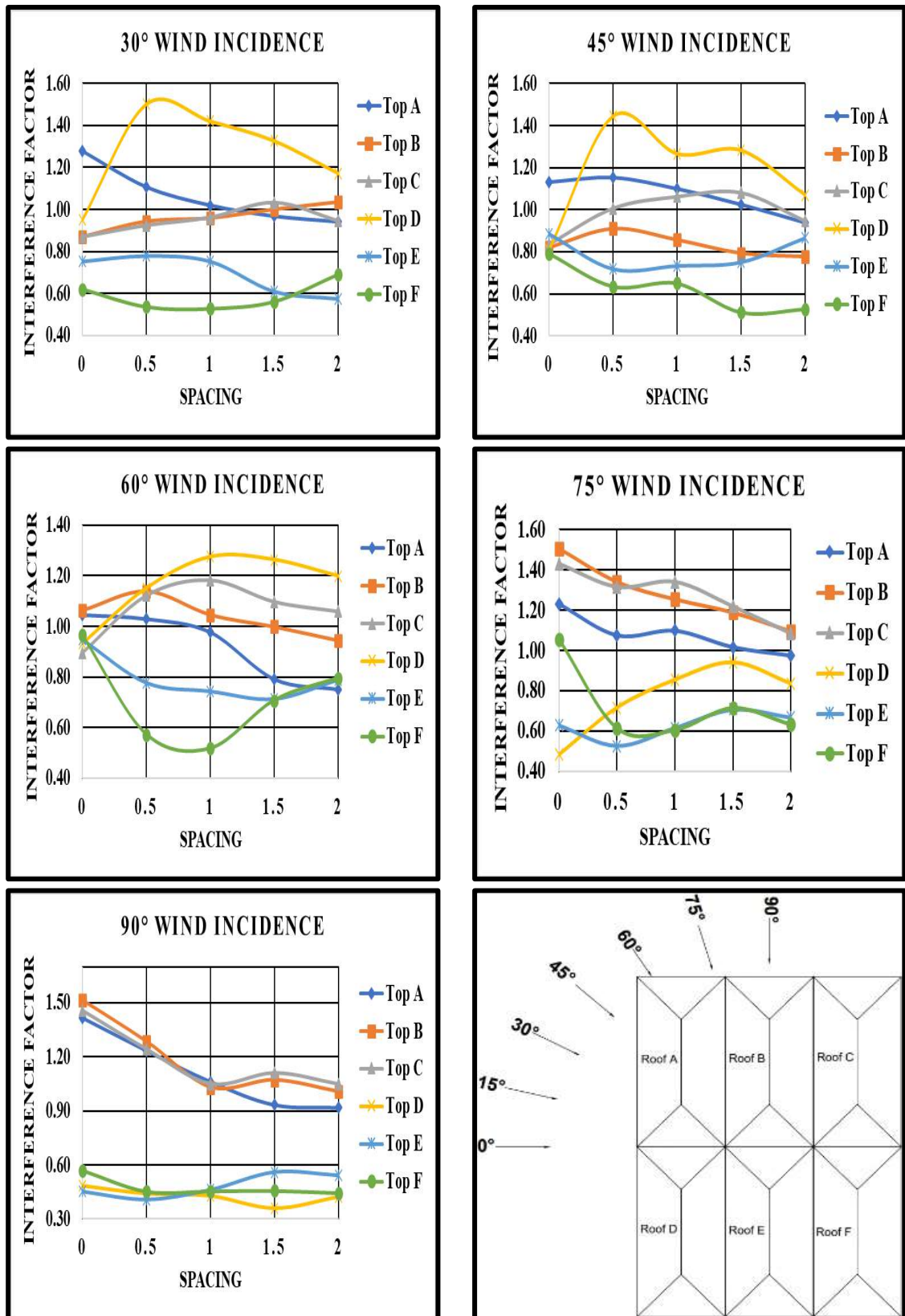
Fig. 7.16(b): Interference Factor for Rectangular Patter of 30° Hip roof

6.3.1.4 Interference Difference (ID)

Sometimes it comes to knowledge that due to interference either pressure or suction on buildings gets reduced such as the action of shielding effect on the roof due to the presence of the interfering building in the upstream direction of the wind flow resulting in the reduction of the pressure or suction. The values of *ID* are calculated for all the hip roofs under variable spacing and wind interval conditions presented in Fig. 7.17. The pattern of variation of *ID* for a hip roof is exactly similar to the variation of pressure coefficient with respect to the variable spacing and different angles of wind attack because *ID* denotes the difference between the pressure coefficient during interfering conditions and isolated conditions. The negative sign of *ID* indicates the increased suction on the roofs due to interference of the upstream or side buildings, and the positive sign of *ID* denotes the reduced suction on the roof. Since it is clearly visible from Fig. 7.17, that initially at 0 spacing, the value of *ID* is less than 1 for all the roofs at all the angles of wind incidences, but it starts moving towards the reduced value i.e., *ID* becomes greater than or equal to 0 resulting in the reduced suction on the roof when spacing is increased from 0 to 0.5B, B, 1.5B and 2B at all the wind incidence angles.
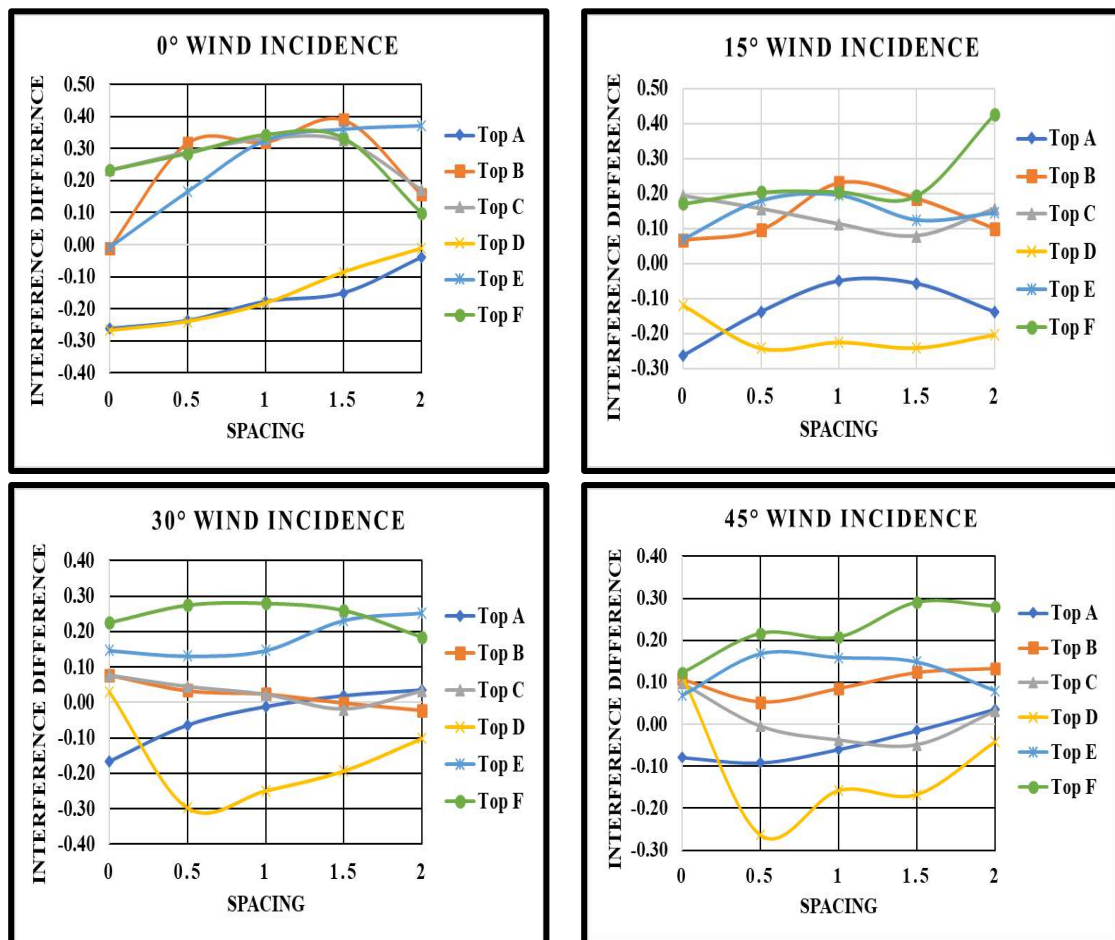
Fig. 7.17(a): Interference Difference for Rectangular Patter of Hip roof
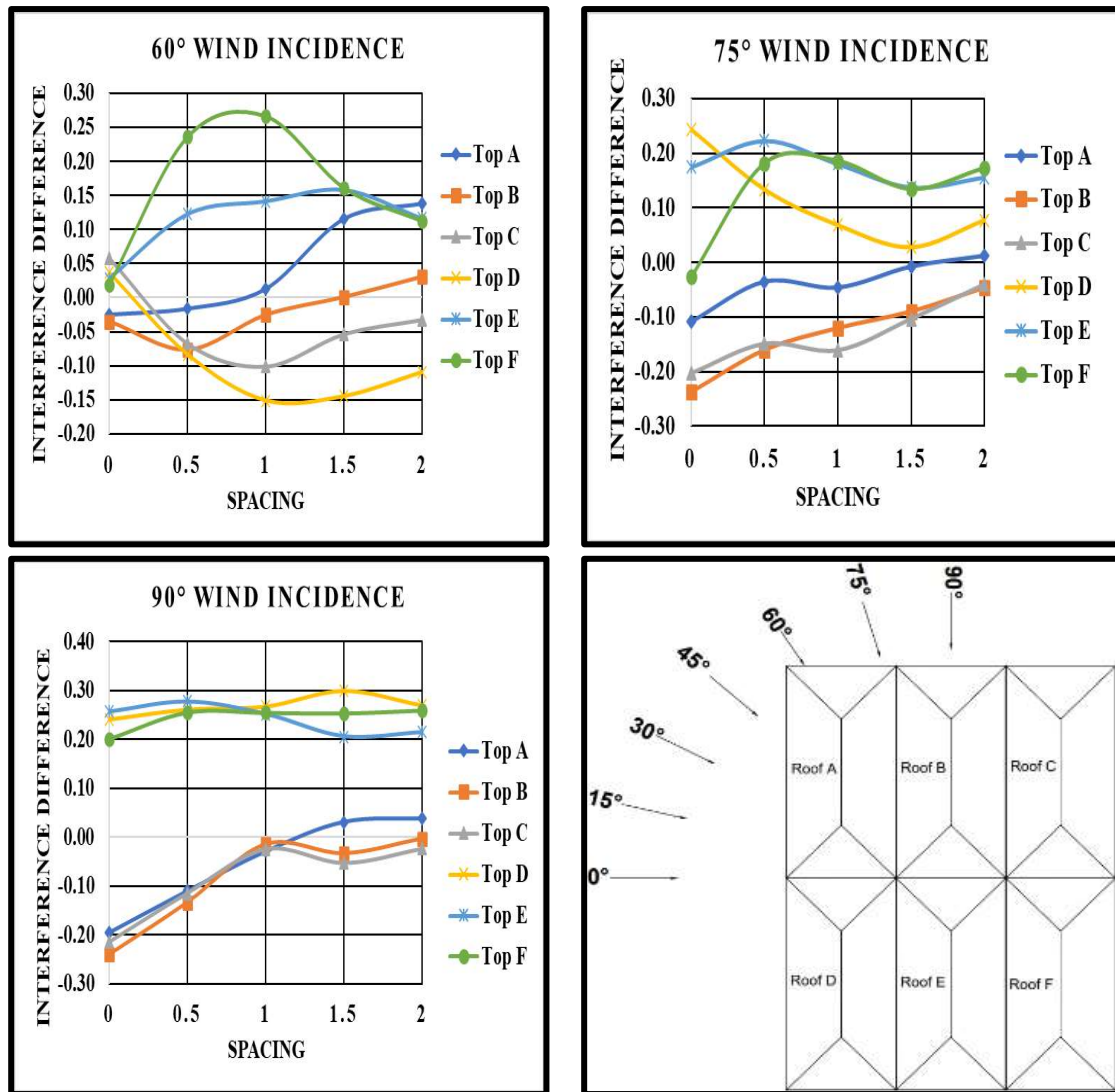
Fig. 7.17(b): Interference Difference for Rectangular Patter of Hip roof

7.1.3.5 Wind Flow Streamlines

The wind flow streamlines for low-rise buildings with 30° hip roofs arranged in rectangular patterns with variable spacing are shown in Fig. 7.18 to 7.22 at different angles of wind incidence, i.e., 0°, 45° and 90°. The streamlines are generated for different wind-induced interference conditions by creating a plane at an eave height of the building, i.e., 150 mm. It is clearly seen from Fig. 7.18 that in the case of zero spacing between the buildings, the wind flow is separated from the upstream wall in a uniform pattern and gets recirculated and the merged in downstream direction or in wake region. By increasing the spacing in between the buildings from zero to 0.5B, B, 1.5B and 2B, the wind starts flowing in between the buildings resulting in reduction of flow circulation in wake region. When the spacing is B, 1.5B and 2B, it is observed that the flow is recirculating in between the buildings during 0°, 45° and 180° angles of wind incidence. The spacing between buildings i.e., 0, 0.5B, B, 1.5B and 2B is proved

to beneficial in reducing the vortices due to wind flow pattern. The vortex generation in wake region of the hip roof is lesser than that of the 30° mono-slope roof.
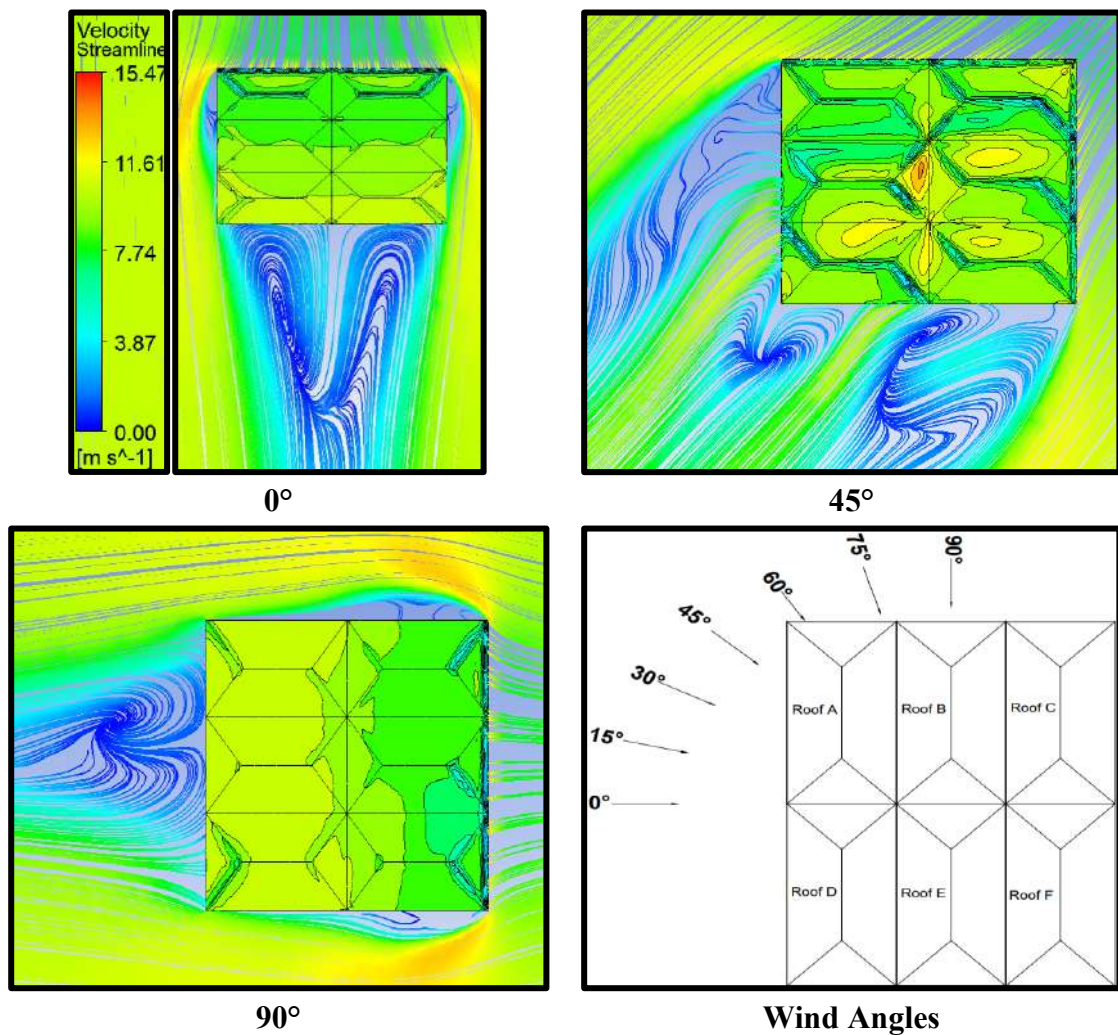
Fig. 7.18: Wind Flow Streamlines for Rectangular Pattern with zero Spacing
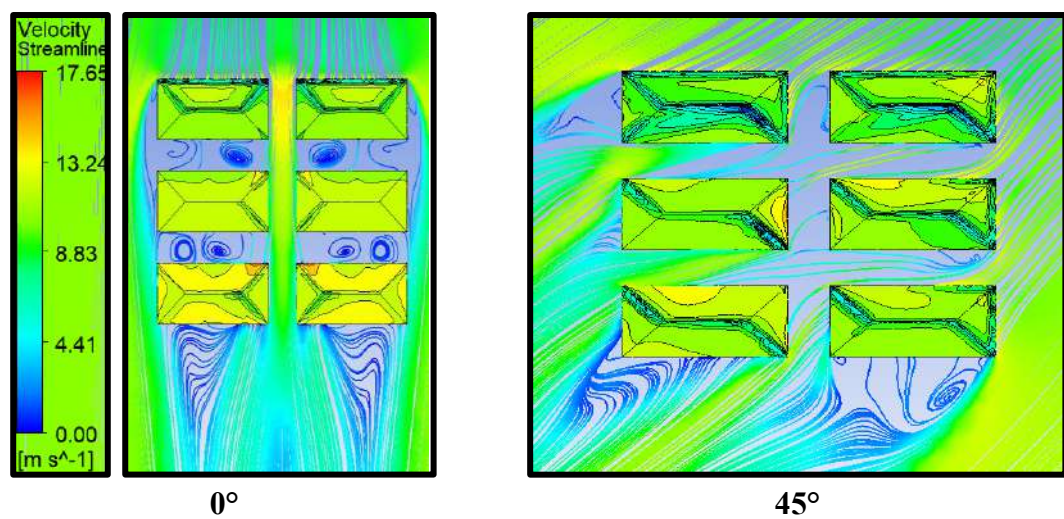
Fig. 7.19(a): Wind Flow Streamlines for Rectangular Pattern with 0.5B Spacing

90°   **Wind Angles**
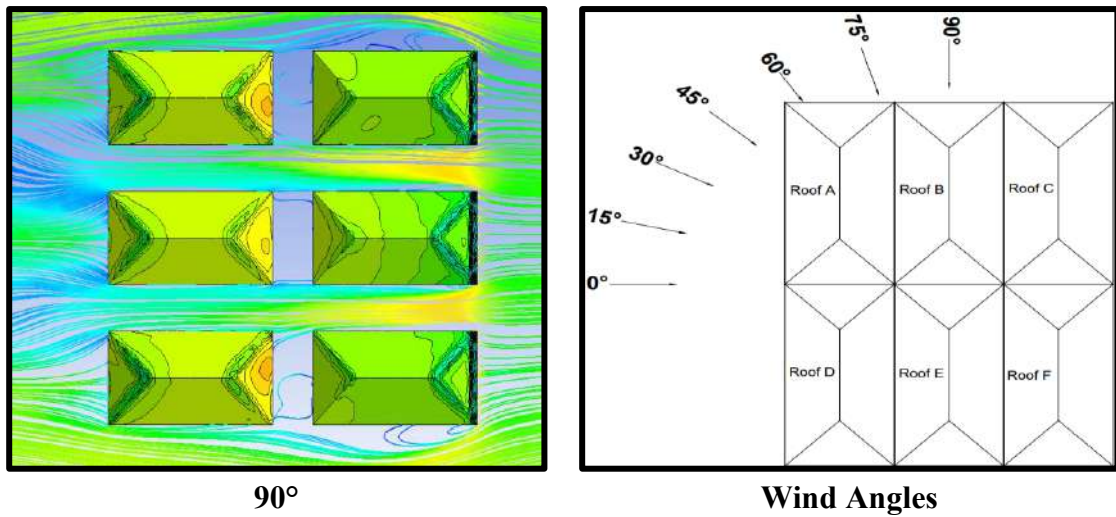
Fig. 7.19(b): Wind Flow Streamlines for Rectangular Pattern with 0.5B Spacing

0°   **45°**

90°   **Wind Angles**
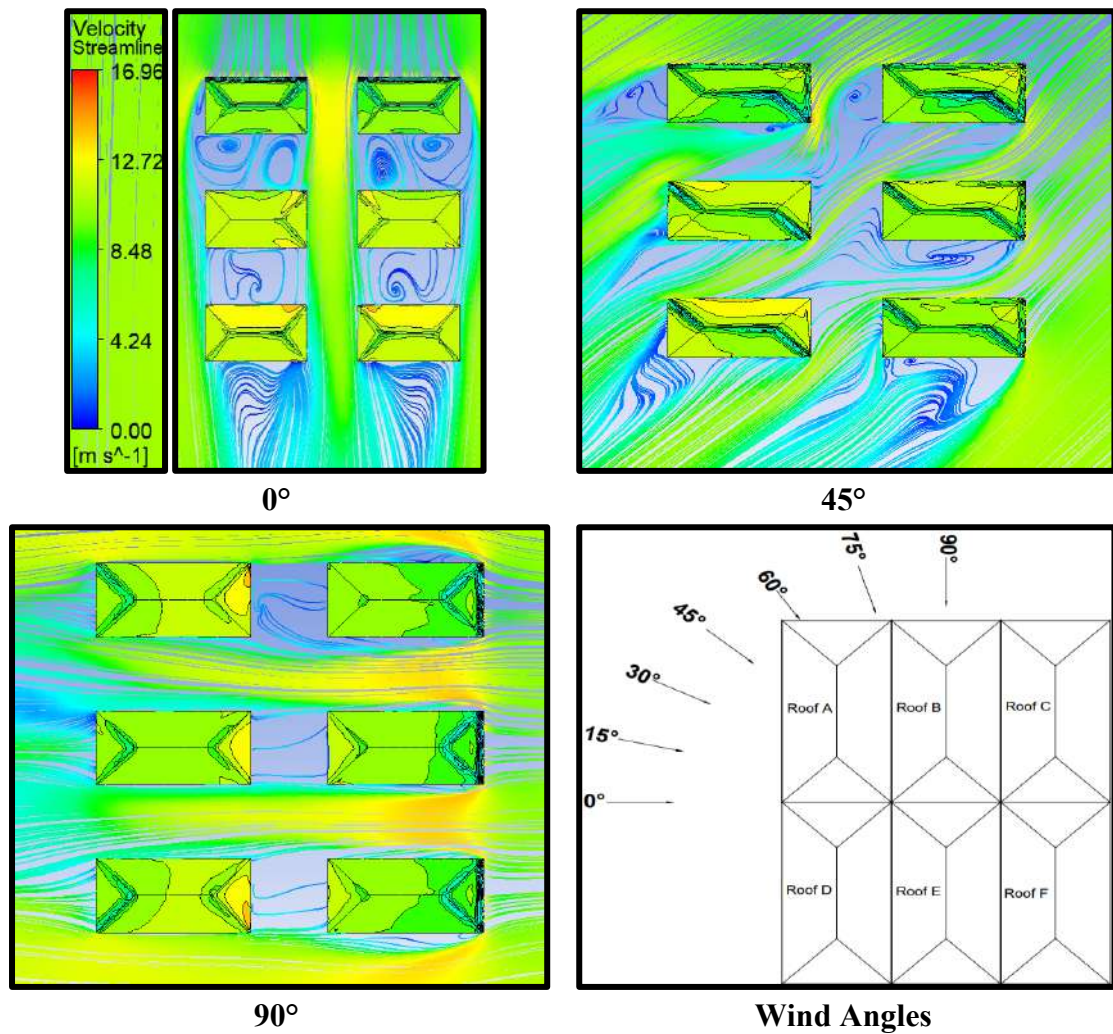
Fig. 7.20: Wind Flow Streamlines for Rectangular Pattern with B Spacing

0°

45°

90°

Wind Angles
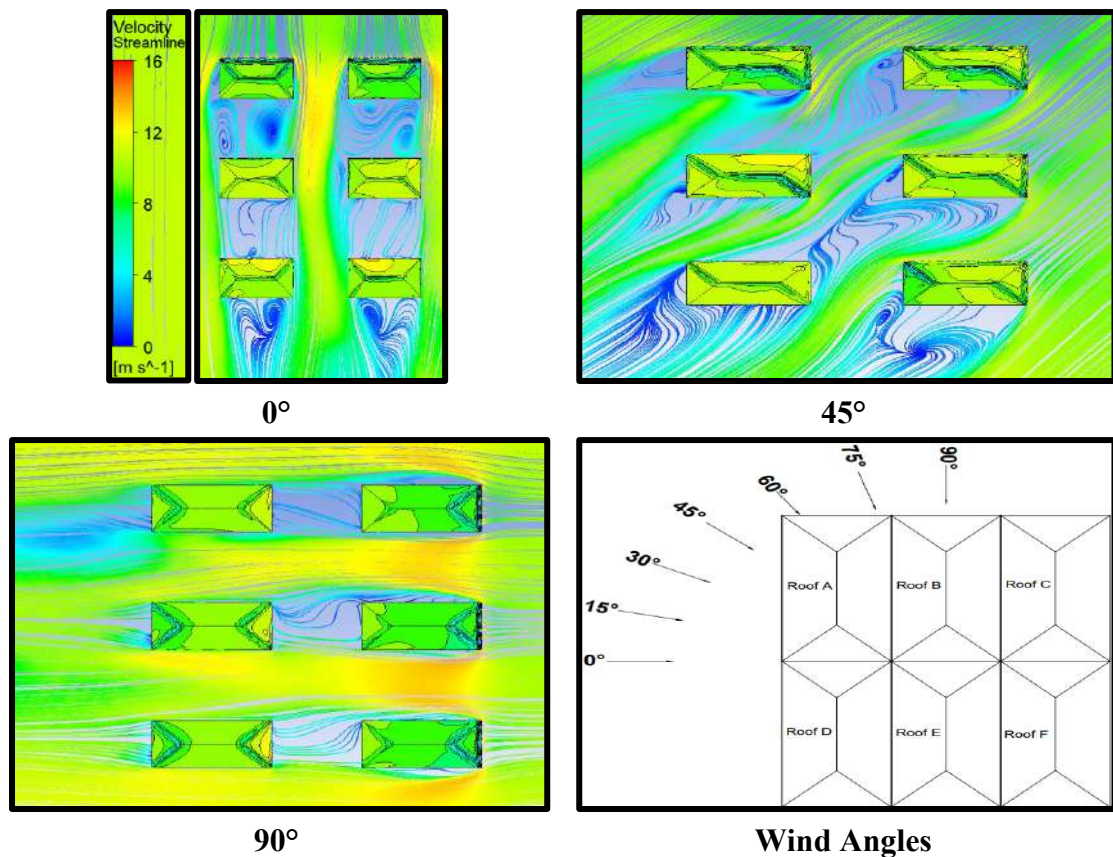
Fig.7.21: Wind Flow Streamlines for Rectangular Pattern with 1.5B Spacing

0°

45°

90°

Wind Angles
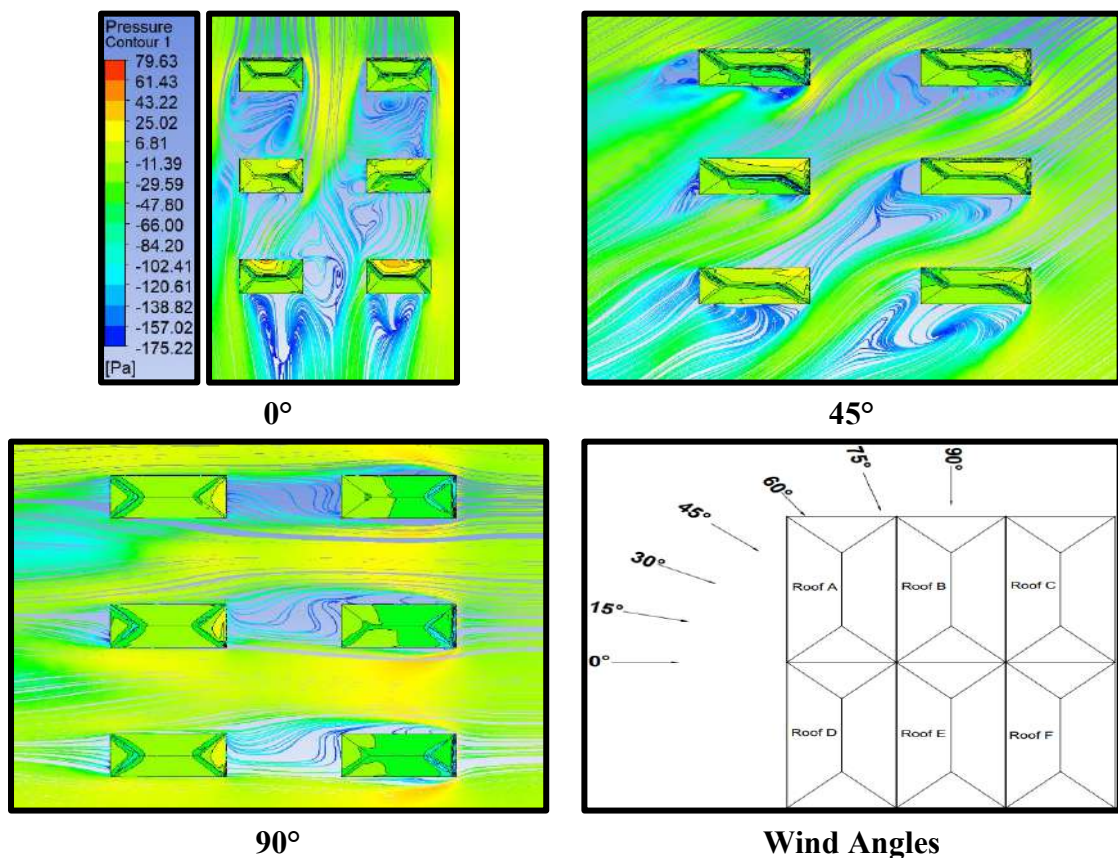
Fig. 7.22: Wind Flow Streamlines for Rectangular Pattern with 2B Spacing

7.3.2 Z Pattern

Similarly to the rectangular pattern, the 30° hip roofs are now arranged in Z pattern of different interfering conditions with variable spacing of 0, 0.5B, B, 1.5B and 2B at different angles of wind attack i.e., 0° to 180° at 15° each interval to find out the wind effects on the roof, discussed below. The Z pattern with 30° hip roof and wind angles are shown in Fig. 7.23.

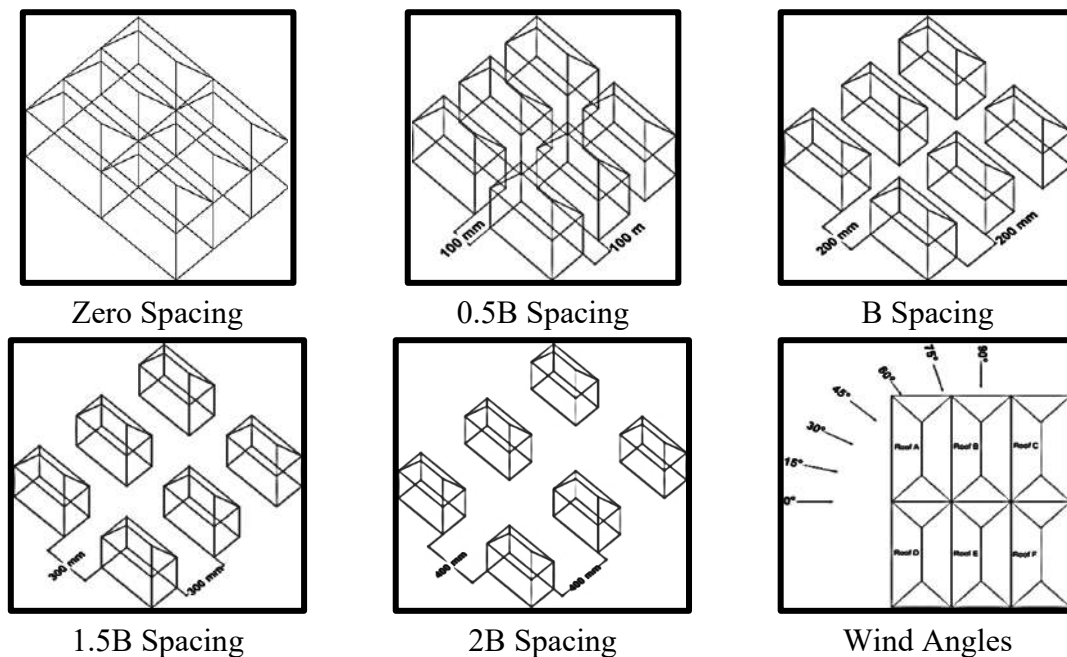|		
Zero Spacing	0.5B Spacing	B Spacing
1.5B Spacing	2B Spacing	Wind Angles
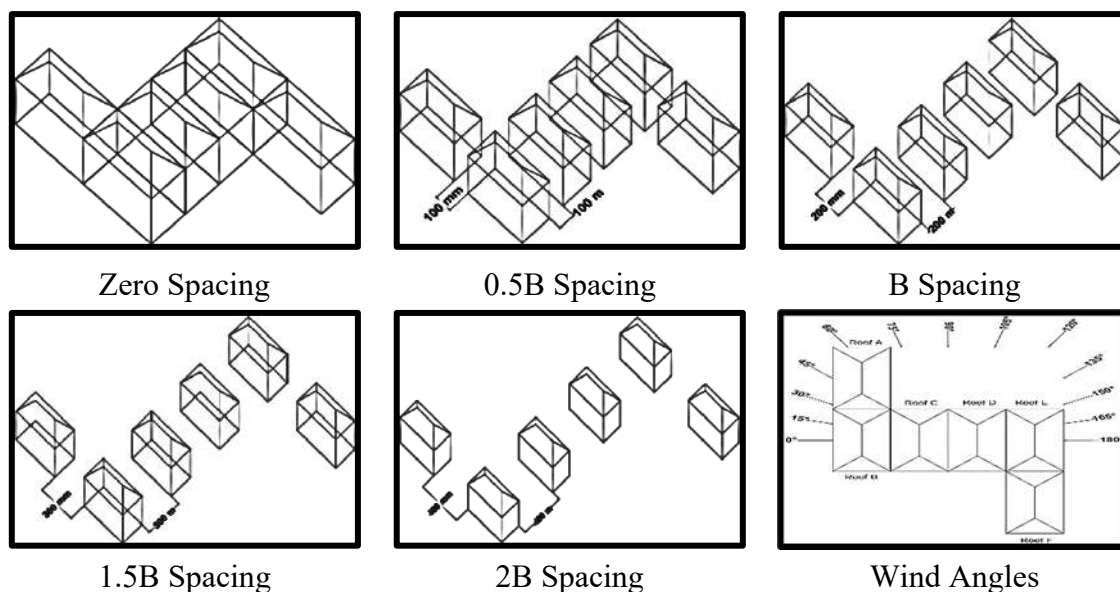
Fig. 7.23: Z Pattern and Wind Angles of 30° Mono-Slope Roof

7.3.2.1 Pressure Contours

The wind-induced pressure contours on the 30° hip roof of low-rise structures are investigated by arranging the low-rise building models in a Z pattern with variable spacing (0, 0.5B, B, 1.5B and 2B) using CFD simulation are discussed here in this section. The pressure contours, roof nomenclature and angles of wind incidences for all the spacing configurations are shown in Figs. 7.24-7.28. It is clearly visible from Figs. 7.24-7.28, that the 30° hip roof is under positive and negative wind-induced pressure distribution during all the wind attacks, i.e., ranging between 0° to 180° at 15° intervals. Spacing between the hip roof from, i.e., 0, 0.5B, B, 1.5B and 2B is beneficial in reducing the pressure distribution on the roofs as shown in Fig. 7.24-7.28, respectively. It is also noticed that the upstream edges and roof ridge line of the 30° hip roofs are under higher negative pressure as compared to the other portions of the roofs. The stability of hip-roof is more in case of interfering conditions than that of the dome, cylindrical and mono-slope roofs. The maximum change in wind pressure distribution i.e., conversion of negative pressure into positive pressure on the roof is noticed during 0.5B and B spacing between the buildings as shown in Figs. 7.25 & 7.26 respectively.

0°

15°

30°

45°

60°

75°

90°

105°

120°

135°

150°

165°

180°
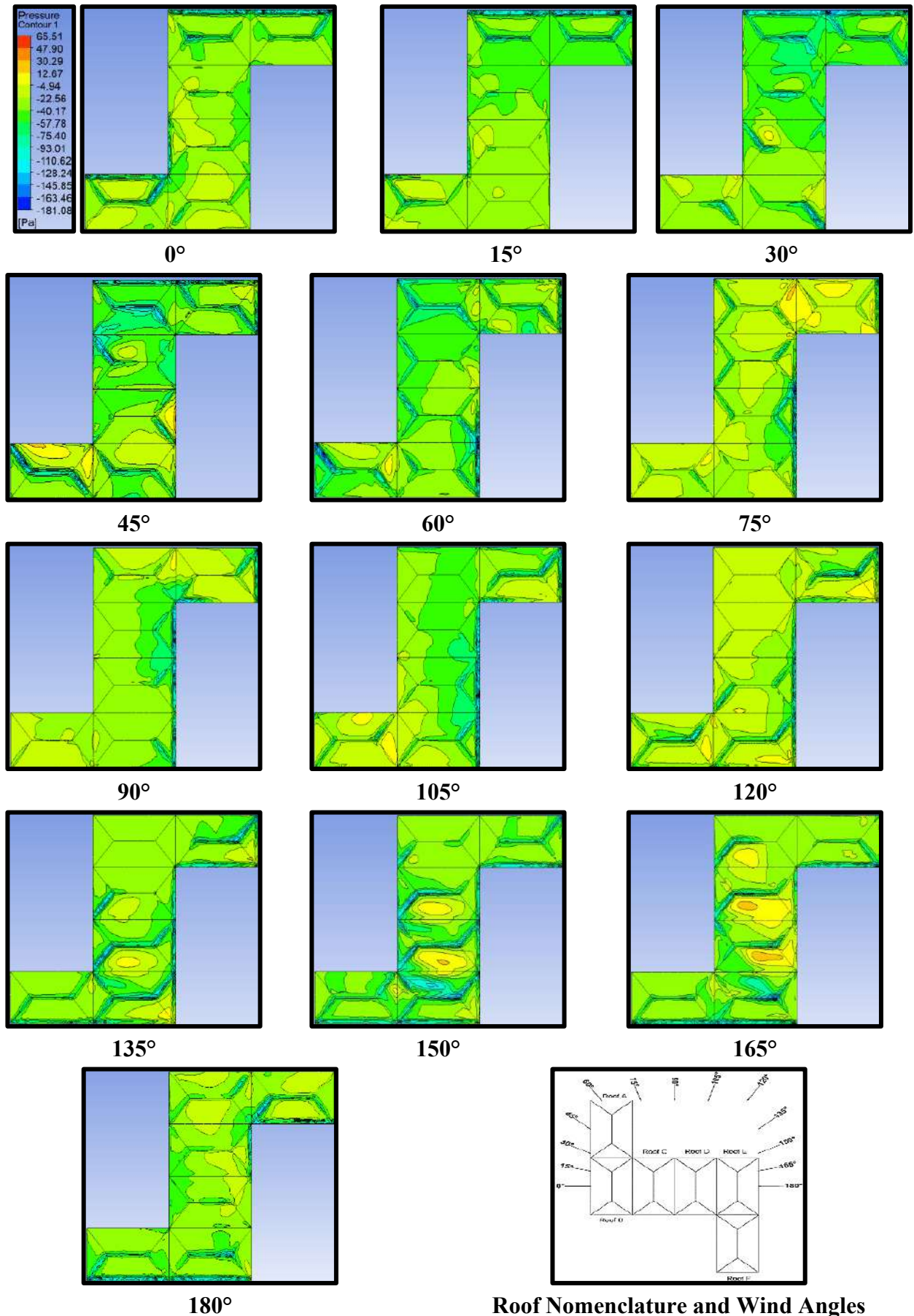
Roof Nomenclature and Wind Angles

Fig. 7.24: Pressure Contours for Z pattern with Zero Spacing

0° **15°** **30°**

45° **60°** **75°**

90° **105°** **120°**

135° **150°** **165°**
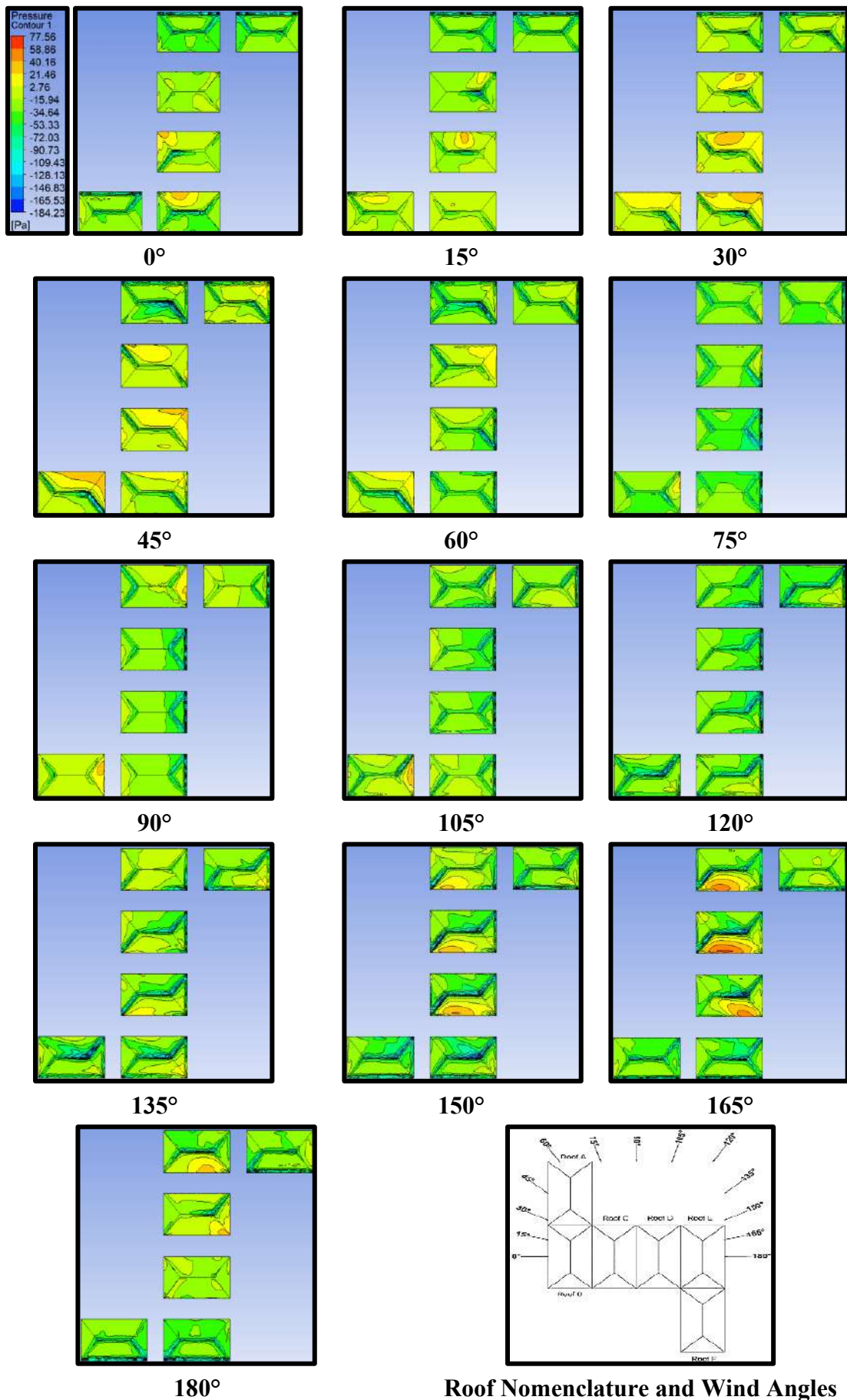
180° **Roof Nomenclature and Wind Angles**

Fig. 7.25: Pressure Contours for Z pattern with 0.5B Spacing

0° **15°** **30°**

45° **60°** **75°**

90° **105°** **120°**

135° **150°** **165°**
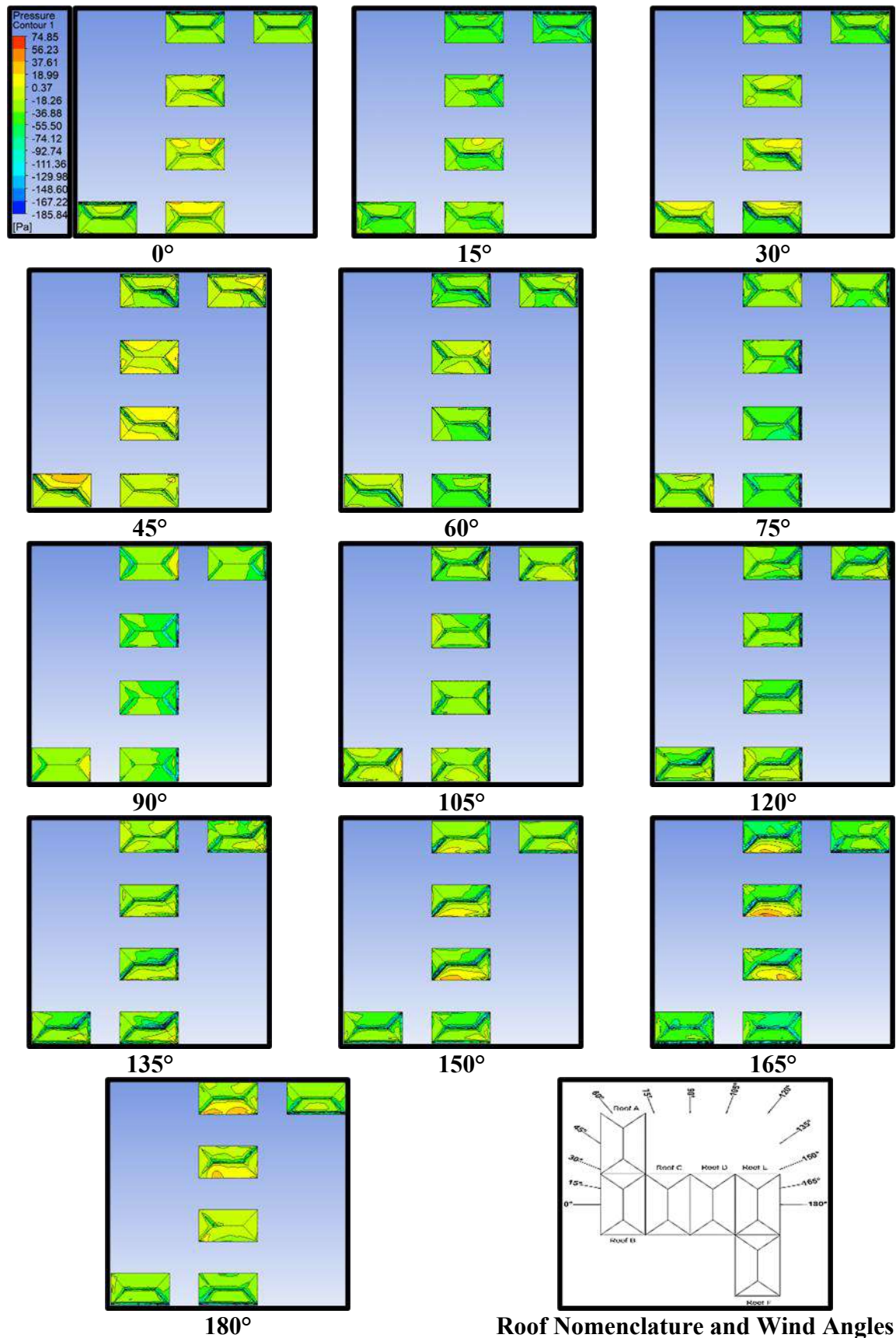
180° **Roof Nomenclature and Wind Angles**

Fig. 7.26: Pressure Contours for Z pattern with B Spacing
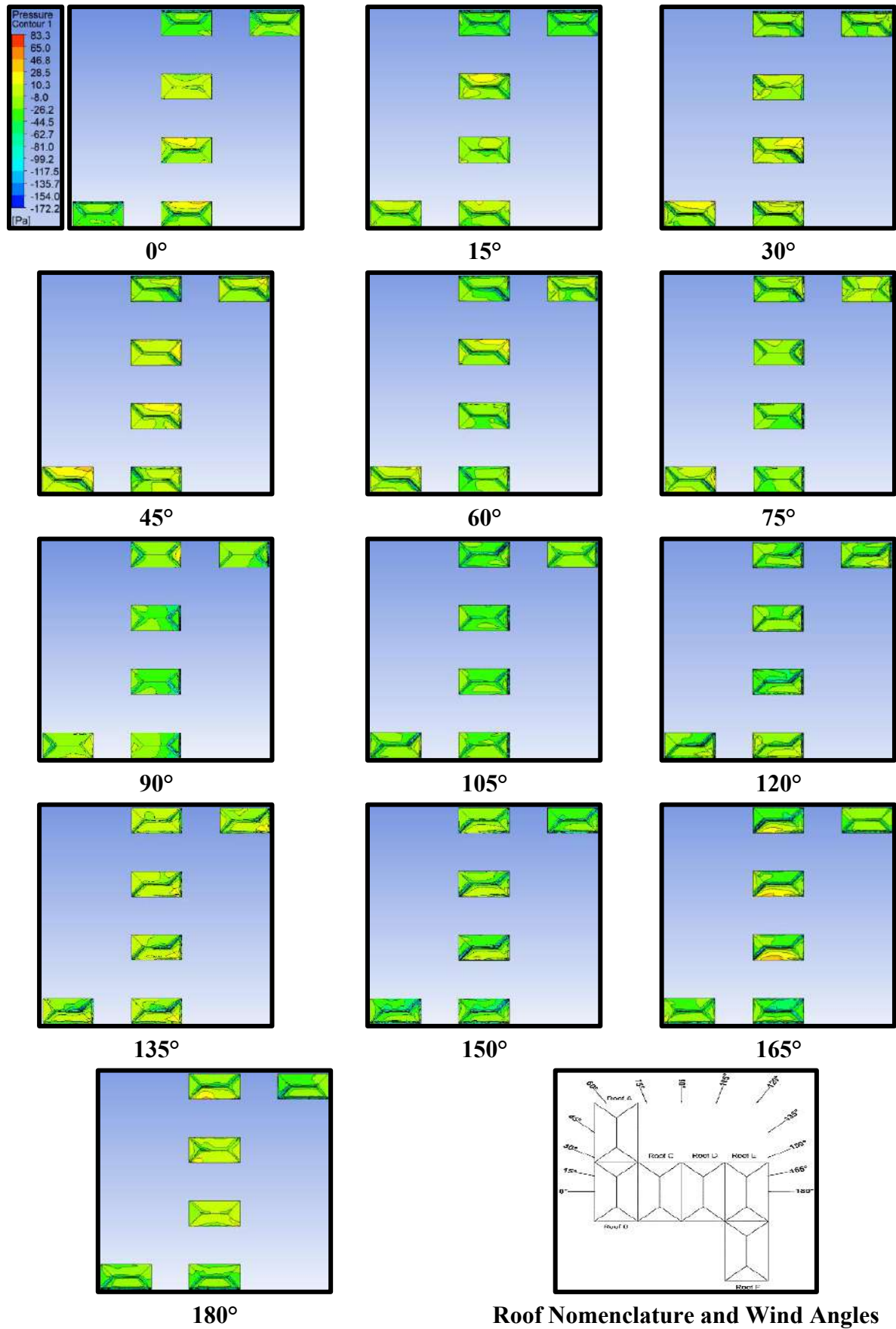
0°　　　　　**15°**　　　　　**30°**

45°　　　　　**60°**　　　　　**75°**

90°　　　　　**105°**　　　　　**120°**

135°　　　　　**150°**　　　　　**165°**

180°　　　　　**Roof Nomenclature and Wind Angles**

Fig. 7.27: Pressure Contours for Z pattern with 1.5B Spacing

0°   **15°**   **30°**

45°   **60°**   **75°**

90°   **105°**   **120°**

135°   **150°**   **165°**
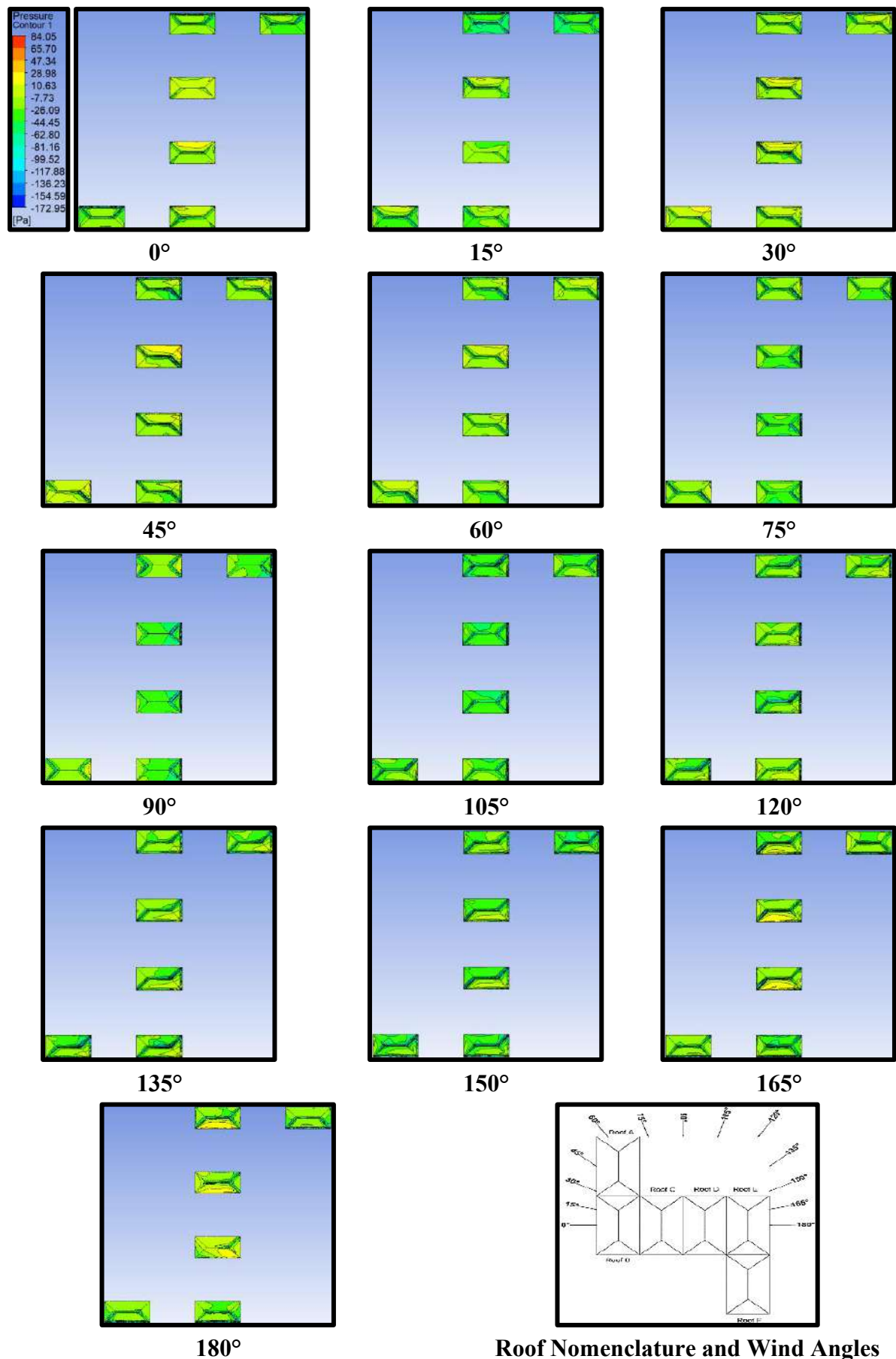
180°   **Roof Nomenclature and Wind Angles**

Fig. 7.28: Pressure Contours for Z pattern with 2B Spacing

7.3.2.2 Pressure Coefficient (C_{pe})

The variation of C_{pe} on the 30° hip roofs of six low-rise buildings arranged in z pattern with variable spacing of zero, 0.5B, B, 1.5B and 2B at different angles of wind interval ranging between 0° to 180° having an interval of 15° each, is shown in Fig. 7.29. At each interval of wind incidence, it is observed that the overall value of C_{pe} is negative in magnitude on all the 30° hip roofs in the case of different spacings between the buildings. The range of C_{pe} on roof A is -0.8 to -0.32 indicating that there is only suction on the roof in which the maximum suction is occurring during 135° angle of wind incidence with 0.5B spacing between the buildings, while the minimum suction on roof A is observed during 60° wind incidence with zero spacing between the buildings. The maximum and minimum suction on roof B is observed when the value of C_{pe} is -0.86 at 45° wind angle with 0.5B spacing and -0.26 at 90° wind angle with 1.5B spacing. The maximum value of negative C_{pe} on roofs C is -0.78 at 135° angle of wind attack when the spacing between buildings is 0.5B, while the minimum negative value of C_{pe} is -0.01, which is almost negligible or zero at 0° wind incidence angle and 2B spacing. The range of C_{pe} for roof D is -0.84 to -0.12, in which the maximum suction is observed during a 120° angle of wind incidence and zero spacing and minimum suction occurs during 0° wind angle and 2B spacing. The roofs E and F are under maximum suction with C_{pe} = -0.86 at 150° wind incidence angle and 0.5B spacing while minimum C_{pe} = -0.22 is for roof E at 0° wind incidence and B spacing and -0.13 is for roof F at 90° wind angle and 0.5B spacing.
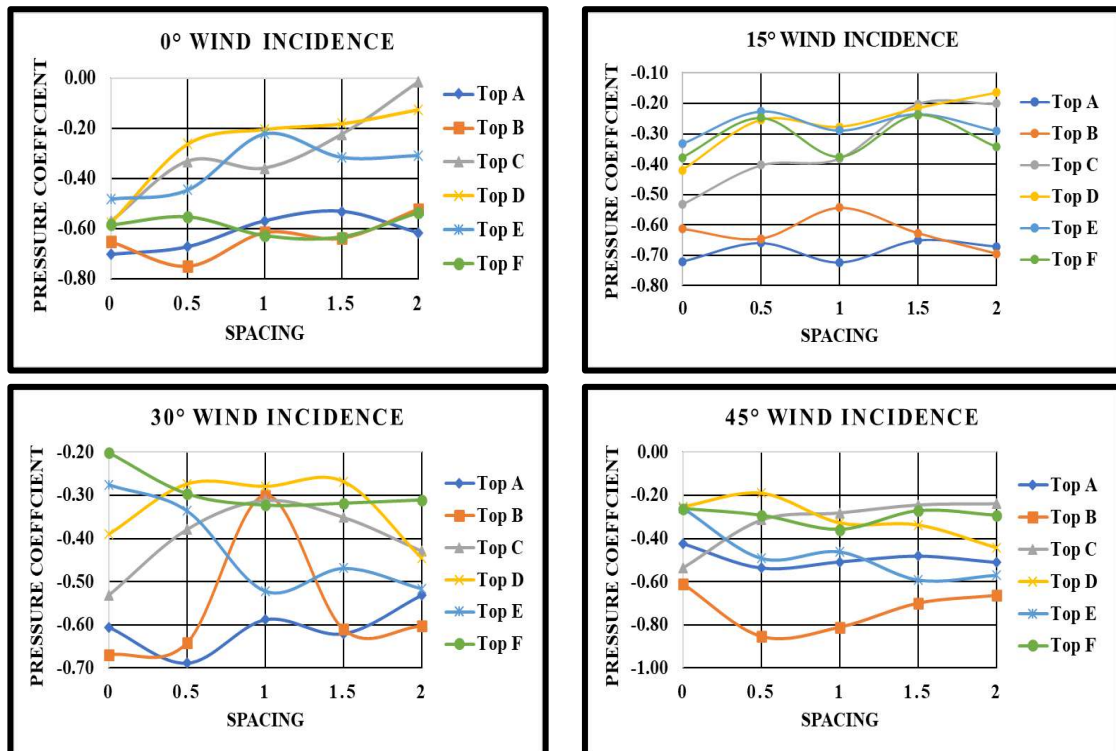
Fig. 7.29(a): Pressure Coefficient for Z pattern of 30° Hip Roof

60° WIND INCIDENCE

75° WIND INCIDENCE

90° WIND INCIDENCE

105° WIND INCIDENCE

120° WIND INCIDENCE

135° WIND INCIDENCE

150° WIND INCIDENCE

165° WIND INCIDENCE
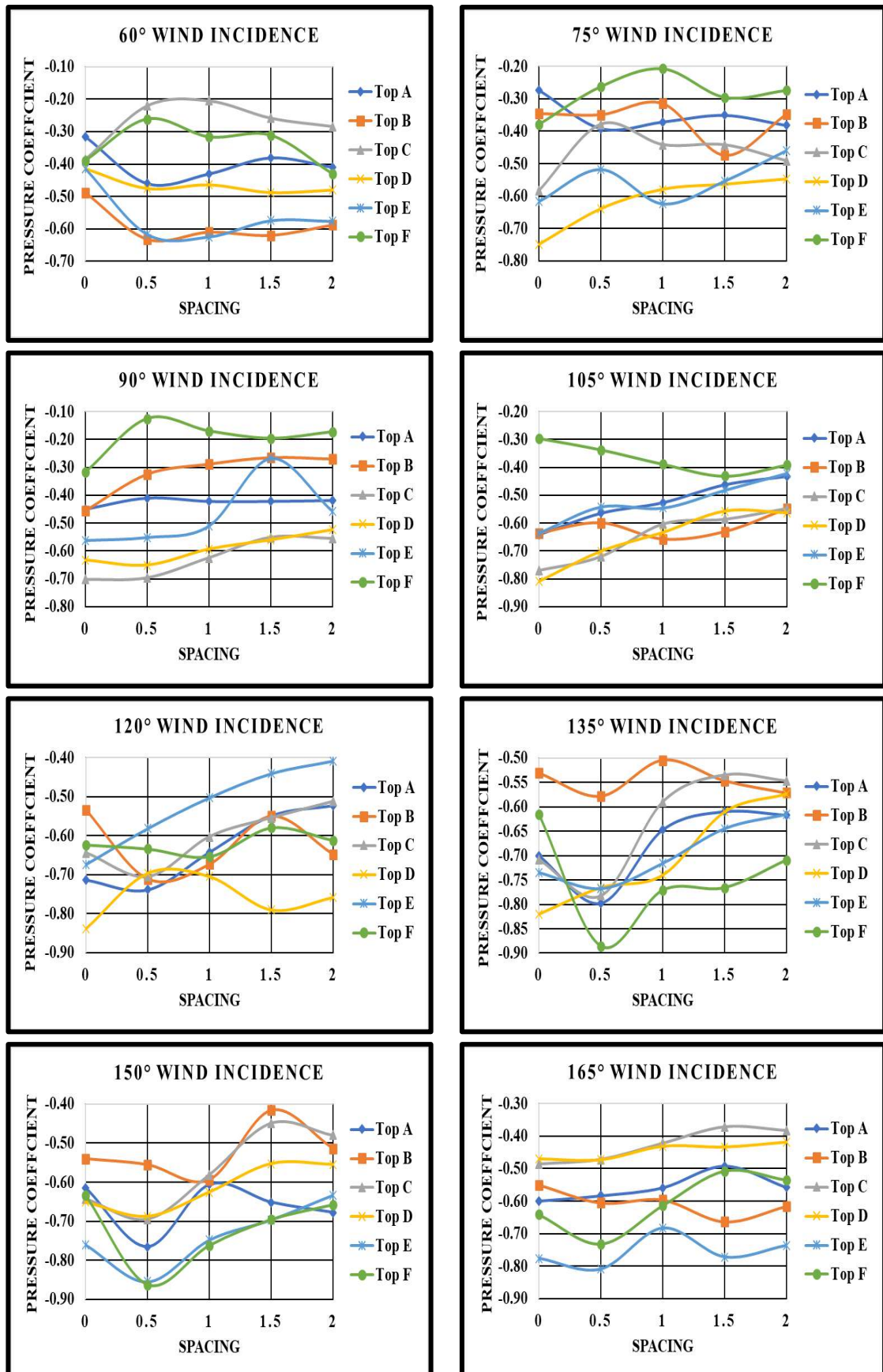
Fig. 7.29(b): Pressure Coefficient for Z pattern of 30° Hip Roof
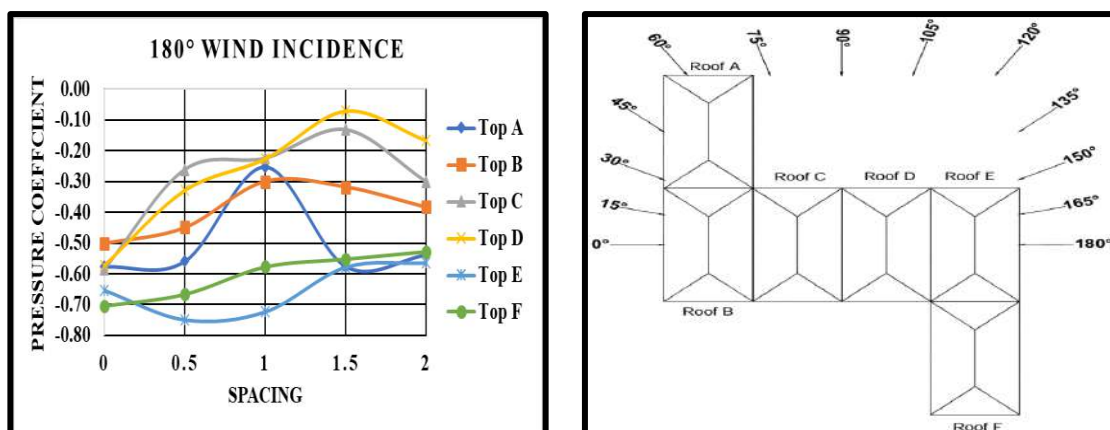
Fig. 7.29(c): Pressure Coefficient for Z pattern of 30° Hip Roof

7.3.2.3 Interference Factor (IF)

The idea of enhancement or reduction of suction or pressure on the roof is given by interference factor (*IF*) due to the presence of low-rise structure in the vicinity. The value of If gets modified with respect to the spacing between the buildings and angles of wind attack. The varying magnitude of *IF* on a 30° hip roof arranged in a z pattern with variable spacing (0,0.5B, B, 1.5B and 2B) at various angles of wind attacks, i.e., 0° to 180° at 15° intervals is shown in Fig. 7.30. The value of *IF* on the roof A keeps on reducing with an increase in spacing from 0 to 2B. Initially, the value of *IF* comes out to be more than 1, indicating the increased suction on roof A but it gets reduced while increasing the spacing till 2B at which *IF* becomes less than 1 indicating the reduced suction on roof A. Similarly to the *IF* of roof A, the value of *IF* for roof B follows the same trend in which its value comes out to be more than 1 when the angles of wind attack are 0°, 15°, 30°, 45°, 60°, 105°, 120° and 165° respectively and starts reducing when spacing between the building in increased from 0 to 2B. Also, the maximum reduction in *IF*, i.e., reduced suction on roof B, is observed at 1.5B spacing at all the wind incidence angles, i.e., 0° to 180° at 15° intervals, as shown in Fig. 7.30. A drastic reduction in the value of *IF* for roof C is observed at 0°, 15°, 30°, 45°, 60°, 75° and 165° angles of wind incidence when the spacing is changed from 0 to 2B, during which *IF* changed from more than 1 to less than 1, indicating the reduced suction on roof C. But, on the rest of the wind incidence angles, the value of *IF* already comes out to be more than 1 and not much changed with respect to the spacing. The variation of IF on roof D follows the same pattern as that of roof B when wind incidence angles are 0°, 15°, 30°, 75°, 60° and 165°, at which the maximum reduction of *IF* takes place when the spacing is 1.5B between the buildings. The value of *IF* for roof E is less than 1 only in cases when the angle of wind incidence is 0°, 15°, 30° and 45°, indicating the reduced suction on roof E due to interference. The reduction in the value of *IF* for roof F with

respect to the spacing is observed when the angle of wind incidence ranges between 15° to 105°, respectively, as shown in Fig. 7.30. The variation of spacing between the buildings is proved to be beneficial which helps in reducing the suction on the roof and greatly influences the nature of wind on roofs. The angle of wind incidence also plays a vital role in changing the magnitude of *IF* on the roof or low-rise structure with a hip roof.

Fig. 7.30(a): Interference Factor for Z Pattern of 30° Hip Roof

Fig. 7.30(b): Interference Factor for Z Pattern of 30° Hip Roof

7.3.2.4 Interference Difference (ID)

The difference between C_{pe} obtained during an interfering condition and C_{pe} obtained during an isolated condition is called as interference difference (*ID*), which gives an exact idea of enhancement or reduction in the wind-induced positive or negative pressure coefficient on the roofs. The variation of *ID* on 30° hip roofs arranged in a z pattern with different spacing ranging between 0 to 2B (where B is the width of a low-rise building) and at various angles of wind incidences ranging between 0° to 180° at 15° intervals is shown in Fig. 7.31. When the magnitude of negative C_{pe} on the roof is increased during interfering conditions, then the value of *ID* comes out to be negative, indicating the increased suction on the roof during interfering conditions, while the value of *ID* is positive, but the magnitude of C_{pe} is still negative on the roofs indicates that the suction on the roof is reduced due to interference of vicinity buildings. This variation of *ID* on 30° hip roof arranged in z pattern with variable spacing with respect to different angles of wind incidences is shown in Fig. 7.31 below.

Fig. 7.31(a): Interference Difference for Z Pattern of 30° Hip Roof

Fig. 7.31(b): Interference Difference for Z Pattern of 30° Hip Roof
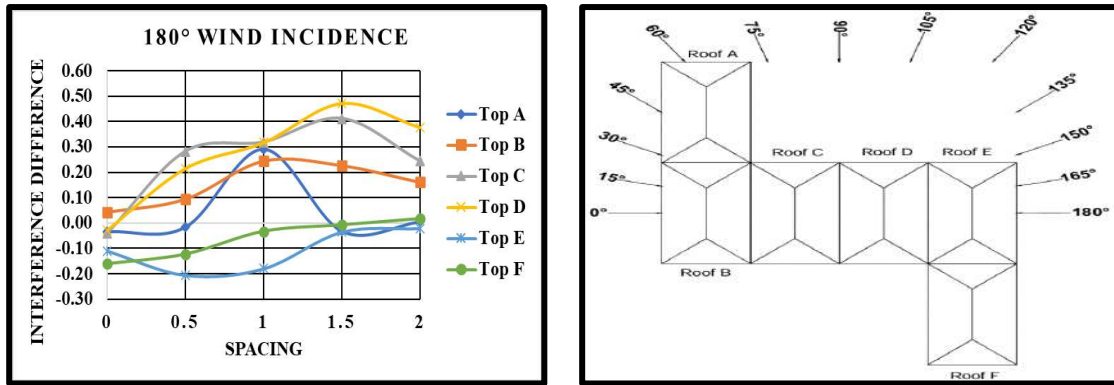
Fig. 7.31(c): Interference Difference for Z Pattern of 30° Hip Roof

7.3.2.5 Wind Flow Streamlines

The wind flow streamlines show how the wind flows around the buildings and is responsible for wind actions on the building walls and roofs. The streamlines for a z-pattern of low-rise buildings with 30° mono-slope roofs at 15° wind intervals are shown in Figs. 7.32 – 7.36. The streamlines for 30° hip roofs are obtained at the eave height (150 mm) of the low-rise structures to analyse the wind effects on the roofs. When the wind strikes the wall and roof surface of the structures, it gets separated from the windward or upstream side, which is responsible for the generation of eddies around the building, after which the flow recirculation and reattachment take place in the wake region of the building or downstream side. In the case of zero spacing, the eddies formation occurs on all sides of the building model other than the windward side. The building model with zero spacing behaves like a single building with multi-spans of 30° hip roofs. The length of the wake region in the downstream direction depends upon the angle of the wind attack and the pattern of the arrangement of the building, in which it is clearly predictable that the length of the wake region is lesser in the case of a rectangular pattern as compared to z pattern. The turbulence in the wind flow pattern is induced in between the buildings when spacing is increased from 0 to 2B, due to which the length of the wake region is reduced as shown in Figs. 7.32-7.36 respectively.

0° 45°

Fig. 7.32(a): Wind Flow Streamlines for Z pattern with Zero Spacing

90°

135°

180°
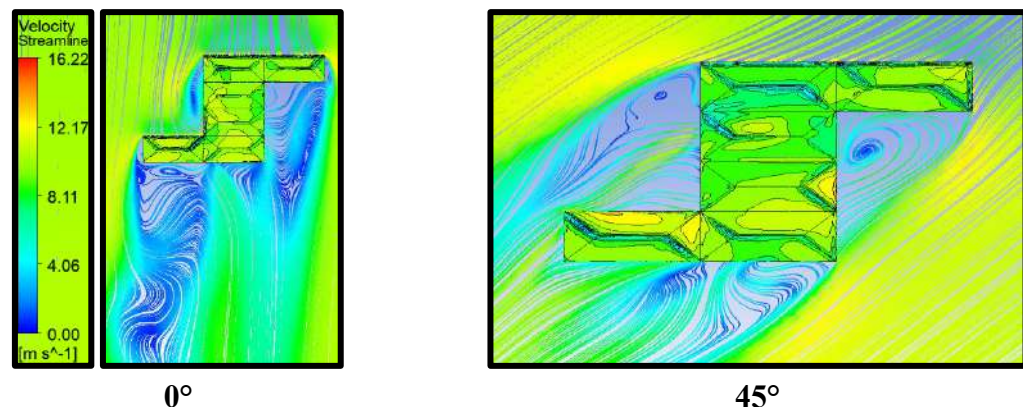
Angles of Wind Incidence

Fig. 7.32(b): Wind Flow Streamlines for Z pattern with Zero Spacing

0°

45°

90°

135°
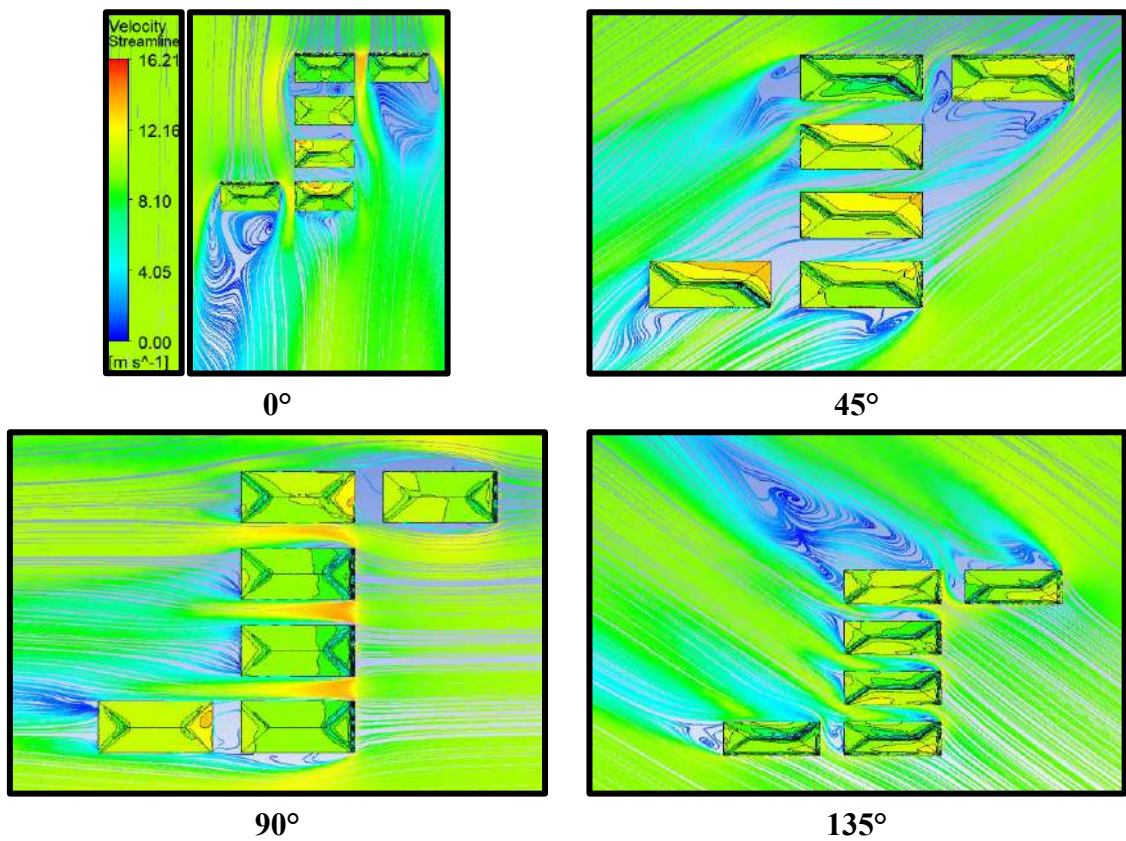
Fig. 7.33(a): Wind Flow Streamlines for Z pattern with 0.5B Spacing

180°
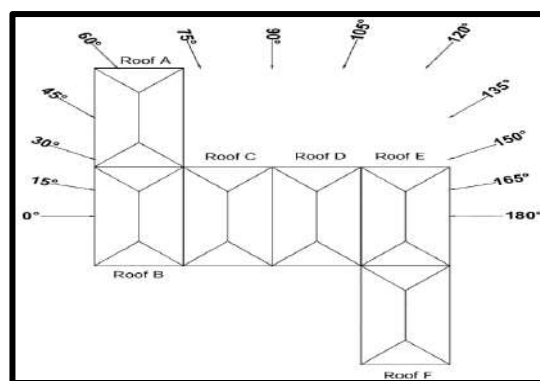
Angles of Wind Incidence

Fig. 7.33(b): Wind Flow Streamlines for Z pattern with 0.5B Spacing

0°

45°

90°

135°

180°
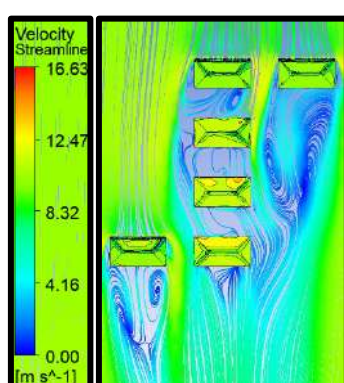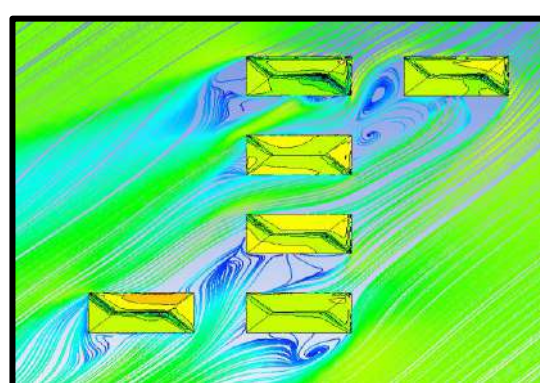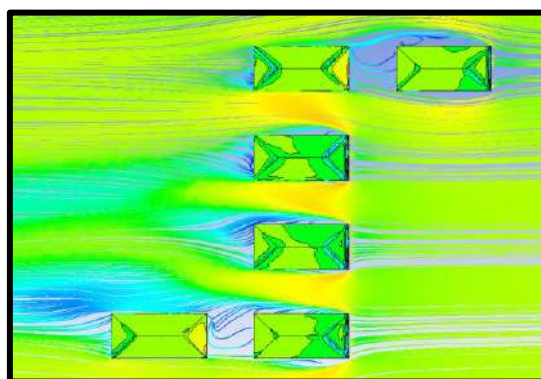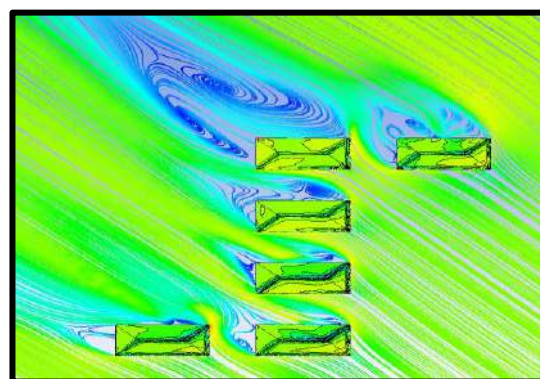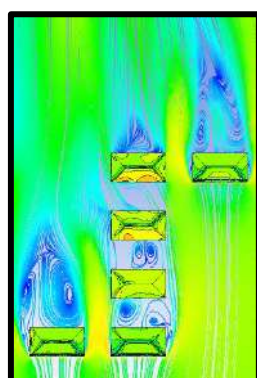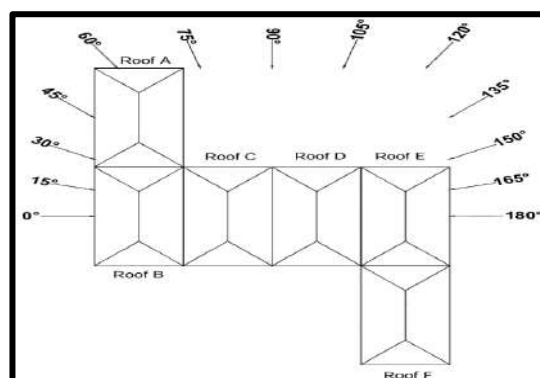
Angles of Wind Incidence

Fig. 7.34: Wind Flow Streamlines for Z pattern with B Spacing

0°

45°

90°

135°

180°

Angles of Wind Incidence
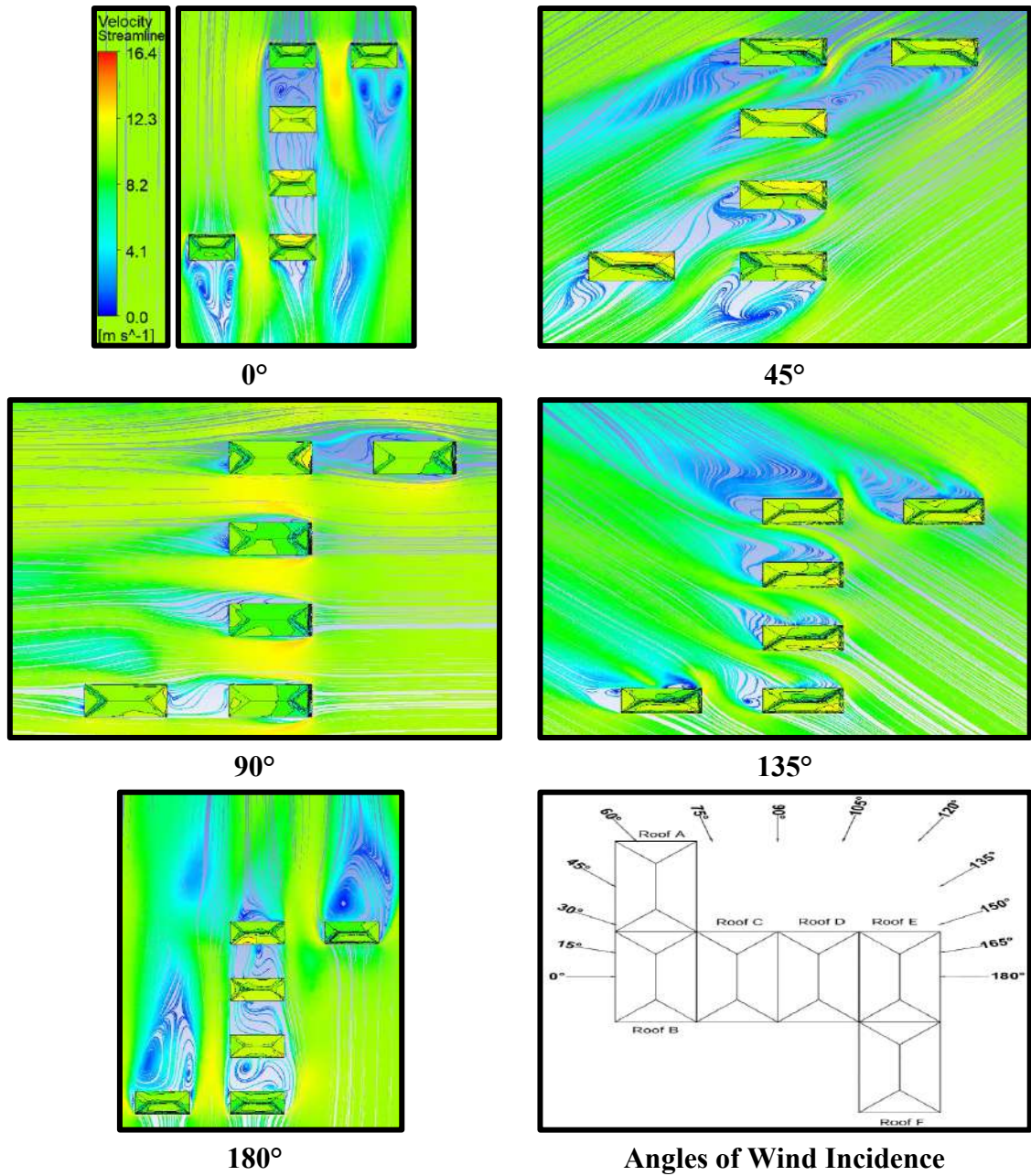
Fig. 7.35: Wind Flow Streamlines for Z pattern with 1.5B Spacing

0°

45°

Fig. 7.36(a): Wind Flow Streamlines for Z pattern with 2B Spacing

90°   **135°**

180°   **Angles of Wind Incidence**
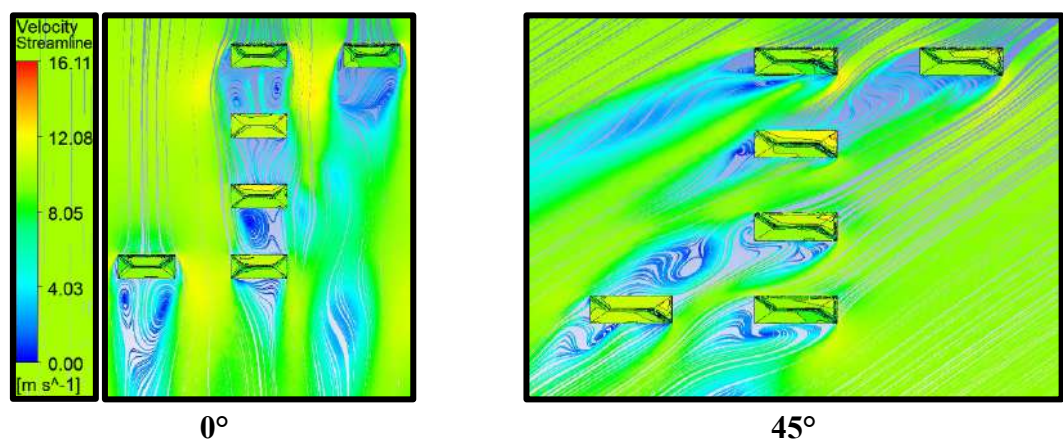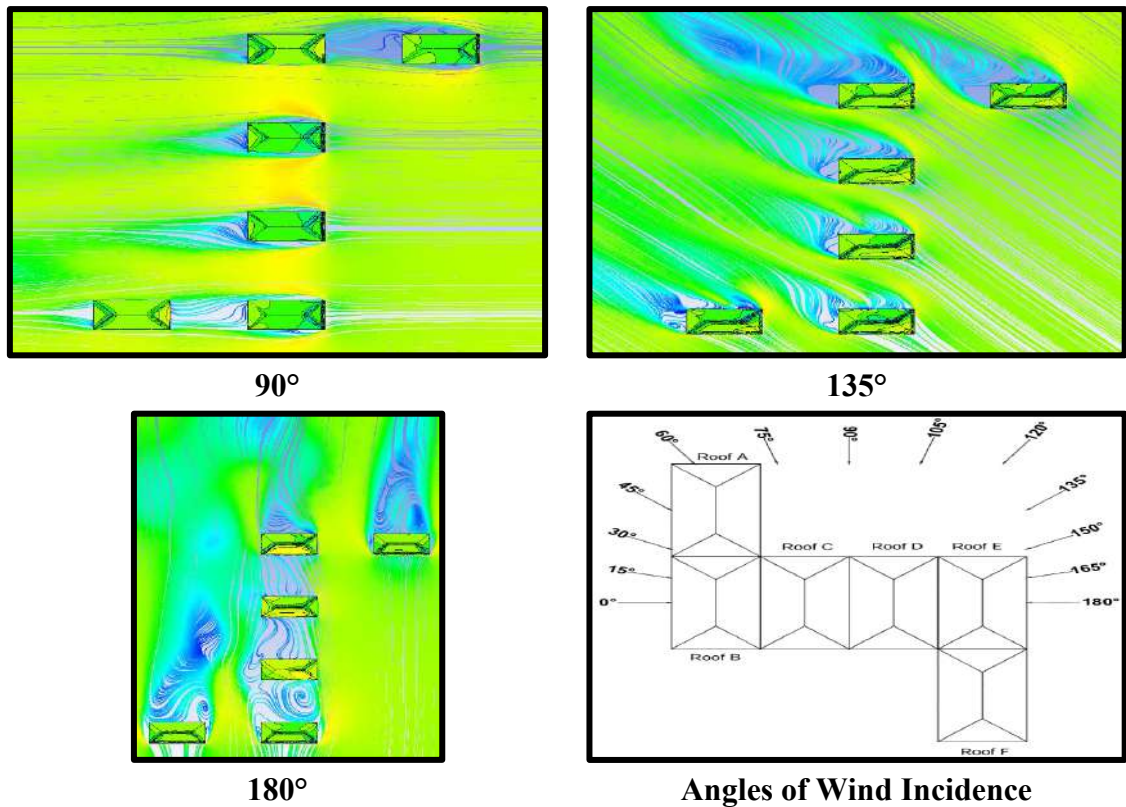
Fig. 7.36(b): Wind Flow Streamlines for Z pattern with 2B Spacing

7.3.3 T Pattern

This section contains a detailed description of the variation of pressure contours, pressure coefficients, *IF* and *ID* over the 30° hip roofs arranged in a T pattern with variable spacing, i.e., 0, 0.5B, B, 1.5B and 2B at different angles of wind incidence such that 0° to 180° at 15° wind interval. The T pattern with 30° hip roof and wind angles are shown in Fig. 7.37.

Zero Spacing   0.5B Spacing   B Spacing

1.5B Spacing   2B Spacing   Wind Angles
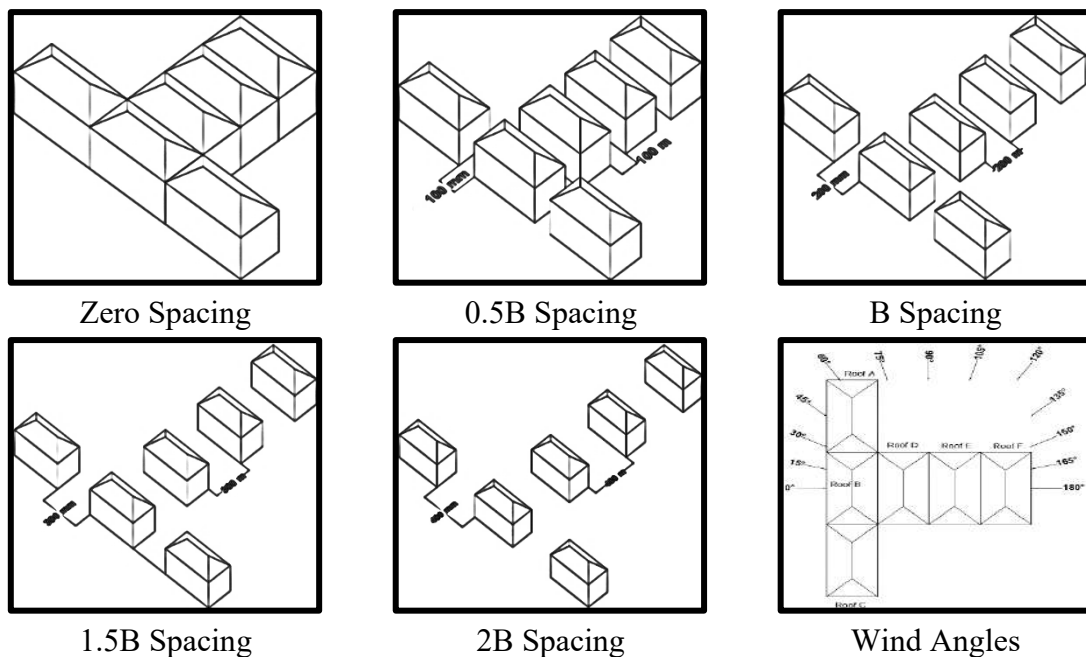
Fig. 7.37: T Pattern and Wind Angles of 30° Mono-Slope Roof

7.3.3.1 Pressure Contours

The wind-induced pressure contours on the 30° hip roof of low-rise structures are investigated by arranging the low-rise building models in a T pattern with variable spacing (0, 0.5B, B, 1.5B and 2B) using CFD simulation are discussed here in this section. The pressure contours, roof nomenclature and angles of wind incidences for all the spacing configurations are shown in Figs. 7.38-7.42. It is clearly visible from Figs. 7.38-7.42, that the 30° hip roof is under negative as well as positive wind induced pressure distribution which make it more stable as compared to dome, cylindrical and mono-slope roofs during all the wind attacks i.e., ranging between 0° to 180° at 15° intervals. Spacing between the hip roof from i.e., 0, 0.5B, B, 1.5B and 2B is beneficial in reducing the pressure distribution on the roofs as shown in Fig. 7.38-7.42 respectively. It is also noticed that the edges (windward, leeward and side edges) and roof ridge line of the 30° hip roofs are under higher negative pressure as compared to the other portion of the roofs. The effects of interference are mostly visible from the roofs which are lying in the single central line of the T-pattern also when the angle of wind attack is 0°, 90° and 180° respectively. The maximum change in wind pressure distribution i.e., conversion of negative pressure into positive pressure on the roof is noticed during 0.5B and B spacing between the buildings as shown in Figs. 7.39 & 7.40 respectively.

Fig. 7.38(a): Pressure Contours for T pattern with Zero Spacing

90°   **105°**   **120°**

135°   **150°**   **165°**

180°   **Roof Nomenclature and Wind Angles**
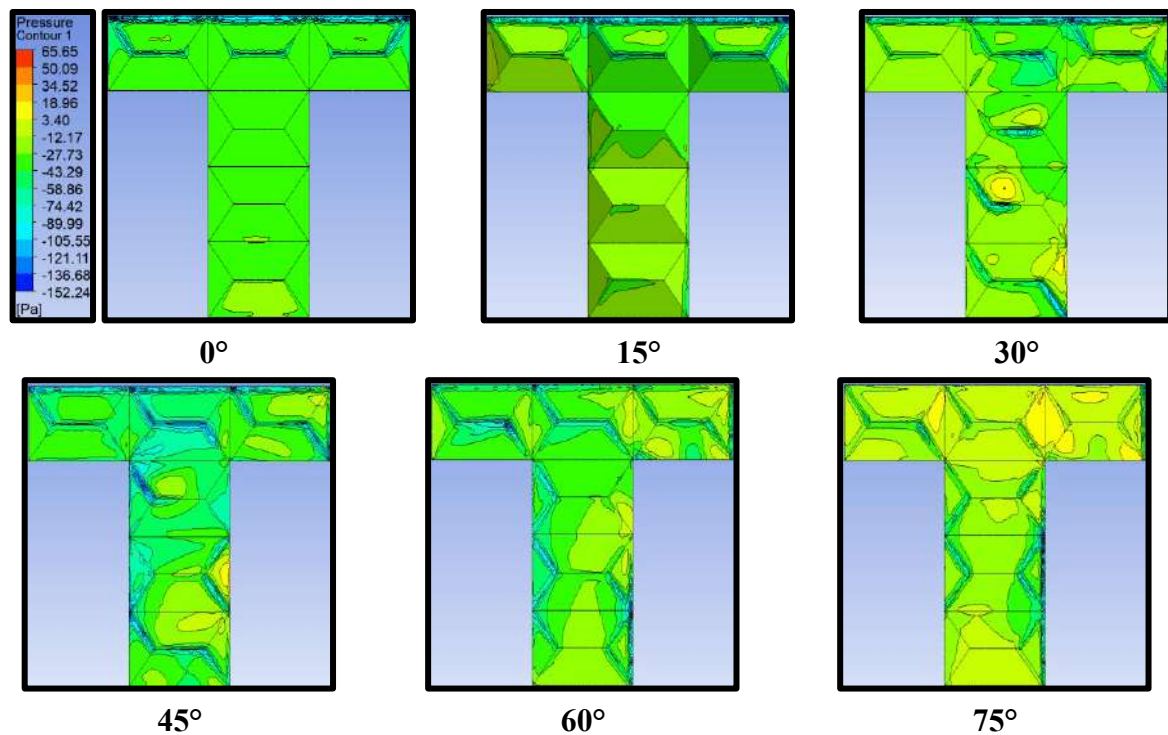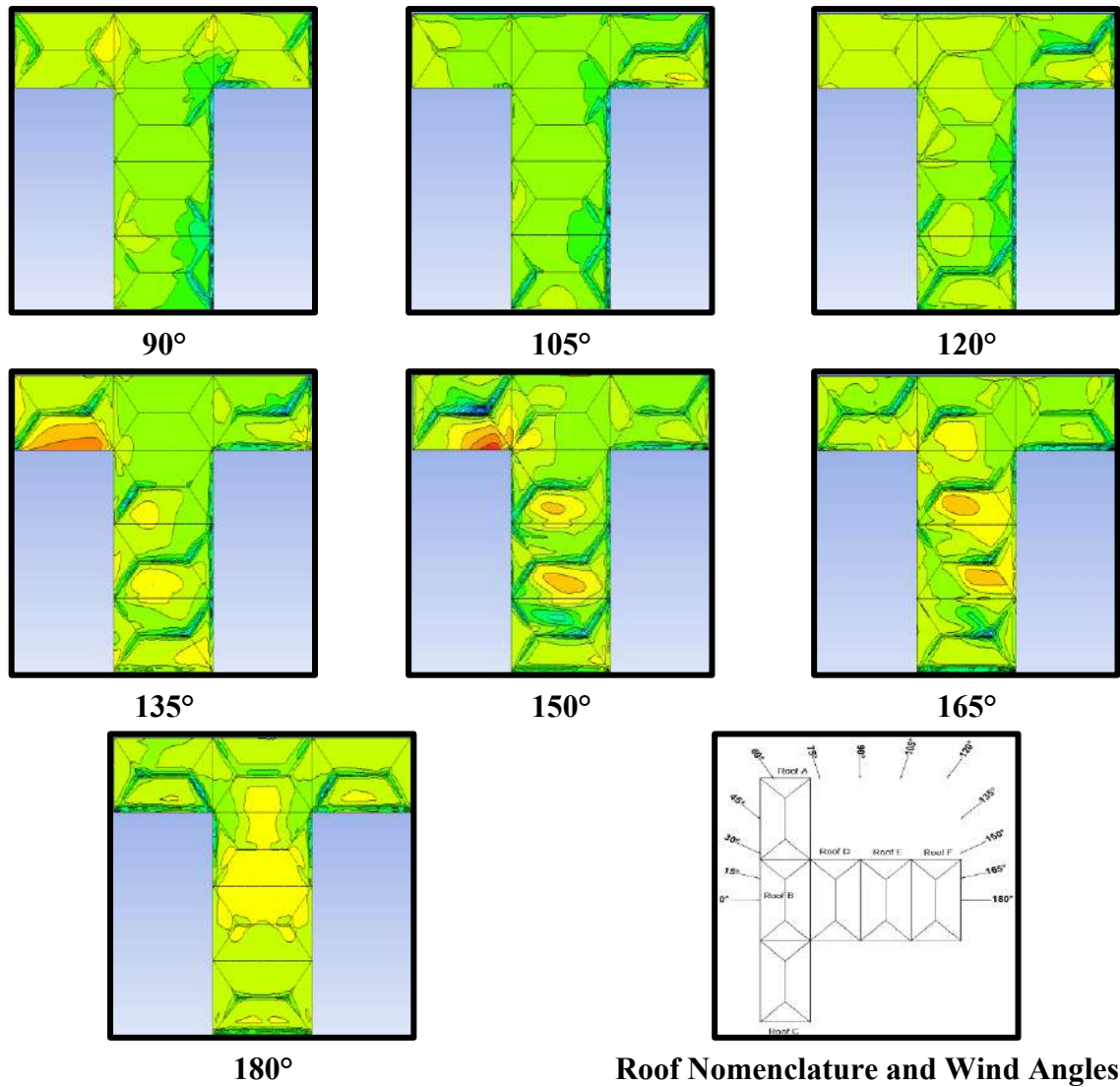
Fig. 7.38(b): Pressure Contours for T pattern with Zero Spacing

0°   **15°**   **30°**
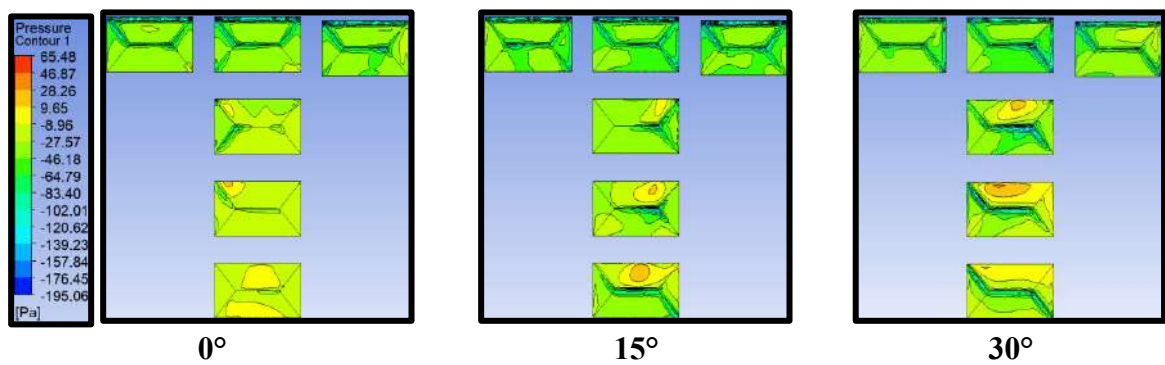
Fig. 7.39(a): Pressure Contours for T pattern with 0.5B Spacing

45° **60°** **75°**

90° **105°** **120°**

135° **150°** **165°**

180° **Roof Nomenclature and Wind Angles**
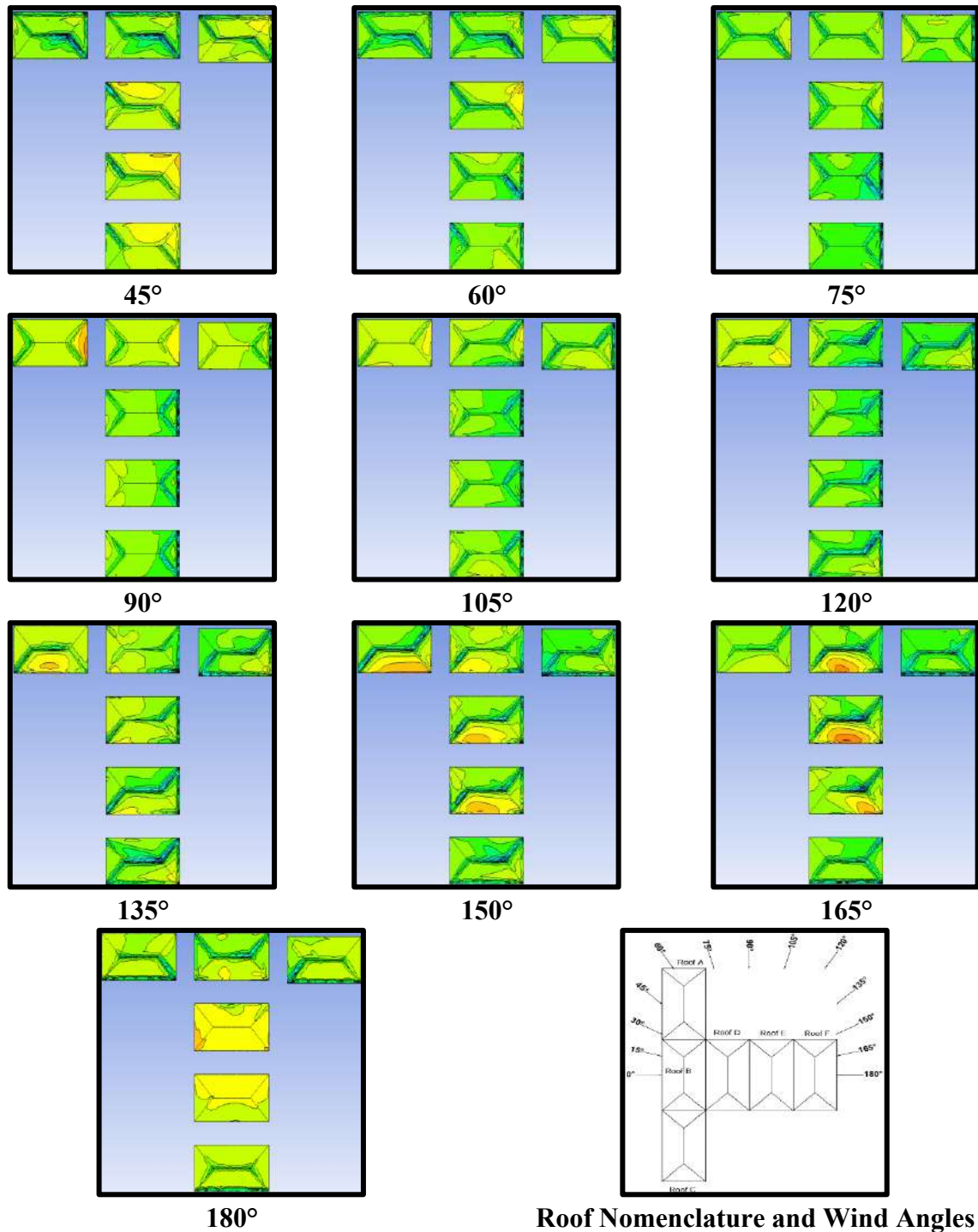
Fig. 7.39(b): Pressure Contours for T pattern with 0.5B Spacing
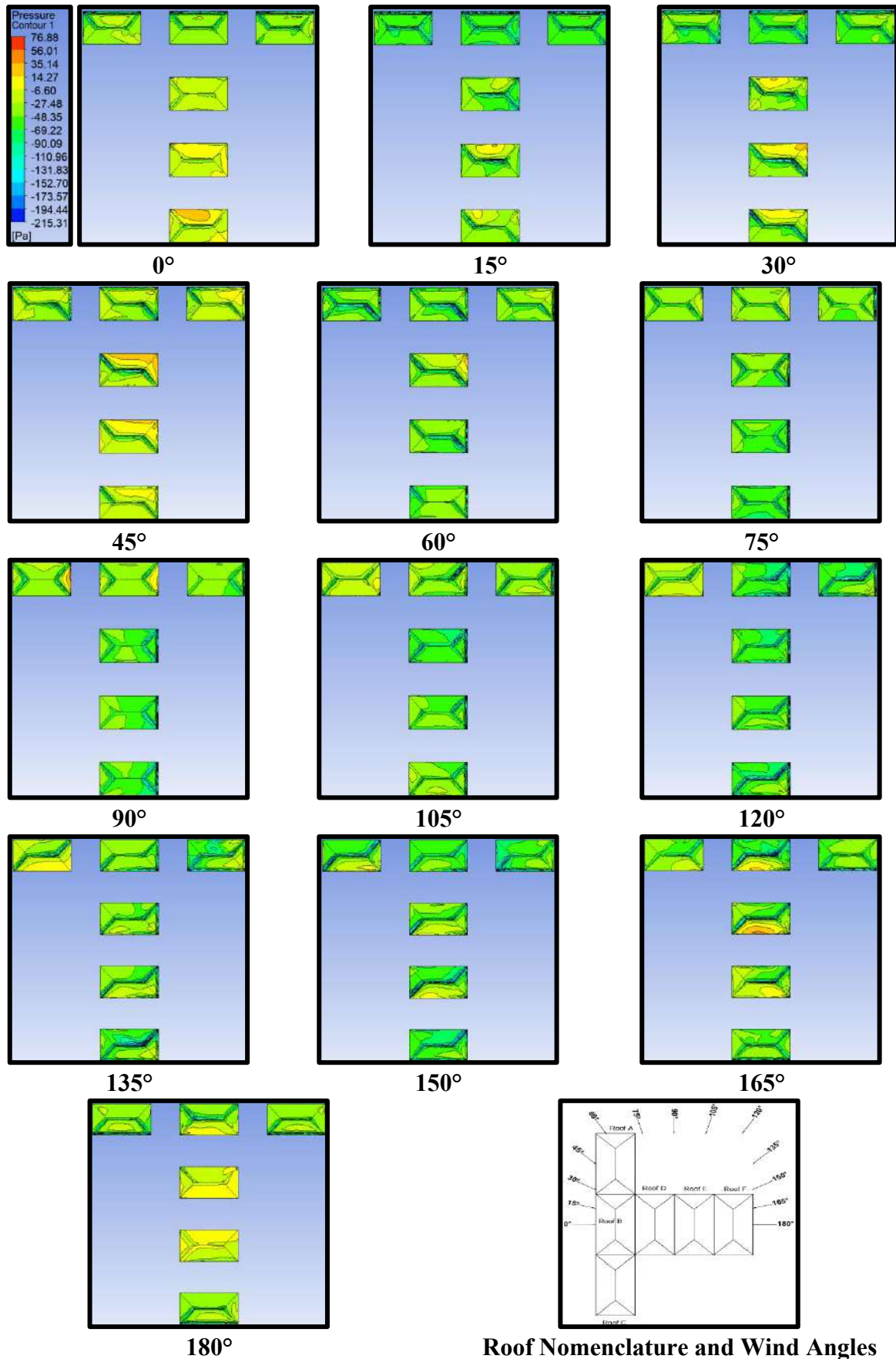
Fig. 7.40: Pressure Contours for T pattern with B Spacing

0° **15°** **30°**

45° **60°** **75°**

90° **105°** **120°**

135° **150°** **165°**

180° **Roof Nomenclature and Wind Angles**

Fig. 7.41: Pressure Contours for T pattern with 1.5B Spacing

0°

15°

30°

45°

60°

75°

90°

105°

120°

135°

150°

165°

180°
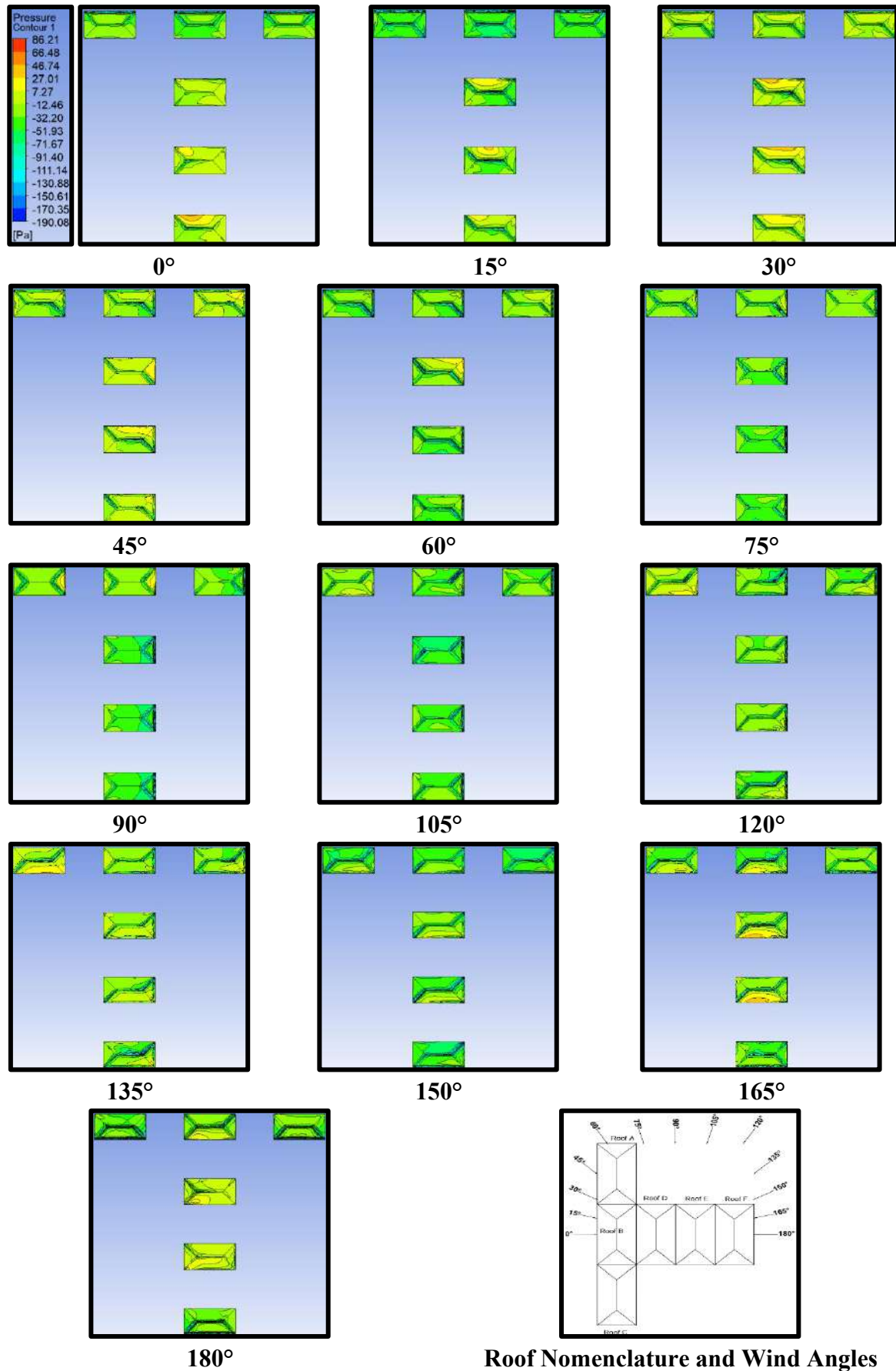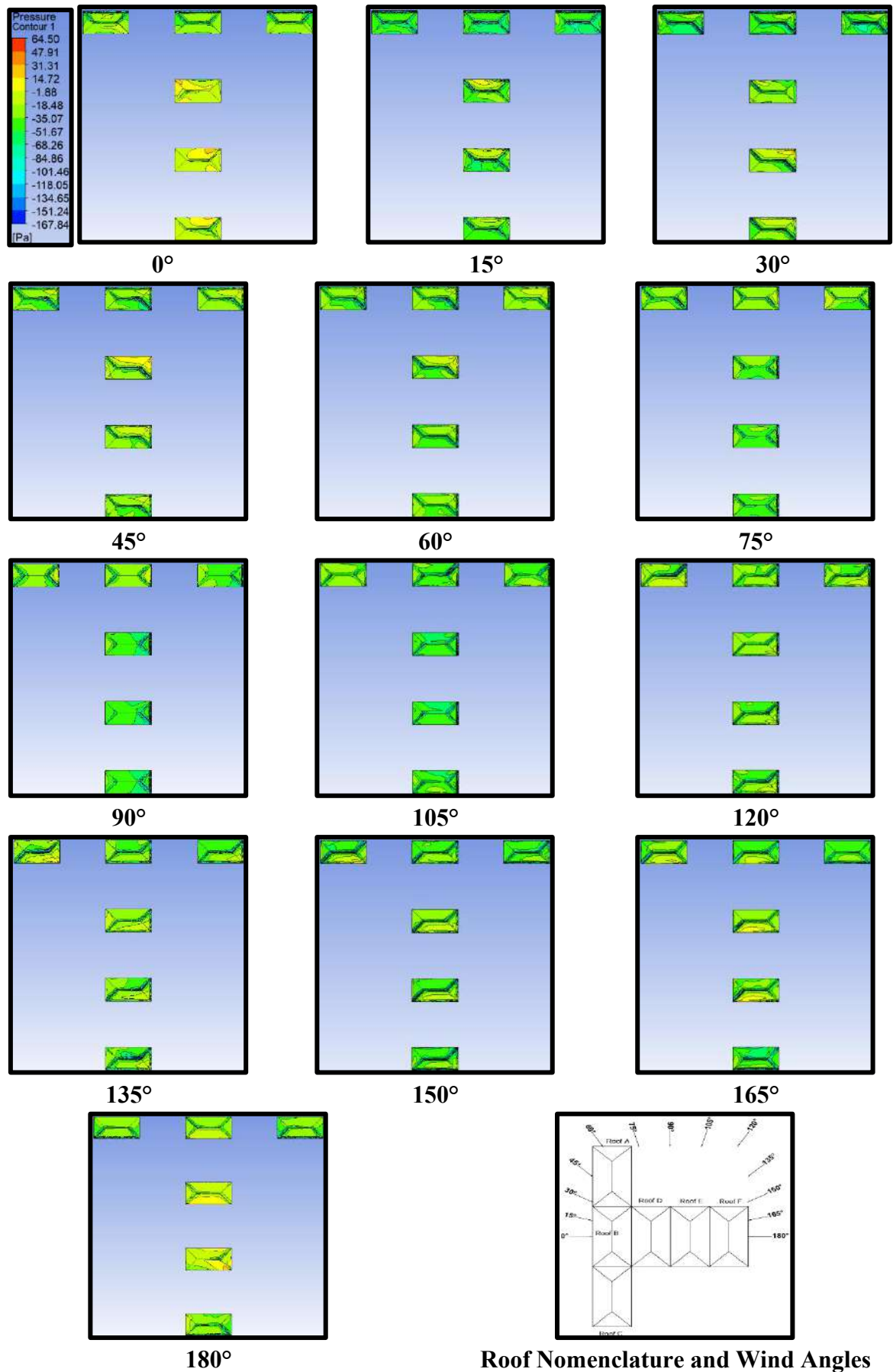
Roof Nomenclature and Wind Angles

Fig. 7.42: Pressure Contours for T pattern with 2B Spacing

7.3.3.2 Pressure Coefficient (C_{pe})

The variation of C_{pe} on the 30° hip roof of six low-rise buildings arranged in T pattern with variable spacing of zero, 0.5B, B, 1.5B and 2B at different angles of wind interval ranging between 0° to 180° having an interval of 15° each, is shown in Fig. 7.43. At each interval of wind incidence, it is observed that the overall value of C_{pe} is negative in magnitude on all the 30° hip roofs in the case of different spacings between the buildings. The range of C_{pe} on roof A is -0.85 to -0.26 indicating that there is only suction on the roof in which the maximum suction occurs during 0° & 150° angle of wind incidence with 0.5B and B spacing between the buildings, while the minimum suction on roof A is observed during 75° wind incidence with zero spacing between the buildings. The maximum and minimum suction on roof B is observed when the value of C_{pe} is -0.89 at 45° wind angle with 0.5B spacing and -0.17 at 90° wind angle with 1.5B spacing. The maximum value of negative C_{pe} on roofs C is -0.85 at 45° angle of wind attack when the spacing between buildings is 0.5B, while the minimum negative value of C_{pe} is -0.16, which is almost negligible or zero at 90° wind incidence angle and 0.5B spacing. The range of C_{pe} for roof D is -0.84 to -0.02, in which the maximum suction is observed during a 105° angle of wind incidence and B spacing and minimum suction occurs during 180° wind angle and 0.5B spacing. Roof E is undergoing maximum suction at 75° wind angle with zero spacing, during which the value of C_{pe} is -0.89, and minimum suction, i.e., C_{pe}, is -0.03 at 180° with 2B spacing.
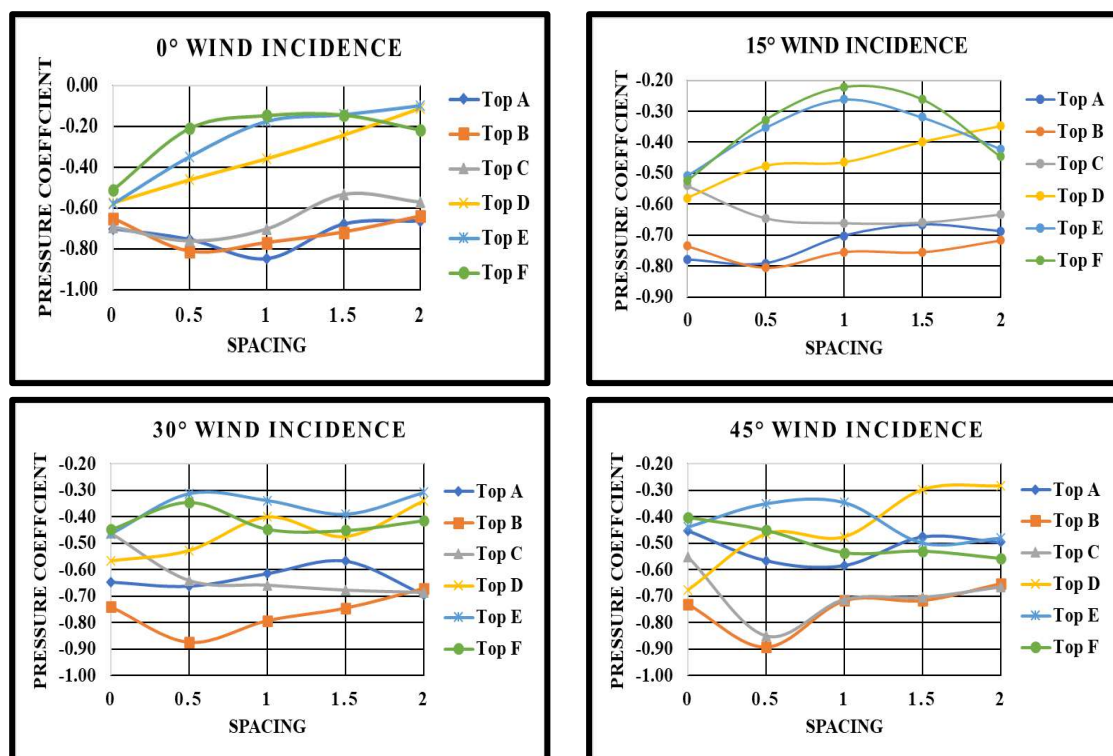
Fig. 7.43(a): Pressure Coefficient for T pattern with variable Spacing
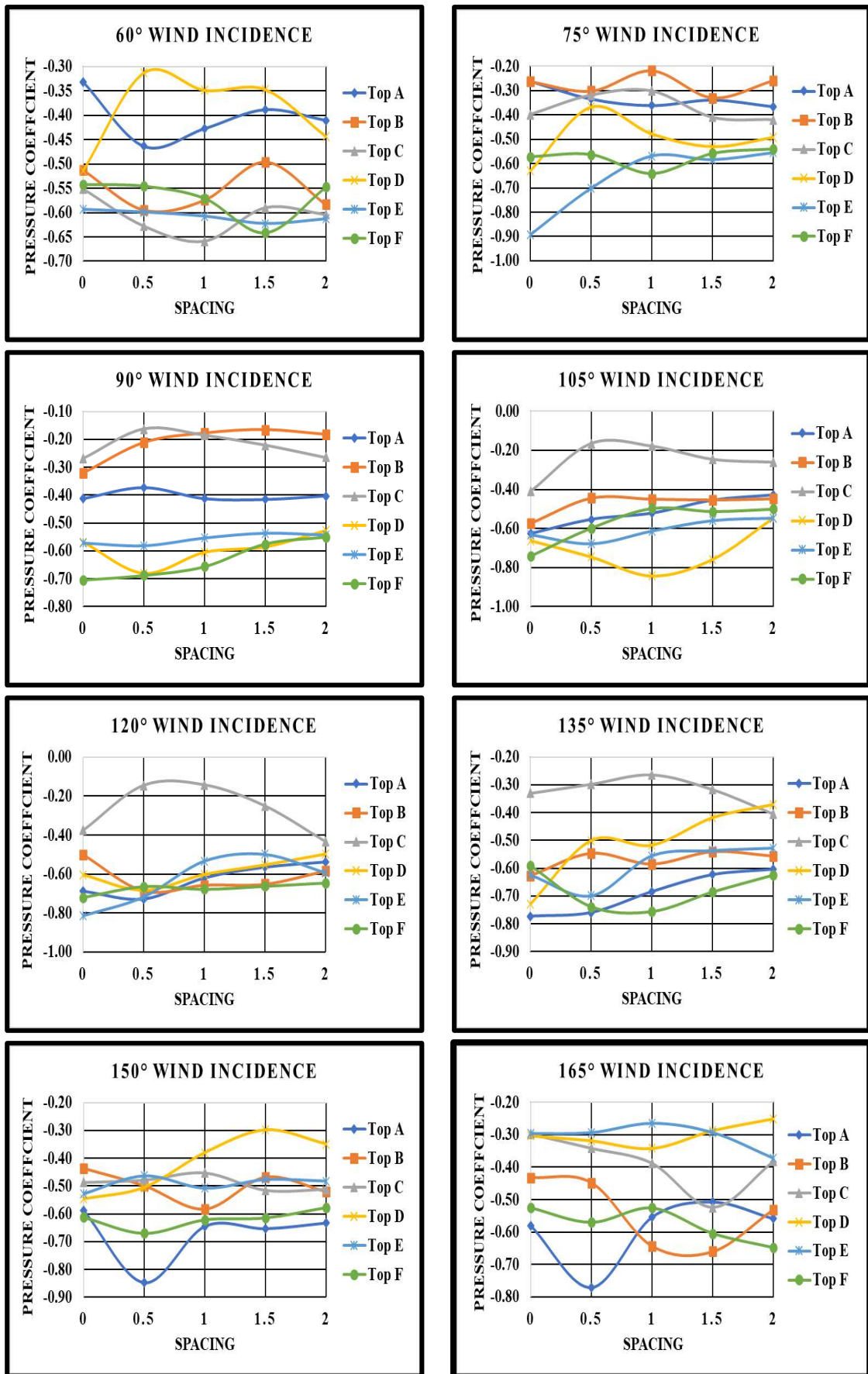
Fig. 7.43(b): Pressure Coefficient for T pattern with variable Spacing
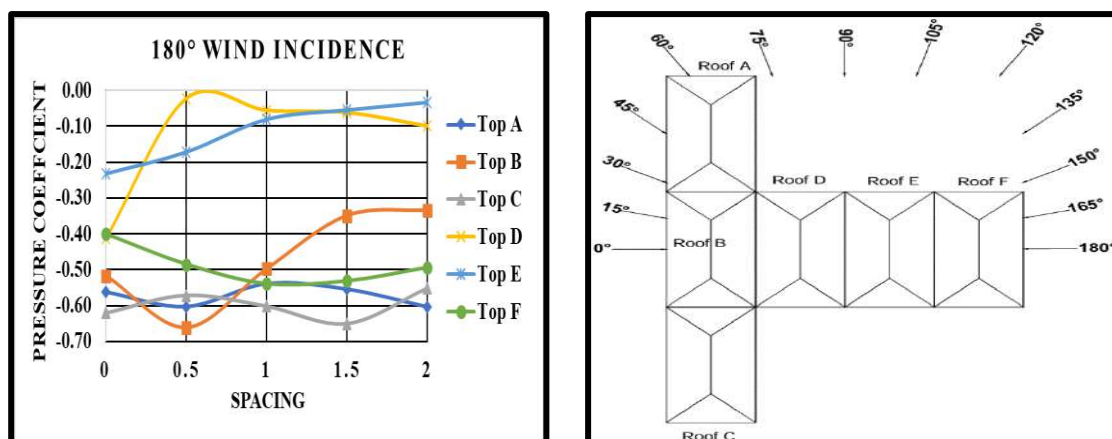
Fig. 7.43(c): Pressure Coefficient for T pattern with variable Spacing

7.3.3.3 Interference Factor (IF)

The idea of enhancement or reduction of suction or pressure on the roof is given by interference factor (*IF*) due to the presence of low-rise structure in the vicinity. The value of *IF* gets modified with respect to the spacing between the buildings and angles of wind attack. The varying magnitude of *IF* on a 30° hip roofs arranged in a T pattern with variable spacing (0,0.5B, B, 1.5B and 2B) at various angles of wind attacks, i.e., 0° to 180° at 15° intervals is shown in Fig. 7.44. The value of *IF* on the roof A keeps on reducing with an increase in spacing from 0 to 2B. Initially, the value of *IF* comes out to be more than 1, indicating the increased suction on roof A at 0° to 30° and 105° to 180° angles of wind incidence with zero spacing, but it gets reduced while increasing the spacing till 2B at which *IF* becomes less than 1 indicating the reduced suction on roof A. On the rest of the wind incidence angles i.e., 45°, 60°, 75° and 90°, the value of *IF* is already less than 1 for roof A. Similarly to the *IF* of roof A, the value of *IF* for roof B follows the same trend in which its value comes out to be more than 1 when the angles of wind attack are 0°, 15°, 30°, 45° and 120° respectively and starts reducing when spacing between the building in increased from 0 to 2B. Also, the maximum reduction in *IF*, i.e., reduced suction on roof B, is observed at 1.5B spacing at all the wind incidence angles, i.e., 0° to 180° at 15° intervals, as shown in Fig. 7.44. The magnitude of *IF* is greater than 1 on roofs C when the angle of wind incidence ranges between 0° to 60° and 180° indicating the increased suction due to interference of buildings existing in the vicinity. The variation of *IF* on roof D follows the same pattern as that of roof B when wind incidence angles are 0° to 60° and 135° to 180°, at which the maximum reduction of *IF* takes place when the spacing is 1.5B between the buildings. The value of *IF* for roof E is greater than 1 when the angle of wind incidence is 0° to 45° and 135° to 180°, indicating the increased suction on roof E due to interference. The reduction in the value of *IF* for roof F with respect to the spacing is

observed when the angle of wind incidence ranges between 0° to 60°, 165° and 180° respectively, as shown in Fig. 7.44. The variation of spacing between the buildings is proved to be beneficial which helps in reducing the suction on the roof and greatly influences the nature of wind on roofs. The angle of wind incidence also plays a vital role in changing the magnitude of *IF* on the roof or low-rise structure with a hip roof.
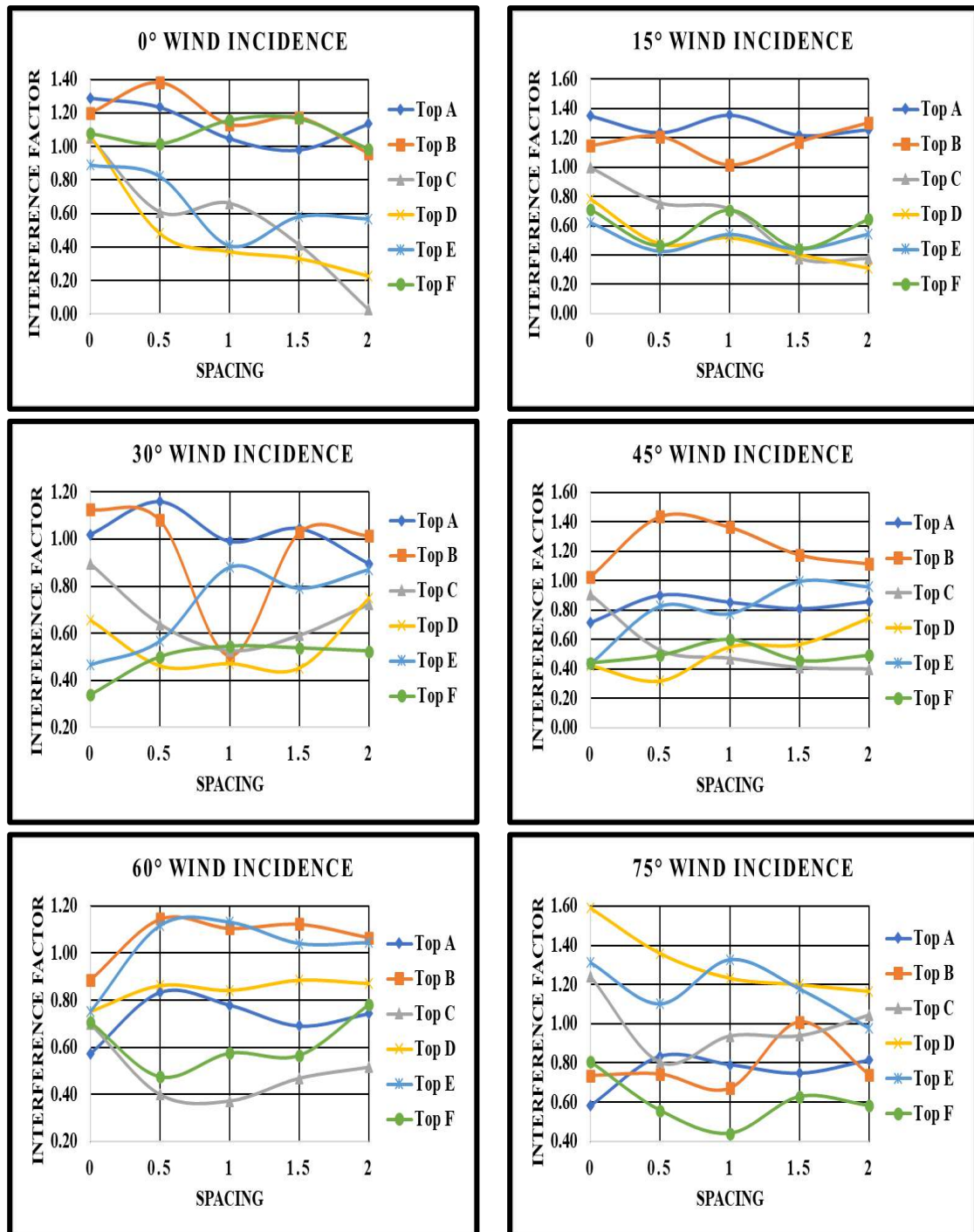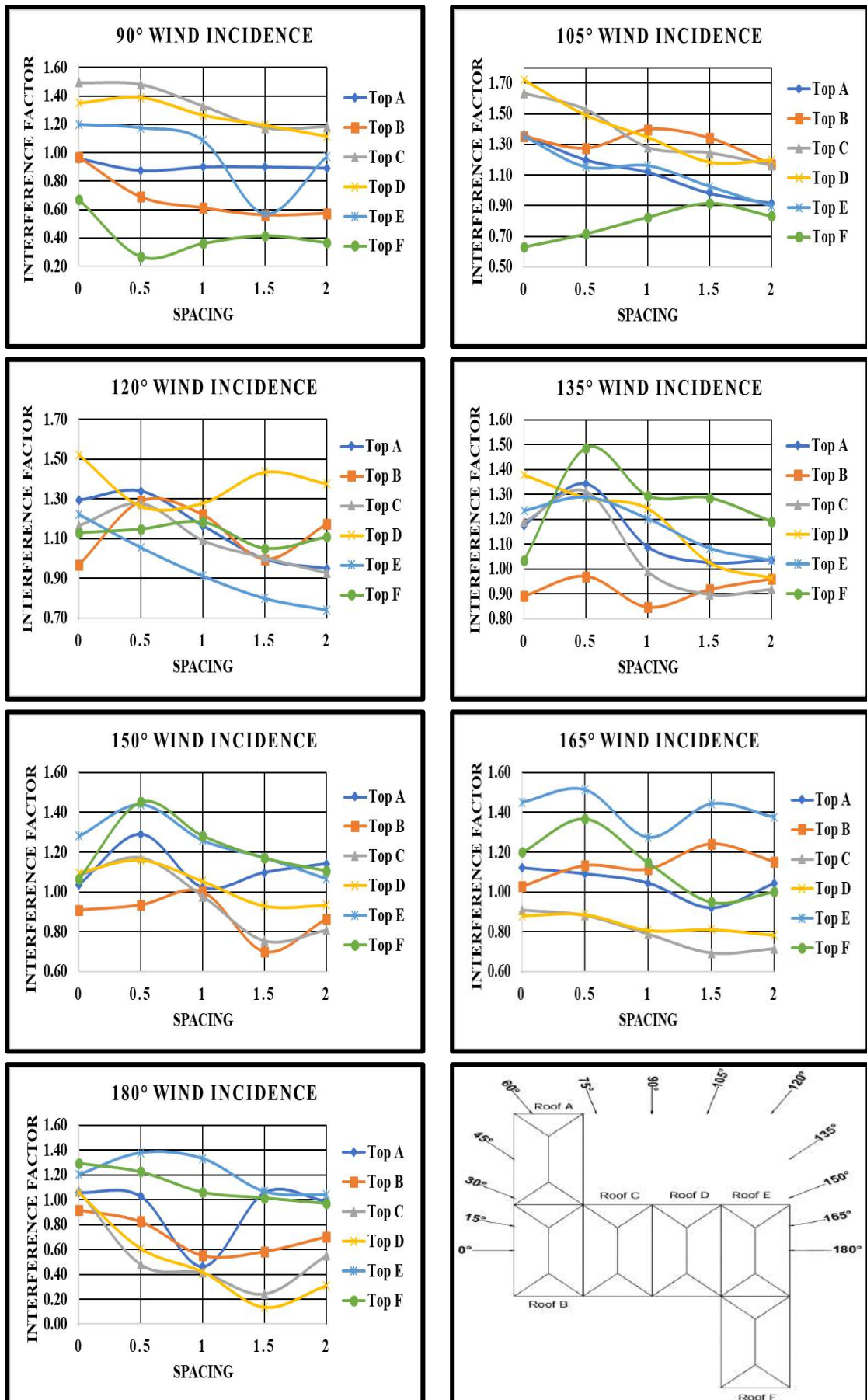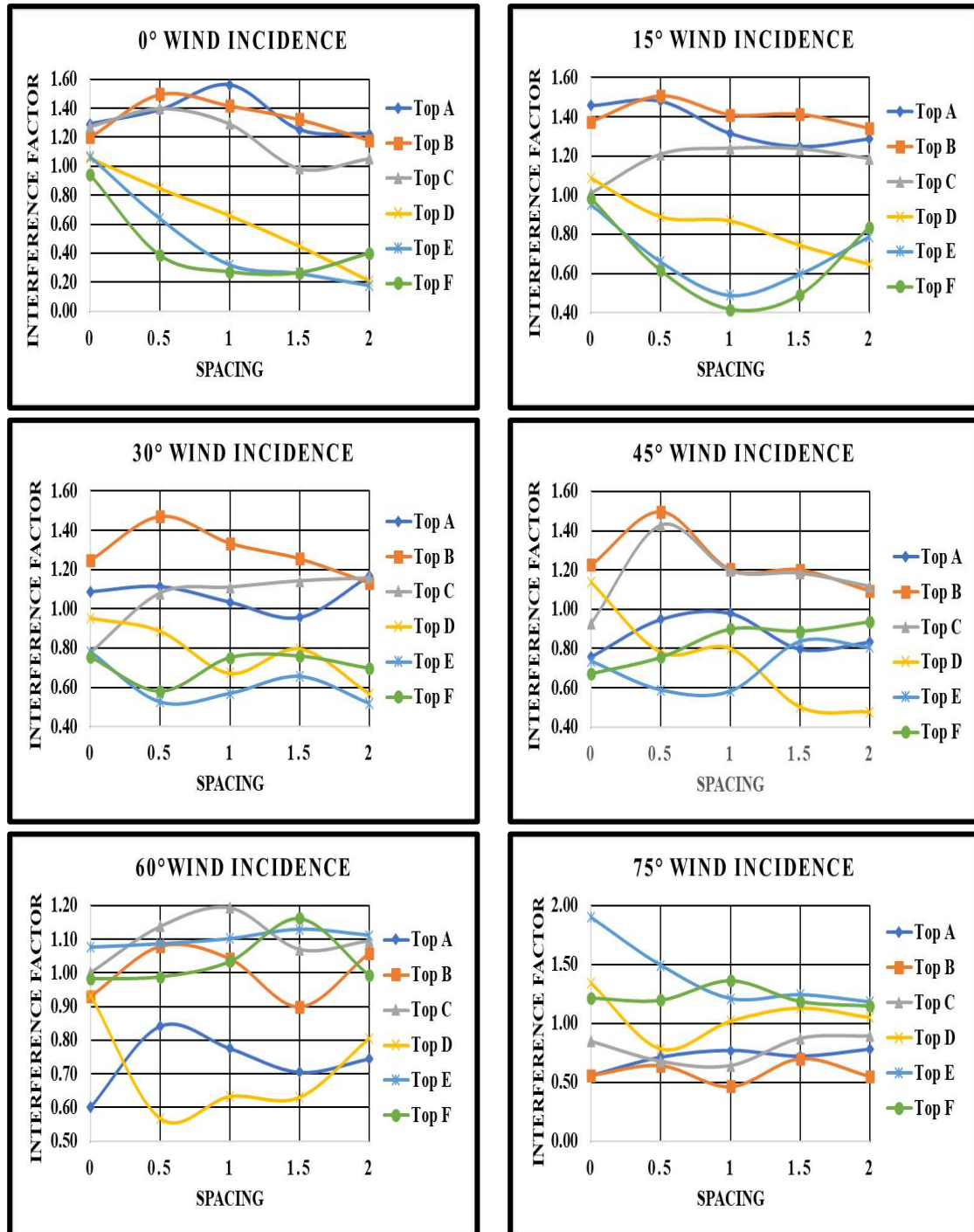

Fig. 7.44(a): Interference Factor for T pattern with variable Spacing
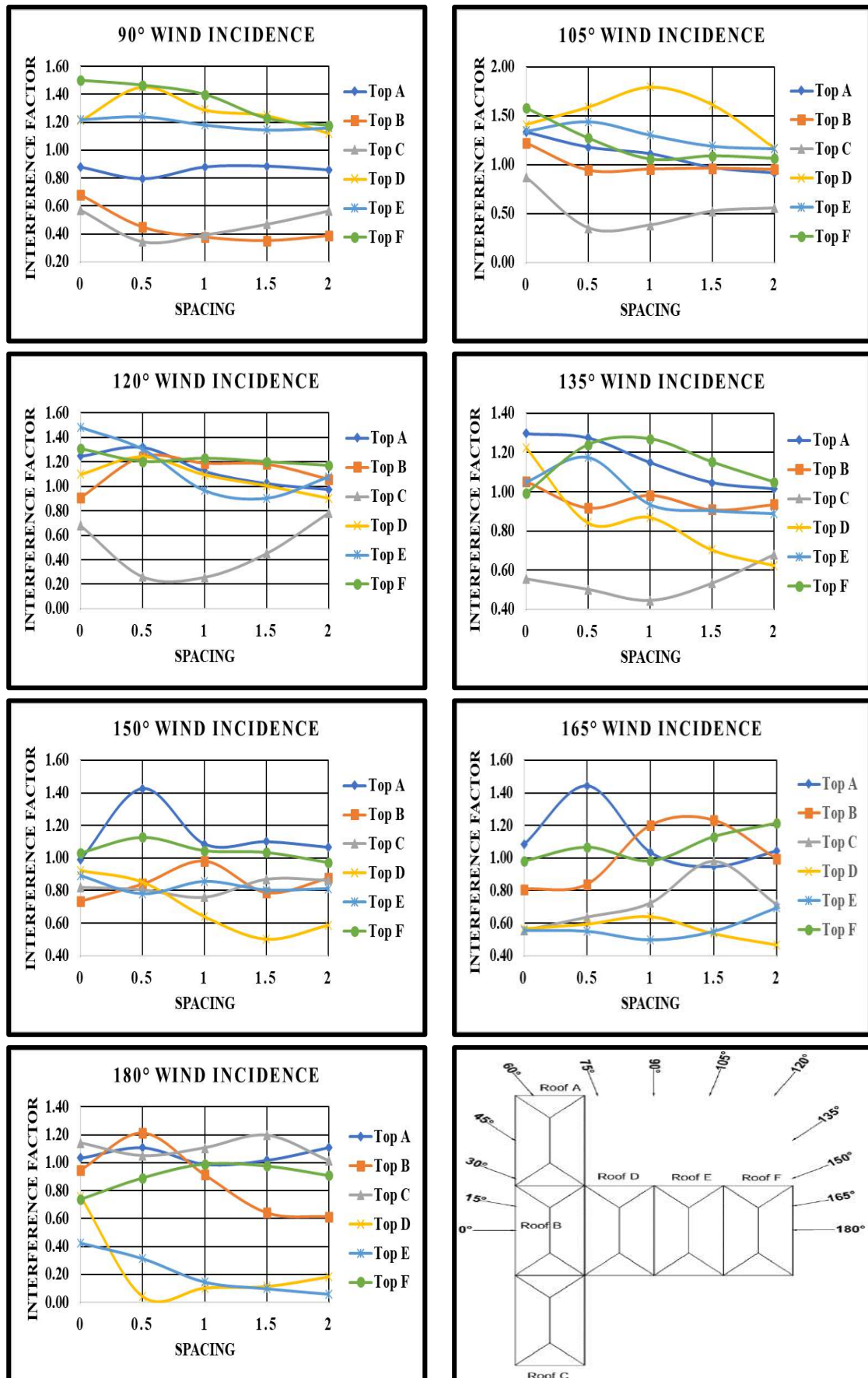
Fig. 7.44(b): Interference Factor for T pattern with variable Spacing

7.3.3.4 Interference Difference (ID)

The difference between C_{pe} obtained during an interfering condition and C_{pe} obtained during an isolated condition is called as interference difference (*ID*), which gives an exact idea of enhancement or reduction in the wind-induced positive or negative pressure coefficient on the roofs. The variation of *ID* on 30° hip roofs arranged in a T pattern with different spacing ranging between 0 to 2B (where B is the width of a low-rise building) and at various angles of wind incidences ranging between 0° to 180° at 15° intervals is shown in Fig. 7.45. When the magnitude of negative C_{pe} on the roof is increased during interfering conditions, then the value of *ID* comes out to be negative, indicating the increased suction on the roof during interfering conditions, while the value of *ID* is positive, but the magnitude of C_{pe} is still negative on the roofs indicates that the suction on the roof is reduced due to interference of vicinity buildings. This variation of *ID* on 30° mono-slope roof arranged in T pattern with variable spacing with respect to different angles of wind incidences is shown in Fig. 7.45 below.
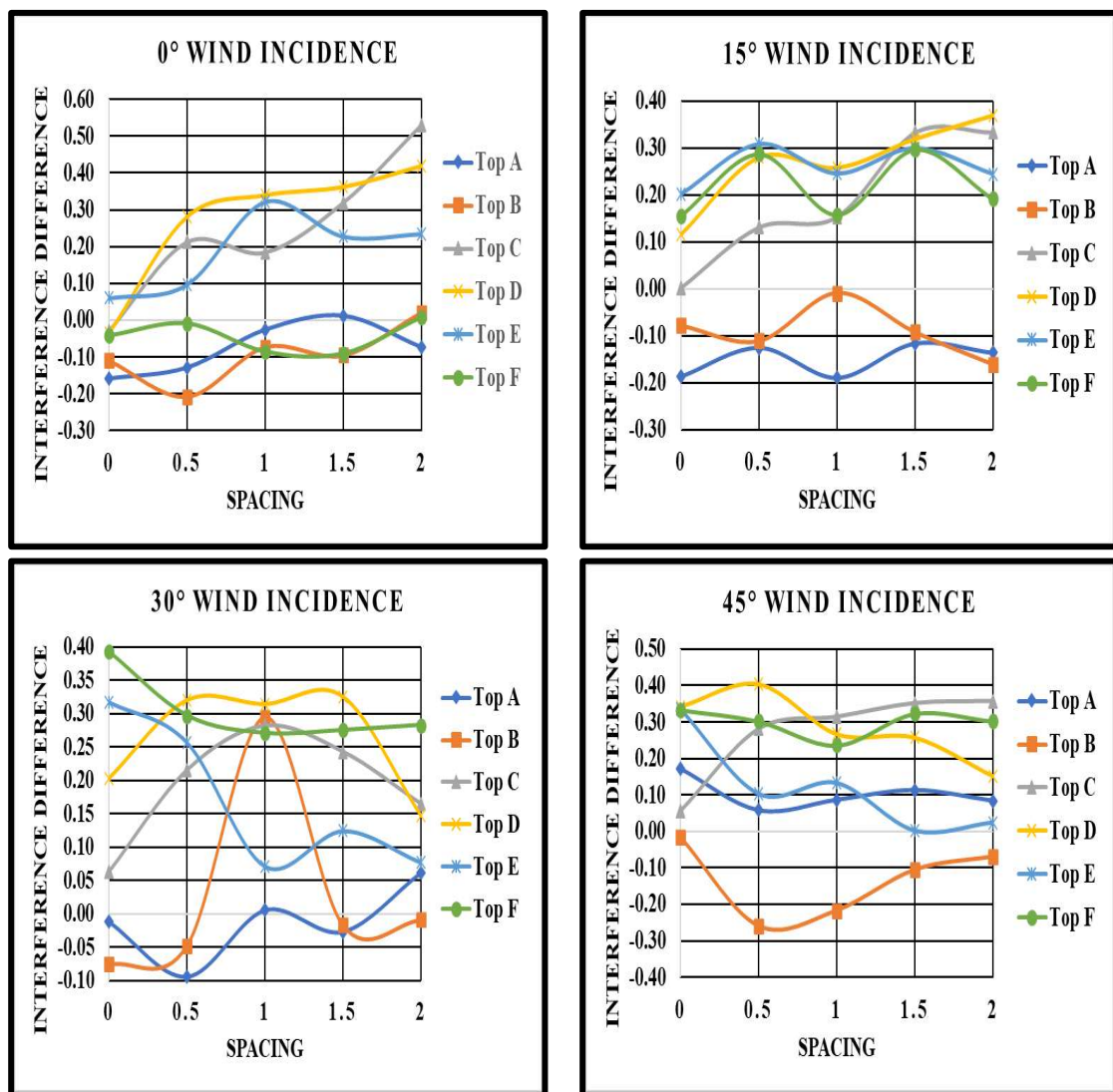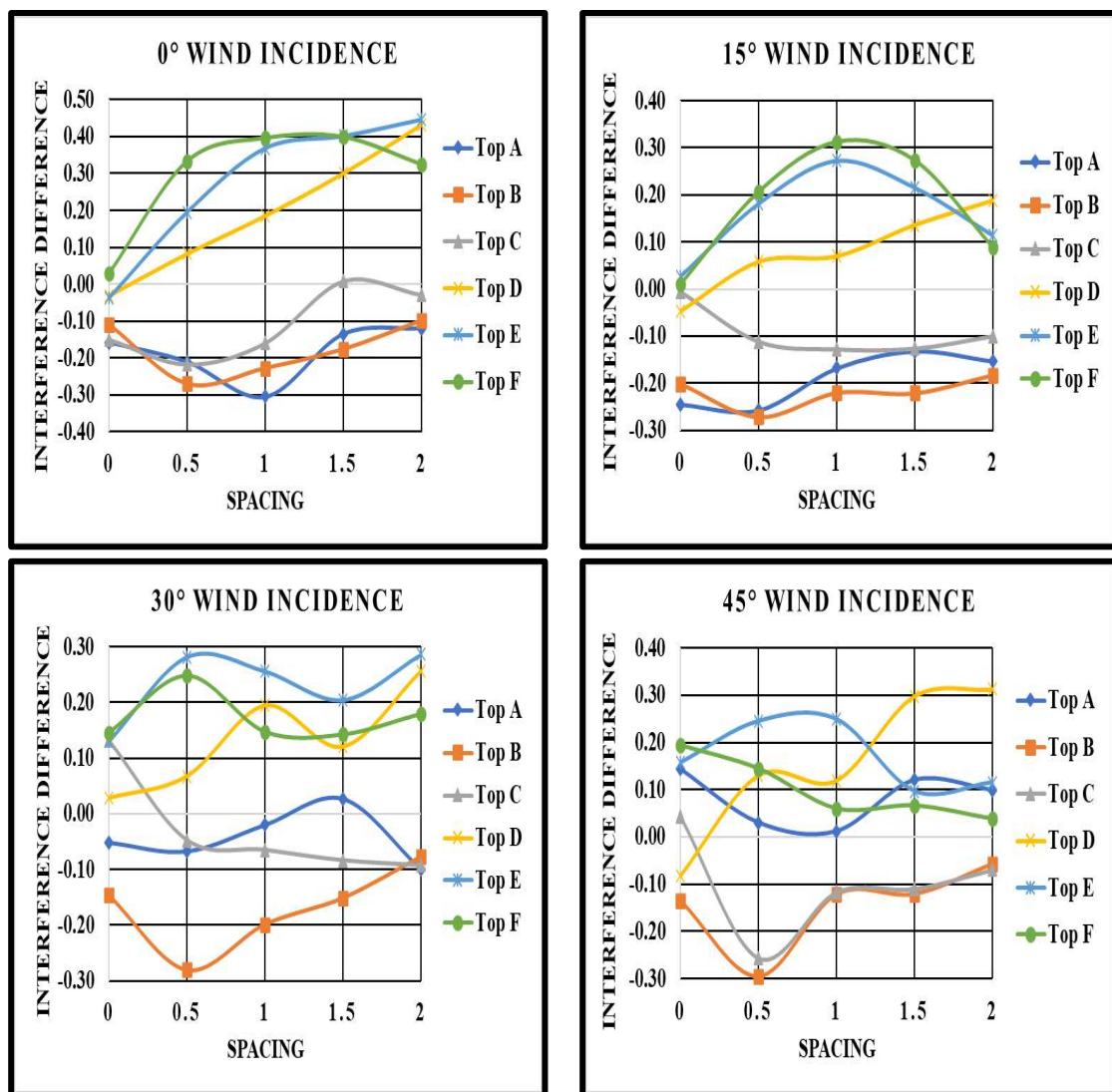

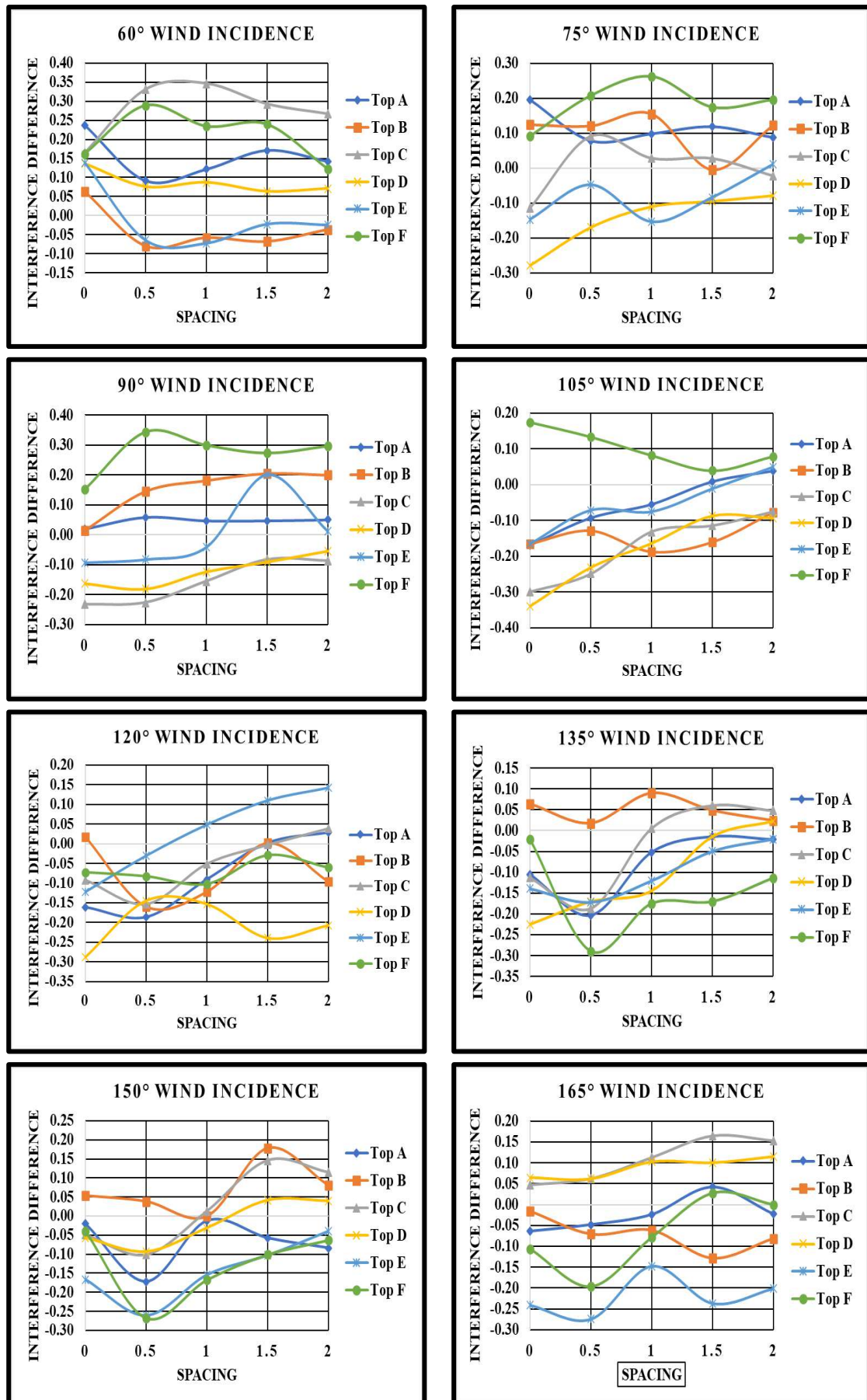
Fig. 7.45(a): Interference Difference for T pattern with variable Spacing
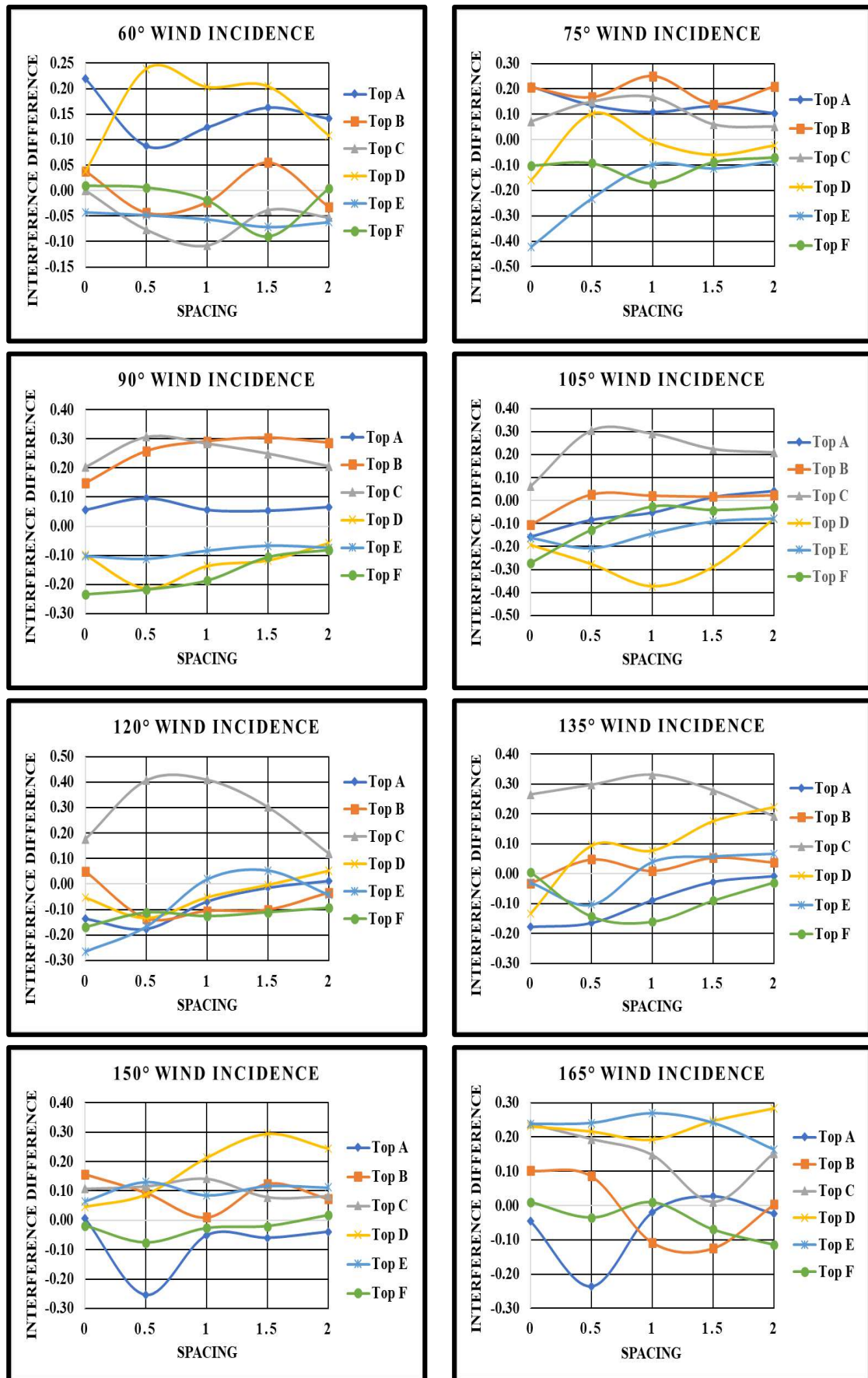
Fig. 7.45(b): Interference Difference for T pattern with variable Spacing
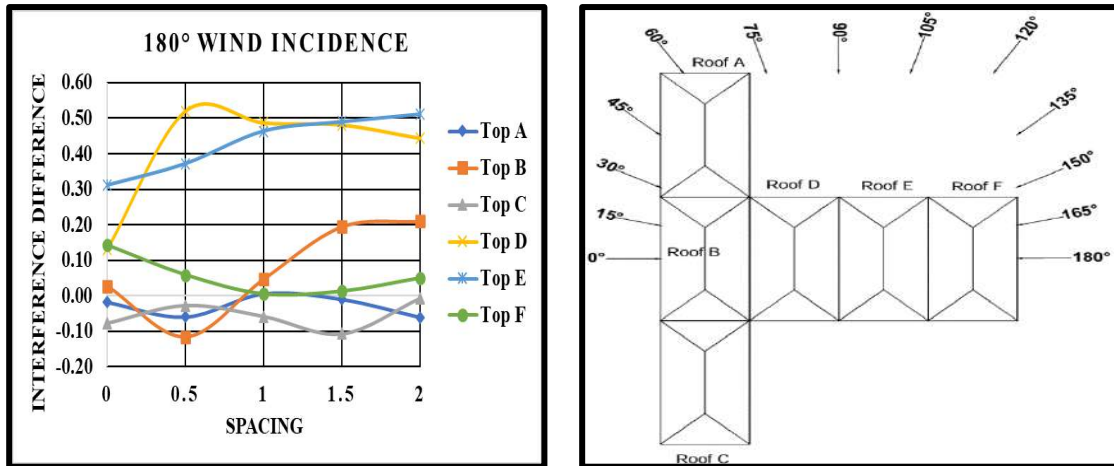
Fig. 7.45(c): Interference Difference for T pattern with variable Spacing

7.3.3.5 Wind Flow Streamlines

The pattern of wind flow around the low-rise structure with hip roofs arranged in a T pattern with variable spacing (0, 0.5B, B, 1.5B and 2B) and at different angles of wind attack (0° to 180° at 45° interval) is shown in Fig. 7.46-7.50. As the wind is flowing around the building, there is a formation of vortex generation in the wake region after striking and separating from the upstream direction at the stagnation point. The formation of wake region is depending upon the angle of wind attack and spacing between the structures. The wake formation is reduced when the spacing between the buildings is increased from 0 to 2B as the wind flow is getting inserted in between the buildings. When there is zero spacing between the buildings, the vortex generation takes place only in the surrounding of the buildings in the downstream direction, but when the spacing is increased from zero to 2B, the flow is inserted between the buildings, resulting in reduced eddies formation and vortex generation in the wake region.

| 0° | 45° |

Fig. 7.46(a): Wind Flow Streamlines for T pattern with Zero Spacing

90°

135°

180°

Angles of Wind Incidence

Fig. 7.46(b): Wind Flow Streamlines for T pattern with Zero Spacing

0°

45°

Fig. 7.47(a): Wind Flow Streamlines for T pattern with 0.5B Spacing

90°

135°

180°

Angles of Wind Incidence
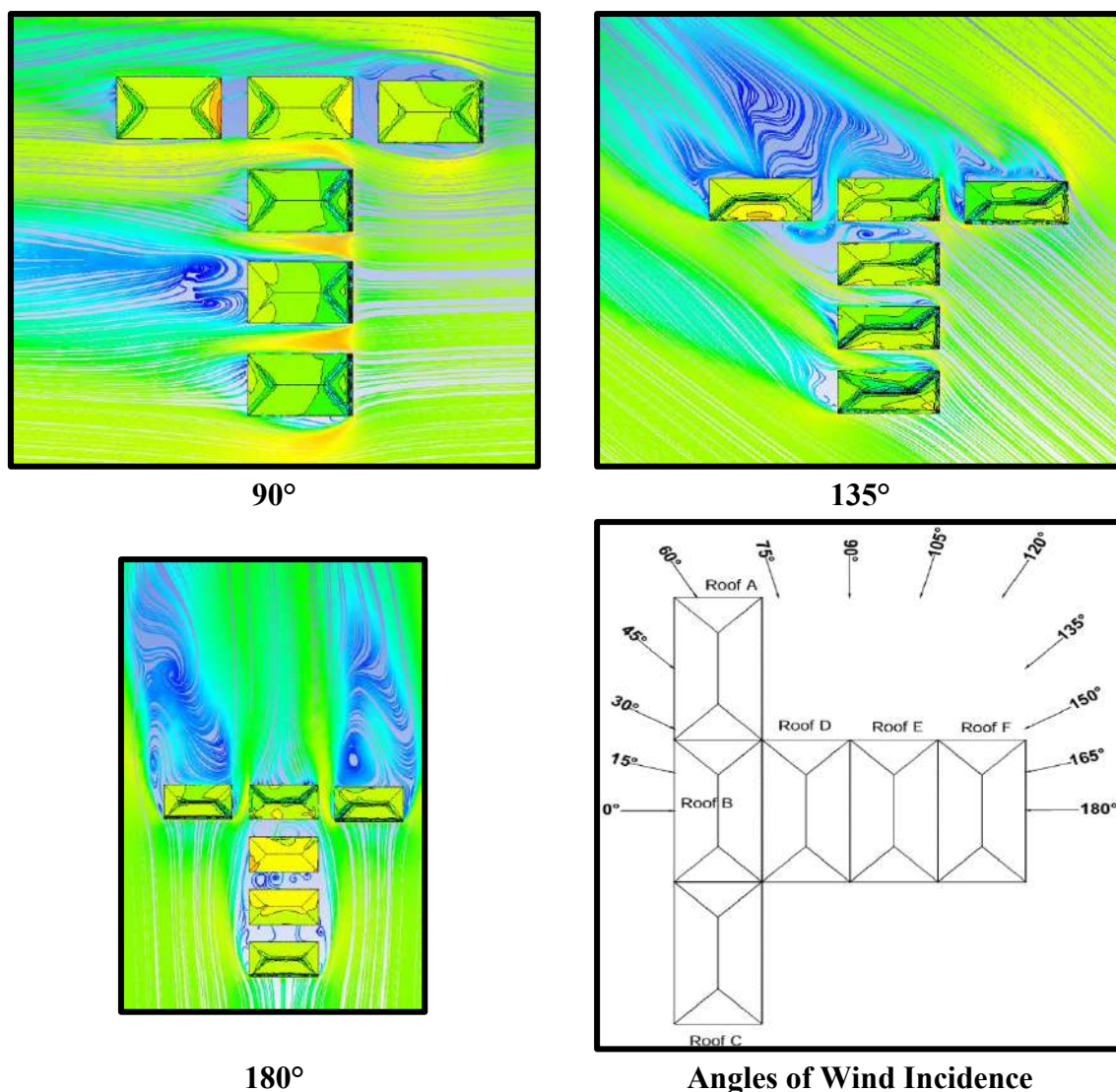
Fig. 7.47(b): Wind Flow Streamlines for T pattern with 0.5B Spacing

0°

45°

Fig. 7.48(a): Wind Flow Streamlines for T pattern with B Spacing

90°

135°

180°

Angles of Wind Incidence

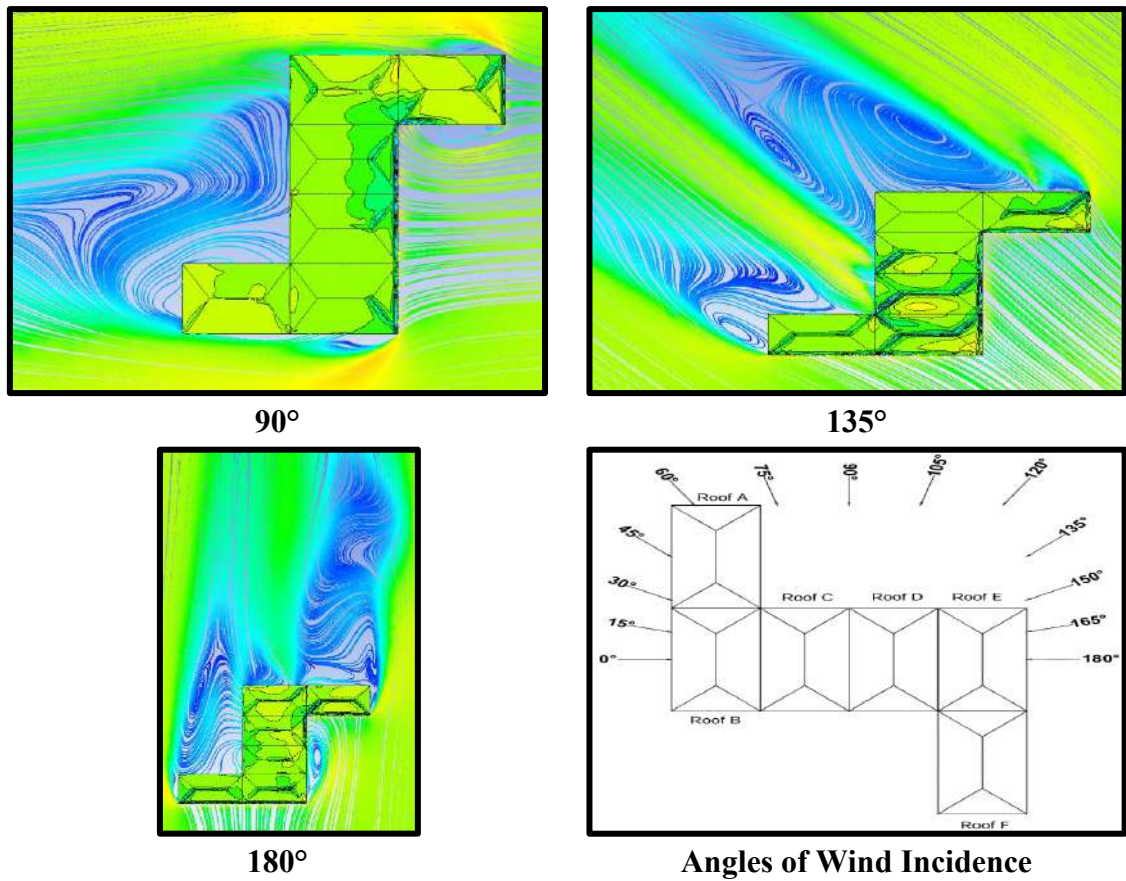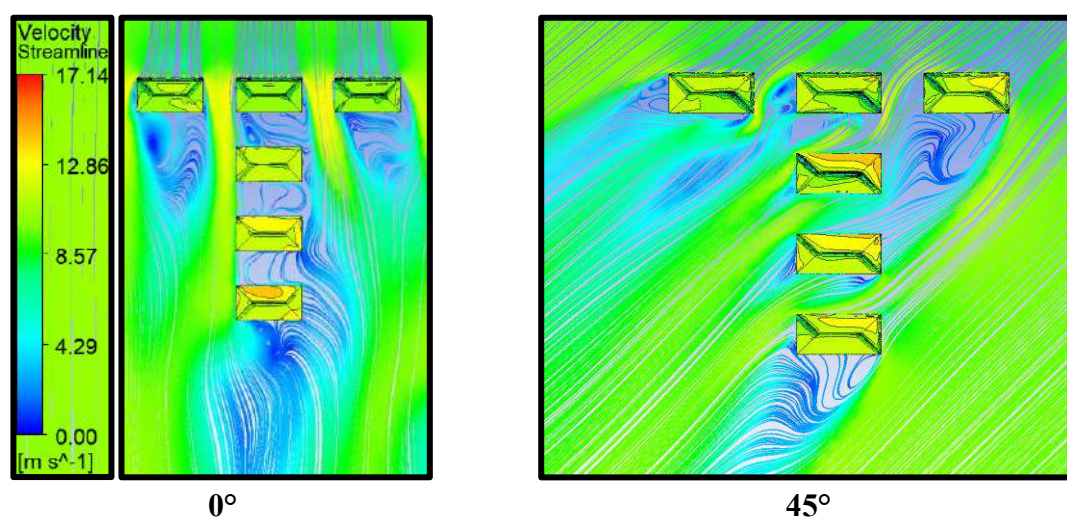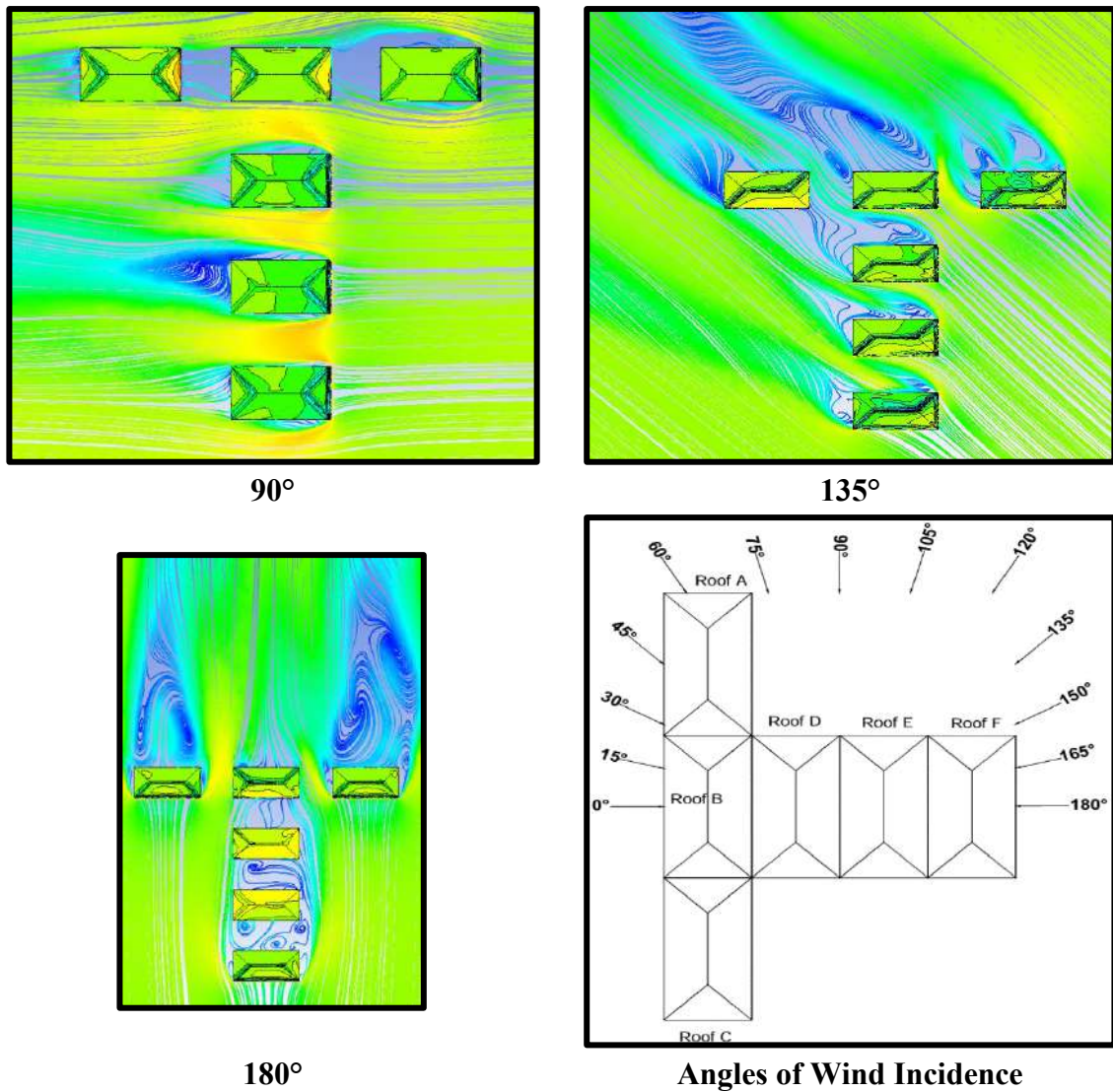**Fig. 7.48(b):** Wind Flow Streamlines for T pattern with B Spacing

0°

45°

Fig. 7.49(a): Wind Flow Streamlines for T pattern with 1.5B Spacing

90°

135°

180°

Angles of Wind Incidence
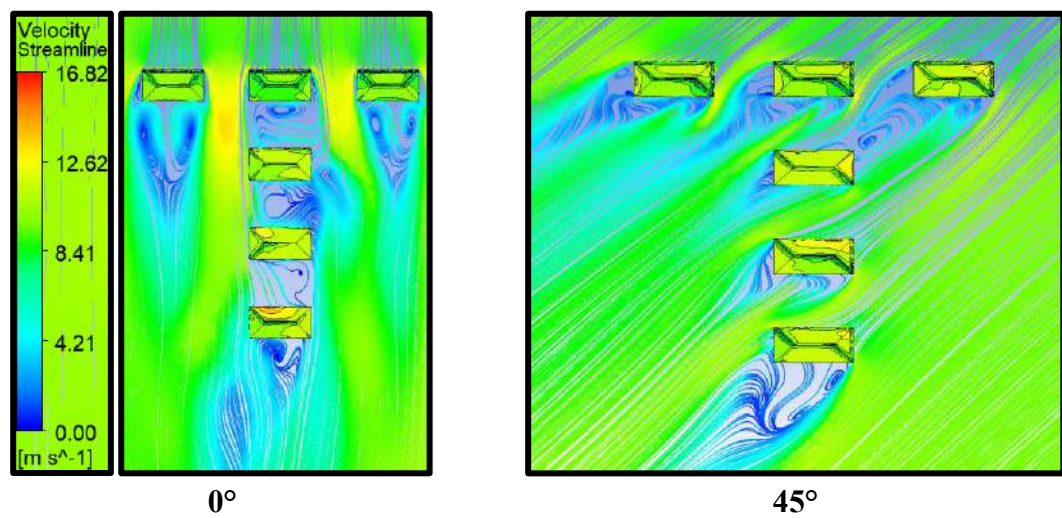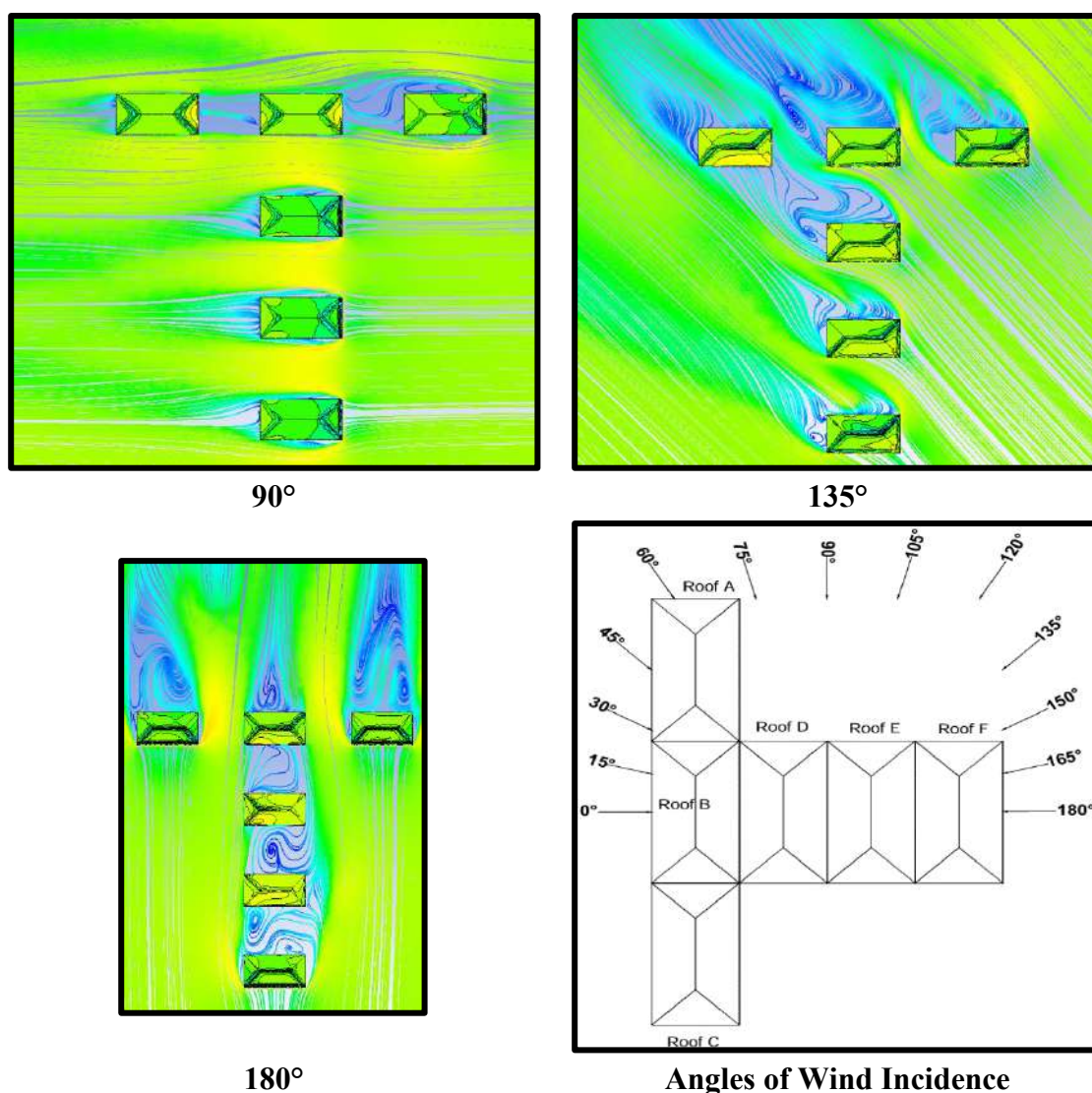
Fig. 7.49(b): Wind Flow Streamlines for T pattern with 1.5B Spacing

0°

45°

Fig. 7.50(a): Wind Flow Streamlines for T pattern with 2B Spacing

90°

135°

180°

Angles of Wind Incidence
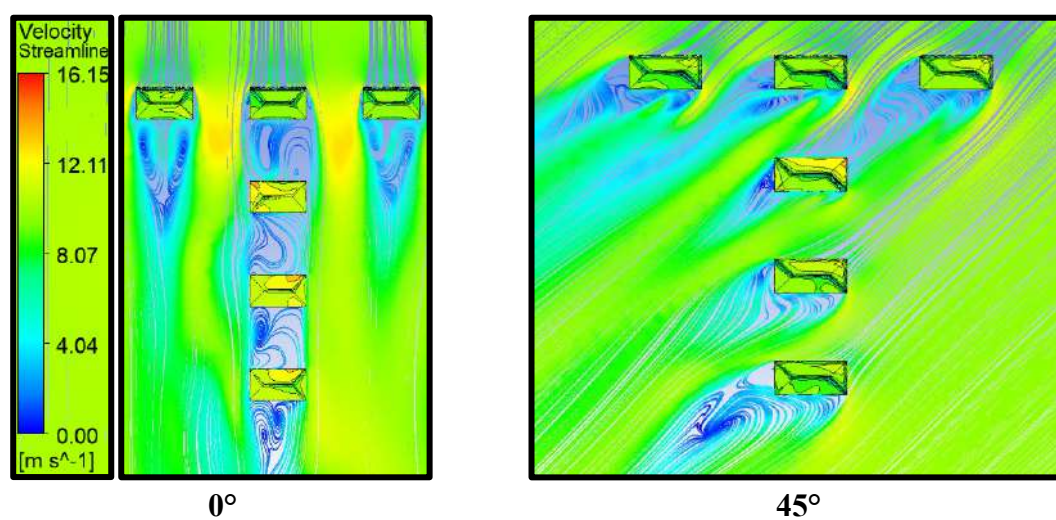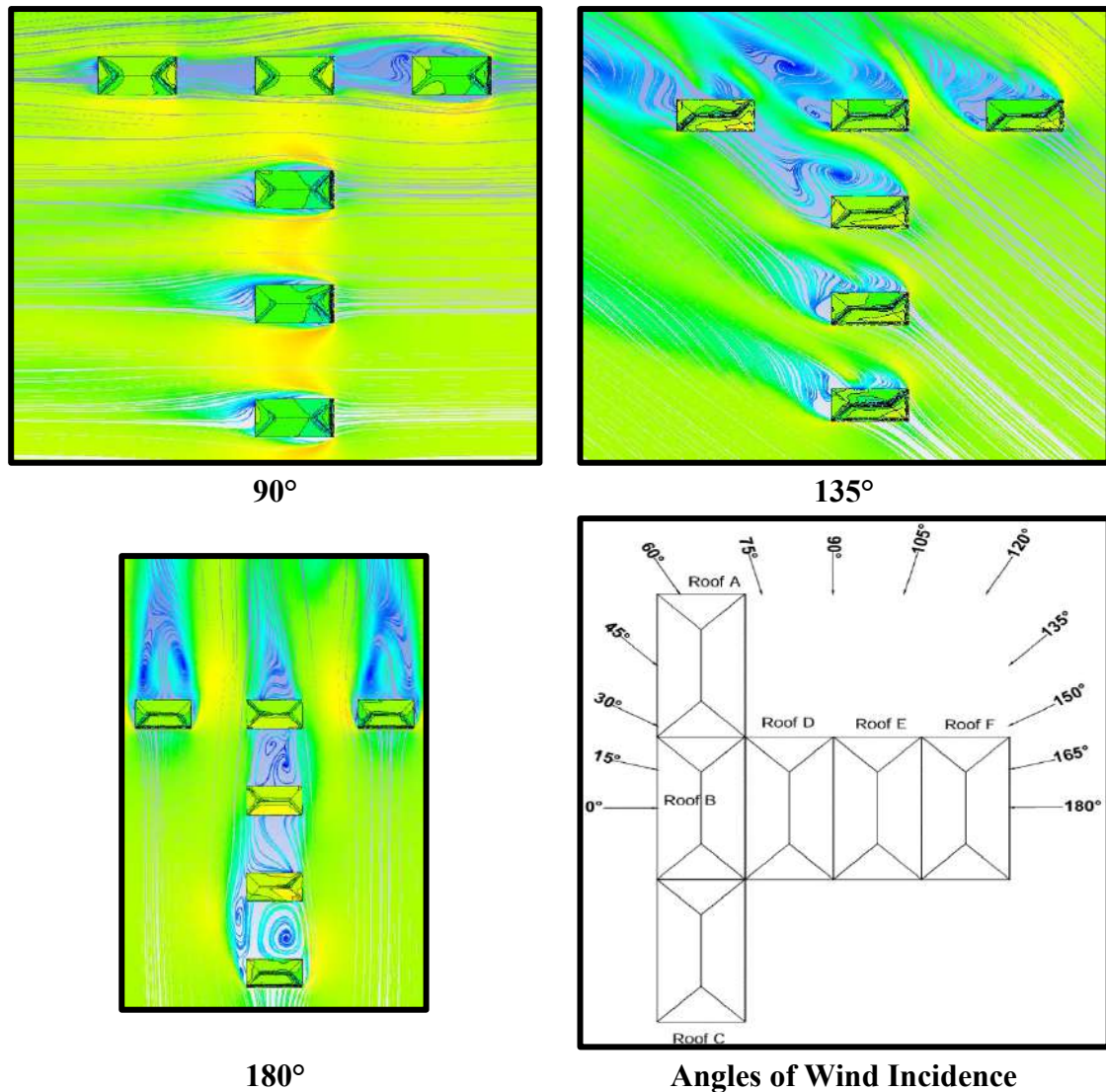
Fig. 7.50(b): Wind Flow Streamlines for T pattern with 2B Spacing

7.4. Conclusions

In conclusion, the study highlights the complex interplay of wind-induced forces on hip roof structures, emphasizing the need for careful consideration of both suction and pressure forces to ensure their stability and safety. The findings indicate that:

A. **Roof Angle and Safety:** A 30° hip roof experiences the lowest suction compared to 10° and 20° roofs, making it the safest among the tested configurations.

B. **Building Spacing and Suction Reduction:** Increasing the spacing between buildings reduces wind-induced suction on hip roofs due to interference effects, with varying reductions observed in rectangular, T, and Z arrangements.

C. The value of C_{pe} ranges between -0.89 to -0.15 in the case of the rectangular pattern, -0.89 to -0.05 for the T pattern and -0.86 to -0.01 for the Z pattern when the spacing

between buildings increased from 0 to 2B indicating the reduced suction on the hip roof because of the interference.

D. The value of *IF* ranges between 1.51 to 0.2 in the case of the rectangular pattern, -1.72 to 0.03 for the T pattern and 1.64 to 0.03 for the Z pattern when the spacing between buildings increased from 0 to 2B indicating the reduced suction on the hip roof because of the interference i.e., 80.18% (in rectangular), 100% (in T pattern) and 98.14% (in Z pattern).

E. The value of *ID* ranges between -0.3 to 0.39 in the case of the rectangular pattern, -0.3 to 0.42 for the T pattern and -0.28 to 0.53 for the Z pattern when the spacing between buildings increased from 0 to 2B indicating the reduced suction on the hip roof because of the interference.

F. **Shape and Layout Influence:** The arrangement of multiple hip-roofed buildings significantly affects wind pressure distribution, underlining the importance of strategic building layouts for minimizing wind loads.

G. **Vortex Shedding Mitigation:** Increased spacing between buildings also reduces vortex shedding, enhancing overall structural safety during wind interference.

H. These insights are crucial for optimizing the design and placement of hip roof buildings, ensuring structural integrity, and minimizing wind-related risks. Building designers should consider roof slope, spacing, and overall layout when addressing wind loads in both standalone and clustered building scenarios.

CHAPTER 8

RESULTS AND DISCUSSIONS ON COMPARISON OF CYLINDRICAL, DOME, MONO-SLOPE AND HIP ROOF

8.1 General

There are several types of roof forms provided for low-rise structures, some of them are cylindrical roof, dome roof, mono-slope roof and hip roof. The mono-slope roof is provided with a roof slope from one side due to which one wall is lower and other wall is higher while the hip roof is provided with same roof slope from all four sides which is divided into 4 different portions, i.e., windward and leeward, both in the form of a trapezoidal section and 2 side slopes in the form of a triangular section. This chapter deals with in-depth comparison pressure coefficient, drag and lift coefficient all the four roofs considered for the present research.

8.2 Comparison of Pressure Coefficient (C_{pe})

The variation of C_{pe} with respect of different angles of wind attack for cylindrical roof, dome roof, mono-slope roof and hip roof is shown in Fig. 8.1. The roof slope of mono-slope roof and hip roof is considered to be 30° for the comparison. The angle of wind attack considered for cylindrical roof and hip roof is ranging between 0° to 90° at 15° interval, for dome roof the angle of wind attack is 0°, 45°, 90° and for mono-slope roof the wind angle is varying from 0° to 180° at 15° interval based on their symmetry about central line.

The maximum negative value of C_{pe} for cylindrical roof is -0.90 corresponding to the maximum suction at 15° wind interval and minimum suction occurs at 90° having the value of C_{pe} = -0.44. The value of negative C_{pe} for dome is more or less same at 0° and 45° wind intervals i.e., -0.53 and -0.59. In case of hip roof, the maximum suction is occurring during wind attack of 45° i.e., C_{pe} = -0.60 and minimum suction is at 75° and 90° having the value of C_{pe} as -0.47. The value of C_{pe} for mono-slope roof is increasing in negative magnitude as the wind angle changes from 0° to 165° in which the maximum suction is occurring at 165° wind attack with C_{pe} value of -0.68.

The cylindrical Roof experiences the strongest suction at the apex and leeward side due to its curved geometry and flow separation. On dome roofs, there is smoother flow compared to cylindrical roofs, leading to less extreme pressure coefficients. The mono-slope roof is under high suction at the leading edge (apex), which makes it vulnerable to wind uplift, and the hip roof proves to be the most aerodynamically stable, with more balanced pressure distribution and less severe suction forces.

From Fig. 8.1, it can predict that the critical angle of wind attack for all the roof is different from each other i.e., 15° for cylindrical roof, 45° for dome roof, 165° for mono-slope roof and 45° for hip roof.
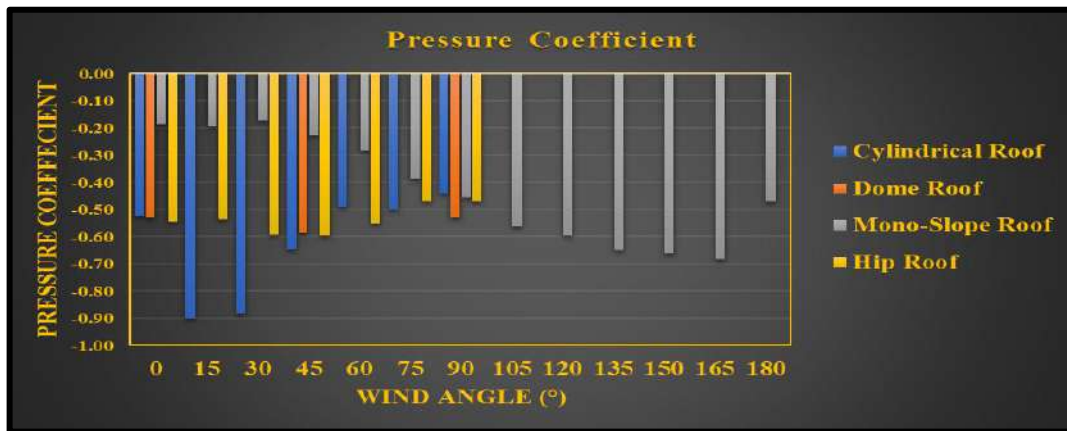
Fig. 8.1: Comparison of Pressure Coefficient

8.3 Comparison of Drag and Lift Coefficients

In wind flow analysis, drag and lift coefficients are significant research variables that are investigated in wind leading and transverse direction. The equations 8.1 & 8.2 show how the design wind pressure and the projected frontal/normal area of the structure are multiplied by the forces acting on the structure both wind leading and transverse direction. Force coefficients in the direction parallel and perpendicular to the direction of wind flow are known as the drag and lift coefficients (C_d and C_l), and they are seen in Figs. 8.2 and 8.3 respectively. These coefficients were determined for the various wind incidence angles in order to examine various roof shapes.

$$C_l = \frac{F_{across}}{0.5 * \rho_{air} * v^2 * L_z * H} \dots\dots\dots\dots\dots\dots\dots\dots\dots\dots\dots\dots\dots\dots\dots\dots\dots\dots\dots\dots (8.1)$$

$$C_d = \frac{F_{along}}{0.5 * \rho_{air} * v^2 * L_x * H} \dots\dots\dots\dots\dots\dots\dots\dots\dots\dots\dots\dots\dots\dots\dots\dots\dots\dots\dots (8.2)$$

Where, F_{across} and F_{along} are the wind forces acting perpendicular and parallel to wind directions, L_z and L_x are the projections length and projection width of the building and H is the maximum height of the building (0.25 m for cylindrical roof building, 0.27 m for mono-slope roof building, 0.21 m for hip roof building and 0.18 m for dome roof building). The fluctuation pattern of C_d and C_l of cylindrical roof and hip roof is similar to each other. The maximum and minimum value of C_d for cylindrical roof building are 0.83 at 90° and -0.62 at 0° respectively while for hip roof building, the maximum and minimum value of C_d are 0.51 at 90° and -0.76 at 0°. In case of mono-slope roof, the maximum and minimum value of C_d are

0.64 at 45° and -1.18 at 180° respectively. The value of C_d -0.85 at 0° and 0.11 at 45° for dome roof building.

The lift coefficient C_l in case of cylindrical roof building is having negative magnitude at all the wind incidence angles as it can be seen in Fig. 8.3. The maximum negative C_l is -0.23 at 30° and minimum is -0.04 at 90° and the maximum value of C_l is 0.24 at 0° and minimum is -0.29 at 45° respectively for hip roof building as shown in Fig. 8.3. Since the dome roof building is symmetric about both the axis, therefore it is having the value of C_l equal to C_d at 45° i.e., 0.11 but C_l at 0° is -0.22. The maximum negative value of C_l = -0.33 is found at 0° and maximum positive C_l = 0.6 at found at 150° in case of mono-slope roof building shown in Fig. 8.3.

The hip roof is most aerodynamically efficient and stable due to its balanced shape, which minimizes both drag and lift. Dome roof experiences lower drag and moderate lift, making it suitable for wind-prone areas. On a cylindrical roof, high lift due to its curved surface makes it vulnerable to wind uplift, though drag is moderate. Mono-slope roof is most vulnerable to wind forces due to its high drag and lift, especially on steep slopes.
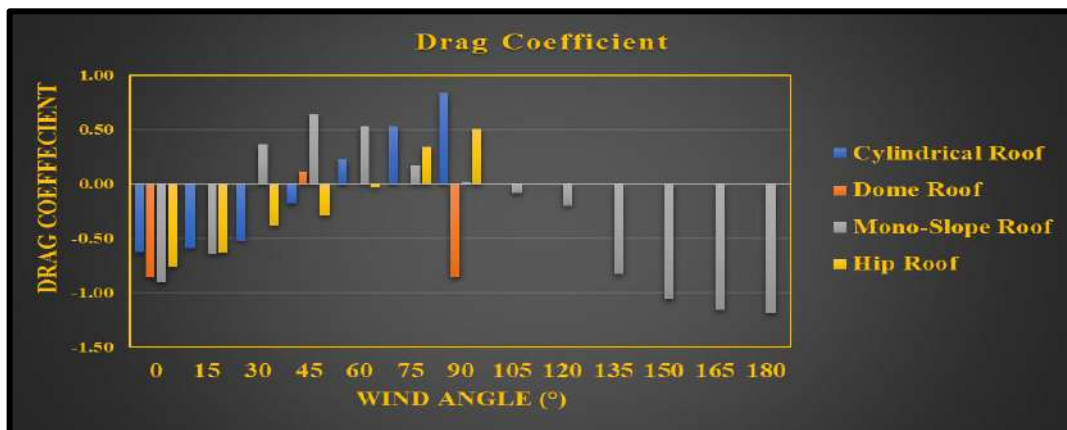
Fig. 8.2: Comparison of Drag Coefficient

Fig. 8.3: Comparison of Lift Coefficient

8.4 Comparison of Wind Flow Pattern on Cylindrical, Dome, Mono-Slope and Hip Roof

The hypothetical routes fluid particles take as they flow vertically around a low-rise building are referred to as "streamlines" in the vertical plane. Since they help engineers and architects comprehend how the wind travels about the building and identify possible weak places, these streamlines are crucial in the construction of low-rise buildings. Computational fluid dynamics (CFD) simulations are frequently used in the design of low-rise structures to evaluate streamlines in the vertical plane. These models may create visualisations of the resulting streamlines and model the wind flow around a building.

The streamlines for all the roof forms considered for the investigation are presented in Fig. 8.4. It has been observed that the cylindrical and dome roof are more behaving like a streamline body to the flow since the wind flow is taking place very smoothly during 0° wind attack. Wind flow follows the curved surface of the cylindrical and dome roof, creating a smooth, continuous flow following the curved shape responsible for low-pressure areas at the apex of the roof. When wind encounters the curved roof of a cylinder, it accelerates as it flows over the apex (similar to how airflow behaves over an air foil). This increase in wind speed at the apex is governed by Bernoulli's principle, which states that an increase in velocity leads to a decrease in pressure. Hence, the suction is higher at the apex. After flowing over the apex, the wind may separate from the roof surface on the leeward side, leading to turbulent flow and a wake region. This separation reduces the effective suction on the leeward portion compared to the apex. The curvature of the cylindrical roof causes streamlines to diverge more at the apex compared to the flatter windward and leeward regions. This results in a pressure distribution where the suction is maximized at the topmost portion of the roof. On the windward side (before the apex), the wind stagnates partially and begins to accelerate as it climbs the curve. The stagnation point at the base of the windward side reduces the suction in this region compared to the apex. On cylindrical or curved roofs, the airflow over the apex can generate stronger vortex shedding or higher shear forces, further enhancing the suction in that area relative to other portions of the roof.

When wind strikes the windward side of the mono-slope roof, the airflow is forced upward along the slope. At the lower edge (base of the slope), the wind velocity is nearly zero, and pressure is at its maximum (stagnation pressure). As the wind flows up the slope, it accelerates, leading to a decrease in pressure (Bernoulli's principle). This creates suction forces (negative pressure) on the windward slope. If the slope is steep, airflow may separate earlier, creating

turbulence near the surface. The apex or top edge of the roof plays a critical role. As the wind flows over the leading edge, it experiences an abrupt change in direction, which causes a sharp increase in wind speed and a strong suction effect. This high suction zone is a critical area for roof design, as it is prone to high uplift forces. Once the wind passes over the apex, the wind often detaches from the roof's surface, especially if the leeward slope is shallow or horizontal. This creates a low-pressure wake region characterized by turbulence and eddies. The pressure in this region is lower than on the windward side, contributing to a net uplift force. The edges of the roof, especially the windward and lateral edges, experience corner vortices due to the interaction of roof and wall surfaces. These vortices generate localized areas of high suction, which can increase the risk of edge lifting or damage if not properly accounted for in the design. If the mono-slope roof has overhangs or gaps at its edges, the wind can interact with these features to amplify uplift forces or create additional turbulence underneath the roof structure.

The wind flow pattern over a hip roof is strongly influenced by its multi-sloped geometry, which helps distribute wind forces more evenly compared to other roof types. When wind approaches the windward side of the hip roof, a stagnation points forms near the lower edge (at the base of the slope), where wind velocity drops to zero and pressure is highest. As the wind flows up the inclined surface, it accelerates, leading to reduced pressure (suction) according to Bernoulli's principle. The gradual slope helps smooth the flow, minimizing sharp pressure gradients and reducing the risk of detachment. At the ridge or apex (the top intersection of the roof slopes), the airflow over the ridge accelerates significantly, creating a zone of high suction (negative pressure). This area is a critical point for uplift forces. The curved geometry of the roof prevents abrupt flow separation, allowing wind to flow smoothly over the apex in most cases. As the wind passes over the apex and moves down the leeward side, depending on the roof pitch, the wind may partially separate from the surface, creating a low-pressure wake region on the leeward slope. The pressure on the leeward side is lower than on the windward side but generally more uniform due to the sloping design. The inclined corners where roof planes meet (the hips) experience unique airflow characteristics. Wind tends to converge along these edges, increasing wind speeds locally and creating slightly higher suction forces compared to flat planes. At the lower edges and corners of the roof, small vortices may form, causing localized turbulence and pressure fluctuations. If the wind direction is oblique to the roof, the side slopes experience lower wind speeds and pressures compared to the directly windward slope. Uneven pressure distribution across the roof can create torsional forces on the structure.
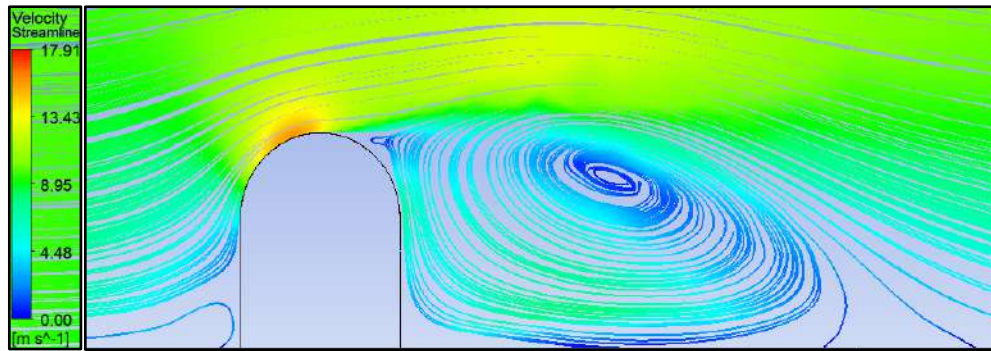
Fig. 8.4(a): Wind Flow Streamlines over the cylindrical roof
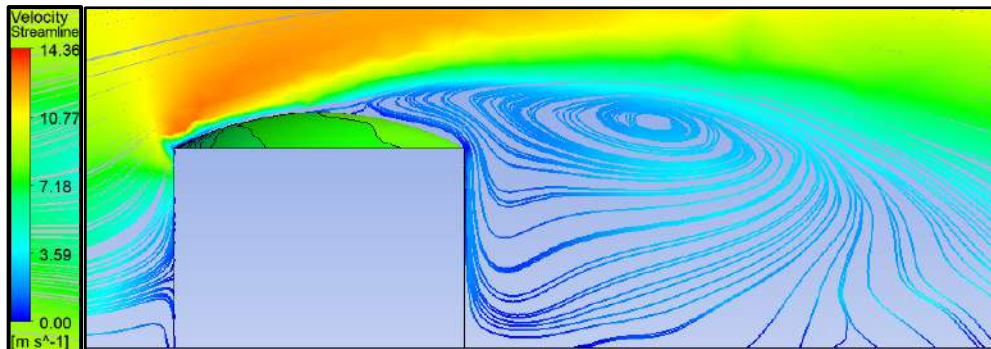
Fig. 8.4(b): Wind Flow Streamlines over dome roof
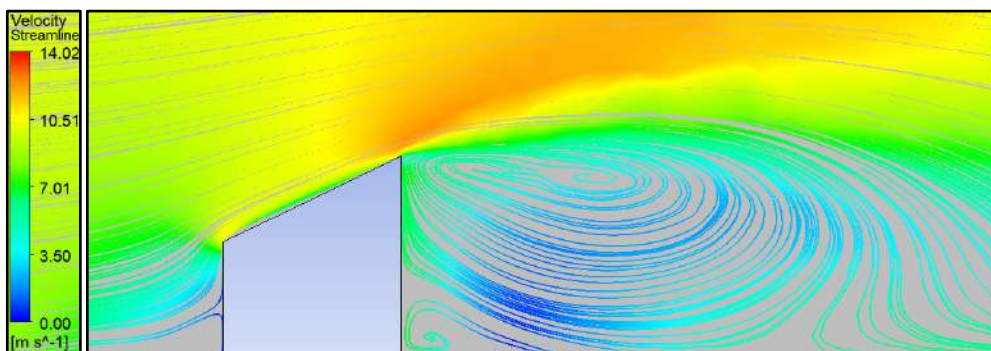
Fig. 8.4(c): Wind Flow Streamlines over mono-slope roof
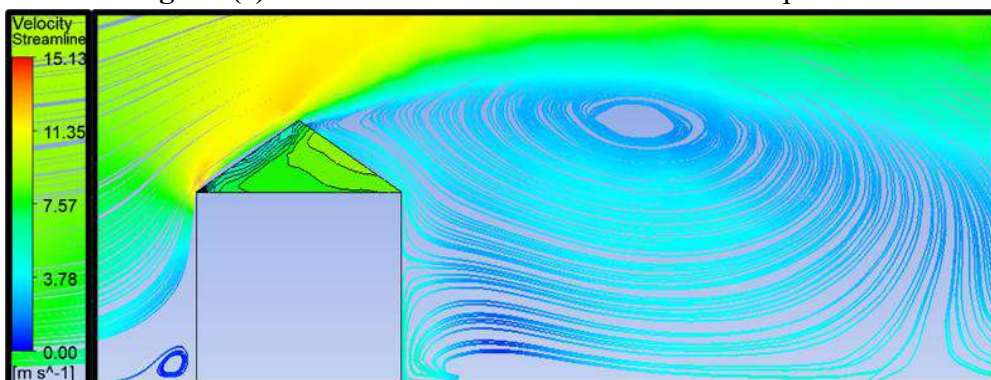
Wind Flow Streamlines over hip roof
Fig. 8.4(d): Wind Flow Streamlines over different roofs

8.5. Comparison of Interference Conditions

It is well known fact that the wind-induced pressure gets modified on the structures due to the presence of surrounding buildings. In present research, the wind-induced pressure is studied on

all the mentioned roofs under different interfering condition as discussed in previous chapters. In this section, the C_{pe}, *IF*, *ID* are compared and presented in table 8.1. The structure designer needs to consider the range of mentioned parameters while designing the low-rise rise structures with roof shapes under different interfering conditions. The comparison of behaviour of various roofs under different interference condition is shown in table 8.2.

Table 8.1 Comparison of Interference Parameters

Interference Pattern	Interference Parameters	Dome Roof	Cylindrical Roof	Mono-Slope Roof	Hip Roof
Rectangular Pattern	C_{pe}	-0.91 to -0.05	-1.02 to -0.08	-1.14 to 0.00	-0.89 to -0.1
	IF	1.7 to 0.12	1.63 to 0.19	3.97 to -0.90	1.51 to 0.2
	ID	0.47 to -0.51	0.73 to -0.36	0.4 to -0.55	0.42 to -0.3
T Pattern	C_{pe}	-0.95 to +0.1	-1.17 to -0.07	-1.0 to 3.8	-0.89 to 0.00
	IF	1.65 to -0.19	2.05 to 0.1	1.78 to -0.48	1.9 to 0.04
	ID	0.63 to -0.36	0.74 to -0.55	0.11 to -1.0	0.52 to -0.42
Z Pattern	C_{pe}	-0.98 to 0.00	-1.29 to -0.05	-1.0 to 0.55	-0.89 to 0.00
	IF	1.87 to 0.01	1.84 to 0.11	3.8 to -0.8	1.72 to 0.03
	ID	0.53 to -0.46	0.73 to -0.44	1.23 to -0.48	0.53 to -0.34

Table 8.2 Comparison of behaviour under different interference conditions

Roof Type	Interference Sensitivity	Key Effects	Overall Stability
Cylindrical Roof	High	Amplified suction at apex, intensified leeward turbulence, vortex shedding	Moderate (requires reinforcement)
Dome Roof	Low to Moderate	Slightly increased suction at apex, minimal wake amplification	High (stable geometry)
Mono-Slope Roof	High	Increased drag and uplift at windward edges, strong turbulence at the leeward side	Low (high risk of damage)
Hip Roof	Low	Slightly increased suction at ridge and edges, balanced pressure distribution	Very High (most stable)

In summary, cylindrical and dome roofs offer excellent wind resistance but less flexible in design. Mono-slope roofs are simple but have a higher risk of wind damage and collapse. Hip roofs offer a balance between wind resistance and design flexibility but are more complex than

mono-slope roofs. The comparison of different roofs based on wind effects, advantages and disadvantages is shown in table 8.3.

Table 8.3 Comparison based on wind effects, advantages and disadvantages

Parameters	Cylindrical Roof	Dome Roof	Mono-Slope Roof	Hip Roof
Wind Effects	Least affected by wind due to curved shape	Similar to cylindrical roofs, wind flows around the dome-shape	Wind can create uplift and detachment risk	Wind can create uplift and detachment risk at the ridge
	Wind flows around the roof, reducing the pressure	Reduced uplift and detachment risk	Increased pressure on the windward side	Increased pressure on the windward side
	Minimal uplift and detachment risk	May experience increased pressure at the base	May experience wind-driven rain and debris damage	May experience wind-driven rain and debris damage
Advantages	Excellent wind resistance	Excellent wind resistance	Simple and cost-effective design	Good wind resistance compared to mono-slope roofs
	Reduced risk of damage and collapse	Reduced risk of damage and collapse	Easy to construct and maintain	Reduced risk of damage and collapse
Disadvantages	Higher construction costs	Higher construction costs	Higher risk of wind damage and collapse	More complex design and construction
	Limited design flexibility	Limited design flexibility	Limited design flexibility	Higher construction costs

CHAPTER 9
CONCLUSIONS

9.1 General

In present research, the wind effects on different types of roofs of low-rise structures have been investigated using Ansys CFX platform in three different phases. Four different roofs i.e., dome roof, cylindrical roof, mono-slope roof and hip roof were considered for the investigation. In first phase, the isolated models of roofs were subjected to different angles of wind attack ranging between 0° to 90° (hip and cylindrical roofs), 0° to 180° (mono-slope roof) and 0° & 45° (dome roof) at 15° wind interval to find out the effects of wind on roofs of low-rise structures. In second phase, different roof configurations of mono-slope roof and hip roof provided with different roof slopes i.e., 10°, 20° and 30° were subjected to wind attack to find out the effect of roof slope. In third phase, the effect of interference has been investigated between the roofs arranged in different configurations i.e., rectangular, Z and T pattern with variable spacing between i.e., zero, 0.5B, B, 1.5B and 2B (where B is width of the building). The results obtained from the study have been discussed in detail in chapter 5, 6, 7 and 8. The conclusions drawn from the research are included in this chapter.

9.2 Conclusions for Dome Roof

a) Current wind load standards provide limited guidance on wind pressure distribution for low-rise domical roofs, covering only a narrow range of wind angles. However, simulations show that wind pressure coefficients vary significantly with wind direction, emphasizing the need for designers to consider the worst-case wind scenario to ensure structural safety and economy.

b) The pressure coefficient (C_{pe}) values taken in the codal provisions are of higher magnitude as compared to the values obtained from experimental and CFD investigation, which means that the codal values are over estimated i.e., 69.81% and less considerate for complex roof shapes.

c) The critical angle of wind attack is 45° during which the maximum suction is occurring on the dome roof.

d) The range of C_{pe} is -0.99 to -0.06 for the rectangular pattern, -0.91 to 0.00 for the Z pattern and -0.88 to -0.04 for the T pattern which keeps on reducing by increasing the spacing between the buildings from 0 to 2B.

e) The range of interference factor (*IF*) is 1.7 to 0.12 for the rectangular pattern, 1.87 to 0.01 for the Z pattern and 1.65 to 0.19 for the T pattern which keeps on reducing by increasing the spacing between the buildings from 0 to 2B.

f) The range of interference difference (*ID*) is -0.41 to 0.47 for the rectangular pattern, -0.46 to 0.53 for the Z pattern and -0.29 to 0.63 for the T pattern which keeps on reducing by increasing the spacing between the buildings from 0 to 2B.

g) The dome roof acts like a streamlined body, which helps reduce the pressure on the roof from higher negative magnitudes to lower negative magnitudes.

h) Since the buildings were shielded from all directions during the rectangular arrangement, the rectangular pattern has proved to be more beneficial during interference than the T and Z patterns.

9.3 Conclusions for Cylindrical Roof

a) Mostly, cylindrical roof experiences a pulling force (suction) rather than a pushing force (pressure), with the strongest suction force occurring at the top of the roof, near the edge facing the wind direction. This highlights the importance of considering wind-induced suction forces when designing and constructing cylindrical roofs to ensure their stability and safety.

b) The critical angle of wind attack, which is responsible for maximum suction on cylindrical roofs, is 15° and 30°.

c) The value of pressure coefficient (C_{pe}) ranges between -1.00 to -0.08 in the case of the rectangular pattern, -1.29 to -0.12 for the Z pattern and -1.17 to -0.05 for the T pattern when the spacing between buildings increased from 0 to 2B indicating the reduced suction on the cylindrical roof because of the interference i.e., 84.90% (in rectangular), 86.79% (in T pattern) and 90.56% (in Z pattern).

d) The value of interference factor (*IF*) ranges between 1.63 to 0.19 in the case of the rectangular pattern, 1.84 to 0.2 for the Z pattern and 2.05 to 0.1 for the T pattern when the spacing between buildings increased from 0 to 2B indicating the reduced suction on the cylindrical roof because of the interference.

e) The value of interference difference (*ID*) ranges between -0.36 to 0.55 in the case of the rectangular pattern, -0.44 to 0.72 for the Z pattern and -0.53 to 0.74 for the T pattern when the spacing between buildings increased from 0 to 2B indicating the reduced suction on the cylindrical roof because of the interference.

f) The distribution of wind pressure on the windward side of rectangular, T, and Z-shaped buildings is similar to that of a single-span building. However, the leeward side (the side

opposite to the wind direction) experiences a relatively uniform suction force, with the maximum suction being approximately half of the pressure on the windward side. This suggests that the windward side provides a shielding effect, reducing the wind pressure on the leeward side.

g) Due to the dominance of the shielding effect in the rectangular arrangement of buildings, the rectangular pattern proves to be more beneficial and stable than that of the T and Z patterns.

h) The wind pressure coefficients, which are used to calculate wind loads on cylindrical roofs, are significantly affected by the angle at which the wind hits the roof. Therefore, designers must carefully determine the most critical wind direction, which will have the greatest impact on the structural system of the curved roof, and use this information to design the roof's structural system to ensure its stability and safety.

9.4 Conclusions for Mono-Slope Roof

a) The pressure distribution over the mono-slope roof is suction in nature.

b) The pressure coefficient on a mono-slope roof is reduced by an increase in roof slope 10°, 20° and 30°. The minimum pressure coefficient (C_{pe}) is obtained for a 30° mono-slope roof.

c) The critical angle of wind attack on mono-slope roof is 165° which is responsible for the maximum suction.

d) The value of pressure coefficient (C_{pe}) ranges between -1.07 to 0.17 in the case of the rectangular pattern, -1.25 to 0.22 for the Z pattern and -1.00 to 0.11 for the T pattern when the spacing between buildings increased from 0 to 2B indicating the reduced suction on the mono-slope roof because of the interference i.e., 84.69% (in rectangular), 89.11% (in T pattern) and 82.03% (in Z pattern).

e) The value of interference factor (*IF*) ranges between 3.97 to -0.91 in the case of the rectangular pattern, 3.81 to -0.85 for the Z pattern and 3.91 to -0.68 for the T pattern when the spacing between buildings increased from 0 to 2B indicating the reduced suction on the mono-slope roof because of the interference.

f) The value of interference difference (*ID*) ranges between -0.56 to 0.38 in the case of the rectangular pattern, -0.45 to 0.4 for the Z pattern and -0.49 to 1.23 for the T pattern when the spacing between buildings increased from 0 to 2B indicating the reduced suction on the mono-slope roof because of the interference.

g) From the arrangement of mono-slope roof buildings in rectangular, Z and T patterns with variable spacing, the rectangular pattern is more beneficial as compared to the Z and T pattern.

9.5 Conclusions for Hip Roof

a) The wind creates a suction force on most of the hip roof, which can pull the roof upwards, while a small area near the windward edge experiences a pressure force, which pushes the roof in the downstream direction. This highlights the importance of considering both pressure and suction forces when designing and constructing hip roofs to ensure their stability and safety.

b) There is a uniform distribution of wind-induced pressure along the long edge over most of the two side slopes. The highest mean suction appears in the area, which is close to the roof corners behind the windward hip ridge.

c) The suction on the 30° hip roof is lowest as compared to 10° and 20° hip roofs, which makes the 30° hip roof safer than other hip roofs.

d) The critical angle of wind attack is 45° at which there was maximum suction on hip roof.

e) The value of pressure coefficient (C_{pe}) ranges between -0.89 to -0.15 in the case of the rectangular pattern, -0.89 to -0.05 for the T pattern and -0.86 to -0.01 for the Z pattern when the spacing between buildings increased from 0 to 2B indicating the reduced suction on the cylindrical roof because of the interference.

f) The value of interference factor (*IF*) ranges between 1.51 to 0.2 in the case of the rectangular pattern, -1.72 to 0.03 for the T pattern and 1.64 to 0.03 for the Z pattern when the spacing between buildings increased from 0 to 2B indicating the reduced suction on the cylindrical roof because of the interference i.e., 80.18% (in rectangular), 100% (in T pattern) and 98.14% (in Z pattern).

g) The value of interference difference (*ID*) ranges between -0.3 to 0.39 in the case of the rectangular pattern, -0.3 to 0.42 for the T pattern and -0.28 to 0.53 for the Z pattern when the spacing between buildings increased from 0 to 2B indicating the reduced suction on the cylindrical roof because of the interference.

h) The shape formed by the arrangement of multiple hip roof buildings influences the way wind pressure is distributed across the roofs. This suggests that building designers and engineers should consider the overall layout and arrangement of buildings when assessing wind loads and designing the structural systems of hip roof buildings.

9.6 Conclusions from the comparison of dome, cylindrical, mono-slope and hip roofs

a) The study highlights that the critical angle of wind attack varies for different roof types due to their geometric configurations and aerodynamics i.e. for cylindrical roof the critical angle is 15°, 45° for dome roof and hip roof and 165° for mono-slope roof.

b) Cylindrical and dome roofs offer excellent wind resistance especially when the angle of wind attack is 0° due to the smooth and streamlined wind flow around the roof but are less flexible in design.

c) Mono-slope roofs are simple but have a higher risk of wind damage and collapse.

d) Hip roofs offer a balance between wind resistance and design flexibility but are more complex than mono-slope roofs.

e) The rectangular pattern arrangement with variable spacing is more beneficial and stable than that of the T and Z patterns.

9.7 Recommendations

a) The findings underscore the need for a more nuanced approach to wind load analysis and design, encouraging designers to consider aerodynamic behavior, interference effects, and realistic wind pressure distributions to ensure the safety and efficiency of domical, cylindrical, mono-slope and hip roof structures.

b) The insights emphasize the need for meticulous wind load analysis and interference consideration in the design and construction of domical, cylindrical, mono-slope and hip roofs and nearby structures.

c) The optimal aerodynamic performance and reduced suction, a 30° mono-slope roof in a rectangular building pattern with increased spacing from zero to 2B, is the most effective configuration.

d) The insights are crucial for optimizing the design and placement of hip roofs, ensuring structural integrity, and minimizing wind-induced risk. Building designers should consider roof slope, spacing and overall layout when addressing wind loads in both standalone and clustered building scenarios.

9.8 Future Scope of work

The present thesis is a numerical research work carried out on the models of low-rise buildings of various roof geometries using Ansys CFX in order to study the influence of geometrical shapes on wind pressure distribution. However, there still exists vast area in which research is required to be carried out in future. Some of the areas which can be explored are listed below.

a) Low-rise buildings with square and rectangular plan are considered in the present study. Buildings with circular plan can also be considered.

b) Four types of roof forms namely domical roof, cylindrical roof, mono-slope roof and hip roof are considered in the present study. Wind pressure distribution on buildings with other roof forms such as conical and skylight roofs can also be investigated.

c) Present study includes clad buildings with different roof forms but with no openings on walls. Effects of openings on both internal and external wind pressures on such buildings can also be studied.

d) Effects of interference between the buildings of same shape and size are studied for certain arrangements. It is possible to consider few more arrangements of them.

e) Only values of mean wind pressure coefficients are reported in this thesis. Values of fluctuating components of wind pressures can also be investigated and reported.

REFERENCES

1. Ahmad, S. and Kumar, K. 2001. "Interference Effects on Wind Loads on Low-Rise Hip Roof Buildings." Engineering Structures 23:1577–89.

2. Ai, Z. T., and Mak, C.M. 2013. "CFD Simulation of Flow and Dispersion around an Isolated Building: Effect of Inhomogeneous ABL and near-Wall Treatment." Atmospheric Environment 77:568–78. doi: 10.1016/j.atmosenv.2013.05.034.

3. Akon, A. F. and Gregory, A. K. 2016. "Mean Pressure Distributions and Reattachment Lengths for Roof-Separation Bubbles on Low-Rise Buildings." Journal of Wind Engineering and Industrial Aerodynamics 155:115–25. doi: 10.1016/j.jweia.2016.05.008.

4. Alrawashdeh, H., and Stathopoulos, T. 2015. "Wind Pressures on Large Roofs of Low Buildings and Wind Codes and Standards." Journal of Wind Engineering and Industrial Aerodynamics 147:212–25.

5. Amreshwar, K. 2005. "Wind Pressure Distribution On Elevated Structures With Curved Roofs." IIT, Roorkee.

6. Bitsuamlak, G. T., Workamaw, W., Edward, L. and Chowdhury, A.G. 2013. "Aerodynamic Mitigation of Roof and Wall Corner Suctions Using Simple Architectural Elements." Journal of Engineering Mechanics 139(3):396–408. doi: 10.1061/(asce)em.1943-7889.0000505.

7. Blaabjerg, F. and Ke, M. 2017. "Wind Energy Systems." Proceedings of the IEEE 105(11):2116–31. doi: 10.1109/JPROC.2017.2695485.

8. Blocken, B., and Carmeliet, J. 2010. "Overview of Three State-of-the-Art Wind-Driven Rain Assessment Models and Comparison Based on Model Theory." Building and Environment 45(3):691–703. doi: 10.1016/j.buildenv.2009.08.007.

9. Blocken, B., and Gualtieri, C. 2012. "Ten Iterative Steps for Model Development and Evaluation Applied to Computational Fluid Dynamics for Environmental Fluid Mechanics." Environmental Modelling and Software 33:1–22. doi: 10.1016/j.envsoft.2012.02.001.

10. Blocken, B., Janssen, W. D. and Hooff, T. V. 2012. "CFD Simulation for Pedestrian Wind Comfort and Wind Safety in Urban Areas: General Decision Framework and Case Study for the Eindhoven University Campus." Environmental Modelling and Software 30:15–34. doi: 10.1016/j.envsoft.2011.11.009.

11. Blocken, B. and Stathopoulos, T. 2013. "CFD Simulation of Pedestrian-Level Wind Conditions around Buildings: Past Achievements and Prospects." Journal of Wind Engineering and Industrial Aerodynamics 121(c):138–45. doi: 10.1016/j.jweia.2013.08.008.

12. Blocken, B. 2014. "50 Years of Computational Wind Engineering: Past, Present and Future." Journal of Wind Engineering and Industrial Aerodynamics 129:69–102. doi: 10.1016/j.jweia.2014.03.008.

13. Blocken, B. 2015. "Computational Fluid Dynamics for Urban Physics: Importance, Scales, Possibilities, Limitations and Ten Tips and Tricks towards Accurate and Reliable Simulations." Building and Environment 91:219–45. doi: 10.1016/j.buildenv.2015.02.015.

14. Blocken, B, and Carmeliet, J. 2004. "A Review of Wind-Driven Rain Research in Building Science." 92(13):1079–1130.

15. Blocken, B., Stathopoulos, T. and Carmeliet, J. 2007. "CFD Simulation of the Atmospheric Boundary Layer: Wall Function Problems." Atmospheric Environment 41(2):238–52. doi: 10.1016/j.atmosenv.2006.08.019.

16. Cermak, J. E. 1990. "Physical-Modeling Investigations for Wind Engineering: Applications beyond Wind-Load Determinations." Journal of Wind Engineering and Inductrial Aerodynamics 36(1):39–52. doi: https://doi.org/10.1016/0167-6105(90)90291-J.

17. Chen, B., Cheng, H., Kong, H., Chen, X. and Yang, Q. 2019. "Interference Effects on Wind Loads of Gable-Roof Buildings with Different Roof Slopes." Journal of Wind Engineering and Industrial Aerodynamics 189:198–217. doi: 10.1016/j.jweia.2019.03.033.

18. Cochran, L. S., and Cermak, J. E. 1992. "Full- and Model-Scale Cladding Pressures on the Texas Tech University Experimental Building." Journal of Wind Engineering and Industrial Aerodynamics 43(1–3):1589–1600. doi: 10.1016/0167-6105(92)90374-J.

19. Davenport, A. G., Surry, D. and Stathopoulos, T. 1977. "'Wind Loads on Low-Rise Buildings." Final Report of Phases I and II - Parts 1 and 2', BL WT Report SS8-19 77, The University of Western Ontario, London, Ontario, Canada, Nov.

20. Davenport, A. G., and Isyumov, N. 1967. "The Application of the Boundary Layer Wind Tunnel to the Prediction of Wind Loading." 201–28.

21. Faghih, A. K. and Bahadori, M. N. 2010. "Three Dimensional Numerical Investigation of Air Flow over Domed Roofs." Journal of Wind Engineering and Industrial Aerodynamics 98(3):161–68. doi: 10.1016/j.jweia.2009.10.012.

22. Fouad, N. S., Mahmoud, G.H. and Nasr, N. E. 2018. "Comparative Study of International Codes Wind Loads and CFD Results for Low Rise Buildings." Alexandria Engineering Journal 57(4):3623–39. doi: 10.1016/j.aej.2017.11.023.

23. Franke, J., Hellsten, A., Schlünzen, H. and Carissimo, B. 2007. "Guideline for the CFD Simulation of Flows in the Urban Environment." COST Action 732 Quality Assurance and Improvement of Microscale Meteorological Models.

24. Garret, J. R. 1984. The Atmospheric Boundary Layer. Cambridge: Cambridge University Press.

25. Ginger, J. D., and Holmes, J. D. 2003. "Effect of Building Length on Wind Loads on Low-Rise Buildings with a Steep Roof Pitch." Journal of Wind Engineering and Industrial Aerodynamics 91(11):1377–1400. doi: 10.1016/j.jweia.2003.08.003.

26. Guha, T. K., Sharma, R. N. and Richards, P. J. 2012. "Internal Pressure in a Building with Multiple Dominant Openings in a Single Wall: Comparison with the Single Opening Situation." Journal of Wind Engineering and Industrial Aerodynamics 107–108:244–55. doi: 10.1016/j.jweia.2012.04.023.

27. Haines, M. and Taylor, I. 2018. "Numerical Investigation of the Flow Field around Low Rise Buildings Due to a Downburst Event Using Large Eddy Simulation." Journal of Wind Engineering and Industrial Aerodynamics 172(July 2017):12–30. doi: 10.1016/j.jweia.2017.10.028.

28. Ho, T. C. E., Surry, D., Morrish, D. and Kopp, G. A. 2005. "The UWO Contribution to the NIST Aerodynamic Database for Wind Loads on Low Buildings: Part 1. Archiving Format and Basic Aerodynamic Data." Journal of Wind Engineering and Industrial Aerodynamics 93(1):1–30. doi: 10.1016/j.jweia.2004.07.006.

29. Holmes, J. D. 1983. Wind Loads on Low Rise Buildings - A Review. Highett, Victoria, Australia.

30. Hooff, T. V., Blocken, B. and Tominaga, Y. 2017. "On the Accuracy of CFD Simulations of Cross-Ventilation Flows for a Generic Isolated Building: Comparison of RANS, LES and Experiments." Building and Environment 114:148–65. doi: 10.1016/j.buildenv.2016.12.019.

31. Hoq, S. M. A., and Judd, J. P. 2021. "Comparison of Wind Tunnel Test Data for Low-Rise Buildings with Main Wind Force Resisting System Design Procedures." Buildings 11(8). doi: 10.3390/buildings11080342.

32. Hoxeya, R. P., Robertsona, A. P., Basarab, B. and Younis, B. A. 1993. "Geometric Parameters That Affect Wind Loads on Low-Rise Buildings: Full-Scale and CFD Experiments." Journal of Wind Engineering and Industrial Aerodynamtcs 50:243–52.

33. Hu, G., Tse, K. T., Kwok, K. C. S. and Zhang, Y. 2015. "Large Eddy Simulation of Flow around an Inclined Finite Square Cylinder." Journal of Wind Engineering and Industrial Aerodynamics 146:172–84. doi: 10.1016/j.jweia.2015.08.008.

34. Jameel, A., Irtaza, H. and Javed, M. A. 1970. "Study of Wind Forces on Low-Rise Hip-Roof Building." International Journal of Engineering, Science and Technology 7(2):43–53. doi: 10.4314/ijest.v7i2.4.

35. Janajreh, I. and Simiu, Ed. 2012. "Large Eddy Simulation of Wind Loads on a Low-Rise Structure and Comparison with Wind Tunnel Results." Applied Mechanics and Materials 152–154:1806–13. doi: 10.4028/www.scientific.net/AMM.152-154.1806.

36. Jensen, M. 1958. "The Modal-Law for Phenomena in Natural Wind".

37. Kasperski, M. 1996. "Design Wind Loads for Low-Rise Buildings: A Critical Review of Wind Load Specifications for Industrial Buildings." Journal of Wind Engineering and Industrial Aerodynamics 61(2–3):169–79. doi: 10.1016/0167-6105(96)00051-7.

38. Kind, R. J. and Wardlaw, R. L. 1979. "Model Studies of the Wind Resistance of Two Loose-Laid Roof-Insulation Systems".

39. Kobayashi, T., Sandberg, M., Kotani, H. and Claesson, L. 2010. "Experimental Investigation and CFD Analysis of Cross-Ventilated Flow through Single Room Detached House Model." Building and Environment 45(12):2723–34. doi: 10.1016/j.buildenv.2010.06.001.

40. Kopp, G. A. and Morrison, M. J. 2018. "Component and Cladding Wind Loads for Low-Slope Roofs on Low-Rise Buildings." Journal of Structural Engineering 144(4). doi: 10.1061/(asce)st.1943-541x.0001989.

41. Krishna, P. 1995. "Wind Loads on Low Rise Buildings-A Review".

42. Kumar, K. S. and Stathopoulos, T. 2000. "Wind Loads on Low Building Roofs: A Stochastic Perspective".

43. Kumar, R. 1991. "Mean Wind Pressure Distribution on Convex Cylindrical Roof." IIT, Roorkee.

44. Lin, J., and Surry, D. 1998. "The Variation of Peak Loads with Tributary Area near Corners on Flat Low Building Roofs." Journal of Wind Engineering and Industrial Aerodynamics 77–78:185–96. doi: 10.1016/S0167-6105(98)00142-1.

45. Lin, J. X., Surry, D. and Tieleman, H. W. 1995. "The Distribution of Pressure near Roof Corners of Flat Roof Low Buildings." Journal of Wind Engineering and Industrial Aerodynamics 56(2–3):235–65. doi: 10.1016/0167-6105(94)00089-V.

46. Liu, J. and Niu, J. 2016. "CFD Simulation of the Wind Environment around an Isolated High-Rise Building: An Evaluation of SRANS, LES and DES Models." Building and Environment 96:91–106. doi: 10.1016/j.buildenv.2015.11.007.

47. Meecham, D. 1992. "The Improved Performance of Hip Roofs in Extreme Winds — A Case Study." Journal of Wind Engineering and Industrial Aerodynamics 43(1):1717–1726. doi: https://doi.org/10.1016/0167-6105(92)90583-V.

48. Meecham, D., Surry, D. and Davenport, A. G. 1991. The Magnitude and Distribution of Wind-Induced Pressures on Hip and Gable Roofs.

49. Mo, J. O., Choudhry, A. Arjomandi, M. and Lee, Y. H. 2013. "Large Eddy Simulation of the Wind Turbine Wake Characteristics in the Numerical Wind Tunnel Model." Journal of Wind Engineering and Industrial Aerodynamics 112:11–24. doi: 10.1016/j.jweia.2012.09.002.

50. Mochida, A. and Lun, I. Y. F. 2008. "Prediction of Wind Environment and Thermal Comfort at Pedestrian Level in Urban Area." Journal of Wind Engineering and Industrial Aerodynamics 96(10–11):1498–1527. doi: 10.1016/j.jweia.2008.02.033.

51. Montazeri, H., and Blocken, V. 2013. "CFD Simulation of Wind-Induced Pressure Coefficients on Buildings with and without Balconies: Validation and Sensitivity Analysis." Building and Environment 60:137–49. doi: 10.1016/j.buildenv.2012.11.012.

52. Moonen, P., Defraeye, T., Dorer, V., Blocken, V. and Carmeliet, J. 2012. "Urban Physics: Effect of the Micro-Climate on Comfort, Health and Energy Demand." Frontiers of Architectural Research 1(3):197–228. doi: 10.1016/j.foar.2012.05.002.

53. Natalini, M. B., Morel, C. and Natalini, B. 2013. "Mean Loads on Vaulted Canopy Roofs." Journal of Wind Engineering and Industrial Aerodynamics 119:102–13. doi: 10.1016/j.jweia.2013.05.001.

54. Ozmen, Y., E. B., and Beeck, J. P. A. J. V. 2016. "Wind Flow over the Low-Rise Building Models with Gabled Roofs Having Different Pitch Angles." Building and Environment 95:63–74. doi: 10.1016/j.buildenv.2015.09.014.

55. Prandtl, L. 1905. "Über Flüssigkeitsbewegung Bei Sehr Kleiner Reibung." Pp. 484–91 in Verhandlungen des III. Internationalen Mathematiker-Kongresses, Heidelberg. Teubner, Leipzig.

56. Prasad, D., Uliate, T. and Rafiuddin, M. A. 2009. "Wind Loads on Low-Rise Building Models with Different Roof Configurations." International Journal of Fluid Mechanics Research 36(3):231–43. doi: 10.1615/InterJFluidMechRes.v36.i3.30.

57. Qiu, Y., Sun, Y., Wu, Y. and Tamura, T. 2014. "Modeling the Mean Wind Loads on Cylindrical Roofs with Consideration of the Reynolds Number Effect in Uniform Flow with Low Turbulence." Journal of Wind Engineering and Industrial Aerodynamics 129:11–21. doi: 10.1016/j.jweia.2014.02.011.

58. Rani, N., and Ahuja, A. K. 2017. "Wind Pressure Distribution on Circular Canopy Roofs." in Resilient Structures and Sustainable Construction, edited by E. Pellicer, J. M. Adam, V. Yepes, A. Singh, and S. Yazdani. ISEC Press.

59. Rani, N. and Ahuja, A. K. 2017. "Effect of Blockage of Wind Loads on Mono-Slope Canopy Roofs." in International Conference on Recent Advances in Civil Engineering (ICRACE 2017).

60. Rani, N. and Ahuja, A. K. 2018. "Wind Loads on Multi-Span Mono-Slope Canopy Roof." in Urbanization Challenges in Emerging Economies.

61. Ricci, M., Patruno, L. and Miranda, S. D. 2017. "Wind Loads and Structural Response: Benchmarking LES on a Low-Rise Building." Engineering Structures 144:26–42. doi: 10.1016/j.engstruct.2017.04.027.

62. Richards, P. J. and Norris, S. E. 2011. "Appropriate Boundary Conditions for Computational Wind Engineering Models Revisited." Journal of Wind Engineering and Industrial Aerodynamics 99(4):257–66. doi: 10.1016/j.jweia.2010.12.008.

63. Saathoff, P., and Stathopoulos, T. 1992. "Wind Loads on Buildings with Sawtooth Roofs." Journal of Structural Engineering 118(2):429–46.

64. Shao, S., Stathopoulos, T., Yang, Q. and Tian, Y. 2018. "Wind Pressures on 4:12-Sloped Hip Roofs of L- and T-Shaped Low-Rise Buildings." Journal of Structural Engineering 144(7):04018088. doi: 10.1061/(asce)st.1943-541x.0002077.

65. Sharma, D., Pal, S. and Raj, R. 2023a. "Effect of Spacing on Wind-Induced Interference on the Roof of Low-Rise Buildings with Cylindrical Roof Using CFD Simulation." Sadhana - Academy Proceedings in Engineering Sciences 48(4). doi: 10.1007/s12046-023-02351-5.

66. Sharma, D., Pal, S. and Raj, R. 2023b. "Numerical Prediction of the Proximity Effects on Wind Loads of Low - Rise Buildings with Cylindrical Roofs." Wind and Structures, An International Journal 4:277–92. doi: https://doi.org/10.12989/was.2023.36.4.277.

67. Sharma, D., Raj, R. and Pal, S. 2023c. "Effects of Roof Shapes on Wind Pressure Distribution of Multi-Span Low-Rise Buildings." Proceedings of International Structural Engineering and Construction 10(1):1–6. doi: 10.14455/10.14455/isec.2023.10(1).str-19.

68. Sharma, D., Raj, R. and Pal, S. 2024. "Effects of Different Types of Roofs under Wind Loads for Low-Rise Structures." in AIP Conference Proceedings. Vol. 030008.

69. Singh, J. and Roy, A. K. 2018. "Wind Pressure Coefficients on Pyramidal Roof of Square Plan Low Rise Double Storey Building." Computational Engineering and Physical Modeling 1(1):1–16. doi: 10.22115/cepm.2019.144599.1043.

70. Singh, J. and Roy, A. K. 2019a. "CFD Simulation of the Wind Field around Pyramidal Roofed Single-Story Buildings." SN Applied Sciences 1(11). doi: 10.1007/s42452-019-1476-2.

71. Singh, J. and Roy, A. K. 2019b. "Effects of Roof Slope and Wind Direction on Wind Pressure Distribution on the Roof of a Square Plan Pyramidal Low-Rise Building Using CFD Simulation." International Journal of Advanced Structural Engineering 11(2):231–54. doi: 10.1007/s40091-019-0227-3.

72. Stathopoulos, T. 1979. "Turbulent Wind Actions on Low-Rise Buildings." University of Western Ontario, Ontario, Canada.

73. Stathopoulos, T. 1987. "Wind Pressures on Flat Roof Edges and Corners." in 7th Int. Conf. on Wind Engineering, Aachen, Germany.

74. Stathopoulos, T., and Surry, D. 1983. "Scale Effects in Wind Tunnel Testing of Low Buildings." Journal of Wind Engineering and Industrial Aerodynamics 13(1–3):313–26. doi: 10.1016/0167-6105(83)90152-6.

75. Stathopoulos, T., Surry, D. and Davenport, M. 1981. "Effective Wind Loads On Flat Roofs." Journal of Structural Division 107(2):291–98.

76. Stathopoulos, T. and Yongsheng, Z. 1993. "Computation Of Wind Pressures On L-Shaped Buildings." Journal of Engineering Mechanis 119(8):1526–41.

77. Stathopoulos, T. 1984. "Wind Loads on Low-Rise Buildings: A Review of the State of the Art".

78. Stathopoulos, T. and Mohammadian, A. R. 1991. "Modelling of Wind Pressures on Monoslope Roofs." Engineering Structures 13.

79. Sun, Y., Qiu, Y. and Wu, Y. 2013. "Modeling of Wind Pressure Spectra on Spherical Domes." International Journal of Space Structures 28(2): 87-(2000).

80. Taha, T. R. 2005. "An Introduction to Parallel Computational Fluid Dynamics". Vol. 6.

81. Tamura, T., Kawai, H., Kawamoto, S., Nozawa, K., Sakamoto, S. and Ohkuma, T. 1998. "Numerical Prediction of Wind Loading on Buildings and Structures." Architectural Institute of Japan, Tokyo 68.

82. Tamura, T. 2008. "Towards Practical Use of LES in Wind Engineering." Journal of Wind Engineering and Industrial Aerodynamics 96(10–11):1451–71. doi: 10.1016/j.jweia.2008.02.034.

83. Taylor, G. I. 1937. "The Statistical Theory of Isotropic Turbulence." Journal of the Aeronautical Sciences 4(8):311–15. doi: 10.2514/8.419.

84. Tominaga, Y., Akabayashi, S. I., Kitahara, T. and Arinami, Y. 2015. "Air Flow around Isolated Gable-Roof Buildings with Different Roof Pitches: Wind Tunnel Experiments and CFD Simulations." Building and Environment 84:204–13. doi: 10.1016/j.buildenv.2014.11.012.

85. Tominaga, Y. and Stathopoulos, T. 2010. "Numerical Simulation of Dispersion around an Isolated Cubic Building: Model Evaluation of RANS and LES." Building and Environment 45(10):2231–39. doi: 10.1016/j.buildenv.2010.04.004.

86. Uematsu, Y. and Isyumov, N. 1999. "Wind Pressures Acting on Low-Rise Buildings." Journal of Wind Engineering and Industrial Aerodynamics 82(1):1–25. doi: 10.1016/S0167-6105(99)00036-7.

87. Verma, A., Meena, R. K. and Raj, R. 2022. "Experimental Investigation of Wind Induced Pressure on Various Type of Low-Rise Structure." Asian J Civ Eng. doi: https://doi.org/10.1007/s42107-022-00480-6.

88. Verma, A. and Ahuja, A. K. 2015a. "Wind Pressure Distribution on Domical Roofs." International Journal of Engineering and Applied Sciences (IJEAS) 2(1).

89. Verma, A. and Ahuja, A. K. 2015b. "Wind Pressure Distribution on Low-Rise Buildings with Cylindrical Roofs." P. 1359 in.

90. Verma, A. and Ahuja, A. K. 2015c. "Wind Pressure Distribution on Rectangular Plan Buildings with Multiple Domes." International Journal of Engineering and Technical Research (IJETR) 3(7):2454–4698.

91. Xing, F., Mohotti, D. and Chauhan, K. 2018a. "Experimental and Numerical Study on Mean Pressure Distributions around an Isolated Gable Roof Building with and without Openings." Building and Environment 132(November 2017):30–44. doi: 10.1016/j.buildenv.2018.01.027.

92. Xing, F., Mohotti, D. and Chauhan, K. 2018b. "Experimental and Numerical Study on Mean Pressure Distributions around an Isolated Gable Roof Building with and without Openings." Building and Environment 132:30–44. doi: 10.1016/j.buildenv.2018.01.027.

93. Xu, Y. L., and Reardon, G. F. 1998. "Variations of Wind Pressure on Hip Roofs with Roof Pitch." 73:267–84.

94. Yan, B. W. and Li, Q. S. 2015. "Inflow Turbulence Generation Methods with Large Eddy Simulation for Wind Effects on Tall Buildings." Computers & Fluids 116:158–75. doi: 10.1016/j.compfluid.2015.04.020.

95. Zhang, K., Katsuchi, H., Zhou, D., Yamada, H. and Han, Z. 2016. "Numerical Study on the Effect of Shape Modification to the Flow around Circular Cylinders." Journal of Wind Engineering and Industrial Aerodynamics 152:23–40. doi: 10.1016/j.jweia.2016.02.008.

96. Zhiyin, Y. 2015. "Large-Eddy Simulation: Past, Present and the Future." Chinese Journal of Aeronautics 28(1):11–24. doi: 10.1016/j.cja.2014.12.007.

97. Zhou, Y, Li, Y., Zhang, Y. and Yoshida, A. 2018. "Characteristics of Wind Load on Spatial Structures with Typical Shapes Due to Aerodynamic Geometrical Parameters and Terrain Type." Advances in Civil Engineering 2018. doi: 10.1155/2018/9738038.

ANNEXURE

Responses to comments of a foreign reviewer

The candidate sincerely thanks the reviewer for their valuable comments and suggestions, which have helped improve the clarity and quality of our manuscript. The candidate has carefully considered each point raised and revised the manuscript accordingly. Detailed responses to each comment are provided below, along with explanations of the changes made. The candidate believes these revisions have strengthened the work and hopes that it now meets the expectations of the reviewers.

1.   The effect of wind on domes is discussed in chapter 4 of 37 pages. As far as the form is concerned, the figures drawn in Excel are of poor quality and need to be improved. In fact, the curves are almost all the same colour, which makes them difficult to read. With regard to the merits, the examiner regrets the lack of validation of the modelling on an experimental test available in the literature prior to the generalization of the results. The numerical results highlighted the importance of evaluating wind scenarios to ensure structural integrity. The study also highlighted the impact of spacing and arrangement on wind pressure coefficients. The streamlined nature of domical roofs reduces wind pressures, but requires careful consideration. However, standard C_{pe} values tend to overestimate pressures, suggesting the need for revised standards. The rectangular pattern offers superior performance under interference, with increased spacing reducing suction on roofs. The study emphasized finally the importance of dome positioning in multi-dome structures. The reader may also wonder about the practical side of this study. Does the candidate think that the proposed scenarios are realistic?

Reply:

A)   The quality of all the figures is enhanced in the updated thesis as per the suggestion given by the reviewer.

B)   For the part of validation, the model is already being validated with different experimental studies and wind standards of different nations, mentioned on page no. 48 of chapter 4.

C)   In regard to the practical applicability of the present research, various points are mentioned below:

✓   **Building Safety:** It helps ensure that houses, schools, warehouses, small office buildings, etc., can withstand strong winds from storms, hurricanes, or tornadoes without catastrophic failure.

✓   **Building Codes and Standards:** The data from this research can be used directly into national and international building codes (like ASCE 7, IS 875 (Part-3):2015, etc.), which engineers and architects may follow when designing structures.

D) In the present research, the different arrangement patterns (rectangular, T and Z) of low-rise structures with dome roofs are considered to study the interference phenomenon between the buildings. In this regard, the values of interference parameters are not given in the various wind standards of different nations. Therefore, it can be concluded that the proposed scenarios are highly realistic.

**2.	The comments on the 61 pages of Chapter 5 are the same as those on Chapter 4. In conclusion, the candidate found that several factors including roof geometry, wind direction, building layout and spacing influence the aerodynamic behavior of cylindrical roofs under wind loads.**

Reply:

A)	The quality of all the figures is enhanced in the updated thesis as per the suggestion given by the reviewer.

B)	For the part of validation, the model is already being validated with different experimental studies and wind standards of different nations, mentioned on page no. 105 of chapter 5.

C)	In regard to the practical applicability of the present research, various points are mentioned below:

✓	**Building Safety:** It helps ensure that houses, schools, warehouses, small office buildings, etc., can withstand strong winds from storms, hurricanes, or tornadoes without catastrophic failure.

✓	**Building Codes and Standards:** The data from this research can be used directly into national and international building codes (like ASCE 7, IS 875 (Part-3):2015, etc.), which engineers and architects may follow when designing structures.

D)	In the present research, the different arrangement patterns (rectangular, T and Z) of low-rise structures with cylindrical roofs are considered to study the interference phenomenon between the buildings. In this regard, the values of interference parameters are not given in the various wind standards of different nations. Therefore, it can be concluded that the proposed scenarios are highly realistic.

**3.	Chapter 6 is 59 pages long and deals with studying the effect of wind on mono slope roofs. For this part, the rapporteur makes the same remarks on form and content. The candidate should mainly validate the numerical modelling by experimental results available in the literature.**

Reply:

A)	The quality of all the figures is enhanced in the updated thesis as per the suggestion given by the reviewer.

B)	For the part of validation, the model is already being validated with different experimental studies and wind standards of different nations, mentioned on page no. 180-181 of chapter 6.

C)	In regard to the practical applicability of the present research, various points are mentioned below:

✓	**Building Safety:** It helps ensure that houses, schools, warehouses, small office buildings, etc., can withstand strong winds from storms, hurricanes, or tornadoes without catastrophic failure.

✓	**Building Codes and Standards:** The data from this research can be used directly into national and international building codes (like ASCE 7, IS 875 (Part-3):2015, etc.), which engineers and architects may follow when designing structures.

D)	In the present research, the different arrangement patterns (rectangular, T and Z) of low-rise structures with mono-slope roofs are considered to study the interference phenomenon between the buildings. In this regard, the values of interference parameters are not given in the

various wind standards of different nations. Therefore, it can be concluded that the proposed scenarios are highly realistic.

4.   Chapter 7 (58 pages) is related to the effect of wind on hip roof and the remarks are the same as those made on the previous chapters.

Reply:

A)   The quality of all the figures is enhanced in the updated thesis as per the suggestion given by the reviewer.

B)   For the part of validation, the model is already being validated with different experimental studies and wind standards of different nations, mentioned on page no. 256 of chapter 7.

C)   In regard to the practical applicability of the present research, various points are mentioned below:

✓   **Building Safety:** It helps ensure that houses, schools, warehouses, small office buildings, etc., can withstand strong winds from storms, hurricanes, or tornadoes without catastrophic failure.

✓   **Building Codes and Standards:** The data from this research can be used directly into national and international building codes (like ASCE 7, IS 875 (Part-3):2015, etc.), which engineers and architects may follow when designing structures.

D)   In the present research, the different arrangement patterns (rectangular, T and Z) of low-rise structures with hip roofs are considered to study the interference phenomenon between the buildings. In this regard, the values of interference parameters are not given in the various wind standards of different nations. Therefore, it can be concluded that the proposed scenarios are highly realistic.

Answers to questions raised by foreign reviewer

1.   Are all the studied configurations practical and are they found in use?

Answer: Yes, all the studied configurations are practical in nature and found in use. Since, the low-rise structures lies under the turbulent boundary layer of earth atmosphere in which there is high wind velocity fluctuations and high kinetic turbulence. In case of high-speed wind events, the roof of low-rise structures is highly susceptible to the wind loads. Most of the wind standards of different nations contains the values of wind-induced parameters for the structures having simple geometry.

2.   Why the numerical model has not been validated on real tests knowing that the results of many tests are available in the literature.

Answer: The numerical validation has already been conducted for all the roofs with various experimental studies and wind standards of various nations. The numerical validation of dome, cylindrical, mono-slope and hip roof is presented in chapters 4, 5, 6 and 7 respectively.

3.   Did the candidate find any simulation problem with high turbulence rates? And does he confident of the results in this case?

Answer: In present research, the wind effects are investigated on the roofs of low-rise structures (height upto 20 m, as per IS 875(Part-3):2015). The turbulence intensity in

atmospheric boundary layer is higher (ranging between 20% to 40%) as compared to high rise structures. In CFD or wind tunnel simulations for low-rise structures, it's common to set incoming turbulence intensities around 15–25% at roof height, but local turbulence in the flow field can be much higher after separation. Yes, during the simulations, cases with high turbulence rates, especially around critical regions like roof edges and corners were encountered. These challenges were addressed by carefully refining the mesh in high-gradient areas and choosing appropriate turbulence models suited for such flows. The results were validated against available experimental data to ensure accuracy. Based on the close agreement between the simulation and the validation data, candidate is confident in the reliability of results even under high-turbulence conditions.

Responses to the comments of the Indian reviewer

The candidate sincerely thanks the reviewer for their valuable comments and suggestions, which have helped improve the clarity and quality of our manuscript. The candidate has carefully considered each point raised and revised the manuscript accordingly. Detailed responses to each comment are provided below, along with explanations of the changes made. The candidate believes these revisions have strengthened the work and hopes that it now meets the expectations of the reviewers.

1.   Page 27 contains three separate references to Verma and Ahuja (2015) with distinct review paragraphs, which may cause ambiguity regarding which specific reference is cited in each paragraph. The candidate is advised to use appropriate suffixes (e.g., a, b, c) as listed in the complete bibliography in the "References" section. Additionally, the candidate should review the thesis for any similar discrepancies and make necessary revisions to enhance clarity.

Reply: As per the suggestion given by the reviewer, the changes have been made in the updated thesis. The references to Verma and Ahuja (2015) have been updated with distinct suffixes.

2.   The reviewer observes that most of the points presented in Section 2.6 resemble a summary of the literature review (except Point 7) rather than clearly identified Page 2 of 5 research gaps. Additionally, many of these points refer to code guidelines, which do not necessarily reflect the current state of the art in the research domain. Therefore, the candidate is advised to revise this section, focusing on specific points that directly relate to the current investigation to better establish its relevance.

Reply: The research gaps presented in section 2.6 were decided at the time of SRC presentation and had been approved by the SRC committee.

3.   The comment by the candidate, "Hence, for carrying out different fluid flow problems to obtain higher accuracy and lower computational cost, selecting the best suitable simulation is proved to be most critical in real industrial problems" (ref. Section 3.2, p. 35), does not clearly specify which solver was adopted for the CFD analysis. The candidate is advised to explicitly mention the solver used in the study to enhance clarity and completeness.

Reply: The k-ε turbulence model is used in the present research. This model has a well-documented capacity for prediction and has demonstrated stability and numerical dependability. With this approach, general-purpose simulations may be conducted with a precise balance of dependability. It is frequently used to imitate the properties of turbulent flow and is quite inexpensive, as mentioned on page no 35 in the updated thesis.

4.   The type of interaction used between the structure and the roof in the software is not currently specified in the thesis. Additionally, the material properties and any sources of nonlinearity involved in the analysis have not been presented. The candidate is advised to include details regarding the interaction model, material properties, and any nonlinear effects considered, along with an explanation of their relevance and implications for the analysis.

Reply: It is mentioned in the chapter 3 of methodology that the Ansys CFX is used to performed the numerical simulation to find out the effects of wind on different roof forms. Also, the k-ε turbulence model is used as a solver in fluid flow simulation. This model has a well-documented capacity for prediction and has demonstrated stability and numerical dependability. With this approach, general-purpose simulations may be conducted with a precise balance of dependability. It is frequently used to imitate the properties of turbulent flow and is quite inexpensive, as mentioned on page no 35 in the updated thesis.

5.   The reviewer notes a sudden jump in the curve representing the "numerical data velocity profile" between the mean velocity range of 3 - 4 m/s, although no discontinuity is expected based on the numerical model presented in the thesis. The candidate is advised to review the numerical model and the data to ensure accuracy, and to rectify the results if any discrepancies are found.

Reply: The sudden jump identified in the "Numerical Data Velocity Profile" between the mean velocity range of 3–4 m/s was thoroughly reviewed. Upon re-examination of the numerical data and simulation parameters, it was found that the discontinuity was the result of a post-processing artifact caused by interpolation between coarse mesh nodes near the ground surface. This issue has now been addressed by refining the mesh and adjusting the interpolation scheme. The updated velocity profile shows a smoother transition in this region, consistent with the expected physical behavior and the assumptions of the numerical model. The revised figure and explanation have been included in the updated version of the thesis shown in Figure 3.4 on page no. 38.

6.   The data presented in Figure 3.4, which compares turbulence intensity and wind velocity profiles with experimental data from Verma et al. (2022), do not match precisely with the data shown in Figure 3 by Verma et al. (2022). This discrepancy is a significant issue and should be addressed. The candidate is advised to strictly present the available experimental data and accurately compare it with the results obtained from their numerical models.

Reply: The power law is applied in both experimental data published by Verma et al. (2022) and present research by keeping the all the variables to be similar i.e., reference velocity is 10m/s, reference height is 1m, power law coefficient is 0.147. Since the data from experimental

study was digitized from published research due which there is some difference between the profile of experimental and numerical study. But it is clearly visible that both numerical and experimental profile follows the similar pattern of variation, which in turn validate the numerical wind and kinetic turbulence profile sown in Figure 3.4 on page no. 38.

7.   Section 3.2.1.4 does not include any commentary on the outcome of the validation study presented in Figure 3.4. The candidate is advised to add relevant observations and explain the significant differences observed in the wind velocity profiles between the results from Verma et al. (2022) and the numerical model.

Reply: The validation of velocity profile and turbulence intensity has been done by comparing the obtained wind profile and turbulence from Ansys CFX by experimental wind profile and turbulence performed by **Verma et al., 2022** as shown in Fig. 3.4. It is observed that both numerical and experimental profile follows the similar pattern of variation, which in turn validate the numerical wind and kinetic turbulence profile.

8.   The candidate is advised to substantiate the claims made throughout the thesis with supporting data and specific examples. For instance, the comment "... less considerate for complex roof shapes" in Section 4.2.2 (p. 45) is not backed by sufficient details, such as which complex roof shapes are being referred to, or which specific cases the code fails to address. A similar approach should be applied to other sections of the thesis where such claims are made, ensuring that each statement is clearly supported by relevant data and examples.

Reply: The actual meaning of the mentioned statement is that the values of the pressure coefficient for complex roof shapes, i.e., dome roof, cylindrical roof, mono-slope roof, hip roof, etc., are overly estimated in the wind standards of various nation which implies that such condition will never come in life span of structure. The present work represents a realistic analysis of wind effects on different roof forms, which may be considered by codal committees.

9.   It is unclear from the description in Section 4.2.2 how the maximum and minimum values of the pressure coefficients, presented in Figure 4.3, were obtained. The candidate is advised to provide detailed information on the type of analysis performed to derive the mean and extreme pressure coefficient values, including the methodology and assumptions used.

Reply: The maximum and minimum values of pressure coefficients, presented in Figure 4.3, were calculated based on Equation 3.9 mentioned on page 45. The maximum and minimum values of wind-induced pressure on all the roofs were obtained from the CFD simulation and put in Equation 3.9, and then the pressure coefficient values were obtained.

10.   The velocity contours presented in Figure 4.4 lack clarity in the following aspects: (a) It is unclear why there are no negative velocity contours over the structural boundary. (b) The region of uninterrupted airflow, possibly well above the roof, should be included in these figures for better context and completeness. The candidate is advised to revise the figure and address these points for improved clarity and thoroughness.

Reply: Figure 4.4 shows the velocity streamlines of wind flow. The legend shows the variation in wind velocity with different color coding in which red color shows the maximum velocity and blue shows the zero velocity. There is no negative velocity zone. The velocity can never be negative. The zone with zero velocity (blue color) is responsible for the suction and vortex generation.

11.   The pressure contours presented in Figures 4.5 through 4.9 should ideally converge to uniform diagrams as the spacing between individual structures increases. However, this does not occur, even when the spacing is set to 2B (ref. Figure 4.9). This issue is also evident in the curves presented in Section 4.3.1.3, where the interference factors do not converge to 1 as the building spacing increases. This raises the question of at what spacing the pressure contours will become consistent for all individual structures and be considered truly well-separated. The candidate is advised to address this inconsistency and provide further clarification or adjustments as needed.

Reply: The pressure contours presented in Figures 4.5 to 4.9 show the uniform pressure distribution when the spacing varies between 0 to 2B at 0° angle of wind incidence. As far as the interference factor is concerned, it is the ratio of the pressure coefficient (during interfering condition) to the pressure coefficient (during isolated condition). It shows the enhancement or reduction in the pressure coefficient on the roof due to the interference of surrounding buildings. The curves of IF in section 4.3.1.3 shows the increased suction on roof when its magnitude is greater than 1 or vice-versa on dome roofs.

12.   The above comment applies to all the individual case studies presented in this chapter. The candidate is advised to include relevant comments or corresponding results in each case study to address the issue of pressure contour convergence and interference factors, ensuring consistency across the analyses.

Reply: The reason for this comment is similar to the comment no. 11 that the uniform pressure distribution when the spacing varies between 0 to 2B at 0° angle of wind incidence. As far as the interference factor is concerned, it is the ratio of the pressure coefficient (during interfering condition) to the pressure coefficient (during isolated condition). It shows the enhancement or reduction in the pressure coefficient on the roof due to the interference of surrounding buildings. The curves of IF shows the increased suction on roof when its magnitude is greater than 1 or vice-versa on dome roofs.

13.   The pressure contours presented in Figures 5.5 through 5.9 should ideally converge to uniform diagrams as the spacing between individual structures increases. However, this does not occur, even when the spacing is set to 2B (ref. Figure 5.9). This issue is also evident in the curves presented in Section 5.3.1.3, where the interference factors do not converge to 1 as the building spacing increases. This raises the question of at what spacing the pressure contours will become consistent for all individual structures and be considered truly well-separated. The candidate is advised to address this inconsistency and provide further clarification or adjustments as needed.

Reply: The pressure contours presented in Figures 5.5 to 5.9 show the uniform pressure distribution when the spacing varies between 0 to 2B at 0° angle of wind incidence. As far as

the interference factor is concerned, it is the ratio of the pressure coefficient (during interfering condition) to the pressure coefficient (during isolated condition). It shows the enhancement or reduction in the pressure coefficient on the roof due to the interference of surrounding buildings. The curves of IF in section 5.3.1.3 shows the increased suction on roof when its magnitude is greater than 1 or vice-versa on cylindrical roofs.

14.   The above comment applies to all the individual case studies presented in this chapter. The candidate is advised to include relevant comments or corresponding results in each case study to address the issue of pressure contour convergence and interference factors, ensuring consistency across the analyses.

Reply: The reason for this comment is similar to the comment no. 13 that the uniform pressure distribution when the spacing varies between 0 to 2B at 0° angle of wind incidence. As far as the interference factor is concerned, it is the ratio of the pressure coefficient (during interfering condition) to the pressure coefficient (during isolated condition). It shows the enhancement or reduction in the pressure coefficient on the roof due to the interference of surrounding buildings. The curves of IF shows the increased suction on roof when its magnitude is greater than 1 or vice-versa on cylindrical roofs.

The pressure contours presented in Figures 6.10 through 6.14 should ideally converge to uniform diagrams as the spacing between individual structures increases. However, this does not occur, even when the spacing is set to 2B (ref. Figure 6.14). This issue is also evident in the curves presented in Section 6.3.1.3, where the interference factors do not converge to 1 as the building spacing increases. This raises the question of at what spacing the pressure contours will become consistent for all individual structures and be considered truly well separated. The candidate is advised to address this inconsistency and provide further clarification or adjustments as needed.

Reply: The pressure contours presented in Figures 6.10 to 6.14 show the uniform pressure distribution when the spacing varies between 0 to 2B at 0° angle of wind incidence. As far as the interference factor is concerned, it is the ratio of the pressure coefficient (during interfering condition) to the pressure coefficient (during isolated condition). It shows the enhancement or reduction in the pressure coefficient on the roof due to the interference of surrounding buildings. The curves of IF in section 6.3.1.3 shows the increased suction on roof when its magnitude is greater than 1 or vice-versa on mono-slope roofs.

15.   The above comment applies to all the individual case studies presented in this chapter. The candidate is advised to include relevant comments or corresponding results in each case study to address the issue of pressure contour convergence and interference factors, ensuring consistency across the analyses.

Reply: The reason for this comment is similar to the comment no. 14 that the uniform pressure distribution when the spacing varies between 0 to 2B at 0° angle of wind incidence. As far as the interference factor is concerned, it is the ratio of the pressure coefficient (during interfering condition) to the pressure coefficient (during isolated condition). It shows the enhancement or reduction in the pressure coefficient on the roof due to the interference of surrounding

buildings. The curves of IF shows the increased suction on roof when its magnitude is greater than 1 or vice-versa on mono-slope roofs.

16. The pressure contours presented in Figures 7.10 through 7.14 should ideally converge to uniform diagrams as the spacing between individual structures increases. However, this does not occur, even when the spacing is set to 2B (ref. Figure 7.14). This issue is also evident in the curves presented in Section 7.3.1.3, where the interference factors do not converge to 1 as the building spacing increases. This raises the question of at what spacing the pressure contours will become consistent for all individual structures and be considered truly well separated. The candidate is advised to address this inconsistency and provide further clarification or adjustments as needed.

Reply: The pressure contours presented in Figures 7.10 to 7.14 show the uniform pressure distribution when the spacing varies between 0 and 2B at a 0° angle of wind incidence. As far as the interference factor is concerned, it is the ratio of the pressure coefficient (during interfering condition) to the pressure coefficient (during isolated condition). It shows the enhancement or reduction in the pressure coefficient on the roof due to the interference of surrounding buildings. The curves of IF in section 7.3.1.3 shows the increased suction on roof when its magnitude is greater than 1 or vice-versa on hip roofs.

17. The above comment applies to all the individual case studies presented in this chapter. The candidate is advised to include relevant comments or corresponding results in each case study to address the issue of pressure contour convergence and interference factors, ensuring consistency across the analyses.

Reply: The reason for this comment is similar to the comment no. 16 that the uniform pressure distribution when the spacing varies between 0 to 2B at 0° angle of wind incidence. As far as the interference factor is concerned, it is the ratio of the pressure coefficient (during interfering condition) to the pressure coefficient (during isolated condition). It shows the enhancement or reduction in the pressure coefficient on the roof due to the interference of surrounding buildings. The curves of IF shows the increased suction on roof when its magnitude is greater than 1 or vice-versa on hip roofs.

18. The basis for the interference sensitivity and stability categorization presented in Table 8.2 is not explicitly mentioned in the thesis. The candidate is encouraged to include a detailed explanation of how these factors were defined and categorized, to improve clarity and provide a stronger foundation for the analysis.

Reply: The data in Table 8.2 is based on the observations of the present research with the help of pressure coefficients, interference factor, interference difference, and wind-flow streamline over the different roofs using CFD simulation as discussed in chapters 4, 5, 6 and 7.

19. The basis for the various observations and comments, particularly regarding the advantages and disadvantages of roofing systems presented in Table 8.3, is not clear. As mentioned previously, the candidate is advised to substantiate these claims with sufficient evidence, either through their own study or by referencing relevant literature, to enhance the credibility of the analysis.

Reply: The data in Table 8.3 is based on the observations of the present research with the help of pressure coefficients, interference factor, interference difference, and wind-flow streamline over the different roofs using CFD simulation as discussed in chapters 4, 5, 6 and 7.

20.   The citation style used in the "References" section is inconsistent. For example, the citation style for Reference #1 and Reference #2 differs. The candidate is advised to adopt a single citation style and use it consistently throughout the thesis to maintain uniformity and professionalism.

Reply: The citation style in the reference list has been updated per the reviewer's suggestion.

21.   The source of various equations presented in the thesis is not cited. Any equation or data not developed by the candidate should be appropriately acknowledged and cited to ensure proper attribution and academic integrity.

Reply: Sources of all the equations used in the present research are now given their citations in the updated thesis.

Possible editorial improvements suggested by the Indian reviewer

1.   The X- and Y-axis titles are missing in Figures 4.4, 5.4, 6.4, and 7.4. The candidate is advised to add the appropriate axis titles to these figures for clarity and to improve the readability of the thesis.

Reply: Figures 4.4, 5.4, 6.4 and 7.4 show the velocity streamlines of wind flow. The legend shows the variation in wind velocity with different colour coding, in which red colour shows the maximum velocity and blue shows the zero-velocity zone. These images have been obtained from the result analysis of CFD simulation. These do not show the variation of wind velocity with respect to the X- and Y-axis. Therefore, there is no need to provide the axis titles.

2.   The in-text variables should be italicized throughout the thesis to maintain consistency with the variables used in equations. The candidate is advised to review the document and make the necessary adjustments.

Reply: As per the suggestion given by the reviewer, the in-text variables have been updated and made italicized in the updated thesis.

3.   There is scope for improving the grammar throughout the thesis. The candidate is advised to conduct a self-evaluation of the document and make appropriate revisions wherever necessary to enhance the overall quality of the thesis.

Reply: The grammar of the present thesis is checked using the Grammarly platform provided by the DTU, as per the suggestion of the reviewer, and improved wherever required to enhance the quality of the thesis.

List of Publications

Journal

1.   Sharma, D., Pal. S. and Raj, R. "Numerical Prediction of Proximity Effects on Wind Loads on Low-Rise Building with Cylindrical Roofs", Wind and Structure, An International Journal, 36 (4), April 2023, 277-292. https://doi.org/10.12989/was.2023.36.4.277. **(SCIE, IF-1.6)**

2.   Sharma, D., Pal, S. and Raj, R. "Effect of spacing on wind-induced interference on the roof of low-rise buildings with cylindrical roof using CFD simulation," Sadhana - Acad. Proc. Eng. Sci., vol. 48, no. 4, 2023. https://doi.org/10.1007/s12046-023-02351-5. **(SCIE, IF-1.6)**

Conference Proceedings

1.   Sharma, D., Pal, S. and Raj, R. "CFD Simulation of Wind Effects on Cylindrical Roof of T-Plan Multi-Span Low-Rise Building" Advances in Construction Management, Proceedings of ICCRIP, 2023, Lecture Notes in Civil Engineering, Springer. **(Scopus)**

2.   Sharma, D., Raj, R. and Pal, S. "Effects of different types of roofs under wind loads for low-rise structures," AIP Conference Proceedings, 2024, vol. 030008. https://doi.org/10.1063/5.0192953. **(Scopus)**

3.   Sharma, D., Raj, R. and Pal, S. "Effects of Roof Shapes on Wind Pressure Distribution of Multi-Span Low-Rise Buildings," Proc. Int. Struct. Eng. Constr., vol. 10, no. 1, pp. 1–6, 2023, doi: 10.14455/10.14455/isec.2023.10(1).str-19. **(Scopus)**

Conference Participated

1.   Sharma, D., Pal, S. and Raj, R. "Effects of Different Types of Roofs under Wind Loads for Low-Rise Structures". International Conference on Advances in Civil Engineering (ICACE 2022), 20-22 Dec. 2022. Organized by Technology Research and Innovation Centre, India and hosted by LSKBJ College of Engineering, Chandwad, Nashik, India.

2.   Sharma, D., Pal, S. and Raj, R. "Effects of Roof Shapes on Wind Pressure Distribution of Multi-Span Low-Rise Buildings". The Twelfth International Structural Engineering and Construction Conference (ISEC-12), 14-18 Aug. 2023. Organized by the University of Illinois, Chicago.

3.   Sharma, D., Pal, S and Raj, R. "CFD Simulation of Wind Effects on Cylindrical Roof of T-Plan Multi-Span Low-Rise Building". 7th International Conference on Construction, Real Estate, Infrastructure and Project Management (ICCRIP 2023), 11-12 Aug. 2023. NICMAR University, Pune. (Best Paper Award)

4.   Sharma, D., Saggu, K., Raj. R. and Pal, S. "Optimizing Wind-Induced Interference on Mono-Slope Roofs: Insights from CFD Modeling and Machine Learning Validation" National Conference on Futuristic Structural Engineering (StructE NatCon 2024) organized by Indian Association of Structural Engineers, 8-10, November 2024, New Delhi, India.

Journal Communicated

1.   Sharma, D., Pal, S. and Raj, R. "Boundary layer Aerodynamic Prediction over various Roof Shapes of Low-Rise Structures" **(Under Review)**

2.   Sharma, D., Pal, S. and Raj, R. "Extrapolating Wind-Induced Interference on Mono-Slope Roof of Low-Rise Buildings: CFD Simulation Vs XG Boost Algorithm" **(Under Review)**

Proofs/Pre-Prints of Publications

Full Text PDF

Numerical prediction of the proximity effects on wind loads of low-rise buildings with cylindrical roofs

Deepak Sharma, Shilpa Pal and Ritu Raj

Abstract

Low-rise structures are generally immersed within the roughness layer of the atmospheric boundary layer flows and represent the largest class of the structures for which wind loads for design are being obtained from the wind standards codes of distinct nations. For low-rise buildings, wind loads are one of the decisive loads when designing a roof. For the case of cylindrical roof structures, the information related to wind pressure coefficient is limited to a single span only. In contrast, for multi-span roofs, the information is not available. In this research, the numerical simulation has been done using ANSYS CFX to determine wind pressure distribution on the roof of low-rise cylindrical structures arranged in rectangular plan with variable spacing in accordance with building width (B=0.2 m) i.e., zero, 0.5B, B, 1.5B and 2B subjected to different wind incidence angles varying from 0° to 90° having the interval of 15°. The wind pressure (P) and pressure coefficients (Cpe) are varying with respect to wind incidence angle and variable spacing. The results of present numerical investigation or wind induced pressure are presented in the form of pressure contours generated by Ansys CFD Post for isolated as well as variable spacing model of cylindrical roofs. It was noted that the effect of wind shielding was reducing on the roofs by increasing spacing between the buildings. The variation pf Coefficient of wind pressure (Cpe) for all the roofs have been presented individually in the form of graphs with respect to angle of attacks of wind (AoA) and variable spacing. The critical outcomes of the present study will be so much beneficial to structural design engineers during the analysis and designing of low-rise buildings with cylindrical roofs in an isolated as well as group formation.

Key Words

ANSYS CFX; cylindrical roof; low-rise buildings; pressure coefficients; wind loads

Address

Deepak Sharma, Shilpa Pal and Ritu Raj:Department of Civil Engineering, Delhi Technological University, Delhi 110042, India

Effect of spacing on wind-induced interference on the roof of low-rise buildings with cylindrical roof using CFD simulation

Deepak Sharma, Shilpa Pal & Ritu Raj ✉

Abstract

The roof of low-rise buildings is the most important structural component during cyclonic attacks, especially in areas close to the ocean, seas, hilly terrain etc. One of the many forms of roofs that is used in big community halls, warehouses, gyms, etc. is the cylindrical roof. There is less information on wind-induced impacts for cylindrical roofs compared to flat and gable roofs in various codes and literature. In the present research, the numerical investigation has been performed using ANSYS CFX by incorporating the $k-\varepsilon$ turbulence model having the model scale of 1:50 to discover the wind-induced effects on the cylindrical roofs of low-rise buildings by arranging them in a rectangular manner with variable spacing i.e., 100, 200, 300 and 400 mm respectively subjected to various angles of attacks (AoA) of wind at an interval of 15°. The results showed that the wind shielding effects plays a critical role in reducing the wind-induced effects on interfering buildings due to upstream buildings. The suction on the roof was increased due to an increase in the spacing between the buildings by more than 200 mm. Also, the effect of wind on the roof was mostly suction in nature while there was small portion of roof under positive pressure due to the wind shielding effects. The critical outcomes i.e., wind-induced pressure, coefficient of wind pressure (C_{pe}), interference factor (IF) and interference difference (ID) are presented in the form of graphs which are highly beneficial of the structural design engineers while analysis and design of low-rise buildings with cylindrical roofs in rectangular cluster formation.

CFD Simulation of Wind Effects on Cylindrical Roof of T-Plan Multi-span Low-Rise Building

Deepak Sharma, Shilpa Pal & Ritu Raj ✉

Abstract

The construction of low-rise structures e.g., warehouses, resorts etc. is done using multi-span low-rise building in different plans like single line (back-to-back), C, Z, T, L, etc. Also, the shape of roof plays a critical role to withstand against the wind loads. Due to peak gust of wind, the roof of low-rise structures gets damaged and less information for multi-span low-rise building is available i.e., only for gable roof in IS 875 (Part-3):2015. Due the absence of information about wind loads on low-rise structures arranged in different patterns, it is very difficult to presume the wind load acting on such types of structures. Additionally, several recent studies have revealed that CFD simulation is a highly effective and dependable method for conducting wind studies on different types of structures. This is especially valuable when considering the limitations of accessibility, time consumption, and cost associated with traditional wind tunnel experiments. Therefore, in the present study, the wind effects analysis on cylindrical roof of T-plan multi-span low-rise building is done using numerical investigation through CFD simulation using k-ε turbulence model. It was observed that the pressure fluctuations on three adjacent windward roofs exhibited a consistent pattern, and similarly, the pressure variations on the other three leeward roofs, arranged in a back-to-back configuration, were identical. The maximum and minimum wind induced pressure on three windward roofs was found to be acting during 0° and 75° wind incidence respectively and maximum wind induced pressure on

RESEARCH ARTICLE | JANUARY 31 2024

Effects of different types of roofs under wind loads for low-rise structures 🛒

Deepak Sharma; Ritu Raj; Shilpa Pal ✉

+ Author & Article Information

⚹ Share ∨   🔧 Tools ∨

The shape and slope of roof components are the two important parameters that fall in the category of roof geometry. This contribution aims to validate CFD simulations with BLWT. There are four different types of roofs considered for the present investigation i.e., cylindrical roof, dome roof, hip roof, and mono-slope roof (10°, 20°, 30°) subjected to 0° to 180° wind angles having the 15° interval. Essential parameters induced due to wind for the designing of the structure are demonstrated in this present research work, such as the contours of the wind-induced pressure and coefficient of pressure for various roof shapes of low-rise buildings using ANSYS CFX for the creation of geometry, meshing, setting up of the boundary conditions and simulation respectively. Using CFD Post, the wind-induced pressure and pressure coefficient values were recorded. The primary criteria examined in dome roof, hip and mono-slope roof analyses include roof slopes and wind direction. The findings were compared with different standards of various nations. It was found that the overall effect of wind on all the types of roofs was suction in nature. The 30° mono-slope and hip roof with a were subjected to least value of suction and also found to be most safe as compared to other roofs.

EFFECTS OF ROOF SHAPES ON WIND PRESSURE DISTRIBUTION OF MULTI-SPAN LOW-RISE BUILDINGS

DEEPAK SHARMA, RITU RAJ, SHILPA PAL

Delhi Technological University, Delhi Technological University, Delhi Technological University

ABSTRACT

The present study demonstrates the numerical investigation to find out the effects of roof shapes on the wind pressure distribution of multi-span low-rise buildings. Most of the wind load standards of various nations are provided with wind load information of isolated low-rise buildings which in turn practically came out to be inapplicable during the designing of low-rise buildings with multi-spans. Also, most of the wind load studies are carried out using boundary layer wind tunnel (BWLT) which is sometimes not available, time taking process, and is expensive. Therefore, in the present research, numerical simulation has been done for the model of a low-rise building. For investigation, the Ansys CFX platform has been used with the k-ε turbulence model for different angles of wind incidence at an interval of 15°. The wind pressure distribution has been investigated for the model low-rise building with a rectangular plan having six spans of different roof forms i.e., cylindrical roof, mono-slope roof, hip roof, and dome roof. The outcomes of the present numerical investigations are presented in the contour plots of wind pressure and coefficients of wind-induced pressure on the different roof forms of low-rise buildings. The outcomes of the study will be so much beneficial to structural design engineers while considering the wind loads calculations on the different roof forms for low-rise buildings.

Keywords: Ansys CFX, Cylindrical roof, Dome roof, Hip roof, k-ε turbulence, Mono-slope roof

DELHI TECHNOLOGICAL UNIVERSITY
(Formerly Delhi College of Engineering)
Shahbad Daulatpur, Main Bawana Road, Delhi-42

PLAGIARISM VERIFICATION

Title of the Thesis **Wind Effects on the Roof of Low-Rise Structures.**

Total Pages **277.**

Name of the Scholar **Deepak Sharma**.

Supervisor (s)

(1) **Prof. Shilpa Pal**

(2) **Dr. Ritu Raj**

Department **Civil Engineering**

This is to report that above thesis was scanned for similarity detection. Process and outcome is given below:

Software used: **Turnitin** Similarity Index: **7%** Total Word Count: **52,713**

Date: **26/12/2024**

Candidate's Signature

Signature of Supervisor (s)

Curriculum Vitae

DEEPAK SHARMA

C-42, Mandawali Fazalpur Unchepar, Delhi-110092
Ph. No.: +91-8376867911
Email.: ds05705@gmail.com,
deepaksharma_2k21phdce02@dtu.ac.in

EDUCATIONAL QUALIFICATIONS

Year	Degree	University	Division
2021-25	Ph.D. Structural Engineering	Delhi Technological University, Delhi	1st
2018	M.Tech Structural Engineering	G.B. Pant University of Agriculture and Technology, Pantnagar, Uttarakhand	1st
2016	B.Tech Civil Engineering	Dr. A.P.J Abdul Kalam Technical University, Lucknow, Uttar Pradesh	1st (Hons.)
2012	Intermediate	CBSE	1st
2010	High School	CBSE	1st

PROFESSIONAL EXPERIENCE

- Worked as a structure design engineer at Pioneer Consulting Engineers Pvt. Ltd., IP Extension, Delhi-110092 from July 2018 till December 2020.

S.No.	Project Name	Client
1	Revised Office Building, Gurugram	Perfect Office Management Services Pvt. Ltd.
2	Group Housing (Paradise-II), Ghaziabad	High End Infratech Pvt. Ltd.
3	INHS Kalyani, 604 Bedded Command Hospital, Vishakhapatnam	Chief Engineer (INDIAN NAVY), MES

In all the above industrial projects I was involved in designing of RCC Beams, Columns, Slab,Foundation, Retaining walls etc. The modelling of structures was performed using ETABS, SAFE and detailing was done using AUTOCAD, utilizing IS456, IS800, IS875 and other supporting standards.

INDUSTRIAL TRAINING

- Summer Internship of 6 weeks at DMRC and Vijay Nirman Pvt. Ltd. in CC64R project.
- Summer Internship of 6 weeks at Rural Engineering Department, Ghaziabad.
- Certified Software training of Autocad and Staad.pro V8i at CETPA INFOTECH Pvt. Ltd.

ACADEMIC PROJECTS

- **B.Tech:** Investigation of Engineering Properties of Soil and Fly Ash Mixes.
- **M.Tech:** Effects on Compressive Strength of Recycled and Natural Aggregate Concrete Using Black Lentil Powder Subjected to Elevated Temperature and Gradual Cooling.
- **Ph.D.:** Wind Effects on the Roof of Low-Rise Structures

PUBLICATIONS

- **Sharma, D.,** Pal. S. and Raj, R. **"Numerical Prediction of Proximity Effects on Wind Loads on Low-Rise Building with Cylindrical Roofs"**, Wind and Structure, An International Journal, 36 (4), April 2023, 277-292. **https://doi.org/10.12989/was.2023.36.4.277.** (SCIE, IF-1.6)

- **Sharma, D.,** Pal, S. and Raj, R. **"Effect of spacing on wind-induced interference on the roof of low-rise buildings with cylindrical roof using CFD simulation,"** Sadhana - Acad. Proc. Eng. Sci., vol. 48, no. 4, 2023, doi: **https://doi.org/10.1007/s12046-023-02351-5.** **(SCIE, IF-1.6)**

- Kumar, A., Meena, R.K., **Sharma, D.** and Raj, R. **"Structural parameters of Wrench – C shape building using CFD"**, International Journal of Construction Management, Taylor & Francis, **https://doi.org/10.1080/15623599.2023.2271218.** **(ESCI, IF-4.5)**

- **Sharma, D.**, Raj, R. and Pal, S. "**Effects of Roof Shapes on Wind Pressure Distribution of Multi-Span Low-Rise Buildings**," Proc. Int. Struct. Eng. Constr., vol. 10, no. 1, pp. 1–6, 2023, doi: https://**doi.org/10.14455/10.14455/isec.2023.10(1).str-19.** **(Scopus)**

- **Sharma, D.,** Pal, S and Raj, R. **"CFD Simulation of Wind Effects on Cylindrical Roof of T-Plan Multi-Span Low-Rise Building"**, Lecture Notes in Civil Engineering, Springer. **https://doi.org/10.1007/978-981-96-4902-0_2** **(Book Chapter, Scopus)**

- **Sharma, D.,** Raj, R. and Pal, S. **"Effects of different types of roofs under wind loads for low-rise structures,"** AIP Conference Proceedings, 2024, vol. 030008. **https://doi.org/10.1063/5.0192953.** **(Scopus)**

- Arya, S.M., **Sharma, D.** and Raj, R. (2024) "**Analysis of Wind Effects on Tall Buildings of Irregular Cross-Sections Using Numerical Simulation**", Computational Analysis of Buildings, Engineering Research Transcripts, Grinrey Publishing, pp. 1–14. doi: https://doi.org/**10.55084/grinrey/ERT/978-81-964105-4-4_1.** **(Book Chapter, Scopus)**

- Mishra, A., Verma, A., Ranjan, A., **Sharma, D.** and Raj, R. (2024) **"CFD Investigation of Aerodynamic Effects on Multi-span Low-rise Structures with Curved Canopy Roofs of Different Apex Height"**, Computational Analysis of Buildings, Engineering Research Transcripts, Grinrey Publishing, pp. 15–42. doi: https://doi.org/**10.55084/grinrey/ERT/978-81-964105-4-4_2.** **(Book Chapter, Scopus)**

- Chaurasia, A.K., Anand, A.K., Meena, A., **Sharma, D**. and Raj, R. (2024) **"CFD Simulation of Wind-Induced Interference Effects on Low-Rise Gable Roof Structure using ANSYS",** Computational Analysis of Buildings, Engineering Research Transcripts, Grinrey Publishing, pp. 63–74. doi: https://doi.org/**10.55084/grinrey/ERT/978-81-964105-4-4_4.** **(Book Chapter, Scopus)**

- **Sharma, D.,** Saggu, K., Raj, R and Pal, S. (2024) **"Optimizing Wind-Induced Interference on Mono-Slope Roof: Insights from CFD Modelling and Machine Learning Validation."** National Conference on Futuristic Structural Engineering, StructE NatCon 2024, 8-10 Nov. 2024, Indian Association of Structural Engineering,

Delhi, India. **(Under Process of Publication, Scopus)**

- Sharma, D., Pandey, S., Thakur, N., Nath, P. and Raj, R. (2024) **"Optimizing Wind Load Performance through Shape Modifications and Corner Configurations in High-Rise Buildings: A Computational Fluid Dynamics Study"** Institution of Engineers India, Series A. **(under revision, Scopus)**

- **Sharma, D.** and Katariya, S.K. (2017) **"Investigation of Engineering Properties of Soil and Fly Ash Mixes"** in **All India Seminar on Advances in Technology to Mitigatethe Effects of Natural Hazards (ATMENH-2017)** organized by **Institute of Engineer's, India, Pantnagar Local Centre.**

- **Sharma, D.** and Katariya, S.K. "Effects on Strength of Natural and Recycled Aggregate Concrete Subjected to Elevated Temperature and Gradual Cooling", International Journal of Current Trends in Engineering and Technology (IJCTET), ISSN: 2395-3152, Vol: 04, Issue: 02 (March-April, 2018).

CONFERENCE PARTICIPATED (NATIONAL/INTERNATIONAL)

- National Conference on Futuristic Structural Engineering, StructE NatCon 2024, 8-10 Nov. 2024, Indian Association of Structural Engineering, Delhi, India.

- Engineering Advances 2024, First International Conference, 12-14, June 2024, Pravara Rural Engineering College, Loni, Ahmednagar, Maharashtra, India in association with Technology Research and Innovation Centre, India, Accra Technical University, Accra, Ghana, Academy of Nanotechnology and Waste Water Innovations, South Africa.

- International Conference on Research Advances in Engineering and Technology (ITechCET 2024), 24-25 May 2024, Musaliar College of Engineering and Technology, Pathanamthitta, Kerala, India.

- International Conference Futuristic and Sustainable Aspects in Engineering and Technology (FSAET, 2023), 28-30 Nov. 2023, Department of Civil Engineering, GLA University, Mathura, Uttar Pradesh.

- 7th International Conference on Construction, Real Estate, Infrastructure and Project Management (ICCRIP 2023), 11-13 August 2023, NICMAR University, Pune, India.

- The Twelfth International Structural Engineering and Construction Conference (ISEC 12), 14-18 August 2023, University of Illinois, Chicago, USA.

- International Conference on Advances in Civil Engineering (ICACE, 2022), 20-22 Dec. 2022, Technology Research and Innovation Centre, India and hosted by LSKBJ College of Engineering, Chandwad, Nashik, India.

CONFERENCE/FDP/SEMINARS (ORGANIZED/VOLUNTEERED)

- Contributed as an organizing committee member in 5-day faculty development programme on **Disaster Preparedness and Risk Reduction,** organized by **Civil Engineering Department, DTU** in collaboration with **National Institute of Disaster Management, 11-15 December 2023.**

- Contributed as a volunteer in organizing **A Motivational Talk on Being an Entrepreneur** by Sh. Narayan Sigh Rao in Civil Engineering Department, DTU on 10th December 2022.

- Contributed as an organizing member of **Second International Conference in Construction Engineering (ICCE 22), 28-30 November 2022 in hybrid mode at Higher Institute of Earthquake Studies and Research (HIESR)-Damascus University, Syria.**

ACHIEVEMENTS/EXTRA-CURRICULAR

- **Research Excellence Award** for SCI/SCIE publication from Delhi Technological University.
- GATE (CE) 2025 Qualified
- **Best Paper Award** in Engineering Advances 2024, First International Conference, Pravara Rural Engineering College, Loni, Ahmednagar, Maharashtra, India in association with Technology Research and Innovation Centre, India, Accra Technical University, Accra, Ghana, Academy of Nanotechnology and Waste Water Innovations, South Africa.
- **Best Paper Award** in ICCRIP 2023, International Conference, NICMAR, Pune, India
- **Bronze Medal** in academics at college level.
- **Consistently in top-3** students of B.tech. civil Engineering in college.
- **Excellence in Conduct Award** in school at intermediate level.
- Two times **First Runner-up** in dance championship in college annual fest.
- Winner of various technical events in college annual fest.

INTERPERSONAL SKILLS

- Disciplined, dedicated and hardworking with an ability to easily adapt to changing work environments and technology.
- Keen learner with ability to learn new knowledge with ease.
- Good inter-personal and communication skills.
- Ability to work in team and at individual level.
- Ability to rapidly build relationship and set up trust.
- Ability to work under pressure and tight schedules.

HOBBIES/INTERESTS

- Listening Music
- Drawing and Sketching
- Dancing

PERSONAL INFORMATION

Mother's Name	:	Smt. Lata Sharma
Father's Name	:	Sh. R.S. Sharma
Date of Birth	:	13 May 1995
Sex and Marital Status	:	Male/ Unmarried
Language Proficiency	:	English, Hindi

REFERENCES

- Prof. Shilpa Pal, Professor, Civil Engineering, Delhi Technological University, Delhi, India, shilpapal@dtu.ac.in
- Dr. Ritu Raj, Assistant Professor, Civil Engineering, Delhi Technological University, Delhi, India, rituraj@dtu.ac.in
- Dr. S.K. Katariya, Associate Professor, Civil Engineering, G.B. Pant University of Agriculture and Technology, Pantnagar, Uttarakhand, drskkatariya@gmail.com

DECLARATION

I do hereby declare that the above information is true to the best of my knowledge.

(Signature)

Name: DEEPAK SHARMA
Place: DELHI